GE Power Systems

Utility Advanced Turbine Systems (ATS) Technology Readiness Testing

Phase 3R

Final Report – Volume 1 Program Overview

June, 2001

Prepared for U.S. Department of Energy
National Energy Technology Laboratory
Morgantown, WV 26507-0880

Prepared by General Electric Company
Power Generation Engineering
Schenectady, NY 12345

DOE Cooperative Agreement No. DE-FC21-95MC31176

Table of Contents

Abstract 1

ATS Final Report – Program Review

Executive Summary 3
- Background 3
- Program Objective Achieved 3
- Program Goals 4
- Program Goals Achieved 5
- Benefits to the Public 6
- H System™ Spin-offs/Flowdown to Other Products 7
- "Design for Six Sigma" Design Process 7
- Compressor 9
- Combustion 10
- Rotor System 10
- Control Systems 10
- Turbine 11

ATS Program Summary 12
- Rationale for the H System™ 12
- ATS Background 12
- Conceptual Design 14
- The Case for Steam Cooling 14
- H System™ Combined Cycle System 16
- Specific Output 17
- System Strategy and Integration 17
- Reliability, Availability, Maintainability (RAM) 19
- Integrated Gasification Combined Cycle 20

Gas Turbine Validation Testing for Low Risk 20
- Compressor 24
- Compressor Test Rig Program 24
- Baseline Compressor 24
- 9H Compressor 25
- 7H Compressor 26
- Combustor Testing 27
- Combustor Design Status 28
- Turbine Design 30
- Materials 32
- Turbine Design Status 32
- Nozzle Cascade Testing 35
- Turbine Rotor Rig Test 37
- Rig Description 38
- Gas Turbine Factory Tests 38

Conclusion 41

List of Figures

1 7H Gas Turbine Being Transported to the Test Stand 4
2 DOE Sponsored H/ATS Technology Flowdown to Other Gas Turbines 8
3 Schedule for ATS Phases 1 through 3R 13
4 Combustion and Firing Temperatures 14
5 Impact of Stage 1 Nozzle Cooling Method 15
6 H Combined Cycle and System Description 16
7 7H and 7FA Footprint Comparison 17
8 Mark VI – ICS Design Integrated with H System™ Design 18
9 Heat Recovery (HR) IGCC Design Block Flow Diagram 21
10 Components Tested During ATS Program 22
11 9H Subscale Test Rig Cross Section 25
12 Comparison of 7H and 9H Rig Flowpaths 26
13 7H Compressor Map 27
14 H Combustion Test Stand – Side View 28
15 Combustion System Cross-Section 28
16 Fuel Injection System Cross-Section 29
17 Combustion Mode Staging Scheme 30
18 NOx Baseload Emissions as a Function of Combustor Exit Temperature 31
19 Comparison of 7H and 9H Flowpaths 32
20 Full Scale Stage 1 Nozzle Heat Transfer Test Validates Design and Analysis Predictions 33
21 Materials Validation Testing in Steam 34
22 Thermal Barrier Coating Durability 34
23 9H Cascade Vane Orientation 36
24 Cross Section of Steam Delivery Rotating Rig 38
25 9H Gas Turbine in Half Shell Prior to First FSNL Test 39
26 7H Gas Turbine Being Assembled 40
27 7H Gas Turbine Being Installed in Test Stand 41

Abstract

The following paper provides an overview of GE's *H System*™ technology, and specifically, the design, development, and test activities associated with the DOE Advanced Turbine Systems (ATS) program. There was intensive effort expended in bringing this revolutionary advanced technology program to commercial reality. In addition to describing the magnitude of performance improvement possible through use of *H System*™ technology, this paper discusses the technological milestones during the development of the first 9H (50Hz) and 7H (60 Hz) gas turbines.

To illustrate the methodical product development strategy used by GE, this paper discusses several technologies that were essential to the introduction of the *H System*™. Also included are analyses of the series of comprehensive tests of materials, components and subsystems that necessarily preceded full scale field testing of the *H System*™. This paper validates one of the basic premises with which GE started the *H System*™ development program: exhaustive and elaborate testing programs minimized risk at every step of this process, and increase the probability of success when the *H System*™ is introduced into commercial service.

In 1995, GE, the world leader in gas turbine technology for over half a century, in conjunction with the DOE National Energy Technology Laboratory's ATS program, introduced its new generation of gas turbines. This *H System*™ technology is the first gas turbine ever to achieve the milestone of 60% fuel efficiency. Because fuel represents the largest individual expense of running a power plant, an efficiency increase of even a single percentage point can substantially reduce operating costs over the life of a typical gas-fired, combined-cycle plant in the 400 to 500 megawatt range.

The *H System*™ is not simply a state-of-the-art gas turbine. It is an advanced, integrated, combined-cycle system in which every component is optimized for the highest level of performance.

The unique feature of an H-technology combined-cycle system is the integrated heat transfer system, which combines both the steam plant reheat process and gas turbine bucket and nozzle cooling. This feature allows the power generator to operate at a higher firing temperature than current technology units, thereby resulting in dramatic improvements in fuel-efficiency. The end result is the generation of electricity at the lowest, most competitive price possible. Also, despite the higher firing temperature of the *H System*™, the combustion temperature is kept at levels that minimize emission production.

GE has more than 3.6 million fired hours of experience in operating advanced technology gas turbines, more than three times the fired hours of competitors' units combined. The *H System*™ design incorporates lessons learned from this experience with knowledge gleaned from operating GE aircraft engines. In addition, the 9H gas turbine is the first ever designed using "Design for Six Sigma" methodology, which maximizes reliability

and availability throughout the entire design process. Both the 7H and 9H gas turbines will achieve the reliability levels of our F-class technology machines.

GE has tested its *H System*™ gas turbine more thoroughly than any previously introduced into commercial service. The *H System*™ gas turbine has undergone extensive design validation and component testing. Full-speed, no-load testing of the 9H was achieved in May 1998 and pre-shipment testing was completed in November 1999. The 9H will also undergo approximately a half-year of extensive demonstration and characterization testing at the launch site. Testing of the 7H began in December 1999, and full speed, no-load testing was completed in February 2000. The 7H gas turbine will also be subjected to extensive demonstration and characterization testing at the launch site.

ATS Final Report-Program Review

Executive Summary

Background

In response to the Department of Energy's Energy Information Administration (DOE/EIA) early 1990's projection that there will be a significant increase in demand for electricity in the US during the next two decades, the DOE initiated the Advanced Turbine Systems (ATS) program to produce advanced power generation gas turbines. These gas turbines would be more fuel efficient, environmentally friendly, and less expensive to operate than the utility gas turbine units available in the early 1990's.

DOE's National Energy Technology Laboratory (NETL) in the Office of Fossil Energy, and the Office of Industrial Programs in the Office of Energy Efficiency and Renewable Energy share responsibility with their industrial partners for development of these revolutionary systems. Expectations for the resulting power generation system are to meet or exceed 60 percent system efficiency in the utility market using natural gas fuel. Although first designed to operate with natural gas, the technology is intended to evolve to full fuel-flexibility, allowing a coal-derived or renewable biomass-based gas to be used. In addition, the system resulting from ATS technology will emit far less nitrogen oxides, carbon dioxide, and unburned hydrocarbons than current gas turbine systems. The ATS program emphasizes reducing the cost of generating electricity with gas turbines, while increasing their efficiency, and lowering emissions. ATS turbines are projected to enter the pre-commercial demonstration stage in 2003, and commercialization is expected in 2004.

By setting stretch goals in a variety of technical areas, the DOE has challenged the gas turbine manufacturers to develop innovative solutions to meet these goals.

Note: The GE Power Systems (GEPS) ATS program is a part of a larger *H System*™ program, which includes the MS9001H (9H, 50 Hz) gas turbine to be exported from the GEPS Greenville, SC manufacturing facility. There was common component technology development for both engines, and as the 9H preceded the MS7001H (7H, 60 Hz) ATS gas turbine in construction and testing, valuable lessons were learned from the initial 9H test program that benefited the 7H design and subsequent testing.

Program Objective Achieved

The overall objective of the Advanced Turbine System (ATS) program Phase 3R (restructured Phase 3 – Technology Readiness Testing) was to develop and demonstrate a highly efficient, environmentally superior, and cost-competitive utility ATS for base-load, utility-scale power generation. In Phase 3R, GE Power Systems did achieve the overall objective by designing and testing components critical to the ATS design, and

incorporating their components into the final *H System*™ design. The full scale 7H (60 Hz) gas turbine was designed, fabricated, and successfully tested at Full Speed, No Load (FSNL) conditions at GE's Greenville, SC manufacturing/testing facility. Figure 1 shows the 7H being transported to the test stand.

Figure 1. 7 H Gas Turbine being transported to the test stand.

Program Goals

DOE support was instrumental in the success of the GE ATS program, providing sufficient and timely financial support to facilitate the extensive development program tasks in a timely manner. Without this extensive support, the H System development would have taken considerably longer to complete, due to internal corporate funding constraints. The DOE support for the ATS also allowed GE to remain competitive (versus foreign utility gas turbine suppliers) in the emerging global high technology utility power generation market. The ATS system developed had the following DOE required program goals:

- System efficiency that would meet or exceed 60 percent, lower heating value basis.
- Environmental superiority and acceptance in severe non-attainment areas under full load operating conditions without the use of post-combustion emissions controls.

Environmental superiority and acceptance in non-attainment areas includes limiting NOx to less than 10 parts per million by volume (dry basis) at 15 percent oxygen, with acceptable carbon monoxide and unburned hydrocarbon emissions.

- Busbar energy costs that are 10 percent less than current (1992) state-of-the-art turbine systems meeting the same environmental requirements.

- Fuel-flexible designs operating on natural gas, but also capable of being adapted to operate on coal (syngas) or biomass (syngas) fuel.

  Reliability-Availability-Maintainability (RAM) that is equivalent to modern advanced power generation systems.

- Commercial systems that could enter the market in the year 2000.

Program Goals Achieved

- System efficiency.

  The GEPS ATS combined cycle (gas turbine and steam turbine in series) system has been designed to achieve 60 percent efficiency when run at the base load design conditions, a significant advance over 1990's levels. This will be achieved by increasing the firing temperature (the combustion gas temperature entering the turbine section) without increasing the combustion temperature through the use of a unique closed-loop cooling scheme that utilizes the superior heat transfer characteristics of steam (compared to air). The first two stages of the turbine are steam-cooled, with the steam being recycled for use in the steam turbine to produce additional power.

  Combined cycle system optimizing studies were used in the design of the ATS power plant. These studies showed that the GE ATS design is on track to achieve the 60 percent efficiency goal. Initial testing of the 7H gas turbine at the Greenville, SC manufacturing site has verified the analytical models. The first full scale *H System*™ will be run at Baglan Bay, UK in 2002.

- Environmental Superiority.

  GEPS has designed and tested a lean premixed natural gas combustion system that meets the ATS NOx goal of 9 ppmvd, with carbon monoxide and unburned hydrocarbons below 20 ppm, without post-combustion clean-up. The combustion system has been demonstrated at full-scale (flow, pressure, temperature) engine operating conditions in a test stand at GE Aircraft Engines in Evendale, OH.

- Busbar energy cost 10% below 1992 cost.

  There are many components that make up the cost of electricity, including capital equipment, fuel, cost of capital/interest rates, and supply and demand. As these

component costs are site specific, there is no one value for energy cost. The high efficiency ATS machine will allow the conversion of fuel energy into electricity greater than 10 percent more efficiently than 1992 levels.

- Fuel Flexible design.

  The GEPS ATS gas turbine has been designed to use natural gas fuel, but the design can evolve to allow use in an integrated gasification combined cycle (IGCC) power system that uses coal-derived syngas, or biomass derived syngas fuel. ATS IGCC performance has been calculated for the 7H power train with coal-based syngas.

- Reliability, Availability, Maintainability (RAM)

  GE has completed a RAM analysis that verifies that the ATS gas turbine is equivalent to GE's current "F" technology gas turbines. As much of the *H System*™ technology is based on proven, established design practices, and new technologies are validated by extensive component design and testing, GE expects that the *H System*™ RAM will be equivalent to current advanced technology gas turbines.

- Commercial Availability by 2000

  The first *H System*™ technology gas turbine for development/commercial use will be the 50 Hz 9H, which is sited at Baglan Bay, UK. This machine will undergo on-site testing, including testing the steam-cooling system under full load conditions for the first time, starting in 2002. The first 60 Hz ATS engine will be located at Sithe Energies, Scriba, NY facility, and will undergo full load development testing in 2003 before entering commercial service.

Benefits to the Public

The ATS gas turbine will provide significant public benefits through improvements in a variety of measurable parameters. These include:

- Lower energy consumption and fuel cost savings - The ATS will lower energy consumption due to its higher efficiency design, and will lead to fuel cost savings by displacing less efficient producers, either as a choice for new capacity installation, or as a retrofit to repower older fossil units.

- Electricity cost savings – The installation of ATS machines will lead to a lower cost of electricity to the grid. The new machines will lower the marginal cost of electricity production over a wide range of capacity factors, and consequently increase the overall competitiveness of U. S. industry and reduce costs to consumers.

  Emissions reduction – By introduction of the ATS machines into the power system grid, there will be a significant reduction in CO2, NOx, and SO2 emissions. Due to

the low emissions design goal and displacement of older power systems that use oil or coal, there will be a quantifiable reduction in emissions.

- Job creation – The projected demand for turbines in the large utility size range will increase production jobs to fulfill this demand, as well as provide additional employment at parts vendors, and in the power plant construction and supply industries.

- Gas turbine export – There is a large potential worldwide demand for the ATS size machines. This demand is projected to be larger than U. S. market requirements in the next two decades. Historically, U. S. manufacturers have provided over half of the worldwide power system gas turbines. Retaining this market share with a competitive product will provide additional employment stability, and improve the U.S. balance of payments account.

- Conservation of land, water resources – As the ATS machines replace older fossil units, there will be a reduction in demand for land and water resources. As the new machines are relatively compact, less land will be required for installation, and there will be less demand for water resources, such as cooling tower makeup water and wastewater discharge.

H System™ Spin-offs/Flowdown to Other Products

The ATS machine (*H System*™) efficiency goal was a major challenge, requiring advancements in virtually all of the components comprising a utility power generation gas turbine. Systematic design and development programs, utilizing the "Design for Six Sigma" methodology, were utilized for all of the engine components.

The following list highlights the major advancements whose technology has become incorporated in GE's corporate database and overall design system. All future GEPS product developments will benefit from this upgrade, and there is an ongoing program to evaluate new technology for incorporation into existing products in a cost-effective manner.

"Design for Six Sigma" Design Process

The *H System*™ was the first GEPS Product to utilize the NPI (New Product Introduction/DFSS [Design for Six Sigma]) design process. The formalization of the design process allows GEPS to benchmark itself against other GE high technology businesses, and to take advantage of improved analytical and experimental techniques that arise in other GE businesses. GE's company-wide quality control program, Six Sigma, has brought about numerous improvements in design philosophy. By using Six Sigma, GE has developed a statistical, data driven-process that focuses on maximizing reliability and availability throughout the entire design process.

During the NPI design phases, optimal performance and specifications are determined for the entire power plant, and then driven down to an individual basis for the gas turbine, compressor, aerodynamic components, and materials selection. For example, when the conceptual design phase is complete, thermodynamic boundary conditions have also been established, and the system design architecture has been identified. Material characterization testing is then completed to obtain early data relative to design requirements.

Within the preliminary design phase, the piece part design definitions are determined. For example, the compressor airfoil shape is defined through balancing aerodynamic and mechanical constraints. Periodic design reviews are conducted for each component to support GE's design practices. These have been derived over years of experience, and in conjunction with GE Aircraft Engines and Corporate Research and Development, guide the designer through process requirements, and benefits of lessons learned.

The immediate beneficiary of the ATS design is the MS7001 FB gas turbine design. This design is using the DFSS design process, and will be the first to incorporate a large number of technical advances initiated in the *H System*™ program. These spin-off or flow-down technologies are shown by component in Figure 2, and are briefly described below.

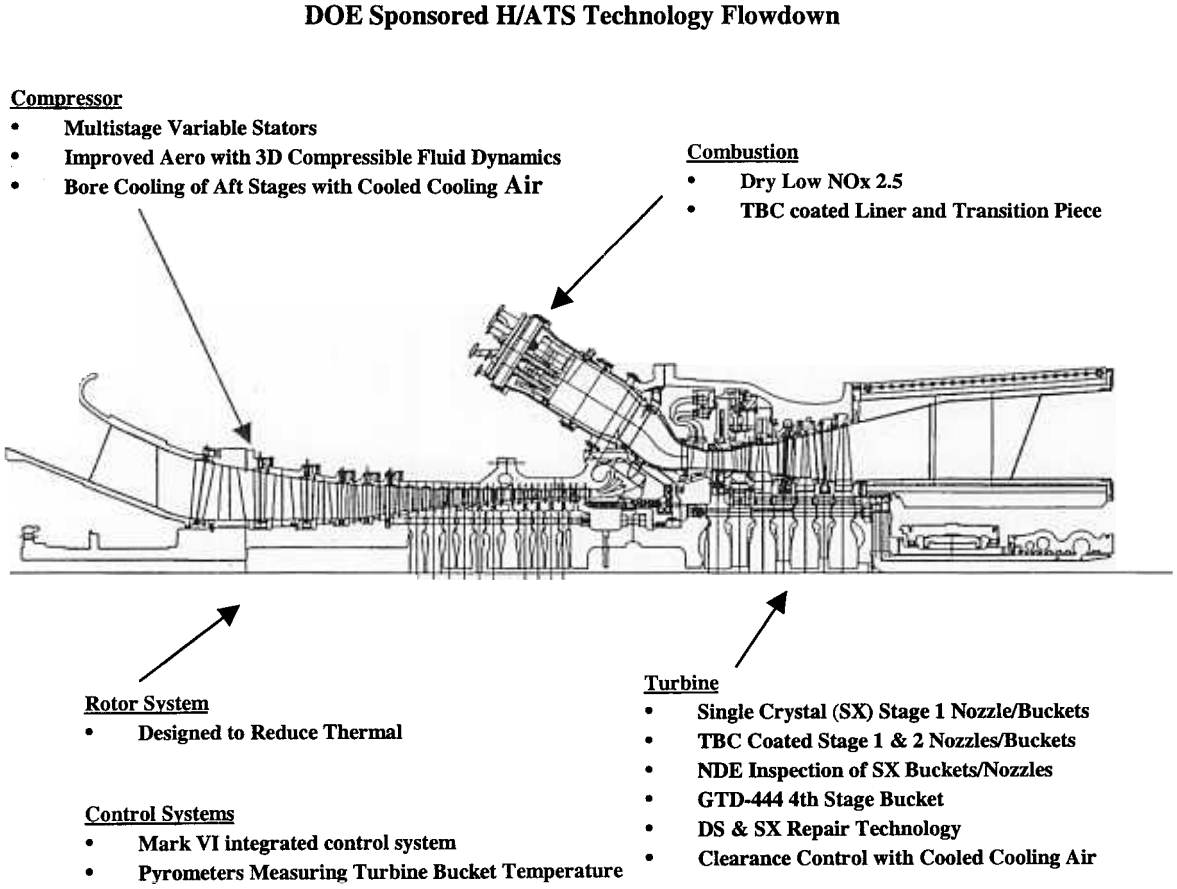

Figure 2. DOE Sponsored H/ATS Technology Flowdown to Other Gas Turbines

Compressor

The *H System*™ compressor provides a 23:1 pressure ratio with 1510 lbs/sec (685 kg/sec) and 1230 lbs/sec (585 kg/sec) airflow for the 9H and 7H gas turbines, respectively. These units are derived from the high-pressure compressor GE Aircraft Engines (GEAE) uses in the CF6-80C2 aircraft engine, and the LM6000 aeroderivative gas turbine. For use in the *H System*™ gas turbines, the CF6-80C2 compressor has been scaled up (2.6:1 for the 7H, and 3.1:1 for the 9H), with four stages added to achieve the desired combination of airflow and pressure ratio. The CF6 compressor design has accumulated over 20 million hours of running experience, providing a solid design foundation for the *H System*™ gas turbine.

The ATS gas turbine required many developments in compressor technology beyond then current GE Power Systems design procedures. These new technologies include: new aerodynamic design for the front and aft sections of the compressor, including a "0" stage for high flow; low radius ratio front stages blade designs; low aspect ratio exit vane design; multiple stage forward spool shaft design; high rabbet rotor design; 7H single through bolt rotor construction; multiple passage rotor air cooling system; multiple stage variable guide vane (VGV) system; new blade axial retention design; trenched casing flowpath design; tri-passage diffuser design (GE patent); and 9H compressor discharge case (CDC) double wall clearance control casing.

All of the ATS compressor developments are now part of GE's corporate design database, and any or all may be utilized in future designs. Of specific interest are the following.

The *H System*™ compressors have several rows of variable stator vanes (VSV) at the front of the compressor, in addition to the variable inlet guide vane (IGV) used on prior GE gas turbines to modulate airflow. These are used in conjunction with the IGV, to control compressor airflow during turndown, as well as optimize operation for variations in ambient temperature.

The *H System*™ compressors also utilized improved 3-D computational fluid dynamic (CFD) tools in the redesign of the flowpath and blade geometry. The 3-D design of the rotor blade root contours improved the air flow, and consequently reduced losses. The three compressor rig tests verified the use of the 3-D CFD tools, and these tools are now part of GEPS design practice. The engineering work stations were linked into a "virtual super computer" for these advanced designs.

The *H System*™ machine compressors have a bore cooling system for the rear stages that utilizes cooled compressor discharge cooling air to regulate the temperature and minimize thermal stress, and allows use of current disk materials (steel wheels instead of Inconel for cost reduction).

Combustion

The *H System*™ can-annular combustor system is a lean pre-mix Dry Low NOx (DLN) system, similar to the GE DLN combustion systems currently used in FA-class service. The H DLN 2.5 combustion system has demonstrated single digit NOx and CO levels at full power conditions in the GEAE full scale test rig. This technology is being fed back into the GE combustor design database. In addition, the uniform flow delivered by the tri-passage diffuser was confirmed during the combustor test program.

The thermal barrier coating (TBC) coated liner and transition piece both required advances in design and part fabrication. Due to the high temperatures encountered, the material for both was changed to GTD-222 from Nimonic-263. TBC was added to both parts to improve part life. The heat treatment process and TBC application methods developed will be utilized in other high-temperature applications.

Rotor System

An analytical computer structural model (using ANSYS) was constructed to develop a response surface for "backbone bending" due to bottom-to-top casing temperature gradients. These gradients distort the case relative to the unit rotor, causing rubbing of the compressor airfoil tips. Using the case distortion model, a refined understanding of the casing behavior was obtained, leading to a redesign of the air ventilation system around the exterior of the gas turbine. This analysis and design changes are being done for the rest of the GE Power Systems gas turbine product line to allow blade clearance reductions and corresponding increased performance.

Control Systems

The *H System*™ uses the Mark VI integrated control system, a full-authority digital controller that manages the operation of the gas turbine, steam turbine, and generator power train and the steam flows between the HRSG, steam turbine, and gas turbine. The Mark VI also schedules distribution of cooling steam to the gas turbine. A diagnostic capability is built into this control system, which also stores critical data in an electronic historian for easy retrieval and troubleshooting. The Mark VI technology has been incorporated into the GE Power Systems control design architecture, and is the baseline control technology for new Power Systems products, and is being incorporated into existing machines.

The *H System*™ uses pyrometers to monitor the stage 1 and stage 2 bucket temperatures in order to detect a sudden loss of steam-coolant. The pyrometers are used because: 1) they respond quickly to the parameter of concern (temperature), 2) all of the buckets come into the field of view, and 3) the response time of the detection system is very fast. The pyrometer system signal is sent to the Mark VI controller, and can shut the engine down if a temperature problem is detected. The pyrometer technology is being incorporated into other (non-steam-cooled) engines for temperature monitoring of turbine

buckets, which allows for condition based maintenance programs for life extension, and consequent lower overall cost of electricity.

Turbine

The *H System*™ uses single crystal steam-cooled nozzles and buckets in the turbine first stage. The closed-loop internal steam-cooling eliminates the film cooling on the gas path side of the airfoil, and consequently increases the temperature gradients through the airfoil walls, resulting in higher thermal stresses on the airfoil materials. Keeping the airfoil wall thickness within specified limits is essential for maintaining material temperature gradients and consequent thermal stresses within allowable limits. Extensive development effort was expended by the casting vendor and GE to develop a process to maximize the stability of the cores at casting temperatures, in order to produce airfoil wall thicknesses within the desired limits. This production procedure is now available for other large single crystal GE gas turbine components.

Thermal barrier coating (TBC) is used on the flowpath surfaces of the steam-cooled turbine airfoils to allow operation at increased turbine inlet temperatures while maintaining airfoil substrate temperatures at levels that meet ATS life goals. Extensive TBC development activities have been completed under the ATS program, including: development of an air plasma spray deposition process developed and patented at GE-CRD; an improved bond coat system and application process; robot motion control software for TBC application; oxidation and mechanical property measurements in a steam environment; and high temperature gradient testing in an e-beam test facility that replicates the surface temperature and thermal gradient expected in the ATS machine. Results of this extensive TBC development and testing are being utilized throughout the GEPS product line, including new machines, and in upgrades to existing machines.

Improved methods for non-destructive evaluation (NDE) have been developed that exceed the capability offered by currently available inspection technology for inspection of the single crystal and directionally solidified ATS turbine airfoils. Results include prototype ultrasonic and infrared systems for airfoil thickness measurements, both of which have been used by the casting vendor for inspection castings of single crystal and directionally solidified airfoils. In addition, digital radiography x-ray inspection techniques were developed to detect internal casting defects. These NDE methods are now available at the casting vendor, and will be used for inspection of GEPS production airfoils.

The 3600 rpm of the 7H gas turbine, as compared with the 3000 rpm for the 9H, coupled with the large diameter, necessitated a change in fourth stage bucket material, as tip creep was projected to be a problem. By switching materials from the 9H GTD-111 to GTD-444, a 300% improvement in creep life was achieved. This material is now available for use on all GE gas turbines, resulting in lower cost of electricity.

The repair of single crystal (SX) and directionally solidified (DS) airfoils is of concern to gas turbine users, as the replacement of these parts is very expensive. Repair techniques have been developed as part of the ATS program to repair airfoil damage, which extends

the useful component life. These techniques are now part of the GEPS materials database, and have been leveraged to other GE programs.

A dedicated cooling air skid is used to heat and cool the inner turbine shell for both the 9H and 7H gas turbines in order to provide rotor tip clearance control for increased efficiency. Clearance control information is now part of the GEPS turbine design database, and is available for other GE programs.

ATS Program Summary

Rationale for the *H System*™

The use of gas turbines for power generation has been steadily increasing in popularity for more than five decades. Gas turbine cycles are inherently capable of higher power density, higher fuel efficiency, and lower emissions than the competing platforms. Gas turbine performance is driven by the firing temperature, which is directly related to specific output, and inversely related to fuel consumption per kW of output. This means that increases in firing temperature provide higher fuel efficiency (lower fuel consumption per kW of output) and, at the same time, higher specific output (more kW per pound of air passing through the turbine).

The use of aircraft engine materials and cooling technology has allowed firing temperature for GE's industrial gas turbines to increase steadily. However, higher temperatures in the combustor also increase NOx production. In the "Conceptual Design" section of this paper, we describe how the GE *H System*™ solved the NOx problem, and is able to raise firing temperature by 200°F / 110°C over the current "F" class turbines *and* hold the NOx emission levels at the initial "F" class levels.

ATS Background

GEPS has completed design, assembly, and initial testing of the 7H 60 Hz ATS steam-cooled gas turbine. This design evolved from early system studies performed over a decade ago, in which a large number of variations in cycle configurations were evaluated prior to settling on the current concept. As a result of having made a basic cycle configuration selection in advance of the initiation of the DOE ATS program, GE did not elect to participate in Phase 1 (Cycle Identification), Figure 3.

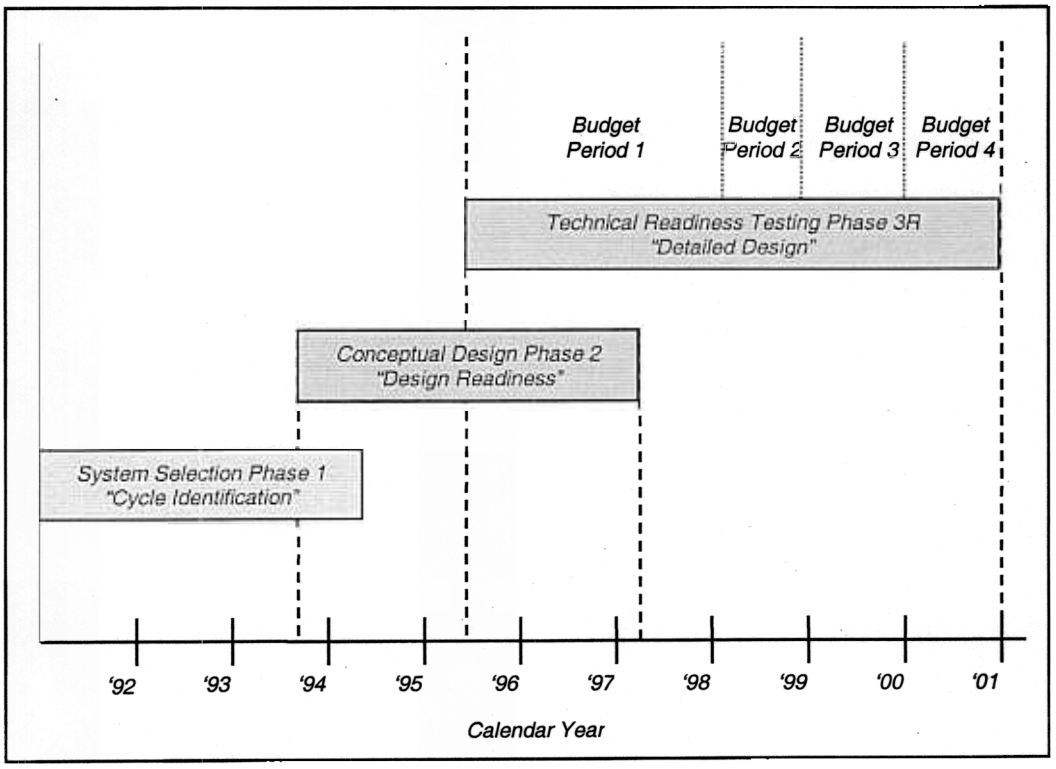

Figure 3. Schedule for ATS Phases 1 through 3 R

A proposal was submitted in 1992 for ATS Phase 2 (Conceptual Design and Project Development), and work began upon contract award in 1993. Through participation in Phase 2, GE was able to analytically and experimentally examine many of the critical technology issues associated with the use of closed circuit steam-cooling in a utility scale gas turbine combined cycle system. These technology issues included materials/steam compatibility, steam cleanliness requirements, heat transfer in steam-cooled rotating components, combined cycle performance, and system startup requirements.

In November 1994, GE submitted a proposal for the Phase 3 (Technology Readiness Testing), and Phase 4 (Pre-Commercial Demonstration) programs and a contract was awarded, with work starting in mid-1995. The design of GE's H technology machines had already begun at that point. In March 1997, DOE issued a Request for Proposal for a restructured program that would extend Phase 3 beyond the December 1997 conclusion date. The restructured program (called Phase 3R) included the Full Speed, No Load (FSNL) testing from Phase 4 of the 7H (60 Hz) ATS machine at the Greenville, SC manufacturing facility. The original Phase 4 was eliminated from the program. Phase 3R is scheduled to conclude in December 2000.

Conceptual Design

The GE *H System*™ is a combined cycle plant. The hot gases from the gas turbine exhaust proceed to a downstream boiler or heat recovery steam generator (HRSG). The resulting steam is passed through a steam turbine, and the steam turbine output then augments that from the gas turbine. The output and efficiency of the steam turbine's "bottoming cycle" is a function of the gas turbine exhaust temperature. For a given firing temperature class, 2600°F / 1430°C for the *H System*™, the gas turbine exhaust temperature is largely determined by the work required to drive the compressor, that is, in turn, affected by the "compressor pressure ratio." The H System's™ pressure ratio of 23:1 was selected to optimize the combined cycle performance, while at the same time allowing for an uncooled last stage gas turbine bucket, consistent with past GEPS practice. The 23:1 compressor pressure ratio, in turn, determined that using four turbine stages would provide the optimum performance and cost solution. This is a major change from the earlier "F" class gas turbines, which used a 15:1 compressor pressure ratio and three turbine stages. With the H System's™ higher pressure ratio, the use of only three turbine stages would have increased the loading on each stage to a point where an unacceptable reduction in stage efficiencies would result. By using four stages, the *H System*™ turbine is able to specify optimum work loading for each stage and achieve high turbine efficiency.

The Case for Steam-cooling

The GE *H System*™ gas turbine uses closed-loop steam-cooling of the turbine. This unique cooling system allows the turbine to fire at a higher temperature for increased performance, yet without increased combustion temperatures or their resulting increased emissions levels. It is this closed-loop steam-cooling that enabled the combined-cycle GE *H System*™ to achieve 60% fuel efficiency while maintaining adherence to the strictest, low NOx standards (Figure 4).

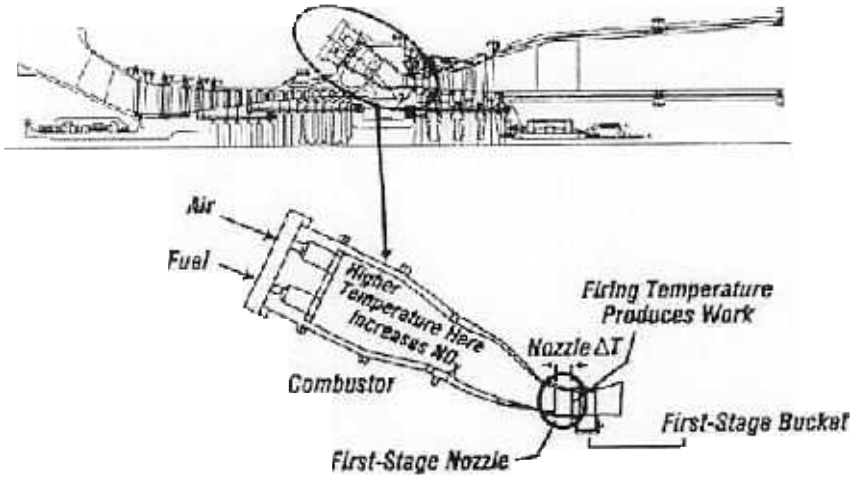

Figure 4. Combustion and Firing Temperatures

Combustion temperature must be as low as possible to establish low NOx emissions, while the firing temperature must be as high as possible for optimum cycle efficiency. The goal is to adequately cool the stage 1 nozzle, while minimizing the decrease in combustion product temperature as it passes through the stage 1 nozzle. This is achieved with closed-loop steam-cooling.

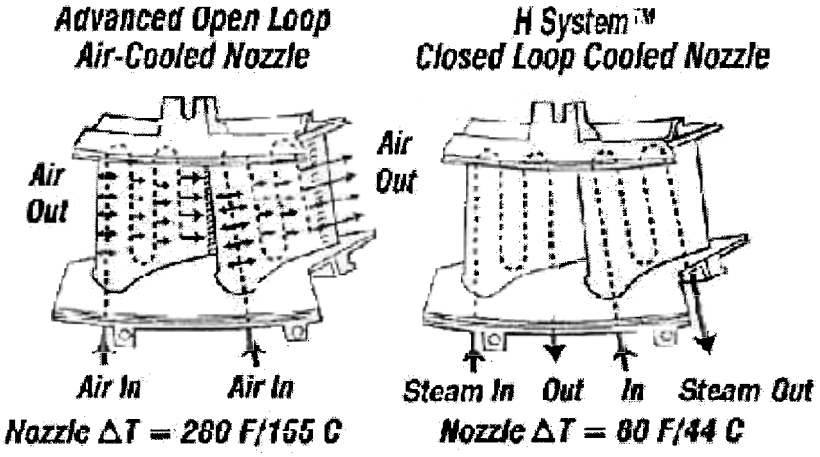

Figure 5. Impact of Stage 1 Nozzle Cooling Method

In conventional gas turbines, with designs predating the *H System*™, the stage 1 nozzle is cooled with compressor discharge air. This cooling process causes a temperature drop across the stage 1 nozzle of up to 280° F/155° C. In *H System*™ gas turbines, cooling the stage 1 nozzle with a closed-loop steam-coolant reduces the temperature drop across that nozzle to less than 80° F/44° C (Figure 5). This results in a firing temperature class of 2600° F/1430° C, or 200° F/110° C higher than in preceding systems, yet with no increase in combustion temperature. An additional benefit of the *H System*™ is that while the steam-cools the nozzle, it picks up heat for use in the steam turbine, transferring what was traditionally waste heat into useable output. The third advantage of closed-loop cooling is that extraction of compressor discharge air is reduced, thereby allowing more to flow to the head-end of the combustor for fuel premixing. In conventional gas turbines, compressor air is also used to cool rotational and stationary components downstream of the stage 1 nozzle in the turbine section. This air is traditionally labeled as "chargeable air," because it reduces cycle performance. In *H System*™ gas turbines, this "chargeable air" is replaced with steam, which enhances cycle performance by up to 2 points in efficiency, and significantly increases the gas turbine output, since more of the compressor air can be channeled through the turbine flowpath to do useful work. A second advantage of replacing "chargeable air" with steam accrues to the H System's™ cycle through recovery of the heat removed from the gas turbine in the bottoming cycle.

H System™ Combined-Cycle System

The *H System*™ combined-cycle system consists of a gas turbine, a three-pressure-level HRSG and a reheat steam turbine. The features of the combined-cycle system, which include the coolant steam flow from the steam cycle to the gas turbine, are shown in Figure 6. The high-pressure steam from the HRSG is expanded through the steam turbine's high-pressure section. The exhaust steam from this turbine section is then split. One part is returned to the HRSG for reheating; the other is combined with intermediate-pressure (IP) steam and used for cooling in the gas turbine. Steam is used to cool the stationary and rotational parts of the gas turbine. The cooling system operates in series with the reheater, with gas turbine cooling steam returned to the steam cycle cold reheat line.

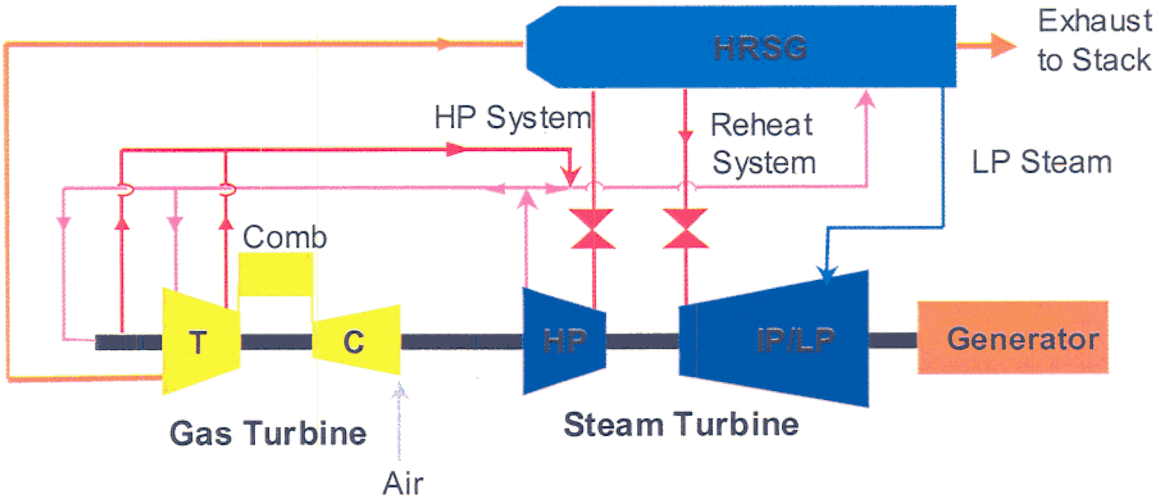

Figure 6. H Combined Cycle and System Description

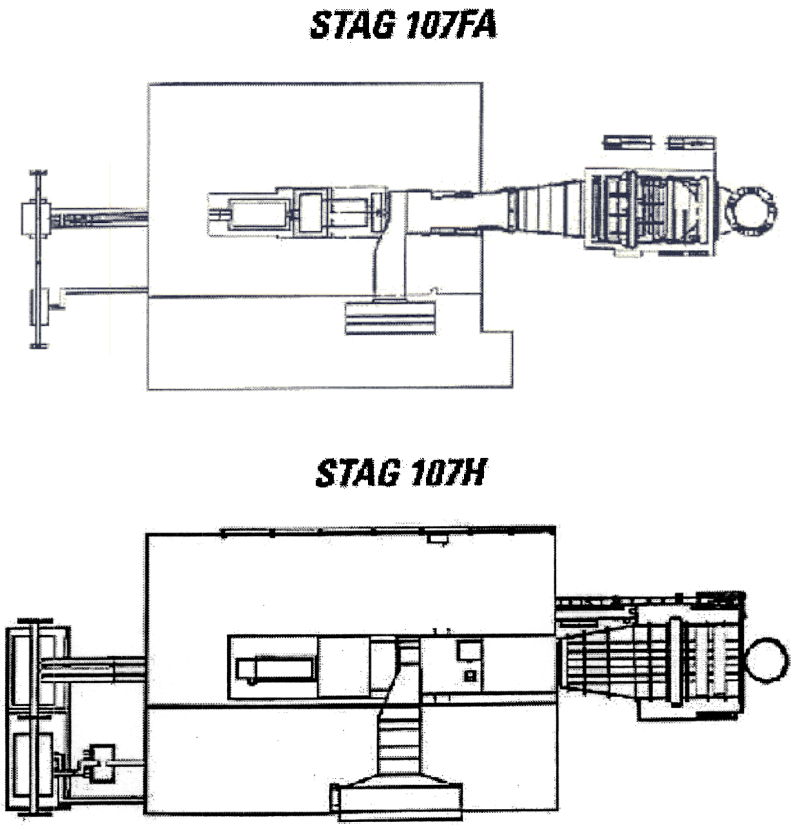

Figure 7. 7H and 7FA Footprint Comparison

Specific Output

One extremely attractive feature of the *H System*™, combined-cycle power plants is the high specific output. This permits compact plant design with a reduced "footprint" when compared with conventional designs, and consequently, the potential for reduced plant capital costs (Figure 7). In a 60 Hz configuration, the H technology's compact design results in a 54% increase in output over the FA plants with an increase of just 10% in plant size. The power density or installed capacity per unit of plot space is increased by 40%, thereby conserving land resources.

System Strategy and Integration

While component and subsystem validation is necessary and is the focus of most NPI programs, other factors must also be considered in creating a successful product. The gas turbine must operate as a system, combining the compressor, combustor and turbine at design point (base load), at part load turndown conditions, and at no load. The power plant and all power island components must also operate at steady state and under transient conditions, from startup, to purge, to full speed. Unlike traditional combined-cycle units, the *H System*™ gas turbine, steam turbine and HRSG are linked into one, interdependent system. Clearly, the reasoning behind these GE *H System*™ components runs contrary to the traditional approach, which designs and specifies each component as

a stand-alone entity. In the *H System*™ the performance of the gas turbine, combined-cycle and balance of plant has been modeled, both steady state and transient; and analyzed in detail, as one large, integrated system, from its inception.

The GE *H System*™ concept incorporates an integrated control system (ICS) to act as the glue, which ties all the subsystems together (Figure 8).

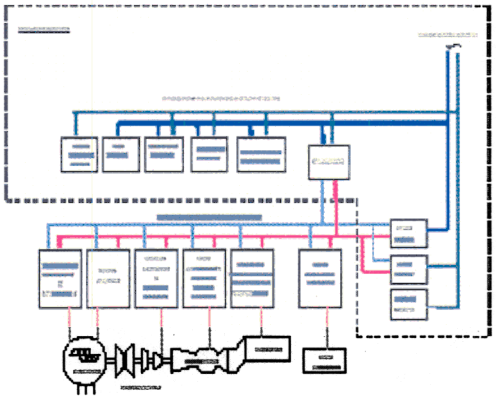

Figure 8. Mark VI – ICS Design Integrated with *H System*™ Design

Systems and Controls teams, working closely with one another as well as with customers, have formulated improved hardware, software, and control concepts. This integration was facilitated by a new, third-generation, full-authority digital system, the Mark VI controller. This control system was designed with and is supplied by GE Industrial Systems (GEIS), which is yet another GE business working closely with GEPS.

The control system for the *H System*™ not only controls operation of the gas turbine, steam turbine and generator power train but also manages steam flows between the HRSG, steam turbine and gas turbine. It also schedules distribution of cooling steam to the gas turbine. A diagnostic capability is built into the control system, which also stores critical data in an electronic historian for easy retrieval and troubleshooting.

The development of the Mark VI and integrated control system has been deliberately scheduled ahead of the H gas turbine to reduce the gas turbine risk. With the help of GE Corporate Research and Development, the Mark VI followed a separate and rigorous NPI risk abatement procedure, which included proof of concept tests and shake down tests of a full combined-cycle plant at GE Aircraft Engines Lynn, Massachusetts factory.

The Systems and Controls teams have state-of-the-art computer simulations at their disposal to facilitate full engineering of control and fallback strategies. Digital simulations also serve as a training tool for new operators.

Simulation capability was used in real time during the 9H Full Speed No Load (FSNL) test in May 1998. This facilitated revision of the accelerating torque demand curves for the gas turbine and re-setting of the starter motor current and gas turbine combustor fuel schedule. The end result was an automated, one button, soft start for the gas turbine, which was used by the TEPCO team to initiate the May 30, 1998 customer witness test.

Reliability, Availability, Maintainability (RAM)

GE's new *H System™* design is the latest development in the evolution toward more efficient, more reliable, (and therefore more productive), electric power generation equipment offerings. This design is currently in its initial offering stage and no full plant operating data are yet available to bear out the engineering predictions for specific power output capability, net plant heat rate, emissions performance, reliability, and availability, which are the principal measures of the long-term "value" of a power plant. GE's target levels of reliability and availability are consistent with the current industry expectations for large combined cycle plants.

The first phase in the *H System™* development process was a thorough assessment of product options, corresponding design concepts, and system requirements. Also crucial in the first phase was careful selection of materials, components and subsystems. These were sorted into categories of existing capabilities or of required technology advancements. The technical risk for each component and subsystem was assessed and abatement analyses, testing, and data requirements were specified. The plans to abate risk and facilitate design were arranged, funded and executed. The second development phase covered product conceptual and preliminary designs. This phase included the introduction of knowledge gained through experience, materials data, and analytical codes from GEPS and GEAE. The *H System™* development program is currently in its third and final phase, Technology Readiness Testing. This phase includes execution of detailed design and product validation through technology rig and full scale component testing. A high degree of confidence has been gained during this third phase through component and subsystem testing, and subsequent validation of analysis codes. The development program will conclude with full-scale gas turbine testing at GE's factory test stand in Greenville, SC, followed by combined cycle power plant testing at the Baglan Energy Park launch site in the United Kingdom for the 9H (50 Hz) machine, and later at Sithe Energies Heritage Station site in upstate New York for the 7H (60 Hz) machine.

It should first be recognized that the controls and accessories support systems typically account for 60% to 80% of a plant's unplanned outage events, and for 50% to 60% of the unplanned outage time. As the new *H System™* machines go into production, the supporting controls and accessories systems are being assembled from the same class of components in the same proven system structures that currently serve the "E" Class and "F" Class product offerings. Much of the *H System™* design is based on proven, established technologies. Designs for the major components of the combined cycle powertrain, including the bearing designs, the evaluation methods for rotor dynamics, the

compressor and turbine blading designs, and the generator field construction methods are all either direct applications of proven design technology or evolutionary refinement of existing designs. It is for these reasons that GE expects that the reliability of the new *H System™* will be fully commensurate with the levels associated with today's "F" Class combined cycle power plants. With maintenance and operations performed at "best practice" levels, the new *H System™* plant should reach its full reliability potential of 97.0% or better.

Integrated Gasification Combined Cycle (IGCC)

One of the ATS program goals is to be a fuel-flexible design, operating on natural gas, but also being capable of operating on coal (syngas), or biomass (syngas). An assessment of the 9H ATS design was performed to determine its ability to accommodate low heating value fuel gas and nitrogen injection for NOx supression, and to determine what IGCC system modifications would be required to utilize this fuel. This approach is also directly applicable to the 7H ATS configuration.

A configuration optimization study of an IGCC power plant design, integrating General Electric's (GE) single shaft combined steam and gas (STAG) 109H combined cycle unit with Texaco's heat recovery coal gasification unit, and Praxair's elevated pressure air separation unit. The full heat recovery IGCC design is preferred for high cost fuels, where high efficiency is important. The cycle analysis and system optimization were performed jointly by GE, Texaco, and Praxair as part of a larger study, the results of which were presented at the October 1999 Pittsburgh Coal Conference. The approach of this study is directly applicable to the 7H ATS 60 Hz configuration.

The oxygen blown type gasification process with conventional low temperature gas cleaning was selected for *H System™* IGCC over the optional air blown type gasification process with hot gas clean-up, since the air blown systems at present are impractical for this size machine. The study was conducted at ISO ambient conditions using a typical sub-bituminous coal. Figure 9 shows the *H System™* IGCC block flow diagram.

Gas Turbine Validation Testing for Low Risk

Although GEPS officially introduced the *H System*™ concept and two product lines, the 9H and 7H gas turbines, to the industry in 1995, *H System*™ technology has been under development since 1992, making extensive use of proven materials, proven design features, and proven heat transfer principles – either from existing GE Power Systems designs, from GE Aircraft Engine designs, or from GE Corporate Research and Development design experience. This extensive experience base was enhanced with a comprehensive technology development and component testing program to validate the *H System*™ design, with encouragement and support of the U.S. Department of Energy.

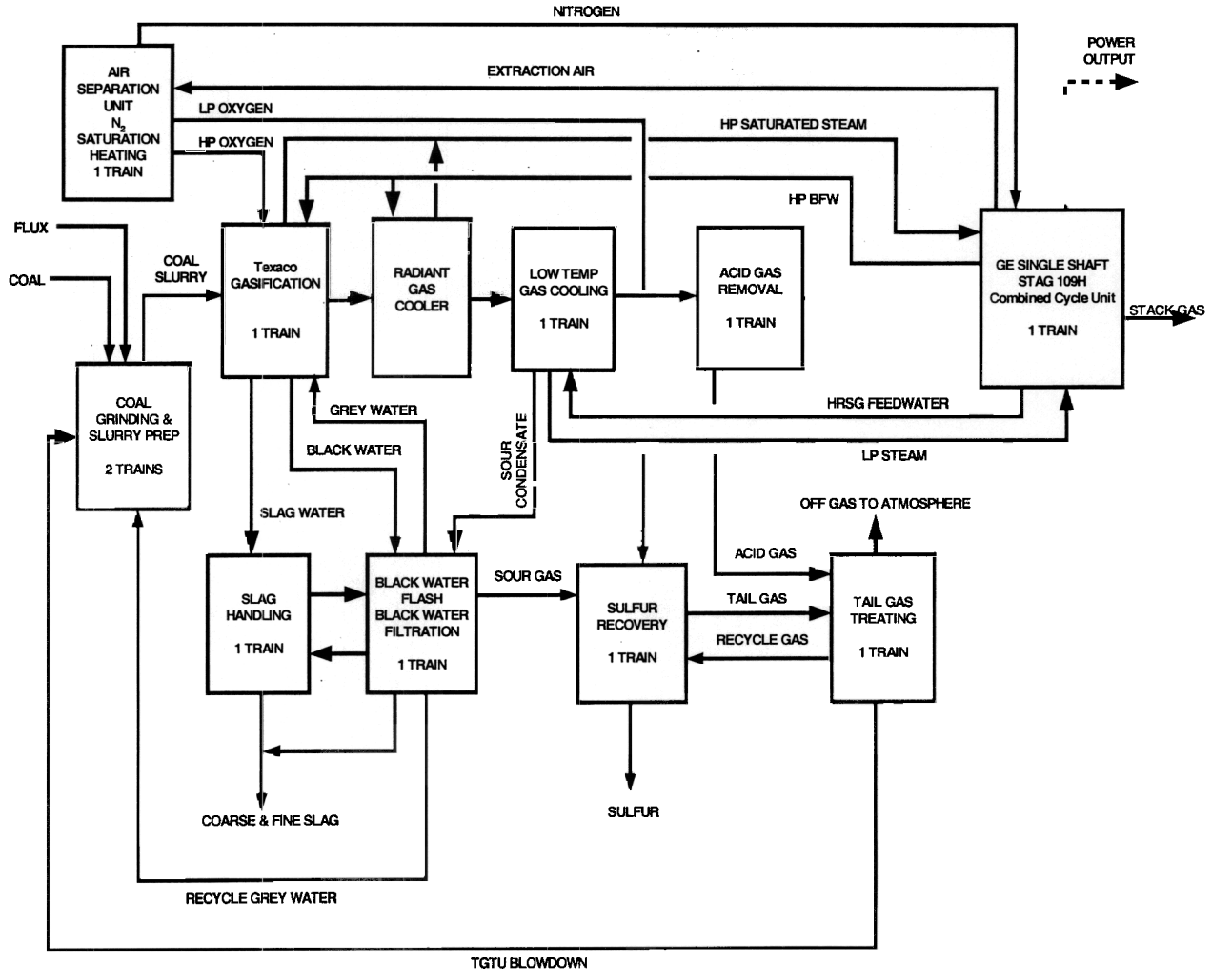

Figure 9. Heat Recovery (HR) IGCC Design Block Flow Diagram

The first phase in the *H System*™ development process was a thorough assessment of product options, corresponding design concepts, and system requirements. Also crucial in the first phase was careful selection of materials, components and subsystems. These were sorted into categories of existing capabilities or required technology advancements. All resources and technological capabilities of GEAE and CRD were made available to the Power Systems' *H System*™ team.

For each component and subsystem, risk was assessed and abatement analyses, testing, and data were specified. Plans to abate risk and facilitate design were arranged, funded and executed.

The second development phase covered product conceptual and preliminary designs, and included the introduction of knowledge gained through experience, materials, data, and analytical codes from GEPS and GEAE.

The *H System*™ development program is currently in its third and final phase, Technology Readiness Testing. This phase includes execution of detailed design and product validation through component and gas turbine testing. Figure 10 shows the ATS machine cross-section with the major subsystem components identified, and Table 1 lists the specific component tests and facility locations.

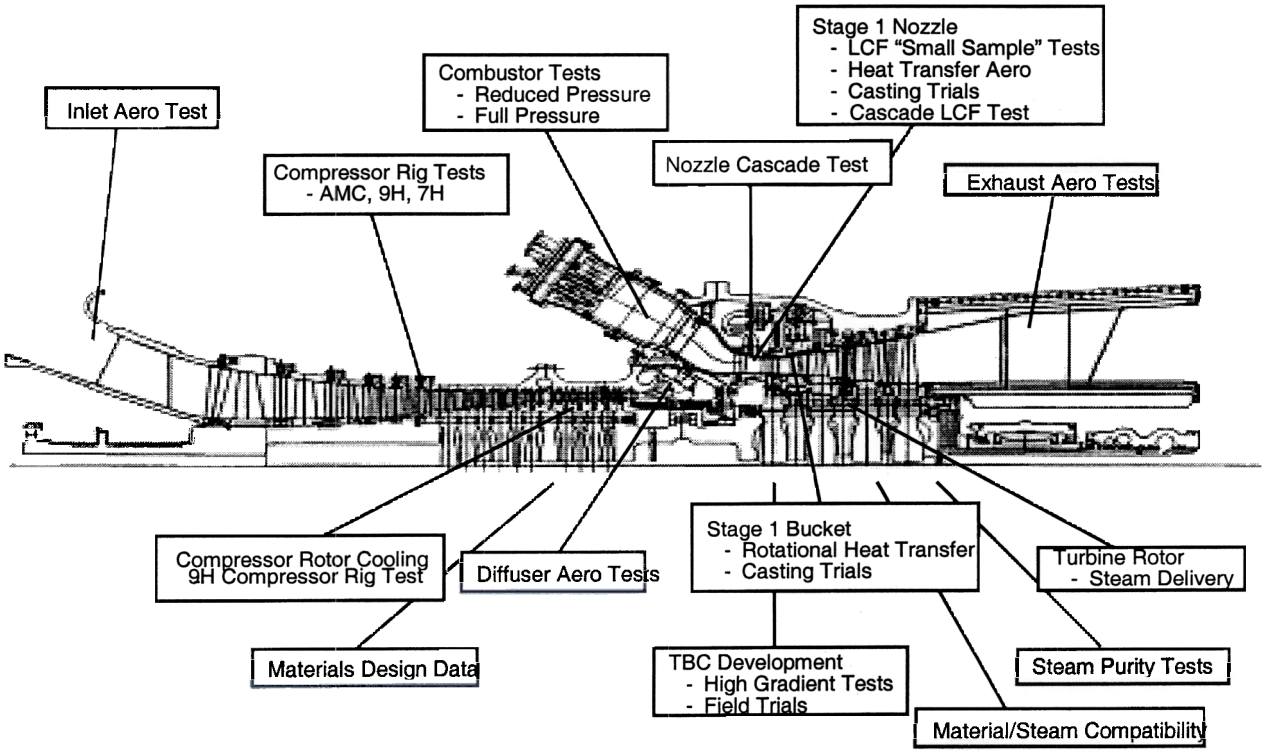

Figure 10. Components Tested during ATS Program

Table 1: GE ATS Component Testing during Phase 3R

Inlet Aero Test		GE Nuovo Pignone, Italy
Compressor Rig Tests	Advanced Machine Compressor (AMC) • 9H • 7H	GEAE, Lynn, MA
Compressor Rotor Cooling Tests	9H Rig Compressor Test	GEAE-Lynn, MA
Combustor Tests	Reduced Pressure Full Pressure	GEPG Lab, CRD, Schenectady, NY GEAE Lab, Evendale, OH GEAE Lab, Evendale, OH
Diffuser Aero Tests		GE-CRD, Schenectady, NY
Nozzle Cascade Test	Nozzle Aerodynamics Nozzle Heat Transfer	GEAE, Evendale, OH
Stage 1 Nozzle Tests	LCF "Small Sample" Tests Heat Transfer Aero Tests Casting Trials Cascade LCF Test-Prototype Cascade LCF Test-Production	GE-CRD, Schenectady, NY GE-CRD, Schenectady, NY Texas A&M GE-CRD, Schenectady, NY Howmet, Hampton, VA GEAE, Evendale, OH GEAE, Evendale, OH
Stage 1 Bucket Tests	Rotational Heat Transfer Casting Trials	GE-CRD, Schenectady, NY GE-CRD, Schenectady, NY Howmet, Hampton, VA
Turbine Rotor Tests	Steam Delivery Component Testing	GEPG Lab, CRD, Schenectady, NY
Exhaust Aero Tests		GE-CRD, Schenectady, NY
Material Design Data		GE-CRD, Schenectady, NY
TBC Tests	High Gradient Tests Field Trials	GE-CRD, Schenectady, NY Virginia Power, VA
Steam Purity Tests		Ocean State Power, Burrillville, RI
Material Steam Compatibility Tests		GE-CRD, Schenectady, NY
Brush Seal Test-Rotating Rig Test		Ocean State Power, Burrillville, RI
9H FSNL 9H FSFL Pre-shipment 7H FSNL		GEPS, Greenville, SC GEPS, Greenville, SC GEPS, Greenville, SC

A high degree of confidence has been gained through this component and subsystem testing and has provided validation of analysis codes. Completion of the development test program resulted in full-scale gas turbine testing at the GEPS factory test stand in Greenville, SC, to be followed by combined cycle power plant development testing at the Baglan Energy Park launch site, in the United Kingdom.

Compressor

The *H System*™ compressors provide a 23:1 pressure ratio with 1510 lb/s (685 kg/s) and 1230 lb/s (558 kg/s) airflow for the 9H and 7H gas turbines, respectively. They are derived from the high-pressure compressor used in GE CF6-80C2 aircraft engine and the LM6000 aeroderivative gas turbine. This compressor design has more than 20 million hours of experience providing reliable operation.

For use in the *H System*™ gas turbine, the 14 stage CF6-80C2 compressor is scaled up (2.6:1 for the 7H, and 3.1:1 for the 9H), with four stages added to achieve the desired combination of airflow and pressure ratio.

In addition to the variable inlet guide vane (IGV) used on prior GE gas turbines to modulate airflow, the *H System*™ compressors have variable stators (VSV) in the front stage of the compressor (9H - 4 VSV, 7H - 5 VSV). They are used in conjunction with the IGV to control compressor airflow during turndown (rpm stays the same, airflow decreases), as well as to optimize engine operation for variations in ambient temperature. A single actuation system, driven by two hydraulic actuators, is used to control both the IGV's and VSV's as a single system.

Compressor Rig Test Program

Although the compressor design was derived from a proven GE aircraft design, a multiphase compressor rig test program was performed at the GE Aircraft Engines (GEAE), Lynn, MA compressor test facility. This facility houses the CF6-size test stand powered by a 33,000 hp steam turbine. Extensive instrumentation and data acquisition/reduction capabilities allowed for monitoring a full range of performance parameters. Test results obtained in the sub-scale (CF6 vs *H System*™) rig are directly applicable to the full-scale design. GE has significant experience in scaling compressors up and down in size.

Baseline Compressor

Three test rigs were used in the *H System*™ compressor validation program. A "baseline" compressor was successfully tested in 1995, validating the use of the 18 stage CF6-based compressor (14 stage CF6 with 4 stages added). Stage 1 and 2 were redesigned from the aircraft configuration, stages 3-12 remained the same, and stages 13 and 14 were redesigned. Stages 15-18 were added. Valuable experience was obtained in running the higher-pressure ratio (20.4:1) machine, with flow, pressure ratio, efficiency, aeromechanics, operability, and turndown all being measured.

9H Compressor

The 9H compressor rig (Figure 11) was run in the GEAE Lynn test facility in 2Q97-3Q97. This compressor was similar to the 1995 design with redesigned stages 1-3, and redesigned stages 15-18. As a result of the redesigned stages, the pressure ratio increased to 23.2:1 (H machine design). The compressor operating parameters were completely mapped, with stall margin meeting or exceeding the 10% requirement throughout the operating range. Power turndown was demonstrated to 3% of design flow, at 100% speed, which more than met design requirements. The VSV settings optimized performance and efficiency. These setting were then used on the full scale 9H during its full speed, no load test in the GE Power Systems test stand in Greenville, SC.

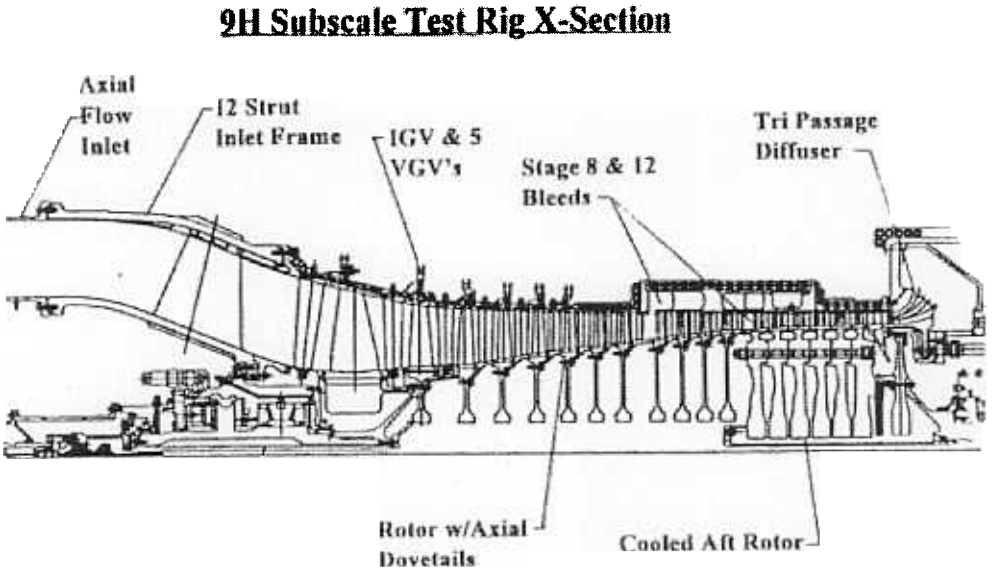

Figure 11. 9H Subscale Test Rig Cross-Section

The aft rotor purge air cooling system operated as predicted. A small amount of compressor discharge air is routed into the compressor bore cavity, and fed between the disks for rear stage cooling, thus providing enhanced design life and improved performance. The rotor purge system controls the environment in the aft rotor to be similar to the FA rotor, as the materials in the *H System*™ compressor wheels are the same as in the FA. The purge system controls thermal gradients in the individual compressor wheels, thus enhancing life and increasing the durability of the rotor. The purge system also leads to improved control of compressor clearance, and thus better efficiency.

All of the compressor airfoils (blade and vanes) achieved all of the design objectives with regard to aeromechanics (vibratory responses). A total of 115 thin film strain gauges were applied to stage 1 through 18, and verified that the 9H compressor had no high vibratory stress modes.

7H Compressor

A comparison of the 7H and 9H flowpaths is shown in Figure 12. The 7H compressor has 18 stages, but is not a pure scale of the 9H (solely based on rpm differences). The 7H has an "zero" stage ahead of the scaled first stage, in order to increase airflow, and the last stage (#18) is omitted. The addition of a larger inlet stage was made to provide more airflow to better position the 7H machine in the marketplace.

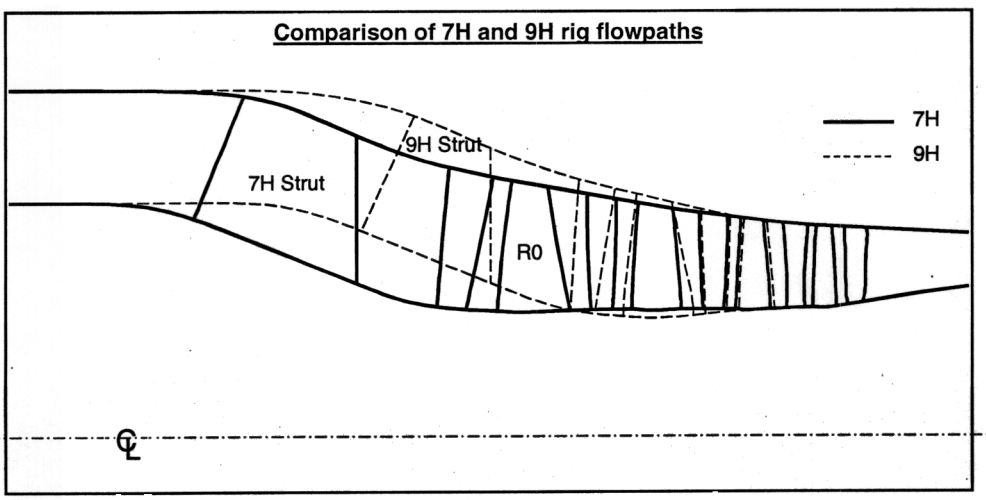

Figure 12. Comparison of 7H and 9H Rig Flowpaths

The 7H compressor rig test was performed at the GEAE, Lynn, MA test facility in 3Q99. The compressor had instrumentation similar to the 9H compressor rig, but did not have the purge air configuration in the rear stages, as that design aspect has already been verified. The 7H rig test had over 800 sensors and accumulated over 150 hours to characterize the compressor's aerodynamic and aeromechanical operations. Key test elements include optimum ganging of the variable guide vanes and stators; performance mapping to quantify airflow, efficiency, and stall margins; stage pressure and temperature splits; start-up, acceleration, and turndown characteristics; and identification of flutter and vibratory characteristics of the airfoils (aeromechanics).

As with the 9H compressor rig, the 7H compressor rig was used to fully map the 7H compressor for Standard, Hot Day and Cold Day performance, start-up bleed conditions, part-speed operability, and power turndown. The VSV scheduling and performance optimization derivatives were determined for use on the 7H FSNL test. Data analysis showed that the 7H compressor rig met all design performance, operability, and aeromechanical goals.

Figure 13 shows the 7H compressor map, with lines of predicted performance and test data plotted on a pressure ratio vs. inlet corrected flow background. The 7H compressor had 1.5% higher flow than predicted, showing growth potential for the 7H.

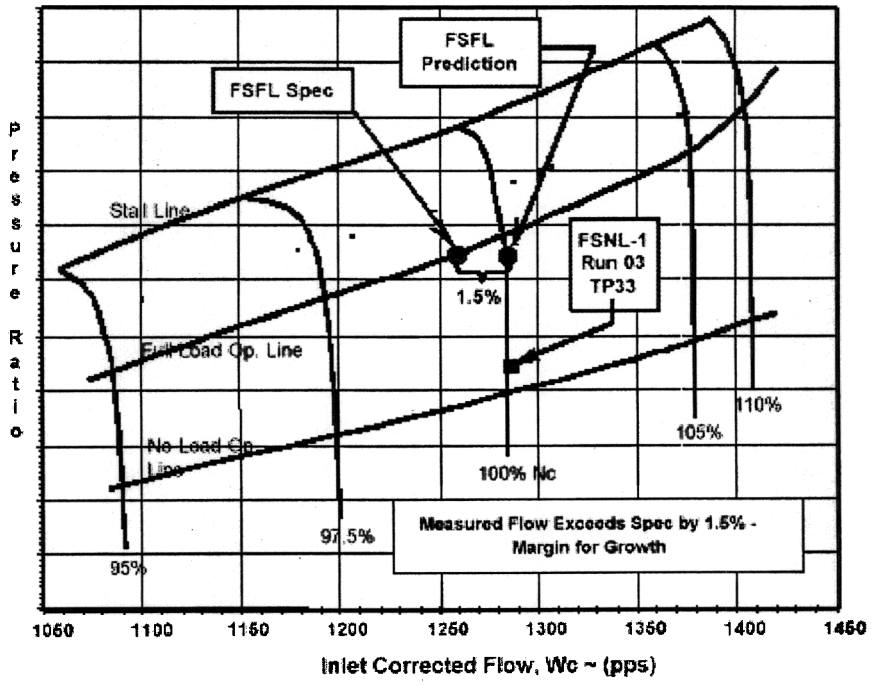

Figure 13. 7H Compressor Map

Combustor Testing

The *H System*™ combustor design is based on the current GE commercial Dry Low NOx (DLN) combustion system, with modifications being made for improved use of air, reduced cooling, and greater load turndown capability. The combustor designs are similar for the 9H and 7H machines, with differences being due to different airflow requirements. (There are 14 combustion cans on the 9H, and 12 on the 7H, which keep airflow requirements roughly equal).

A full-scale combustion test rig was constructed at the GE Aircraft Engine facility in Evendale, OH. This rig allowed testing at full pressure, temperature, and flow conditions for both the 9H and 7H engine combustor systems, and provided excess capacity to test for hot day and over-speed conditions. The combustor test stand is shown in Figure 14, and shows the arrangement of a single combustor can, transition piece, and downstream cooled nozzle bar system (to simulate turbine nozzle blockage). Instrumentation, plenum inlet, and exhaust ports are also shown. The rig also has the capability to use heated fuel.

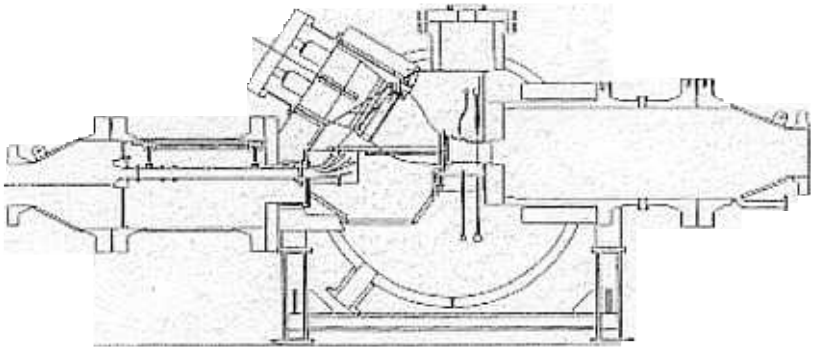

Figure 14. H Combustion Test Stand – Side View

Combustor Design Status

Figure 15 shows a cross-section of the combustion system. The technical approach features a tri-passage radial prediffuser which optimizes the airflow pressure distribution around the combustion chambers, a GTD222 transition piece with an advanced integral aft frame mounting arrangement, and impingement sleeve cooling of the transition piece. The transition piece seals are the advanced cloth variety for minimum leakage and maximum wear resistance. The flowsleeve incorporates impingement holes for liner aft cooling. The liner cooling is of the turbolator type so that all available air can be allocated to the reaction zone to reduce NOx. Advanced 2-Cool™ composite wall convective cooling is utilized at the aft end of the liner. An effusion-cooled cap is utilized at the forward end of the combustion chamber.

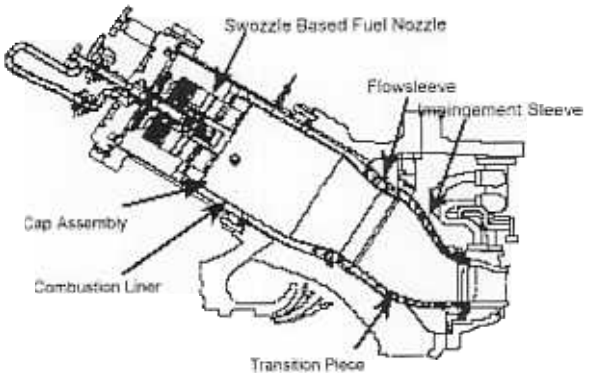

Figure 15. Combustion System Cross-Section

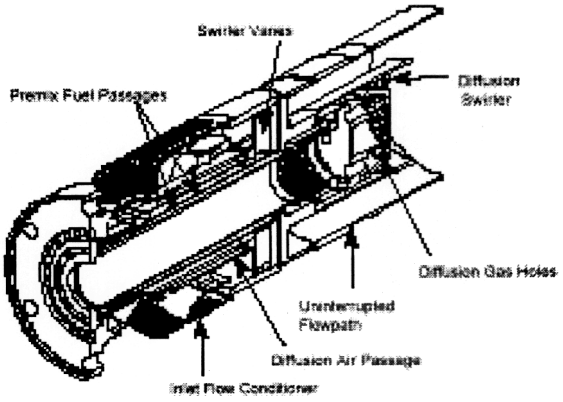

Figure 16. Fuel Injection System Cross-Section

The *H System*™ fuel injector is shown in Figure 16, and is based on the *swozzle* concept. The term *swozzle* is derived by joining the words "swirler" and "nozzle." The premixing passage of the swozzle utilizes swirl vanes to impart rotation to the admitted airflow, and each of these swirl vanes also contains passages for injecting fuel into the premixer airflow. Thus, the premixer is very aerodynamic and highly resistant to flashback and flameholding. Downstream of the swozzle vanes, the outer wall of the premixer is integral to the fuel injector to provide added flameholding resistance. Finally, for diffusion flame starting and low load operation, a swirl cup is provided in the center of each fuel injector.

The *H System*™ combustor uses a simplified combustion mode staging scheme to achieve low emissions over the premixed load range while providing flexible and robust operation at other gas turbine loads. Figure 17 shows a schematic diagram of the staging scheme. The most significant attribute is that there are only three combustion modes: diffusion, piloted premix, and full premix mode. These modes are supported by the presence of four fuel circuits: outer nozzle premixed fuel (P4), center nozzle premixed fuel (P1), burner quaternary premixed fuel (BQ), and diffusion fuel (D4). The gas turbine is started on D4, accelerated to Full Speed No Load (FSNL), and loaded further. At approximately 20-35% gas turbine load, two premixed fuel streams P1, and P4, are activated in the transfer into Piloted Premix. After loading the gas turbine to approximately 40-50% load, transfer to full premix mode is made and all D4 fuel flow is terminated while BQ fuel flow is activated. This very simplified staging strategy has major advantages for smooth unit operability and robustness.

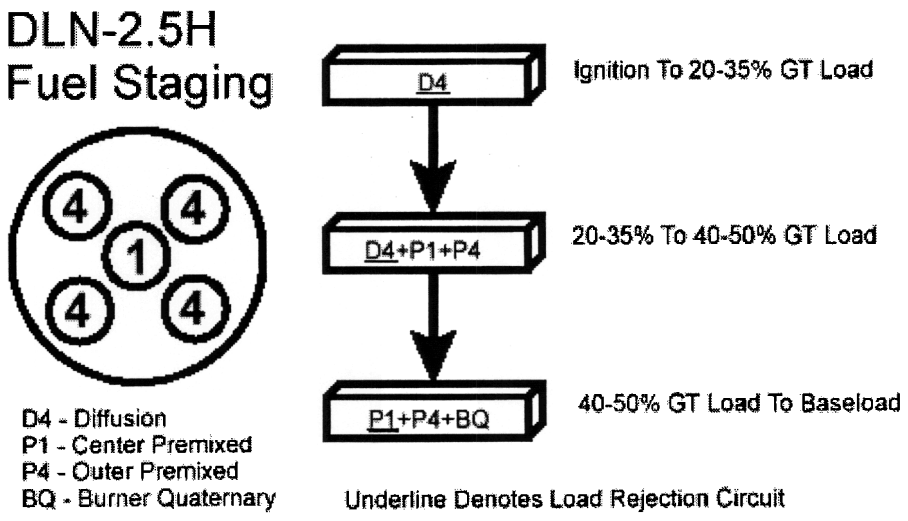

Figure 17. Combustion Mode Staging Scheme

The *H System*™ combustor was developed in an extensive test series to ensure low emissions, quiet combustion dynamics, ample flashback/flameholding resistance, and rigorously assessed component lifing supported by a complete set of thermal data. In excess of thirty tests were run at the GEAE combustion test facility, in Evendale, Ohio, with full pressure, temperature, and airflow. Figure 18 shows typical NOx base load emissions as a function of combustor exit temperature. The *H System*™ components have significant margin in each case. In addition, hydrogen torch ignition testing was performed on the fuel injector premixing passages. In all cases the fuel injectors exhibited well in excess of 30 ft/s flameholding margin after the hydrogen torch was de-activated. In addition, lifing studies have shown expected combustion system component lives with short term Z-scores between 5.5 and 7.5 relative to the combustion inspection intervals on a thermal cycles-to-crack initiation basis. Thus, there is a 99.9% certainty that component lifing goals will be met.

Turbine Design

The *H System*™ turbine design employs optimized 3D geometry with closed-loop steam-cooling in the first- and second-stage rotational and stationary airfoils. As mentioned previously, steam-cooling will allow the firing temperature of the *H System*™ gas turbine to increase to 2600F/1430C, while retaining the same part life specifications as the current GE gas turbine products.

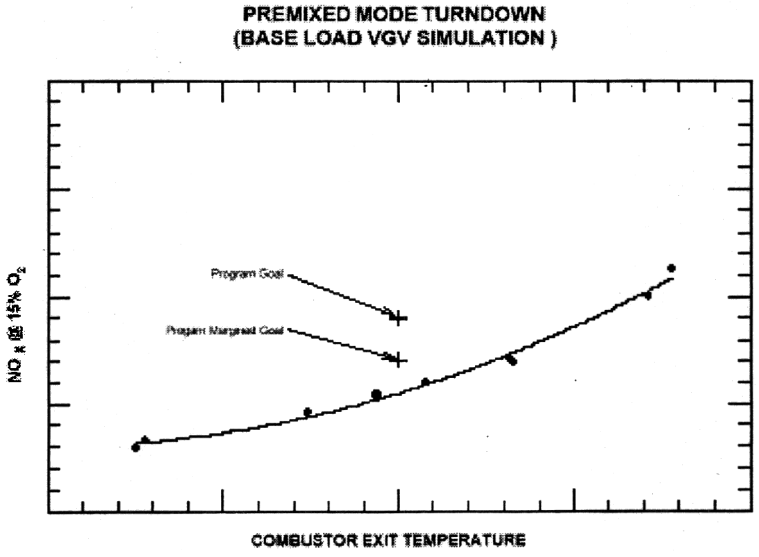

Figure 18. NOx Baseload Emissions as a Function of Combustor Exit Temperature

The lack of airfoil film cooling dilution flow in the turbine results in a higher exhaust temperature for a given firing temperature. However, the maximum exhaust temperature is fixed due to material limits (to proven F-Class materials). In order to maintain a prescribed turbine exhaust gas temperature, the compressor pressure ratio needs to be increased relative to a conventional air-cooled machine. The cycle pressure ratio for the *H System*™ machines was selected to be 23:1, which is significantly higher than previous GE single shaft machine designs. The 23:1 ratio also complements the higher firing temperature, as there is an optimum pressure ratio for a given firing temperature.

In early conceptual design studies, the benefits/drawbacks of a three-stage versus four-stage turbine were compared. However, detailed cycle analysis showed that the high stage loading requirements needed to drive a 23:1 compressor resulted in lower turbine efficiency, and the 60% combined cycle efficiency goal would not be met. The turbine efficiency penalty due to high stage loading outweighed the benefit of reduced cooling flow requirements of the three-stage design. Therefore, the four-stage design was selected.

The remainder of the conceptual design phase focused on defining the flow path and airfoil counts that would yield maximum performance, while aiming for maximum commonality between the 50 Hz (9H) and the 60 Hz (7H) machines. Historically, GE's 50 Hz machines are 1.2 geometric scales of the 60 Hz machines. As most, but not all, key aerodynamic and mechanical characteristics will scale, the additional development work needed to execute a scaled design is relatively small compared to the design effort need for two independent designs.

The approach taken on the *H System*™ machines differs from the traditional GE approach. In order to minimize manufacturing and assembly complexity on the rotor and

steam supply system, the maximum level of geometric commonality between the 7H and 9H was sought. The 20% speed difference between the two machines implies a 40% difference in aerodynamic loading, and in mechanical loading (speed-squared relationships) for a common flow path design. In practice, it was not possible to meet aerodynamic and mechanical requirements by using common flow paths for both applications. The final flow path selection maintains commonality between the key rotor and steam delivery features, even though the flowpaths deviate somewhat (see Figure 19). The 7H, due to its higher speed, has lower aerodynamic loading, but higher mechanical stresses.

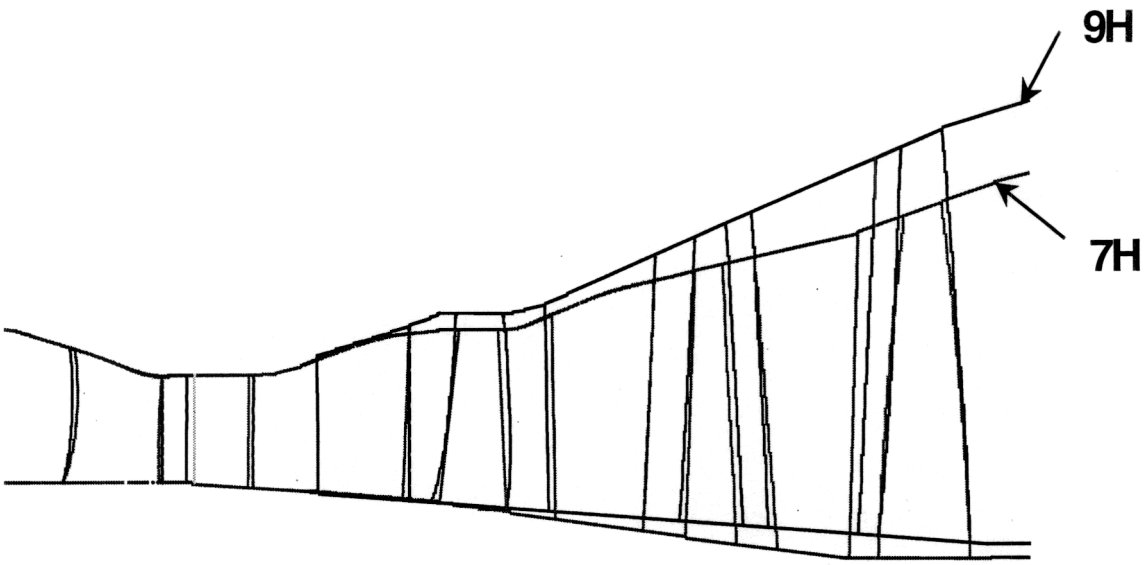

Figure 19. Comparison of 7H and 9H Flowpaths

Turbine component testing consisted of: extensive materials testing, heat transfer tests, a nozzle cascade test rig, and a turbine rotor steam delivery test rig. The buckets were vibration tested at GEAE, and run in the full speed, no load tests at Greenville, SC. These tests are described below.

Materials

Turbine Design Status

The turbine operates with high gas path temperatures, providing the work extraction to drive the compressor and generator. Two of the factors critical to reliable, long life are the turbine airfoil's heat transfer and material capabilities. When closed circuit steam-cooling is used, as on the H turbine, the key factors do not change. However, the impact

of steam on the airfoil's heat transfer and material capabilities must also be considered. For many years, the U.S. Department of Energy (DOE) Advanced Turbine System has provided cooperative support for GE's development of the *H System*™ turbine heat transfer materials capability and steam effects. Results have fully defined and validated the factors vital to successful turbine operation. A number of different heat transfer tests were performed to fully characterize the heat transfer characteristics of the steam-cooled components culminating with the full-scale nozzle cascade testing at the GE Aircraft Engines test facility. Figure 20 shows the stage 1 nozzle cascade test rig used for internal cooling heat transfer validation.

Figure 20. Full Scale Stage 1 Nozzle Heat Transfer Test Validates Design and Analysis Predictions

An extensive array of material tests has been performed to validate the material characteristics in a steam environment. Testing has included samples of base material and joints and the testing has addressed the following mechanisms: cyclic oxidation, fatigue crack propagation, creep, notch low-cycle fatigue and low-cycle fatigue (Figure 21).

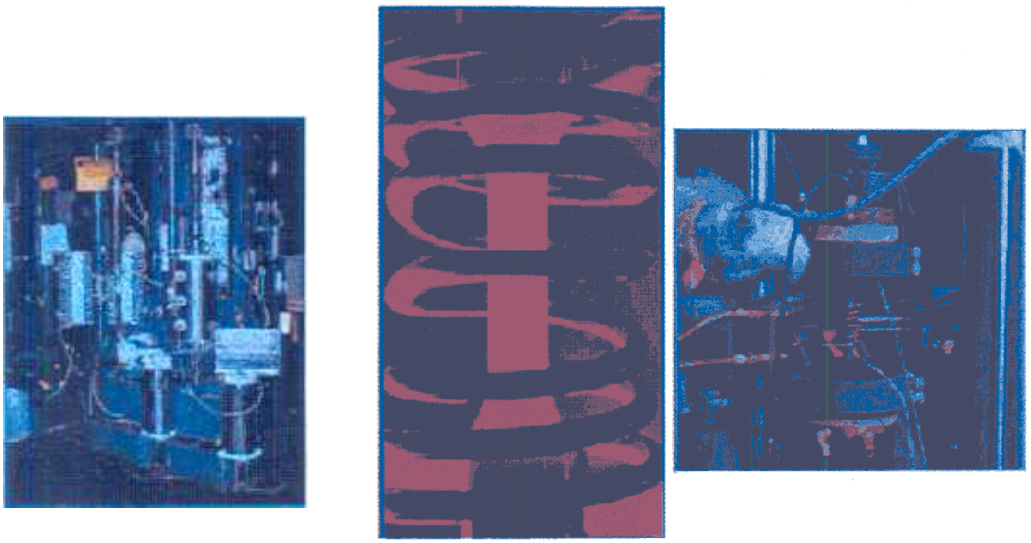

Figure 21. Materials Validation Testing in Steam

Thermal barrier coating (TBC) is used on the flowpath surfaces of the steam-cooled turbine airfoils. Life validation has been performed using both field trials (Figure 22) and laboratory analysis. The latter involved a test that duplicates thermal-mechanical conditions, which the TBC will experience on the *H System*™ airfoils.

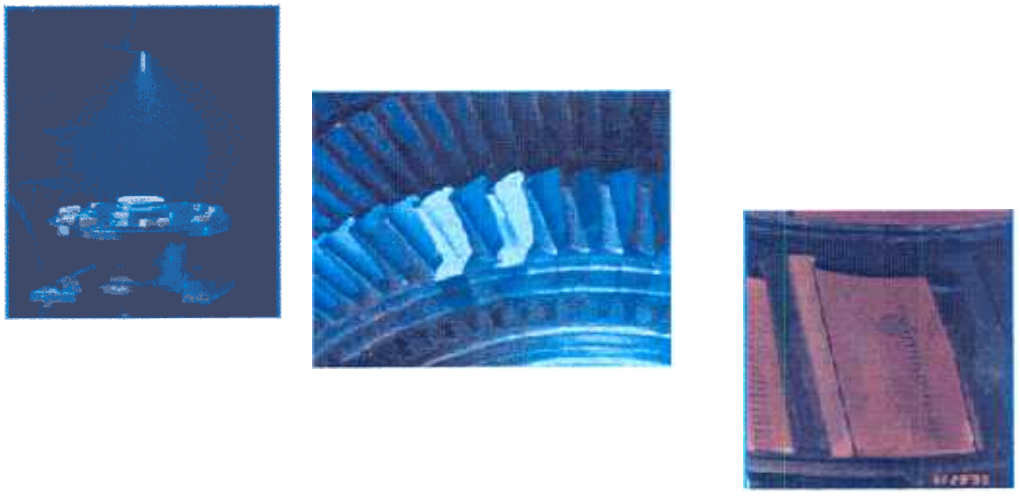

Figure 22. Thermal Barrier Coating Durability

Long-term durability of the steam-cooled components is dependent on avoidance of internal deposit buildup, which is, in turn, dependent on steam purity. This is accomplished through system design and filtration of the gas turbine cooling steam. Long-term validation testing, completed at an existing power plant, has defined particle size distribution and validated long-term steam filtration. As further validation, specimens duplicating nozzle cooling passages have initiated long-term exposure tests. A separate rotational rig is being used for bucket validation. The *H System*™ turbine airfoils have been designed using design data and validation test results for heat transfer, material capability and steam-cooling effects. The durability of ceramic thermal barrier coatings has been demonstrated by three different component tests performed by CRD: "Furnace cycle", "Jet engine thermal shock " and electron beam thermal gradient.

The electron beam thermal gradient test was developed specifically for GEPS to accurately simulate the very high heat transfers and gradients representative of the *H System*™ gas turbine. Heat transfers and gradients representative of the *H System*™ gas turbine have also been proven by field testing of the enhanced coatings in E- and F-class gas turbines.

Nozzle Cascade Testing

The *H System*™ stage one nozzle was designed using GE's design practice database, with validation tests for heat transfer, material properties, and steam-cooling effects. These test results were incorporated into detailed 3-dimensional aerodynamic, thermal, and stress models as part of the design process. As further validation, full-size, steam-cooled stage 1 nozzle segments were tested at full *H System*™ operating conditions in a nozzle cascade test rig.

The test rig is located at GEAE's Evendale, OH facility, and shares the control room and airflow facilities with the combustor test rig. Details of the rig are show in Figure 23. The nozzle cascade test rig consists of two stage 1 airfoils downstream of an *H System*™ combustor and transition piece. The flowpath to contours on either side of the two nozzle segments are formed by two water-cooled copper endwalls. A four-phase test program was designed to characterize combustor behavior, verify aerodynamic performance, measure heat transfer characteristics, and accumulate low-cycle fatigue (LCF) cycles. Correlation of the nozzle cascade test data with design predictions validated the 9H and 7H steam-cooled hardware.

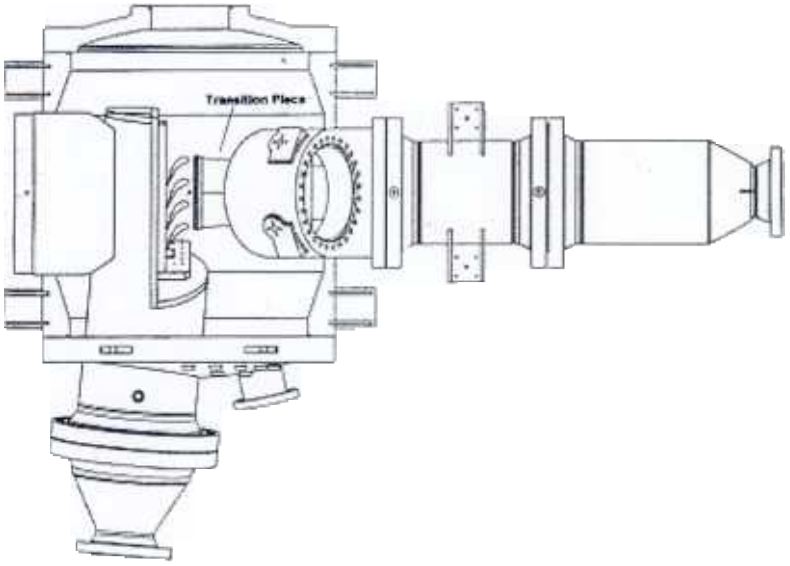

Figure 23. 9H Cascade Vane Orientation

Phase 1 involved combustor mapping and characterization of the combustion system, and an overall facility shakedown. The initial testing was completed in 1995 to map the temperature profile at the exit of the transition piece (entrance to the nozzle cascade). Additional combustor testing was performed in 1Q97 to confirm temperature profiles at the high and low end points of the LCF cycle to be used in phase 4.

Phase 2 consisted of a cascade aerodynamic test, in which the rig was run at full air flow conditions to determine the external Mach member distribution on the airfoil surfaces. This parameter is important in establishing nozzle external heat transfer coefficients as well as verifying the aerodynamic quality of the test configuration. This phase was successfully completed in 3Q95.

In Phase 3, the heat transfer test, several hundred internal cavity metal temperature, and steam temperature and steam pressure sensors, and external temperature and pressure sensors were used to validate the stage one nozzle internal heat transfer and flow circuit predictions. The testing was conducted under steady state and transient operating conditions that closely match the operation of the production engine. Testing ran for over 100 hours, and over 30 data points were taken. Test data results were analyzed and compared to a detailed flow and three-dimensional heat transfer analysis of the nozzle. Phase 3 testing was completed in 1Q97.

Phase 4, the low cycle fatigue (LCF) test, involved cyclic operation of the test rig to simulate periodic start-up and shutdown of the engine during commercial operation. The rig was operated between two steady state points: one at a low thermal stress state, and the other at a high thermal stress state. Testing was performed to determine the durability of the thermal barrier coating (TBC) on the nozzle and to test the nozzle durability in

both fully coated and spalled conditions (hardware was pre-spalled to evaluate this effect) to establish any crack propagation behavior. It was found that cracks occurred only in the pre-spalled areas, and did not grow. Nozzle cascade hardware is shown in Figure 16 of the Materials section.

The nozzle cascade test results were correlated with the analytical predictions used in the nozzle design. It was found that there was very close agreement between the two, thus validating the design methodology for all of the steam-cooled turbine hardware.

Turbine Rotor Rig Test

The *H System*™ machines are designed to have steam-cooled rotating hardware, specifically the stage 1 and stage 2 turbine buckets, which are fed by a steam delivery system through the rotor assembly via the aft shaft. This steam delivery system relies on "spoolies", tubular spool-shaped seals that connect the steam delivery system to the flowpath airfoils, to deliver steam to the buckets without detrimental leakage, which would lead to performance loss and adverse thermal gradients within the rotor structure. The basic concept for power system steam sealing is derived from many years of successful application of spoolies in the GE CF6 and CFM56 aircraft engine families.

In the conceptual design phase, material selection was made only after considering the effects of steam present in this application. Coatings to improve durability of the spoolie were also tested. These basic coupon tests and operational experience provided valuable information to the designers.

In the preliminary design phase, parametric analysis was performed to optimize spoolie configuration. Component testing began for both air and steam systems. The spoolie was instrumented to validate the analysis. Again, the combination of analysis and validation tests provided confirmation that the design(s) under consideration were based on the right concept. Over 50 component tests have been conducted on these spoolies, evaluating coatings, lateral loads, fits, axial motion, angular motion, temperature and surface finish.

The detailed design phase focused on optimization of the physical features of the subsystem, spoolie-coating seat. In addition, refined analysis was performed to allow for plasticity lifecycle calculations in the region of the highest stresses. This analysis was again validated with a spoolie cyclic life test, which demonstrated effective sealing at machine operating conditions with a life of over 20,000 cycles.

Spoolies were also used on the *H System*™ FSNL gas turbine tests. During the 9H Full Speed, Full Load pre-shipment testing, compressor discharge air flowed through the circuit. This is typical of any no-load operation. Assembly and disassembly tooling and processes were developed. The spoolies were subjected to a similar environment with complete mechanical G loading. Post-testing condition of the seals was correlated to the observation made on the component tests. This provided another opportunity for validation.

A Steam Delivery Rotating Rig (Figure 24) was used to evaluate the mechanical integrity and wear characteristics of the rotor steam delivery hardware. The rig was subjected to repeated speed and thermal cycles in order to simulate the centrifugal loading and startup thermal interactions between the steam delivery hardware and the rotor wheels in order to provide accelerated lifecycle testing.

Leak checks were performed pre-test and post-test, and no appreciable change in leakage was detected. Spoolies were removed as part of the post-test inspection, and they showed only minimal wear.

Rig Description

As shown in Figure 24, the Steam Delivery Rotating Rig consists of a series of three turbine disks and two spacers, which are modifications of existing components, and new forward and aft shafts.

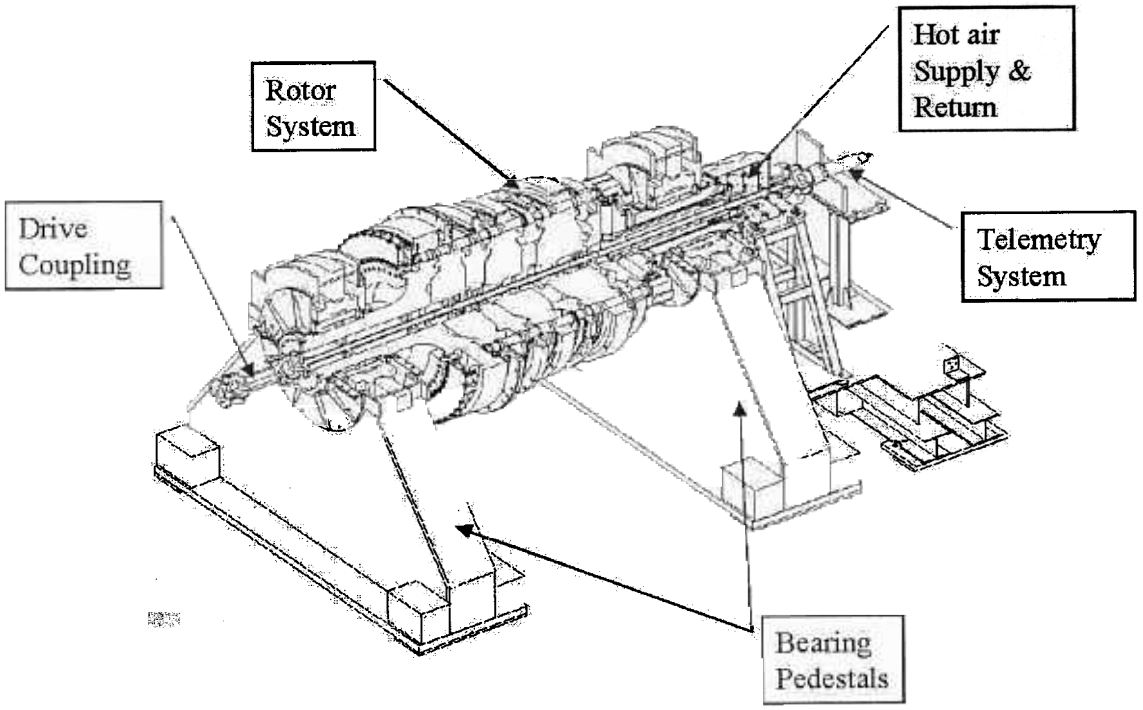

Figure 24. Cross-section of Steam Delivery Rotating Rig

Gas Turbine Factory Tests

The first six years of the GE *H System*™ validation program focused on sub-component and component tests. Finally, in May 1998, the program moved on to the next stage, that of full-scale gas turbine testing at the Greenville, South Carolina factory (Figure 25).

The 9H gas turbine achieved first fire and full speed and, then, over a space of five fired tests, accomplished the full set of objectives. These objectives included: confirmation of

rotor dynamics, vibration levels and onset of different modes, compressor airfoil aero-mechanics, compressor performance, including confirmation of airflow; and efficiency scale-up effects versus the CF6 scale rig tests, measurement of compressor and turbine rotor clearances, and demonstration of the gas turbine with the Mark VI control system. The testing also provided data on key systems: bearings, rotor cooling, cavity temperatures and effectiveness of the clearance control systems. Following the testing, the gas turbine was disassembled in the factory and measured and scrutinized for signs of wear and tear. The hardware was found to be in excellent condition. The 9H gas turbine was rebuilt with production turbine airfoils and pre-shipment tests performed in October and November 1999. This unit was fully instrumented for the field test to follow and, thus, incorporated over 3500 gauges and sensors.

Figure 25. 9H Gas Turbine in Half Shell Prior to First FSNL Test

This second 9H test series took seven fired starts and verified that the gas turbine was ready to ship to the field for the final validation step. Many firsts were accomplished. The pre-shipment test confirmed that the rotating air/steam cooling system performed as modeled and designed. In particular, leakage, which is critical to the cooling and life of the turbine airfoils and the achievement of well-balanced and predictable rotor behaviors, was well under allowable limits. Compressor and turbine blade aeromechanics data, were obtained at rates of up to 108% of the design speed, clearing the unit to run at design and over-speed conditions. Rotor dynamics were once again demonstrated, and

vibration levels were found to be acceptable without field balance weights. The Mark VI control system demonstrated full control of both the gas turbine and the new *H System*™ accessory and protection systems.

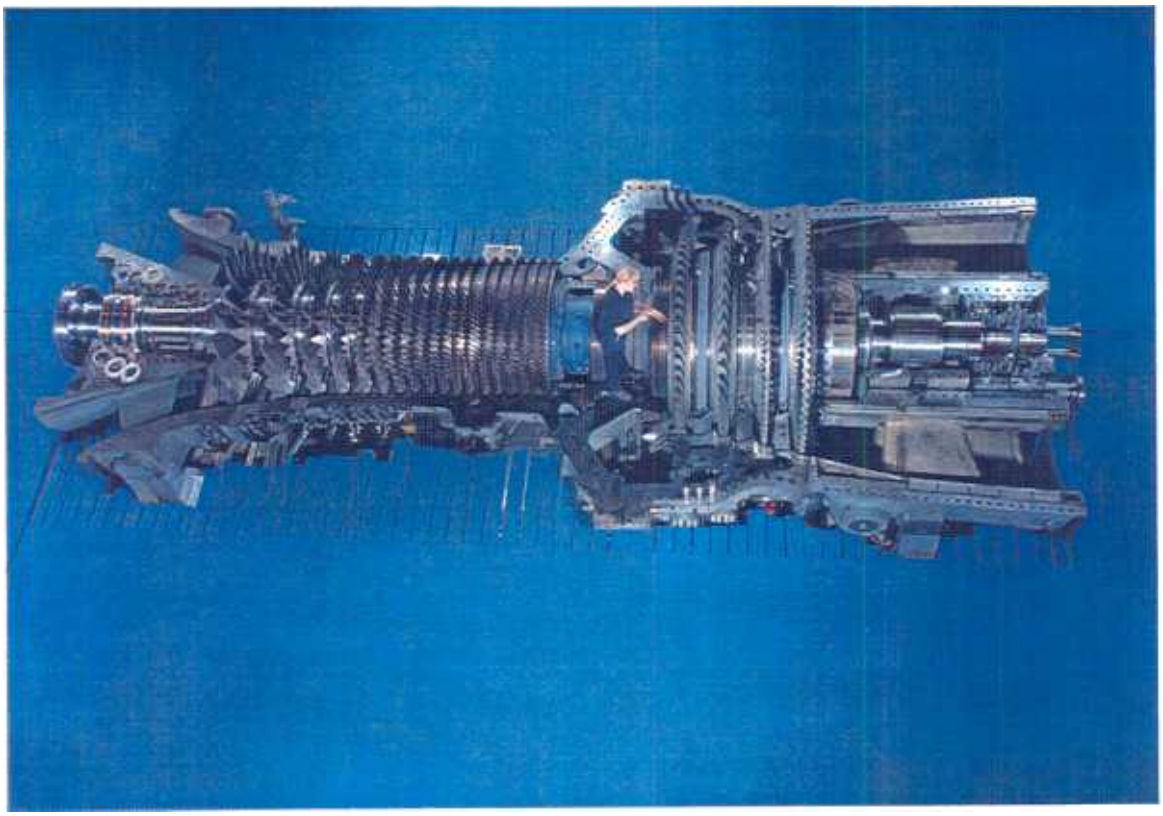

Figure 26. 7H Gas Turbine Being Assembled

The first 7H gas turbine was assembled (Figure 26) and moved to the test stand in December 1999 (Figure 27). This 7H went through a test series similar to that for the first 9H factory test. However, the 7H not only covered the 9H test objectives described earlier, but also ran separately with deliberate unbalance at compressor and turbine ends to characterize the rotor sensitivity and vectors. The rotor vibrations showed excellent correlation with the rotor dynamic model and analysis. The 7H gas turbine is now back in the factory for disassembly and inspection, following the same sequence used for the 9H.

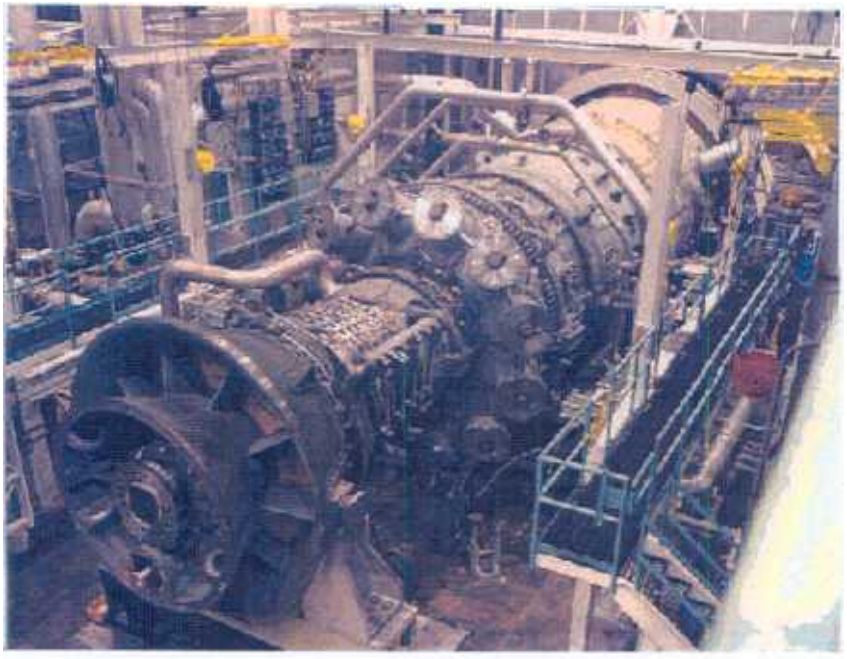

Figure 27. 7H Gas Turbine Being Installed in Test Stand

Conclusion

GE Power Systems has completed work on the DOE Advanced Turbine Systems program, and has achieved the program goals. A full scale 7H (60 Hz) gas turbine has been designed, fabricated, and successfully tested at Full Speed, No Load conditions at GE's Greenville, SC manufacturing/test facility.

The GE *H System*™, combined cycle power plant creates an entirely new category of power generation systems. Its innovative cooling system allows a major increase in firing temperature, which allows the combined cycle power plant to reach record levels of efficiency and specific work, while retaining low emissions capability, and with reliability parameters comparable to existing products.

The design for this "next generation" power generation system is now established. Both the 9H (50 HZ) and the 7H (60 Hz) family members are currently in the production and final validation phase. The extensive component test validation program, already well underway, will ensure delivery of a highly reliable combined cycle power generation system to the customer.

GE Power Systems

Utility Advanced Turbine Systems (ATS) Technology Readiness Testing

Phase 3R

Final Report – Volume 2 Technical Report

June, 2001

Prepared for U.S. Department of Energy
National Energy Technology Laboratory
Morgantown, WV 26507-0880

Prepared by General Electric Company
Power Generation Engineering
Schenectady, NY 12345

DOE Cooperative Agreement No. DE-FC21-95MC31176

Table of Contents

1 Executive Summary 1

2 Final Report 11
2.1 (NE) NEPA (National Environmental Policy Act) [S,G] 11
2.2 (GT) Gas Turbine Design [S,C,A,G] 14
2.2.1 (GTAD) Aerodynamic Design [A] 14
2.2.2 (GTFF) Gas Turbine Flange to Flange Design [S,C,A] 26
2.2.2.1 (GTFFCP) Compressor Design [S,A] 26
2.2.2.2 (GTFFCB) Combustor Design [S,C,A] 33
2.2.2.3 (GTFFTR) Turbine Rotor Design [S] 39
2.2.2.3.1 (GTFFTR) Turbine Rotor Mechanical Analysis [S,G] .. 44
2.2.2.3.2 (GTFFTR) Wheel Forging Stress Analysis [C] 46
2.2.2.3.3 (GTFFTR) Rotor Steam Circuit Analysis {S,C] 49
2.2.2.3.4 (GTFFTR) Turbine Rotor Shaft Temperature Analysis – #2 Bearing [S,C] 54
2.2.2.3.5 (GTFFTB) Bucket Temperature Monitoring [S,C] 55
2.2.2.3.6 (GTFFTR) Rotor Component Flow Tests [C] 56
2.2.2.4 (GTFFTB) Turbine Bucket Design [S,C] 61
2.2.2.4.1 (GTFFTB) S1B and S2B Wheel Dovetail Analysis [S] 68
2.2.2.4.2 (GTFFTB) S3B and S4B Tip Shroud Design Optimization [C] 69
2.2.2.4.3 (GTFFTB) Bucket Wide Grain Sensitivity Analysis [C] 71
2.2.2.4.3.1 (GTFFTB) Bucket Robust Design and Life Assessment [S,C] 72
2.2.2.4.3.2 (GTFFTB) S1B Forced Response Analysis [C] 74
2.2.2.4.4 (GTETIH) Bucket Tip Treatment Heat Transfer [C] 76
2.2.2.4.5 (GTFFTB) S1B and S2B Air/Steam Coolant Transition Analysis [C] 83
2.2.2.4.5.1 (GTFFTB) Loss of Steam Cooling Algorithms for Full Load Operation [C] 85
2.2.2.4.6 (GTETEH) S1B External Heat Transfer [C] 86
2.2.2.4.7 (GTETIH) Bucket Platform Cooling Model Validation [S,C] 87
2.2.2.4.8 (GTETIH) S1B Leading Edge Turbulator Tests [C] 90
2.2.2.5 (GTFFTS) Turbine Stator Design [S] 91
2.2.2.5.1 (GTFFTS) Turbine Stator Robust Design [S] 99
2.2.2.6 (GTFFST) Structures Design [S,C,A] 103
2.2.2.6.1 (GTFFSTEF) Exhaust Diffuser Performance [C] 105
2.2.2.6.2 (GTFFST) Steam Box CFD Analysis [C] 106
2.2.2.7 (GTFFMS) Mechanical System Design [S] 109
2.2.2.7.1 (GTFFMS) Transient Gas Turbine Cycle Model [S] ... 112

2.2.2.8 (GTFFPP) On-Base and External Piping Design [G] 115
2.2.2.9 (GTFFIT) Instrumentation and Test [S,G] 120
2.2.2.9.1 (GTFFIT) Instrumentation and Test [S,G] 120
2.2.3 (GTET) Technology Validation [C] 132
2.2.3.1 (GTETNC) First-Stage Nozzle Design [C] 132
2.2.3.1.1 (GTETNC) Nozzle Cascade CFD Analysis [C] 132
2.2.3.1.2 (GTETEH02) Combustion-Generated Flow Effects on Heat Transfer [C] 133
2.2.3.2 (GTETRS) Rotor Steam Transfer [C] 139
2.2.3.3 (GTETSE) Rotor-Bucket Steam Transfer Spoolie [C] 140
2.2.3.4 (GTETRH) Rotational Heat Transfer [C] 143
2.2.3.4.1 (GTETRH01) Turbine Rotational Heat Transfer [C] . 143
2.2.3.4.2 (GTETRH) Rotational Effects on Bucket Mixing Ribs [C] 148
2.2.3.4.3 (GTETRHTPD) Bucket Cooling Circuit Rotational Pressure Drop Test [C] 151
2.2.3.4.4 (GTETRH) Rotating Trailing Edge Heat Transfer Tests [C] 152
2.2.3.5 (GTETIH03) Surface Enhanced Internal Heat Transfer [C] 155
2.2.3.5.1 (GTETS2NHT) S2N Trailing Edge Flow Test [C] 155
2.2.3.5.2 (GTETTE) S2B Trailing Edge Testing [C] 157
2.2.3.5.3 (GTETIH04) S1N Outer Band Liquid Crystal Heat Transfer Tests [C] 163
2.2.3.5.4 (GTETIH04) S1N Convex Cavity Heat Transfer Tests [C] 166
2.2.3.5.5 (GTETIH05) Bucket Tip Closed Circuit Cooling [C] 168
2.2.3.5.6 (GTETLE) Bucket Leading Edge Heat Transfer Testing [C] 171
2.2.3.5.7 (GTETIH03) S1N Surface Enhanced Internal Heat Transfer [C] 174
2.2.3.5.8 (GTETIH03) S1N Trailing Edge Flow and Heat Transfer Tests [C] 177
2.2.3.5.9 (GTETBKHT) High Reynolds Number Turbulator Static Heat Transfer Test [C] 181
2.2.3.5.10 (GTET) Impingement Degradation Effects [C] 184
2.2.3.5.11 (GTETIH) Production Airfoil Flow Checks [C] 186
2.2.3.5.12 (GTETIH) Nozzle Fillet Heat Transfer [C] 189
2.2.3.5.13 (GTETIH) S1N and S2N Endwall Heat Transfer [C]. 191
2.2.3.5.14 (GTETIH) Production Stage 1 Nozzle Cooling Circuit Flow Checks [C] 193
2.2.3.6 (GTETEH) Surface Roughness and Combustor-Generated Flow Effects on Heat Transfer [C] 194
2.2.3.6.1 (GTETEH04) S1N Heat Transfer for Production Aero with TBC Spall Effects 197
2.2.3.6.2 (GTETEH03) Surface Roughness Effects on Heat Transfer [C] 198

2.2.3.7 (GTETCP) LCF Coupon Tests [C] 206
2.2.3.7.1 (GTETCP) LCF Nozzle Coupon Life Validation Tests [C] 206
2.2.3.8 (GTETSP) Steam Particulate Deposition [C] 208
2.2.3.8.1 (GTETSP) Steam Particulate Rotational Deposition [C] 208
2.2.4 (GTMT) Materials Technologies [S] 213
2.2.4.1 (GTMTSE) Steam Effects on Mechanical Properties [S] 213
2.2.4.2 (GTMTSO) Oxidation Due to Steam [S] 215
2.2.4.3 (GTMTCE) Corrosion Rate Evaluations of Airfoil Overlay Coatings [S] 216
2.2.4.4 (GTMTBV) Compressor Blades and Vanes Materials and Processes [S] 218
2.2.4.5 (GTMTVG) Compressor Variable Guide Vane System Design Support and Process Development [S] 220
2.2.4.6 (GTMTCS) Compressor Structural Materials and Process 221
2.2.4.7 (GTMTRF) Turbine Rotor Forging Materials and Processes [S] .. 222
2.2.4.8 (GTMTRS) Turbine Rotor Spoolies and Transfer Devices Materials and Processes [S] 225
2.2.4.9 (GTMTSB) Structural Bolting [S] 226
2.2.4.10 (GTMTTA) Turbine Airfoils Materials and Processes [S] 227
2.2.4.10.1 (GTMTTA) Airfoil NDE [C] 233
2.2.4.11 (GTMTCB) Combustion Materials and Processes [S] 237
2.2.4.12 (GTMTST) Turbine Structures Materials and Processes [S] 238
2.2.4.13 (GTMTSH) Turbine Shells [S] 239
2.2.4.14 (GTMTSR) Seal Technology [S] 240
2.2.4.14.1 (GTFFTSESV) Hot Gas Path and Transition Piece Cloth Seals [C] 240
2.2.4.14.2 (GTETBS) Steam Gland Brush Seals [C] 243
2.2.4.14.3 (GTEBS) 7H Stage 3 Nozzle Brush Seals [C] 245
2.2.4.15 (GTMTAR) Airfoil Repair [S] 248
2.2.5 (GTTT) Thermal Barrier Coating Technology [S] 249
2.2.5.1 (GTTTSD) Coating System Development [S] 249
2.2.5.1.1 (GTTTSD) Effects of TBC Surface Finish on Drag [C] 262
2.2.5.2 (GTTTRR) TBC Risk Reduction [S] 263
2.2.5.3 (GTTTDD) TBC Design Data and Life Analysis [S] 268
2.2.5.3.1 (GTFFTB) Bucket TBC Roughness and Spall Characterization [C] 274
2.3 Combined Cycle Integration [S] 276
2.3.1 (CCUA) Unit Accessories [S] 276
2.3.2 (CCCL) Controls [S] 283
2.3.3 (CCRA) Reliability, Availability, and Maintainability (RAM) Analysis [S] 289
2.3.4 (CCSD) Combined Cycle Systems Design [S] 294
2.4 (MF) Manufacturing Equipment and Tooling [G] 299

2.5 (IG) Integrated Gasification and Biomass Fuel [S] 303
2.6 (DE) Pre-Commercial Demonstration 311
2.7 (PM) Program Management [S] 311

List of Figures

1-1	7H ATS Gas Turbine Cross Section	1
1-2	Schedule for Phase 1 through 3R	2
1-3	Phase 3R Timeline of Significant Events	4
1-4	ATS Combined Cycle Power Plant	5
1-5	An Isometric Drawing of the ATS Gas Turbine	6
1-6	Validation Testing of the ATS Gas Turbine	7
1-7	Phase 3R Work Breakdown Structure	9
2.2.1-1	Comparison of 7H and 9H Rig Flow Paths	16
2.2.1-2	Comparison of 7H and 9H Compressor Performance Maps	17
2.2.1-3	Comparison of 7H and 9H Flow Paths	23
2.2.1-4	Smith Diagram	23
2.2.1-5	7H Blade Airfoil Casings	24
2.2.1-6	9H Stage 1 Nozzle Heat Transfer Coefficient Study	24
2.2.1-7	7H Stage 1 Blade Contours Showing Radial Gas Temperature	25
2.2.1-8	7H Stage 1 Turbine Characteristics	25
2.2.2.1-1	7H Compressor New Technologies	27
2.2.2.1-2	AMC Rig #3 for 7H Compressor Design Evaluation	31
2.2.2.2-1	H Combustion System Cross Section	34
2.2.2.2-2	H Swozzle Fuel Injector	35
2.2.2.2-3	DLN-2.5 Fuel Staging	36
2.2.2.2-4	Combustor Development Rig Cross Section	36
2.2.2.2-5	Typical Nox Base Load Emissions Data	37
2.2.2.2-6	Typical Combustion Dynamics Data	38
2.2.2.3-1	Steam Delivery Rotating Cross Section	42
2.2.2.3-2	Typical Cycle	43
2.2.2.3.6-1	Schematic of the Manifold Test System	58
2.2.2.4-1	Comparison of 7H and 9H Flow Paths and Stage 1 Bucket Profile	64
2.2.2.4-2	Representative Finite Element Modeling – Stage 1 Bucket	65
2.2.2.4-3	FEA Dynamic Analysis of Mode Shapes	66
2.2.2.4-4	Bucket Joining and Assembly for 7H Stage 1 Bucket	67
2.2.2.4-5	Tip Hole Closure Using GE Proprietary Welding Technology	68
2.2.2.4.2-1	7H Stage 3 Bucket Local Creep Analysis Model	71
2.2.2.4.4-1	Blade Tip Cascade Rig	78
2.2.2.4.4-2	Blade Tip Cascade Cross Section	79
2.2.2.4.4-3	Tip Seal Geometries	80
2.2.2.4.4-4	Stage 2 Bucket Tip Cascade	81

2.2.2.4.4-5	Sample Midchord Seal Strip Heat Transfer Results	81
2.2.2.4.8-1	Liquid Crystal Test Model of S1B Leading Edge Cooling Surfaces	91
2.2.2.5-1	9H Baglan Bay Turbine Cross Section	97
2.2.2.5-2	Typical Steam Cooled Nozzle Cross Section	97
2.2.2.5-3	Typical Trailing Edge Cooling Hole	98
2.2.2.5-4	Stage 1 Nozzle Assembly	98
2.2.2.5-5	Stage 1 Nozzle Cascade Test Rig	99
2.2.2.6.2-1	Original Scroll Geometry for CFD Analysis	107
2.2.2.8-1	ATS Gas Turbine – ISO	117
2.2.2.8-2	ATS Gas Turbine – Right Side	118
2.2.2.8-3	ATS Gas Turbine – Left Side	119
2.2.3.1.2-1	Turbulence Variation with Reynolds Number	136
2.2.3.1.2-2	Smooth Airfoil Comparison	137
2.2.3.1.2-3	Rough Surface Comparison	138
2.2.3.2-1	Schematic Diagram of Test Rig	141
2.2.3.3-2	Spoolie Test Matrix	142
2.2.3.3-3	Spoolie Life as a Function of Angulation, Interference, and Steam Temperature	142
2.2.3.4.1-1	Rotating Bucket Rig	145
2.2.3.4.1-2	Photo of Rotating Rig	145
2.2.3.4.1-3	Rotating Bucket Rig Flow Schematic	146
2.2.3.4.1-4	Rotating Bucket Rig Cross Section	147
2.2.3.4.2-1	Rotating Bucket Rig with Mixing Ribs Cross Section	150
2.2.3.4.4-1	Bucket Trailing Edge Cooling Channels	153
2.2.3.4.4-2	Trailing Edge Rotating Rig Cross Section	154
2.2.3.5.1-1	Sample Heat Transfer Test Result for S2N Trailing Edge at Lab Conditions	156
2.2.3.5.2-1	Bucket Trailing Edge	158
2.2.3.5.2-2	Bucket Tip Turn Region	159
2.2.3.5.2-3	Bucket Trailing Edge Cavity Rig Flowpath	161
2.2.3.5.3-1	S1N Outer Band Liquid Crystal Rig	164
2.2.3.5.4-1	S1N Heat Transfer Test Section	167
2.2.3.5.5-1	Bucket Tip Closed Circuit Cooling Rig Schematic	169
2.2.3.5.5-2	Smooth Tip Turn Endwall Heat Transfer	170
2.2.3.5.5-3	Surface Enhancement on Tip Turn Endwall Heat Transfer	171
2.2.3.5.6-1	Bucket Leading Edge Heat Transfer Model	172
2.2.3.5.6-2	Copper Block with Geometry of Leading Edge Formed by Wire Electrical Discharge Machining	174
2.2.3.5.6-3	Test Section Consists of Stack-up of EDM'ed Blocks Inside of a Low Thermal Conductivity G10 Fiberglass Board Shell	174

2.2.3.5.8-1 Lab-scale S1N Trailing Edge Model Liquid Crystal Test 179
2.2.3.5.9-1 High Reynolds Number Turbulated Passage Test Section 182
2.2.3.5.9-2 Section A-A Construction 183
2.2.3.5.9-3 Flow Loop at Texas A&M's Turbomachinery Laboratory 183
2.2.3.5.12-1 Example of 10X Fillet Region Impingement Test Model 190
2.2.3.6-1 Cold Flow Wind Tunnel Cross Section Views 196
2.2.3.6.2-1 Airfoil Heat Transfer Coefficients with Ra = 4.5 Microns and High Tu 202
2.2.3.6.2-2 Effect of Surface Roughness with Re_{cx} = 4.7e6 and Tu = 9 203
2.2.3.6.2-3 Airfoil Mach Distribution with Trip Locations 203
2.2.3.6.2-4 Effect of Modeled Spallation Trip on Pressure Side Heat Transfer 204
2.2.4.10.1-1 Photograph of a Prototype Ultrasonic System for Wall Thickness Measurement in Single Crystal Nickel-Based Super-alloy Turbine Airfoils for the ATS Gas Turbine 235
2.2.4.10.1-2 Photograph of a Prototype IR System for Wall Thickness Measurement in Single Crystal and Directionally Solidified Nickel-Based Super-alloy Turbine Airfoils for the ATS Gas Turbine 235
2.2.4.10.1-3 Digital Radiograph of a Portion of a Single Crystal Casing for the ATS Gas Turbine 236
2.2.4.14.1-1 Hot Gas Path Seals in a Turbine 241
2.2.4.14.3-1 Brush Seals Configuration for 7H S3N 246
2.2.5.1-1 Thermal Barrier Coating Microstructures 257
2.2.5.1-2 Robotic Manipulation Scheme for Coating Advanced Turbine Systems Components 257
2.2.5.1-3 Deposition of Thermal Barrier Coating on the ATS Stage One Nozzle at GE-CRD 258
2.2.5.1-4 ATS Stage One Nozzle After Deposition of Thermal Barrier Coating 258
2.2.5.1-5 Reactor for Depositing CMAS Protective Coating at GE-CRD 259
2.2.5.1-6 ATS Stage One Nozzle Before and After Deposition of CMAS Protective Coating 260
2.2.5.1-7 Process Steps for Using CNC Grinding to Create the Desired Ceramic Coating Thickness Profiles on ATS Turbine Components 260
2.2.5.1-8 Control of Air Plasma Deposition Process for Thermal Barrier Coating 261
2.2.5.1-9 Quality Flowdown and Flowup as Applied to Development of Thermal Barrier Coating for the Advanced Turbine System 261
2.2.5.2-1 Electron Beam High Thermal Gradient Test Rig 266
2.2.5.2-2 Electron Beam High Thermal Gradient "Tophat" Test Specimen 267
2.2.5.3-1 Degradation Modes for Thermal Barrier Coating 272
2.2.5.3-2 Path to Develop Coating Life Prediction Models 273
2.2.5.3-3 Tests Used for Predicting Thermo-Mechanical Fatigue Life of Thermal Barrier Coating on Gas Turbine Components 273

2.3.1-1	Completed 9H Cooling Air Cooling Skid for Baglan Bay	278
2.3.2-1	Integrated Control System	285
2.3.2-2	H System Complex Cycle	286
2.3.2-3	S107H/S109H Cold Start Loading Profile, Single Unit	287
2.3.2-4	Integrated 9H Simulation Model Non-Real Time	287
2.3.2-5	Integrated 9H Simulation Model Non-Real Time	288
2.3.3-1	Design for Reliability (DFR) Process Map	290
2.3.3-2	Failure Modes and Effects Analysis (FMEA) Form	291
2.3.3-3	Lube Oil Reliability Block Diagram Model	291
2.3.4-1	Overview of the GEPS ATS Integrated Steam Cooling System	294
2.3.4-2	Typical S107H/S109H Hot Start Loading Profile	296
2.3.4-3	Typical S107H/S109H Cold Start Loading Profile, Single Unit	296
2.3.4-4	GEPS H Combined Cycle Configuration, Showing Two Different Steam Turbines	297
2.5-1	Heat Recovery (HR) IGCC Design Block Flow Diagram	305

List of Tables

1-1	Components and Locations Involved in Phase 3R Testing	8
2.2.4.4-1	403Cb+ LCF Test Matrix at 950°F, A=+1, frequency = 20 cpm	218
2.2.4.4-2	403Cb+ LCF Test Matrix at 850°F, A=+1, frequency = 20 cpm	219
2.2.4.4-3	403Cb+ HCF Test Matrix	219
2.2.4.4-4	403Cb+ Creep Test Conditions	219
2.2.4.9-1	403Cb+ Stress Relaxation Test Conditions	227
2.5.1	Design Basis	304
2.5-2	Overall 9H IGCC Performance	309

ACRONYMS USED IN GE ATS REPORT

ACC - active clearance control
AEC - Automated Eddy Current
ANSYS - *finite element software*
APS - air plasma spray
ATS - Advanced Turbine System
AWS - aft wheel shaft
CAC - cooling-air cooling
CAD - computer-aided design
CC - compressor case
CDC - compressor discharge case or casing
CDD - compressor discharge diffuser
CFD - computational fluid dynamics
CMAS - calcium-magnesium-aluminum-silicate
CMM - coordinate measuring machine
CNC - computer numeric control
CNRC - Canadian National Research Council
CRD - GE Corporate Research and Development
CSMP - Coordination through Short Motion Programming
CTP - critical-to-process
CTQ - critical-to-quality
CVD - chemical vapor deposition
DFSS - design for six sigma
DLN - dry low NOx
DOE - U.S. Department of Energy
DTA - differential thermal analysis
DTC - design to cost
DVC - dense vertically cracked
EA - Environmental Assessment
EB - electron beam
EDM - electron discharge machine
EDR - electronic data release
EIS - Environmental Impact Statement
EPRI - Electric Power Research Institute
FBD - Free Body Diagram
FCGR - fatigue crack growth rate
FCP - fatigue crack propagation
FCT - furnace cycle test
FEA - finite element analysis
FEM - finite element model
FETC - Federal Energy Technology Center
FFT - Fast Fourier Transform
FMEA - failure modes effects analysis
FONSI - Finding of No Significant Impact
FPI - fluorescent penetrant inspection
FPQ - first piece qualification
FSFL - full speed, full load
FSNL - full speed, no load
GASP - gravity-assisted shot peening
GEAE - GE Aircraft Engines
GEPG - GE Power Generation
GEPS - GE Power Systems
GTAW - gas tungsten arc weld
GTCC - gas turbine combined cycle
HCF - high cycle fatigue
HIP - hot isostatically pressed
HP - high-pressure
HRSG - heat recovery steam generator
HVOF - high velocity oxy-fuel
IGCC - integrated gasification combined cycle
IGV - inlet guide vane
IP - intermediate-pressure
IP&D - process and interface drawing; process and instrumentation drawing
IR - infrared
IT - Inverse Time
KCC - key control characteristic
KCP - key control parameter
KNP - key noise parameter
LCF - low cycle fatigue
LCVT - liquid crystal video thermography
LH - lower half
LUT - Laser Ultrasound
NDE - nondestructive evaluation
NDT - nondestructive testing

NEPA - National Environmental Policy Act
NETL - National Energy Technology Laboratory
ORNL - Oak Ridge National Laboratory
P&ID - process and interface drawing; process and instrumentation diagram
QDC - Quality Data Collection
QFD - quality function deployment
RAM - reliability, availability, and maintainability
SEM - scanning electron microscopy
SLA – stereo lithography apparatus
SSPM - steady state performance model
SSRT - slow strain rate tensile
STP - Segment Time Programming
STEM – shaped tube electrolyte machining
TBC - thermal barrier coating
TBO - time-between-outages
TC - thermocouple
TCP - Tool Center Point
TDM - thermal dynamic model
TDS - thermal dynamic simulation
TEM - transmission electron microscopy
TIG - tungsten inert gas
TMF - thermomechanical fatigue
TP - transition piece
UAB - Utility Advisory Board
UG - UniGraphics
UH - upper half
VGV - variable guide vane
VPS - vacuum plasma spray
VSV - variable stator vane
YFT - *fluids analysis software*

Section 1 Executive Summary

The overall objective of the Advanced Turbine System (ATS) Phase 3 Cooperative Agreement between GE and the U.S. Department of Energy (DOE) was the development of a highly efficient, environmentally superior, and cost-competitive utility ATS for base-load utility-scale power generation, the GE 7H (60 Hz) combined cycle power system, and related 9H (50 Hz) common technology. The major effort was expended on detail design. Validation of critical components and technologies was performed, including: hot gas path component testing, sub-scale compressor testing, steam purity test trials, and rotational heat transfer confirmation testing. Processes were developed to support the manufacture of the first system, which was to have been sited and operated in Phase 4, but will now be sited and operated commercially by GE. This change resulted from DOE's request to GE for deletion of Phase 4 in favor of a restructured Phase 3 (as Phase 3R) to include full speed, no load (FSNL) testing of the 7H gas turbine. Technology enhancements that were not required for the first machine design but will be critical for future ATS advances in performance, reliability, and costs were also initiated. Long-term tests of materials to confirm design life predictions continued for the duration of the program. A schematic of the GE 7H ATS machine is shown in Figure 1-1.

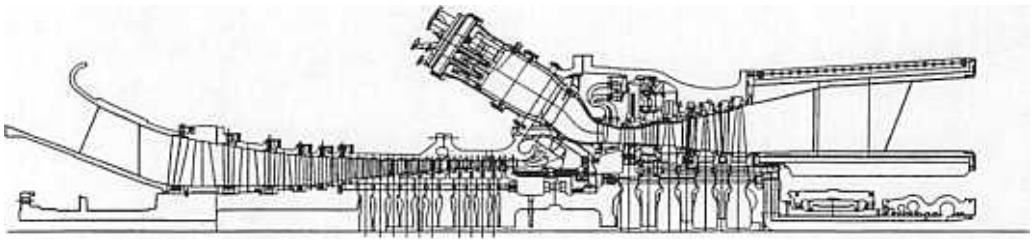

Figure 1-1. 7H ATS Gas Turbine Cross Section

Note: The GE Power Systems (GEPS) ATS program is a part of a larger *H System*™ program, which includes the MS9001H (9H, 50 Hz) gas turbine to be exported from the GEPS Greenville, SC manufacturing facility. There was common component technology development for both engines, and as the 9H preceded the MS7001H (7H, 60 Hz) ATS gas turbine in construction and testing, valuable lessons were learned from the initial 9H test program that benefited the 7H design and subsequent testing.

Background

In the early '90's, GE recognized the need to introduce new technology to follow on to the "F" technology the Company introduced in 1988. By working with industry and DOE, GE helped shape the ATS program goal of demonstrating a gas turbine, combined-cycle system using natural gas as the primary fuel that achieves the following targets:

- System efficiency exceeding 60 percent lower heating value basis.

- Environmental superiority under full-load operating conditions without the use of post-combustion emissions controls. Environmental superiority includes limiting NOx to less than 10 parts per mission by volume (dry basis) at 15 percent oxygen.
- Busbar energy costs that are 10 percent less than current state-of-the-art turbine systems meeting the same environmental requirements.
- Fuel-flexible designs operating on natural gas but also capable of being adapted to operate on coal-based, distillate, or biomass fuels.
- Reliability-Availability-Maintainability (RAM) that is equivalent to modern advanced power generation systems.
- Commercial systems that could enter the market in the year 2000.

DOE designed the original ATS program in four phases:

Phase 1 - System Selection
Phase 2 - Conceptual Design and Product Definition
Phase 3 - Technology Readiness Testing
Phase 4 - Commercial Utility Scale Demonstration

Figure 1-2 shows the scheduling for the entire ATS program with a restructured Phase 3 (Phase 3R) and the elimination of Phase 4. Phase 3R was divided into four Budget Periods. Budget Period 1 was the original Phase 3.

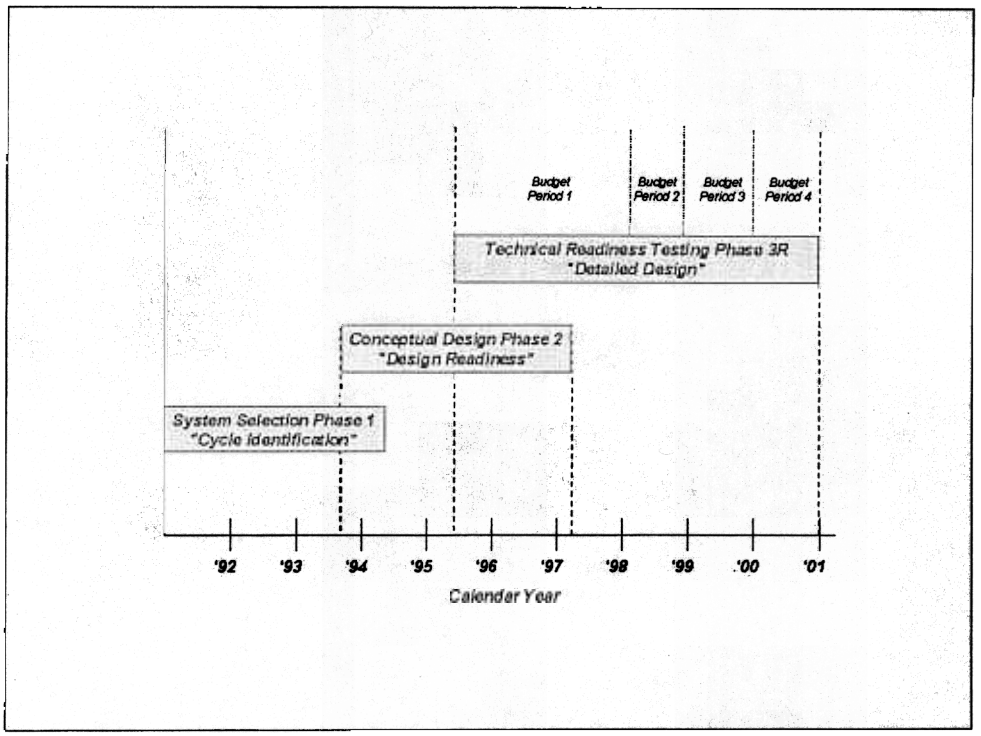

Figure 1-2. Schedule for Phase 1 through Phase 3R.

In Phase 1, DOE invited power generation equipment suppliers to propose a system concept that would meet ATS goals. Although awarded a Phase 1 activity, GE decided not to spend DOE funds in this area, since the Company had already completed cycle selection studies, and was working on a preliminary design.

A proposal for Phase 2 was developed and submitted. This proposal focused on developing the technologies needed for GE's advanced design. Upon contract award, GE began technology development under the ATS Phase 2 program in late 1993. This phase was completed in 4Q96, and the Final Reports were submitted in 2Q97.

In November 1994, GE submitted a proposal for the Phase 3 (Technology Readiness Testing) and Phase 4 (Pre-Commercial Demonstration) programs. The design of GE's H technology machines had already begun at that point. In September 1995, DOE awarded the Phase 3 Cooperative Agreement to GE.

In March 1997, DOE issued a Request for Proposal for a restructured program that would extend Phase 3 beyond the December 1997 conclusion date. The restructured program (called Phase 3R) featured continued component design and development, and Full Speed No Load (FSNL) testing of the 7H (60Hz) ATS machine at the Greenville, SC manufacturing facility. The original Phase 4 (Commercial Utility Scale Demonstration) was eliminated.

GE responded to DOE in July 1997 with a proposal for a restructured ATS program. Subsequently, GE submitted a final revised proposal to DOE in December 1997. Negotiations with DOE regarding the restructured ATS program concluded in late March 1998 with the execution of a modified Cooperative Agreement for the ATS program, which extended through December 31, 2000. A Continuation Application to this Cooperative Agreement was submitted in September 1998 to cover Budget Periods 3 and 4 (remainder of program), with negotiations for Budget Period 3 being concluded in December 1998. Another Continuation Application to this Cooperative Agreement was submitted in September 1999 to cover Budget Period 4, with negotiations being concluded in December 1999.

Subsequent to the signing of the Phase 3R Cooperative Agreement in 1998, the 9H (50Hz) FSNL test program was initiated. The 9H FSNL test program continued into 1999, testing incremental modifications to the engine. Information derived from this testing was used to update the design system for both the 9H and 7H ATS engine programs.

The 7H ATS FSNL test program was completed in February, 2000, and has verified all CTQ's (critical to quality parameters determined before testing). CTQ's included were compressor operating performance (air flow and efficiency), aeromechanics, rotor dynamics, operability, turndown, startup characteristics, and Mark VI control system operation.

Program Schedule

Figure 1-3 shows the timeline of major component test milestones in the Phase 3R program. The tests shown led to the successful completion of the 7H FSNL test in 1Q00.

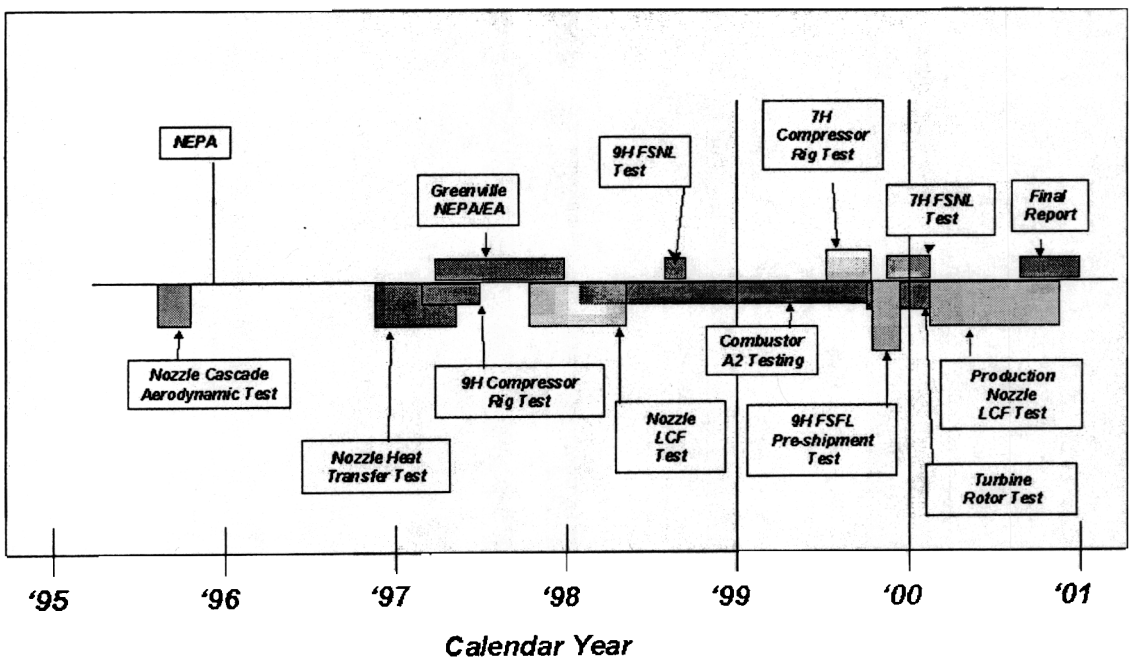

Figure 1-3. Phase 3R Timeline of Significant Events

Phase 3R Overview

The Phase 3R program provided the design for the ATS power plant. In the broadest terms, this design encompasses the entire power plant as pictured in Figure 1-4. Specifically, the Phase 3R program provided the detailed design of those components of a combined cycle power plant that are unique to H technology. This scope included detailed design of the gas turbine and gas turbine related accessories, and detailed specifications of the steam turbine, generator, materials shipped direct (MSD), accessories, controls, HRSG, and Balance of Plant (BOP).

The scope was accomplished for both the 7H (60 Hz) and 9H (50 Hz) power systems.

The engineering required in preparation for manufacturing the 7H and 9H gas turbines was included in the Phase 3R program, as well as engineering supporting the FSNL testing for both gas turbines. Engineering in support of pre-shipment FSNL testing of the 7H and 9H gas turbines has also been included, as important information results from first FSNL operation.

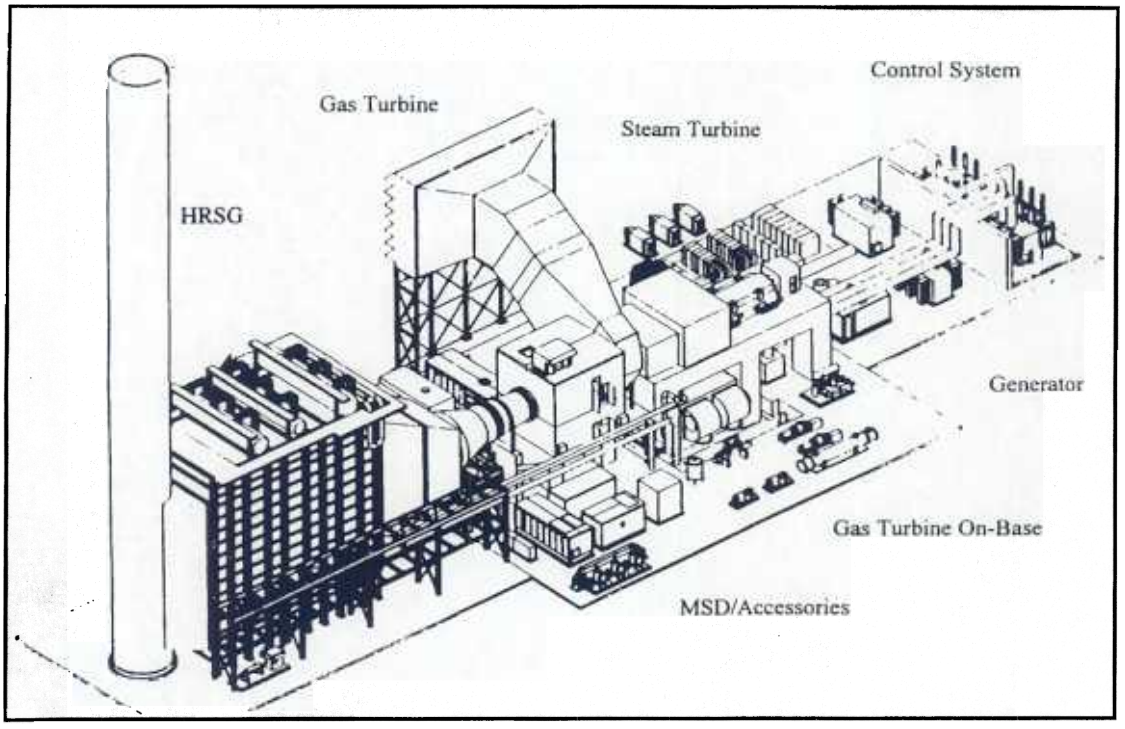

Figure 1-4. ATS Combined Cycle Power Plant

Central to the ATS combined cycle system is the H technology gas turbine, which is shown in Figure 1-5. Both a 60 Hz (7H) and a 50 Hz (9H) design were completed. Significant components comprising this gas turbine design are the compressor, combustion system, turbine rotor, turbine buckets, turbine stator, turbine structures, and on-base piping.

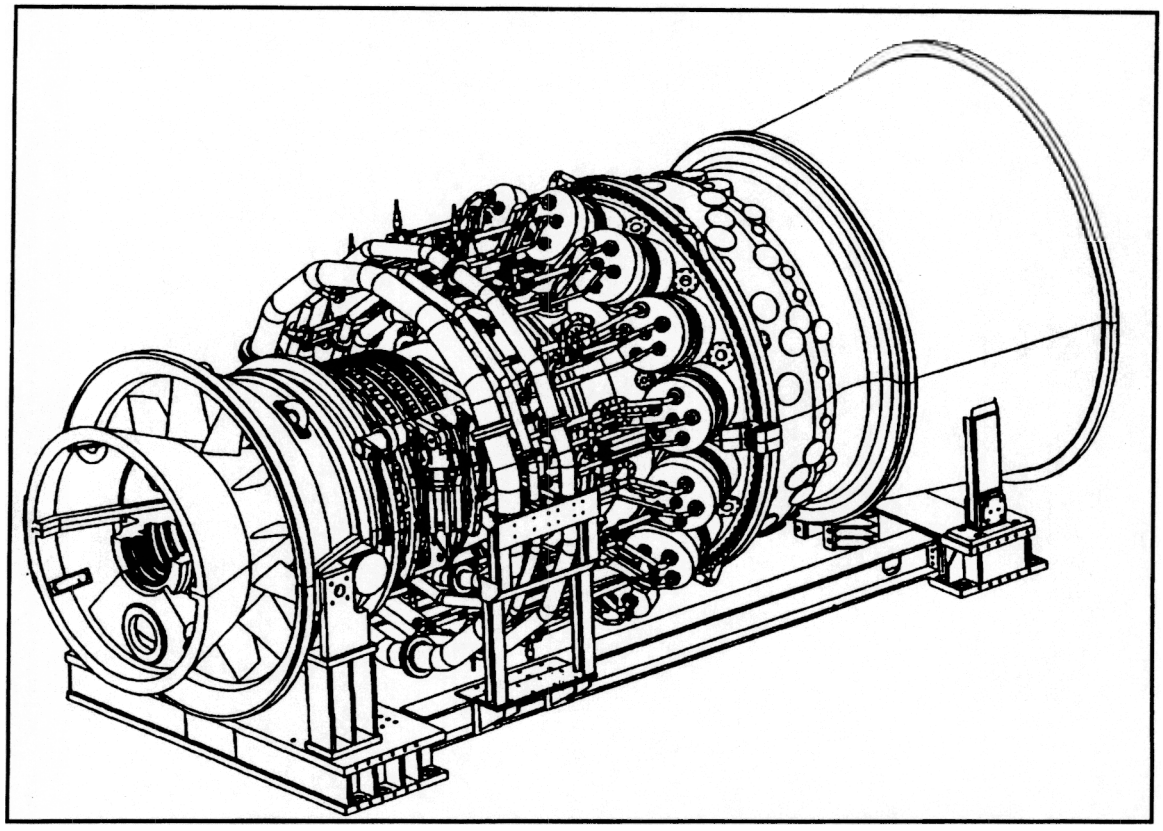

Figure 1-5. An Isometric Drawing of the ATS Gas Turbine

Since the gas turbine is the most critical part of the new H technology power system, extensive testing was performed to validate the design, confirm performance, and assess the life of the components. Figure 1-6 shows the completed validation testing of the gas turbine components that were performed under Phase 3R. These tests validated the 7H and 9H gas turbine designs at the component level. Table 1.1 shows the locations and status of the Phase 3R component testing. Both gas turbine systems were tested in the Greenville, SC factory at FSNL conditions.

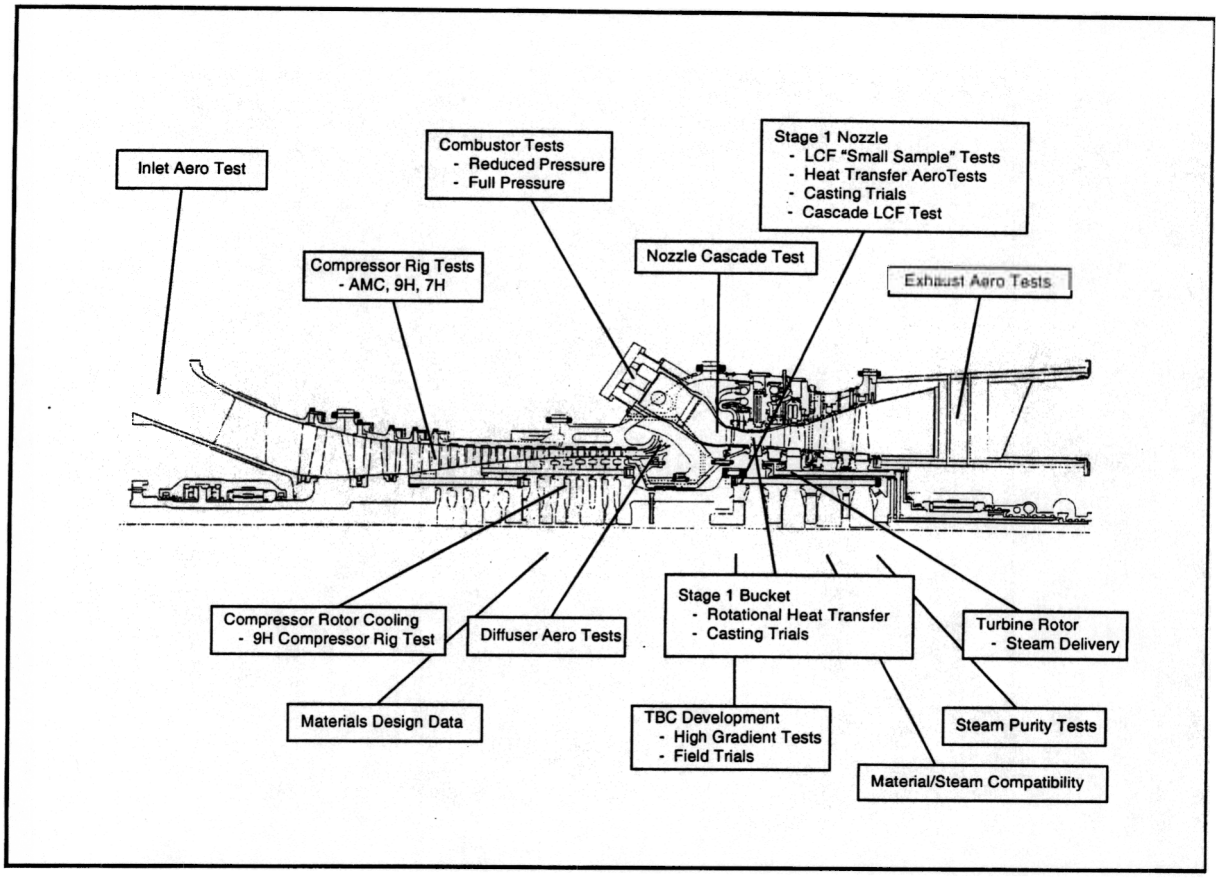

Figure 1-6. Validation Testing of the ATS Gas Turbine (See Table 1.1).

7H ATS FSNL Test Description

The fully instrumented MS7001H prototype unit was installed in GE's gas turbine test stand in Greenville, SC for the FSNL test. The test stand equipment included all accessory systems needed to support FSNL operation. Selected sensors on the unit that were used for FSFL demonstration test activity were connected to the test stand data system. Standard production control system, performance, and monitoring instrumentation was installed, and signals were recorded to establish baseline data for production 7H units. After the unit was installed, and mechanical, electrical, and unfired cranking checks were completed, the 7H prototype was fired and accelerated to FSNL. Data were recorded during startup transient conditions, as well as at the steady-state FSNL point. Data was recorded during the shutdown transient.

Table 1.1. Components and Locations Involved in Phase 3R Testing

Inlet Aero Test		GE Nuovo Pignone, Italy
Compressor Rig Tests	Advanced Machine Compressor (AMC) • 9H • 7H	GEAE, Lynn, MA
Compressor Rotor Cooling Tests	9H Rig Compressor Test	GEAE-Lynn, MA
Combustor Tests	Reduced Pressure Full Pressure	GEPG Lab, CRD, Schenectady, NY GEAE Lab, Evendale, OH GEAE Lab, Evendale, OH
Diffuser Aero Tests		GE-CRD, Schenectady, NY
Nozzle Cascade Test	Nozzle Aerodynamics Nozzle Heat Transfer	GEAE, Evendale, OH
Stage 1 Nozzle Tests	LCF "Small Sample" Tests Heat Transfer Aero Tests Casting Trials Cascade LCF Test-Prototype Cascade LCF Test-Production	GE-CRD, Schenectady, NY GE-CRD, Schenectady, NY Texas A&M GE-CRD, Schenectady, NY Howmet, Hampton, VA GEAE, Evendale, OH GEAE, Evendale, OH
Stage 1 Bucket Tests	Rotational Heat Transfer Casting Trials	GE-CRD, Schenectady, NY GE-CRD, Schenectady, NY Howmet, Hampton, VA
Turbine Rotor Tests	Steam Delivery Component Testing	GEPG Lab, CRD, Schenectady, NY
Exhaust Aero Tests		GE-CRD, Schenectady, NY
Material Design Data		GE-CRD, Schenectady, NY
TBC Tests	High Gradient Tests Field Trials	GE-CRD, Schenectady, NY Virginia Power, VA
Steam Purity Tests		Ocean State Power, Burrillville, RI
Material Steam Compatibility Tests		GE-CRD, Schenectady, NY
Brush Seal Test-Rotating Rig Test		Ocean State Power, Burrillville, RI
9H FSNL 9H FSFL Pre-shipment 7H FSNL		GEPS, Greenville, SC GEPS, Greenville, SC GEPS, Greenville, SC

ATS Phase 3R Work Breakdown Structure

A block diagram of the Phase 3R Work Breakdown Structure (WBS) is provided in Figure 1-7. This is a subset of the complete WBS that was used by GE to manage the development of the 7H and 9H systems. A character code is used to identify each work element, with two characters for each level of the WBS. For example, 7HGTFFTB is the work element on the 7H Gas Turbine Flange-to-Flange product Turbine Buckets.

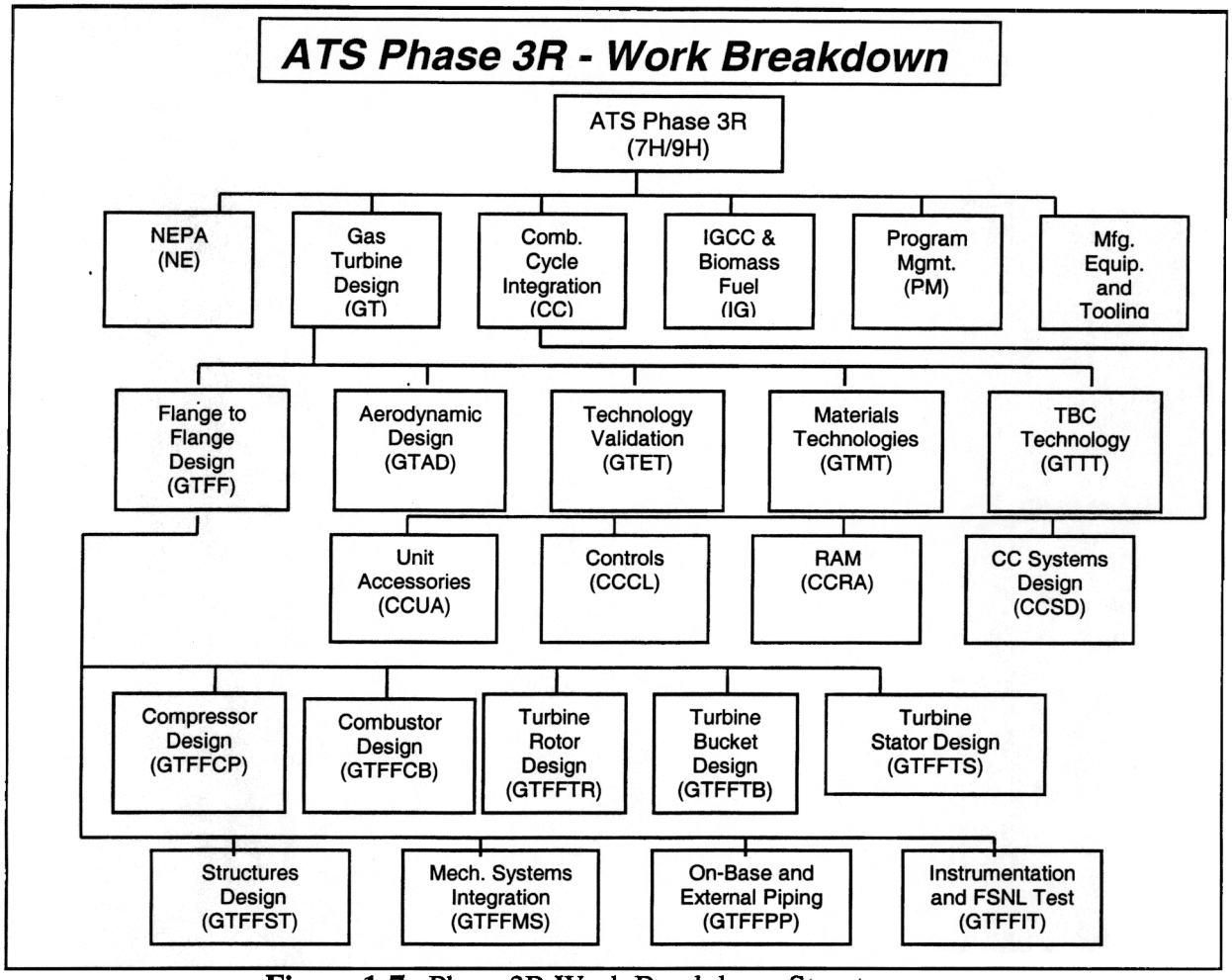

Figure 1-7. Phase 3R Work Breakdown Structure

ATS Phase 3R Statement of Work

The overall objective of the Advanced Turbine Design System (ATS) Phase 3R Cooperative Agreement between GE and the U.S. Department of Energy (DOE) was the development of the GE 7H and 9H combined cycle power systems. The major effort was be expended on detailed design. Validation of critical components and technologies were performed, including: hot gas path component testing, sub-scale compressor testing, steam purity test trials, and rotational heat transfer confirmation testing. Processes were developed to support the manufacture of the 9H and 7H gas turbines at Greenville, SC, and the first 7H system that was tested to FSNL conditions. Technology enhancements that were not required for the first machine design, but will be critical for future ATS advances in performance, reliability, and costs were initiated. Long-term tests of materials to confirm design life predictions continued. The GE component performing the work for each WBS task is indicated after each title:

GE Power Systems-Schenectady	[S]
GE Corporate Research and Development	[C]
GE Aircraft Engine-Evendale	[A]
GE Power Systems-Greenville	[G]

Section 2 Final Report

Section 2.1 (NE) NEPA (National Environmental Policy Act) [S,G]

Objective

Draft topical reports were prepared by GE that provided the relevant Environmental, Health, and Safety information related to the engineering development and testing activities of the WBS, as required for the National Environmental Policy Act (NEPA) assessments to be generated by DOE. Separate topical reports were furnished as follows:

- Comprehensive topical reports covering all major engineering development testing sites other than the FSNL test.
- A generic Environmental Information Volume (EIV) for a potential "greenfield" siting of the ATS machine.
- A topical report specifically related to manufacturing and FSNL testing of GE's 7H gas turbine at Greenville, SC.

DOE reviewed each report, and advised the Participant of the acceptability of the report, or the need for additional information. A final topical report was then submitted.

Introduction/Background

The U. S. Government requires all contractors to have a safety and health program in place for each location where work will be performed. In addition, an environmental protection plan is required for each location where testing will occur. This plan will address the applicable federal, state, and local regulatory requirements, and is adequate to address the project work site.

The environmental, health, and safety (EH&S) information provided by the contractors is used by DOE to prepare the appropriate NEPA documentation for the proposed project. The EH&S information includes:

- A brief, non-confidential description of the project, including project objectives, project schedule, map locations, description of existing facilities, and a description of facilities to be constructed for the project. If appropriate, the contractor will provide process flow diagrams, plan and elevation views, and sizes and capacities for major equipment. In addition, a discussion will be included covering the quantities and types of materials to be used in the project including feedstocks, utilities, fuels, reactants, products, effluents, unrecovered materials, and solid waste.

- Discussion regarding current environmental characteristics of the site(s), and any potential environmental impacts from the project. The discussion will include compliance with federal, state, and local environmental regulations pertaining to the following categories: air quality; water resources; land use; pollution prevention; waste management; ecological impacts; biodiversity; socioeconomic impacts; archaeological, cultural, and historical resources; noise; occupational, safety and health; cumulative impacts; and a summary of environmental impacts.

- A table that identifies all federal, state, and local permits and licenses required for the project. The table will provide information on the permitting and licensing schedule and current status of each permit and license, and on the allowable releases of solid, liquid, and air pollutants under the permit(s) and license(s).

Discussion

Separate ATS Phase 3 (Technology Readiness Testing) environmental, health, and safety reports were prepared for each location where component testing was planned. These locations were: GE Power Systems' main plant facility in Schenectady NY; GE Aircraft Engines' facilities in Evendale, OH; and GE Aircraft Engines' facilities in Lynn, MA. These reports were prepared by the consulting firm of ERM-Northeast, Inc., as a subcontractor to GEPS.

The report prepared by the GE Corporate Research and Development Center (GE-CRD) covered the related activities at GE-CRD facilities in Niskayuna, NY, as well as the test activities to be conducted at Ocean State Power in Burrville, RI, and at Texas A&M University in College Station, TX under the direction of GE-CRD.

An ATS Phase 4 (Pre-Commercial Demonstration) "Generic" Environmental Information Volume (EIV) was prepared for the 7H Base Reference Plant. It was unknown at the time whether the ATS site would be an addition to or repowering of the current gas and steam turbines at an existing power generation facility, a retrofit of other power equipment, or a new installation at an undeveloped "greenfield" site. Consequently, the EIV addressed the environmental impacts of the proposed actions to the extent that the impacts could be characterized in a non-site specific manner.

The ATS program was restructured in 1997, with the Phase 4 Commercial Utility Scale Demonstration being eliminated, and the full speed, no load (FSNL) test of the 7H (60 Hz) ATS machine being added to a restructured Phase 3 (Phase 3R).

As part of the Phase 3R program, an environmental, health, and safety (EH&S) assessment was required before the ATS 7H FSNL test program could be initiated at GE's Gas Turbine Manufacturing Facility in Greenville, SC. The EH&S assessment was prepared by International Technology Corp. as a subcontractor to GEPS. The report covered: a general description of current site operations and EH&S status; a description of the proposed ATS 7H-related activities, and a discussion of the resulting environmental, health, and safety and other impacts to the site and surrounding area; a listing of permits and/or licenses required to comply with the federal, state, and local regulations for proposed 7H- related activities; and an assessment of adequacy of current and required permits, licenses, programs, and/or plans.

The results of the Greenville, SC EH&S study were used by DOE to prepare an Environmental Assessment (EA) for the Greenville facility. The EA analyzed the potential impacts of the fabrication, assembly, and testing program. Based on this analysis, DOE determined that the proposed ATS activity was not a major Federal action significantly affecting the quality of the human environment, within the meaning of the

National Environmental Policy Act of 1969, and therefore issued a Finding of No Significant Impact (FONSI).

Summary/Conclusion

Environmental, health, and safety reports documenting the meeting of appropriate federal, state, and local requirements were prepared for all locations where GE ATS-related engineering design and testing took place. Reports for the following locations were submitted and approved by DOE:

GEPS - Schenectady, NY
GEPS - Greenville, SC
GEAE - Evendale, OH
GEPS - Lynn, MA
GE - CRD - Niskayuna, NY
GE - CRD - Ocean State Power, Burrville, RI
GE - CRD - Texas A&M University, College Station, TX

The most extensive environmental, health, and safety study was conducted for the GE Gas Turbine Manufacturing Facility in Greenville, SC, where the ATS 7H gas turbine assembly and FSNL testing took place. The facility met all federal, state, and local requirements, and DOE issued a Finding of No Significant Impact (FONSI) for the facility.

Technology Application

The NEPA report provides documentation that GE Power Systems is in compliance with all applicable environmental, health, and safety laws and regulations, and has the required permits and licenses necessary for compliance.

Section 2.2 (GT) Gas Turbine Design [S,C,A,G]

Section 2.2.1 (GTAD) Aerodynamic Design [A]

Objective

To achieve ATS performance goals, two separate eighteen stage compressors based on CF6-80C2 technology and two four-stage turbines were designed. Advanced aerodynamic technology pioneered at GEAE was applied to each stage to maximize performance and meet mechanical design requirements required by steam cooling technology. The 7H (60 Hz) and 9H (60 Hz) machines have similar flow paths and common rotor technology, but required different aerodynamic designs. Performance requirements for the 7H and 9H compressor and turbine aerodynamics are the same.

ATS Compressor Aerodynamic Design

Introduction/Background

This section covers the aerodynamic design and validation of the compressors for the MS7001H (7H) and MS9001H (9H) compressors. Both compressors have 18 stages and are derived from scaling the General Electric CF6-80C2 aircraft engine compressor, with new or modified designs where required.

The 9H compressor was designed to meet a required airflow of 1514 pps at full speed full load (FSFL), ISO day conditions, at a pressure ratio of 23.2:1. The design incorporates one variable inlet guide vane (VIGV) and four stages of variable stator vanes (VSV). The 7H compressor was designed to meet a required airflow of 1255 pps at FSFL, ISO day conditions, also at a pressure ratio of 23.2:1, this design incorporates one VIGV and five stages of VSVs.

A series of three sub-scale rig tests were carried out to validate the designs, before running the full-scale machines.

Discussion

A series of three Advanced Machine Compressor (AMC) compressor rigs (AMC001/1, AMC002/1(9H), and AMC003/1(7H)) were designed to support the development of the full-scale 7H and 9H compressors.

AMC001/1 was an 18 stage design (numbered 1 to 18) with a design point pressure ratio of 20.4:1, and was tested at CF6 size. The flowpath and airfoil geometry for the first two stages were redesigned from the CF6-80C2 compressor, utilizing 3-D computational fluid dynamic (CFD) tools. The stages from 3 to 12 were the same as the CF6 design, with some restaggering of the airfoils to account for differences in bleed flows between the two compressors. Stages 13 and 14 were redesigns of the CF6 airfoils, and stages 15 to 18 were completely new designs.

This compressor was tested to demonstrate the suitability of an aero-derivative compressor for a combined cycle power generation application, and formed the foundation for the balance of the H program compressor development. The aerodynamic goals of the test were to map the compressor performance, in terms of flow, pressure ratio and efficiency, over the entire range of operation, i.e. high speed, power turn down, and in the start-up region. The rig compressor was tested for 229 hours at the General Electric Aircraft Engines, Lynn, MA, full-scale test facility, between January and April 1995, and 591 data points were recorded.

Measured performance was very close to the design objective in respect to airflow and efficiency, and with surge margin exceeding the minimum requirements. Power turn down (PTD) operation was demonstrated down to 50% of nominal design flow, by closing the VIGV and four VSVs as a gang, with acceptable operability. Utilizing the gang of variable vanes, instead of the VIGV alone for PTD operation, yielded greater operating efficiency and more favorable pressure and temperature distributions in the front stages of the compressor. This eliminated the need for inflow bleed heating in the product machine for protection against icing during PTD operation.

AMC002/1 was also an 18 stage design (numbered 1 to 18) with a design point pressure ratio of 23.2:1, and was also tested at CF6 size, approximately a one third scale of the 9H compressor. The flowpath and airfoils of the front three stages were redesigned from AMC001/1 due to the requirement for increased airflow and pressure ratio. Stages 4 to 14 were as AMC001/1, with some minor redesigns for frequency tuning, and rotors 13 and 14 restaggered, due to a change in bleed flow. The rear stages were all new airfoils due to the change in pressure ratio and flow from AMC001/1. The new airfoils in this compressor utilized 3D aerodynamic design for increased efficiency and stability.

This compressor rig employed all new disks with axial dovetail slots (as used in the product compressor). It also had a unique rotor aft block (stages 13-18), which incorporated an aft cooling circuit that models the product line rotor. This rig also incorporated a tri-passage diffuser, and a bleed after stator 12, used for turbine cooling and start-up in the 9H product compressor. This compressor rig was tested at the GEAE-Lynn test facility between June and August 1997, with the same aerodynamic objectives as AMC001/1, plus the validation of the tri-passage diffuser performance. The rig ran for 160 hours, and 525 data points were recorded.

The measured performance met the requirements of airflow, efficiency, and surge margin at full power conditions. PTD operation was demonstrated down to 50% of nominal design flow by closing the VIGV and four VSVs as a gang, again with acceptable operability. Some optimization of the VSV schedule was also attempted to try and gain more performance, without compromising the operability of the compressor.

AMC003/1 was another 18 stage design, with a design point pressure ratio of 23.2:1. The 7H compressor is approximately two-and-a-half times larger than the CF6 sized rig compressor. At rig scale, the airflow requirement of the 7H compressor is approximately 13% higher than that of the 9H compressor. This increase was achieved by the addition of a zero stage ahead of the first stage, and the removal of the last stage to maintain a total of 18. Consequently, the stage numbering of the 7H compressor is 0 to 17.

At rig size, the flowpaths from stator 2 inlet to stator 14 exit are common between AMC002/1 and AMC003/1. The increased airflow of AMC003/1 required an increase in the flowpath area in the front and rear of the compressor to control the Mach numbers in these regions, and keep the same entry conditions into the diffuser as on the 9H compressor. The addition of the zero stage and the change in the flowpath, required new airfoil designs up to, and including, the third stage rotor. The change in the work distribution through the compressor led to a reduction in the number of airfoils in stages 14 to 17, which were also new designs. As on AMC002/1, the new airfoil designs utilized 3D aerodynamic design methodology. The airfoils from stator 3 to stator 14 were the same designs as used on AMC002/1. An additional bleed was added at stator 15, to closely match the design of the 7H product compressor.

A comparison of the rig front-end flowpaths is shown in Figure 2.2.1-1 below.

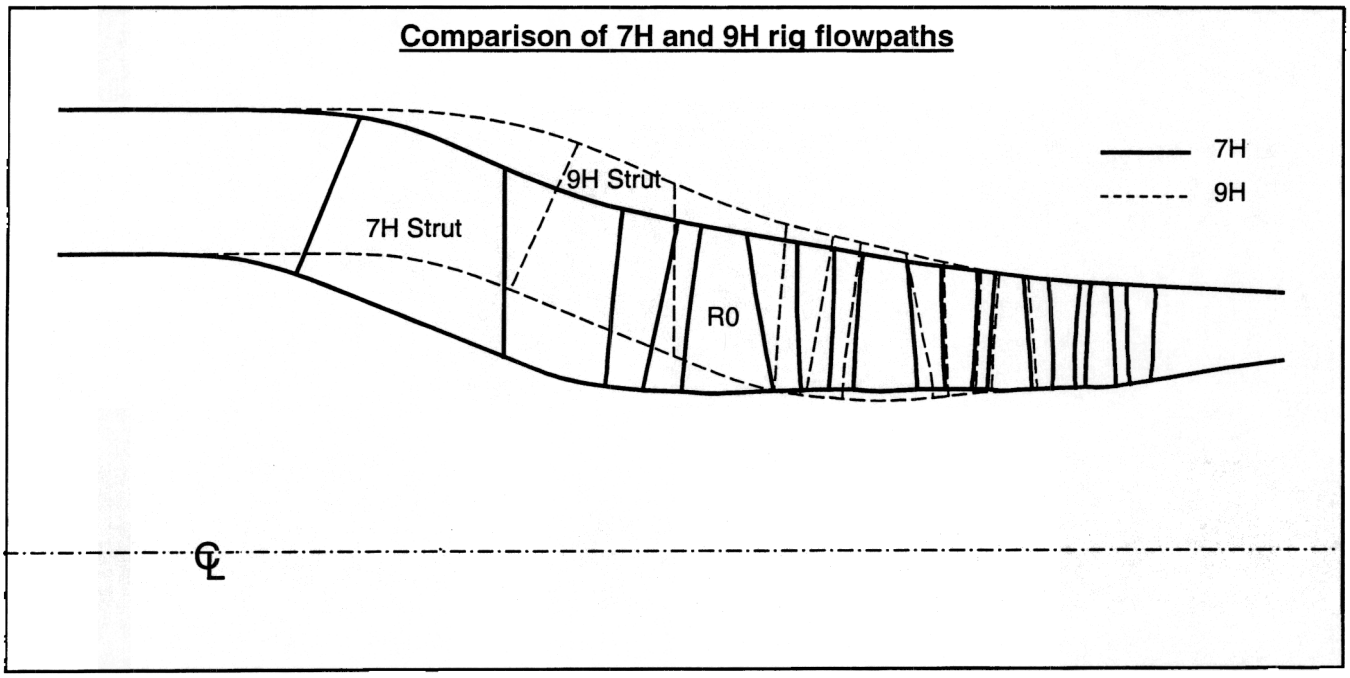

Figure 2.2.1-1. Comparison of 7H and 9H Rig Flowpaths

The AMC003/1 compressor rig was similar in mechanical design to AMC001/1, in that the CF6 style circumferential dovetail slots were used on the mid-stages, and a simple conical diffuser incorporated the tri-passage diffuser of the product design having been successfully tested on AMC002/1. This rig was again tested at GEAE, Lynn, between June and August 1999, for 150 hours, and 803 data points were recorded. The objectives of the test remaining the same as before, and once again all the performance requirements were met, or exceeded. As on AMC002/1 some VSV optimization was attempted to try to improve the compressor's performance.

The full power compressor maps are shown below in Figure 2.2.1-2, non-dimensionalized around their design points, for comparison.

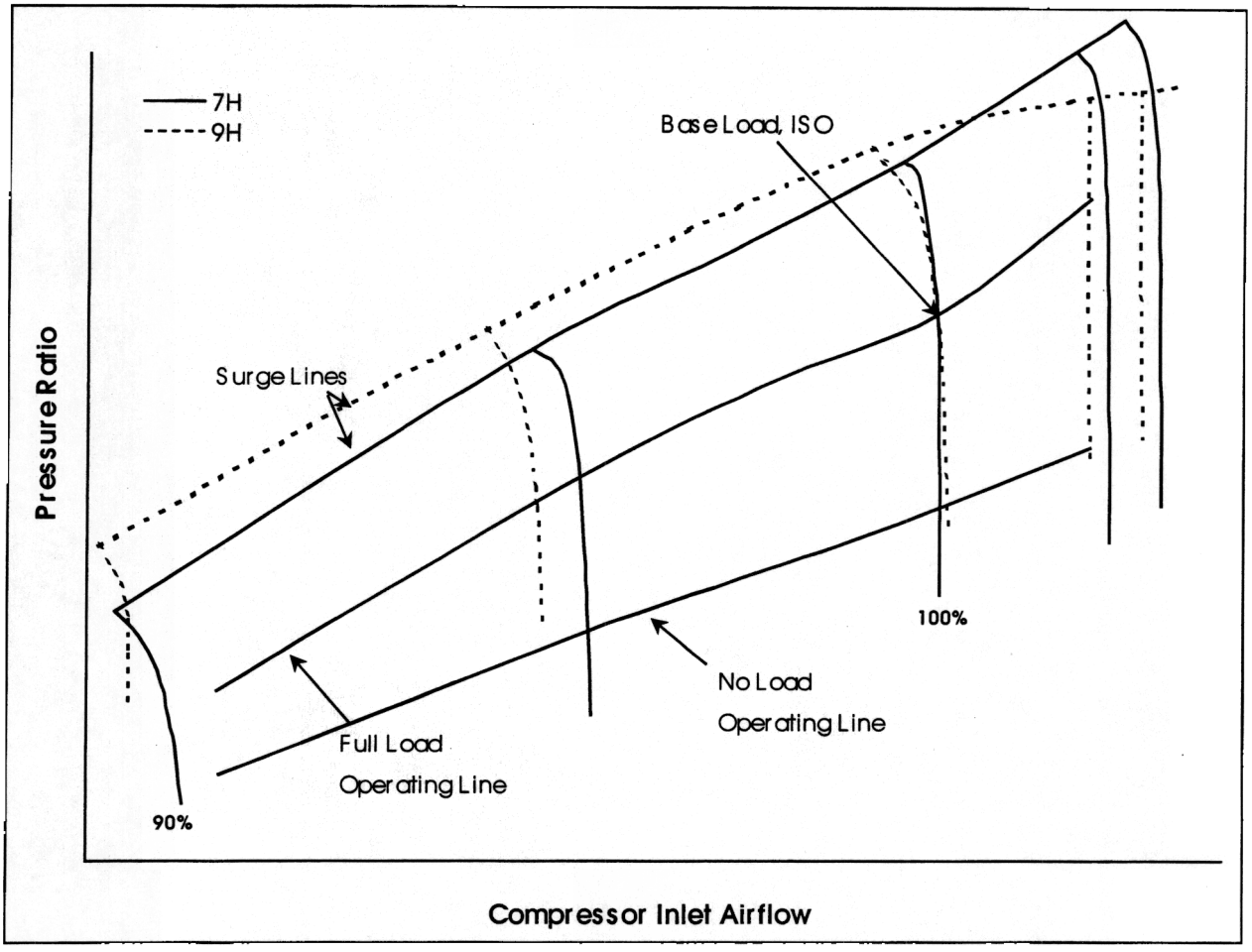

Figure 2.2.1-2. Comparison of 7H and 9H Compressor Performance Maps

All three compressor rigs were extensively instrumented with overall performance measurement instrumentation, casing static pressure taps, and stator leading edge pressure and temperature sensors. These measurements led to a good aerodynamic understanding of the internal stage matching of the compressor and validation of the compressor aerodynamic models. High-speed pressure transducers were also used to help identify the stage initiating surge at the various conditions tested. A number of the rotors used clearanceometers to determine their running tip clearances, which is essential to know, since tip clearance has a large impact on the surge margin and efficiency of a compressor.

The compressor rigs were approximately one third scales of the 7H and 9H compressors. Reynolds numbers and size effects influence a compressor's performance, so some assumptions had to be made as to the performance of the product size compressors, given the performance of the rig compressors. The two full-speed, no-load (FSNL) tests of the 9H and the one FSNL test of the 7H have validated the assumptions for the change in flow and efficiency predicted when scaling up a compressor.

Summary/Conclusions

A series of three sub-scale compressor rigs were designed and tested in support of the 7H and 9H compressor designs, and demonstrated the applicability of an aero-derivative compressor in a combined cycle power generation application.

The three compressors demonstrated their required performance at their respective design points, and met their requirements on surge margin. Power turn down operation was proven down to 50% of nominal design point flow, with acceptable operability.

The performance assumptions made when scaling from the rig size compressors to the product size were validated by the full-speed, no-load tests carried out after the rig testing was complete.

ATS Turbine Aerodynamic Design

Introduction/Background

The turbine aerodynamic requirements and steam cooling concept are integrated in the H technology turbine aerodynamic design. Both H-technology turbines were developed for GE's next generation product line gas turbines, targeting a combined cycle efficiency above 60% while maintaining low emissions, high durability, and competitive manufacturing cost. The leap in combined cycle performance compared with the current F-technology is realized by steam cooling the first and second stages of the turbine nozzles and buckets. Two closed loop steam systems were introduced, one stationary and one rotating, that circulate steam through the hot gas path components, and after cooling these components, delivers increased temperature steam back into the steam cycle. This novel cooling approach significantly reduces the amount of compressor air needed for cooling, and therefore has a positive effect both on combined cycle performance, and on NOx formation.

Discussion

Steam Cooled Turbine Stages - Stage Count Selection

The steam cooling of the first and second stages of turbine nozzles and buckets, accomplished by two closed loop circuits, also reduces the need for compressor air bleed cooling of the turbine stages. This lack of airfoil film cooling dilution flow in the turbine also results in higher exhaust temperature for a given firing temperature. However, the maximum exhaust temperature is fixed due to material limits (to proven F-class materials). In order to maintain a prescribed turbine exhaust gas temperature, the compressor pressure ratio needs to be increased relative to a conventional air cooled machine. The cycle pressure ratio for the H-technology turbines was selected to be 23:1, which is significantly higher than previous GE single shaft turbine designs. The 23:1 ratio also complements the higher firing temperature, as there is an optimum pressure ratio for a given firing temperature.

In early conceptual design studies, the benefits/drawbacks of a three-stage versus a four-stage design were compared. A significant amount of aerodynamic design work was initially carried

out on a three-stage concept, but detailed analyses showed that this concept would not meet the goal of 60% combined cycle efficiency. The turbine efficiency penalty due to the high stage loading outweighed the benefit due to reduced cooling flow requirements of the three-stage design. Hence, a four stage concept was selected.

Commonality between 50Hz and 60Hz machines

The remainder of the conceptual design phase focused on defining flow path and airfoil counts that yield maximum performance, but also striving towards maximum commonality between the 50Hz (9H) and 60Hz (7H) machines. Traditionally, GE's 50 Hz machines are 1.2 geometric scales of the 60 Hz machines. Most, but not all, key aerodynamic and mechanical characteristics will scale, and the additional development work needed to execute a scaled design is relatively small compared with the design effort needed for two independent design efforts. The approach taken on the H-technology machines, however, was different from this traditional approach. In order to minimize manufacturing and assembly complexity on the rotor and steam supply system, the maximum level of direct geometric commonality between the 7H and 9H was sought. The 20% speed difference between the two turbines implies a 40% difference in aerodynamic loading ($\square H/2U^2$) and in mechanical loading (AN^2) for a common flow path design. In practice, it was not possible to meet aerodynamic and mechanical requirements by using common flow paths for both applications. The final flow path selection (Figure 2.2.1-3) maintains commonality between the key rotor and steam delivery features, even though the flow paths deviate somewhat in the aft stages. The 7H, due to its higher speed, has lower aerodynamic loading, but higher mechanical stresses.

Mean line optimization

The work per stage, stage reaction levels, and airfoil counts were optimized using GE Aircraft Engines conceptual design software that includes a mean line efficiency prediction code, a prediction tool for gas temperature profiles, and routines for predicting required cooling flows. The conventional aerodynamic design system had to be modified to incorporate the effect of steam cooling. An optimization script was wrapped around this system of conceptual aerodynamic prediction codes and a target function, which was a combination of maximizing turbine efficiency and minimizing required cooling flows. Resulting stage loadings are presented in the Smith diagram (Figure 2.2.1-4).

Airfoil design

The detailed airfoil design was developed by an integrated design team focused on meeting key requirements for aerodynamic performance, heat transfer, aeromechanics and producibility. The hot airfoil shape was defined on stream surfaces of revolution, and were initially analyzed using S1-S2 analysis codes. The axi-symmetric analysis included modeling of cooling, leakage and purge flows and had a radial mixing model for the temperature profile. Radial equilibrium included effects of airfoil lean and blockage. GE Aircraft Engine geometry generation tools for rapid parametric generation of internal airfoil geometry were utilized such that full 3D

aerodynamic, heat transfer and mechanical analysis could quickly be generated on any candidate airfoil. Advanced 3D CFD models were used to parametrically investigate profile shapes and airfoil stack. Three dimensional aerodynamic design features, as pioneered by GE Aircraft Engines, were implemented throughout the turbine, but are most pronounced for the first stage, for which the aerodynamic loading is the highest and the airfoil aspect ratios are the lowest. Blade airfoil castings are shown in Figure 2.2.1-5.

Stage 1

Stage 1 nozzle steam cooling requirements limit the maximum external heat transfer coefficient allowed on the airfoil suction surface. A study was done on varying nozzle solidity, as one parameter to control external heat transfer coefficient. As the solidity is reduced, the increased airfoil loading will drive up the heat transfer coefficients beyond what can easily be accommodated using a steam cooling concept (Figure 2.2.1-6). The resulting solidity is somewhat higher than it would be, had it been optimized for performance, but the loss in performance due to high solidity is negligible. Both the nozzle and blade airfoil shapes were optimized using 3D CFD tools to maximize turbine efficiency. The 3D aerodynamic design of stage 1 improves the stage efficiency by 1 point relative to a conventional design, and the radial temperature migration in the blade passage is reduced, resulting in a lower heat load on blade platforms and shrouds.

Stage 2

Due to modest aerodynamic stage loading, very small performance improvement potential for 3D aerodynamics was predicted for this stage. Hence, the stage 2 airfoil shapes were maintained relatively linear for producibility and simplicity. Both stages 1 and 2 blades are unshrouded, and steam cooled. Conventional air cooled blades typically feature a squealer tip that contributes to reducing overtip leakage flow, and therefore has a positive impact on the performance. For the steam cooled blades, however, the squealer tip design was abandoned for durability reasons, and the sensitivity of tip clearance on turbine efficiency can therefore be expected to be somewhat larger than is the case for a conventional air cooled design. This has been addressed by adopting an active clearance control system for the first two stages.

Stage 3

Stage 3 and 4 airfoils have higher aspect ratios than the first two stages, and profile loss becomes a relatively more important driver on stage efficiency than secondary loss. The 3D optimizations were therefore focused on minimizing profile loss by utilizing nozzle compound lean and airfoil vortexing to locally avoid excessive Mach number levels, and also to avoid very low hub reaction. Mechanical requirements on the stage 3 blade, inherent from using STEM drilled cooling holes, required close to linear leading and trailing edges in order to effectively cool these edges. High rim stresses on these airfoils required consideration to the tip shroud design, such that the tip shroud effectively seals the leakage over the tip but does not introduce unnecessary weight and stresses in the airfoil.

Stage 4

The last stage is uncooled, and is characterized by high mechanical rim load, as indicated by high values of the A*N^2 parameter (annulus area * rpm^2). The high airfoil and disk stresses were controlled by minimizing the blade height while still maintaining sufficiently low turbine exit Mach number in order to provide good aerodynamic performance, and sufficient flow growth capability. Nevertheless, high axial Mach number was a key aerodynamic consideration for the blade design. Highly stressed airfoils typically result in airfoils with thick hub sections to relieve the root stress. At high axial Mach number, the hub blockage can introduce significant loss. For the aerodynamic design of the fourth stage, nozzle lean and a controlled vortex design were used to balance the radial aerodynamic loading distribution such that the tip chord could be minimized. Less weight in the tip of the airfoil reduces the pull stress, and reduces the requirement for an exceedingly thick hub section.

3D aerodynamic analysis for heat transfer design

After calibration against available prototype test data, a methodology of stacking single blade row CFD solutions was devised that calibrates well against available measured temperature profiles. The prediction for each blade row utilizes inlet boundary conditions from the mass averaged solution of the upstream blade row and scaled to the 1D mass average of the axi-symmetric model at the corresponding plane. The exit condition is simply taken from the axi-symmetric model. Cooling and leakage flows are modeled by means of source terms in the mass, momentum and energy equations. This has shown to accurately model cooling flow impact on aerodynamic performance, flow angle deviation and radial temperature migration. An example of radial temperature migration on the 7H stage 1 blade pressure and suction surfaces is presented in Figure 2.2.1-7. Gas temperatures for heat transfer boundary conditions were taken directly from the 3D analysis.

Generation of turbine stage characteristics for cycle modeling

Off-design turbine stage performance maps were developed for implementation into the overall gas turbine cycle deck to predict gas turbine performance at varying load and ambient temperature conditions. The turbine maps were also utilized for transient cycle modeling, which was needed for properly assessing component life and transient clearances in the gas turbine. The methodology for predicting these turbine characteristics is based on a 1D off-design turbine map prediction code developed by GE Aircraft Engines, but modified for the specific needs of GE Power Systems. The software generates a map of stage total-to-static efficiency and flow coefficient versus stage total-to-static pressure ratio and velocity ratio parameter. The off-design loss models have been verified against a number of turbine rigs, but also directly against GE Power Systems field test data. An example of 7H stage 1 characteristic is displayed in Figure 2.2.1-8.

Summary/Conclusions

Two four stage steam cooled turbines were designed as part of the H machine program, incorporating closed lop steam cooling in the first two stages. Traditionally, GE's 50 Hz machines are 1.2 geometric scales of the 60 Hz machines. Most, but not all, key aerodynamic and mechanical characteristics will scale, and the additional development work needed to execute a scaled design is relatively small compared with the design effort needed for two independent design efforts. The approach taken on the H-technology machines, however, was different from this traditional approach. In order to minimize manufacturing and assembly complexity on the rotor and steam supply system, the maximum level of direct geometric commonality between the 7H and 9H was sought.

The work per stage, stage reaction levels, and airfoil counts were optimized using GE Aircraft Engines conceptual design software that includes a mean line efficiency prediction code, a prediction tool for gas temperature profiles, and routines for predicting required cooling flows.

GE Aircraft Engine geometry generation tools for rapid parametric generation of internal airfoil geometry were utilized such that full 3D aerodynamic, heat transfer and mechanical analysis could quickly be generated on any candidate airfoil. Advanced 3D CFD models were used to parametrically investigate profile shapes and airfoil stack.

Off-design turbine stage performance maps were developed for implementation into the overall gas turbine cycle deck to predict gas turbine performance at varying load and ambient temperature conditions. The turbine maps were also utilized for transient cycle modeling, which was needed for properly assessing component life and transient clearances in the gas turbine.

Technology Application

Advanced 3D aerodynamic technology has been applied to the design of the 7H and 9H turbines to maximize performance and meet mechanical design objectives required by steam cooling technology.

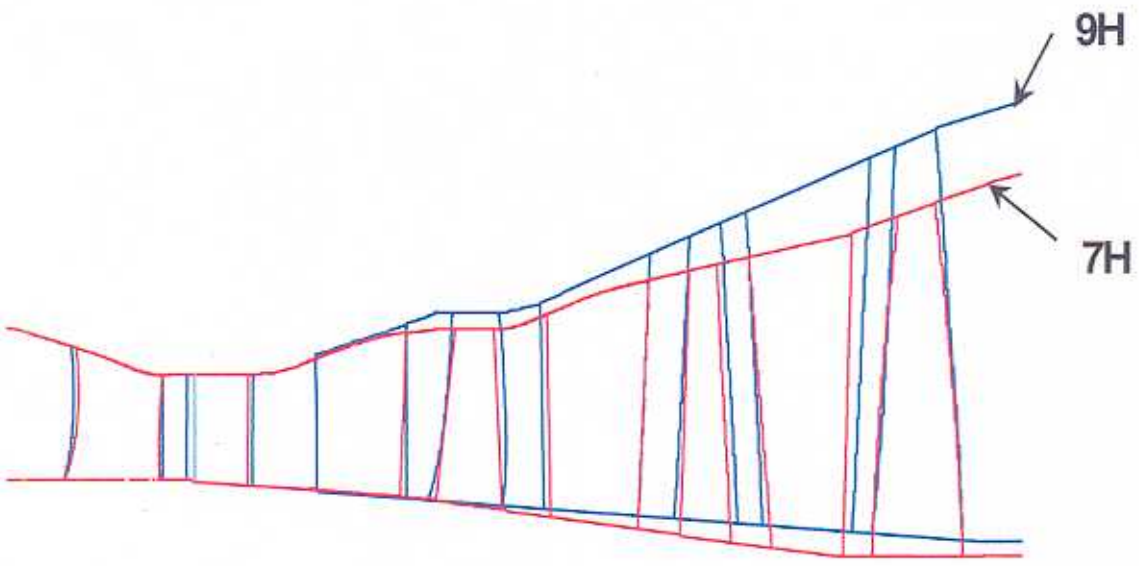

Fig 2.2.1-3. Comparison of 7H and 9H flow paths

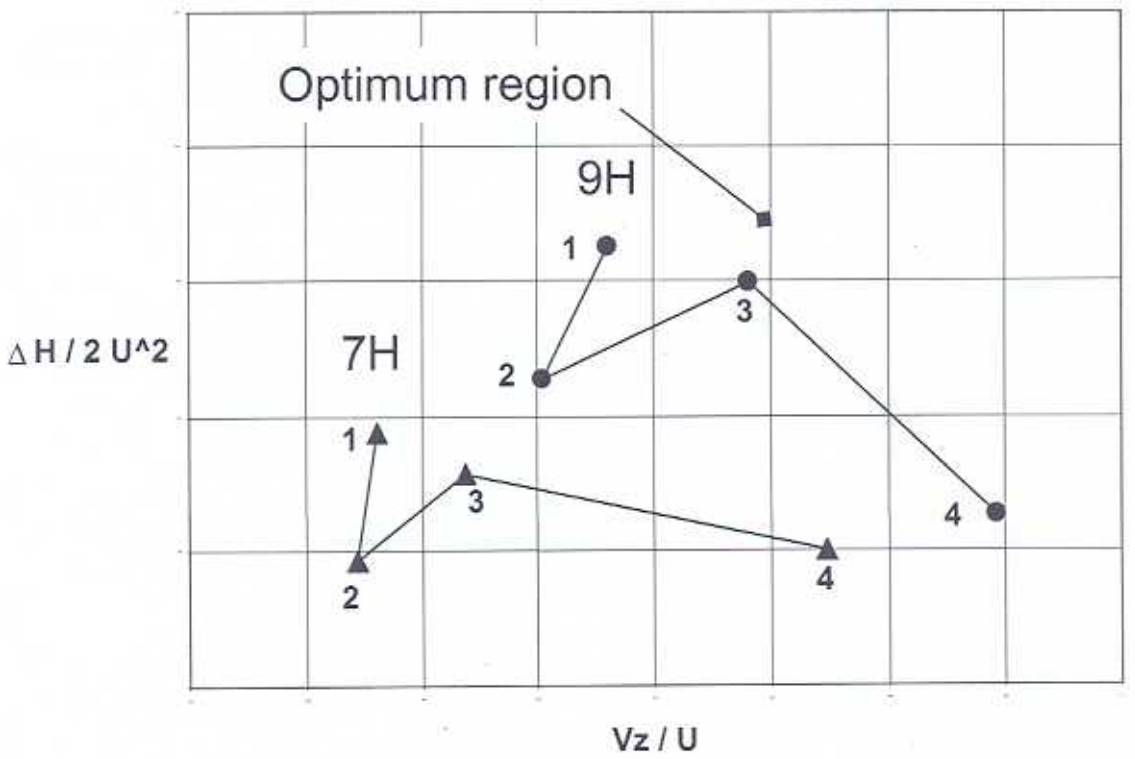

Fig 2.2.1-4. Smith diagram

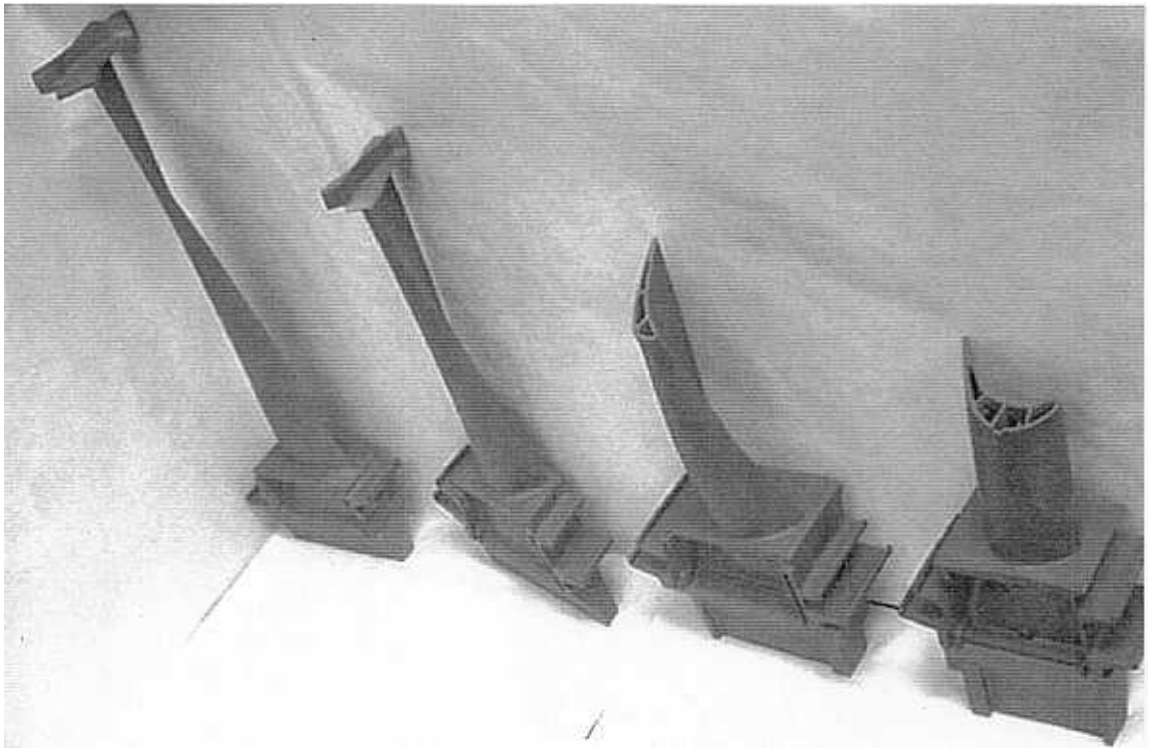

Fig 2.2.1-5. 7H blade airfoil castings

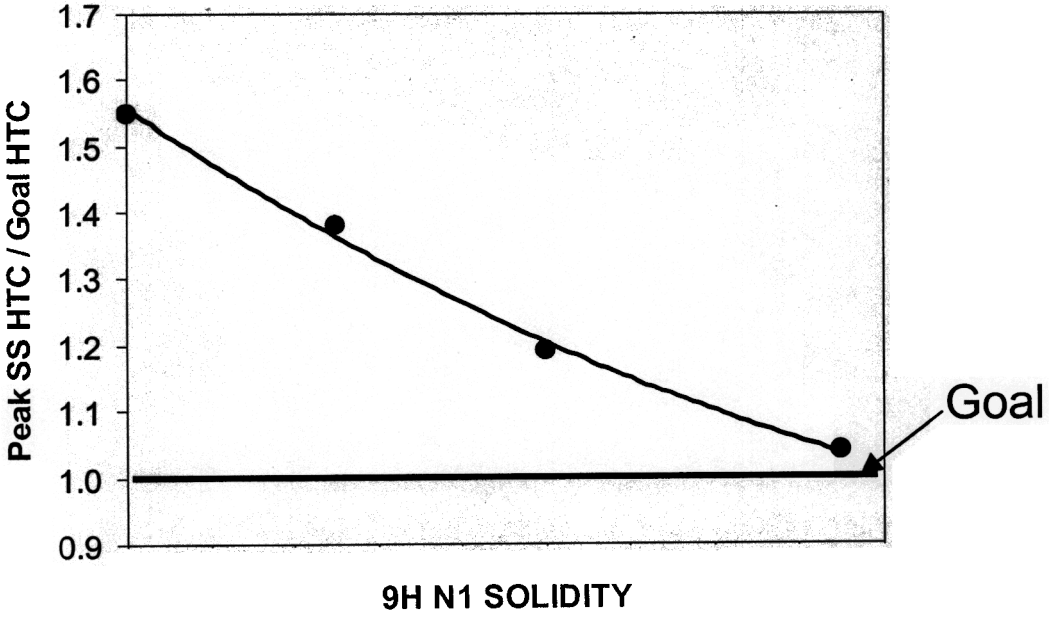

Figure 2.2.1-6. 9H stage 1 nozzle heat transfer coefficient study

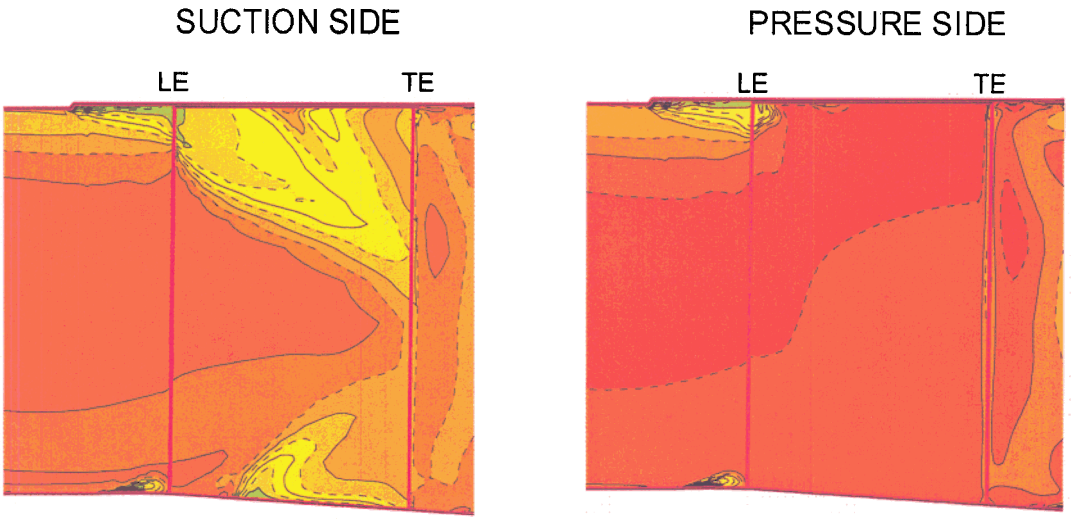

Figure 2.2.1-7. 7H Stage 1 Blade Contours Showing Radial Gas Temperature

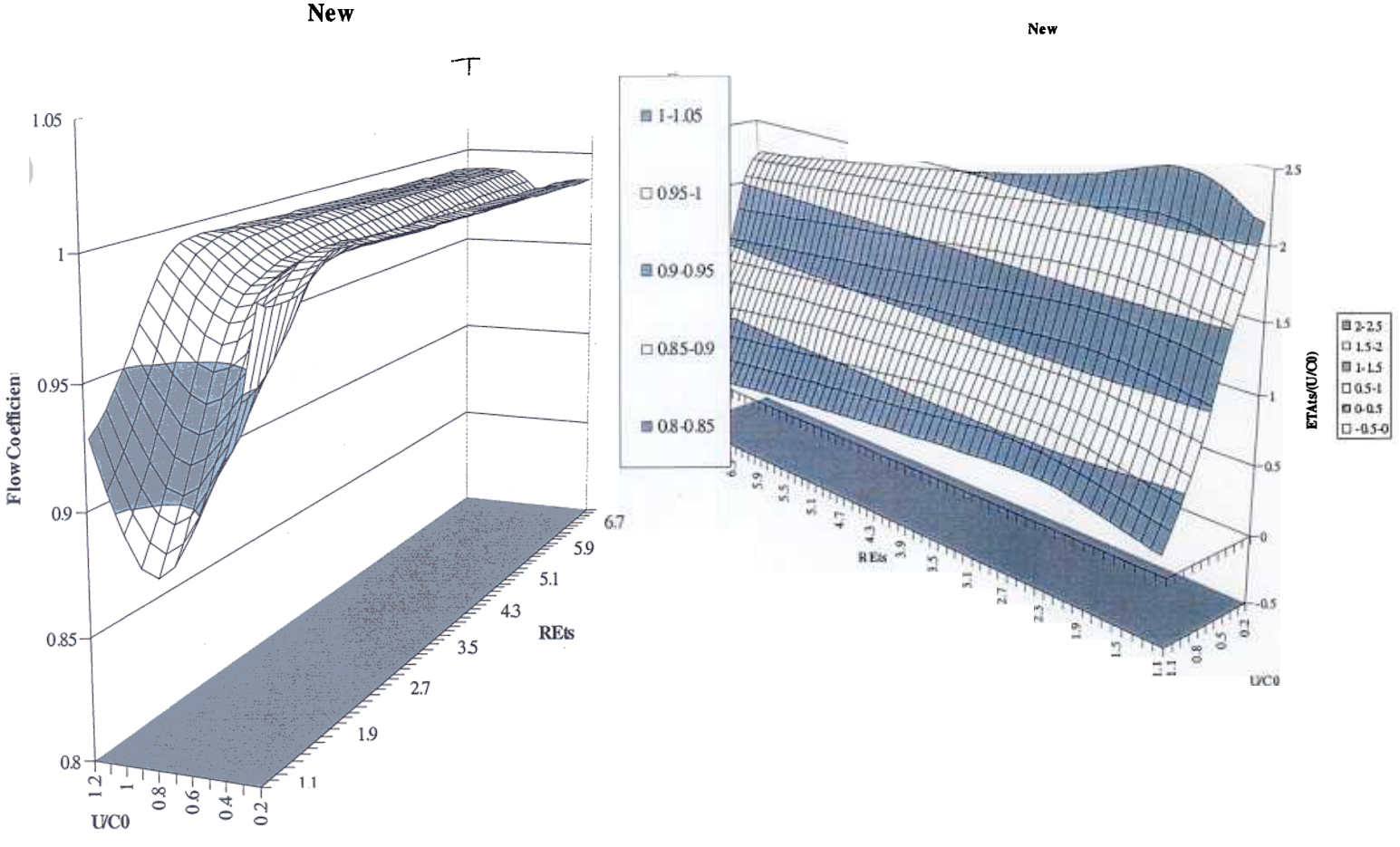

Figure 2.2.1-8. 7H Stage 1 Turbine Characteristic

Section 2.2.2 (GTFF) Gas Turbine Flange to Flange Design [S,C,A]

Section 2.2.2.1 (GTFFCP) Compressor Design [S,A]

Objective

The objective of this task was to design 7H and 9H compressor rotor and stator structures with the goal of achieving high efficiency at lower cost and greater durability by using proven GE Power Generation heavy-duty use design practices. The designs were based on the GEAE CF6-80C2 compressor. Transient and steady state thermomechanical stress analyses were run to ensure compliance with GEPG life standards. Drawings were prepared for forgings, castings, machining, and instrumentation for full speed, no load (FSNL) tests of the first unit on both 9H and 7H applications.

Compressor rig tests will be performed at the GEAE-Lynn, MA test facility to verify the base 18 stage compressor design, the 9H compressor including tri-passage diffuser and rotor cooling proof of concept, and the 7H compressor with the redesigned "0" stage.

Introduction

The ATS gas turbine design required many new developments in compressor technologies beyond current GE Power Generation gas turbines (See Figure 2.2.2.1 - 1: 7H Compressor New Technologies). These new technologies include: 1) new aerodynamic design for the front and aft sections of the compressor, 2) low radius ratio front stages blade designs, 3) low aspect ratio exit vane design, 4) multiple stage forward spool shaft design, 5) high rabbet rotor design, 6) 7H single through bolt rotor construction, 7) multiple passage rotor air cooling system, 8) multiple stage variable guide vane (VGV) system, 9) new blade axial retention design, 10) trenched casing flowpath design, 11) 3-passage diffuser design, and 12) 9H compressor discharge case (CDC) double wall clearance control casing.

The development procedures of these technologies included seven tollgate phases, namely: 1) product option identification, 2) requirement and resources, 3) conceptual design, 4) preliminary design, 5) detail design, 6) production and design validation, and post shipment test and monitoring. During each phase, numerous design reviews and tollgate reviews have been held to ensure all design intents have been met.

In parallel with the compressor development, three compressor rigs were designed to verify the ATS compressor concept, and were discussed in Section 2.2.1 During the rig testing, aerodynamic performance, efficiency, and aeromechanics data were collected and analyzed. All lessons learned from the test have been incorporated in the full size production design.

The product validation, including 9H FSNL and FSFL pre-shipment , and 7H FSNL testing have been completed. The post test reviews, as well as tear down inspections, have been performed. The results indicated that the ATS compressor has met all design intents. All lessons learned from the FSNL tests will be incorporated into the FSFL design and testing.

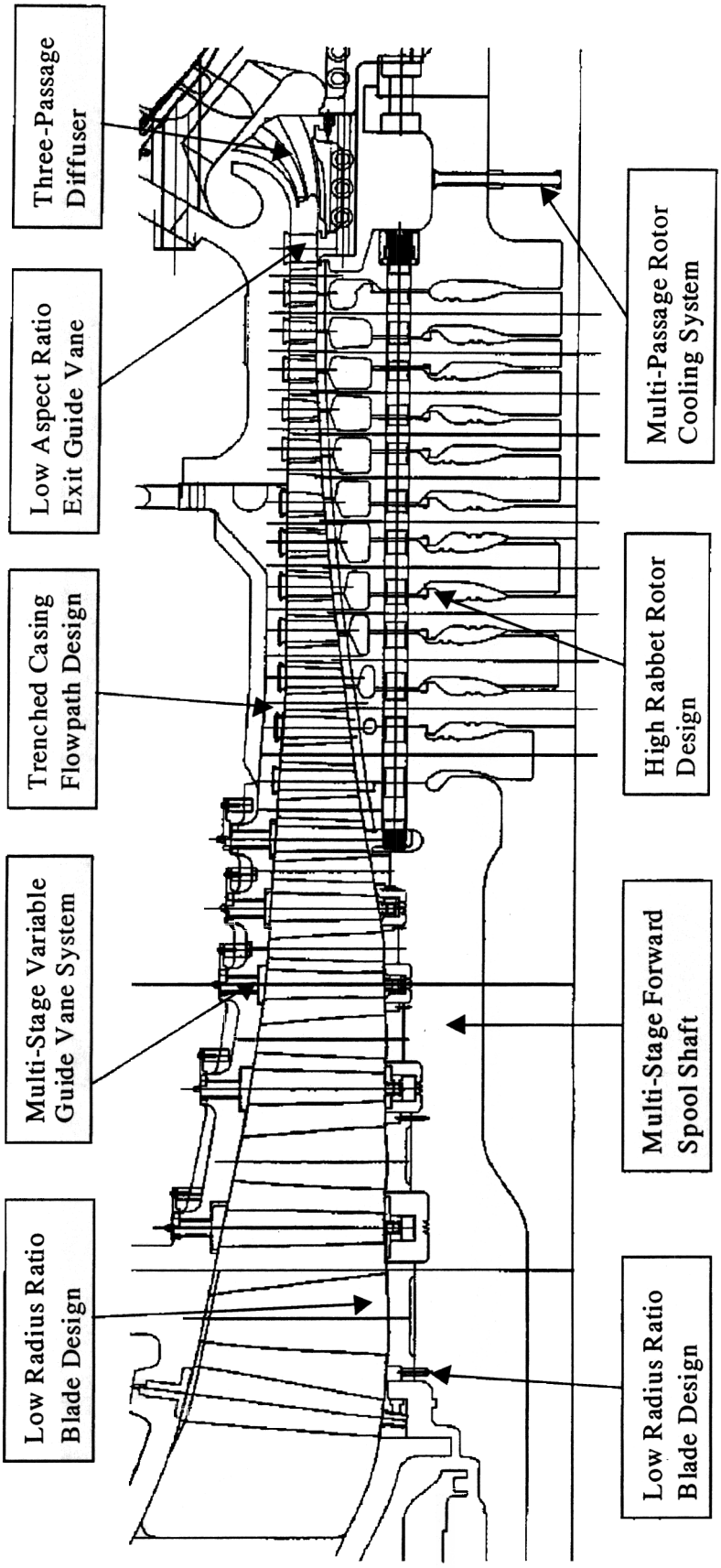

Figure 2.2.2.1 - 1: 7H Compressor New Technologies

Discussion

Compressor Flowpath and Blade Design

The H compressor was designed based on the GEAE CF6-80C2 aircraft engine. However, an aerodynamic redesign of the front and aft sections of the compressor was necessary to increase the flow rate.

The 7H compressor flowpath incorporates lessons learned from GEAE CF6-80C2 engine, the 9H compressor rig, and 9H FSNL testing. By adding a stage "0" in the front end of the compressor, the flowpath has been enlarged to allow more flow rate in meeting the 7H power generation requirement. The blade axial spacing was also increased to improve their aeromechanical behavior.

The redesigned stages include the IGV, and stages 1, 2, 3, 14, 15 16 and 17 blades and vanes. The detail airfoil stress analysis, including vibratory and static finite element analysis for all blades has been carried out. The final machining drawings were issued for every blade and vane by 1Q99.

The blade supplier was down-selected based on a combination of technical ability, cost, and schedule commitment. The manufacturing processes for rotor blades and stator vanes were reviewed and finalized. All forging materials were purchased. The manufacturing of all blades and vanes was completed, and they were delivered to GE for assembly by 3Q99.

The test results from the compressor rig and FSNL testing showed no aeromechanics problems during startup, steady state operation, or during shut down. All design goals have been met.

Compressor Rotor Design

The 7H compressor rotor has incorporated many first-of-a-kind design features. These features include: 1) multiple stage forward spool shaft design, 2) high rabbet rotor design, 3) 7H single through bolt rotor construction, and 4) multiple passage rotor forced air cooling system.

The compressor rotor design analysis, including two dimensional heat transfer and stress analyses, low cycle fatigue, high cycle fatigue, fracture mechanics, creep, burst, rotor dynamics, bolt sizing, rotor structure and rabbet integrity, blade retention, and dovetail slot sizing, was conducted to support the release of forging and machining drawings. All forging drawings and final machining drawings for each stub shaft and wheel were issued by 2Q99.

Rotor suppliers were down-selected based on a combination of technical ability, cost, and schedule commitment. The manufacturing processes for each spool shaft and wheel were reviewed and finalized. All forging materials were purchased. The manufacturing of all rotor hardware was completed delivered to GE for assembly by 3Q99.

The test results from rig and FSNL testing showed that the H compressor rotor design, both the rotor hardware and the multiple passage air cooling system, has met all the design intents.

Compressor Structure Design

The H compressor structure includes the inlet casing and number 1 bearing, compressor mid casing, and the compressor discharge casing and inner barrel. The 7H compressor flowpath design was frozen so that layouts of the inlet, mid-compressor, compressor discharge casings, and the tri-passage diffuser could be completed.

Electronic data releases (EDR's) fully describing the casing castings as 3D electronic solid models were conveyed to the selected suppliers, who were down-selected based on a combination of technical ability, cost, and schedule commitment. Design analysis was completed for each casing, including blade containment, thermal transients, low cycle fatigue (LCF), creep, applied loads (normal and emergency shipping), internal cooling flows, weld life, normal modes, and bolt/flange sizing.

In order to enhance the producibility of the compressor discharge casing (CDC), a single wall casing was used for 7H design. Based on data analysis from the 9H test program, the rotor cooling flow passage was simplified to minimize the pressure loss. This new design concept was validated upon review of the 7H FSNL test results.

Detailed machining drawings defining all the required features for the 7H FSNL compressor casing were issued. These included all the drawings for the inlet, compressor case, VGV system, CDC, tri-passage diffuser, and CDC inner barrel. All machining operations were completed at the suppliers. Modified machining drawings for prototype test instrumentation were issued for all components, and instrumentation provisions were incorporated into the machining operations.

A detailed, internal design review was conducted to determine that the designs conformed to accepted GE Design Practices. The review showed that the designs met all the design goals and requirements. Detailed lifing analysis was also completed. Action items from these reviews were incorporated into the casing drawings without schedule impact.

In addition, detailed rotor/stator clearance analysis, including the effects of 3D geometry variation, enclosure temperature variation, stator tube 1G sag, hard stalls, and thermal transients was completed, and minimum clearances required to prevent unacceptable rubbing were established.

All hardware passed the GE quality review for First Piece Qualification (FPQ). In particular, the diffuser dimensional control and material quality were excellent. This represented a significant improvement in producibility from the original 9H concept. All hardware was shipped to Greenville for assembly. Unit assembly drawings, including the

stator arrangement, clearance drawing, unit bolting and doweling, unit jacking and alignment, were initiated and assembly operations were completed during 3Q99.

Multiple Stage VSV System

In addition to the variable inlet guide vane (IGV) used on prior GE gas turbines to modulate airflow, the H machine compressors employ multiple rows of Variable Stator Vanes (VSV) in order to improve the compressor aerodynamic performance and airfoil aeromechanics behavior. There are six variable vane rows, (IGV, and VSV 0 to VSV 4), in the 7H VSV system.

Kinematics studies were performed for each VSV to determine the VSV schedule and to evaluate the VSV angle sensitivity to part tolerance. The results showed that the current manufacturing tolerances meet the desired system sensitivity requirements.

Rig tests were conducted to evaluate the proposed VSV schedule. In addition, numerous tests were performed in achieving an "optimized" VSV schedule. The 7H FSNL test results confirmed the rig test findings. All airfoil stresses were below the design limits. No rotating stall was observed during the test.

Compressor Rig Tests

Three compressor rigs were designed, built, and tested to verify the ATS compressor concept. The first one (Advanced Machine Compressor, AMC001), validated the use of an aircraft design with variable vanes and additional stages in a power generation application. The second one (AMC002) validated the 9H compressor design. The third one (AMC003) was the 7H ATS design validation vehicle. Details are discussed in Section 2.2.1. The cross section of AMC003 is shown in Figure 2.2.2.1 – 2.

The rig design used the same vigorous design procedure as the production design. The compressor design analyses included blade vibratory and static analyses, blade containment, thermal transient, two dimensional heat transfer and stress analyses, low cycle fatigue, high cycle fatigue, fracture mechanics, creep, burst, rotor dynamics, rotor structure and rabbet integrity. Design reviews were held to ensure all design integrity and intents were met.

All AMC003 final drawings, including all blades and vanes, disks, and casings, were issued. The suppliers were down-selected and the manufacturing of all parts was completed by 1Q99. The AMC003 rig assembly was started in 1Q99, and completed in mid 2Q99.

The AMC003 test began in late 2Q99, and was completed in mid 3Q99. Six test phases, including mechanical checkout, initial performance assessment, VSV optimization, part speed operability, power turndown mapping, and high speed surge mapping, were successfully completed. The test results indicated that the 7H compressor design has met all design goals in the compressor performance, efficiency and airfoil aeromechanics behaviors.

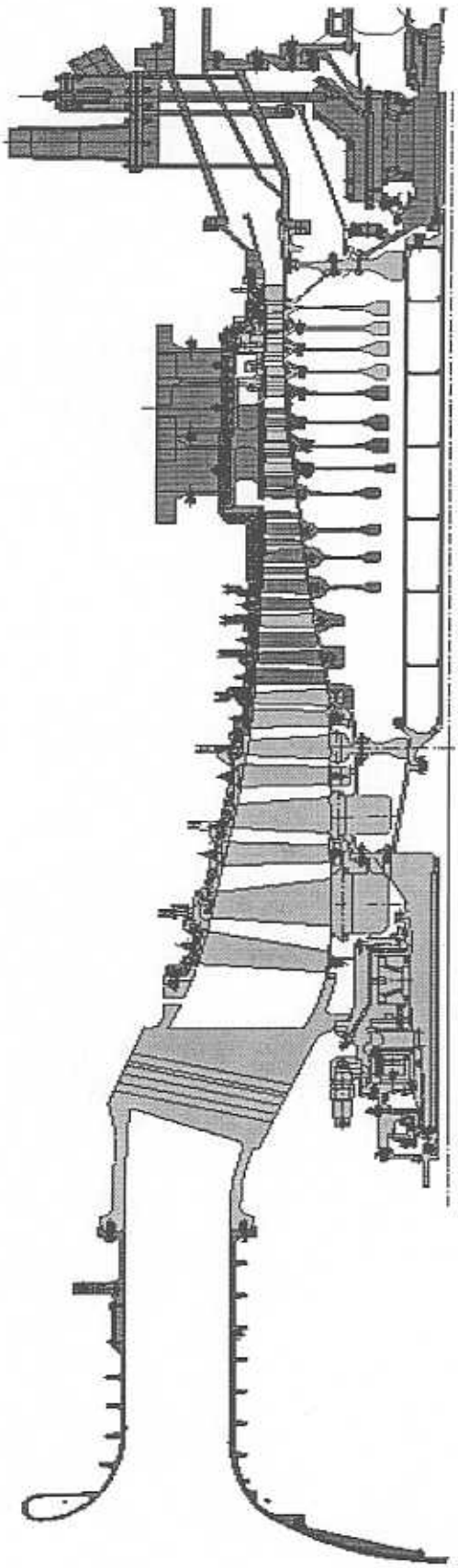

Figure 2.2.2.1 - 2 AMC Rig #3 for 7H Compressor Design Evaluation

Production Compressor Validation Tests and Teardown Inspections

Production validation testing includes FSNL and FSFL pre-shipment tests. To date, one 9H FSNL test, one 9H FSFL pre-shipment test, and one 7H FSNL test have been successfully completed. The 7H ATS FSNL test was conducted in 1Q00. Five test runs were conducted during the FSNL test, and all aeromechanics goals were achieved.

Optimized startup and shut down procedures as well as optimized VSV schedules were obtained during the FSNL test program. The test results showed that the rotor and stator instrumented blade responses were low, and were consistent with the AMC003 rig test results. All were within the design limits.

The data reduction from the light probes also showed that there were no blade instability or stripe mode problems encountered during the test, which ranged from zero to 105% of the design speed.

The other components in the compressor structure, including the VSV system, inlet casing, compressor casing, and number 1 bearing, have demonstrated the design integrity and performances meeting the design intents. In summary, the entire compressor design was successfully demonstrated during the FSNL test.

A teardown inspection was performed after the 7H FSNL test. The inspected compressor parts included all blades and vanes, inlet casing, compressor casing, compressor discharge casing, number 1 bearings, all VSV assemblies, and entire rotor shafts and wheels. The results indicated all parts met their design intents except for some tip rubs in the front stage blades, and some wear marks in the S17 slot that were observed during the teardown.

In order to avoid the tip rubs, the tip configurations of all front stages from R0 to R3 have been redesigned. The affected blades were reworked during 3Q00, and be evaluated during the 7H FSFL pre-shipment test.

The wear marks in the S17 slot were caused by the rigid body motion of S17 vanes. A new segment S17 design was introduced to address this issue. The affected vanes were reworked into segmented assemblies during 3Q00, and be evaluated during the 7H FSFL pre-shipment test

Summary/Conclusion

The ATS compressor design included two compressors, namely 9H and 7H.compressors. Both have undertaken very vigorous design tollgate procedures and design reviews to ensure that all design integrity and design intents were met. The ATS compressor design also called for many new developments in compressor technologies beyond current Power Generation gas turbine practice. The successful implications of these state-of-art

design technologies have distinguished the H compressors from current technology gas turbine compressors.

The successful validation test program, which included three rig tests, the 9H FSNL test, 9H FSFL pre-shipment test, and the 7H FSNL test, demonstrated that the ATS compressor development has achieved all design goals.

Technology Application

The compressor design (aerodynamic and mechanical) and rig test results establish the basis for the 7H and 9H compressor production hardware.

Section 2.2.2.2 (GTFFCB) Combustor Design [S,C,A]

Objective

The objective of this task is to design a combustor based on the commercial DLN2.6 combustion system, with modifications made for improved use of available air and reduced cooling. This design will be similar for both the 7H and 9H machines. It will be configured to ensure the ability to use preheated fuel. Rig testing of full-scale and scaled components will be conducted at 7H and 9H cycle conditions. The final configuration will be validated in single-combustor, full-scale tests under full operating conditions.

The premixer-burner design will be optimized to use minimum pressure drop, achieve required fuel/air mixing, maintain stable flame, and resist flashback. The basic design will be developed and evaluated in full-scale, single-burner tests and then implemented in full-scale combustors. The ability to meet high cycle fatigue (HCF) life goals depends on understanding the effects and interrelationships of all combustion parameters. Existing dynamics models used in parallel with laboratory-scale and full-scale testing will be used to predict combustor dynamic behavior.

Chamber arrangement, casings, cap and liner assemblies, flame detectors, and spark plugs will be designed and analyzed to ensure adequate cooling, mechanical life, and aerodynamic performance. Fuel nozzles will be designed for operation on gas alone or on gas with distillate as a backup fuel. The transition piece will be designed and integrated with the design of the machine mid-section, transition duct cooling, and mounting.

A full-scale, single-combustor test stand will be designed and fabricated to verify performance of the combustion system. Facility modifications will be made to support the test. These include installation of the test stand, installation of high-temperature stainless steel air piping, an additional air heater, control systems, upgrades to the combustion video system, and tooling.

Background/Introduction

The *H System™* can-annular combustion system is a lean pre-mix DLN-2.5H system similar to GE Dry Low NOx (DLN) combustion systems in FA-class service today. Fourteen combustion chambers are used on the MS9001H and twelve combustion chambers on the MS7001H. DLN combustion systems have demonstrated the ability to achieve low NO_X levels in field service and are capable of meeting the firing temperature requirements of the H gas turbine while obtaining single-digit NO_X and CO emissions.

Figure 2.2.2.2-1 shows a full length cross section of the combustion system. The technical approach features a tri-passage radial prediffuser which optimizes the airflow pressure distribution around the combustion chambers, a GTD222 transition piece with an advanced integral aft frame mounting arrangement, and impingement sleeve cooling of the transition piece. The transition piece seals are the advanced cloth variety for minimum leakage and maximum wear. The flowsleeve incorporates impingement holes for liner aft cooling. The liner cooling is of the turbolator type so that all available air can be allocated to the reaction zone to reduce NOx. Advanced *2-Cool™* composite wall convective cooling is utilized at the aft end of the liner. An effusion cooled cap is utilized at the forward end of the combustion chamber.

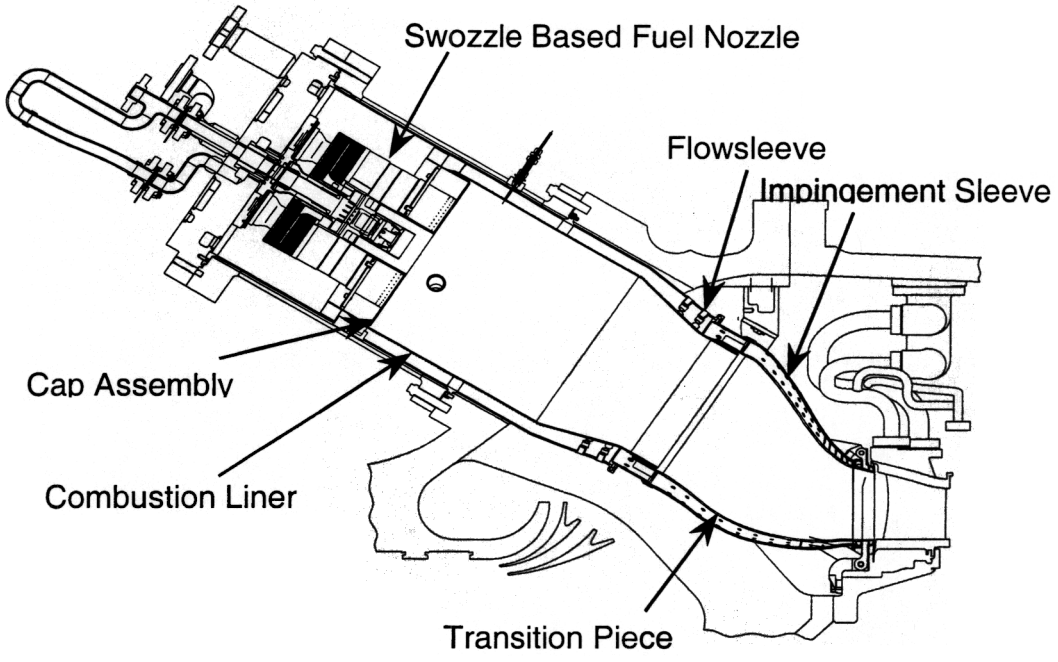

Figure 2.2.2.2-1. H Combustion System Cross Section

The *H System™* fuel injector is shown in Figure 2.2.2.2-2. Based on the *swozzle* concept [the name *swozzle* is derived by joining the words *swirler* and *nozzle*], the premixing passage utilizes swirl vanes to impart swirl to the admitted airflow. These same swirl vanes each also carry two passages for injecting fuel into the premixer airflow. Thus, the premixer is very aerodynamic and highly resistant to flashback and flameholding. The outer wall of the premixer downstream of the swozzle vanes is integral to the fuel injector for added flameholding resistance. In addition, in the center of each fuel injector, an air curtain swirl cup is provided for diffusion flame starting and low load operation.

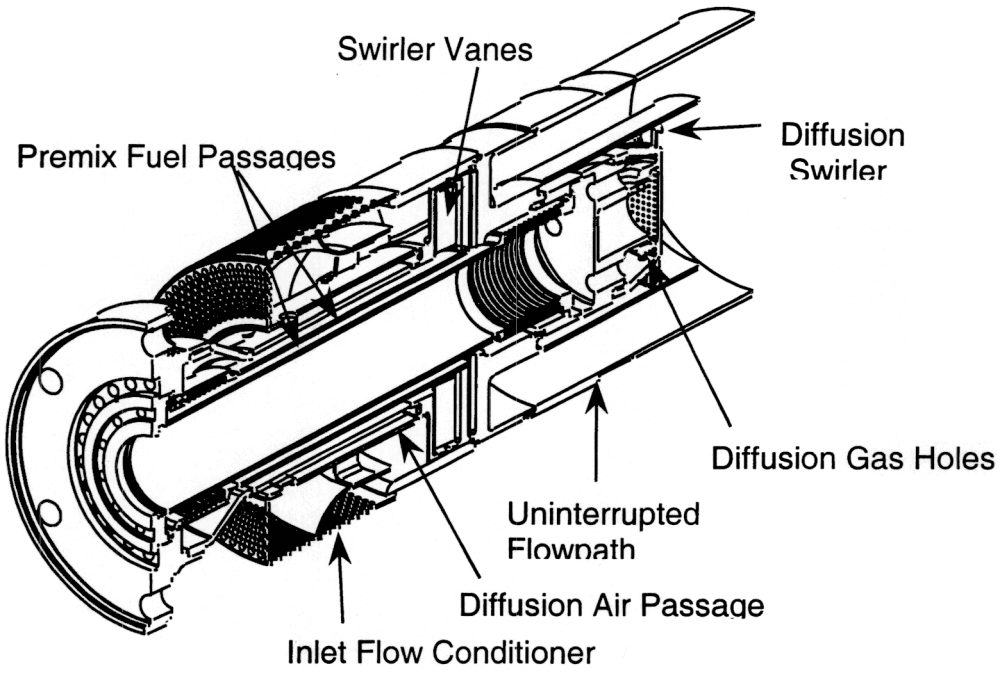

Figure 2.2.2.2-2. H Swozzle Fuel Injector

The *H System™* combustor uses a simplified combustion mode staging scheme to achieve low emissions over the premixed load range while providing flexible and robust operation at other gas turbine loads. Figure 2.2.2.2-3 shows a diagram of this staging strategy. The most significant attribute is that there are only three combustion modes: diffusion, piloted premix, and full premix mode. These modes are supported by the presence of four fuel circuits: outer nozzle premixed fuel (P4), center nozzle premixed fuel (P1), burner quaternary premixed fuel (BQ), and diffusion fuel (D4). The gas turbine is started on D4, accelerated to Full Speed No Load (FSNL), and loaded further. At approximately 20-35% gas turbine load, two premixed fuel streams P1, and P4, are activated in the transfer into Piloted Premix. After loading the gas turbine to approximately 40-50% load, transfer to full premix mode is made, and all D4 fuel flow is terminated while BQ fuel flow is activated. This very simplified staging strategy has major advantages for smooth unit operability and robustness.

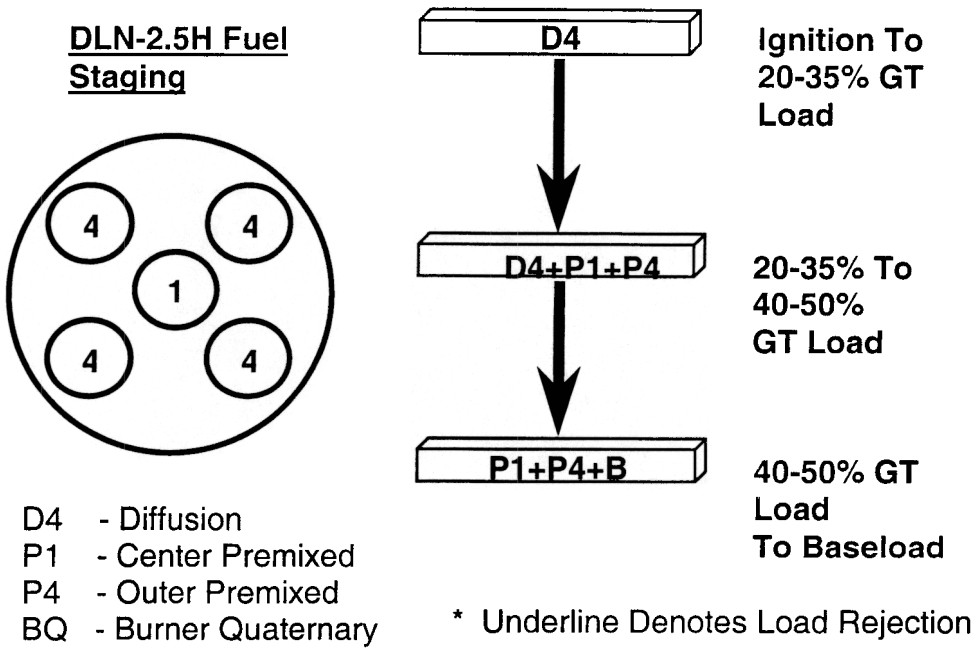

Figure 2.2.2.2-3. DLN-2.5 Fuel Staging

The *H System™* combustor was developed in an extensive test series to ensure low emissions, quiet combustion dynamics, ample flashback/flameholding resistance, and rigorously assessed component lifing supported by a complete set of thermal data. In excess of thirty full pressure, temperature, and airflow tests were run at the combustion test facility at GEAE in Evendale, Ohio, shown in Figure 2.2.2.2-4.

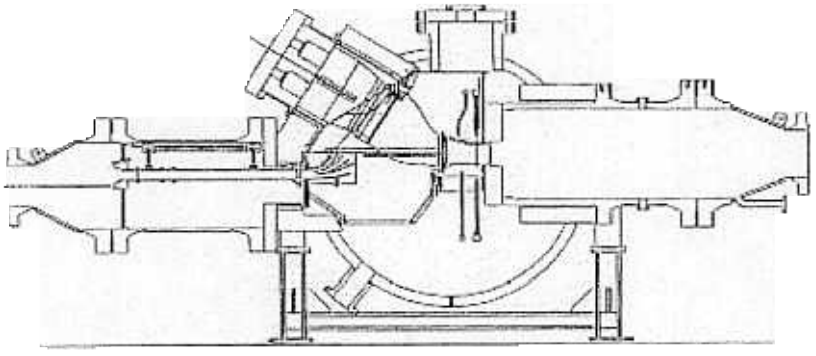

Figure 2.2.2.2-4. Combustor Development Rig Cross Section

Figure 2.2.2.2-5 shows typical NOx base load emissions as a function of combustor exit temperature and Figure 2.2.2.2-6 shows the comparable combustion dynamics data. In addition, hydrogen torch ignition testing was performed on the fuel injector premixing passages. In all cases the fuel injectors exhibited well in excess of 30 ft/s flameholding margin after the hydrogen torch was de-activated. In addition, lifing studies have shown expected combustion system component life goals will be met with margin.

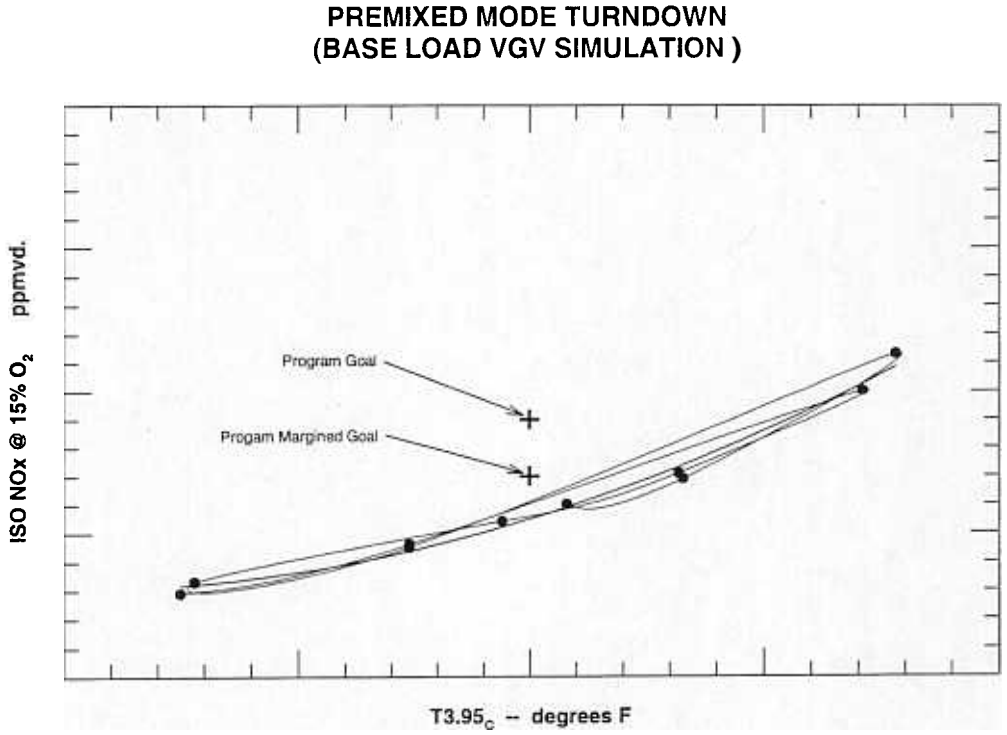

Figure 2.2.2.2-5. Typical NOx Base Load Emissions Data

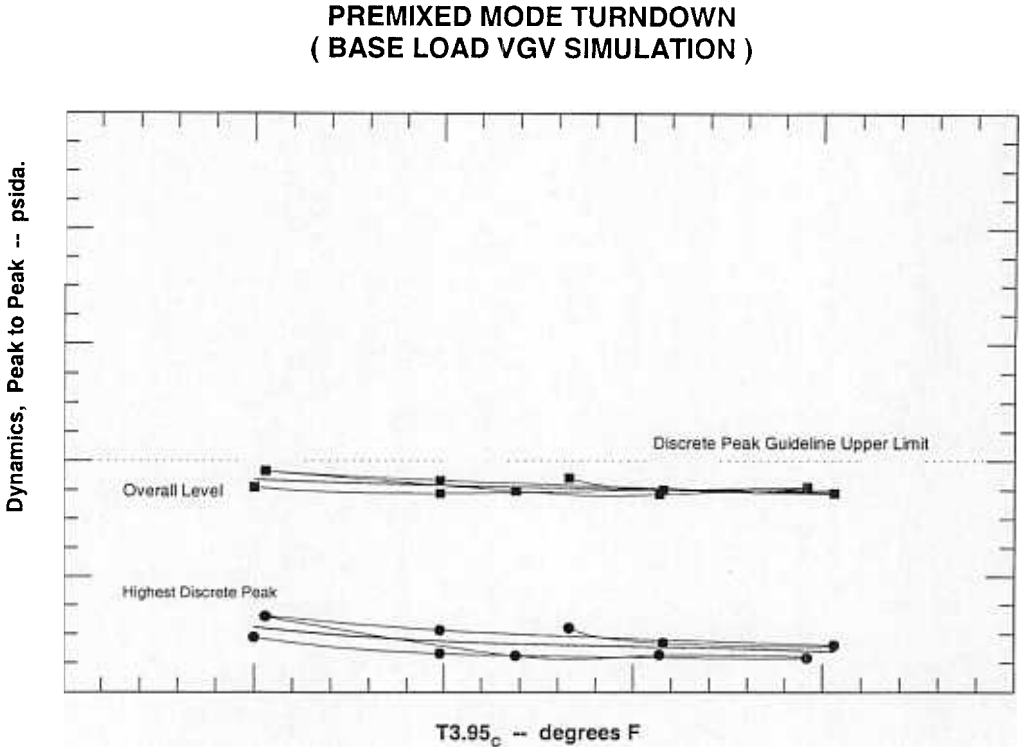

Figure 2.2.2.2-6. Typical Combustion Dynamics Data

Summary/Conclusion

A combustion system was developed that met the ATS single digit NOx emission goal with no post-combustion cleanup. The can-annular system is a lean premix design, utilizing five fuel injectors per combustor can in a staged ignition sequence. This simplified staging has demonstrated major advantages for smooth unit operability and robustness.

A full scale rig (full pressure, temperature, flow) was constructed at the GE Aircraft Engines facility in Evendale, OH, and over thirty development tests were run. The resulting combustor development demonstrated single digit NOx and low combustor dynamics, along with ample flashback/flameholding resistance, and component life assessments.

Technology Application

Design and development of the combustion system is required for the ATS gas turbine to meet the low emissions targets at the high cycle conditions of inlet temperature, pressure, air flow, and outlet temperature, all of which are greater than those of any of GE's developed products.

Section 2.2.2.3 (GTFFTR) Turbine Rotor Design [S]

Objective

The objective of this task was the design of turbine rotor components (wheels, spacers, aft shaft, transition discs, coolant systems, and fastening devices). Transient and steady-state stress analyses were used to calculate parts lives. Rotor and system vibratory characteristics were evaluated. The coolant flow circuit for routing the cooling steam to and from buckets was designed, and its performance calculated. Test results were incorporated concurrently. Drawings and specifications were developed in preparation for manufacturing.

A modified 7F turbine rotor was fitted with production steam delivery hardware, and run to simulate full-scale 7H and 9H centrifugal loading and transient thermal interactions between steam delivery hardware and rotor wheels. Testing accumulated start/stop cycles on the steam delivery hardware, measured movement of the axial tubes, determined wear characteristics between hardware with and without dry film lube, observed spoolie wear due to cyclic operation, and measured changes in steam leakage over time due to cyclic operation.

Turbine Rotor Design Analysis

Introduction/Background

Analytical models are required to facilitate the design of the steam cooled turbine rotor components (wheels, spacers, aft shaft, transition discs, coolant systems, and fastening devices). These models are calibrated by comparing test data with predicted performance values, and adjusting the computational algorithm to reflect the measured values.

Discussion

Turbine rotor transient heat transfer models of both the 7H and 9H rotors were constructed, and were used to predict the turbine rotor operational characteristics. These models included a partial lumped fluid element (LFE) methodology used to study transient and steady state conditions. The 9H FSNL and FSFL pre-shipment units were run and met all test objectives. Excellent quality data were obtained from the densely instrumented turbine rotor, and data reduction and analysis were initiated for comparison to pre-test predictions. The 9H and 7H thermal models were updated based on the results from the 9H FSNL, FSFL pre-shipment, and 7H FSNL testing data analysis. In this updating process, the 9H marriage flange D nuts were determined to produce excessive heating due to windage, and consequently the nuts were redesigned.

The 7H rotor was disassembled following the FSNL test in preparation for instrumentation of the rotor for follow-on FSFL testing. The accurate heat transfer models previously constructed were used to help in the disassembly process, as the robust design of the rotor rabbets required sophisticated methods to determine when the mating components had reached optimum thermal conditions for piece part removal.

Several Design of Experiments (DOE) studies of the 7H turbine bucket dovetail designs were conducted. These studies included: the second-stage dovetail shape DOE that developed the optimized shape of the dovetail tangs; the third-stage dovetail slot bottom shape DOE that developed the optimized shape of the dovetail slot bottom; and the second-stage dovetail slot bottom shape DOE that developed the optimized shape of the dovetail slot bottom. The 7H fourth-stage dovetail shape is the same as the 9H fourth-stage (and the 9FA third-stage) dovetail shape.

Several additional DOE studies were completed to modulate the exhaust frame blowers for rabbet control. The steam system pressure drop DOE was completed, which optimized the steam system sizing.

The 7H and 9H preliminary life assessments, including LCF and fracture mechanics analysis, were completed. The 7H turbine wheel bolt hole fracture life problem was resolved by utilizing further refinement in the bolt hole lifing methodology. Three-dimensional models were created for all major components. Two-dimensional, time-dependent thermal loading boundary conditions were analytically swept onto these models to generate stress concentration factors for three-dimensional features. These stress concentration factors were used in a low cycle fatigue (LCF) program to automatically calculate LCF life throughout the turbine rotor structure. Rotor lifing will continue. This process will be automated by developing scripts and software packages to streamline the process.

A gravity sag analysis was conducted in conjunction with the rotor/casing alignment. Using laser alignment procedures, the rotor sag models for both the 9H and the 7H rotors where accurately verified, and the alignment to the casing was calibrated for future assemblies.

Summary/Conclusion

Analytical turbine rotor heat transfer models were constructed for the 9H and 7H configurations to facilitate design of all turbine rotor components (wheels, spacers, aft shaft, transition discs, coolant systems, and fastening devices). FSNL test data analysis was used to verify and update these models.

Design of Experiment studies were performed for the 7H turbine bucket dovetail designs. Turbine rotor life assessments, including LCF and fracture mechanics, were completed.

Turbine Steam Delivery Rotating Rig

Background/Introduction

The "H" advanced machines are designed to have steam cooled stage 1 and 2 turbine buckets which are fed by a steam delivery and retrieval system through the turbine rotor assembly via the aft shaft. In order to verify this design concept, the Turbine Steam Delivery Rotating Rig was designed and constructed. The rig was operated to evaluate

the mechanical integrity and wear characteristics of the rotor steam delivery hardware by subjecting the hardware to repeated speed and thermal cycles. The rig was designed to simulate simultaneous centrifugal loading and start up thermal interactions between steam delivery hardware and the rotor wheels. Throughout testing, wear patterns on the steam delivery system due to this loading will be monitored.

Discussion

A modified 7F turbine rotor, shown in Figure 2.2.2.3-1, was fitted with production steam delivery hardware, and run to reproduce anticipated full-scale 7H and 9H centrifugal loading and transient thermal interactions between steam delivery hardware and rotor wheels. Testing accumulated start/stop cycles on the steam delivery hardware, measured movement of the axial tubes, determined wear characteristics between hardware with and without dry film lube, observed spoolie wear due to cyclic operation, and measured changes in steam leakage over time due to cyclic operation. (Spoolies are the tubular seals that connect the steam delivery piping to the manifolds.)

All testing of the steam delivery testing in the rotating rig was completed by the end of 2Q00. The goal was to run 140 cycles on the hardware to simulate the first run of the 9H rotor. The total cycle count at the completion of testing was 201 cycles, thus providing a healthy margin.

Many modifications were made to the GEPS Engineering Lab wheelbox facility to achieve this number of cycles. Wheelbox overheating (due to windage heating) was controlled by testing the rotor in a vacuum, as well as supplying cooling air to vital components and instrumentation. The temperature in the wheelbox was kept below 180F throughout testing.

Failures of the electromagnetic clutch were also of concern during testing. This issue was dealt with by installing monitoring instrumentation and feedback loops to the clutch. The monitoring included bearing temperature, cooling water temp, cooling water pressure, cooling water flow, water detection in bearing cavity, vibrations and current usage. The clutch performed flawlessly throughout the remainder of the testing.

Another area of concern was rotor dynamics. Once the wheelbox temperature was reduced, the dynamic response of rotor came back to within predicted limits. Occasionally during testing, the rotor rig was shut down due to facility problems. These 'hot' shut downs resulted in a slight bow in the rotor. In all cases, rotor restart was achieved by accelerating the rotor slowly, thereby keeping the vibrations below predetermined limits.

Throughout the testing there were never any problems with the steam delivery hardware. Stresses and vibrations stayed well within limits. The movement of the steam delivery hardware due to thermal ratcheting behaved as predicted. Pre and post test leakage measurements were made, and no appreciable change in leakage could be seen.

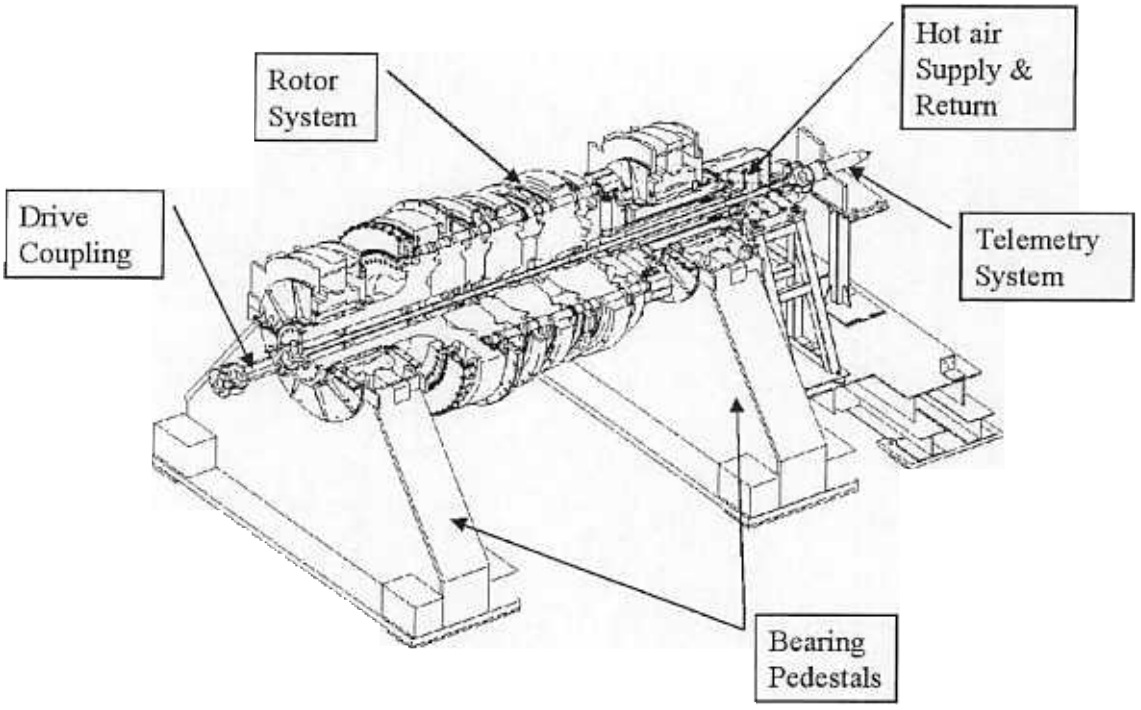

Figure 2.2.2.3-1. Steam Delivery Rotating Cross Section

A typical test cycle is shown in Figure 2.2.2.3-2. Each cycle lasted approximately 30 minutes. The rig was stabilized at approximately 500 rpm, with ambient air flowing through the system. The rig was then accelerated to 4200 rpm. When the rotor reached 90% of the 4200 rpm goal, (3780 rpm), hot air (1000F) was injected into the rotor's steam cooling system hardware. The rotor was held at 4200 rpm for approximately 5 minutes as the rig hardware increased in temperature. When the rig hardware temperature limit was reached, ambient air was injected into the steam circuits to cool the rotor, and the rig was decelerated back to 500 rpm to begin a new cycle. A braking system was used to reduce the rpm, and thus reduce the cycle time.

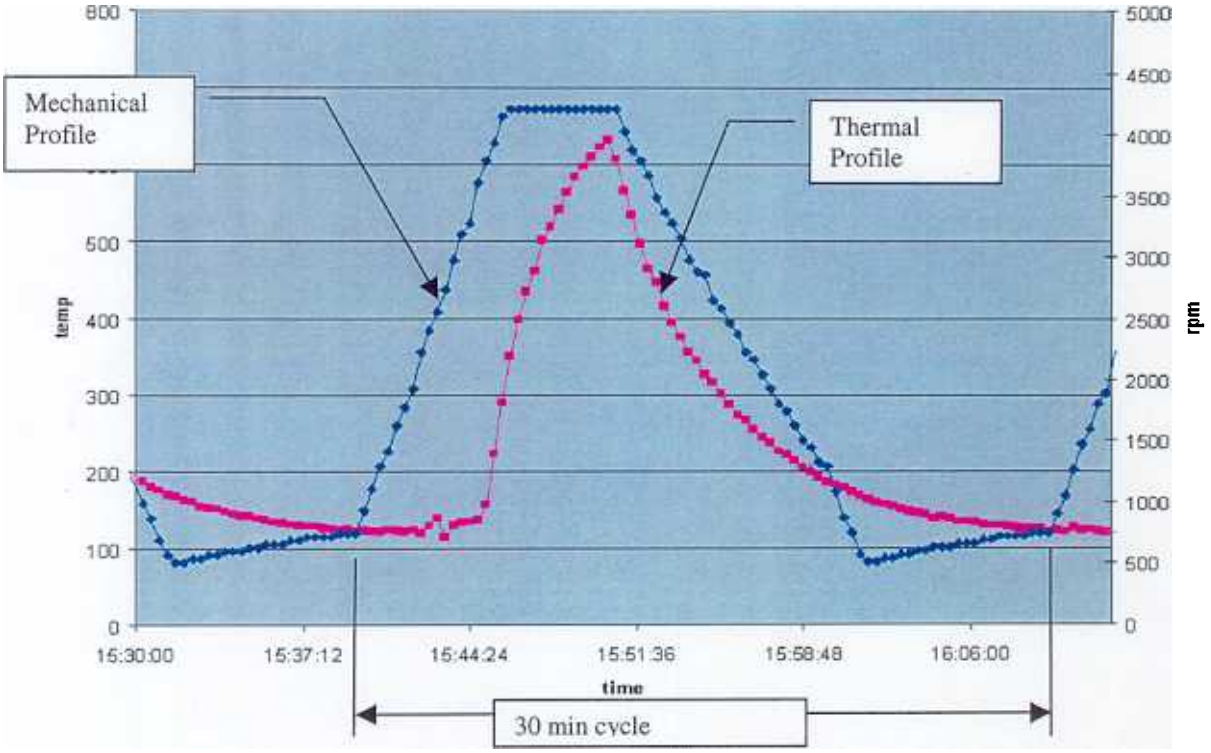

Figure 2.2.2.3-2. Typical Cycle

Summary/Conclusion

Testing of the Steam Delivery Rotating Rig has been completed, with all of the program goal items being accomplished. Actual cycle count was 201 cycles, giving a comfortable margin over the 140 minimum required cycles.

Leak checks were performed to monitor any change in leakage due to spoolie wear or mating surface wear. The leak check performed pre test and post test could not detect any appreciable difference in leakage over the test duration. Spoolies were removed as part of the post test inspection. These spoolies showed only minimal wear, as expected.

The wear patterns on all the mating surfaces are being examined, and the differences being recorded. The rotor had a mixture of parts with and without dry film lube. There was no evidence of excessive wear on any surfaces. Visual observations along with the wear patterns on the steam hardware confirms the predicted 'stick-slip" relative motion between the steam hardware and the mating hardware.

Technology Application

The turbine rotor analysis and design effort defined the basis for the 7H and 9H production hardware. The turbine rotor rig test program validated the rotor steam cooling design.

Section 2.2.2.3.1 (GTFFTR) Turbine Rotor Mechanical Analysis [S,G]

Objective

The objective of this task was to provide thermal and mechanical design and analysis support for rotor components of the ATS gas turbine. Analyses were performed to determine temperature, displacement, and stress distributions for various components of the rotor. Initial designs and concepts were analyzed, compared, and modified to meet design specifications with respect to stress levels, low cycle fatigue (LCF) life, yielded volume, residual displacement, and rabbet closure.

Introduction/Background

Extensive analytical design effort was employed in the design of the steam cooled turbine rotor components. For example, over 150 different configurations of the second-stage rotor in 2D were evaluated under mechanical as well as thermal loadings using the ANSYS finite element program. Design analyses were completed for all of the turbine rotor components to ensure that they would meet all of the performance and life requirements.

Discussion

Plane-stress analyses were performed on various cross sections of the 2-3 spacer to determine hoop stress levels near the steam and feed holes. A parametric study was completed assessing the effect of steam hole size and location for one of the cross sections. A minimum required ligament length was established between the steam hole and outer radius. Steam hole radius was determined to be less important than the radial location of the steam hole. On the basis of these results, two other cross sections of interest were examined under centrifugal loading conditions. Both cross sections produced acceptable stress levels. Plane-stress analyses were also performed on the 2-3 spacer under combined centrifugal and thermal loading conditions simulating transient and steady-state thermal conditions. Three cross sections were examined for each case and all stress levels were found to be acceptable. The 2-3 spacer is expected to meet life requirements and no problems are foreseen.

Thermal and structural analyses of the end cap of the bore tube were run. A number of modifications to the end cap of the bore tube were evaluated, including the base design with a radial undercut, an axial hole at the center, and a combination of the two. Thermal as well as structural analyses were performed. The design with an axial hole at the center showed the best performance with respect to stress reduction because the vanes are freer to grow as a result of thermal expansion. This design was selected.

Stress analyses were performed to determine the influence of steady-state thermal distributions as well as the bolt clamp load on the embossment flange opening/closing of the second-stage rotor. It was found that flange closing is not significantly affected by the amount of bolt clamp load. An increase to almost triple the normal bolt clamp load is required to close the gaps under steady-state thermal conditions. During steady-state thermal conditions, the flanges remain closed when no heat transfer takes place in the cooling holes. When heat transfer does occur, the amount of opening was found acceptable.

Plane-stress analyses of four cross sections of the transition disk were performed. A review was conducted of the stress levels obtained in the transition piece based upon plane-stress; i.e., pie slices of various cross sections. The stress levels obtained from these analyses were within design limits from both yielding and life perspectives.

The automation of the GEPS lifing procedures that was applied to the ATS gas turbine included several significant steps. The first step was the accurate calculation of mechanical and thermal stress concentration factors (Kt) for rotors and spacers at various critical locations. The 3D stress state was then obtained for all rotors and spacers using these Kt's. An independent Fortran program was written to use these stresses, and then apply the GEPS lifing methodologies to compute LCF life numbers for ATS rotors and spacers. The LCF life was obtained at various critical locations on all rotors and spacers for 3600 rpm (7H speed).

Axisymetric studies of the two aft shaft concepts were completed and some 3D analyses were performed in order to examine hoop stresses near the steam holes. Based on the results of this study, a concept was chosen for the ATS gas turbine aft shaft. The concept chosen has inherent design characteristics which make it very robust for the anticipated tuning rabbet loads. In addition, this concept will be less susceptible to low cycle fatigue failure.

There were a number of 3D analyses conducted to evaluate the 3D stress effects. A 3D model of the stage 1-2 spacer was used to evaluate the structural response under a series of rabbet loads and rim loads. The stresses under normal operating conditions were found to meet design criteria.

Nonlinear 3D stress analyses of the axial tube spoolies for the steam delivery system were performed. These analyses included the contact interference to the wheel hole, the effects of thermal transients and initial interferences, as well as plasticity and creep. The analyses focused on stresses caused by angulation resulting from differential heating of the wheels.

Nonlinear 3D stress analyses were also performed on the first- and second-stage bucket spoolies for the steam delivery system. The methodology developed for the axial tube spoolies was used. A design of experiments (DOE) approach was used to assess design variables with the model. The analyses established the proper interference fit to be used and indicated that the design was acceptable for drawing release to manufacturing. The

current spoolie analysis methodology was also applied to a wear test specimen that survived 20,000 cycles at high interference and load. Assembly interference dimensions were computed to obtain required sealing and fatigue life. These results became the design limits for the production designs.

A complex 3D ANSYS stress model of the bucket steam supply manifold was built. The model incorporated internal geometry, non-constant wall thickness, and fillets. Analyses were performed for speed and pressure loading. Some investigations were made into the effect of reducing the spacer rabbet length, which would lead to less support for the manifold. As more data became available on interacting components, boundary conditions were enhanced.

A series of 3D stress analyses was performed on the manifold, investigating ways of strengthening the walls to withstand the pressure loading while minimizing additional weight. Analyses were also performed to investigate the additional stress produced in the manifold caused by the centrifugal effect of the axial tube. The effects of isolating the through-tubes that feed steam to the first-stage buckets, and of using a central support were investigated. Using this information, a new 3D ANSYS finite element model of the feed manifold was built and analyzed. This model incorporated all the latest design changes. The model was detailed and included the variations in wall thickness, fillet radii, and local thickening caused by stops. The analysis exhibited stress levels that were subsequently verified by FSNL test data.

Summary/Conclusion

Thermal and mechanical design and analysis support were completed for the steam cooled turbine rotor components. Analyses were performed to determine temperature, displacement, and stress distributions for these rotor components, including: spacers, bore tube, embossment flange, transition disk, aft shaft, spoolies, and bucket steam supply manifold. Initial designs and concepts were analyzed, compared, and modified to meet design specifications with respect to stress levels, low cycle fatigue (LCF) life, yielded volume, residual displacement, and rabbet closure.

Technology Application

The analysis performed and the resulting design features were used to robustly design an ATS gas turbine rotor that meets cycle life requirements.

Section 2.2.2.3.2 (GTFFTR) Wheel Forging Stress Analysis [C]

Objective

The objective of this task was to assess the significance of residual stresses introduced during forging and post forge heat treatment with respect to overspeed design limits for IN706 and IN718 forgings used to produce turbine rotor disks.

Introduction

Past experience from overspeed tests on a 7FA first-stage turbine wheel (IN706) indicated the possibility of large residual stresses in the wheel forgings after heat treatment. If present, these residual stresses could have an effect on fatigue life as well as residual displacements in the turbine wheels. The effect on residual rabbet deflections is particularly important since rabbet opening/closure as well as rabbet loading and local plasticity may be affected. These affects have not been previously quantified and as a result are not part of present design methodology. As a result, this effort was undertaken to assess the significance of these residual stresses and if necessary, include them in the design of the ATS turbine wheels. The investigation plan was to carry out the residual stress calculation on the 7FA wheel first in order to correlate the analysis with available test data. If the simulation was validated by this correlation, the same procedure would then be applied to the ATS wheels.

Discussion

The starting point for this task was the thermal analysis of the heat treatment process for the 7FA first-stage turbine wheel forging. This thermal analysis included simulation of the quenching, aging, and cooling processes after forging. Information from the literature was used for temperature, convection, and radiation boundary conditions for the quenching and thermal aging processes. The cooling rates defined from these analyses were used to design tests that produced stress-strain and creep response data necessary to adequately model material response throughout the forging thickness. The temperature history from the heat treatment analysis was also used as input for the subsequent stress analysis to determine the residual stresses introduced during quenching, aging and cooling of the 7FA wheel material.

The results of the stress analysis of the quenching process showed that the peak residual stresses introduced during this event are on the order of 690 MPa (100,000 psi).

The thermal stress analysis of the aging process of the 7FA first-stage wheel was carried out first ignoring creep effects. Coupling these results with the time values introduced during the transient thermal analysis, stress and strain data as a function of time were approximated to determine appropriate test conditions for creep and stress relaxation tests. These creep and relaxation tests were conducted using IN706 material and the results indicated that little relaxation should be expected to occur during the aging process. For that reason the simulation of the machining and subsequent overspeed pre-spin of the 7FA first-stage wheel was performed using the plastic strain results from the of the time independent aging analysis, ignoring any creep strain that may have developed. After cooling from the aging temperature, the inelastic strains were then mapped onto the machined wheel shape to determine the final residual stress levels in the wheel prior to the overspeed pre-spin. Plastic strains at the end of the aging process were mapped onto the machined shape using the GEAE code Siesta. An overspeed analysis was then performed using SUSAN that included these residual stresses in order to determine their effect on residual growth, plasticity, and fatigue life.

An overspeed analysis ignoring residual stress effects was also carried out. In the 7FA first-stage wheel, residual growth after overspeed was underpredicted by a factor of two

when residual stresses were ignored. The new analysis procedure, which includes residual stress from the quenching and aging process, predicted a residual radial growth close to that obtained experimentally.

A simulation of the 7FA turbine wheel within a rotor system for a typical start-up was also carried out for three cases: a pure elastic analysis, an elastic plastic analysis, and an elastic plastic analysis with the effects of the forging process, the machining process and the pre-spin included. The elastic and elastic plastic results were very similar, but the analysis with the forging and pre-spin history showed significant differences in comparison to the analyses ignoring residual stress. For the analysis including residual stress, areas around the bore were at smaller stress levels than were indicated if residual stresses were ignored. However, regions near the rabbet fillets showed significantly larger stress when residual stress was included. The effect of forging and pre-spin residuals is apparently very location- and process-dependent.

After completing the 7FA analysis, a similar analytical process was applied to the second stage 7H turbine wheel forging. A heat transfer analysis simulating the quenching and aging process of the 7H gas turbine second-stage wheel was completed. Tensile tests were performed on specimens undergoing the same thermal history seen in the quenching and aging process. Stress-strain curves were generated as a function of temperature for specimens that underwent the quenching thermal cycle alone as well as for specimens that underwent both the quenching and aging thermal cycles. These stress-strain data were used as input for thermal stress analyses simulating the quenching and aging process of the 7H gas turbine second-stage wheel.

Following the thermal analysis, a thermal stress analysis simulating the quenching process of the 7H second-stage wheel was carried out. Peak radial and hoop stress levels predicted for the 7H second stage turbine wheel were similar to those seen in the 7FA first-stage wheel. A thermal stress analysis simulating the aging process of the 7H second-stage wheel was also completed. Peak radial and hoop stress levels predicted from this analysis were higher than those seen in the 7FA first-stage wheel.

The stress and strain results from the 7H second-stage analysis were then used as bounds for performing creep tests on the IN718 material (ATS second stage).

Summary/Conclusion

Stress analyses were carried out to simulate the quenching and thermal aging processes after forging as well as subsequent machining processes for both 7FA and 7H turbine wheels. Stress relaxation experiments indicated that little relaxation occurs during the aging process and creep strain could be ignored in the simulation. Results of these analyses indicated that these post forging processes introduced significant residual stress in turbine wheels. Furthermore, when the overspeed pre-spin was simulated using elasto-plastic constitutive models, it was found that the predictions of residual radial growth after this pre-spin agreed closely with experiment. In comparison, a similar analysis ignoring residual stress underpredicted radial growth by a factor of two. Stress analysis was also carried out to simulate the response of a 7FA turbine wheel within a rotor system for a typical start-up. Analyses which included the residual stress effects of

forging and pre-spin processes were significantly different than those which ignored these residual stresses. Stresses near the bore were significantly lower when residual stresses were included. However, regions near the rabbet fillets showed significantly larger stresses. When residual stress results for a first stage 7FA turbine wheel were compared with similar analyses simulating a second stage 7H turbine wheel, it was found that stresses induced during the quenching process were quite similar. In contrast, the residual stresses induced during thermal aging were higher for the 7H wheel than the 7F. The conclusion of this investigation was that the residual stresses associated with forging processes are significant and can be process dependent.

Technology Application

Residual stresses due to wheel forging were considered during the engineering design process for the ATS turbine wheels.

Section 2.2.2.3.3 (GTFFTR) Rotor Steam Circuit Analysis [S, C]

Objective

The objective of this task was to assess rotational and 3D effects on the flow within the rotor steam circuit components whose performance is strongly dependent on these effects. The steam distribution into the buckets, for example, depends on the performance of the manifolds to ensure that the buckets are adequately cooled. Hydraulic losses can be better estimated when 3D effects are considered. The rotational and 3D effects were assessed using computational fluid dynamics (CFD).

CFD techniques were applied to determine 3D and rotational effects in critical components of the 9H and 7H rotor steam cooling circuit. Component performance (e.g., pressure drop and flow distribution) was established, and means for improving component performance were investigated.

Introduction

The rotor steam circuit analysis used two complementary approaches. One is a general, overall system model, consisting of a 1-dimensional network model of the system built using a hydraulic network solver called YFT. This approach requires the knowledge of hydraulic performance parameters of the individual components that make up the network. This information is supplied by the second, more detailed approach, that employs 3-dimensional Computational Fluid Dynamics (CFD) tools to study the individual components of the steam distribution system.

Discussion

Overall network model

The network model was used to screen several distribution system configurations on the basis of overall hydraulic performance.

The YFT model of the steam distribution baseline concept included all the components of the steam delivery system housed in the gas turbine. The design was significantly altered in several critical areas; e.g., the radial distribution module, the axial tube arrangement, and the bucket manifold pieces. The performance characteristics of the baseline concept were defined, and a preliminary attempt at reducing its pressure losses was made. Three other alternate designs, with various degrees of departure from the baseline, were conceptualized and analyzed. With some optimization, all the designs can be made to meet the overall pressure drop requirement.

As part of the design definition process, a careful study of the arrangement of the radial tubes connecting the bore tube with the axial tubes was undertaken.

The overall design definition process of the steam delivery system also considered the manifold area of the network. YFT models of three candidate manifold designs were created. With the aid of these models, the hydraulic performance of the alternate concepts, including pressure drop and leakage, was evaluated.

The baseline concept for the steam manifold was selected. This design did not compromise the flow distribution between the first- and second-stage buckets or between same-stage buckets. The detail CFD model of this component was used to confirm this preliminary assessment. Additionally, this design offered an improved assembly method over the other concepts; the rabbet retention was based on proven technology, and it was an overall lower risk design based on previous similar manifold analyses. Reduction of leakage sites in this concept and further optimization of its overall impact on the combined cycle were also addressed in this study.

Detailed component analyses

The CFD activity focused on five major components of the steam distribution circuit: the supply manifold, the return manifold, the inlet to the bore tube, the supply side endcaps, and the return side encaps of the bore tube.

Supply and return manifolds

Solid models of the interior fluid space of the 9H bucket supply manifold were generated with Unigraphics. Parasolids versions of these models were meshed for CFD computation using the unstructured-grid solver NOVAK3D. The models included a long section of the axial inlet tube and extensions for the spoolies to allow the flow to develop before boundary conditions are applied. In the early stages of the study, the buckets were not simulated. Many CFD models of the supply and return manifolds were created as the manifold designs evolved. The primary objective of the CFD simulations was to determine the magnitude of the flow maldistribution introduced by the manifolds in each bucket. A second objective was to verify the 1D pressure drop relations used in the overall steam delivery circuit YFT model.

The original baseline design, the T-design, was evaluated first. It displayed significant flow maldistribution to the buckets. The next design, the delta-wing concept, showed a significant improvement in flow distribution. The presence of the buckets, however, was expected to introduce a significant corrective factor.

Using 1D analyses, the geometric characteristics of orifices exhibiting pressure drops equivalent to those found in the first- and second-stage buckets were established and the NOVAK3D grid was updated. The original T-shape supply manifold design was improved, using the lessons learned in the first phase of the project, and analyzed. The flow distribution showed slight deviations among the buckets. The maldistribution due to the return manifold was addressed next.

Concurrent with these CFD analyses, the definition of details in the supply and return manifolds was carried out using 1D analyses to assess trade-offs between performance and design robustness.

As the design of other components around the manifold evolved, constraints on the volume of the manifolds emerged. New models of the evolving designs were created and CFD results indicated a combined supply and return manifold impact on flow maldistribution that was somewhat larger than previously predicted. New modifications were recommended and a new fabricated design evolved. CFD analyses confirmed the adequacy of the flow distribution from bucket to bucket and an acceptable pressure drop performance.

The results of the CFD and 1D analyses were implemented in the design process. Pressure drop analyses indicated that an adequate safety margin is available in the YFT steam circuit model.

Following iterations involving other mechanical considerations, the final concept for the cast design of the 9H return manifold was analyzed. This design incorporated all the recommendations that resulted from the previous CFD analyses of the 9H return manifold. The CFD code CFX was used to solve the discretized governing equations on the unstructured grid built from the part UniGraphics (UG) model. The design improvements for the fabricated design were incorporated in this cast design, and the improvement in its hydraulic performance was evident. The pressure drop introduced by the manifold is below the critical-to-quality (CTQ) value, and the bucket flow maldistribution due to the combined effects of the supply and return manifolds is significantly lower than required for bucket life.

The CFD analysis of the fabricated 7H supply and return manifolds was also completed, and the results were very encouraging. The pressure drop in each 7H manifold was lower than the target set for the 9H manifolds as a result of the realignment of first-stage and second-stage incoming jets, the more aerodynamic contour of the manifolds, and the addition of guide vanes—all lessons learned during the 9H design activity.

After completing the studies of the fabricated designs, the first cast design concepts for the 7H supply and return manifolds were analyzed to establish a baseline performance. Lessons learned during the fabricated concept study were incorporated with very encouraging results: low pressure losses and nearly uniform bucket flow distributions.

Boretube supply and return sides

CFD analyses of the original bore inlet and supply end cap designs were completed. Results of these analyses confirmed flow swirl patterns previously predicted by earlier preliminary CFD analyses, and pressure losses in the range predicted by the YFT

analyses. A redesign of the end caps, driven by manufacturing and inspectability issues, was initiated, and preliminary assessment of pressure drop penalties was performed using 1D analyses. CFD analyses of the alternate bore tube inlet section were performed. In addition to the baseline inlet design, a larger opening was also considered. The larger opening did not exhibit any undesirable back-flows through the inlet area and did improve the hydraulic performance of the bore inlet section (lower pressure drop, improved cross-sectional velocity distribution in the annulus, and slightly lower swirl angle). Analysis of the supply end cap was completed.

Results of CFD simulations of the bore inlet tube static test geometry showed excellent agreement with test results. With no flow swirl, the two approaches predict virtually the same loss coefficient for the inlet into the bore tube.

Following a series of redesign efforts, the CFD simulation of the resulting 7H and 9H supply bore tube designs was also completed and documented. Starting with a description of the CFD model common to both designs, boundary conditions and results for each scenario were derived. The combination of the different rotational speeds in the two designs and the identical scroll concept and flowrates led to an inlet flow in the 7H with an underswirl that was not present in the 9H. The result was markedly different flow swirl angles in the bore tube annulus and correspondingly different pressure drop profiles.

The hydraulic performance of the 9H design is better than that of the previous 9H design. Despite the fact that the previous design operated at a lower flowrate, the pressure drop at the entrance and past the strut were lower in the current design. The value of the swirl that develops just upstream of the strut is similar to the predicted value for the previous 9H bore tube design. The passage of the flow around the strut causes a drop in the swirl angle. Frictional losses downstream of the strut cause a slow decay in the flow swirl angle. The boretube entrance pressure drop is slightly higher in the 7H than in the 9H. This result was expected as the flow enters with a relative swirl in the 7H, whereas in the 9H the flow is perfectly radial (in the relative frame of the rotor). The difference, however, is slight. On the other hand, the pressure drop past the strut is substantially lower in the 7H design than in the 9H design because of the lower flow swirl angle in the 7H configuration. The swirl angle for the 7H design remained at a significantly lower value than the results obtained from the 9H calculation. The strut did not exert as great an influence on this parameter as it did for the 9H.

The CFD analysis of the steam circuit rotor return bore tube was also conducted. The loss coefficient is very close to the value predicted by the modified 1D approximation employed in the overall YFT circuit model. Rotational effects were controlled well by the guide vanes at the inlet to the return bore tube.

Other CFD analysis

Concerns over a potential backflow from the compressor main flow path led to a CFD analysis of the high-pressure packing upstream cavity was performed. This area is not part of the steam distribution circuit, but potential adverse thermal consequences forced a close examination of this area. In the course of the solution process it was necessary to impose a fictitious wall on part of the outlet that leads to the compressor flow path to

prevent inflow through this exit boundary. This is an indication of the possibility of flow reversal through this outlet and, hence, from the compressor flow path. This led to a closer examination of the flow in the neighboring region, and indeed evidence of this potential flow reversal near the stator wall is present. It has been determined that the amount of flow reversal predicted by the analysis is less than 5% of the net outflow and therefore is not expected to carry any adverse consequences. Furthermore, a design feature present in the design but not modeled in the analysis may further reduce this potential flow reversal or completely eliminate it.

Summary

In summary, CFD runs of the baseline supply and return bucket manifold concepts were performed. Results show adequate flow distribution into first- and second-stage buckets. The hydraulic performance of the supply manifold based on CFD results matched the 1D estimates in the overall system analysis. Design modifications were implemented in order to meet pressure drop requirements in the return manifold.

A design review of the steam distribution system was conducted in which all CFD analyses of the rotor inlet section, supply endcap and radial tube, supply and return manifold, return radial tube and endcap, and return bore tube were presented. No open items resulted from the review.

In a separate task, tests of the supply and return manifolds in a non-rotating rig were conducted to establish a benchmark against which the CFD results could be compared. The test configuration of the supply manifold was meshed for CFD analysis. The CFD code CFX was used to predict the flow distribution in the manifold under test conditions.

Comparison with supply manifold test data was completed and results were very satisfactory. All test flowrate data were predicted within an acceptable tolerance. Flow distribution and pressure drop data were compared.

Technology Application

The results of this task define the hydraulic performance of the overall steam distribution circuit and of the individual components it comprises. Performance predictions of various designs were used in tradeoff studies to select the baseline concept of the overall steam distribution strategy and the specific design of the scroll, and the supply and return manifolds. Drawings were issued that incorporate the design modifications arrived at through the performance of this task. As the design of the component evolves in response to mechanical constraints, this task ensures that hydraulic performance is not compromised. This task also identifies performance improvements to achieve critical-to-quality criteria (CTQs).

Section 2.2.2.3.4 (GTFFTR) Turbine Rotor Shaft Temperature Analysis - #2 Bearing [S,C]

Objective

The objective of this task was to investigate design options that would result in a minimum temperature of the shaft surface in contact with oil and/or air oil mist, and a maximum thermal gradient in the area of the oil seals in the #2 bearing.

The allowable temperatures in the seal forward of the bearing are limited due to the accelerated decomposition of lubricating oil at high temperatures. Thermal gradients are also limited in that uneven thermal expansion of the shaft that would adversely affect seal clearances and performance.

Introduction/Background

It is important to keep the turbine rotor shaft surface temperatures as cool as possible to minimize the thermal gradients that cause uneven thermal expansion, and consequent seal clearance variations.

Discussion

Four distinctly different designs were investigated individually and in combination: (1) addition of an extra 6 inches in shaft length, with the additional material added before the forward seal, (2) an axial air gap annulus between the shaft and feed cooling steam, (3) forced air cooling, with cooling air entering through radial holes between the bearing housing and the steam box, traveling axially under the bearing and seal areas, and exiting through radial holes forward of the bearing housing, and (4) addition of a circumferential groove to inhibit thermal flux.

Temperatures in the seal were significantly reduced using a combination of air gap isolation and forced air cooling. Using assumed boundary conditions, a single cavity of still air produced 50% of the required thermal reduction. The addition of forced air cooling through a second axial cavity further reduced seal area maximum temperatures. A small notch cut in the surface of the shaft forward of the seal provided an effective barrier for the transport of the heat. This notch combined with an air gap and forced air cooling provided the lowest temperatures in the model.

Summary/Conclusion

The configuration selected was incorporated into the turbine rotor design, and was validated during the FSNL test program.

Technology Application

All the design options evaluated in this study were considered for ATS turbine rotor design in a detailed follow-up study using a fluid element analysis approach to better simulate the heat transfer boundary conditions in the current modeling effort.

Section 2.2.2.3.5 (GTFFTB) Bucket Temperature Monitoring [S,C]

Objective

The objective of this task was to provide the steam-cooled rotor buckets with protection against a loss-of-steam-coolant event. The protection system will provide a timely signal enabling the turbine to be shut down with minimal damage.

Introduction

Timely detection of a loss of steam cooling event was identified as a fundamental necessity early in the engineering development of the ATS gas turbine. Pyrometers were chosen as the primary means of steam-cooled bucket protection. Several other technologies were investigated (e.g., tracer leaks, vibrational signatures, steam pressures, and steam flowrates) but were discarded in favor of monitoring the bucket temperatures using pyrometers attached to the outer casing of the turbine with a direct line-of-sight view of the buckets. Pyrometers offer significant advantages: (1) they respond to the bucket parameter that is of most concern (i.e., temperature); (2) all the buckets in a stage come into the field of view of a single fixed pyrometer; and (3) the detection system has a rapid response time. Line-of-sight was recognized as the method for achieving long-term pyrometer stability.

Discussion

In order to acquire basic experience in the operation of pyrometers in a gas turbine environment, test pyrometer systems were installed at two commercial sites. Long-term trending of the pyrometer signal and short-term reproducibility of the data affirmed the applicability of this technique to steam-cooled bucket protection.

Component design was completed for line-of-sight pyrometer access for both the first- and second-stage buckets on the ATS gas turbine, and final specifications for the pyrometers were established.

The bucket surfaces that will be monitored by the pyrometers in the ATS gas turbine are TBC coated. Since pyrometry is an optical measurement technique which requires data characterizing the observed surface, TBC data was required. Optical properties of TBC and TBC-coated buckets returned from field testing were measured and the results applied to a model to estimate the surface temperature of the TBC from pyrometer data.

It was discovered that accurate temperature measurements using pyrometers required a "marking system" on the bucket surfaces to provide a datum for the pyrometer data. Platinum "marks" were identified as an approach to providing this datum. In order to test

this approach, the second-stage buckets in the full-speed full-load (FSFL) pre-shipment test were equipped with platinum marks to aid in the estimation of surface temperature and to verify the line of sight. Test data were recorded during the test program, and data analysis was conducted. This marking system was shown to be successful based on accumulated data from this test.

Summary/Conclusion

Pyrometer technology has been developed as the method for detecting loss of steam cooling in the ATS gas turbine. Data collected from pyrometers at two air cooled commercial sites showed that this was a viable approach. Component design was completed and pyrometer specification for the ATS gas turbine was identified. Necessary optical data characterizing TBC covered buckets was measured. A platinum marking technique was devised and implemented to establish a measurement datum on the bucket surfaces to be monitored. The pyrometers were used to collect data during the FSFL pre-shipment test. The monitoring approach was verified.

Technology Application

Pyrometers will be used in the ATS gas turbine to monitor steam-cooled turbine blades during operation. This will allow for timely detection of insufficient steam coolant flow into the buckets.

Section 2.2.2.3.6 (GTFFTR) Rotor Component Flow Tests [C]

Objective

To ensure proper steam flow through the rotor steam cooling circuit selected components from the system were tested to determine their flow characteristics. The supply and return manifolds were tested to determine their pressure loss and the manifold distribution flow uniformity. Tests were conducted to evaluate the possibility that cooling system flow turbulence might cause excessive wear and induce vibration in combination with the system natural frequency response. Selected sections of the steam circuit were tested to determine if there were significant flow-induced pressure oscillations present, and system acoustic frequency response was measured in a field test. The pressure loss and flow uniformity data was used to validate the accuracy of the CFD and YFT design codes.

Four types of tests were conducted: manifold flow testing, dynamic pressure testing, bore tube dynamic pressure testing, and bore tube acoustic resonance field testing. Each of these areas is discussed in the following sections.

Introduction and Background

Manifold Flow Testing

Manifolds are used in the steam cooling system to distribute flow to and from the buckets. The supply manifold has one steam inlet and multiple outlets to the buckets,

both forward to the first stage and aft the second stage. The return manifold collects the flow from the multiple buckets and connects it to one return. It is critical to bucket cooling that the manifold provide an equal and uniform distribution of flow to each bucket. The purpose of the manifold flow testing is to determine if the manifold designs (supply and return) causes a maldistribution of the flow or excessive pressure loss and hence bucket cooling flow loss. Additionally, the experimental data is used to validate the CFD and YFT design codes which are used to simulate the effects of the rotor rotation that this static flow testing cannot model.

Dynamic Pressure Testing

A concern is that coherent flow instabilities (i.e., tones) coupled with system natural frequency response could accelerate wear and fatigue of cooling system parts, particularly the spoolie seals used to seal between the various coolant delivery components.

Bore Tube Dynamic Pressure Testing

Flow induced vibration is also a concern in the inlet portion of the bore tube, a component used to collect the cooling flow from the stator and pass it forward toward the turbine wheels. Because the bore tube has struts that span the inlet annulus and the inlet flow crosses the struts with a varying angle of attack, this area was of greatest interest.

Bore Tube Acoustic Resonance Field Test

The effect of flow induced oscillations coupled with system acoustic resonance can greatly accelerate mechanical wear and fatigue. Flow induced pressure oscillation were measured in earlier tests and this test measures the system acoustic response.

Discussion

Manifold Flow Testing

Figure 2.2.2.3.6-1 shows a schematic of the manifold flow test stand. The configuration shown is for a supply manifold test. Air flow is provided from a single-stage centrifugal compressor. Flow enters the test stand at location 1 as shown in the schematic. The flow passes through a metering tube and ASME orifice that measures the total mass flow going into the manifold. At the inlet to the manifold there is a kiel probe (7) which measures the manifold inlet total pressure. Flow goes up through the manifold (8) and exits through the multiple bucket metering tubes (9&12). At the ends of each of the bucket tubes there is an orifice (10&13). The bucket metering tube orifices are calibrated and they are used to determine the bucket mass flow uniformity. The flow exiting the bucket tubes is vented to atmosphere. All flow tests were conducted at atmospheric conditions using ambient temperature air as the flowing fluid.

To test the return manifold the supply manifold is replaced with the return manifold and flow is simply reversed. The tube shown at (1) is connected to the inlet side of the compressor and flow is sucked through the return manifold.

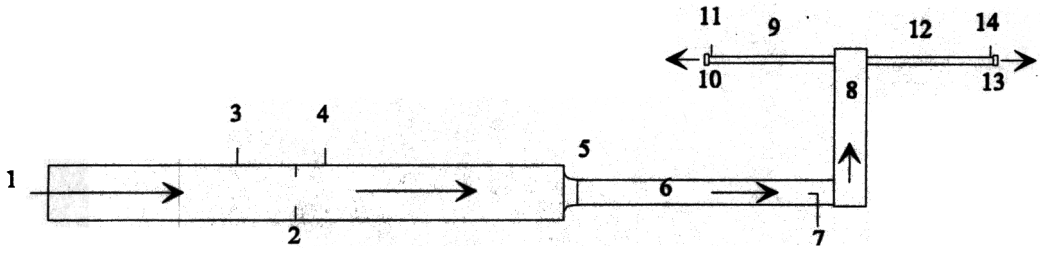

1. Flow enters the mass flow metering tube from the compressor
2. ASME orifice is used to measure total mass flow
3. Upstream orifice pressure measurement
4. Down stream orifice pressure and temperature measurement
5. Eliptical inlet to axial tube
6. Axial supply tube
7. Kiel probe measures total pressure at manifold inlet
8. SLA full scale supply manifold
9. Second stage tube 17 inches long, 1 of 6
10. Second stage tube flow metering orifice, 1 of 6
11. Second stage orifice pressure tap, 1 of 6
12. First stage tube 23 inches long, 1 of 6
13. First stage tube flow metering orifice, 1 of 6
14. First stage orifice pressure tap, 1 of 6

Figure 2.2.2.3.6-1. Schematic of the Manifold Test System

Two acrylic SLA models were constructed, one for the supply manifold and one for the return manifold. The internal dimensions of the model were maintained so as to replicate the flow geometry. The external dimensions were allowed to increase so that the acrylic model would be strong enough to withstand the test pressures.

Design specifications for pressure drop and flow uniformity were determined by calculations of flow using CFD and YFT. Flow uniformity compared the variation of the individual flow (flow to each bucket) to the overall average. Test were conducted at three different flow rates, the design flow rate and ±10% from the design.

Dynamic Pressure Testing

Testing of the steam circuit to determine whether system dynamic pressures have a detrimental effect on spoolie joint performance was completed.. A test was devised and built to measure the dynamic pressures in a portion of the steam supply system. The test included an axial tube, a supply manifold, a bucket tube, and a bucket. There were three spoolie couplings: one connecting the axial tube to the inlet of the manifold, one connecting the exit of the manifold to the bucket tube, and one connecting the bucket

tube to the inlet of the bucket. Seven dynamic pressure transducers were installed in the system to measure the dynamic pressure that acts on the spoolies.

Testing was done with air at atmospheric pressure and temperature. Six flow rates were chosen to emulate steam flow for the range of gas turbine operating conditions. The flow rates were chosen matching the Mach numbers from the machine conditions to the model condition. Dynamic pressure data were taken from each pressure transducer at each of the six flow settings. The data was reduced and plotted to show the spectral content, amplitude, and frequency of each pressure transducer at each flow setting. Test were conduced to determine the effect of component misalignment. During these tests the axial tube was deliberately misaligned and the tests were repeated.

Bore Tube Dynamic Pressure Testing

The bore tube dynamic pressure testing was focused on flow instabilities that may cause excessive wear of cooling system parts. The concern is that the flow passing through the bore tube supply passage and passing over the support struts may produce discrete tones that could couple with the system natural frequency response. The flow-induced pressure oscillations were evaluated in this test; the bore tube system natural frequency response (or system resonance) was evaluated in a field test. To investigate these oscillations, a full-scale model of the bore tube was constructed. The bore tube was connected to a test stand where an earlier bore tube design was tested. Dynamic pressure transducers were installed at seven locations in the bore tube. A shakedown test was completed, and the model and test stand performed as expected. As a result of other mechanical testing, a design change in the bore tube was deemed necessary and the dynamic testing of the flow configuration was stopped.

Bore Tube Acoustic Resonance Field Test

Measurements of the bore tube acoustic resonance were made in the 9H gas turbine at the GEPS Greenville, SC, facility. The objective of these tests was to search the bore tube supply and return ducts for acoustic resonances that might exist and lead to high-cycle fatigue and cracking or other operational problems. The approach was a combination of experimental and analytical techniques.

Loudspeakers were set into specially designed baffles, and the supply and return ducts were individually excited with high-level, broadband noise. Microphones measured the acoustic frequency response of the bore tube acoustic cavity at several locations in both ducts. Many individual peaks indicating resonances were observed, not all of which could be categorized.

Using a combination of analytical methods, a number of these resonances with particular modes of acoustic standing waves in the bore tube were identified. Then frequency-scaling was performed on these resonance peaks to estimate the peaks expected under the temperatures and pressures of actual turbine operations.

Summary/Conclusions

Manifold Flow Testing

The supply manifold performance was within the specification for uniformity of flow distribution and pressure loss. Consequently the supply manifold flow design was excepted. Also, the data from the supply manifold test compared very well with the calculated CFD results and verified the accuracy of the CFD code.

The return manifold met the design specification for pressure loss but did not meet the design specification for the uniformity of flow distribution. The data from the test of the return manifold compared very well with the calculated CFD results and verified the accuracy of the CFD code. As a result, the manifold design was modified to achieve uniform flow distribution through the manifold. The redesign of the supply manifold was accomplished using CFD modeling, and because of the verified accuracy of the CFD code no further testing was deemed necessary.

Dynamic Pressure Testing

In general all of the flow conditions tested were very quiet. Coherent dynamic pressure oscillations were either not present, at insignificantly low pressure or at a high frequency that would not excite mechanical vibration. The data was used as input for mechanical vibration analysis where mechanical motion and wear can be predicted.

Bore Tube Dynamic Pressure Testing

There is no plan to resume testing with the new design.

Bore Tube Acoustic Resonance Field Test

None of the resulting scaled frequency peaks stood out as potentially harmful, as they did not correspond with known structural or flow-induced excitations of the turbine. The excitation of the remaining unidentified modes was not thought to be a problem because of the lack of an observed or calculated driving frequency in turbine operation.

Technical Application

Manifold Flow Testing

Data was provided to ensure proper design of the supply and return manifolds as well as validation of the CFD and YFT design code.

Dynamic Pressure Testing

Dynamic pressure data coupled with system acoustic resonance data is used to minimize wear of cooling system parts due to flow induced vibration.

Bore Tube Dynamic Pressure Testing

None.

Bore Tube Acoustic Resonance Field Test

The test provide design information to lower the risk of accelerated wear and mechanical fatigue due to flow induced oscillations coupled with acoustic resonance response.

Section 2.2.2.4 (GTFFTB) Turbine Bucket Design [S,C]

Objective

The objective of this task is the design of buckets for the four rotating stages. The heat transfer and material databases for steam-cooled first- and second-stage buckets continue to expand and will be integrated concurrently with the design. Cooling passages will be sized consistent with manufacturing practicalities and the bucket life requirements. Flow variation and consistency will affect life calculations and will be considered. Current practices for thermomechanical steady-state and transient analyses, dynamics and vibration analysis (which can deal with anisotropy), and corrosion/oxidation analysis will apply throughout. Drawings and specifications will be developed in preparation for manufacturing.

Introduction/Background

The bucket design and development process involves the completion of work through seven tollgates namely: 1) product option identification, 2) requirement and resources, 3) conceptual design, 4) preliminary design, 5) detail design, 6) production and design validation, and 7) post shipment test and monitoring. During each phase, numerous design reviews and tollgate reviews were held to ensure that the design intent had been met. To date, two full speed no-load (FSNL) tests have been completed on the 9H machine, and one FSNL test has been completed on the 7H. The bucket designs for both the 7H and 9H have been completed, with bucket casting production to follow. The design of the buckets for the 7H was able to leverage the design, testing, and associated technologies used for developing the 9H.

Discussion

The ATS gas turbine design calls for steam cooled buckets on the first two stages, an air cooled bucket for the third stage and an uncooled bucket for the fourth stage. The 1st and 2nd stages both have ceramic thermal barrier coating systems to reduce the operating metal temperatures to acceptable levels. Figure 2.2.2.4-1 shows a comparison of the 7H and 9H flowpaths. A comparison of airfoil shapes is also shown for stage 1, along with airfoil counts for each row. It should be noted that the 7H blade chords are smaller for the same airfoil radial length. The 7H airfoils are sized for the reduced gas path mass flow as well as the higher mechanical (rotational) loadings.

Stage 1 Buckets

The 9H stage 1 bucket cooling design consists of a main cooling circuit (with a nine pass serpentine), a trailing edge cooling circuit and a platform cooling circuit circuit, all cooled by steam. The 7H stage 1 bucket is very similar except that with the shorter airfoil axial chord, only a six pass serpentine is required for the main cooling circuit. The main cooling circuit and the platform cooling circuit are both formed by casting ceramic cores in an investment (lost wax) casting process. The trailing edge cooling circuit is formed by chemically eroding two holes through the trailing edge portion of the airfoil by an electro-chemical machining process also known as Shaped Tube Electro-chemical Machining (STEM), where two tubular shaped electrodes are used to chemically form a tubular passages to very tight tolerances. In both cases, an advantage is gained in the use

of steam and its superior heat transfer properties at the conditions used. Rig tests, both static and rotating, have been used to prove out and validate the cooling concepts under similar conditions i.e. Reynolds numbers, Prandtl numbers, rotation and buoyancy numbers. The material of choice for both the 7H and 9H stage 1 buckets is single crystal N5 for its superior creep and low cycle fatigue (LCF) properties.

Finite element analysis was used extensively in the turbine bucket design process, being utilized for both thermal modeling (Figure 2.2.2.4-2), and aeromechanic analysis and mode prediction (Figure 2.2.2.4-3).

Stage 2 Buckets

The 9H and 7H stage 2 bucket cooling designs are identical in concept. It consists of a main cooling circuit (with a 6 pass serpentine) and a platform cooling circuit circuit, the former cooled by steam, the latter with air. The main difference between the 7H and 9H designs pertains to the higher centrifugal loads of the 7H machine, with larger load carrying cross sectional areas as the radial cross sections get closer to the machine centerline and rotational axis. Rig tests, both static and rotating, have been used to prove out and validate the cooling concepts under similar conditions i.e. Reynolds numbers, Prandtl numbers, rotation and buoyancy

Stage 3 and 4 Buckets

The 9H and 7H stage 3 bucket cooling designs are identical tip shrouded designs typical of GE industrial gas turbine last stage buckets. Cooling air extracted from the compressor is delivered through the turbine case, through the third stage nozzle and then delivered into the rotating blade row via an inducer. The buckets themselves are cooled though radial passages machined through the airfoil exiting at the tip. The stage 4 buckets represent an additional stage to typical GE machines and is an uncooled, longer airfoil, tip shrouded bucket. Again, the main difference between the 7H and 9H designs pertains to the higher centrifugal loads of the 7H machine, requiring larger load carrying cross sectional areas as the radial cross sections get closer to the machine centerline and rotational axis.

Major Design Challenges

Aeromechanics

It was found that for the 9H during the FSFL pre-shipment test in Grenville, SC, that the 7^{th} and 8^{th} modes of the 1^{st} stage buckets were fairly responsive to a 2X engine order of the nozzle vane wake stimulus. The response was judged acceptable for further testing at FSNL conditions. An analysis was conducted to compute the response under full load and design point temperature operating conditions by coupling the computational fluid dynamic analysis to a forced response modal analysis to compute the levels of structural strain at full load. Extensive reviews concluded that operation for full speed and full load operation could continue, and that the expected strain levels would be acceptable. Moreover, it was also found that the margin to the 2^{nd} torsional mode of the stage 1 bucket was less than desired. The commercial replacement 9H stage 1 buckets, as well as the 7H stage 1 buckets, incorporated the results of FSNL test data reduction by incorporating design features for improved avoidance of these modes (2^{nd} torsion and 7^{th}

and 8th modes identified as 4th flex and 1st three stripe respectively). Similarly, the stage 2 buckets of the 7H were found to have inadequate margin between the 2nd torsion mode and the upstream nozzle passing frequency. Redesigns were initiated which improved these margins.

Mechanical Design

The 7H and 9H stages 1 and 2 buckets, being on the same disk rim radii, but with the 7H operating at 20% higher rotational speeds, introduces a mechanical design challenge for design engineers to keep centrifugal load induced stress levels to acceptable levels while keeping overall bucket weight as low as possible (i.e. keep the disk rim loads manageable). Three dimensional finite element analyses and sub-modeling were used extensively to ensure that stress levels were kept within acceptable limits. Optimization studies using GE Six Sigma tools were employed to keep a balance between bucket overall weight, bucket stress levels, and aeromechanics responses.

Joining Technology and Joint Design

Investment casting of turbine blading with ceramic cores requires that cores have sufficient support within the shell system so that the cores can withstand wax injection pressures and pressures developed during the pour of molten metal during investment casting. This requires therefore that all openings used to hold the ceramic cores be closed subsequent to casting. This necessitated the development of brazing, and other proprietary joining technologies to ensure crack free weld and braze joints required by having a closed circuit cooling system. These joining techniques are used to close the openings shown on Figures 2.2.2.4-4, and 2.2.2.4-5.

Wall Thickness Dimensional Control

Keeping wall thicknesses in the airfoil within specified limits is necessary and essential for keeping through the wall temperature gradients and thermal stresses within design limits. The core designs were closely coordinated with HOWMET to maximize the stability of the cores at casting temperatures, and to maximize production of airfoil wall thicknesses within the desired limits.

Platform Cooling Design

At high turbine inlet temperatures, bucket platforms are subject to high thermal stresses. Management of thermal stresses to prevent thermal fatigue at platforms has become necessary at the ATS machine inlet temperatures. The 9H stage 1 buckets used for the FSFL pre-shipment test incorporated a single jet impingement backside cooling with film coverage from the discharged air. An improved cooling concept that uses bypass steam bled from the main coolant passage to cool the platforms is present in both the 7H and 9H production designs. Similar to the FSFL pre-shipment design, shank cavity air will be discharged as air film for additional cooling of any remaining hot spots. The 7H and 9H stage 2 buckets incorporate cooling schemes involving air. For the 7H, a single jet impingement concept is utilized, while for the 9H, a baffle plate impingement concept will be used.

Summary/Conclusions

- The 9H bucket design concepts were successfully tested through two rounds of full speed, no load test at the Greenville, SC factory without any major issues. Minor issues involving the stage 1 bucket response for three stripe and fourth flex modes to 2X nozzle passing excitation precipitated redesigns of the commercial replacement hardware for avoidance of frequency crossings.
- Extensive analysis and reviews were carried out to ensure that continued operation with the hardware installed for no load tests would have no issues at full load testing at the 9H launch customer site.
- The bucket designs have completed the detail design phase. Product definition for the construction of investment casting tooling has also been completed.
- Casting tooling (i.e. wax patterns and core dies) have been completed on the four steam cooled bucket designs.
- The 7H completed no load testing in February, 2000. The 7H production stage 1 buckets have completed the first round of casting trials at the supplier.
- Sufficient frequency margins have been designed into the 7H steam cooled buckets to preclude aeromechanics issues for the upcoming additional no-load and full load testing of the 7H.

Technology Application

The design and development of turbine buckets are required for the ATS turbine to ensure that the buckets deliver power to the turbine shaft and that they meet the stated part life requirements.

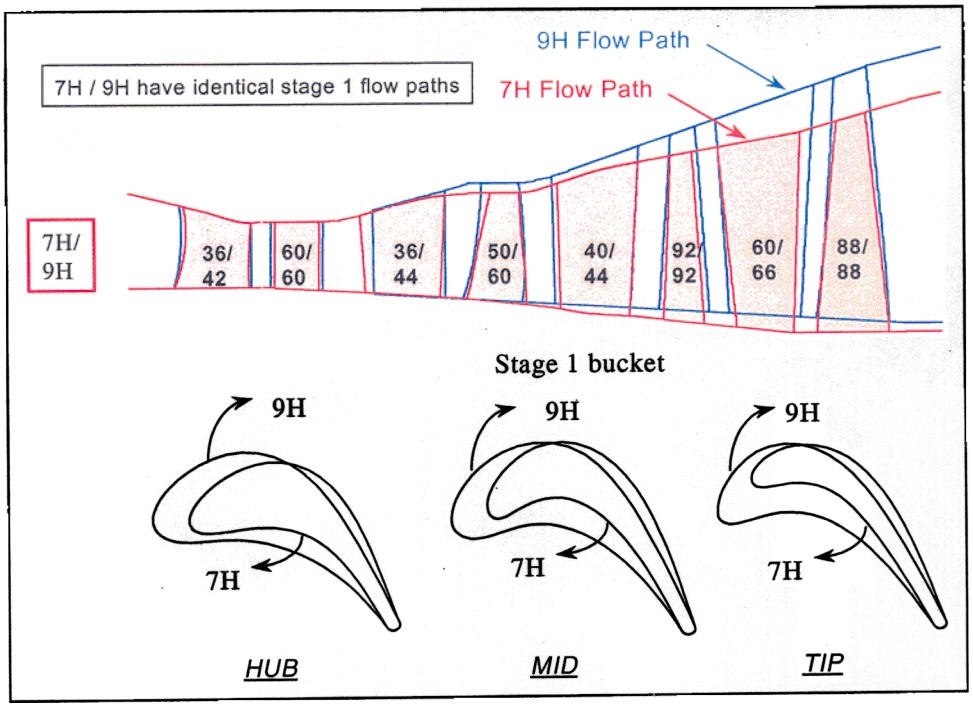

Figure 2.2.2.4-1. Comparison of 7H and 9H Flowpaths and Stage 1 Bucket Profile Comparison

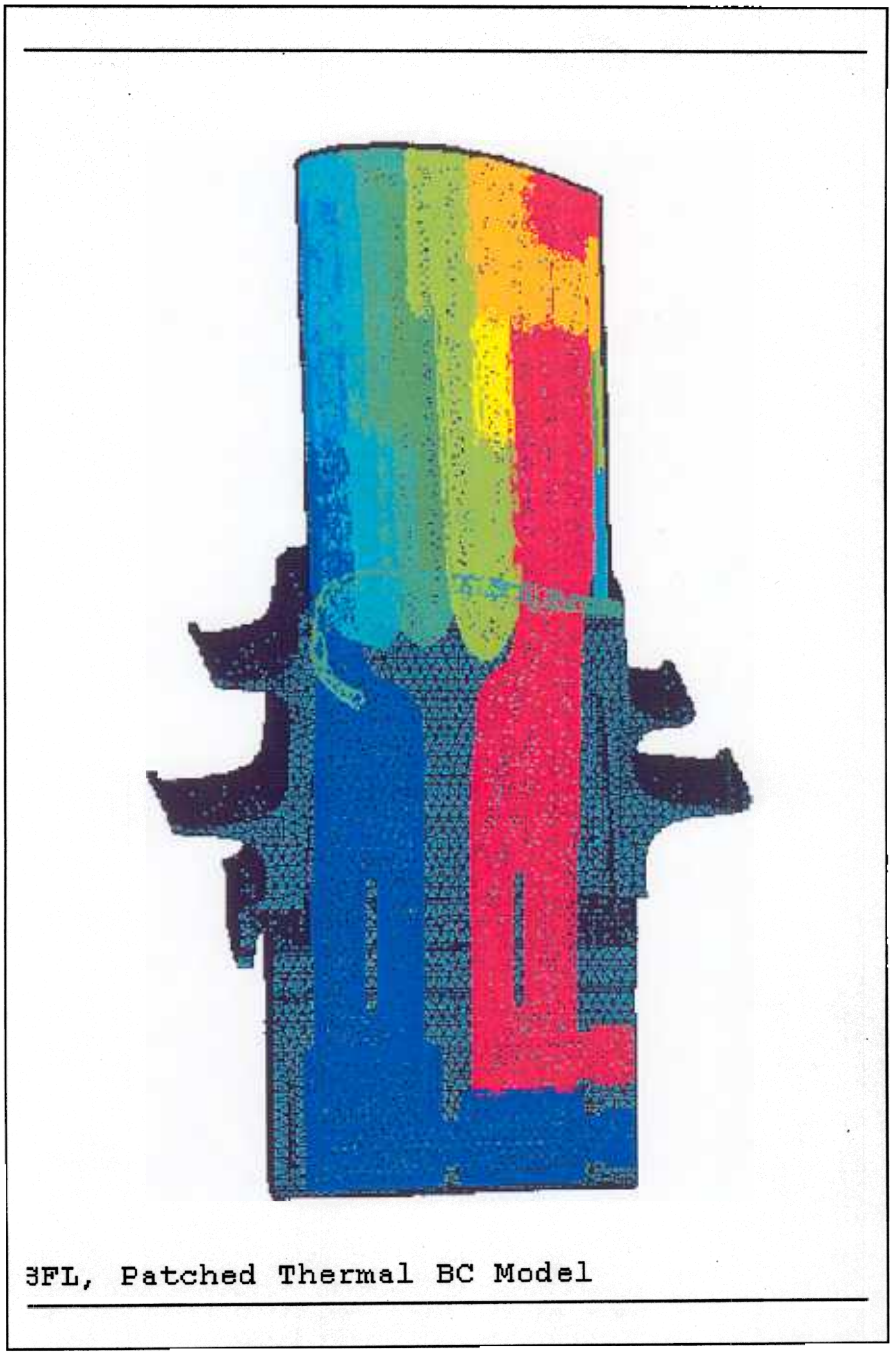

Figure 2.2.2.4-2. Representative Finite Element Modeling – Stage 1 Bucket

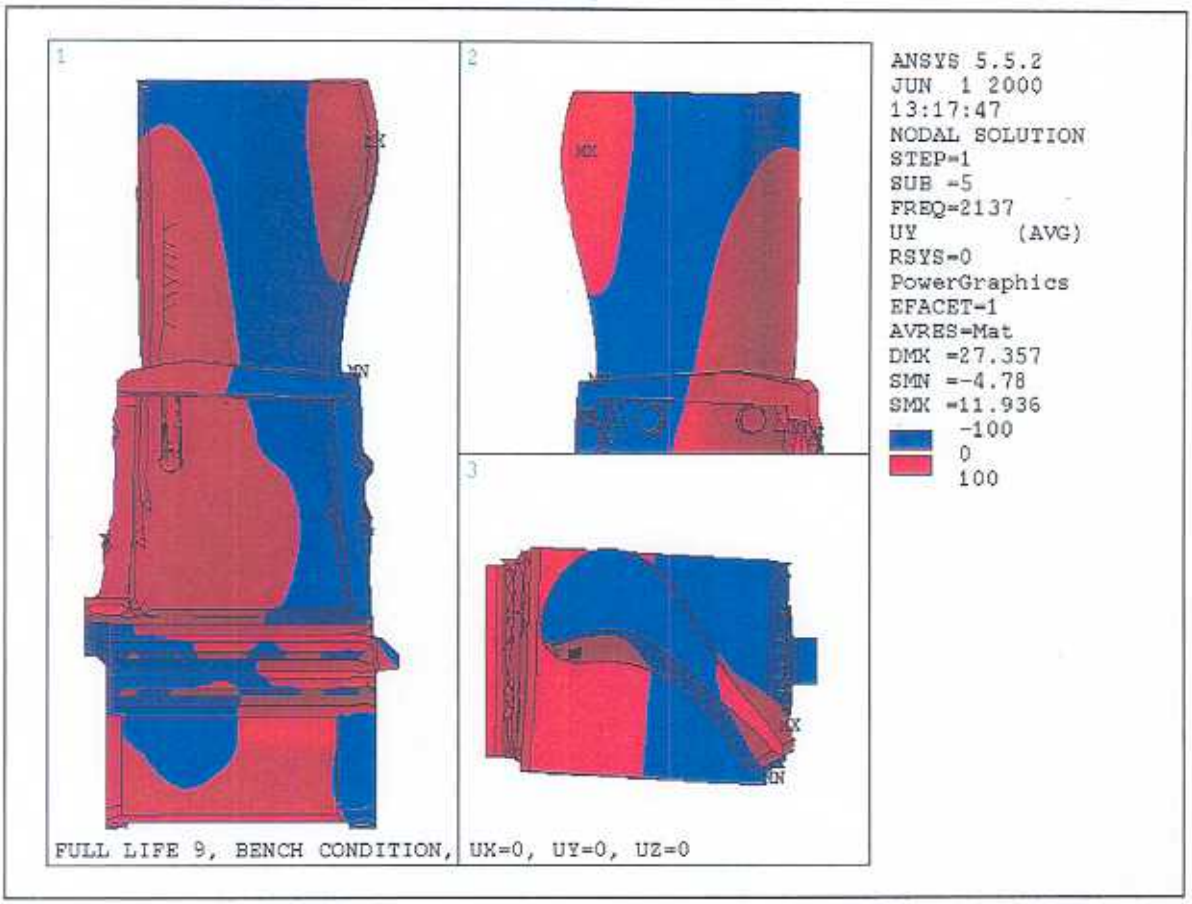

Figure 2.2.2.4-3. FEA Dynamic Analysis of Mode Shapes

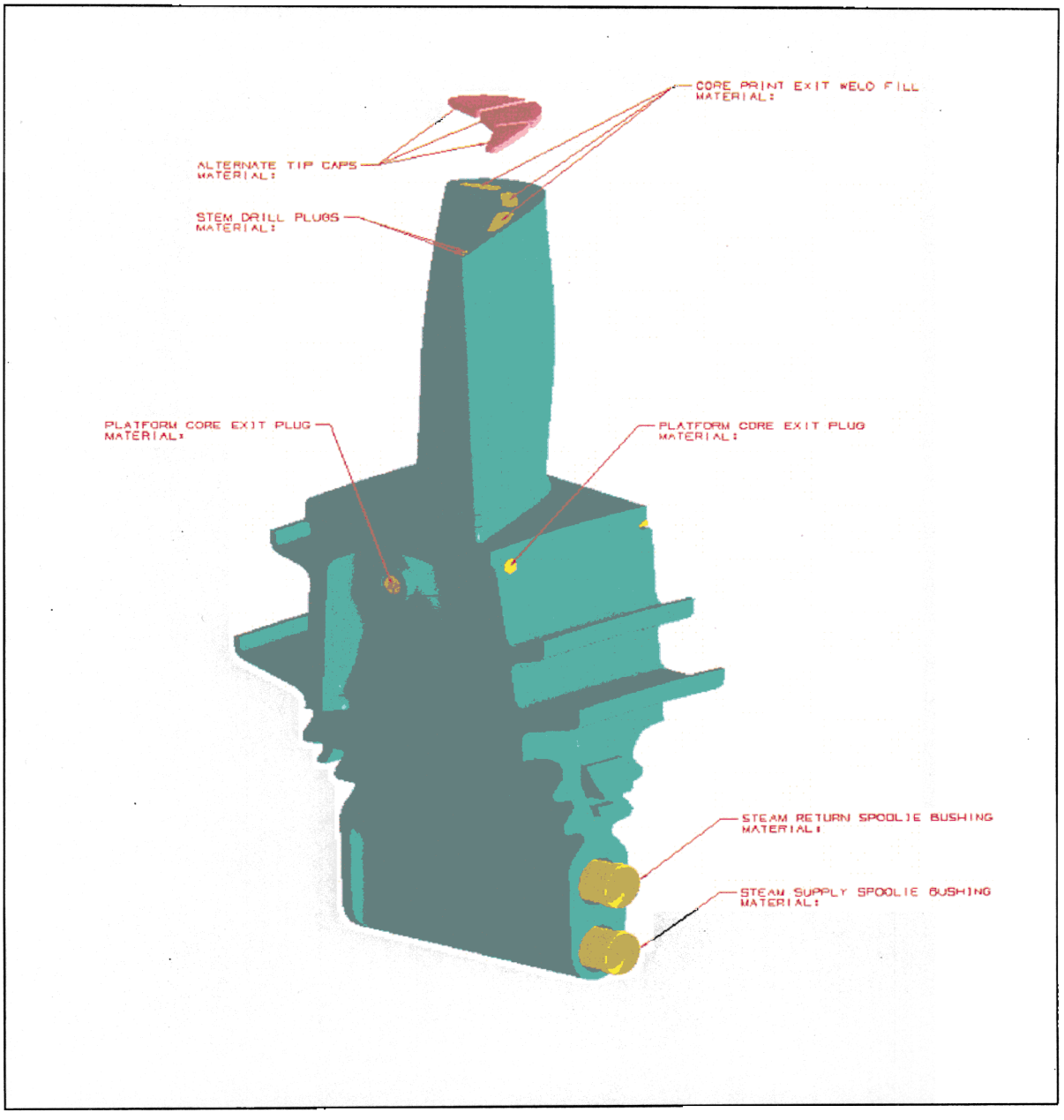

Figure 2.2.2.4-4. Bucket Joining and Assembly for 7H Stage 1 Bucket

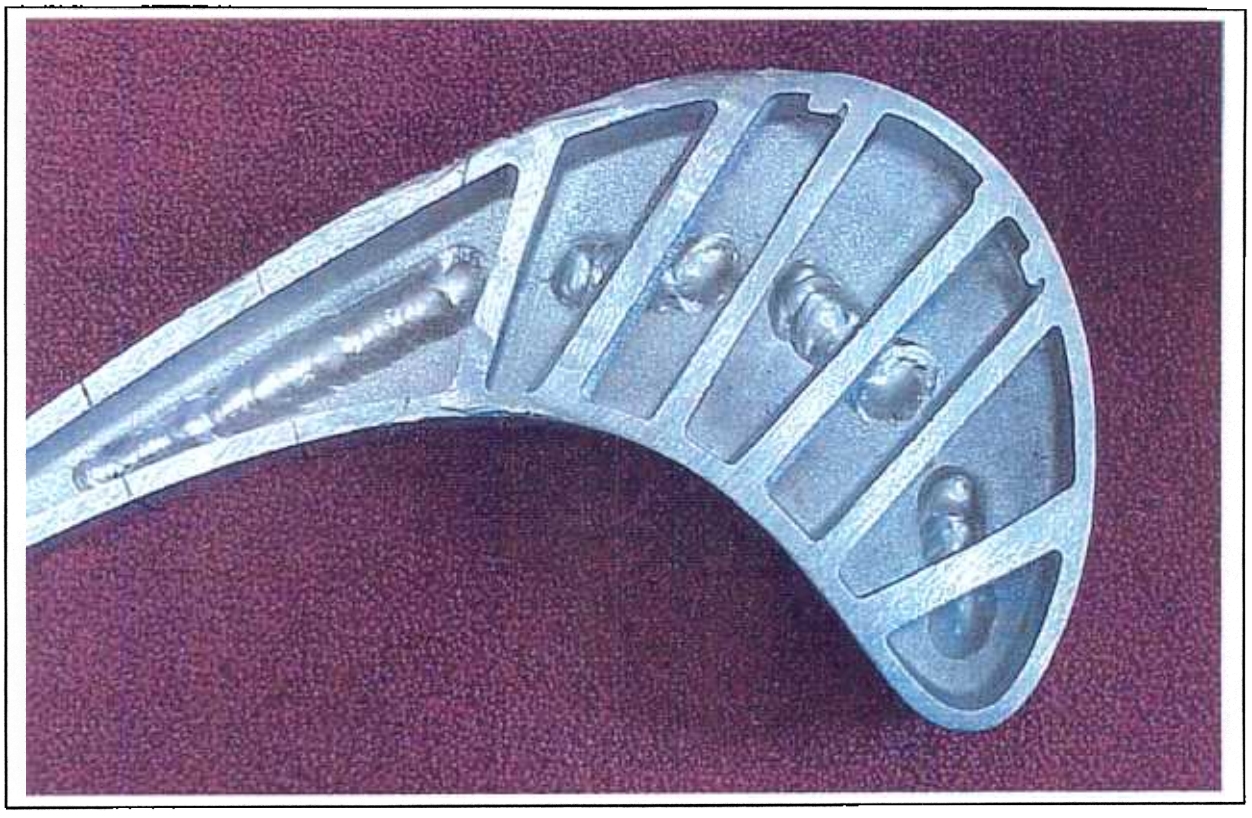

Figure 2.2.2.4-5. Tip Hole Closure Using GE Proprietary Welding Technology

Section 2.2.2.4.1 (GTFFTB) S1B and S2B Wheel Dovetail Analysis [S]

Objective

The objective of this task is to perform 3D thermomechanical analyses of ATS gas turbine rotor dovetails, bolt holes, and steam-cooling holes. The dovetails are highly stressed and, in addition, there are severe thermal gradients in the dovetail region. Detailed 3D stress analyses are required to ensure that the dovetails and the wheels meet design guidelines.

Introduction/Background

Wheel dovetails are highly stressed, and have severe thermal gradients. Detailed 3D finite element analyses are required to ensure that the dovetails , wheels, and buckets meet GEPS design guidelines.

Discussion

A detailed 3D finite element model of a 9°sector of the second-stage wheel was built. The wheel sector model contained approximately 28,000 brick elements. The finite element model of the bucket contained approximately the same number of elements, and included thebucket internal cooling channels.

A 3D steady-state thermal analysis of the assembled wheel/bucket was performed as a coupled thermomechanical analysis. The mechanical loading was due to the centrifugal effects. The thermal boundary conditions were applied on all external surfaces, as well as on the internals of the bucket cooling channels. The thermomechanical coupling was used because of the heat transfer from the bucket to the wheel.

Effective and principal stresses were plotted for mechanical as well as steady-state thermomechanical loadings. The areas of focus in the buckets were in the dovetail region. The stresses due to the centrifugal loading were further increased by the thermal stresses due to the temperature difference between the cooling steam on the input and output side. On the wheel, the areas of focus were in the dovetail, in the dovetail slot bottom, and at the center of the bolt hole.

Summary/Conclusion

Results indicate that the dovetails and wheelposts are serviceable for the duty expected. Subsequent FSNL test data analysis verified this dovetail/wheel/bucket design.

Technology Application

The dovetails were highly stressed and, in addition, there were severe thermal gradients in the dovetail region. Detailed 3D stress analyses were required to ensure that the dovetails and the wheels meet design guidelines for the ATS turbine rotor.

Section 2.2.2.4.2 (GTFFTB) S3B and S4B Tip Shroud Design Optimization [C]

Objective

The objective of this task was to optimize stresses and creep deflections in the 9H third- and fourth-stage bucket shrouds. Detailed 3D bulk creep analyses were needed to ensure that the stresses were within the required limits for creep life.

Introduction/Background

The integral bucket tip shroud contributes to the damping of vibratory stimuli, as well as forms the outer boundary of the gas path. High temperatures and stresses in this region have led to the need for full 3D bulk and/or local creep analyses of the bucket tip shroud to avoid large deflections or deformation that could result in shingling or curling. The

amount of strain in the tip shroud, the rupture limit of the material, and the radial displacement of the tip shroud determine creep life acceptability.

Discussion

The ATS third- and fourth-stage buckets were analyzed, and the stresses in the shrouds were compared with the stresses in a bucket that has been running in a customer engine for an extended period of time (the "reference" shroud). The third-stage bucket shroud was analyzed in 1996, but at that time, the analytical model did not include a full-length model of the airfoil. This was corrected in the present analyses. The ANSYS models for the buckets contained 15,000-20,000 3D hex elements each. The number of elements had to be limited because of the time that would be consumed in 3D creep analyses.

The correct boundary conditions between buckets at the shroud/shroud contact were determined. Four different boundary conditions were examined, from no contact at the shroud/shroud contact area to modeling three consecutive contacting buckets with no friction in the contact areas. Elastic analyses of the three buckets were performed with all four boundary conditions. The results showed that the ATS fourth-stage shroud had higher stresses than the reference shroud. However, since the fourth-stage shroud is operating at a lower temperature than the reference shroud, the stress levels were acceptable. The stresses in the third-stage shroud were relatively high and the shroud is operating at a relatively high temperature. It was therefore recommended to Engineering Design that the height of the rail on the third-stage shroud be increased.

Additionally, 3D local creep analyses were completed for the 7H stage 3 buckets (Figure 2.2.2.4.2-1) and completed for the 7H stage 4 buckets.

Summary/Conclusion

The 9H Stage 3 and 4 bucket tip shroud designs were optimized to meet bulk creep life requirements. Results of the 9H design have been incorporated into the 7H Stage 3 and 4 buckets, and detailed 3D local creep analyses were utilized to confirm and optimize creep life capability.

Technology Application

The analyses performed in this task were incorporated into the shroud designs of the 7H and 9H ATS gas turbine third- and fourth-stage buckets.

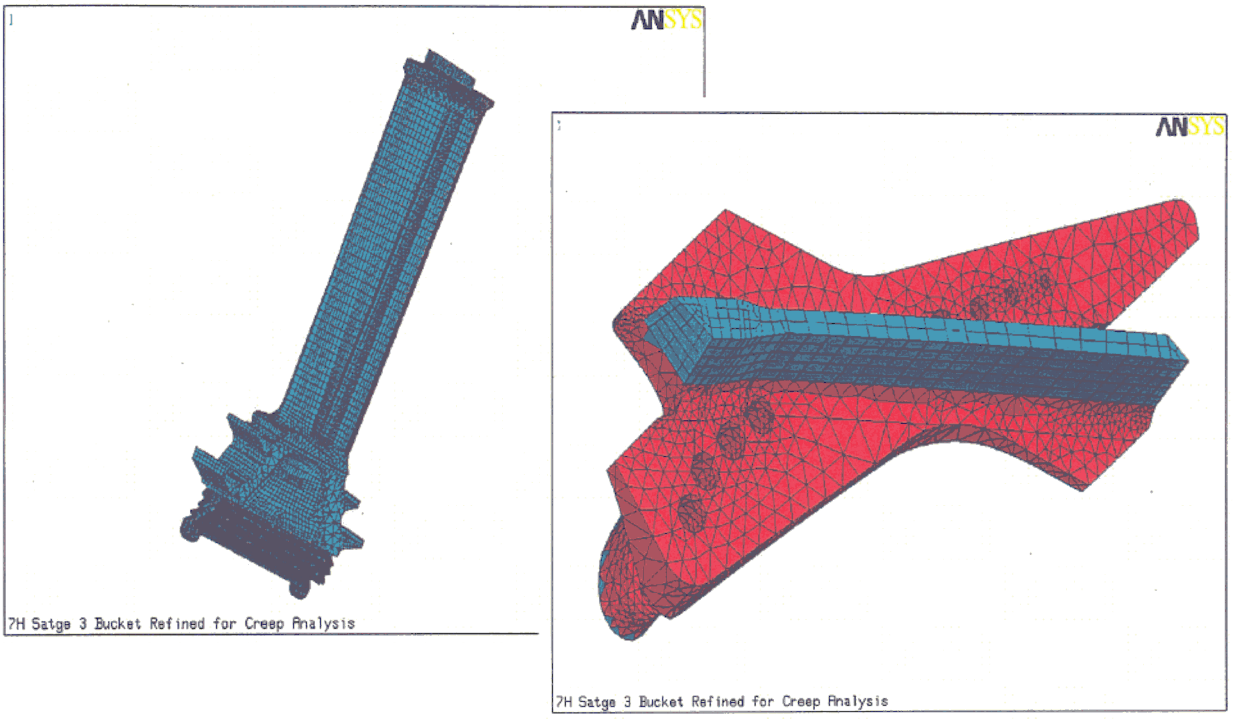

Figure 2.2.2.4.2-1. 7H Stage 3 Bucket Local Creep Analysis Model

Section 2.2.2.4.3 (GTFFTB) Bucket Wide Grain Sensitivity Analysis [C]

Objective

The objective of this task was to show the effect on natural frequency of the variations in grain size and orientation of 9H fourth-stage buckets. If the variations in natural frequency could be shown to be non-critical, bucket yield would be improved.

Introduction/Background

When a single wide grain is present in a directionally solidified (DS) casting, it can make the casting behave more like a single crystal than a DS, multi-grained, casting. In a DS casting, the transverse material properties reflect the multi-grain structure of the material and are a weighted average of the off-axis properties of single crystal material. When a single wide grain dominates the others, the properties of the material approach those of the dominant grain and can deviate significantly from the DS properties. This has the potential for changing the natural frequencies of the bucket.

Because of the variations that can occur, limits are placed on the number, size and orientation of the grains. Buckets that fall outside the proscribed limits are scrapped, resulting in a very costly addition to the total manufacturing cost of the turbine.

Discussion

In order to determine the effect of wide, or dominant, grains on bucket natural frequencies, an analytical design of experiments (DOE) was developed and carried out. The baseline case represented the extreme edge of what would be accepted under the existing specification. A five-grain ANSYS model was used to examine several cases. Three effects were studied: 1) grain size and distribution, 2) dominant grain secondary orientation, and 3) off-axis primary orientation. The grain size and distribution in the model were selected based on data supplied by the casting vendor.

Thirteen cases were analyzed spanning the expected variations in location of the single large grain, the physically real, bounding, secondary orientations, and 15-degree primary orientations. The large grain size was fixed at 40% of the chord width at the root. One of these cases was the baseline DS bucket. Eight cases were 0-degree and 45-degree secondary orientations of five evenly distributed grains, one large grain at the leading edge, one large grain at the trailing edge and two large grains: one at the leading edge and one at the trailing edge. The remaining four cases were 15-degree primary orientations of the five evenly distributed grains toward the leading edge, trailing edge, pressure side and suction side.

The methodology used in analyzing the bucket was:

a. Apply the five grain material distribution to the baseline mesh.
b. Apply the appropriate material orientations to each grain in the airfoil and shank.
c. Conduct the analysis.
d. Post Process in order to obtain natural frequencies and mode shapes.

Various ANSYS macros were written in order to perform the above step.

Summary/Conclusion

The results of this study show that the variations in the natural frequency response of the 9Hbucket are accepatable given the variations in the casting process that lead to wide grains and non-zero secondary and primary orientations. Results of this study are published in a n internal GE CRD Final Report, dated September 30, 1996.

Technology Application

The results of this study were used to relax grain width requirements on the 9H gas turbine buckets significantly improving bucket yield.

Section 2.2.2.4.3.1 (GTFFTB) Bucket Robust Design and Life Assessment [S,C]

Objective

The objective of this task was to use finite element analysis and Design of Experiments (DOE) techniques to quickly estimate bucket life, identify optimized bucket critical-to-

quality criteria (CTQs), and statistical distributions of bucket CTQs given statistical distributions of bucket parameters. The main reason for doing this work was to obtain robust bucket designs that are minimally sensitive to manufacturing tolerances and will therefore meet all life requirements.

Introduction/Background

A method was required for designing steam cooled buckets that would produce hardware that met life and performance requirements, while being minimally sensitive to manufacturing tolerances, thus maximizing production casting yields.

Discussion

The DOE analyses for the first-stage bucket robust design and life assessment, and second-stage bucket life assessment were completed. The factors included in the DOE analyses were: metal wall thickness, airfoil TBC thickness, bond coat thickness, TBC thickness in the leading edge, secondary orientation angle, primary orientation angle about the axial axis of the machine, and primary orientation angle about the tangential axis of the machine. These DOE analyses yielded prediction equations for alternating pseudo-stress, temperature, and low cycle fatigue (LCF) life in a spreadsheet-based life assessment tool that was used to assess the life of production buckets. Robust design and probabilistic analyses were performed using the first-stage bucket equations to determine optimum wall thickness and reliability curves for LCF life in critical first-stage bucket locations, given current production parameters. Similar analyses were conducted for the second-stage bucket. A series of DOE analyses that focused on increasing life in critical regions of the second-stage bucket was also performed.

Similar analyses, based on tools developed in this task, were utilized in the 7H bucket designs.

Summary/Conclusion

The robust design and life assessment of the full speed, no load (FSNL) 9H and 7H first- and second-stage buckets were completed. Successful real time lifing of castings enabled on-time shipment of the castings. Modifications to the bucket geometry, particularly wall thickness in the root fillet and shank regions, led to designs that will meet life requirements.

Technology Application

The results of this study were used on the ATS gas turbine in order to assess bucket performance, and obtain optimized factor settings and statistical distributions of the CTQs, given the distributions of the factors. The results of this study were used on the ATS gas turbine design primarily as a means of improving bucket yield.

Section 2.2.2.4.3.2 (GTFFTB) S1B Forced Response Analysis [C]

Objective

The objective of this task is to develop an engineering approach for predicting the forced response of stage 1 buckets to the excitation due to stage 1 nozzle passing frequencies. Three bucket modes are of specific interest. The resulting analysis will be applied to both Full Speed No-Load and Full Speed Full-Load operating conditions.

Introduction

Current design methodology does not require the prediction of the stains associated with the forced response of turbine airfoils from a first principles basis. Instead, natural frequencies are calculated and buckets are designed so that these frequencies are separated from known excitations expressed in terms of multiples of the machine rotational speed. However, the ability to carry out a forced response analysis based on fundamental aerodynamics does have engineering use and a situation where such a tool could provide valuable information was encountered during development of the ATS gas turbine. An 84 order aeromechanical response of the S1B was observed during FSFL pre-shipment tests. Although the response was only 30% of engineering limits at the test conditions, the question arises as to whether the response at the FSFL test conditions, which would be different, would pose any risk for the ATS gas turbine. To provide engineering information for risk assessment, a fundamental, aerodynamics based forced response analysis was formulated and carried out. The approach was applied to the test conditions associated with the FSFL pre-shipment test first and measured strain response from this test were compared with the predictions in order to assess analysis credibility. The analysis approach was also carried out using the test conditions associated with FSFL in order to assess risk in that test.

Discussion

Three potential excitation mechanisms for the response observed during FSFL pre-shipment tests were identified. These excitation mechanisms were: (1) 2x S1N count; (2)1x S1 shroud count; (3) 6x combustor count. The nozzle excitation was viewed as the most likely and was examined first. Subsequently the shroud excitation mechanism was also examined. Examination of the combustor excitation would have required data which was not available. No examination of that mechanism was undertaken.

Data from the FSFL pre-shipment tests indicated that there were two modes with substantial response (although significantly below design limits) at the operating speed of the machine. The bucket frequency of most concern is described as the 1st 3-stripe mode. This latter mode became the focus of the investigation.

The analytic procedure to examine the 2x nozzle count excitation included the following steps. ANSYS modal analysis was carried out to quantify the structural mode of interest. This natural mode of mechanical response was mapped onto the CFD grids so that modal normalized aerodynamic forces could be calculated after the CFD analysis was complete. Steady state CFD solutions for both the stage 1 nozzle and the stage 1 bucket were produced. The results from the steady-state CFD solution for the nozzle were used

to analytically define the unsteady forcing functions which this flow would exert on the S2B. Using these forcing functions, a linear perturbed response of the S2B can be established using the steady state S2B CFD solution. The nodal forces derived from this analysis can then be used in conjunction with the mechanical response mode to define the normalized modal force amplitude associated with this mode. Strain gage data from a previous test at full-speed, no-load conditions were used to estimate total damping during that test. CFD analysis at the FSFL pre-shipment conditions defined the aerodynamic damping contribution to this measured total damping factor. It was assumed that the total damping was composed of a structural damping component that was not dependent upon machine operating state and an aerodynamic damping component that was dependent on machine operating conditions but could be calculated from CFD analyses using the appropriate machine operating conditions. Once all these variables were defined, the forced response of the bucket at any geometric position could be established using the ANSYS natural mode and simple linear forced response dynamic analysis.

The first mechanism of excitation considered in this analysis was 2x-nozzle-count. The steady state solution for the flow about the first stage nozzle was accomplished using viscous flow assumptions. However, numerical difficulties prevented an adequately converged viscous CFD solution from being attained for the flow in the stage 1 bucket. Since experience has shown that without a fully converged solution for the steady bucket flow, an unsteady flow solution cannot be defined, the decision was made to use an inviscid analysis for the bucket. The nozzle flow solution, which provides the unsteady stimulus for the bucket, was still calculated with fully viscous analysis. Total modal damping for the bucket response observed in the FSNL2 test was estimated from experimental data. Aerodynamic damping levels were calculated using the CFD code and found to be small in comparison to the total damping value. As a result, it was possible to assume that the damping factor for the FSFL response was the same as that observed for FSNL2 conditions.

The bucket frequency of most concern is described as the 1st 3-stripe mode and is excited at the operating speed of the machine. Using the modal response associated with this frequency, the unsteady flow solution derived from the CFD analysis and the experimentally estimated damping factor, the forced response of the S1B at FSNL2 conditions was calculated and compared to measured strain response from the FSNL2 tests. The response predicted by the CFD analysis was found to be 1/13 the mean value of the measured bucket response in the FSFL pre-shipment test. A similar prediction was made to determine the expected response at FSFL conditions. Although the response was predicted to be 3.8 times higher at the FSFL test conditions, the large discrepancy between prediction and observed response at FSFL pre-test conditions led to the conclusion that there is not enough evidence to believe that the 2x-nozzle-count excitation is driving the observed S1B response.

A CFD based analytical procedure was also devised to assess the possibility of excitation due to 1x-shroud count excitation. The assumption behind this driving mechanism is that the shroud shape will deviate from a perfect cylinder, especially at FSFL pre-shipment test operating conditions. Based on measurements of the noncircularity of the shrouds at these conditions, the analysis based on shroud excitation predicted a modal response of the S1B at these conditions that was ½ to 5/8 of the mean measured response of the

bucket. Although the analysis is not standard, this prediction is much closer to the observed response during FSFL pre-shipment testing. The expected response at FSFL due to this shroud excitation mechanism is predicted to be smaller than at pre-shipment test conditions for two reasons. First, for the same deviation from circularity, the CFD analysis predicts that the response at FSFL would be lower. Second, at FSFL conditions, the deviation of the shroud shape from circularity is also less, and as a result the response is also expected to be diminished.

Summary/Conclusion

An analytic procedure was developed to predict the forced response of the S2B in the first 3-stripe mode from fundamental aerodynamic mechanisms. Excitation from mechanisms associated with 2x nozzle count and 1x shroud count were examined. When compared to measurements taken during the FSFL pre-shipment test, the response from the 2x nozzle count excitation was small. Although the response at FSFL conditions was predicted to be over 3 times higher, those levels would not be an issue based purely on the analytic results. The analysis of 1x shroud excitation produced results that were much closer to observed response during the pre-shipment tests. This response was predicted to be less significant at FSFL operating conditions.

Technology Application

A successful methodology of predicting forced response of turbine buckets will allow a priori prediction of response at arbitrary machine operating conditions and provide an engineering tool for risk assessment. The results of this analysis provide experience in validating such an engineering approach. The results were also used for risk assessment of aeromechanical response of the S1B during the FSFL test.

Section 2.2.2.4.4 (GTETIH) Bucket Tip Treatment Heat Transfer [C]

Objective

The bucket tip regions of the ATS turbine remain a critical design issue affecting both turbine performance and life. Since the blades utilize no external film cooling, a tip design must be verified that minimizes both the tip hot gas leakage and the tip external heat loading, while also providing some shroud rub protection for the internal steam-cooling circuit. Standard squealer tip geometries are thought to provide inadequate rub protection and can be difficult to cool without film, while a plain tip geometry will not provide adequate leakage sealing.

This task continued design verification and design improvement for the first- and second-stage blade tips. A blade tip heat transfer cascade was used with new or modified blade tip geometries to design and verify the appropriate tip heat transfer and seal arrangements in conjunction with manufacturing and cooling requirements. Specifically, this task determined the external heat transfer coefficient distributions on the blade tip and on the airfoil surface near the blade tip using steady-state liquid crystal techniques in a blade tip cascade.

Introduction / Background

While decades of research have been dedicated to the study and development of efficient aerodynamics and cooling techniques for turbine airfoils, there remain regions which retain a somewhat more uncertain design aspect requiring more frequent inspection and repair. One such region particular to high-pressure turbines is the blade tip area. Blade tips are comprised of extended surfaces at the furthest radial position of the blade, which are exposed to hot gases on all sides, typically difficult to cool, and subjected to the potential for wear or even hard rubs against the shroud. The sensitivity of turbine efficiency to blade tip clearance can be significant, causing a strong desire on the part of the designers to improve efficiency by decreasing tip-to-shroud operating clearances, or by implementing more effective tip leakage sealing mechanisms. There are several blade tip designs in current use within the industry, including flat unshrouded blade tips, unshrouded tips with various forms of squealer rims, and shrouded blade tips (attached shrouds). No matter the design choice selected for any particular turbine blade tip, a detailed knowledge of the flow field and tip heat transfer is required to achieve the proper balance of elements for efficiency with durability. The flow in and around turbine blade tips has been under investigation much longer than the heat transfer aspects, spurred by its great impact on efficiency for both turbines and compressors. Heat transfer on turbine blade tips has been a subject of consistent research over the past fifteen years. For the parameter ranges tested, the average tip heat transfer has been found to be only a weak function of the rotational speed; i.e., the average heat transfer was mainly determined by the pressure driven flow through the tip gap. Far more limited experimental data have been reported in either stationary or rotating cascade environments.

Previous to the present work, no full-surface heat transfer distributions have been obtained for blade tips. Due to the increased sensitivity of the ATS turbine, which utilizes no film cooling for the bucket tips, it is considered crucial to provide full-surface data on tip heat transfer for design purposes.

Discussion

Texas A&M University Blade Tip Cascade

During the first year of this task, 1996-7, CRD and Texas A&M University worked together to design and fabricate a blade cascade facility in the University's Turbomachinery Laboratory. Texas A&M University constructed a blade tip cascade to model the tip heat transfer for the first-stage blade of the ATS turbine. The cascade was composed of two flow passages and three airfoils scaled so that the appropriate Reynolds number and Mach number distributions would be obtained. Heat transfer testing was based on transient liquid crystal methodology, using a blowdown test capability. During 4Q96, 1Q97, and 2Q97, Texas A&M concentrated on completion of the required test scope from 1996, including tip heat transfer for two geometries with high and low freestream turbulence intensity, near-tip surface heat transfer, shroud pressure measurements, and freestream turbulence intensity measurements. The final report for the work performed at Texas A&M was completed. This effort was concluded with the attainment of test results for tip heat transfer coefficients. Texas A&M provided two sets of tip heat transfer results for two geometries at two freestream turbulence intensity levels. The Texas A&M project was not continued by CRD due to lack of confidence in

the technical results. This stemmed from two sources. First, the application and calibration of the liquid crystal surfaces was not believed to be controlled to the degree required for high quality data. Second and most importantly, the design of the heated test airfoil was such that the initial thermal gradients within the pre-flow airfoil tip were as much as 25 C from leading edge to trailing edge, causing a violation of the required thermal boundary conditions for the test methodology being employed.

CRD Blade Tip Cascades

During 1997-8, a rebuilding of the Texas A&M cascade within CRD's test facilities was completed and tested. This cascade (Figure 2.2.2.4.4-1) includes features added for more flexibility in testing. To avoid problems encountered in the past with flow and thermal boundary conditions, this blade tip cascade uses a steady-state heat flux method with surface heaters to establish the heat transfer conditions rather than the transient blowdown method used by Texas A&M.

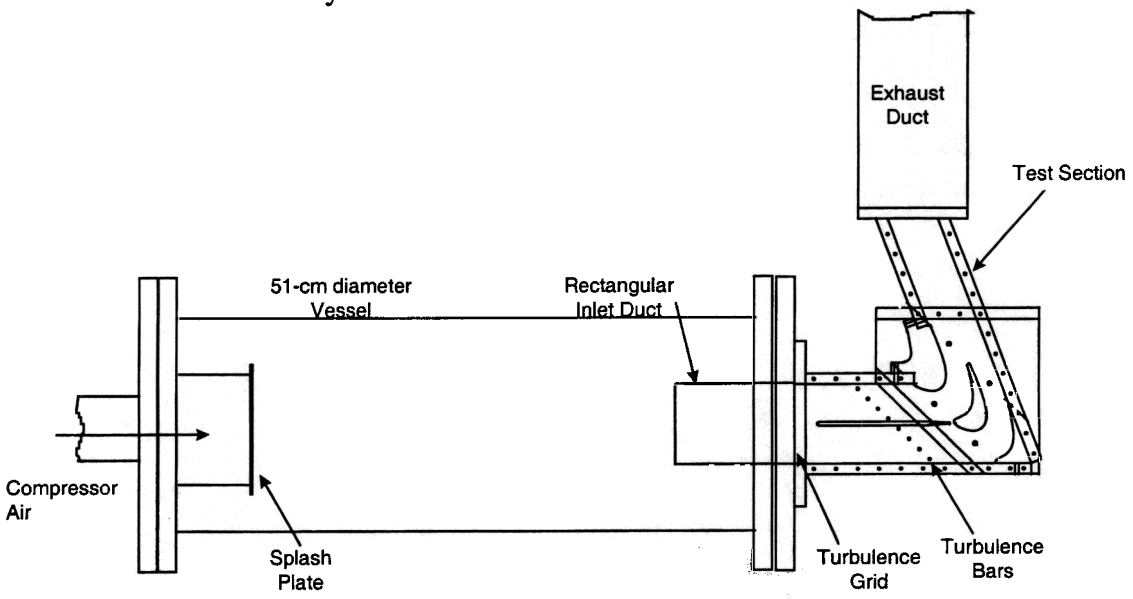

Figure 2.2.2.4.4-1. Blade Tip Cascade Rig

All planned testing for both pressure and heat transfer distributions was completed using the rig show. Pressure distributions were obtained around the profile of the center test airfoil at both the midspan and very close to the tip gap. The pressure profile without a tip gap clearance is very close to the design intent for this bucket section, while the pressure profile with a nominal tip gap clearance shows a more aft loaded aerodynamic profile indicating higher leakages in the aft regions as would be expected. Further pressure distributions were obtained on the tip surface for nominal, as well as lesser and greater, tip clearances. Distributions were also measured on the opposing shroud surface. All pressure results showed a heavy loss as the flow enters the tip clearance, followed by a recovery prior to exiting on the suction side of the tip.

Heat transfer measurements were made using the steady-state liquid crystal technique. An etched foil heater was used to provide a uniform heat flux. Heater local temperatures were measured using a Mylar-backed 0.005-inch-thick liquid crystal sheet applied over the heater with a thin layer of adhesive (0.001 inch). The liquid crystal used was Halcrest

R40C5W, which was calibrated for hue vs. temperature. An RGB camera was used to take both calibration and test images, and the results were reduced to temperatures. A wattmeter was used to measure heater power. The temperature drop through the adhesive and Mylar was then calculated to obtain airfoil tip local temperatures. Heat transfer coefficients were measured on approximately 75% of the flat surface of the blade. A heat loss test was performed and the loss into the airfoil was approximately 8 to 10% of the total power into the heater. All results were corrected for this loss.

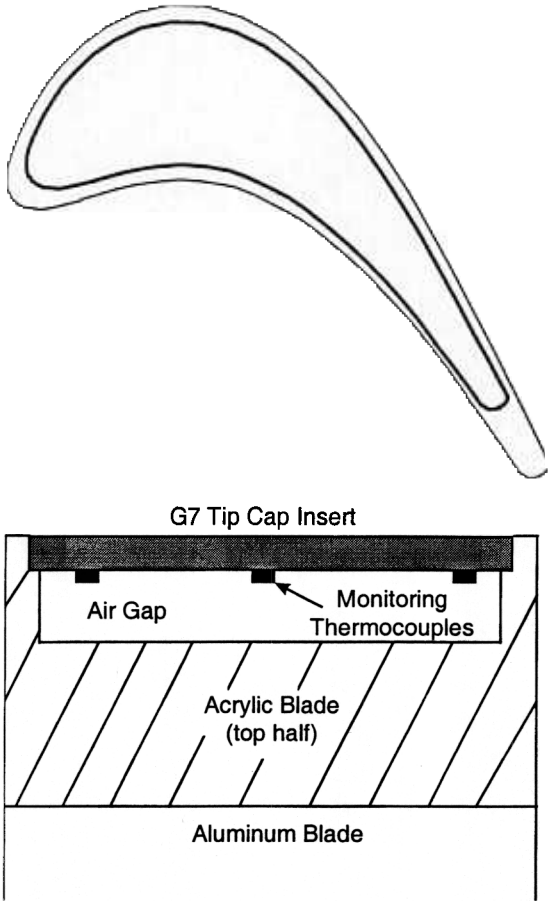

Figure 2.2.2.4.4-2. Blade Tip Cascade Cross Section

A smooth radiused edge (R.090 inch) blade tip was tested as well as four alternative tip seal geometries. Heat transfer coefficients varied slightly with tip gap in the leading edge region of the blade but converged near the trailing edge. The heat transfer and pressure measurements for the tip seal geometries (Figure 2.2.2.4.4-3) showed improvements in leakage and a reduction in heat transfer. A smooth square-edged blade tip and two alternative tip seal geometries were tested and the results compared with the results obtained earlier with the radiused smooth tip.

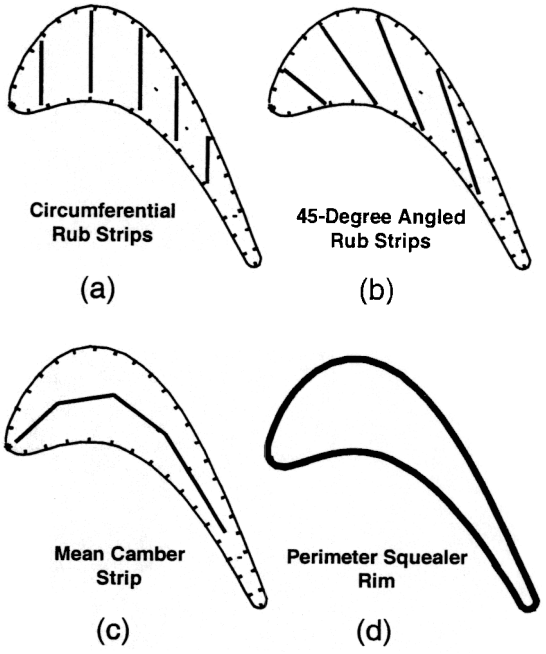

Figure 2.2.2.4.4-3. Tip Seal Geometries

The results may be summarized as follows: (1) A square-edged smooth tip blade had a reduction in leakage but higher heat transfer coefficients. (2) The first alternative geometry, a full perimeter squealer of a height equal to half the nominal tip gap, had a reduction in leakage but a slight increase in heat transfer values. The increase in heat transfer appeared to be due to the flow reattaching on the blade tip. (3) The second alternative tip sealing geometry had a reduction in leakage and heat transfer coefficients. All details of these tests and results may be found in two references which have been published:

Bunker, R.S., Bailey, J.C., and Ameri, A.A., 1999, Heat Transfer and Flow on the First Stage Blade Tip of a Power Generation Gas Turbine Part 1: Experimental Results, *Journal of Turbomachinery*, Vol. 122, pp. 263-271.

Bunker, R.S. and Bailey, J.C., 2000, Blade Tip Heat Transfer and Flow with Chordwise Sealing Strips, *Fourth ISHMT / ASME Heat and Mass Transfer Conference*, Pune, India.

During 1999, a second blade tip cascade was constructed and tested which more nearly represents the thinner aerodynamic sections of the Stage 2 Bucket. The entire facility was designed and fabricated in a similar manner to that described above. Tip treatments, however, were restricted to chordwise features due to the smaller tip area involved. The second cascade rig is shown in Figure 2.2.2.4.4-4.

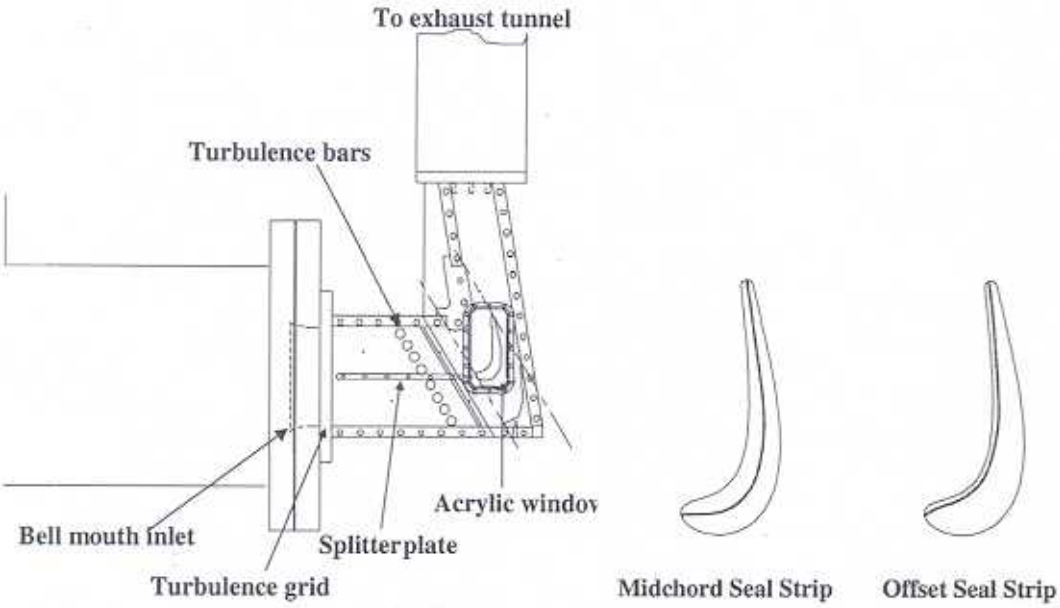

Figure 2.2.2.4.4-4. Stage 2 Bucket Tip Cascade

During this test series it was determined that a simple midchord sealing strip provided good reduction of tip leakage flows as well as a reduced heat loading on the tip. A typical lab-scale test result for heat transfer coefficients is shown in Figure 2.2.2.4.4-5 with a midchord seal strip (W/m2/K). Details of this cascade and test results may be found in the published reference:

Bunker, R.S. & J.C. Bailey. 2000. Blade Tip Heat Transfer and Flow with Chordwise Sealing Strips. *In* Proceedings 8th ISROMAC Conference, Honolulu, Hawaii.

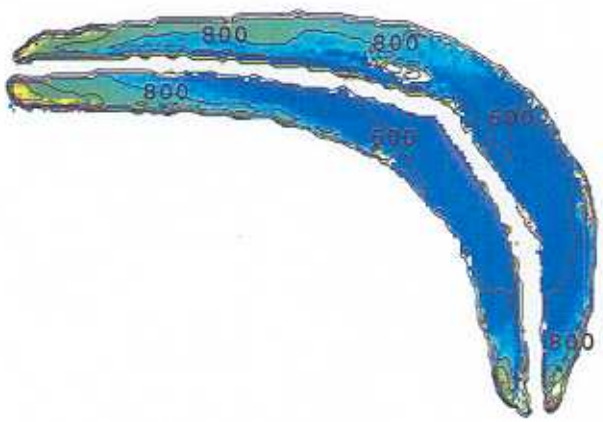

Figure 2.2.2.4.4-5. Sample Midchord Seal Strip Heat Transfer Results

Summary/Conclusion

Relative to the first blade tip cascade test series with the wider aerodynamic section representative of the Stage 1 Bucket, the following conclusions were reached:

- In this stationary cascade model, the pressures measured on the airfoil in the near-tip region form a good basis for determining the overall pressure driven tip leakage flows. Details of the pressure field on the tip surface are required to fully explain the heat transfer results, even for the simple case of a flat blade tip.
- Shroud pressure measurements agree well with the tip surface pressures in this setting, showing much the same local characteristics.
- Tip entry flow for the sharp edge case exhibits differing character at various positions along the pressure side, with a marked high entry loss region in the midchord-to-aft region. Addition of a small tip edge radius serves to redistribute this entry effect and lead to greater leakage at nominal clearance (as deduced from higher tip heat transfer levels).
- The tip geometry and flow field demonstrate a characteristic central sweet spot of low heat transfer which extends into the midchord region and toward the suction side. A pressure side entry separation vortex aft of the sweet spot creates a significant enhancement to heat transfer aft of the sweet spot. Large heat transfer coefficient gradients are observed at outlying suction side peripheral areas in the forward half of the airfoil tip.
- An increase in the approach freestream turbulence intensity level from 5 to 9% raises the overall tip heat transfer by about 10%, moreso in the aft portion of the tip (~20%) and less in the forward areas (~0%).
- The addition of a small edge radius to the tip perimeter causes the tip heat transfer to increase by about 10% in most areas, presumably due to higher allowed tip leakage flow.
- Decreasing the tip clearance C by 38% of the nominal value results in a decrease of some 10% in heat transfer, while an equivalent increase in tip clearance results in a 10% increase in heat transfer.
- Certain regions of the present tip model appear to conform to a simple pressure driven heat transfer behavior similar to that of entry flow into a sudden contraction, but with significant local modifications due to the 3D nature of the flow.
- Four configurations of tip treatments for the reduction of tip leakage flows were tested to determine the resulting tip heat transfer coefficient distributions. Tip strips designed to reduce tip leakage flow act as both turbulators and seal strips.
- Circumferential strips increase heat load to the tip by 20 to 25%, and angled strips increase heat load by 10 to 15%, over that associated with a smooth tip surface.
- Angled strips provided the lowest tip heat transfer of the tip treatment cases tested. This geometry represents a compromise between the circumferential and camberline strips.
- The perimeter squealer rim reduces overall tip heat load below the level observed with a smooth tip surface at the same clearance. Little difference in heat transfer is seen in the sweet spot, due to the large tip thickness relative to the squealer height. However, substantial heat transfer reduction is present in the midchord and aft regions where the squealer acts as the more traditional labyrinth seal.

Relative to the second blade tip cascade test series with the thinner aerodynamic section representative of the Stage 2 Bucket, the following conclusions were reached:

- The smooth tip surface demonstrates a characteristic forward sweet spot of low heat transfer. A pressure side entry separation vortex aft of the sweet spot creates a significant local enhancement to heat transfer. Large heat transfer coefficients are observed in the 40 to 80% axial chord locations where the pressure differentials across the tip are the greatest.
- Use of a simple chordwise sealing strip serves to increase the resistance to tip gap flow leakage, even when the nominal clearance above the strip is the same as that for the smooth tip surface. A strip placed near the pressure side of the tip surface provided better reduction in regional tip pressure differential.
- Location of the chordwise sealing strip can result in very different heat loads to the blade tip. The midchord sealing strip provided the lowest heat transfer coefficient distributions for this tip geometry. While the forward portion of the tip remains little altered, the high-leakage aft portions were significantly changed, apparently due to the formation of flow separation zones on either side of the strip.
- Placement of the chordwise sealing strip near the tip pressure side actually enhanced tip heat load, restricting its benefit to tip leakage reduction only.
- Alteration of the sealing strip height for a constant clearance gap dimension provided little change to either pressure or heat transfer coefficient distributions.
-

Technology Application

The results from the testing performed under this task have been used directly in the design of the first- and second-stage turbine bucket tips to improve tip performance and provide more accurate assessments of tip life. Tip sealing geometries shown to have lower heat loads and/or less gap leakage may be incorporated into the design process as permitted by manufacturing constraints.

Section 2.2.2.4.5 (GTFFTB) S1B and S2B Air/Steam Coolant Transition Analysis[C]

Objective

The objective of this task was to determine the time required for switching from air cooling to steam cooling to keep thermal stresses in the ATS gas turbine first- and second-stage buckets within acceptable levels. Three-dimensional transient thermomechanical analyses of the first- and second-stage buckets were run during the transition from air to steam cooling. Predicted temperature and stress responses were used to evaluate the effect of the coolant change on the bucket life and to recommend control system modifications, if necessary.

Introduction

Transition from air to steam cooling after the ATS gas turbine is started is a unique event with little past experience available to establish its effect on life of the hot gas path parts. This task was undertaken to provide engineering estimates of the effect of that event on the stress and life of the first and second stage turbine buckets. The analysis in this task was carried out using a new thermal analysis code, ANSYS LFE, which required benchmarking its predictions against previous calculations. After analysis benchmarking

and air-to-steam transition analysis, the models were also used to assess the thermomechanical and life effects of loss-of-steam-cooling.

Discussion

The first step in this task was to benchmark the new thermomechanical tools being applied to the analysis. The automation process for steady-state thermomechanical analyses, using ANSYS/LFE, of the ATS gas turbine first-stage bucket was completed and validated at full speed, full load (FSFL) conditions. Comparisons of temperature predictions between ANSYS/LFE and previous YFT and ANSYS iterative calculations showed good agreement. A computer program was also developed to scale the bucket external heat transfer boundary conditions (h and T). The boundary condition scaling was based on the FSFL heat transfer predictions as well as the firing temperature, core flow-rate, and air properties at the desired operating condition. This procedure was later used to generate boundary conditions for the ATS gas turbine first-stage bucket robust design activities. The analysis process was then used to evaluate the steady-state performance of the first-stage bucket at part load, where the air-to-steam transition occurs. The gas path thermal boundary conditions were obtained by scaling the FSFL convective film coefficients and temperatures, while the internal boundary conditions were evaluated using ANSYS/LFE.

The details of the air-to-steam transition process were defined using the transient cycle predictions for a cold start and the transient rotor performance. The transient rotor predictions of temperature at the bucket inlet and pressure drop across the bucket during the air-to-steam transition were used in the analyses. The bucket inlet temperatures and flow-rates were obtained from the rotor model and step-changed from the steady-state air values to the steady-state steam values. The transport properties of the internal coolant were also step-changed from air to steam at the transition time. The computed temperature distributions were used as thermal loading for structural analyses to determine the time, location, and magnitude of the peak component stress from which life estimates were made. These analyses were updated as necessary to reflect design changes as they occurred.

After completing the analysis of the first stage bucket response during air-to-steam transition, the ANSYS/LFE model was also used to predict the effect of loss of steam cooling on the bucket. Steady-state and transient thermomechanical analyses were run to evaluate the impact of reduced coolant flow on bucket performance, and to estimate the required shutdown time in the event of a total loss of coolant.

After consideration of the first stage bucket, the ANSYS/LFE model of the second-stage bucket was completed. Surface elements were created in the bucket internal cooling passages, and the LFE elements were generated. The ANSYS/LFE model of the second-stage bucket airfoil was completed and bench-marked against the design basis ANSYS model at FSFL conditions. Air-to-steam transition and loss of coolant analyses were performed.

Summary/Conclusion

The results for both first- and second-stage buckets showed that the stresses during the normal air-to-steam transients were within acceptable levels. However, proper control of this process will have to be provided if the buckets are to meet LCF life requirements. In

addition, the buckets would only survive a loss-of-cooling condition for a very brief period.

Technology Application

Results from this analysis were used to define air-to-steam transition control during startup.

Section 2.2.2.4.5.1 (GTFFTB) Loss of Steam Cooling Algorithms for Full Load Operation [C]

Objective

The objective of this task was to evolve control logic developed for the air-cooled FSFL pre-shipment test to maturity for steam-cooled full-load conditions and to complete the final code algorithms.

Introduction

Loss of steam cooling in the ATS gas turbine would be a critical event which needs to be detected and acted upon within the control logic of a steam cooled gas turbine. Appropriate control logic to rapidly detect cooling leaks above a threshold level was developed and demonstrated for air cooled operation of the steam delivery system during the FSFL pre-shipment tests. The next step in the evolution of this control logic is to define and create similar code for the actual steam-cooled FSFL operating conditions.

Discussion

The first step in this task was to reach agreement with GEPS engineering representatives upon the required algorithm updates necessary to accommodate control at normal full-speed full-load operating conditions. This discussion led to several specific goals and decisions. First, the present algorithms must be amended to operate with steam cooling. It was also decided that the algorithm will be altered to handle flow measurements made with venturi sensors as opposed to annubar. These flow measurements must be established to be accurate for either steam or air cooling. Finally, individual cooling flow fault detection algorithms will be written for stator-1, stator-2 and rotor, each utilizing a common software functional module.

Work was initiated on two subtasks: (1) revision of the backup algorithm, and (2) development of a concept to calibrate the measurement and control algorithms for commercial sites and operating conditions. Four previously developed algorithms for controlling a loss of steam event were originally assessed during FSNL testing. Two of the algorithms offer detection plus fault isolation and were designed to handle transients between operating points. The remaining two algorithms were intended to be simple and easily understood by an operator. The plan was to eventually down-select to two algorithms. An algorithm handling transients between operating points has been selected. Test results during FSNL indicated that the two original simple algorithms did not work effectively during operating point transitions. As a result, there was a need to revise one of these simple algorithms to incorporate an additional system dynamic model accounting for transients. The revisions required for this second backup algorithm have been defined. Controls and Accessory Systems Engineering will code this algorithm. A Chief Engineer's Review has been rescheduled for late August 2000. Options for calibrating

the model parameters within the algorithm have been defined and proposed. The algorithms are being prepared for test using a simulator to characterize algorithm performance under expected FSFL operating characteristics.

Summary/Conclusion

This task is ongoing at the writing of this final report and will be completed by 12/00. When complete, it will form the basis of an effective and validated method for control in the event of a loss of steam cooling event.

Technology Application

The control algorithms developed in this task will be validated at full-speed full-load conditions and used as part of the control system for the commercial product.

Section 2.2.2.4.6 (GTETEH) S1B External Heat Transfer [C]

Objective

The ATS turbine first-stage bucket is highly loaded, both aerodynamically and thermally. It is crucial that the external heat loading for this component be predicted accurately. A non-conservative design heat load may result in a low life part design, while a too conservative heat load will lead to over-utilization of steam coolant. As the heat load distribution is a major contributor to the bucket cooling design and its effectiveness, an accurate determination of the external heat transfer distribution is required to minimize the impact of other variable factors in the design.

This task was intended to provide external heat transfer coefficient distributions for the pitch section of the ATS turbine first-stage bucket. Cascade slave hardware was manufactured by CRD for installation into the Transonic Blade Cascade facility at NASA Glenn Research Center, Cleveland. NASA will perform flow and heat transfer tests with a smooth airfoil, and report heat transfer distributions at the design Reynolds number. Rough surface testing was optional in this program. This task is being carried out in conjunction with CRD's Research Alliance with NASA Lewis (no funds are exchanged in this Alliance).

Introduction/Background

While GE maintains design tools for the prediction of turbine airfoil external heat transfer coefficients, the increased importance of the external heat loading for the non-film cooled buckets of the ATS machine was felt to warrant obtaining additional experimental validation data. As part of the CRD – NASA Alliance program in Turbine Heat Transfer, it became mutually beneficial to GE and NASA to perform a heat transfer cascade test in the existing transonic facility at Glenn RC. This facility has the ability to run non-dimensional parameter tests at engine conditions using nearly the full size scale of the Stage 1 Bucket. As a consequence, the NASA facility can provide full surface heat transfer data via liquid crystal imaging while varying a number of key parameters, such as Reynolds number, angle of attack, and freestream turbulence. The opportunity for this test by NASA was not to be passed up.

Discussion

CRD's work scope for this task was completed. Fifteen solid slave airfoils for the 9H turbine first-stage bucket (midspan section) were fabricated for NASA's Transonic Blade Cascade Facility. Two of these airfoils were instrumented with an array of static pressure measurement holes. A separate airfoil mold was fabricated for NASA to make the heat transfer test airfoil. Two copper airfoil end pieces were also fabricated for NASA to be used as buss-bars for power delivery to the test airfoil heater. All required airfoil data were delivered to NASA.

As of early 2000, NASA Glenn is roughly two years behind the original schedule for this task. They have recently completed the initial test to measure the Mach number distribution for this airfoil at the design condition. The match of cascade Mach number distribution to design intent is very good. During the remainder of 2000, NASA will be concentrating on completion of the heat transfer measurements. For further information on the NASA facility and the specific type of tests to be performed, refer to the following paper:

Giel, P.W., Bunker, R.S., VanFossen, G.J., and Boyle, R.J., 2000, "Heat Transfer Measurements and Predictions on a Power Generation Gas Turbine Blade", 2000-GT-209, IGTI Conference, Munich, Germany.

Summary/Conclusion

This task is not yet finalized on the part of NASA Glenn. No design heat transfer boundary conditions can be verified until the NASA tests have been completed.

Technology Application

The results of this task will be used to verify the predicted design external heat loading for the first-stage bucket. Where the experimental results deviate significantly from the design predictions, changes in the blade coolant flow may be made to achieve a more efficient design.

Section 2.2.2.4.7 (GTETIH) Bucket Platform Cooling Model Validation [S,C]

Objective

The objective of this task was the quantification of the first- and second-stage platform cooling design, including the principal features of impingement onto a roughened surface, film extraction, and shank leakage. A scaled liquid crystal test model was designed to investigate effects of parameter ranges of the first-stage bucket, with built-in variability for the most important features. Gas turbine roughness levels were compared to smooth surface tests. CFD modeling was also performed to incorporate the effects of rotation.

Introduction/Background

The higher firing temperature of the ATS-class machines, combined with the flatter combustor exit radial gas temperature profiles of power turbines, is necessitating the use of active cooling for the turbine Stage 1 Bucket platform, and perhaps also for the Stage 2 Bucket platform. In general, this situation will become more common as firing

temperatures are increased for either new products or upgrades. Traditionally, bucket platforms in power turbines and HPT blade platforms in aircraft engine turbines have not required active cooling, and so this represents a new turbine cooling application. Recent high thrust versions of the GE90 engine have begun to add limited platform cooling via the inclusion of discrete film holes fed from the air cavity beneath the adjoining platforms of adjacent blades, which simply means the use of wheelspace purge air or blade coolant impeller air. To solve this challenge, the ATS design presently employs a combination of active cooling and film cooling for the platform. The pressure differential which exists from the forward wheelspace to the aft wheelspace is used to drive the platform cooling air.

At a first glance, impingement heat would seem to be a fairly well understood and documented case. However, the present scenario involves several complicating factors which place it outside the available literature database. These include the fact that the impingement is restricted within a prescribed cavity geometry and location, the desired impingement surface will contain a specific type of roughness, and certain design parameters are desired to be variable to allow for design changes. Also unique to the present case, is that the entire platform surface heat transfer distribution is required for full design analysis. The objectives of this experimental study are threefold: (1) provide the required design heat transfer data for the current S1B platform design, (2) formulate and validate an appropriate transfer function describing the primary impingement region heat transfer as affected by the major parameters, and (3) investigate the means by which improved platform cooling can be achieved within the current basic design constraints.

Discussion

The platform test model design is a 3X scale of the first-stage bucket platform underside cavity. The model includes features for coolant delivery, and coolant extraction through both film holes and shank leakage ports. The liquid crystal heat transfer measurement technique requires special features on this model. Etched pattern surface heaters were applied to the primary cooled region of the platform. The heaters were then covered with a very thin layer of Copper to spread the heat flux as a uniform thermal boundary condition for the test.

Simple free-surface impingement tests were first performed without the platform cavity portion of the model for comparison to impingement behavior reported in the literature. These tests established the uniformity of the test surface heat flux. The nominal design case with a smooth surface was tested.

The bucket platform test model is a mainly acrylic model which represents the bucket-to-bucket cavity region just below the platform. The model is a 3X scale of the cavity region utilizing a cross-section taken from the 9H S1B design drawings at a location just beneath the actual platform metal on the cold side. The model cavity is linear in the turbine radial direction. The model does not include casting features which cause the real bucket casting to have a radially contoured cavity below the platform. Such features were judged to be of second order importance with respect to the flow field and heat transfer on the immediate platform underside surface.

The test model has three regions on the platform cold side surface: (1) the area between the bucket pressure side and the damper pin, (2) the area between the damper pin and the adjacent bucket suction side, and (3) the film cooling hole area which encompasses both

pressure and suction side film rows. Region #1 on the pressure side of the platform is the area covered by a heater and liquid crystals, and so is the region of data acquisition for this study. The damper pin is also a 3X scale of the S1B hardware, in both size and shape, and so presents the proper blockage to flow which might otherwise proceed easily from the pressure side to the suction side. Region #2 is merely an open area for these tests, which helps to model the volume of the cavity. Region #3 is a metal plate and can be seen to be recessed into the acrylic. The interior surface of this plate is flush with the acrylic. The plate is of the appropriate thickness to maintain the same L/D ratios for the film cooling holes as is present in the S1B design. The rows of film holes have been sized to achieve the same nominal relative flow rates expected in the S1B design, but in a manner which allows all model film rows to be discharged to atmospheric pressure (room pressure).

The test model has a single inlet flow. Two exit flows are maintained, one being the total of the film row flows and the other being the aft shank leakage. The shank leakage flow is controlled in the model tests by feeding the two shank tubes to a single control valve, which is then followed by a float rotameter. Both the inlet flow rate and the shank leakage flow rate are measured, thus the total of the film cooling holes flow rate is also known.

A series of heat transfer tests were performed with variation of the primary parameters of Reynolds number, flow splits, impingement geometry, and surface roughness. All data was fit to a simple transfer function to predict the impingement heat transfer boundary condition for design use.

CFD analyses of the platform cavity region flow and heat transfer were executed with engine-scale geometry and conditions, including rotation. Data post-processing was completed, and the results provided to the GEPS design team. In general, for the specific cooling design and strength involved in this technology, CFD heat transfer results for the platform cold-side surfaces were within about 20% of the experimental results obtained in the stationary model tests, except for the immediate impingement zone. The disagreement in the primary impingement region is not surprising, given the limitations of CFD modeling. The addition of rotational effects in the CFD flow and heat transfer predictions had negligible effect (i.e., no detrimental effects) on the resulting heat transfer cooling performance for the platform region of interest.

Summary/Conclusion

The result of this task was the selection of the most appropriate platform cooling geometry for the first set of turbine hardware, as well as the definition of desired cooling features for improvement. Design boundary conditions were generated for use in bucket analyses, and subsequent thermal and stress calculations performed. A viable platform cooling method was the final result.

Technology Application

Because of the higher firing temperatures of the ATS turbine and the relatively flat radial temperature profiles experienced by large power turbines, bucket platform cooling requires more attention than in previous turbines. Specifically, the first- and second-stage bucket platforms require active cooling to assure component design life. The detailed local heat transfer coefficients measured in this model test, along with the variation of

key cooling parameters, will be used to provide the most robust platform cooling with optimization of coolant usage.

Section 2.2.2.4.8 (GTETIH) S1B Leading Edge Turbulator Tests [C]

Objective

The serpentine cooling flow circuits of the first- and second-stage buckets of the ATS gas turbine have complicated flow configurations with 45° and 90° turbulators. Design flow analytical models include several empirical friction factors and heat transfer coefficients. A database for the leading edge passage of the serpentine circuit with 90° turbulators was developed.

The objective of this task is to correlate friction factor and heat transfer coefficient data for leading edge passages with 90° turbulators. The accuracy of the correlations developed will determine the need for additional tests with the 7H leading edge turbulated passage, first-stage bucket geometry.

Introduction/Background

The nature of the steam cooling circuit for the Stage 1 Bucket of the ATS turbine is such that the leading edge passage has a critical role in determining the overall bucket flow circuit pressure loss, as well as the life of the part. It is therefore crucial that the correlations used to determine both heat transfer and friction factors for turbulated passages of leading edge regions be examined in detail to assure the degree of required accuracy in design predictions.

Discussion

The friction factor and heat transfer coefficient data existing in the GE Aircraft Engines and CRD database and in the open literature were collected and analyzed. The data were correlated using passage geometric variables and the flow Reynolds numbers. The results obtained imply that the heat transfer Nusselt number correlation has an acceptable uncertainty. The friction factors, however, do not correlate to the degree required in the desired parameter ranges to assure accuracy for design of the flow circuit.

Tests were conducted to evaluate turbulator geometries for the first-stage bucket leading edge passage by performing non-rotating heat transfer and pressure drop tests at high Reynolds numbers on scale models of the leading edge passage. The test rig was designed and built to model the 50% span location of the first-stage bucket leading edge cavity. Heat transfer and friction were measured over a range of Reynolds numbers applicable to the H gas turbine for both smooth walls and walls with five different turbulator geometries. The heat transfer and pressure drop results from this task (shown in Figure 2.2.2.4.8-1) have been used in the design of the first-stage bucket in the H gas turbine.

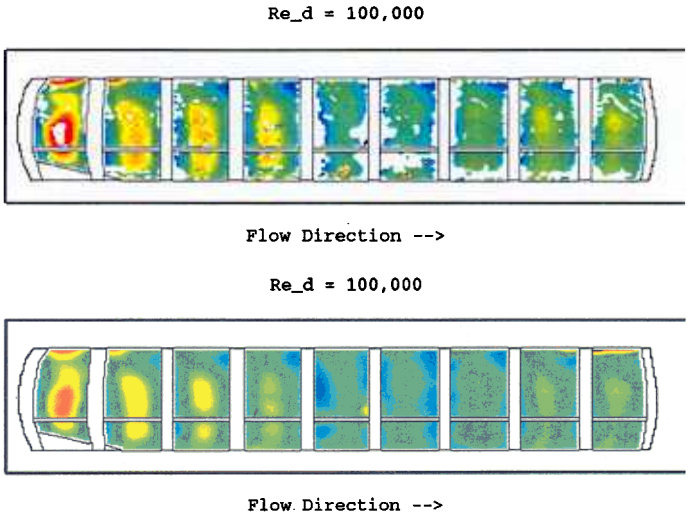

Figure 2.2.2.4.8-1. Liquid Crystal Test Model of S1B Leading Edge Cooling Surfaces

Summary/Conclusion

The friction factors must be experimentally verified by running flow tests with a cast leading edge passage to determining the relation to the existing correlation predictions for design use.

Technology Application

The correlations developed were incorporated into a database for leading edge passages with 90° turbulators that can be used in future design considerations. The additional friction factor data have improved confidence in the developed correlation.

Section 2.2.2.5 (GTFFTS) Turbine Stator Design [S]

Objective

The inner and outer turbine shells will be designed, including a turbine stator cooling system to provide rotor/stator clearance control. A closed-circuit coolant delivery and return system for the turbine flowpath stator components will be designed. Component, subassembly, and assembly flow tests will be incorporated concurrently. Implications for handling equipment (crane and manipulators) will be included in design considerations.

Steam-cooled turbine nozzles will be designed. Thermomechanical transient and steady-state analyses will be run to determine parts lives. Material, manufacturing, and heat transfer database expansion is planned and will be integrated concurrently.

Shrouds will be designed. Sealing systems will be selected for minimum leakage. Thermal and structural analysis of equiaxed or anisotropic materials will be applied as appropriate.

Calculations will be made of all flow in the cooling systems, including leakage flows, to support performance, thrust balance, and component temperature calculations.

Design of hot-gas-path seals will be based on laboratory tests. Seals developed for transition piece-to-nozzle segment and intersegment interfaces will be evaluated in cascade tests. Both sealing and wear performance will be assessed. Manufacturing drawings and specifications will be produced.

Full scale prototype and production nozzles will be tested in a nozzle cascade facility at GEAE-Evendale, OH. The test facility features two closed-loop steam cooled nozzles and aerodynamic sidewall pieces downstream of a full-scale H system combustor and transition piece, run at full pressure, flow, and temperature conditions to determine nozzle heat transfer and low cycle fatigue characteristics.

Background

The primary function of the nozzles is to turn and accelerate the high temperature, high pressure, low velocity combustion gases into the downstream turbine blade rows. The nozzles accomplish this using airfoil shapes spaced around the circumference of the engine.

The ATS turbine design calls for many new developments in the turbine stator technologies that go beyond current power gas turbines. These new technologies include: 1) new aerodynamic design of the flow path and airfoil shapes to maximize efficiency, 2) steam cooling of the stage 1 and stage 2 turbine stator nozzle assemblies, including the airfoils and inner and outer bands, 3) thin walled castings, 4) TBC technology development to make coatings that can withstand the ATS environment and meet design life, and 5) ASME boiler codes for pressure vessels given that steam is being used a the primary coolant for the stator.
Note: The focus of the ATS program has been on the design and production of the steam cooled stage 1 and stage 2 nozzle hardware. Stages 3 and 4 were designed as part of the overall H machine development program, using GE's current design system.

Many design and development phases have been completed during the design and manufacture of the steam cooled turbine stators. New processes and development tools were created, and satisfy the design requirements for life and durability. During each phase of the development, reviews were conducted to assure that strict control and design intent had been met.

The 9H steam cooled prototype hardware has been assembled into the turbine stator structure. Information derived from the FSNL testing has been incorporated into the hardware during final assembly. The stators were instrumented to fully verify the design integrity at FSFL conditions. Testing at full load conditions will be completed once the unit is installed on site for full product verification.

Discussion

Aerodynamic Design

For the ATS turbine, a new set of highly efficient airfoil shapes were required to accommodate the high performance demanded by the cycle and program goals. The Turbine Aerodynamic Design group determined the airfoil shapes using three dimensional computational fluid dynamic (CFD) design tools pioneered at GE Aircraft Engines, utilizing analysis based upon cycle, temperature, and other variables that would allow the ATS turbine to produce the needed output and performance. The H machines represent one of the first applications of sophisticated three dimensional CFD airfoils used in the turbine section of industrial gas turbines. The stage 1 nozzle throat area or minimum flow area sets the machine operating line and compressor pressure ratio. The second stage nozzle turns the combustion gas between the first and second stage buckets, plus provide a sealing interface between the stator structure and turbine rotor. Figure 2.2.2.5-1 shows a cross sectional slice of the ATS turbine.

Mechanical Design and Analysis

Once the airfoil contours were developed, they were given to Engineering Design to perform analysis and lifing calculations. Both structural and thermal analyses were completed on several design iterations in order to optimize many variables that could affect the durability of the nozzles. In each case, steam cooling was utilized on the inner and outer bands, plus the majority of the airfoil. The trailing edge utilized compressor exit air as the cooling medium, with some air being diverted to the wheel spaces on the rotor. Figure 2.2.2.5-2 shows a typical airfoil cross section of a steam cooled nozzle. Once completed, the shape was given to Manufacturing to develop tooling and processes in order to meet the requirements set forth by Engineering Design.

Manufacturing

The nozzles used for the ATS program utilized many advanced manufacturing processes for the first time. The first stage nozzle is a single crystal superalloy casting, and the second stage nozzle is an equiaxed superalloy casting, and both required significant casting development work to allow their successful manufacture. Although the airfoil material is widely used on other turbine programs, the requirement for thinner walls on these airfoils and bands made fabrication much more difficult. Extensive development was completed at the casting vendor in order to fabricate the castings in the required amount of time.

Because the first and second stage nozzles are predominantly cooled with high pressure steam, the nozzles must create a boundary between the cooling steam and the flowpath post-combustion air. To create the nozzle pressure vessel, significant post-cast processing is required. The post-cast processing is focused around sophisticated machining, joining and coating processes. Significant development work was also required during the post-cast machining, joining and coating cycles to produce hardware that would meet design requirements.

Materials Development

Materials testing was also a large part of the nozzle development effort. The characterization of material behavior in a steam environment was an important part of the design validation and characterization. This work was carried out at GE's Corporate Research and Development Center, and in the GEPS Materials Lab, and is reported separately.

Cooling Scheme

The first and second stage nozzles airfoil cooling systems employed both air and steam in the overall design. The steam system within the airfoils and the inner and outer bands utilizes two main cooling concepts. One method is by impingement cooling, where steam is forced through small holes in jets to impinge on the airfoil cavity walls. The other method utilizes a forced convective cooling or duct flow. A shaped core plug is inserted into one of the cavities, and is attached at either the outer or inner wall depending upon the direction of the steam flow. The inner and our bands are cooled through impingement cooling. The steam within this system is closed loop in combination with both series and parallel circuits, and is fed back to the steam cycle after passing through the nozzles.

The air cooled trailing edges used technology currently in use on other Power Generation gas turbines. Specially machined holes allow the air from the turbine rotor aft cavity to cool the bulk of the trailing edge. A telescoping hole, as it has been nicknamed, use a two diameter hole through the metal in the trailing edge. Figure 2.2.2.5-3 shows a cross section of the airfoil with the telescoping hole cross section. A large diameter leaves the air cavity and traverses most of the trailing edge. At the exit of the cooling hole, a sudden change to a slightly smaller diameter, helps to increase the cooling effectiveness where needed.

Thermal Barrier Coating

A thermal barrier coating is applied to the flowpath surface of each nozzle. The thermal barrier coating allows a significant temperature drop to take place before the coating to metal interface. The thermal barrier coating along with the backside cooling allows management of the nozzle metal temperature during all engine operating conditions.

Each nozzle segment was cast as a single piece in order to facilitate TBC coating of the entire gas path surface of the nozzle. A new TBC coating was created in order to provide thermal protection in the severe flow path conditions occurring at FSFL operation, and provide the part with a lasting durability. This new coating built upon experience encountered in current Power Systems power turbines, with additional new manufacturing processes and components being developed. The TBC applied to the H machine hot section was the result of this development and has given the parts a good surface finish with a durable coating.

Welding

Since the nozzle segments are considered to be pressure vessels, special consideration had to be made when welding on attachments and making structural changes. New welding processes were developed that introduced lower heat into the parts to reduce the amount of distortion seen during assembly. Once the segment welding was completed, a final machining operation was performed that would allow them to be assembled within the inner turbine shell. A diaphragm, which interfaces with the rotor, is also attached to the second stage nozzle during this final assembly step. Figure 2.2.2.5-4 shows a finished set of stage 1 nozzles assembled into the inner turbine shell.

Nozzle Cascade Testing

The H machine stage one nozzle was designed using GE's design practice database, with validation tests for heat transfer, material properties, and steam cooling effects. These test results were incorporated into detailed 3-dimensional aerodynamic, thermal, and stress models as part of the design process. As further validation, full-size, steam cooled stage 1 nozzle segments were tested at full H machine operating conditions in a nozzle cascade test.

The test rig is located at GEAE's Evendale, OH facility, and shares the control room and airflow facilities with the combustor test rig. The nozzle cascade test rig consists of two 9H stage 1 airfoils downstream of an H machine combustor and transition piece. The flowpath contours on either side of the two nozzle segments are formed by two water cooled copper endwalls. Figure 2.2.2.5-5 shows the nozzle cascade test rig.

A four-phase test program was designed to characterize combustor behavior, verify aerodynamic performance, measure heat transfer characteristics, and accumulate low-cycle fatigue (LFC) cycles. Correlation of the nozzle cascade test data with design predictions validated the 9H and 7H steam cooled hardware.

Phase 1 involved combustor mapping and characterization of the combustion system, and to perform a general facility shakedown. The initial testing was completed in 1995 to map the temperature profile at the exit of the transition piece (entrance to the nozzle cascade). Additional combustor testing was performed in 1Q97 to confirm temperature profiles at the high and low end points of the LCF cycle to be used in Phase 4.

Phase 2 consisted of a cascade aerodynamic test, in which the rig was run at full air flow conditions to determine the external Mach member distribution on the airfoil surfaces. This parameter is important in establishing nozzle external heat transfer coefficients as well as verifying the aerodynamic quality of the test configuration. This phase was successfully completed in 3Q95.

In Phase 3, the heat transfer test, several hundred internal cavity metal temperature, and steam temperature and steam pressure sensors, and external temperature and pressure sensors were used to validate the stage one nozzle internal heat transfer and flow circuit

predictions. The testing was conducted under steady state and transient operating conditions that closely match the operation of the production engine. Testing ran for over 100 hours, and over 30 data points were taken. Test data results were analyzed and compared to a detailed flow and three-dimensional heat transfer analysis of the nozzle. Phase 3 testing was completed in 1Q97.

Phase 4, the low cycle fatigue (LCF) test, involved cyclic operation of the test rig to simulate periodic start-up and shutdown of the engine during commercial operation. The rig was operated between two steady state points: one at a low thermal stress state, and the other at a high thermal stress state. Testing was performed to determine the durability of the thermal barrier coating (TBC) on the nozzle and to test the nozzle durability in both fully coated and spalled conditions (hardware was pre-spalled to evaluate this effect) to establish any crack propagation behavior. It was found that cracks occurred only in the pre-spalled areas, and did not grow. The nozzle cascade test results were correlated with the analytical predictions used in the nozzle design. It was found that there was very close agreement between the two, thus validating the design methodology for all of the steam-cooled turbine hardware.

FSNL (Full Speed No Load) Testing

Two full-scale 9H, and one full-scale 7H development tests were run to support the validation of the H design. The tests were performed in GE's Industrial Gas Turbine facility in Greenville, SC. The tests were run at no load conditions, so there was no steam cooling of the hot gas path components. Regarding the stages one and two nozzles, the testing allowed demonstration the assembly techniques and handling requirements required for the steam cooled nozzles as part of an overall steam cooled system.

Summary/Conclusion

The ATS turbine program has brought into being a new level of design capabilities and manufacturing processes for nozzle design. New casting technology has led to better process controls that can be applied to other Power Generation turbine programs. Coating technology development has produced a new type of coating that can withstand more severe conditions in the flow path than current coatings. Welding and attachment technologies have been improved with new tools and methods. Design tools were also created that gave new insight on how to analyze and predict steam cooled nozzle lives, both thermally and mechanically. Full life verification will start to be quantified once the prototype unit has been assembled at the field site and the test program is initiated. Several instrumented segments in the nozzle arrangement will record metal, gas, and steam temperatures, and steam pressures. This information will then be used to compare predicted values versus actual to ensure that design life has been fulfilled.

Technology Application

The turbine stator analysis and design effort defined the basis for the 7H and 9H production hardware.

Many of the Manufacturing processes developed on the ATS power turbine can be applied to other power generation turbines to help increase part life and manufacturing cycles. Design tools and methodology can be used on current power turbines as well. All information learned from the full speed full load testing will be applied towards upgrades and future uprates of the ATS platform.

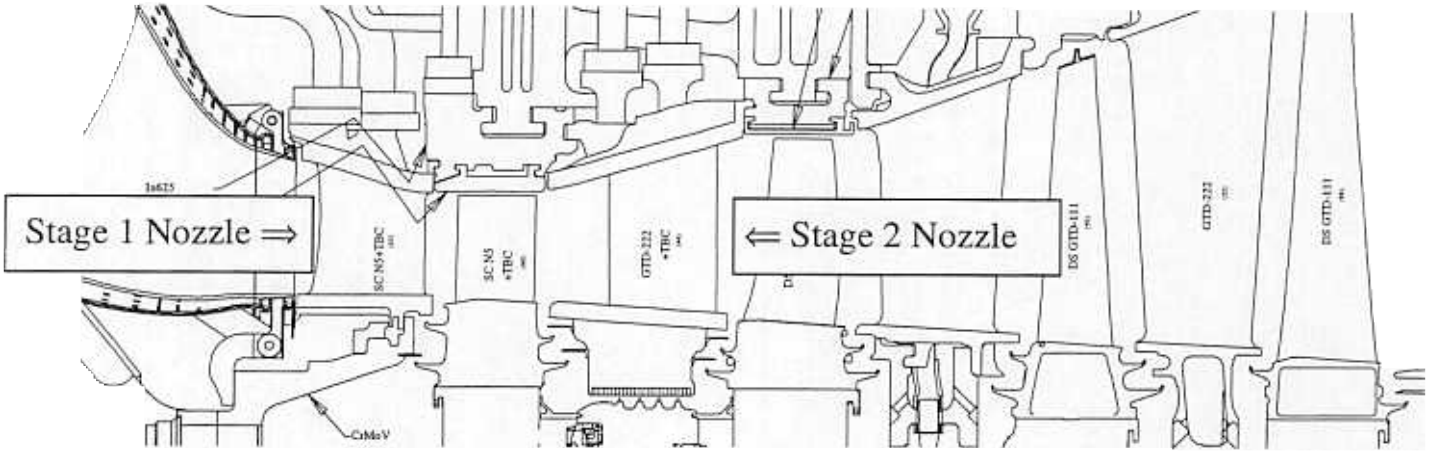

Figure 2.2.2.5-1: 9H Baglan Bay Turbine Cross Section

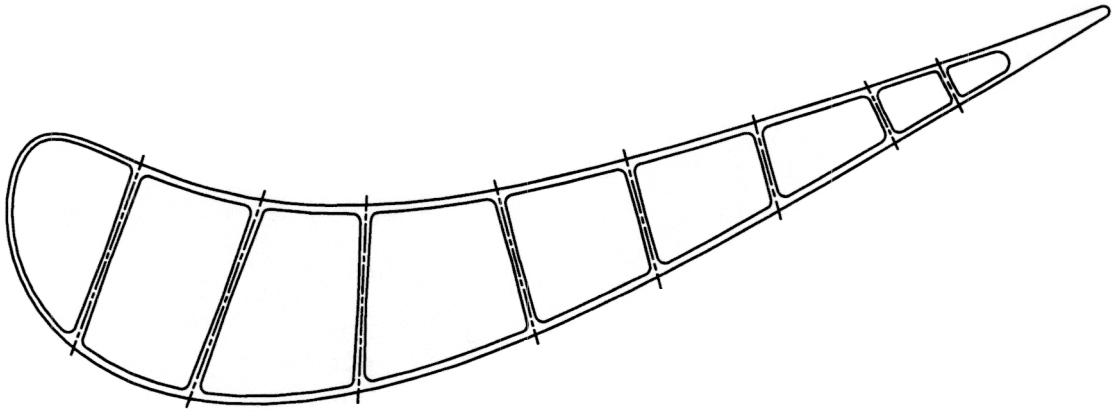

Figure 2.2.2.5-2: Typical Steam Cooled Nozzle Cross Section

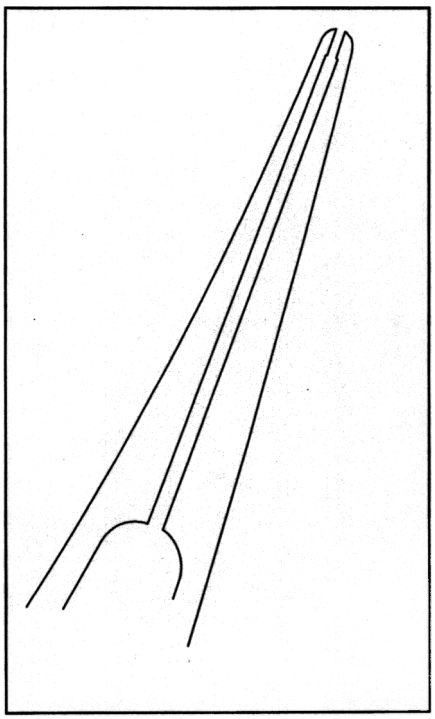

Figure 2.2.2.5-3: Typical Trailing Edge Cooling Hole

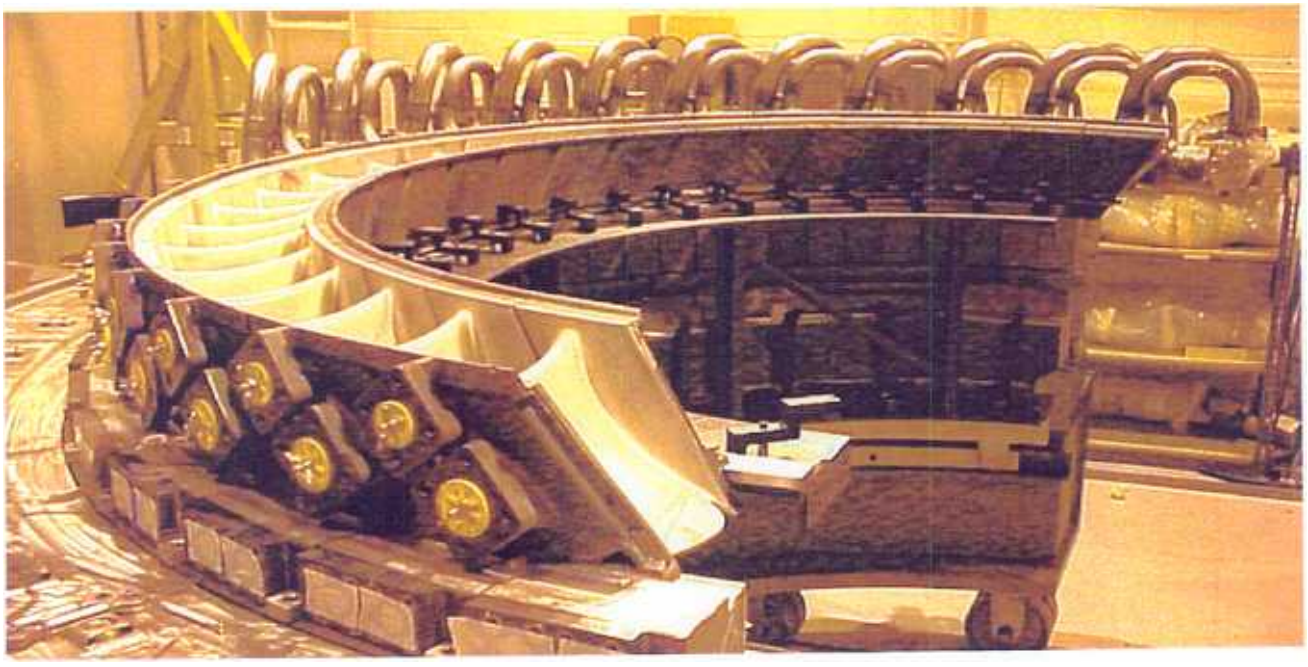

Figure 2.2.2.5-4: Stage 1 Nozzle Assembly

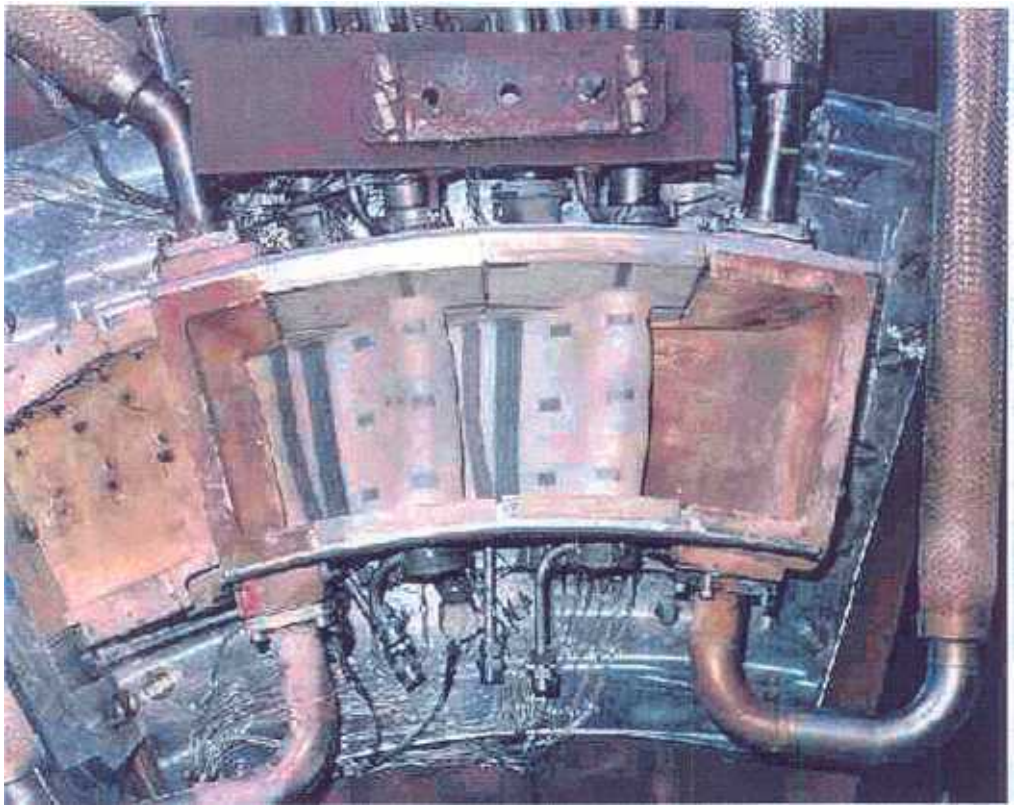

Figure 2.2.2.5-5: Stage 1 Nozzle Cascade Test Rig

Section 2.2.2.5.1 (GTFFTS) Turbine Stator Robust Design [S]

Objective

The objective of this work was to develop and apply robust design methods for the development of steam-cooled components of the advanced gas turbine. The goal of this effort was to achieve high standards of performance, quality, and reliability for these components by performing the following tasks during the product development cycle: (1) apply, and develop as needed, the robust design methodology to first- and second-stage nozzles; (2) apply the robust design methodology to some of the steam- and air-cooled stator components (e.g., first-stage shroud and turbine inner shell); (3) provide consulting and support for applying the robust design methodology to some of the critical rotor components (e.g., manifold, steam tube bushings, and spoolie); (4) provide consulting and support for integration of design, manufacturing, and assembly; and (5) train the GEPS staff on the concepts, methods, and tools for achieving robust design.

A "robust design" is a design that satisfies the product performance requirements in an optimal manner and also exhibits minimal sensitivity to variabilities arising from various sources, such as manufacturing processes and tolerances, material behavior, operating environment, in-service damage, and maintenance and repairs. The methodology consists of the following key steps: (1) identification of critical-to-quality (CTQ) characteristics,

key control parameters (KCPs), and key noise parameters (KNPs); (2) definition of the Design of Experiment (DOE) matrices for KCPs and KNPs; (3) execution of the DOE matrices through analysis, testing, prototyping, and/or manufacturing; (4) statistical analysis of the DOE data to develop response surfaces, (5) optimization using response surfaces to determine optimal KCPs that meet the CTQ requirements and minimize sensitivity to variations; (6) performing Monte Carlo analysis to quantify the likelihood of meeting CTQ requirements under various noise conditions; (7) improving the part's producibility and assembly by specifying wide manufacturing and assembly tolerances; and (8) validating the design developed through analysis and/or testing. The methodology was demonstrated successfully on a number of real-life complex applications and was applied to steam-cooled components of the ATS gas turbines.

Introduction/Background

It was necessary to develop an analytical design process that would produce high casting yields while also meeting engine requirements for performance, quality, and reliability. With the help of GE-CRD, (see Section 2.2.2.4.3.1), a "robust design" process was developed to meet the objectives of this task.

Discussion

Robust design efforts were focused on (1) generating new finite element models (FEMs); (2) parameterizing and updating the existing FEMs; (3) developing robust design formulations by identifying performance critical-to-quality characteristics (CTQs), key control parameters (KCPs), and key noise parameters (KNPs); (4) developing design of experiments (DOE) matrices and executing them through finite element analyses; (5) carrying out statistical analysis of the DOE results, developing response surfaces and optimizing the CTQs for their means and variances; (vi) performing Monte Carlo analysis using response surfaces and a probabilistic analysis code; (6) documenting progress made in this reporting period; and (7) providing consulting services to GEPS staff on robust design for the following components:

First-Stage Nozzle

Statistical analyses were run for the second-phase DOE to develop response surfaces at each finite element node for stress, temperature, and life. Response surfaces were validated against independent DOE runs. Robust design studies were performed by optimizing the variances and mean values of LCF life at critical nodes using response surfaces and an in-house optimization code. Monte Carlo analysis was also carried out to calculate the probability of meeting LCF life requirements at various nodes. Sensitivities to gas path temperature, steam temperature, and steam flowrate were computed for optimizing system efficiency with minimal effect on LCF life.

A third-phase DOE study, which included variability in gas path and coolant temperatures, convective heat transfer coefficients, and crystal orientations, in addition to metal wall and TBC thicknesses, was executed. The data obtained were analyzed, and response surfaces for stress, temperature, and life at each node were developed and

verified. Monte Carlo analysis was performed to calculate the probability of attaining certain LCF life value in the presence of different types of variability. Robust design studies were performed to maximize mean LCF life at each finite element node, and to minimize life sensitivity with respect to variations, including manufacturing tolerances. The finite element model was further updated to incorporate certain design changes and to refine the mesh in certain critical areas of interest including adding new features.

A fourth-phase DOE was designed and executed for lifing the castings received from the vendor. Response surfaces were developed using the finite element results from these runs, and were also verified using independent DOE runs. A spreadsheet tool was developed based upon these response surfaces that enabled rapid estimation of LCF lives, given the coordinate measuring machine (CMM) data for various castings at the vendor site.

A GE quality effort called "design for six sigma" (DFSS) was applied in several areas, including response surfaces for system-level tradeoff studies between low cycle fatigue (LCF) life and combined-cycle efficiency and for steam-cooled joint design between the outer sidewall and cover.

Second-Stage Nozzle

A finite element model comprising airfoil, inner and outer sidewalls, inner and outer fillets and covers, diaphragm, and hook portion was developed. Finite element models of individual singlets were combined to create a doublet, per design requirements. Boundary conditions were applied to the finite element model, and a thermal-structural analysis was performed to ensure that the model produced adequate results.

A DOE study for improving LCF life was completed. The study results obtained for stress, temperature, and life were statistically analyzed. DFSS quality tools were applied to the second stage nozzle design.

First-Stage Shroud

A first-phase DOE study was performed. This required developing macros for updating the finite element model to implement changes in geometry, boundary conditions, and other analysis parameters of interest. Statistical analysis of the DOE results was carried out to identify parameters that have significant influence on life. A second-phase Design of Experiments was executed on the first-stage shroud. Results were analyzed to determine the sensitivity of various parameters, KCPs as well as KNPs, to LCF life.

Rotor Components

Spoolie Design: Robust design analysis was developed. DOE matrix and parameters were defined; analysis of the DOE data was performed; DOE runs resulted in reduced stresses, thus improving the part life.

Main Steam Tube: Several DOE matrices and their parameters were defined and executed. As a result of the analysis, stresses were significantly reduced, thereby improving part life to meet requirements.

Manifold: DOE matrix and parameters were defined. Analysis runs were performed. The results were used to evolve the design concept/configuration. A design was identified that analytically meets the requirements related to design as well as manufacturing.

Flanges: DOE matrix and parameters were defined using mixture design concepts. Analyses of the DOE runs were performed. The results were analyzed to minimize the flange openings. Based upon these findings, the flow circuit was modified to ensure that the flanges remain closed.

Turbine Inner Shell

A robust design approach was defined, and DOE matrices and parameters were identified. ANSYS analyses were carried out for both mechanical and thermal conditions. Data were analyzed to identify parameters that had a significant influence on the performance variables. Two-dimensional thermal results were substantiated with three-dimensional analyses.

Summary/Conclusion

Robust design methods were developed and applied to the development of steam-cooled components of the 9H and 7H gas turbines. This effort resulted in a design system that satisfied the product performance requirements in an optimal manner, and also exhibited minimal sensitivity to variability arising from various sources, such as manufacturing processes and tolerances, material behavior, operating environment, in-service damage, and maintenance and repairs.

Technology Application

Results were used in the development of part drawings in terms of nominal dimensions and manufacturing tolerances, LCF life assessment of as-cast parts to be received from vendors, quantifying the confidence level in meeting the CTQ requirements under various sources of variations, and improving part producibility by widening manufacturing tolerances.

Section 2.2.2.6 (GTFFST) Structures Design [S,C,A]

Objective

The objective of this task was to design the exhaust frame and diffusers, steam gland, and aft bearing housing. Instrumentation and test plans for component model, factory, and field testing were prepared.

Background

The introduction of steam cooling to the turbine rotor components required significant design revisions to the traditional design of GE Power Systems gas turbine aft end structural components in order to accommodate the required changes in steam piping configuration, improved sealing technology, improved aerodynamic performance, and structural design considerations. These design revisions were introduced using the seven step New Product Introduction Tollgate Process. This process allows innovative designs to be developed, while ensuring that a disciplined approach is maintained, that the design solutions use well grounded design fundamentals, and utilize the extensive GE Power Systems experience base, were possible. New design features are validated using component testing, and during full scale FSNL unit testing.

Discussion

From a general gas turbine architecture standpoint, the fundamental change to the exhaust structures is due to the rearranging of the aft bearing housing lube and cooling systems to accommodate the introduction of rotor steam cooling. A cross section of the aft end of the gas turbine is shown in Figure 2.2.2.6-1, illustrating the relative position and size of the structural components.

This layout revision accommodates placement of the steam gland at the aft end of the bearing housing to introduce and extract steam from the rotor steam bore tube. Figure 2.2.2.6-2 shows the steam gland and steam entry and extraction ports. The steam gland needs to be supported structurally within the exhaust frame, which introduces additional length to the exhaust frame. It also interfaces with large steam piping runs that displace the area traditionally used for the aft bearing cooling air and oil lube piping. Figure 2.2.2.6-3 shows a cutaway isometric view of the exhaust frame inner barrel area with the steam pipe to steam gland interface.

In the H machines, the bearing cooling air and lube oil piping flow systems have been redesigned from the current practice of being piped directly to the bearing housing aft end through the large manways and open inner barrel of the diffuser. The exhaust frame has been designed for the bearing cavity cooling air, fire protection, and bearing/turbine instrumentation to be directed through nine hollow struts, while the tenth and larger strut (or King strut) provides space for the lube oil introduction and drain at the bottom centerline. This fundamental concept of using the frame struts as a conduit for secondary flow systems is similar to that used in the turbine rear frames in jet engine designs at GEAE and elsewhere.

During this ATS development phase, several design/technology advances have been demonstrated in the areas of exhaust frame cooling, steam sealing, and diffuser performance. Two main areas required component validation testing due to their fundamental changes to previous industrial gas turbine design: 1) diffuser performance and acoustics with steam pipes crossing the flowpath, and 2) sealing for high pressure steam using brush seals.

Due to the fundamental change in the piping layout with steam pipes being the only rear-end piping, the diffuser was changed from a strutted piece to non-strutted. The steam pipes do not need to be protected from the high temperature gas path, because they are already at high temperature due to the internal steam flow. The resulting non-strutted diffuser has allowed for better optimization of the pressure-recovery flowpath for performance. However, this non-strutted diffuser feature requires the steam piping to cross the gas path, which could result in performance or acoustic problems. Figure 2.2.2.6-3 shows the diffuser and rotor steam delivery and return pipes that cross the flowpath. These concerns were tested during 1997 and 1998 in the GE-CRD mechanical systems lab facilities. The test verified that no piping vortex shedding-driven acoustic issues existed, and that the exhaust diffuser shape and design could be optimized for high pressure-recovery performance. The testing also verified that the exhaust frame/diffuser strut profile, which includes the King strut, would not disturb the pressure profiles of the upstream rotating equipment.

Brush seal steam testing was another significant component test program completed by the exhaust structural component area at CRD. These tests focused on advancing brush seal technology for higher performance, and a more robust mechanical design method of sealing compared to the traditional labyrinth seal packing designs. Specifically, the test focused on steam at the temperature and pressures ranges beyond GE experience in other gas turbine and steam turbine brush seals applications. This testing was completed between 1998 and 2000. Results of tests have optimized the brush seal parameters (number of seals, brush wire density and materials, surface clearances, stability, etc.) for introduction in both the steam feed to return and the steam feed to the low pressure steam turbine extraction locations. Figure 2.2.2.6-4 shows the brush sealing arrangement for the steam gland

Additional advances were made in detail design analysis, particularly in the area of the steam gland. The aerodynamic and mechanical design features were designed using detailed finite element analysis in both computation fluid dynamics (CFD), for setting the steam introduction scroll and rotor inlet flowpath, and in the structural designs. CFD analysis was completed at GE-CRD during 1996 and 1997 to determine the flow pressure distribution so that a steady pressure profile would be maintained (with minimal circumferential variation) for low performance losses as the steam is introduced to the rotor. Structural analysis of the steam gland was performed to validate the transient and steady state structural behavior of the steam gland. Figure 2.2.2.6-5 shows the three dimensional finite element model of the steam gland.

For the overall machine tests, all pre-test Critical To Quality (CTQ) objectives were successfully achieved in the exhaust structures during the 9H FSNL and FSFL pre-shipment test programs, as well as on the 7H FSNL test. During the test programs, all major structural component temperatures were monitored to allow comparison with pre-

test predictions. No major anomalies were experienced, with thermal response and temperature distributions within expected limits.

Capacitance clearance probes were used to measure the turbine and compressor clearances at four circumferential locations and three axial locations, and at one axial location in the turbine. Additional clearance probes were mounted in the steam gland to measure the radial clearance between the steam gland and bore tube. The average measured clearance compared well with prediction, both transiently and at steady state FSNL conditions at all axial locations.

The units were disassembled and inspected after test. Teardown inspection showed some rubbing in the upper half compressor and compressor discharge casing, which was expected due to the higher than predicted rotor lift.

Summary/Conclusion

The design and verification testing of the exhaust frame, steam gland, and aft bearing housing have been successfully completed. All of the components were fabricated, assembled, and tested in full scale engine tests at the GE Power Systems Greenville, SC test facility.

Technology Application

This analysis and design effort establishes the basis for 9H and 7H structure designs.

Section 2.2.2.6.1 (GTFFSTEF) Exhaust Diffuser Performance [C]

Objective

The requirements for the ATS gas turbine exhaust diffuser include: (1) improved base load pressure recovery performance compared with earlier GE exhaust diffuser designs and (2) operation without acoustic resonance at any operating point of the gas turbine. The objectives of this task were to test ATS gas turbine exhaust diffuser geometries for pressure recovery performance and to verify that the design selected did not excite acoustic resonances.

The test program included the installation and test of a scale-model diffuser with flow path geometries and components compatible with the ATS gas turbine. Specifically, the cost-saving idea of internal insulation required axial ribs in the walls of the diffuser flowpath. Impact on pressure recovery was measured. Several other tests were performed, each with the aim of characterizing and maximizing performance. The exhaust diffuser designs were tested to verify that no acoustic resonances are excited.

Introduction/Background

One of the goals of the ATS program is reduced cost of electricity. Cost of electricity is a function of gas turbine first cost, overall efficiency of the combined cycle plant, and maintenance cost. The exhaust diffuser impacts each of these. One cost reduction idea implemented in the ATS gas turbine is to internally insulate the exhaust diffuser outer wall. Flow path effects of the internally insulated concept could impact exhaust diffuser

pressure recovery, a factor in the overall efficiency of the plant. Overall flowpath design within the exhaust diffuser impacts pressure recovery also. Exhaust diffuser resonances can impact maintenance costs by affecting the durability of exhaust diffuser components. These aspects motivated this test program to characterize diffuser pressure recovery and acoustic behavior.

Discussion

This task involved scale model testing of exhaust diffuser configurations for the ATS gas turbine. Essential to the test program was the ability to match inlet Mach number and inlet swirl angle, both of which typically vary with gas turbine load. Inlet conditions affect both pressure recovery and acoustic resonance.

Two scale models were used in the test program. Initially an existing 1/9-scale model was used to study acoustic resonance behavior. Following the preliminary testing with this model, a new 1/13.2-scale model was designed and constructed. This model was used for most of the test program. Instrumentation included wedge probes to characterize inlet flow conditions, static pressure taps for pressure recovery data, and unsteady pressure transducers for acoustic resonance data. Ink injection and tufts were used for flow visualization.

Summary/Conclusion

The following are the key results from this test program:

- At full speed no load, part load, and base load conditions, no acoustic resonances are anticipated. This allows for low noise emissions and good exhaust diffuser life.
- The internally insulated design concept was found to not significantly degrade pressure recovery performance. The cost benefits and performance impact of this approach are both understood.
- Overall pressure recovery of the ATS gas turbine diffuser design was found to be greater than that of prior designs.
-

Technology Application

The results from this series of scale-model gas turbine exhaust diffuser tests were used to establish several diffuser design features, including the feasibility of an internally insulated exhaust frame, a less expensive option than external insulation. Data were used to design a diffuser with the required pressure recovery, enhancing the overall combined-cycle plant efficiency. These tests verified that the final design was free from acoustic resonances.

Section 2.2.2.6.2 (GTFFST) Steam Box CFD Analysis [C]

Objective

The objective of this task was the design of a steam delivery system as part of the 9H/7H steam cooling design. A steam gland was designed to bring the cooling steam from a stationary inlet pipe onboard a rotating shaft. Steam entered the steam gland through an axial inlet pipe. The pipe turned 90° so that the resulting flow traveled tangent to the rotor shaft and into an inlet scroll. The inlet scroll cross-sectional area was sized to match the

steam velocity to the rotor tangential velocity. As the steam traveled around the scroll circumferentially, some steam was extracted into rotor slots. A 3D CFD analysis was required to define the appropriate geometry of the steam gland inlet scroll that resulted in a nearly uniform radial outflow from the scroll circumference.

Introduction/Background

The scroll or steam gland is a stationary component that brings the cooling steam onboard the rotating boretube. Its purpose is to provide a uniform flow distribution around the periphery of the boretube entrance region and to impart a tangential velocity to the steam, that matches the rotational speed of the bore tube.

Discussion

Unigraphics (UG) models were employed to create unstructured 3D grids of various scroll configurations (Figure 2.2.2.6.2-1). The 3D CFD code NOVAK, successfully used in previous ATS applications, was the tool employed in this analysis. Starting with the original configuration, and in an attempt to improve the circumferential variation of the radial outflow, seven concepts were studied. The "continuous scroll outlet" concept came closest to meeting the uniform mass flow distribution. Pressure drops in all concepts are very similar and confirm the value predicted by the YFT model of the complete steam distribution circuit.

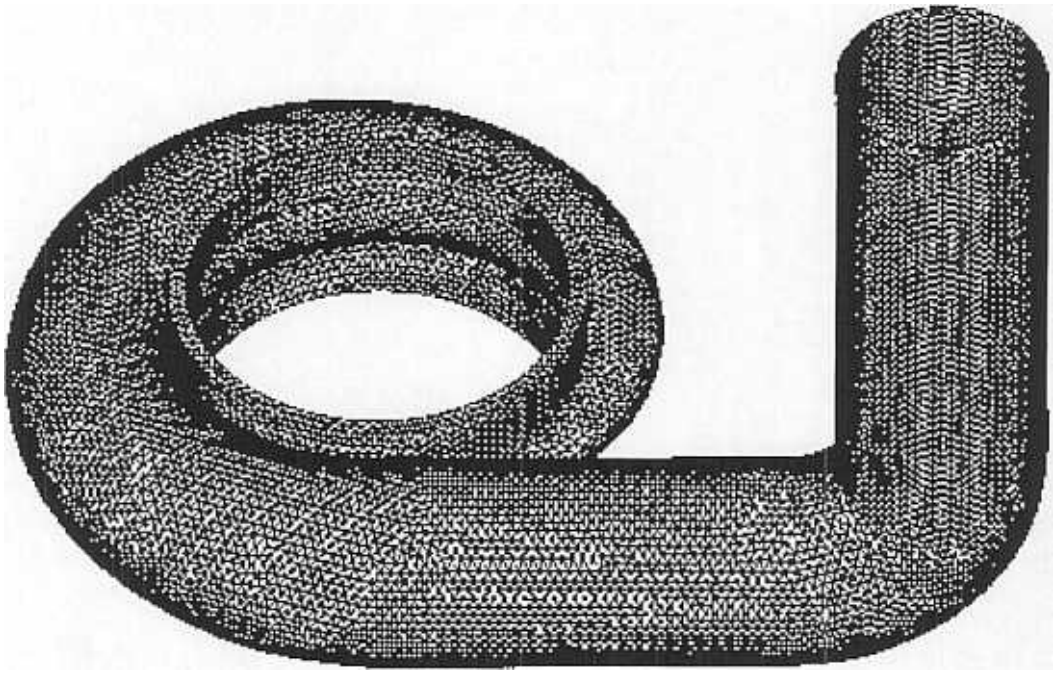

Figure 2.2.2.6.2-1. Original scroll geometry for CFD analysis

Combined with the scroll performance is the behavior of the flow as it enters the annular passage of the rotor. The conditions at the inlet to the entrance hole are specified based on the scroll analysis results.

To confirm the results obtained with NOVAK3D and to assess the effect of the constant exit static pressure assumption required by NOVAK3D, TfC (another CFD code) was used to solve both the original and "continuous scroll outlet" concepts. Both TfC and NOVAK predict a better performance for the modified design, as measured by the standard deviation of the velocity profiles about their mean. Although the comparison between the NOVAK and TfC solutions is satisfactory, the root of the differences was investigated and found to be the differences in the flow predictions in the elbow region of the design. The NOVAK flow pattern indicates a stronger recirculation downstream of the elbow than predicted by TfC. The effect of the exit static pressure on the solution was evaluated by running TfC in the "uniform exit pressure" mode (similar to NOVAK's) and then again with the "non-uniform exit pressure" option. The results of this effort were documented and presented in a design review of the steam gland design. No outstanding issues in this area were identified. The proposed continuous scroll outlet concept was used as the baseline design.

Summary/Conclusion

Following a series of redesigns, the baseline design of steam gland has been proven adequate to uniformly introduce the cooling steam into the rotating components of the steam distribution system. The steam tangential velocity matches the rotational speed of the 9H boretube.

Technology Application

The results of this study have had an impact on the design of the scroll geometry and confirmed its proper performance in meeting the desired uniform flow distribution. The analysis of the entrance to the rotor served three purposes: it incorporated rotational effects and confirmed the 1D analyses of the YFT study of the steam distribution system; it pointed to the relative insensitivity of the current design to variation in the inlet conditions of the flow; and, with the prediction of the relative swirl angle, obstacles in the annular passage were designed to be aligned with the incoming steam.

Section 2.2.2.7 (GTFFMS) Mechanical System Design [S]

Objective

The objective of this task was to perform system level studies to optimize cost and performance. Performance, cost, weight, and other system level integration issues were monitored and tracked. A flange-to-flange cross-section drawing was maintained, and all mechanical interfaces were controlled. All gas turbine systems, as well as the technical requirements for accessories, were defined and specified.

Introduction/Background

A series of Metrics were developed to report the status of major systems requirements, which include performance level in terms of efficiency/heat rate, output, emissions, reliability/availability, and Design to Cost. Additionally, a master schedule was developed that was used as the benchmark to monitor the component design interface definition, and also to track component fabrication, delivery, and assembly schedules.

Discussion

System level studies were performed for the 9H and 7H machines to optimize cost, performance, weight, size, maintainability, reliability, and manufacturability with the objective of minimizing Cost of Electricity. Performance, cost, weight, and other system level and integration issues were monitored and tracked.

The maintainability, reliability, and availability (RAM) team worked to ensure that all of the results derived from current field operation were incorporated into the 9H/7H designs. RAM and failure modes effects analysis (FMEA) studies were completed, and goals were established for both H machines consistent with the respective Product Specifications.

A full-scale mockup of the midsection, including the compressor discharge casing (CDC), combustion transition piece, and steam piping was fabricated. This mockup was used in assembly and maintainability trials, with feedback to Design Engineering to ensure that assembly and maintainability issues were incorporated into designs prior to hardware procurement.

The 9H and 7H mechanical interface drawings, which included the internal and external interfaces, were updated and modified. The 7H aerodynamic flowpath drawing was completed, establishing a basis for the initial cross-section drawing. Detail design and supporting technology development that benefited both the 9H and 7H turbines was completed. Performance estimations were updated to reflect the new component designs. Engineering milestone and manufacturing schedules were updated, reflecting the current hardware production cycles and customer requirements.

The 9H detail design was completed, and hardware was manufactured and assembled to support the FSNL test program. The testing was completed on time after meeting all test objectives. The gas turbine operated flawlessly, and the test stand operated successfully with minor problems as the system checkouts were completed. Information obtained

from the 9H testing was incorporated into the 7H gas turbine design, and the 7H FSNL test program planning. Potential customers and DOE representatives were witnesses to the testing at the GEPS site in Greenville, SC.

A second FSNL test (the FSFL pre-shipment test) of the 9H was successfully completed in November 1999 that demonstrated the aeromechanics of the hot gas path buckets, the rotor steam delivery system, and the improved rotor structure that incorporated lessons derived from the F fleet experience. Speed sweeps to 105% were completed, clearing the 9H unit of aeromechanical constraints. Steam delivery system leakage testing demonstrated leakage levels substantially below the design requirements. The rotor structure demonstrated repeatable acceptable vibration characteristics. Additionally, low temperature gradients around the unit were demonstrated.

During testing of the 9H FSFL pre-shipment machine, opportunities were identified to improve the robustness of the bore tube design. These changes were successfully designed, built, and installed prior to the unit being shipped in December 2000 to the Customer Site.

The Systems Integration of the 9H was completed, and the hardware was shipped to the Customer Site. To ensure fully integrated configuration, minimize unit trips, and maximize the data obtained during the FSFL characterization test, a series of Systems Reviews were initiated early in the year. These reviews continued throughout the year, and are being continued into 2001 to ensure closure of all issues identified and incorporation of any benefits into the 7H.

During the year, there were a series of design reviews held on the Steam Turbine, Generator, and Balance of Plant equipment, for both the 9H and 7H. The integration of these systems were reviewed, and a stage test is to be conducted in Winter/Spring of 2001 validating the controls software and equipment.

The 7H completed the Conceptual Design tollgate and received the formal business review and go-ahead. Cost, schedule, risk, and performance metrics were reviewed and updated to support the requirements of this tollgate. All material was released and suppliers were selected, initiating the manufacturing process. The systems review team, which included engineering, manufacturing, sourcing, and maintainability personnel, met throughout the program to review the merits of various system issues, and determine whether incorporation of these ideas met system goals. The cross-section drawings were updated for the 7H, reflecting conceptual design configuration and interface decisions.

Detail design of the 7H was completed, and then component hardware manufacture was completed, allowing the start of unit assembly. Cost, schedule, risk, and performance metrics were reviewed and updated. Tollgate progress was measured, and the 7H program successfully passed the preliminary design tollgate review in May 1999. 7H system level studies continued to be performed to optimize cost, performance, weight, size, maintainability, reliability, and manufacturability. Performance, cost, weight, and other system level and integration issues were continuously monitored and tracked.

Cross-section drawings for the 7H were completed, reflecting the final design configuration and interface decisions. Hot and cold cross-sections were made available for use.

The 7H gas turbine full speed, no load (FSNL) test was completed in February 2000 without any major issues being identified. Compressor flow, efficiency and aeromechanics were demonstrated. Rotor behavior was stable, and the dynamics were well behaved and within limits. The use of stage 15 bleed was characterized, and the clearance control system was demonstrated.

Minor modifications to bearing clearances and VGV schedules were made during the test runs to address some minor issues. The test was completed within the planned timeframe, and customer witness tests were completed. Prior to removal from the test stand, a major customer event was conducted.

The 7H unit was removed and shipped back to Assembly for teardown and inspection. Inspections of the unit and rotor indicated no unexpected anomalies. The unit was partially disassembled to allow for modifications to allow additional instrumentation. The stator hardware and compressor rotor are now complete, and are awaiting production turbine airfoils to complete manufacturing.

The 7H design of full life hardware continued and the design of tooling for the turbine airfoil castings started.

To improve the installation, commissioning, and characterization testing to maximize the test data quality, a number of initiatives were started.

Cleanliness was identified as an area of concern and much attention was devoted to ensure cleanliness of the components from the vendor through installation. This is of particular importance on a machine that uses steam cooling for stage 1 and 2 buckets and nozzles.

Systems Integration across the various control systems and skids was identified as an opportunity for improvement and action was taken by creating Systems Owners as single points of contact responsible for the success of their assigned systems.

The completion of the P&ID's for the 9H and the completion of the same documents for the 7H factory test has helped resolve many issues. The P&ID's for the first 7H customer are being completed now, well in advance of the need date, to reap the benefits accruing of having early complete and fully reviewed documentation.

Summary/Conclusion

A system of Master Schedule and a series of Metrics were created, and were used as the benchmark to monitor the component design interfaces, and also to track component fabrication, delivery, and assembly schedules. System level studies were performed to optimize cost, performance, weight, and other system level integration issues. A flange-to-flange cross-section drawing was maintained, and all mechanical interfaces were controlled. All gas turbine systems, as well as the technical requirements for accessories, were defined and specified. Successful FSNL and FSFL pre-shipment tests on the 9H and FSNL testing on the 7H have verified the System studies, integration and performance.

Technology Application

The lessons learned from the FSNL testing of the 9H and 7H have been incorporated into both production designs. A cross-functional systems review team will ensure that field experience lessons learned are incorporated into the component designs, thus optimizing performance, cost, weight, size, maintainability, reliability, and manufacturability.

Section 2.2.2.7.1 (GTFFMS) Transient Gas Turbine Cycle Model [S]

Objective

The objective of this task was to evaluate computer platform and software options to best support the integration of a transient gas turbine model into a combined cycle simulation. Transient gas turbine modeling was reviewed, with input from both GEPG and GEAE. From this brief study, it was determined that a new transient model of the ATS machine was necessary in order to reflect more accurately the aerodynamic and thermal behavior. This work assisted GEPS Engineering in developing the new transient model with a steady-state accuracy goal of approximately +/- one percent. The model was designed to be included in overall power plant simulations.

Introduction/Background

This activity is focused on developing a detailed transient aero-thermal model for the gas turbine portion of the ATS power plant. Such a model is be an integral part of the design process, providing detailed information on the transient operation of the gas turbine within the larger context of the combined cycle power plant. This information is used in turn to verify and validate the design of the gas turbine, as well as support the development and validation of the operational strategy for the combined cycle system, and the actual control system software.

Discussion

During the course of Phase 3 of the ATS program, the basic design of the transient gas turbine cycle model has been formulated, several iterations on the design have been developed, and the resulting model utilized in the context of a larger combined-cycle power plant simulation model.

In concluding this phase of the effort, the GE Power Generation Technology (PGT) NPI Systems and Systems Performance groups have published two software releases of the 9H transient gas turbine cycle model, and one release of the 7H model. These models have been modified by the Controls, Accessories and Systems Engineering (CASE) group to run in the real-time combined-cycle model with minimal compromise to steady-state performance, and to add dynamic volume, inertia, and thermal effects to the gas turbine model for true transient performance operation. CASE also functions as the combined-cycle plant transient model owner and integrator.

The latest 9H model supplied by PGSE – August 1999 – was updated based on the most recent (June 1999) steady-state Design Computer Software release. It incorporated additional features beyond the steady-state and (or) 1st transient release predecessor, including:

- Extended and smoothed the high-speed compressor maps (AMC002/1 rig) down to 80% Nc
- Added part-speed compressor performance maps, bleed effects, and surge limit line fit from AMC002/1 rig data.
- Added closed-circuit air cooling and exhaust re-injection effects [including as-shipped and commercial configuration models]
  Extended 4th stage turbine flow coefficient and efficiency maps to higher expansion ratio and velocity ratio to cover all startup and cold day points.
- Added a stage 4 mach number exit limit to simulate exhaust strut choking at high power on a cold day

The latest 7H transient model from PGSE - November 1999 – was based on the then current steady-state model (there has since been an April 2000 steady-state release). It incorporated several of the 9H features above (mach number limit, closed-circuit air cooling, and extended fourth stage turbine map) which had not yet been applied to the 7H steady-state model. Work is continuing on this model to match the 7H FSNL data and to add recent updates from the steady-state model.

While this model does not include all of the features and subsystems from the steady-state model, checkout of the 9H model over a large envelope of base-load through FSNL points produced a very good average error of 0.24% KW and 1.2 deg F exhaust temperature relative to the steady-state model.

Checkout versus the steady-state model below FSNL is not possible due to steady-state model map limits. Low speed results are based on the best-available compressor and turbine information available (rig and/or blade row model results).

As mentioned above, the gas turbine transient cycle model has been modified for inclusion in a larger integrated combined-cycle model representative of the 9H power plant. Besides the gas turbine and its key accessory subsystems, this model also includes subsystem models representing the steam turbine, the heat recovery steam generator, and the piping, valves, and pumps connecting these subsystems. This model integration activity has evolved in two distinct stages. In the first and current stage, the compressor maps and certain key details from the turbine portion of the model have been extracted and used to calibrate a simpler model to support real-time simulation.

The second stage involves bringing more details of the turbine and combustor into the integrated, real-time combined-cycle simulation model. This phase was completed during the 4th quarter of 2000.

These integrated combined-cycle simulation models are currently being used to

- Develop and validate the control system algorithms for the Mark VI Integrated Control System (ICS), the 9H control system hardware platform
- Develop suitable operational strategies for the startup and shutdown of the 9H combined-cycle power plant
- Assist with the verification of design information for plant equipment, such as valves, piping, and heat exchangers

Summary/Conclusion

A transient gas turbine cycle model has been developed for both the 9H and 7H versions of the Advanced Turbine System gas turbine. These models have been derived from steady-state aero-thermal cycle deck models for these machines, with suitable extensions to provide transient operation over the entire speed/load operating range.

These models have been and will continue to be used in the simulation of the combined-cycle operation of the 9H and 7H power plants. They have been adapted and modified as required for real-time simulation of the combined-cycles for both 9H and 7H versions, and in this context have proven essential to the process of developing the operational strategy for the ATS combined-cycle power plant.

The real-time models derived from the transient gas turbine cycle models have furthermore been used in the development and validation of the control system application software for the Mark VI/ICS, the control system platform for the ATS.

Technology Application

The transient gas turbine cycle model has been used within the larger context of the integrated 9H combined-cycle simulation model to help define and verify the operational strategies for the power plant. It is also being used in this context for the development and verification of the actual control system software.

The transient gas turbine cycle model is also being used in the development of advanced strategies for monitoring and controlling key internal parameters within the gas turbine itself.

Simulation models for the both 9H and 7H versions of the advanced turbine system have been developed, and the transient gas turbine cycle model is central to both of these efforts.

Section 2.2.2.8 (GTFFPP) On-Base and External Piping Design [G]

Objective

The objective of this task was to design piping for fuel, air, steam, water, and oil systems. A turbine base was also designed for securing the ATS gas turbine to the foundation.

Introduction/Background

An objective of this task was the design of piping for fuel, air, steam, water, and oil systems. The piping designs are driven by the increased Systems requirements of the ATS gas turbine for output and efficiency. These requirements result in larger piping and the use of non standard piping materials due to high temperature. A new turbine base was also designed for securing the ATS gas turbine to the foundation. The turbine base must be capable of handling and transferring much larger loads than in previous gas turbine designs. This requirement is complicated by the limited space available to the turbine base because of the machine shipping envelope, the increased number of systems requiring piping for fluid transport, the piping size and quantity, and the foundation interface limits. Figure 2.2.2.8-1 through Figure 2.2.2.8-3 show key piping hardware as well as the turbine base.

Discussion

As discussed above, the functional specifications of the ATS gas turbine increased all Systems requirements to fulfill those specifications. The design and manufacturing activities were carried out using established and proven General Electric Quality practices. Major milestones for the program were the Full Speed No Load (FSNL) testing performed in Greenville, SC. There have been three FSNL tests (gas turbine only, no steam turbine, generator, or heat recovery steam generator included) performed. For the following discussion, they will be identified as 9H FSNL, 9H FSFL pre-shipment,

and 7H FSNL.

The 9H FSNL, 9H FSFL pre-shipment, and 7H FSNL testing occurred May 1998, October 1999, and January 2000, respectively. The turbine base and all major production piping systems covered under this section were exercised during these tests with the exception of production fuel gas and steam cooling piping. Production fuel gas piping was not installed due to the use of test stand (non-production) combustion hardware. Steam cooling piping hardware could not be used due to steam not being part of the test stand configuration for FSNL testing. The plan is to verify and validate both the production fuel gas and the steam cooling piping systems during Full Speed Full Load demonstration testing in the field.

The testing was successfully completed with no major issues for the installed hardware. There were several items identified as lessons learned from each test that were incorporated into to the piping systems designs prior to the subsequent test. These lessons learned consisted of design changes for ease of manufacturing, assembly, test, maintenance, and reliability such as piping routing and support changes to minimize vibration. All lessons learned will be incorporated into the final designs prior to each machine shipment to the first customer.

Summary/Conclusion

The primary objectives of this task were to design piping for fuel, air, steam, water, and oil systems as well as a turbine base for securing the ATS gas turbine to the foundation. The design and manufacturing activities were carried out using established and proven General Electric Quality practices. Major milestones for the program were the 9H FSNL, 9H FSFL pre-shipment, and 7H FSNL tests performed in Greenville, SC. The turbine base and all major piping systems covered under this section were exercised during these tests with the exception of production fuel gas and steam cooling piping. The plan is to verify and validate both the production fuel gas and the steam cooling piping systems in the FSFL demonstration testing. The testing was successfully completed with no major issues for the installed hardware. There were several items identified as lessons learned from each test. These lessons learned consisted of design changes for ease of manufacturing, assembly, test, maintenance, and reliability. All lessons learned will be incorporated into the final designs for each first unit Customer.

Technology Application

The turbine base and piping designs require the consideration of new ideas in this technology application. The turbine base must be capable of handling and transferring much larger loads than in previous gas turbine designs. This requirement is complicated by the limited space available to the turbine base because of the machine shipping envelope, the increased number of systems requiring piping, the piping size and quantity, and the foundation interface limits. The piping design challenge is driven by the increase in the number of fluid systems, the increase in piping size, and the use of higher temperature materials in order to achieve higher gas turbine output and efficiency.

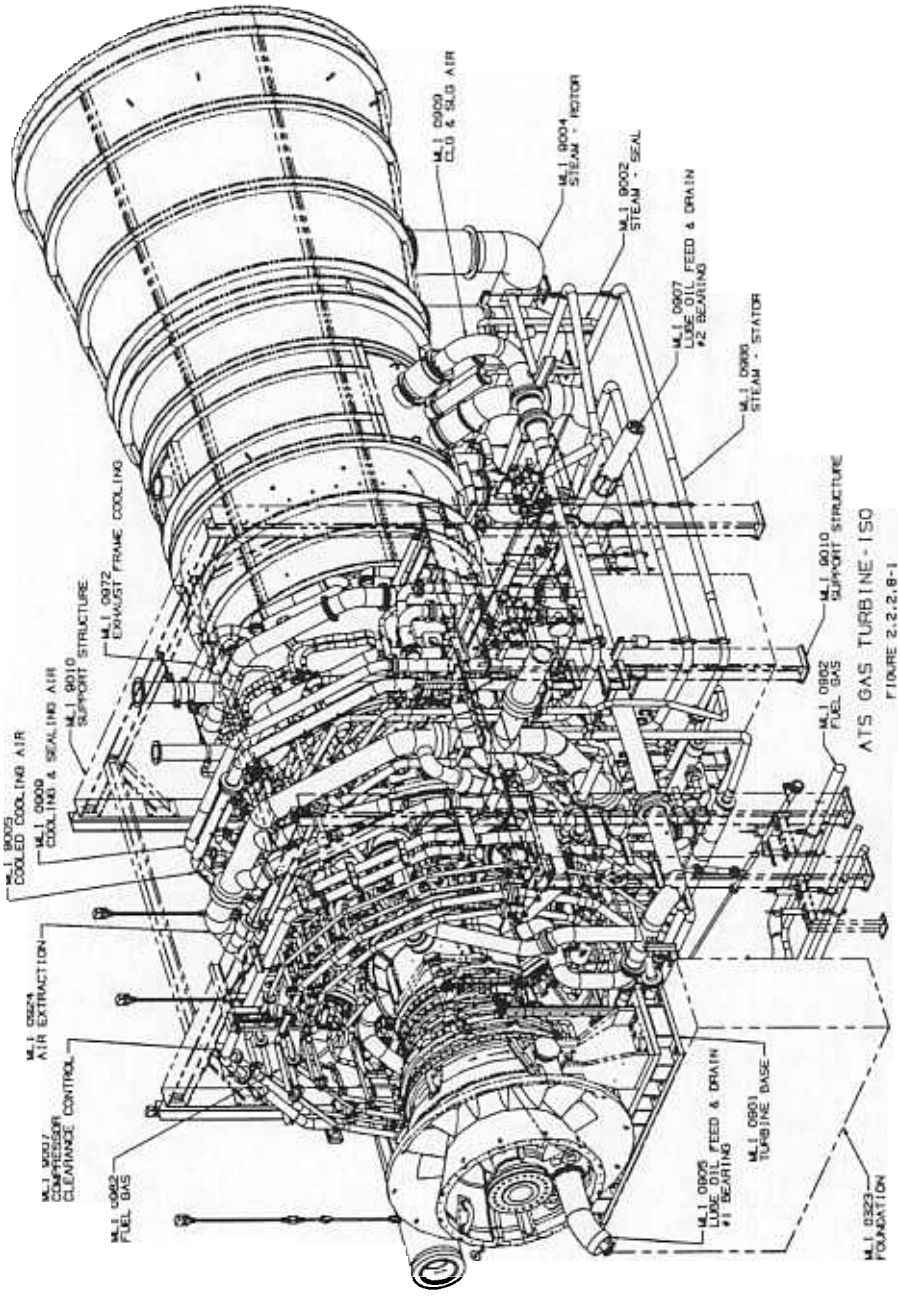
MLI 0959
CLO & SLG AIR
MLI 9004
STEAM - ROTOR
MLI 9002
STEAM - SEAL
MLI 0907
LUBE OIL FEED & DRAIN
#2 BEARING
MLI 0900
STEAM - STATOR
MLI 9010
SUPPORT STRUCTURE
MLI 0962
FUEL GAS
MLI 0323
FOUNDATION
MLI 0903
TURBINE BASE
MLI 0905
LUBE OIL FEED & DRAIN
#1 BEARING
MLI 0962
FUEL GAS
MLI 9007
COMPRESSOR
CLEARANCE CONTROL
MLI 0924
AIR EXTRACTION
MLI 9005
COOLED COOLING AIR
MLI 0909
COOLING & SEALING AIR
MLI 9010
SUPPORT STRUCTURE
MLI 0972
EXHAUST FRAME COOLING
ATS GAS TURBINE - ISO
FIGURE 2.2.2.8-1

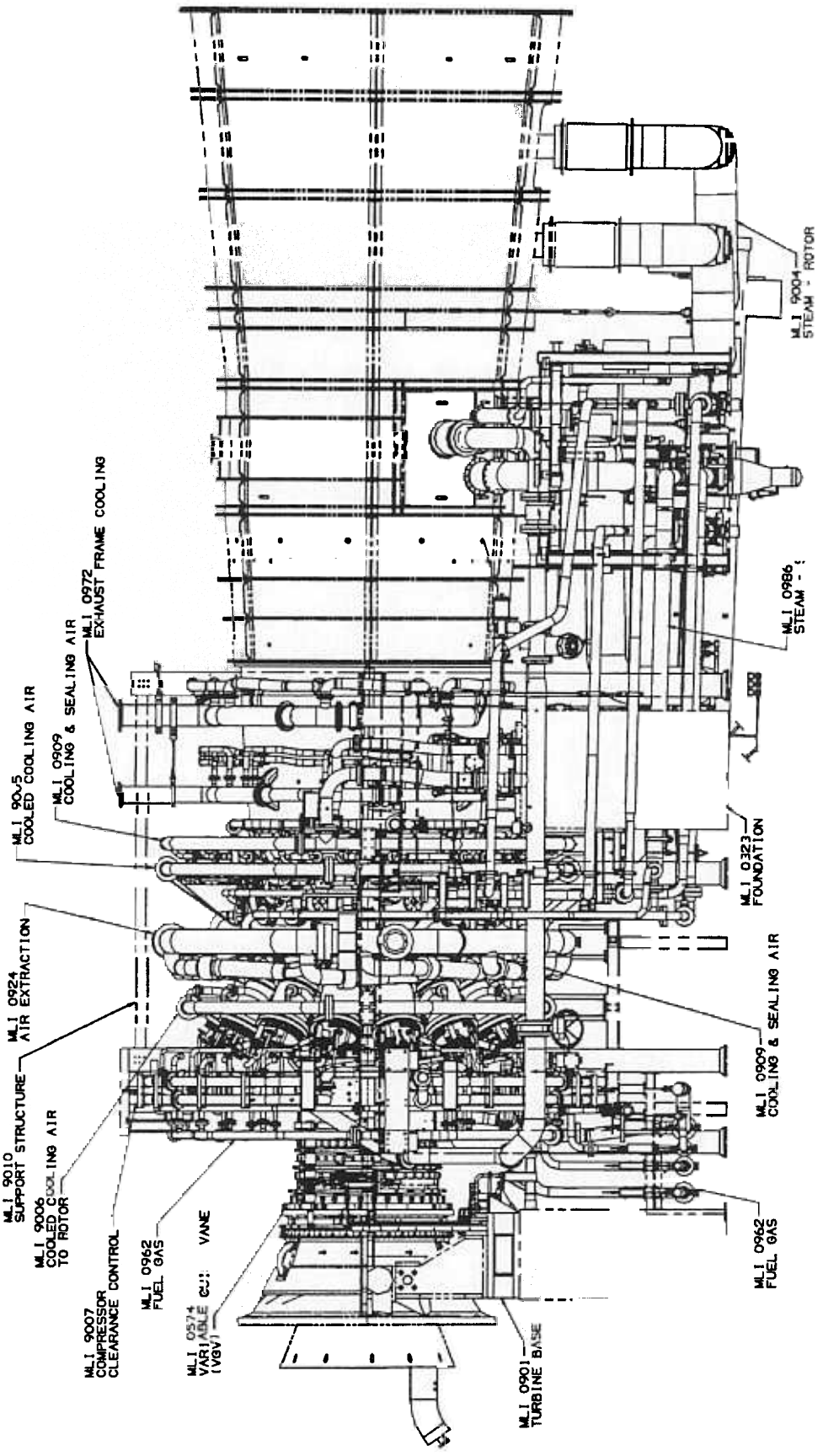

ATS GAS TURBINE-RIGHT SIDE

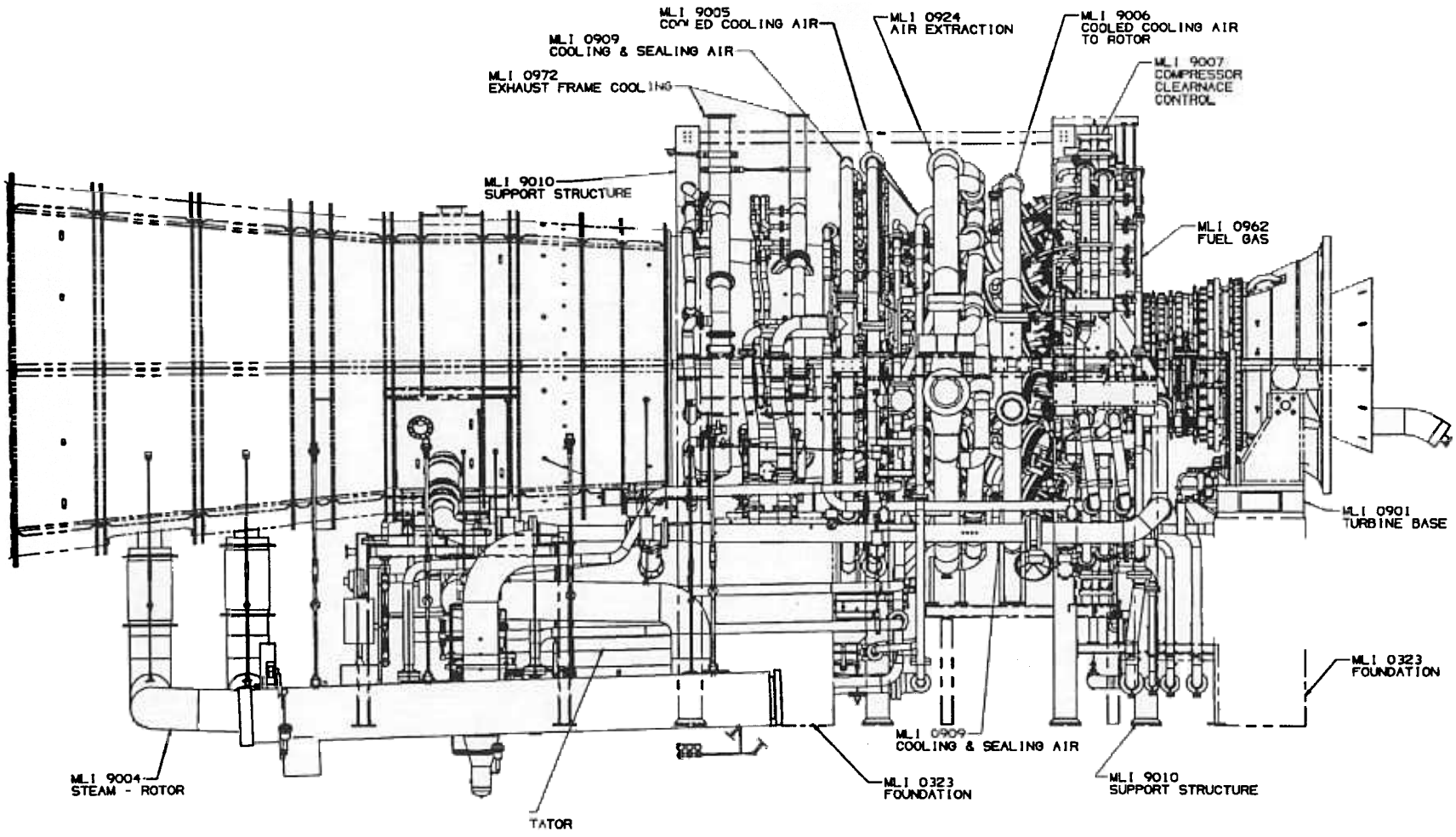

ATS GAS TURBINE-LEFT SIDE

FIGURE 2.2.2.8-3

Section 2.2.2.9 / 2.2.2.9.1 (GTFFIT) Instrumentation and Test [S,G]

Objective

The objective of this task was to instrument and conduct field tests that validate the ATS gas turbine design for mechanical integrity, operating performance of the unit, and establish emissions performance. Test plans were formulated, and instrumentation was specified. Compressor and turbine rotor telemetry systems were developed and acquired.

Introduction / Background

As the H machines are designed to operate in combined cycle only, (steam is needed for cooling), only factory no load testing (part power using air cooling) was done. Full speed, no load (FSNL) factory tests were conducted at the Greenville, SC manufacturing facility to validate the MS 9001H (9H, 50Hz) and MS 7001H (7H, 60Hz) gas turbine configurations for design mechanical integrity and performance. The first 9H test was conducted in June, 1998, and the second, called the Full Speed Full Load (FSFL) pre-shipment test was conducted in November, 1999. The 7H FSNL test was conducted in February, 2000.

The three factory no load tests are described in this report. Each test section contains its own test objectives, applied instrumentation list, test run summary, and test result summary. The instrumentation for the various gas turbine components and systems was defined by Engineering Design, and successfully applied for each test. The instrumentation telemetry system performance was validated during these factory tests.

Discussion

I. First factory test

MS9001H FSNL (First 9H Full Speed No Load Factory Test)

Test Objectives:

The first 9H full speed no load (FSNL) test objectives (CTQs - Critical to Quality parameters) were:

1. Validate the compressor performance, blade aeromechanics and start sequence
2. Validate low rotor vibration and bearing operational characteristics
3. Validate clearance control system
4. Determine shutdown characteristics
5. Calibrate compressor clearance probes

Gas Turbine Configuration for the 9H FSNL Test

The flange to flange gas turbine was built with production compressor rotor disks and airfoils (stator and rotor blades), limited life turbine hot gas path components (nozzles, shrouds and buckets), a modified MS 9E combustion system configured to fit the MS 9H turbine, a new Mark VI control, and new power plant accessory skids. Stationary and rotating steam cooling circuit piping were not installed, however the turbine rotor steam cooling hardware was installed (to understand steam cooling hardware impact on rotor dynamics).

The FSNL test configuration (drive train) included the flange to flange gas turbine connected to the starting means through an instrumented (telemetry) coupling, and a steady rest bearing and shaft. This is the first prototype unit with five variable stator vanes (VSV), which are ganged and moved in unison with Stage 2 serving as a master vane for VSV openings and closings.

The starting device in the test stand had an 8000 HP main motor with a 40 HP turning gear motor (to turn rotor at 2.9 rpm), and a 75 HP pony motor to turn the rotor at 155 rpm.

The power plant related equipment includes the two-sided air inlet, single exhaust and a number of gas turbine accessory skids. In the new test stand at the Greenville plant, the standard production gas turbine skids were installed together with H-specific gas turbine skids such as active clearance control, cool cooling air and Variable stator HPU (hydraulic power unit).

Instrumentation

A selected number of compressor rotor blades and stator vanes were strain gauged, and the compressor casings had dynamic pressure probes, and light probes for blade tip deflection measurement. A selected number of compressor wheels had thermocouples installed to monitor the cooled cooling air circuit. The sensors required to determine compressor performance (pressure, temperature and airflow) were monitored and recorded by the factory test stand quality assurance (QA) system.

The list of sensors installed for various components is shown on the table below. The list includes gas turbine standard and protective instrumentation sensors.

Gas Turbine Component / System	9H FSNL
Turbine Shaft	
Turbine Buckets	
Turbine Rotor Steam Cooling	
Compressor Rotor	X
Compressor Stator	X
Structures	X
Bearings	X
Turbine Nozzles	
Turbine Shrouds	
Turbine Secondary Flow	
Combustor	
Performance	X
X = Instrumentation applied for the 9H FSNL test	

Test Runs and Major Events

RUN #	DATE	MAJOR EVENT / OUTCOME
1	5/6/ thru 5/9/98	* First crank to 32.5% (unfired) speed * Establish crank and purge speed
2	5/11 thru 5/28/98	* On 5/11, flex coupling inoperative, unit shut down * Restart on 5/19 reached FSNL successfully During 5/19 run, with unit at FSNL, lubrication oil cooler heat exchanger leak - unit shut down * Restart on 5/26 with new oil heat exchanger
3		* Customer demo test run # 3 - canceled
4	5/30/98	* Successful customer run
5	6/2/98	* Compressor VSV changes S3 & S4 -> 4 deg open
5A	6/3/98	* Compressor IGV 6 deg closed and S1 ->4 deg open * VSV closed from full open position.
6	6/4/98	* IGV -> 10 deg closed and S1->4 deg open
6A	6/5/98	* IGV ->6 deg closed, S1->4 deg open and S2 ->4 deg open * 104% speed swing for compressor aero mechanics * First fired shut down. For all other runs, the unit was shut down by "e stop / trip button"

Total fired hours = 12.8
Total number of fired starts = 8

Test Results

The unit ran successfully. The measured compressor air flow was 2.2% great than predicted. The compressor stage one rotor blade dynamic response exceeded the design limit during the first start up in the acceleration phase. Additional runs were made to understand and resolve the dynamic response problem.

Closing the compressor inlet guide vanes (reduce compressor inlet flow) during acceleration resolved the dynamic response problem. (The subsequent 9H FSFL pre-shipment test implemented this information, and revised the stator vane schedule and linkage for the start up acceleration phase). All other compressor stages (rotor blades and stator vanes) were within acceptable dynamic stress levels, with the exception of stage 4 and 6 rotor blades, which exceeded the design limits for dynamic response. Blade tip modifications were defined that would resolve the high dynamic responses, and be verified during the FSFL pre-shipment test.

The Mark VI control, and all accessory skids, including the new H specific clearance control skid, and the cooled cooling air skid, performed satisfactorily as predicted.

Turbine rotor vibratory modes observed during test were as predicted. Bearing thrust loads were within design limits. However, bearing losses were higher than predicted, as observed in the bearing oil temperature rise. This finding indicated the need for a larger bearing oil cooler for FSFL pre-shipment testing.

The compressor wheel cooling (purge) circuits performed as predicted.

The starting means torque converter, motors and steady rest bearing performed satisfactorily. The shell and tube type of heat exchanger was used for the rest of the testing and was successful.

The second stage shroud dynamic response was significantly low based on strain gage observations. The clearance control system worked as intended. The measured turbine and compressor airfoil tip clearances were as predicted.

The firing temperature calculations obtained from the Robust Estimator and PERF2U computer programs were confirmed to be reasonably accurate, and matched with the first stage nozzle measured temperatures.

II. Second Factory Test

MS9001H FSFL Pre-Shipment Factory Test

Test Objectives (CTQs) for 9H FSFL Pre-Shipment were:

1. Validate compressor performance, blade aeromechanics and start sequence
2. Validate turbine bucket aeromechanics, rotor thermal evaluation and steam delivery component dynamics
3. Validate steam cooled system integrity
4. Validate low rotor vibration
5. Validate bearing operational characteristics
6. Validate turbine and compressor clearances and shell distortion
7. Validate Mark VI TMR (triple modular redundancy)
8. Calibrate compressor flow probes
9. Validate telemetry system
10. Validate steam cooling protection software

Gas Turbine Configuration for FSFL Pre-Shipment Test

The flange to flange gas turbine was built with a production full life compressor, turbine rotor and Mark VI control system. It had limited life hot gas path components (nozzles, shrouds, and inner turbine shell), and a modified MS 9E combustion system configured to fit the MS 9H turbine. The 9H unit was installed in the test stand in Greenville, SC with all skids and starting means. The 9H FSFL pre-shipment test configuration (drive train) include the flange to flange gas turbine connected to starting means through an instrumented (telemetry) coupling, and a steady rest bearing and shaft. This prototype unit had five variable stator vanes, which are ganged and moved in unison with stage 2 as a master vane for variable stator vane (VSV) openings and closings. The active clearance control system and cooled cooling air for compressor rotor structure were from the FSNL test. The rotating steam cooling circuit hardware and piping were installed. As in the 9H FSNL test, the turbine stage 1 and 2 nozzle steam cooling hardware was not installed.

The test stand starting device had an 8000 HP main motor with 40 HP turning gear motor (to turn rotor at 2.9 rpm), and a 75 HP pony motor to turn rotor at 155 rpm.

The power plant related equipment included the two-sided air inlet, single exhaust, and a number of gas turbine accessory skids. In the test stand at the Greenville plant, the standard production gas turbine skids were installed together with H-specific gas turbine skids such as active clearance control, cool cooling air, and variable stator HPU (hydraulic power unit).

Instrumentation

A selected number of compressor rotor blades (stage 1 rotor blades), stator vanes, turbine buckets, and steam tubes were strain gauged for areomechanical measurements. The compressor casing had light probes (for compressor blade tip deflection measurement), a pyrometer (for second stage turbine bucket temperature measurement), and dynamic pressure probes. A selected number of wheels (both compressor and turbine) had thermocouples to monitor the metal temperatures.

The list of sensors installed for various components are shown in table below. The list includes gas turbine standard and protective instrumentation sensors. The compressor performance required sensors are monitored and recorded by factory test stand QA (quality assurance) system and also Mark VI Historian.

Gas Turbine Component/ System	9H FSFL Pre-Shipment	9H FSFL
Turbine Shaft	X	X
Turbine Buckets	X	X
Turbine Rotor Steam Cooling	X	X
Compressor Rotor	X	X
Compressor Stator	X	X
Structures	X	X
Bearings	X	X
Turbine Nozzles		X
Turbine Shrouds		X
Turbine Secondary Flow	X	X
Combustor		X
Performance	X	X
FSFL = Full speed full load field test (at customer's site)		
FSFL pre-shipment test		
X = Instrumentation applied		

Test Runs and Major Events

RUN #	DATE	MAJOR EVENT / OUTCOME
0	10/21/99	* First crank to 30 % (unfired) speed * Established crank and purge speed
1	10/22/99	* First fire attempt, gas stop ratio valve problem Logic revised from 25 seconds delay to 6 seconds * Unit fired during second attempt * Accelerated to 3143 rpm
01	10/24/99	* Removed cone and ring from bore tube, and accelerated to 960 rpm * Placed balance weight opposite original weight and accelerated to 360 rpm
04	10/26/99	* Unit accelerated to 2496 rpm with normal shutdown, (11 minutes fired time)
05	10/27/99	* Unit accelerated to 2485 rpm with normal shutdown, (10 minutes fired time).
1.1	10/28,29	* Kalman filter tests (steam path leakage tests) Activated valves for leakage before and after, and found no leakage * Tested Cooled Cooling Air (CCA) and Air Cool Steam Cool (ACSC) flow modulations * Made leakage flow studies with VSV modulations * Checked rotor dynamics and wheel space temperatures * Ran aero performance and normal (fired) shut down.
2.1	11/1,2	* Ran CCA and CCS (Clearance Control System) tests * Bearing oil flow tests * Steam path leakage tests ACSC and VSV modulation with various leakages * Rotor dynamics and W/S Temps.
4.1	11/5/99	* Accelerated unit to 108% max speed, with unit trip * and hot restart * Ran aero performance for National grid code * High speed - 105% Nc (corrected speed) performance * Ran steam detection flow variations and blockage tests

Total fired hours = 17

Total number of fired starts = 7

6 fired shut downs and 1 trip (108% speed)

Test Results

1. FSFL pre-shipment test ran successfully, meeting pretest planned CTQs (objectives).
2. The compressor airflow and efficiency were confirmed as pretest prediction.
3. The compressor inlet flow probes (to be used for field test) were calibrated successfully
4. Met one condition of the National Grid Code (NGC) under frequency requirements (in view of compressor surge margin.
5. The compressor cooled cooling air (CCA) flow and rotor temperatures performed as expected.
6. Bucket aeromechanics and temperatures at steady state no load conditions are acceptable.
7. Mark VI control system was successful in terms of software, hardware, interface, data collection and TMR (triple modular redundancy).
8. All accessory skids, including CCS (clearance control system), CCA and HPU (hydraulic power unit), performed satisfactorily.
9. AWS (aft wheel space) heating system for shut down was successful and will be installed for field unit to understand full load shut down.
10. Steam cooling leakage and blockage tests DFSS (design for Six Sigma) were successful in selecting the field protection system.
11. Rotor critical speed measurements met pretest predictions. Based on bearing oil flow DFSS, it is recommended to reduce oil flow and reduce power.
12. Wheel space temperatures were within design limits. Needs improvement in thermocouple installation and check out for field unit.
13. Turbine clearance DFSS (Design for six sigma experiments) was successful in deriving a transfer function and this will be used to control clearance in field with CCS (clearance control system) and CCA (cool cooling air) skid's temperature adjustments.
14. The turbine casing temperatures were as predicted.
15. The instrumentation and data acquisition system, especially the new telemetry system, was successful in providing reliable data.

III. Third factory test

MS7001H FSNL First 7H Full No Load Factory Test

7H FSNL Test Objectives:

1. Confirm the compressor rig test results (validate compressor performance, VSV schedule, and aero mechanical stability).
2. Validate Compressor rotor cooling system.
3. Understand rotor dynamics.
4. Validate bearing operational characteristics
5. Validate clearance control system
6. Determine starting/shutdown characteristics

Gas Turbine Configuration for the 7H FSNL Test:

The flange to flange 7H gas turbine contained a production compressor rotor and airfoils (stator and rotor blades), limited life turbine hot gas path components (nozzles, shrouds and buckets), a 9E combustion system modified to fit the 7H turbine, a new Mark VI control, and new power plant accessory skids. The FSNL test configuration (drive train) included a flange to flange gas turbine connected to the starting means through an instrumented (telemetry) coupling spool and flexible couplings and shaft. This prototype unit has six variable stator vanes including the IGV (inlet guide vane), which are ganged and moved in unison with stage 2 as a master vane for VSV (variable stator vanes) openings and closings.

The starting device in the test stand had an 8000HP main motor with a 40 HP turning gear motor (to turn rotor at 2.9 rpm) and a 75 HP pony motor to turn rotor at 155 rpm.

The power plant related equipment includes the two-sided air inlet, single exhaust and number of gas turbine skids. In the test stand at the Greenville plant, the standard production gas turbine skids were installed together with H-specific gas turbine skids such as active clearance control, cool cooling air, and variable stator HPU (hydraulic power unit).

Instrumentation

A selected number of compressor rotor blades (RO) and stator vanes were strain gauged. The compressor casings had dynamic pressure probes for blade tip deflection measurement and a selected number of compressor wheels had thermocouples to monitor the internal temperatures.

The list of sensors installed for various components is shown in the table below:

Gas Turbine Component / System	7H FSNL
Turbine Shaft	
Turbine Buckets	
Turbine Rotor Steam Cooling	
Compressor Rotor	X
Compressor Stator	X
Structures	X
Bearings	X
Turbine Nozzles	
Turbine Shrouds	
Turbine Secondary Flow	
Combustor	
Performance	X
X = Instrumented components	

Test Runs & Major Events

RUN #	DATE	MAJOR EVENT / OUTCOME
0	1/21/2000	* First crank to 12% speed * Restart and accelerate to 31.1% speed * Established crank and purge speed * Conducted "dry fire" run
1	1/27/2000	* First fire, unit to 3600 rpm with VSV at 18.5 degrees and no bleed through stage 15 * Check out fired shut down sequence
2	1/31/2000	* Second fired run to 100% speed. * Conducted stage 15 bleed and VSV variation DOEs (design of experiments). * Ran CCS tests with temperature variation of 575, 500 and 400F. * Ran aero mechanical speed swing (100%-105.1%-100%). * Unit shutdown with VSV at 18.5 degrees (60% closed).
3	2/7/2000	* Third fired run to check rotor dynamics * Exhaust frame strut cooling flow direction reversed. * Fired shut down with 18.5 degrees VSV and stage 12 bleed open @ 90% corrected speed.

4	2/8/2000	* Fourth fired run, to understand rotor sensitivity for compressor end unbalance (345 gm). * Successfully completed CCA DOEs (design of experiments). Varied CCA temperatures and cooling flow variations at 100% speed. * Ran max speed to 104% for "rotor dynamic" studies. * Shut down with 18.5 VSV and stage 12 bleed open @ 90% corrected speed
5	2/11/2000	* Fifth fired run for turbine end unbalance sensitivity with 650 gm unbalance at turbine aft end. * Held unit at 100% speed for 38 minutes and fuel gas pressure to 200 psi, forced to have fired shut down. * Ran hot restart and conducted DOEs for VSV variation and stage 15 bleed flow changes. * Conducted speed swing from 98% to 104% speed * First trip from 104% speed to check both "Rotor dynamics" and "Control primary overspeed system".

Total fired hours = 17.9

Total number of fired starts = 6

Test Results

1 7H FSNL test ran successfully, meeting all planned CTQs (critical to quality) without any significant test problem.

2. The compressor air flow and efficiency were confirmed with pretest prediction based on Lynn 7H compressor rig test.

3. The compressor blade aeromechanics response was below design level during start up and steady state. The shutdown response was brought to the design level by modifying the shutdown sequence (closed VSV (variable stator vanes) and stage 14 bleed open at 90%Nc (corrected speed)).

4. The compressor rotor thermal response was as predicted, and the CCA (cool cooling air) system performed as intended to meet the rotor temperature response. CCA DOEs were successful in optimizing the compressor rotor temperatures.

5. Initially, high vibration was noted in the unit rotor due to lightly loaded thrust bearings. Resolution was achieved by reducing thrust bearing axial spacing from 18 to 12 mils.
6. The Mark VI control system and all test stand skids operated successfully as design intended.
7. DOEs were performed for the CCS (clearance control system). The tests were successful in establishing the bucket tip clearance to CCS temperature relation, which will be required for field unit performance optimization.
8. The wheel space temperatures were below design limits. The stage 1 forward, stage 3 forward/aft and stage 4 aft data will be evaluated to understand the difference between pretest prediction and actual test results.
9. The first stage bucket capacitance probes were successful in establishing the rotor dwell speeds during the test. For the FSFL (full speed full load) field test, it is recommended to have capacitance probes and strain gauges together to establish the strain levels to deflection relation.
10. The instrumentation and data acquisition systems were successful, providing reliable data. The on line data reduction capability enhanced the test related decisions.

Summary/Conclusions

1. Three factory tests validated both MS9001H and MS7001H compressors for operating performance (air flow and efficiency) and the mechanical integrity of all components.
2. These tests also validated gas turbine operability in terms of performance, rotor dynamics, Mark VI control system, and all accessories (including clearance control skid, cooled cooling air skid, and variable vane actuating system).
3. The instrumentation was successful in terms of providing reliable data.
4. The new telemetry system performance was validated, and this successful system will be used for the 9H and 7H FSFL field tests.

Technology Application

These are test plans to establish the instrumentation requirements for 7H and 9H FSNL and FSFL tests.

Section 2.2.3 (GTET) Technology Validation [C]

The overall objective of this task was to provide confirmation of critical component design and technology. The validations included hot gas path component testing, sub-scale compressor testing, steam purity test trials, and rotational heat transfer testing. Technology enhancements that were not required for the first machine design but will be critical for future ATS advances in performance, reliability, and costs were conducted.

Section 2.2.3.1 (GTETNC) First-Stage Nozzle Design [C]

Section 2.2.3.1.1 (GTETNC) Nozzle Cascade CFD Analysis [C]

Objective

The objective of this task was to apply a fully viscous 3D computational fluid dynamics (CFD) analysis to predict the flow and aid in the generation of heat transfer boundary conditions for the first-stage Nozzle Cascade Test. This validated CFD tool became the vehicle to apply the Nozzle Cascade Test data to the actual machine design problem.

Introduction

The stationary components of the Advanced Turbine System (ATS) are critical to achieving the overall performance goals for the system. The thermal and mechanical design limitation of the first-stage nozzle airfoils defines the maximum conditions at which the gas turbine can be operated and thus influences the limits on performance and output.

The Nozzle Cascade Test Stand employs a full-sized combustor, a transition piece, and a first-stage nozzle segment with three passages. The three passages are created by two actual nozzle segments and two end walls. The cascade efflux is discharged into a water quench through a 106-cm (42-in) diameter duct.

One of the specific test objectives was to establish the static pressure distribution (or Mach number distribution) within the test passages to allow interpretation of heat transfer data to be obtained in a subsequent test. To this end, a CFD model of the test assembly was created with the aim of employing the data collected during the pressure tap test to validate the analytical methodology. The validated tool could then be used to predict conditions during the heat transfer test and for the real machine design

Discussion

The data from the pressure tap test (which yielded strictly aerodynamic information such as static pressures around the airfoils and along the OD and ID wall) and the predictions of the 3D CFD code NOVAK3D were compared, and a detailed internal document was written. The agreement between the CFD predictions and the pressure tap test data was very good, especially in view of the large range of Mach numbers present in the computational field (from very low subsonic to transonic) and the complicated geometry of the test setup. One of the most interesting predictions confirmed by the test data was the non-periodicity of the data. This comparison served to validate NOVAK3D as a

predictive tool for future tests as well as for the actual machine design under different conditions.

Boundary conditions were determined for the pre-test predictions of the heat transfer test series for the first-stage nozzle cascade test program. The CFD results were subsequently used to simulate the aerodynamic characteristics on the ID and OD walls of the nozzle cascade. The primary predictive tool for heat transfer coefficients along the walls requires information about variation of aerodynamic conditions outside the boundary layer formed on the walls. To this end, NOVAK3D was run with representative transition piece inlet temperatures and pressures for various combustor operation modes. Results were cast in the form of static pressure and temperature variations along streamlines adjacent to the walls. The streamlines were selected as close as possible to the walls but avoiding secondary flows such as horseshoe vortices. The data in this form was processed and used in conjunction with a boundary layer code to determine heat transfer coefficients.

Summary/Conclusion

The NOVAK3D package offers the flexibility to mesh complex geometries with minimum degree of approximation. The general agreement between the test data and the code predictions adds confidence to the application of NOVAK3D to the other nozzle cascade and heat transfer test and to the actual engine design.

Technology Application

The validation of NOVAK3D predictive capabilities provides a valuable tool to evaluate the impact of design modifications and off-design performance of ATS nozzles in particular. It also contributes to a more realistic calculation of heat transfer coefficients and consequently enhances the heat transfer predictions in complex geometries.

Section 2.2.3.1.2 (GTETEH02) Combustion-Generated Flow Effects on Heat Transfer [C]

Objective

The objective of this task was to evaluate the freestream turbulence intensity incident upon the ATS first-stage nozzle airfoil, and the effect of this turbulence level on the airfoil heat load. This turbulence intensity level and its character have a major and direct bearing on the heat load for the nozzle airfoil and endwall.

Introduction / Background

The importance of airfoil surface roughness and freestream turbulence intensity on vane and blade heat loading characteristics has been known for many years. Both factors are considered to be major contributors to the undesirable but inevitable increase in airfoil heat loads from idealized conditions to engine representative conditions. In the past, turbine designers relied heavily upon engine experience to dictate the conservatism required to be incorporated into successive designs, such that surface roughness and turbulence intensity effects would be accounted for at least approximately. In more recent years, designs seeking to squeeze out every percent of efficiency require more detailed knowledge of the specific effects, the distributions with location, the alterations

with flow conditions, and the interactions amongst effects. Of even more importance is the concurrent requirement to design airfoils for full life and high reliability. The approaching goal is of course the ability to computationally predict such effects on heat transfer. While the effect of surface roughness, or surface finish, has been relatively well studied for its impact on aerodynamic performance, the effect on heat transfer has been mostly limited to idealized flat plate or tube geometries. Likewise, while the effect of freestream turbulence intensity has been and continues to be studied mostly in situations of flat plates, cylinders in crossflow, or with controlled pressure gradients, the impact on airfoil heat transfer of engine-like turbulence is a topic receiving increased recent attention.

The present experimental study utilizes a transonic linear vane cascade to obtain airfoil heat transfer coefficient distributions for a higher range of Re_{CX} representing larger, higher output gas turbines. A range of surface roughnesses from R_a of 0.4 to 4.5 μm is tested with varying Tu of 4 to 13%. A cold flow mock combustor of the Dry Low NOx type is used to provide large scale turbulence effects specific to the ATS turbine inlet nozzle.

Discussion

The present study utilizes a linear vane, or turbine inlet nozzle, cascade comprised of five airfoils and four flow passages. The test airfoil has an axial chord length of 7 cm, a chord length of 12.75 cm, and a leading edge diameter of 2.2 cm. The span of the cascade flowpath is a constant 9.04 cm, giving a throat aspect ratio of nearly 5. The inlet flow angle is zero degrees, while the exit flow angle is about 77.5 degrees. The cascade is fabricated from an aluminum frame with stainless steel test airfoils for a maximum operating inlet total pressure of about 5 atmospheres at room temperature. The cascade proper is preceded by a flow preparation vessel which houses a variety of upstream configurations. For the tests reported herein, this vessel contains a splash plate at its inlet to distribute the supply air within the vessel, a scaled combustor liner, and a transition piece both made from sheet metal. The combustor liner model is of the Dry Low NOx (DLN) type having no dilution or film cooling air injection. The transition piece transfers the flow from the circular liner geometry to the rectangular cascade inlet dimensions. These two sections combine for a length of about 124 cm, with individual lengths of 68 cm (liner) and 56 cm. Higher cascade inlet freestream turbulence levels are obtained by one of two devices. Perforated plates may be placed at a location 4.5 cm upstream of the airfoil leading edge plane, or a set of scaled DLN-type swirlers may be set into the upstream end of the combustor liner. This latter configuration results in a cold flow combustor mockup, generating both upstream swirl and large scale turbulence more typical of a turbine. The cascade is supplied by the combined output of three house compressors giving a maximum total flow of about 8 kg/sec. An in-line ASME standard orifice station is located upstream of the facility to provide total flow rate. Inlet and exit pneumatic control valves are used to set the pressure and overall pressure ratio for the cascade. For the present testing, the airfoil pressure ratio was kept at a constant value of 1.86 (total inlet pressure over static exit pressure).

The cascade is transonic, operating with an inlet Mach number of about 0.11 and an exit Mach number of 0.98. The inlet total pressure ranges from 214 kPa to 475 kPa depending on the test setpoint. The inlet temperature is essentially that of the compressor discharge, varying from 13 to 30°C depending on the season. These conditions result in cascade Re_{Cx} from 2.2 to 4.8 •10^6, or Re_C of 4.0 to 8.7 •10^6. The cascade operates under a constant pressure ratio distribution condition with changes in Re being affected by changing the pressure (density) level of the air. The pressure ratios shown are the local ratio of static pressure to the total inlet pressure. The middle three airfoils of the cascade comprise the instrumented section. The two airfoils adjacent to the center airfoil are used to monitor the static pressure distribution of the flow passages bounding the center airfoil. Each of these airfoils has pressure or suction side static pressure taps at the airfoil midspan, which are updated through a Scanivalve system every few seconds. Prior to any heat transfer tests, the central airfoil shown with thermocouples was replaced with an airfoil having static pressure taps on both the pressure and suction surfaces. With all three pressure-instrumented airfoils installed, the back wall of the cascade was adjusted to obtain flow periodicity for the central two flow passages.

Three upstream configurations were used to generate various levels and type of inlet freestream turbulence. The "no-plate" case is that without perforated plates or swirlers. Two types of perforated plates were used, the "small hole" plate having 0.508 cm diameter holes on 0.635 cm centers for an open area of 58%, and the "large hole" plate having 0.635 cm diameter holes on 0.953 cm centers for an open area of 40%. The swirler system uses a full set of premix / diffusion swirlers far upstream. A TSI hot-film probe was placed midway between two airfoils along the leading edge plane, with its axis perpendicular to the mainstream direction. Because such probes are normally operated very near atmospheric pressure, an in-situ 'calibration' was used to determine the turbulence intensity under the present pressurized conditions. Since the average inlet freestream velocity is known from an orifice mass flow rate measurement, and is in fact the same for each test point (i.e., Reynolds number is changed via pressure level, not flow rate), hot-film DC voltage measurements from each Reynolds number were plotted against inlet freestream mass velocity ρV to obtain the variation with pressure (density). The resulting variation is very nearly linear (each case has a correlation coefficient of 0.997) and due only to changes in pressure, not velocity. The hot-film AC rms voltage indicates the changes due to velocity fluctuations at a given pressure level, assuming negligible density fluctuations. The resulting turbulence intensities, or AC mass velocity divided by DC mass velocity, are shown as a function of cascade Re_{Cx}.

Figure 2.2.3.1.2-1 shows curves for each plate configuration, with each case showing a variation in Tu decaying with increasing Re_{Cx}. The greatest Tu level achieved is about 13% at low Re_{Cx}. The maximum Tu level at high Re_{Cx} is about 9%. Because the plates are spaced 7 and 9 hole diameters upstream of the airfoil leading edge (considered a minimum for jet merging), there may be anisotropic turbulence at the cascade inlet. No Tu was obtained for the swirler system, as the hot-film probe could not respond accurately for the apparently larger scale turbulence. Turbulence length scales were not measured.

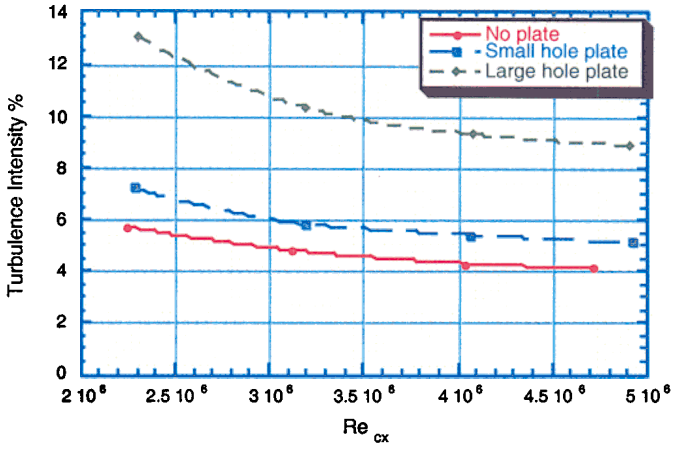

Figure 2.2.3.1.2-1. Turbulence Variation with Reynolds Number

The effect of cascade inlet freestream turbulence intensity on airfoil heat transfer has been observed in the results primarily with respect to the stagnation point region. A comparison is shown in Figure 2.2.3.1.2-2 of the four Tu cases tested for the smooth airfoil at an Re_{cx} of 4.8 $\bullet 10^6$. Smooth surface stagnation point heat transfer increases with Tu for the non-combustor cases, in a similar fashion to previously established relationships of $TuRe_D^{0.5}$. Specifically, the present smooth surface stagnation point Frössling numbers, Fr(0), agree with the correlation of Lowery and Vachon (1975) for the case without the use of a perforated plate. For the elevated Tu cases where a perforated plate has been used, the current Fr(0) data lie in the range of 1.5 to 2.2, which exceeds most reported data of Lowery and Vachon (1975), VanFossen and Ching (1994), and Ames and Moffat (1990). It must be pointed out though, that the perforated plate spacing ahead of this cascade could very well result in anisotropic turbulence, particularly for the large hole plate. Stagnation region heat transfer also follows this same behavior within about $\pm$1.5 cm of the stagnation point. Outside of this region, Tu begins to have varying effect on heat transfer. The pressure side heat transfer is less affected by Tu, but shows a consistent increase with Tu over the whole side. Suction side transition location is moved forward by Tu, but the strength or duration of transition is essentially the same for all non-combustor Tu. The decay of freestream Tu is evident in that the suction side heat transfer coefficients all come together toward the aft end of the airfoil.

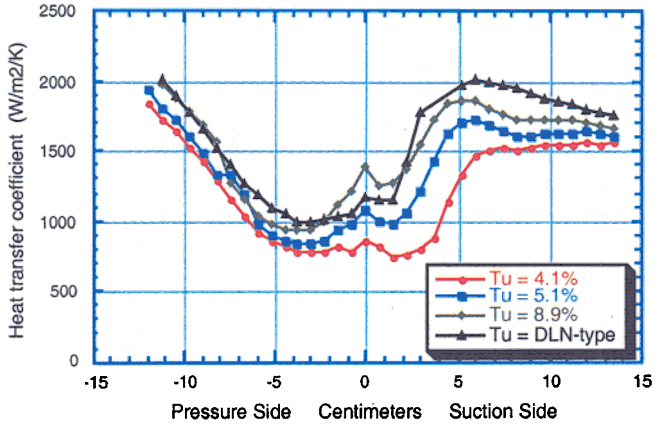

Figure 2.2.3.1.2-2. Smooth Airfoil Comparison

The heat transfer present with the mock combustor turbulence is markedly different in two respects. First, the stagnation region heat transfer is lower than that produced by a plate with Tu of about 9%. This may indicate that the turbulence length scale from the mock combustor is much larger than that of the perforated plate, and of the same magnitude or greater than the airfoil leading edge diameter of D=2.2 cm. Experiments by Britter et al (1979), measured the distortion of turbulence around a circular cylinder. They found that the turbulence vorticity (eddies) were distorted by the mean flow interaction with the cylinder, or blocked by the presence of the cylinder. As the Λ/D ratio decreases (small scale eddies relative to the cylinder size), the eddies are distorted by the very high strain rates. When the Λ/D ratio is large though, the cylinder will effectively block the eddy for a distance of about Λ from the cylinder, resulting in a lower heat transfer as compared to the small scale eddies. This could also be a factor in why the hot-film anemometer did not provide a reliable Tu measurement. The remaining pressure side heat transfer is about the same for the mock combustor Tu. Second, the suction side transitions more abruptly, pushing the entire heat transfer distribution higher, yet coming back to the same trailing edge value.

The cascade was tested with various turbulence-generating means placed upstream of the airfoils, including a scaled cold-flow mockup of a DLN combustor system. Tests were conducted for both smooth and rough airfoil surfaces. Under rough surface conditions, (Figure 2.2.3.1.2-3), the mock combustor was shown to produce essentially the same airfoil heat transfer as was obtained with a large-hole perforated plate placed very close to the airfoil leading edge plane. Hot-film turbulence intensity measurements were made in this cascade environment. The large-hole perforated plate yielded an intensity of approximately 9% at the airfoil leading edge location under design flow conditions. The DLN combustor system produced turbulence with apparent large eddy scale so that hot-film measurement was not considered. However, these results indicate that airfoil heat

transfer distributions measured through the use of a large-hole perforated plate of the type used here are representative of the DLN system influence on airfoil heat transfer.

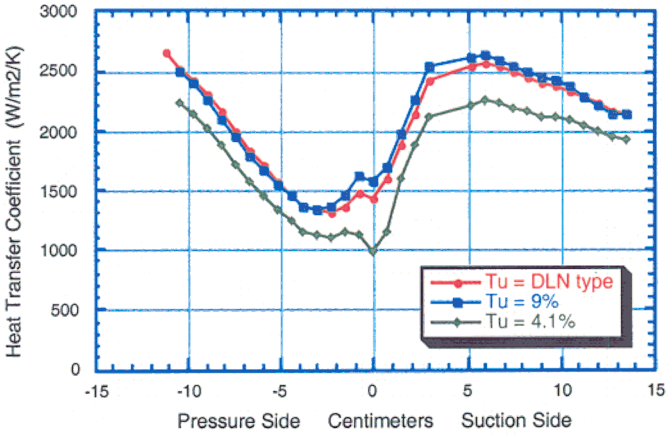

Figure 2.2.3.1.2-3. Rough Surface Comparison

Summary/Conclusion

Comparisons of smooth surface stagnation point heat transfer to available correlations showed mixed agreement, with the best overall agreement provide by the correlation of Ames and Moffat (1990, "Heat Transfer with High Intensity, Large Scale Turbulence: The Flat Plate Turbulent Boundary Layer and the Cylindrical Stagnation Point", Stanford Report HMT-44). This finding is significant for the current design in that the large-scale turbulence effect on airfoil stagnation region heat transfer is substantially greater than that normally assumed for airfoils.

The main point to notice under conditions of elevated roughness, is that the mock combustor Tu produces the same airfoil heat transfer as that obtained with the perforated plate, with only a small leading edge difference. The fact that the apparently very different conditions of Tu and length scale produced by these two devices gives the same result, lends some confidence to the use of plate or grid type Tu heat transfer results to turbine design applications. More information on this cascade may be found in the publication:

Bunker, R.S., 1997, "Separate and Combined Effects of Surface Roughness and Turbulence Intensity on Vane Heat Transfer", 97-GT-135, 1997 International Gas Turbine Conference, Orlando, FL.

Technology Application

The ATS cascade test results have been incorporated directly into the ATS first-stage nozzle design. Comparison of results with both high-turbulence-generating perforated

plates and a DLN combustor system cold-flow mockup have verified the applicability to design of heat transfer results from the former method.

Section 2.2.3.2 (GTETRS) Rotor Steam Transfer [C]

Objective

For stable cooling of the turbine buckets, static flow tests were conducted to validate the steam flows in the circuit to and from the buckets, through the rotor. These tests established flow losses for the unique components in the steam delivery circuit.

Introduction

Engineering analysis is a heavily used tool in the design of gas turbines, especially for the steam cooled ATS gas turbine. However, experience and validation of these tools is necessary for their confident use. There are many aspects of the ATS gas turbine which represent first-time applications for engineering predictive tools. The rotor steam delivery system is a good example of a situation where the components have not been analyzed in the past and accuracy is unconfirmed. Steam inlets, "spoolie" seals, and unique geometry in the steam supply manifolds are several examples of such situations. Pressure losses in these geometries must be defined in order to validate the engineering tools used to design flow in the steam delivery system. The tests described here had two primary purposes. First, they provided initial characterization of various configurations, allowing design tradeoffs. Second, they provided an approach to validation of the pressure losses in these geometries for use in predictive engineering methods The tests carried out here were done on non-rotating systems and compared to analysis. This validation process then allowed the engineering predictive codes to be applied to the rotational situations encountered in the ATS gas turbine.

Discussion

Flow tests were completed for various steam inlet geometries, where the steam first comes on board the rotor. These tests helped to characterize the pressure losses with various configurations and establish a preferred design compromise. The results show good agreement with analytical model results.

Downstream of this steam inlet the flow splits into multiple passages, at the same time turning and changing the flow area. Again, for the flow losses in this region to be accurately represented, a rig test was required. This part of the circuit was added to the flow rig and run with favorable results.

The various components of the steam system are connected together with "spoolie" seals. These components offer both forward- and backward-facing lips that provide additional sources of pressure loss to the system. These components were also flow tested for pressure loss, and the results were used to validate the analytical system flow model.

The steam supply manifolds are used to distribute steam to the buckets. Due to the unique geometry of this component, pressure losses were measured to determine the effects on the supply of cooling steam to the buckets. A flow test rig was used to test and

characterize the pressure losses in the manifolds and to help validate the analytical models of the rotational effects on the steam flows. The test data from the supply manifold test raised questions regarding the calibration of the metering orifices used. Portions of the test were rerun, yielding results that showed acceptable agreement between test and analysis.

A steam return manifold was also tested. In parallel, CFD analysis was run for these test conditions to establish the validity of the analysis methodology.

The static flow tests and the CFD analyses were compared to test data, and analytic procedures were defined and validated.

Summary/Conclusion

Pressure losses in various components of the steam delivery system with unique geometries were characterized. These tests provided results used for initial design tradeoffs and also provided a basis for validating engineering predictive analysis which could then be extended to new design studies. Inlets, "spoolie" seals, and manifolds were studied experimentally. Comparisons were made between these static tests and comparable analyses, allowing the extension of the predictive techniques to rotating environments.

Technology Application

Rotor steam transfer tests are used to evaluate the design optimum for the 7H and 9H turbine bucket cooling.

Section 2.2.3.3 (GTETSE) Rotor-Bucket Steam Transfer Spoolie [C]

Objective

The primary seals in the H machine are tube seals (spoolies), which are needed to accommodate misalignment between the components due to tolerance stack-up and thermal growth in the rotor steam circuit. The leakage through these seals is expected to change over the life of the H machine and thus have a significant effect on its performance. For example, an initial improvement in sealing ability is expected as the mating surfaces seat themselves. This sealing ability is then expected to degrade with increased wear of the seals. Additionally, cyclic centrifugal loading due to turbine startup and shutdown can cause fatigue cracks that significantly increase leakage.

The objectives of this task were (1) to validate the design of the spoolie by determining the leakage rate as a function of wear and fatigue and (2) to determine the design and service factors that have the strongest effect on leakage through the spoolie.

Introduction

A high-temperature (1000°F), high-pressure test rig (600 psi), capable of simulating spoolie operating conditions during service in the H machine was built at CRD. The test facility includes a DI water plant which provides high purity filtered water to a boiler and superheater. This combination is capable of delivering either superheated steam or heated

high pressure air to the test specimen. The boiler and superheater are connected to the test rig by heat traced, insulated, stainless steel piping and includes a high temperature, 2μm particulate filter upstream of the test rig. The test rig was designed with removable inserts so that both large (manifold) and small (bucket) spoolies can be tested. The rig was heated and insulated so that the specimen and cooling fluid can be maintained at a uniform temperature during testing. In addition, the rig was modified to provide an alternating side load to simulate the variation in centrifugal force during machine startup/shutdown. The leakage past the spoolie flows through an 8 μm particulate filter into a leakage manifold. The leakage manifold volume was critically designed: small enough to minimize the response time of the system, yet with a sufficiently large cross sectional area to reduce the flow velocity to levels where the effects of dynamic pressure are negligible. The manifold had nine critical flow venturies that measured leakage rates (flow) over five orders of magnitude. These venturies were controlled by hermetically sealed bellow valves. The exhaust was collected under a slight vacuum and continually drained. A schematic of the rig capabilities is shown in Figure 2.2.3.2-1 below.

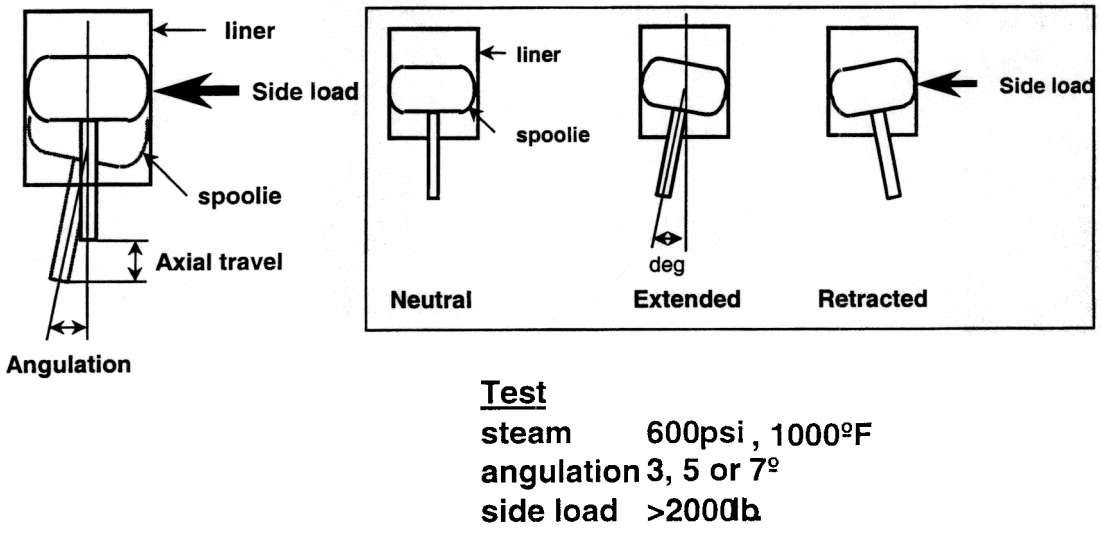

Figure 2.2.3.3-1. Schematic Diagram of Test Rig.

A 2^3 design of experiments was developed to determine the effect of steam temperature, joint interference and degree of angulation on spoolie life. The test matrix is shown in Figure 2.2.3.2-2 below.

Test #	Temp, F	Angle, deg	Inter. inch
1	700	5	.015
2	700	3	.015

3	1000	3	.011
4	1000	3	.015
5	900-950	5	.015
6	700	5	.011
7	700	3	.011
8	900-950	5	.011

Figure 2.2.3.3-2. Spoolie Test Matrix

Results

Testing successfully demonstrated the durability of spoolie coating in a steam environment.

Results from the design of experiments showed that spoolie life increases with decrease in angulation, increase in steam temperature, and increase in joint interference as shown below.

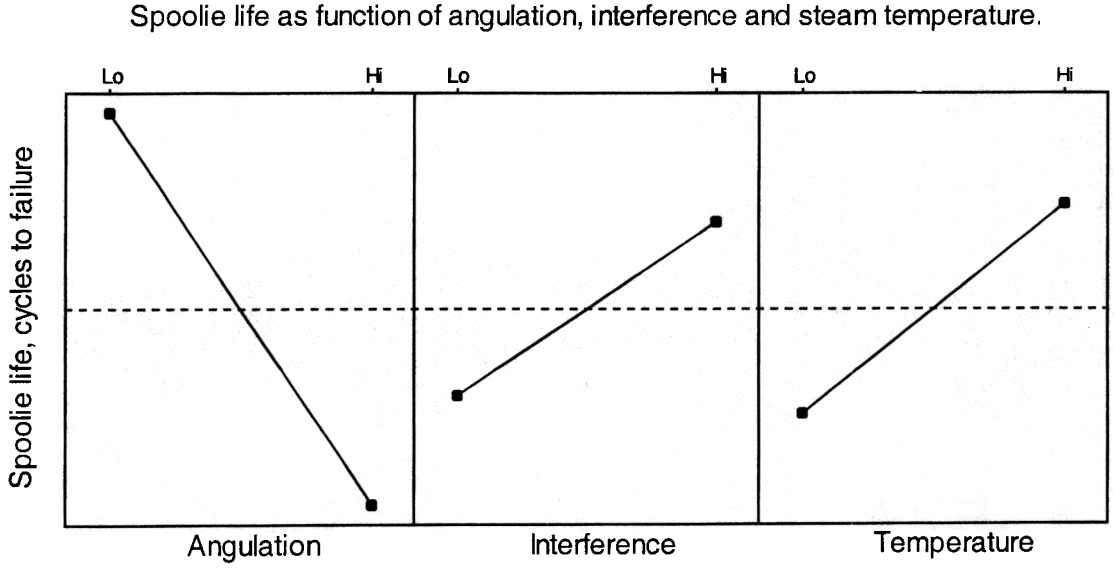

Figure 2.2.3.3-3. Spoolie life as a Function of Angulation, Interference, and Steam Temperature

Technology Application

The results of this task will be used to predict spoolie life and performance in service. In addition, failure analysis will help improve spoolie design through use of superior materials and design parameters.

Section 2.2.3.4 (GTETRH) Rotational Heat Transfer [C]

Section 2.2.3.4.1 (GTETRH01) Turbine Rotational Heat Transfer [C]

Objective

Prior to this program, only a limited database was available on the effect of rotation on heat transfer in turbine blade cooling passages. At the conditions present in the ATS turbine, major extrapolation of the existing data was required. To extend the data to the range of Reynolds and Buoyancy numbers present in the ATS turbine, measurements of the local heat transfer coefficients under these conditions were obtained in a low aspect ratio rectangular blade cooling passage with and without turbulators. One objective of this task was to construct, install, and test a 6.6:1 aspect ratio cooling passage in the full-scale CRD rotating test rig over a range of Buoyancy numbers previously obtained in the low aspect ratio passage. In parallel, a sub-scale test rig was employed to evaluate alternate turbulator designs in order to identify the best configuration for subsequent evaluation in the full-scale test rig.

Introduction/Background

Cooling of gas turbine buckets to ensure adequate life margin at advanced engine conditions of pressure and temperature requires that the internal heat transfer as influenced by rotation be known with sufficient accuracy. The existing database, comprised of information readily available in the open literature, has limited advanced design applicability considering the range of geometric and fluid-thermal dimensionless parameters of interest. Studies conducted by computational fluid dynamics (CFD) have demonstrated that as the range of such parameters is extended, the characteristics of the predicted heat transfer capability change significantly, even to the extent that bucket cooling designs which perform adequately at state-of-the-art conditions are marginal or unacceptable at advanced conditions. It must be noted, that while CFD may be used as a tool for gauging such general trends, it is not yet sufficiently accurate to replace the experimental design data, especially at extended conditions.

Rotational effects on heat transfer are of concern in gas turbines and compressors for both the hot gas flow paths and the internal cooling flow channels. In view of the major factor such rotating channel flows have on the cooling of the turbine buckets, special attention must be paid to both the radial inflow and outflow passage heat transfer for all surfaces of the internal channels, as well as for various aspect ratios and orientations of channels as they typically appear in designs. Although the published data generally cover the parameters of interest to currently operating machines, they do not extend to the operating conditions of the ATS steam-cooled, closed-circuit turbine buckets. Missing from such data are channels of large aspect ratio such as those encountered in the midchord region of many designs, and channels of triangular low aspect ratio and spatial orientation such as those in the bucket trailing edge region. The typical database parameters for designs include Rotational numbers from 0 to 0.5, Buoyancy numbers from 0 to 1, Reynolds numbers up to 75,000, and aspect ratios of 1:2 to 2:1. Now consider the range of parameters required for the design of the ATS turbine, which includes Rotational numbers from 0 to 0.5, Buoyancy numbers from 0 to 5, Reynolds numbers up to 500,000,

and aspect ratios of 1:8 to 7:1. Combining these parameter ranges with the need for turbulation to enhance heat transfer further, and the requirement for experimental validation of such rotating heat transfer becomes clear.

Further introduction on this topic can be found in the publication: Staub, F.W., Maddaus, A.D., and Tekriwal, P.K., 1995, "Rotational Effects on Heat Transfer at Advanced Engine Conditions," 95-GT-417, 1995 International Gas Turbine Conference, Houston, TX.

Discussion

The general test rig and facility layout is depicted in Figures 2.2.3.4.1-1 to 2.2.3.4.1-4. A more complete description of the facility and operation may be found in the referenced paper 95-GT-417. The test section, or payload, is mounted in the Rotating Heat Transfer Test Facility at the furthest extent of one arm. The radius at the duct inlet is 48.4 inches. R-134a refrigerant is supplied to the duct by a compressor at flow rates up to 1 lbm/s. The arm is rotated up to 800 RPM and is monitored for excessive vibrations. The entire arm is housed within an insulated box. The air inside the insulated box is heated to roughly the temperature of the duct walls to reduce conduction heat losses from the payload to the environment.

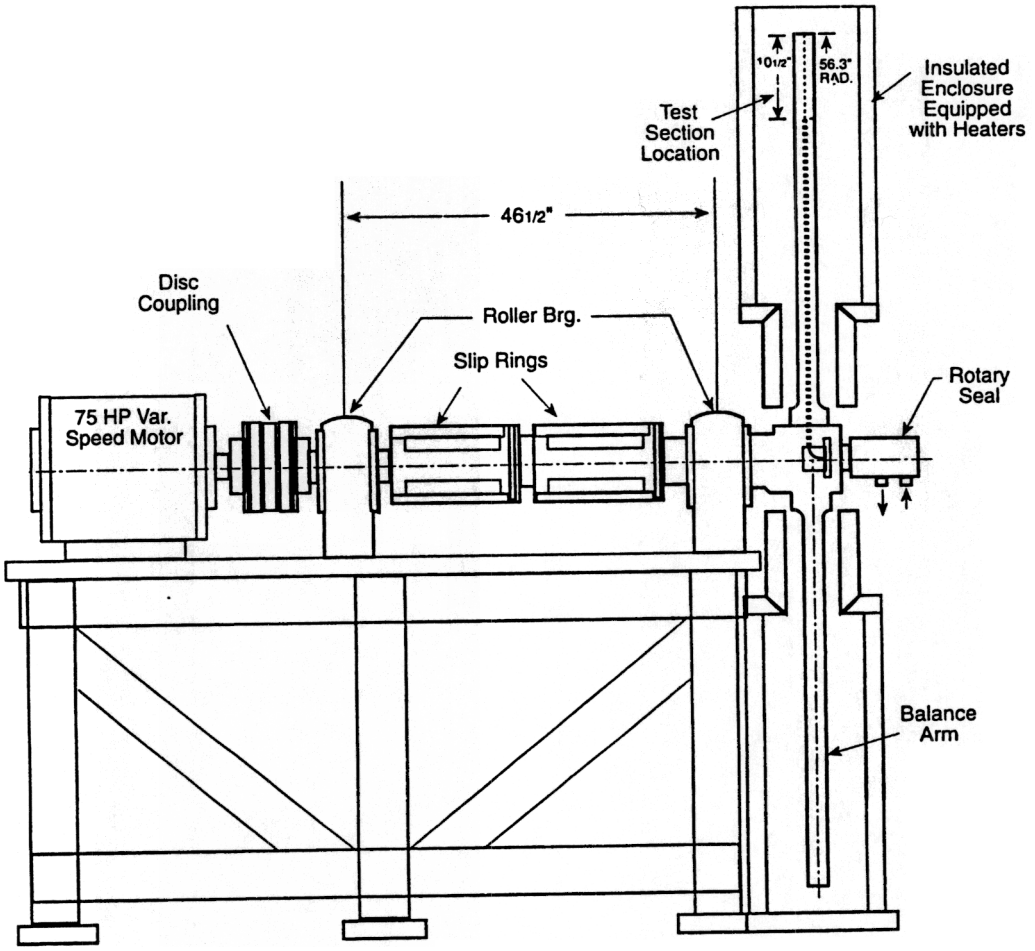

Figure 2.2.3.4.1-1. Rotating Bucket Rig

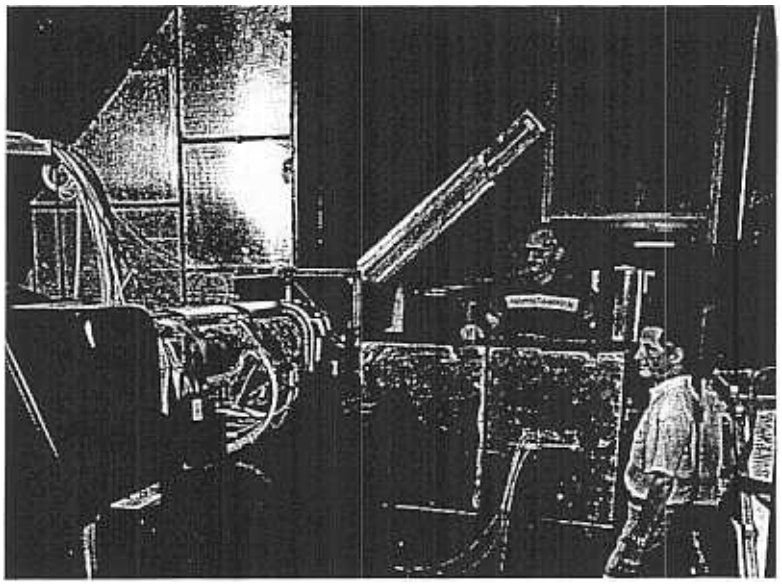

Figure 2.2.3.4.1-2. Photo of Rotating Rig

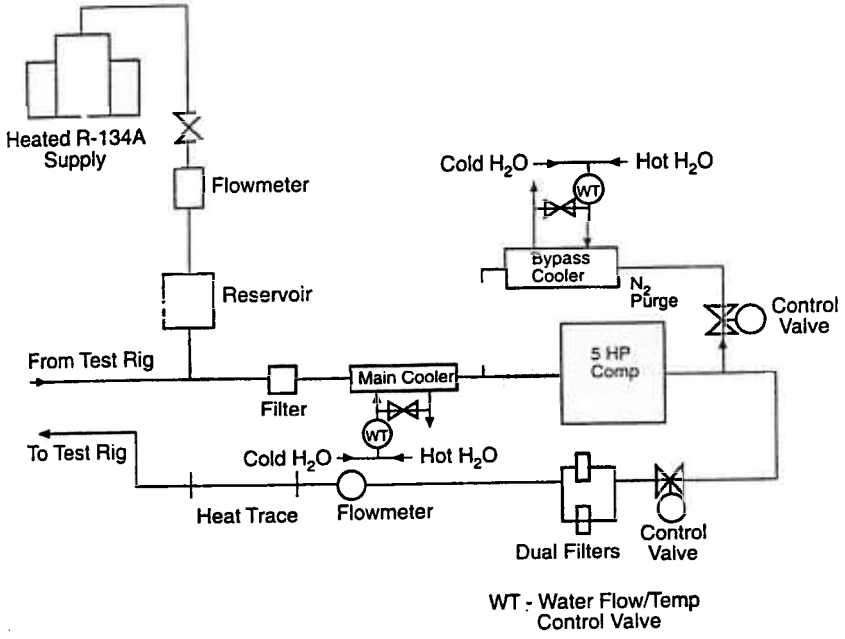

Figure 2.2.3.4.1-3. Rotating Bucket Rig Flow Schematic

During a typical run, the flow rate is set until the desired Reynolds number is achieved. The flow rate is measured with a turbine flow meter. After achieving the proper Reynolds number, the arm is spun at an estimated rotational speed. Then the heaters are turned on and the duct walls heated until they all average ~50°F (or the target temperature differential) warmer than the bulk flow temperature. The bulk temperature is measured with two thermocouples at the inlet manifold and two at the exit manifold. To compute the local bulk temperature at any given radial station in the test duct, the inlet and exit mean temperatures are linearly interpolated.

After this initial temperature balance is reached, the rotational speed, and usually also the heater inputs, are adjusted until the desired Buoyancy number is achieved. Again, Reynolds number and temperature uniformity are all checked and the control settings iterated upon until the desired Reynolds number and Buoyancy number are met with the duct walls all at roughly the same temperature. At this point, 5 minutes worth of data are recorded. The data on all signals is then averaged over this 5 minutes before reducing the data. The heater output is determined by measuring the heater current with Yokogawa Model 2534-10 power meters. The heater resistances are pre-measured using a 4-wire resistance measurement technique for high precision. The cal-rod heaters are supplied with AC voltage, while the foil heaters are supplied with DC voltage.

A significant amount of heat is conducted to or from each heater to neighboring heaters, external payload structures, and other spurious conductive paths. Two separate 2-D conduction analyses were performed in ANSYS to model the radial and circumferential conduction paths separately. Also, the test section was evacuated and some runs were obtained to measure the heat lost from the payload to the box air as a function of RPM.

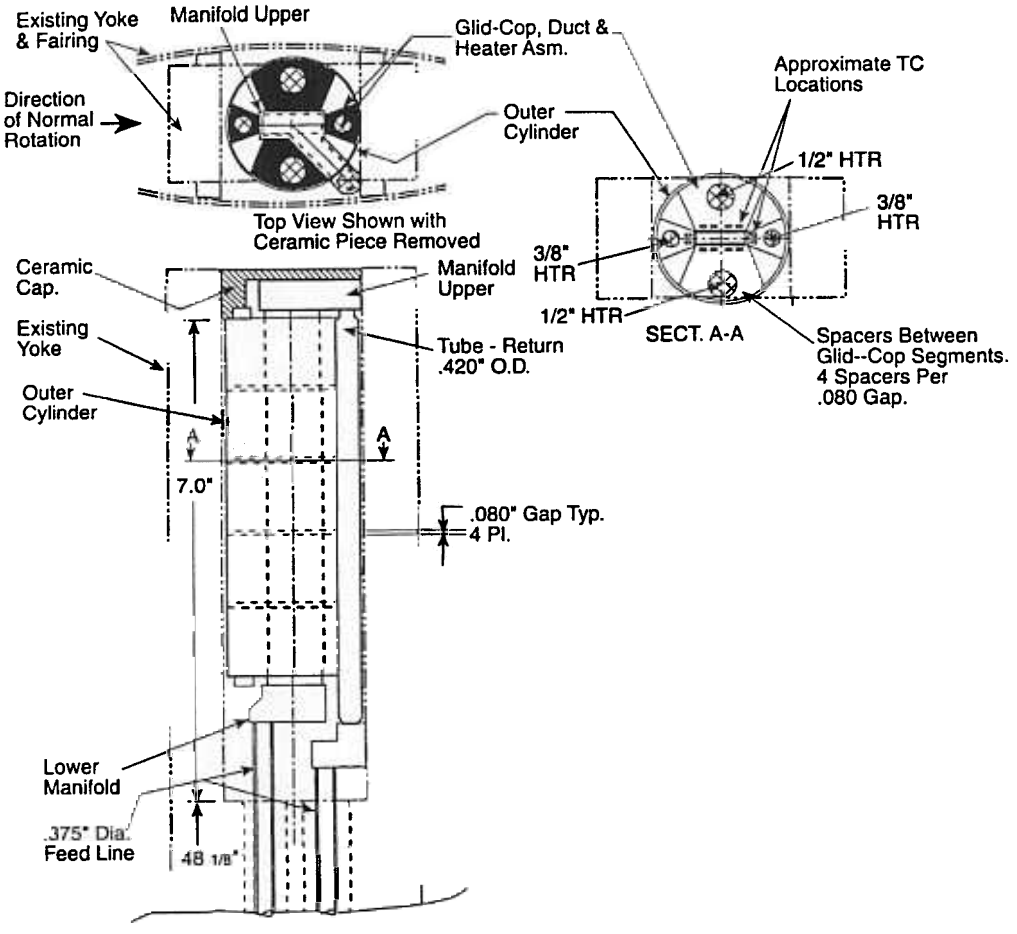

Figure 2.2.3.4.1-4. Rotating Bucket Rig Cross Section

The arm inlet and exit pressures are measured with 300 and 200 psia pressure transducers, respectively. However, the pumping of the arm leads to significant

compression of the working fluid by the time the fluid reaches the test duct. The test duct pressures are then estimated using the pumping parameters of the radial duct flow.

The measurement of the local heat transfer coefficient in a turbulated high aspect ratio duct of 6.6:1 was completed in the full-scale rotational test facility. A total of approximately 270 tests covered a range of Reynolds numbers and Buoyancy numbers. Both radial outflow and inflow heat transfer data were obtained for the leading and trailing walls of the channel (representing bucket pressure and suction side walls). Each end of the duct contained 180-degree bends to model the turning that occurs within serpentine cooling passages. The effect of rotation on the turbine bucket tip, internal surface heat transfer coefficient was also determined.

The evaluation of alternate turbulator configurations in the low aspect ratio passage was carried out in parallel using the small-scale test rig that allowed low cost changes to be made using thin-film heaters and thermocouples on each of the four duct walls. Alternate turbulator designs were cemented to the thin-film heaters using a soluble cement. Buoyancy numbers and Reynolds numbers were attained in the small-scale test rig, where the emphasis was on the relative performance of the various turbulator configurations. The height and pitch of the turbulators were independently investigated, and several innovative designs were considered to improve the heat transfer coefficients in radial outflow on the lead side. More details on this facility and its capabilities can be found in the paper:

Willett, F.T. and Bergles, A.E., 2000, "Heat Transfer in Rotating Narrow Rectangular Ducts with Heated Sides Oriented at 60° to the R-Z Plane", 2000-GT-224, Int. Gas Turbine Conference, Munich.

Summary/Conclusion

Design data has been obtained of direct applicability to the ATS turbine and the thermal design of the rotating bucket cooling systems. Comparison of the heat transfer coefficient data for an aspect ratio 6.6:1 passage with that of a lower aspect ratio passage (or one at differing flow conditions) has confirmed that significantly different behavior is present than would be predicted from a simplistic extrapolation of existing data. It is therefore essential to the success of this design that accurate knowledge of detailed heat transfer under engine design conditions be obtained. This also points to the need for additional testing of rotating channels for various other differing aspect ratios and/or channel orientations.

Technology Application

The data obtained in the full-scale test rig were employed to design bucket cooling passages that avoid the low performance operating range. The data obtained on the effect of alternate turbulator configurations in the small-scale test rig were employed in design tradeoff analyses for the 7H and 9H steam cooled buckets.

Section 2.2.3.4.2 (GTETRH) Rotational Effects on Bucket Mixing Ribs [C]

Objective

The addition of mixing ribs to turbine blade radial cooling passages was found to provide a more robust thermal design, without the severe reduction in performance measured previously, when evaluated in sub-scale models at low Reynolds numbers. Since this design improvement was scheduled for use in the ATS gas turbine, design data that incorporate this change were obtained at full-scale conditions in the operating range of interest.

A full-scale turbulated test passage of an appropriate aspect ratio 3.3:1 was constructed that was similar to the one tested previously except for the addition of the new mixing rib geometry. This passage was evaluated in the full-scale rotational test rig over the range of dimensionless parameters present in the ATS gas turbine.

Introduction / Background

It is well documented in open literature, that under certain conditions within rotating channels the heat transfer coefficients present on the lead wall (suction side) may be severely reduced below the level which would otherwise exist without rotation. This effect is due to the interaction of buoyancy forces with the rotational forces, and can in extreme cases reverse the flow inside the channel along one wall. This is a highly undesirable condition. In addition to quantifying the rotating channel heat transfer distributions for the actual conditions and geometries present in the ATS turbine bucket designs, it is desired to improve upon the conventional turbulated designs in a manner which reduces such undesirable rotational effects. One method of approach is through the use of mixing ribs.

Discussion

The full-scale test passage, incorporating mixing ribs in addition to a previously tested turbulator configuration with aspect ratio of 3.3:1 was designed, constructed, and installed, and is shown in Figure 2.2.3.4.2-1. An unheated passage of the same cross section as the heated passage was installed upstream of the test passage and connected with the test passage by a 180° turn. This arrangement provides a realistic inlet velocity distribution to the test passage, as in a serpentine cooling design. Similar to the passage tested without mixing ribs (Section 2.2.3.4.1), the four passage sides were independently heated electrically using thin-foil heaters, and had enough thermocouples to allow the evaluation of the local heat transfer coefficient on each passage side. The thermocouples on the leading and trailing sides provide the radial variation of the heat transfer coefficient over fourteen equal radial lengths.

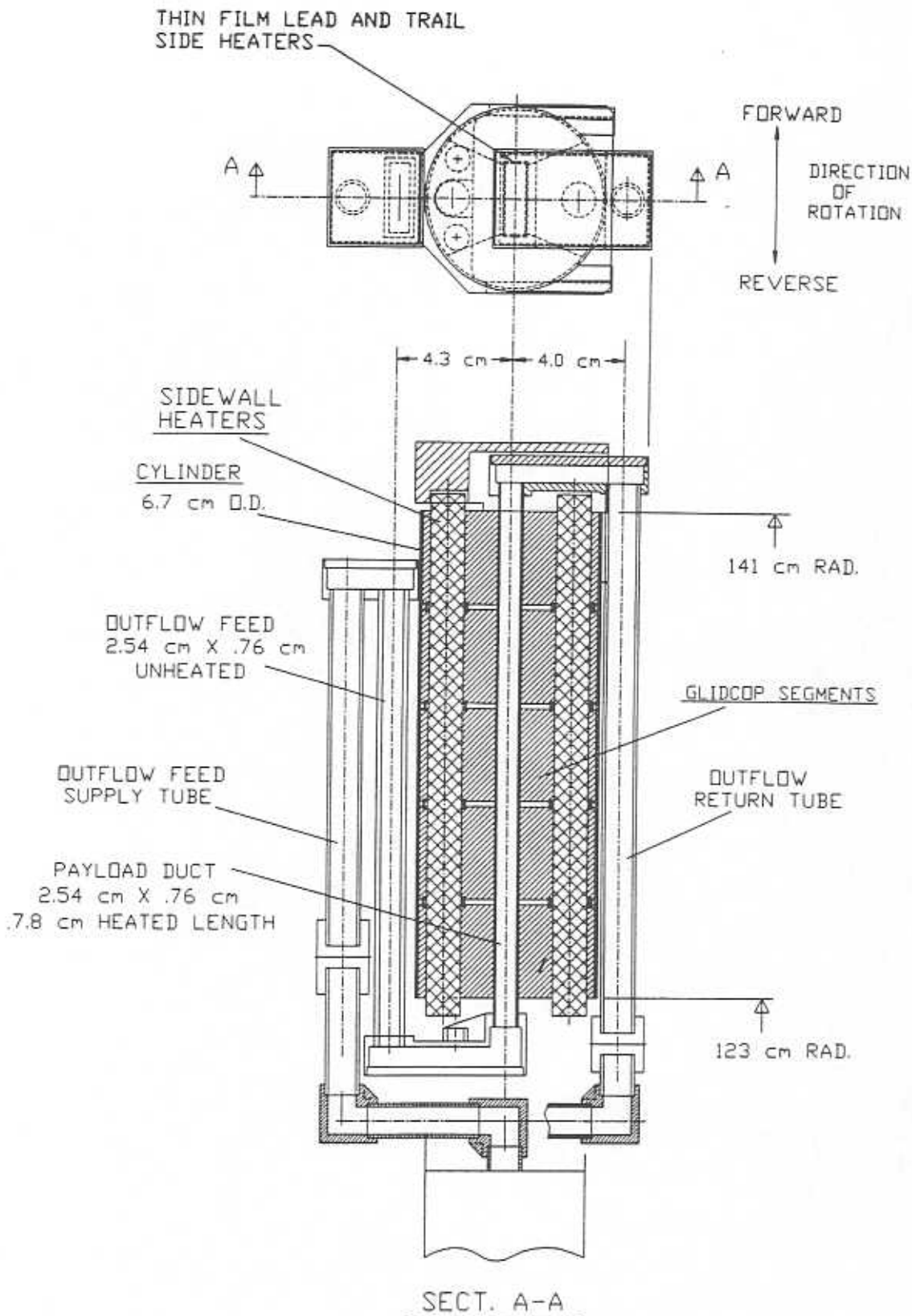

Figure 2.2.3.4.2-1. Rotating Bucket Rig with Mixing Ribs Cross Section

The mixing ribs installed in the turbulated test duct in the full-scale test rig were evaluated over the Buoyancy number range of interest at Reynolds numbers up to 300,000. The data confirmed the benefit of using mixing ribs at high Buoyancy numbers and also showed that the radial location of the ribs has a significant effect on the leading and trailing side heat transfer. Additional small-scale tests were run to evaluate a range of mixing ribs configurations.

Summary/Conclusion

The use of mixing ribs within the rotating cooling passages of the turbine buckets has been experimentally validated and quantified for design purposes. An associated benefit to heat transfer on the lead and trail walls was realized, in addition to the elimination of the typical tendency to reversed flow.

Technology Application

The new turbulator and rib design is being employed to reduce the bucket cost and to yield a more robust design with improved performance at high Buoyancy numbers.

Section 2.2.3.4.3 (GTETRHTPD) Bucket Cooling Circuit Rotational Pressure Drop Test [C]

Objective

The objective of this task is to determine the effect of rotation on the pressure drop in a radial bucket cooling passage. Computational fluid dynamics (CFD) predictions of the effect of rotation on bucket cooling passage heat transfer and pressure drop indicate a significant effect of the Buoyancy number on pressure drop. Since the bucket pressure drop is a major fraction of the total system pressure drop involving the coolant, it was deemed necessary to measure this effect using the full-scale test rig.

The high aspect ratio turbulated duct assembly was instrumented to measure the pressure drop between the inlet and outlet manifolds. Appropriate heaters were employed on the pressure measurement lines to avoid condensation of the working fluid and to minimize the density corrections required due to temperature differences between the measurement lines and the test duct. This allowed the differential pressure transducer to be mounted near the rotational axis, where no transducer correction for centrifugal effects was required. The pressure drop for both radial outflow and radial inflow was measured.

Introduction/Background

The use of a closed-circuit, steam-cooled system for the ATS turbine airfoils puts constraints on many combined cycle system parameters associated with the delivery and return of the steam. Both the gas turbine nozzles and the buckets must be designed for operation with a maximum steam pressure drop in the individual flow circuits of the components. This requirement dictates that the pressure drop within the rotating cooling channels of the turbine buckets be known for all design conditions. While pressure losses within stationary passages are relatively easy to predict, those in rotating channels can be

confounded by the same conditions which complicate the heat transfer, namely buoyancy and rotational forces. It is therefore essential that experimental validation of such pressure losses be obtained.

Discussion

The full-scale rotational test facility consists of a rotating arm equipped with a yoke to hold the test section, and suitable passages for the working fluid, power leads, and thermocouples. For the measurements carried out in this investigation, only the leading and trailing sides of the test duct were heated in order to more closely simulate the conditions in the application. The test section geometry of channel aspect ratio 6.6:1 was utilized, as described in Section 2.2.3.4.1.

The results obtained showed a strong effect of the Buoyancy number on pressure drop with a larger effect in radial outflow. These results have been reported for designers in the form of a correlation that relates the ratio of the pressure drop with rotation to the pressure drop without rotation, with the Buoyancy number as the correlating variable.

Summary/Conclusion

Pressure drops have been measured for both radial inflow and outflow conditions within a high aspect ratio, turbulated channel for a range of rotational conditions. As with the heat transfer, the pressure drop is found to be significantly altered over that which would exist under stationary conditions.

Technology Application

The new pressure drop correlation, which includes the effect of the Buoyancy number, is now in use in the evaluation of alternate coolant passage designs and in the evaluation of the flow-pressure drop characteristic of the ATS turbine bucket cooling system.

Section 2.2.3.4.4 (GTETRH) Rotating Trailing Edge Heat Transfer Tests [C]

Objective

A number of tests were conducted to measure the heat transfer coefficients in the cooling passages of buckets. The completed tests focused on rectangular turbulated ducts (some with mixing ribs) of various aspect ratios representative of the range of geometries of cooling passages in most of the cooling circuit. The trailing edge cavities of the buckets, however, have a more triangular shape, and also have the difficult task of cooling the trailing edge. Validation of the ATS gas turbine second-stage bucket trailing edge passage is required primarily because of the strong effect of rotation on radial outflow, but also because of geometrical differences. The objective of the current task was to measure the heat transfer coefficients in a constant-area duct that captures all of these features. Tests were performed in the full-scale rotational test rig.

Introduction/Background

Previous studies of the heat transfer in smooth and turbulated rectangular ducts of various aspect ratios have shown that rotational effects can be quite significant, and in fact

sometimes detrimental. Rotational outflow was found to be particularly sensitive to rotational effects. These data have proved invaluable during the design of most serpentine cooling passages in turbine buckets.

Trailing edge cavities present a unique challenge. They have very high aspect ratios (or low depending on the point of view), are non-rectangular, and are not parallel to the axis of rotation. In the current open literature, there are little or no data pertaining to trailing edge channel cooling for aspect ratios of more than 1:2, and certainly no data for the flow conditions of the ATS turbine closed-circuit cooling system. Therefore, the rectangular-duct databases do not provide the bucket designer the data needed for confident cooling-side heat transfer predictions in these trailing edge ducts.

Discussion

The trailing edge heat transfer test section utilizes the same Full-Scale Rotating Test rig as described earlier in Section 2.2.3.4.1. The Stage 2 Bucket trailing edge passage has many complicating geometric features that affect heat transfer: changing area, changing shape, twist (or orientation relative to axis of rotation), and turbulated walls. The goal of this test was to assess the effect of rotation on the heat transfer in a duct representative of this passage. Therefore, a much simplified geometry was selected for the test duct, but one which retains the salient features necessary to generate quality design data. A schematic representation of the bucket trailing edge is shown in Figure 2.2.3.4.4-1, and the rotating rig cross section is shown in Figure 2.2.3.4.4-2.

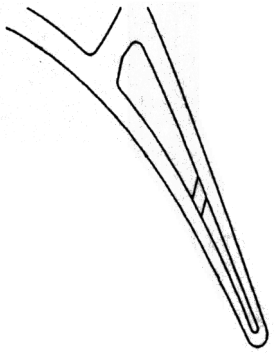

Figure 2.2.3.4.4-1. Bucket Trailing Edge Cooling Channels.

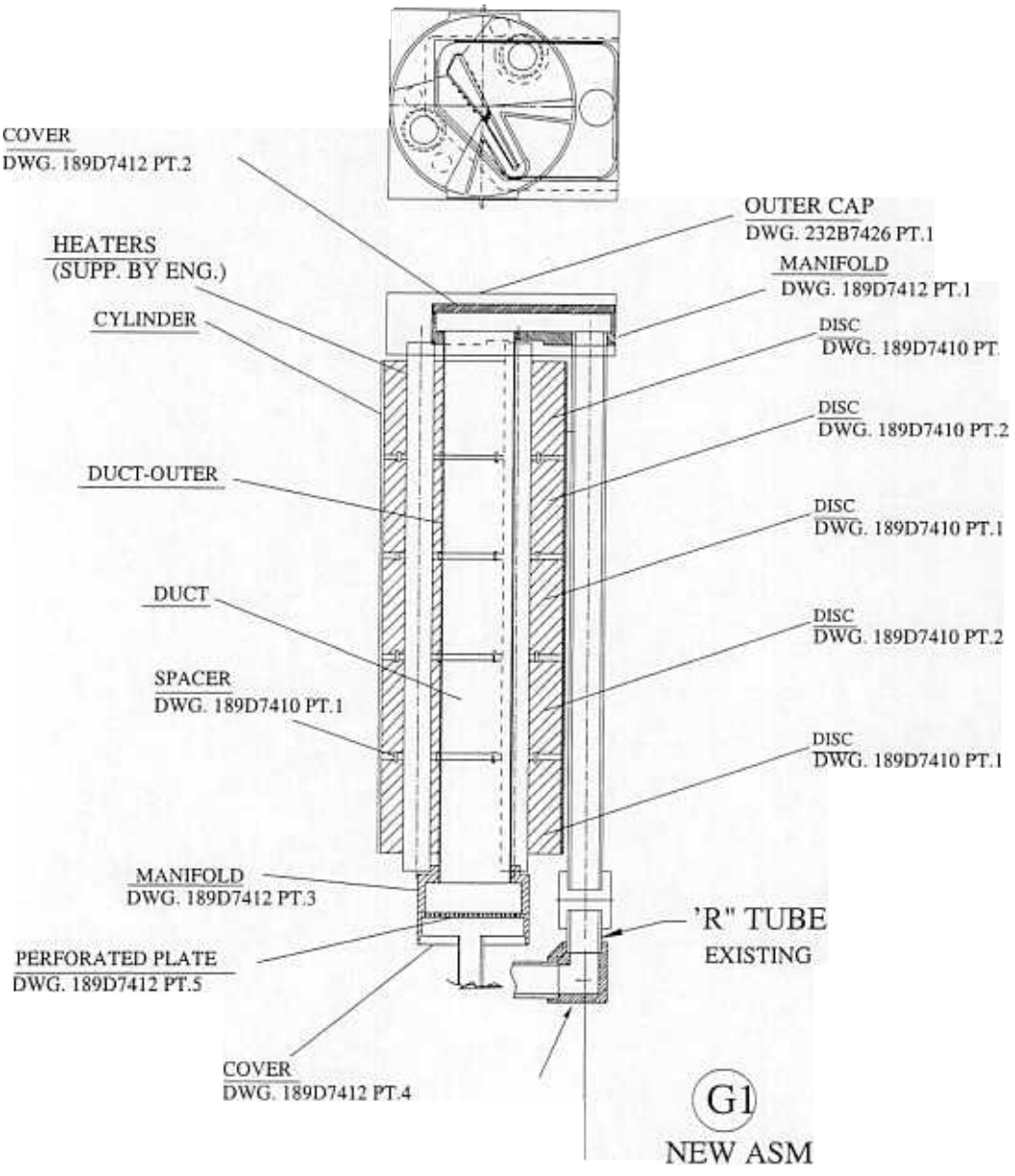

Figure 2.2.3.4.4-2. Trailing Edge Rotating Rig Cross Section

The basic configuration is similar to the previous payloads. Flow is always radially outward in this payload. Flow enters the payload through a lower manifold, which was significantly enlarged to help guarantee uniform flow entering the duct. The inlet manifold was fitted with a perforated plate and steel screen to help distribute the flow evenly. Also, a circular metal shim baffle was welded to the screen immediately above the inlet tube to prevent a jet of flow from impinging the duct inlet. Inlet velocity uniformity was checked on an inlet mockup prior to construction to optimize this screen and baffle arrangement.

The main test duct is wire and plunge electro-discharge machined from stainless steel. The pressure and suction side walls in the larger end are each heated by a single

CALROD heater embedded in a stack of five GLIDCOP blocks. These blocks are brazed to the outside duct walls and have Type-K sheathed thermocouples brazed inside near the duct wall. Each block has two thermocouples for redundancy. Due to the high conductivity of the blocks, these thermocouples provide measures of the heat transfer coefficients roughly averaged over the area of the block-duct braze interface. The pressure and suction sides of the narrow region are each heated by a full-length Constantan foil heater. A pair of foil Type-K thermocouples are epoxied to the back side of the foil heaters at each of five radial stations. These thermocouples can provide more localized measures of heat transfer coefficients, but in this report are averaged together to characterize the overall heat transfer coefficients.

Testing was performed with Reynolds numbers and Buoyancy numbers varied over the range of interest. Significant variations in heat transfer with changes in rotation and buoyancy parameters were found for the various regions in the duct. This was true of both the radial position in the duct and the axial location within a radial section. The use of strictly stationary channel data would incorrectly predict the thermal performance by a large margin.

Summary/Conclusion

Design condition heat transfer data has been obtained for the specific case of bucket trailing edge cooling passages under flow conditions expected in the ATS turbine. Once again it has been determined that such validation data is essential for accurate design.

Technology Application

Results from these tests will be used to update cooling heat transfer boundary conditions for stress and life calculations for the second-stage bucket, and will also be used to reassess the heat transfer coefficients used in the first-stage bucket trailing edge.

Section 2.2.3.5 (GTETIH03) Surface Enhanced Internal Heat Transfer [C]

Section 2.2.3.5.1 (GTETS2NHT) S2N Trailing Edge Flow Test [C]

Objective

The objective of this task was to perform heat transfer tests in the trailing edge region of the second-stage nozzle using an acrylic model built in 1995. The purpose of the work was to generate a cooling scheme that would (1) even out the coolant side heat transfer coefficients along the channel and (2) yield results that are comparable to or better than the turbulent pipe flow correlation predictions.

The model keeps the important geometric variables of the passage close to the actual design. It has thin-foil heaters on both the suction and pressure sides, and liquid crystals to determine the temperature distributions. Tests were conducted to investigate the triangular passage performance with several turbulator designs.

Introduction/Background

While a fairly extensive database exists in the open literature concerning heat transfer and friction factors within turbulated channels of cooled turbine airfoils, such data has concentrated primarily on rectangular or square channels. This data cannot in all cases be extended to applications within high-aspect ratio channels, nor especially channels of triangular cross section. The trailing edge region of any cooled turbine airfoil represents a case outside the database, and so requires validation of the specific design conditions, as well as investigation for the optimal turbulated configuration.

Discussion

Several series of tests were conducted with the second-stage nozzle trailing edge triangular cooling passage model. Since the cross section of the trailing edge varies with location, the model was divided into three regions. Three thin-foil heaters cover the inlet, middle, and exit regions of the trailing edge. Six static pressure taps were drilled to measure static pressure distributions. Holes were also provided for the insertion of thermocouples to measure temperatures.

Several color photographs of the exit region were taken during these tests. Knowing the color-to-temperature calibration of the liquid crystals used allowed conversion of the colors to wall temperatures. Knowing the heat dissipated by each heater and the wall and air temperatures enabled calculation of the heat transfer coefficients corresponding to the specific colors (e.g., gold/yellow or green). A sample is shown in Figure 2.2.3.5.1-1.

Five series of tests were conducted to determine the optimal turbulator design. Based on comparisons of the results of these tests, a turbulator configuration was chosen that provided the required average heat transfer enhancement and friction factor increase.

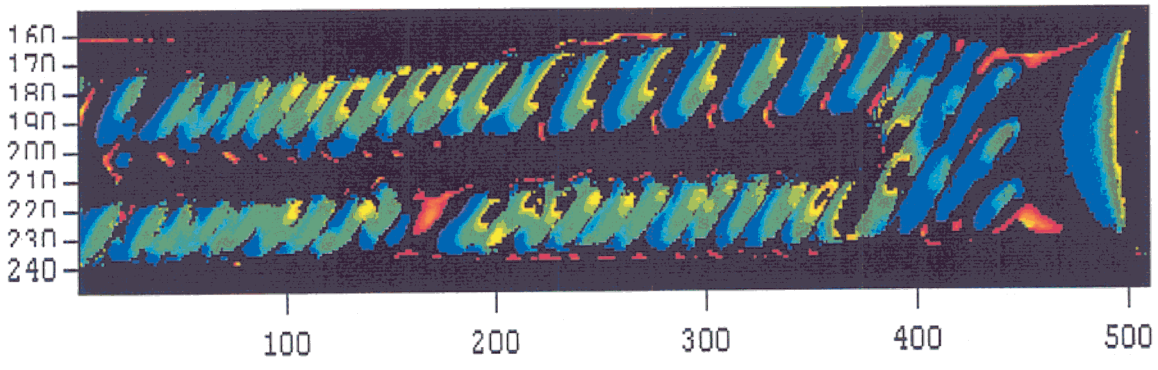

Figure 2.2.3.5.1-1. Sample Heat Transfer Test Result for S2N Trailing Edge at Lab Conditions

Summary/Conclusion

The experimental investigation successfully determined an appropriate trailing edge cooling configuration for the Stage 2 Nozzle. Design boundary conditions in a scaled up form for the engine have been employed in the final S2N calculations.

Technology Application

The test results for cooling passages in the second-stage nozzle trailing edge cooling circuit provided the necessary design information and turbulator configurations for the ATS second-stage nozzle. This allowed the design to obtain the desired heat transfer enhancement for the passages, and to channel the cooling flow near the apex of the triangular flow passage near the trailing edge region effectively.

Section 2.2.3.5.2 (GTETTE) S2B Trailing Edge Testing [C]

Objective

The initial task objective was to provide adequate experimental data to verify the performance of the second-stage bucket trailing edge cooling circuit. Because film cooling and trailing edge bleed cooling are incompatible with the ATS gas turbine objective of closed circuit cooling, the bucket trailing edge must be cooled completely by convection in the trailing edge cavity. The geometry and flow conditions in the trailing edge cavity are different from any analyzed and tested previously. The heat transfer coefficients in the cavity are determined experimentally using a scale model. The experimental results are used to guide and improve the design of the bucket.

The trailing edge tip turn region received specific attention in order to optimize its design. The objective here was to determine the heat transfer coefficients within the second-stage bucket trailing edge tip turn region for the current design, and to modify and test the geometry for longer life design. Modifications included re-positioning of the internal flow turning vane, resizing of the vane, and reshaping the casting to produce a turning flow passage internally. An existing liquid crystal test model of the region was used in stationary testing.

As work progressed, the objective was revised. The final objective was to verify detailed predictions of flow distribution in the trailing edge cavity of the second-stage bucket. Measurements were made at numerous static pressure taps in the trailing edge cavity and the cavity immediately downstream of the trailing edge cavity. These data were used to refine the 1D flow models used to predict internal bucket cooling flows. Measurements were made on a 2X model of the trailing edge tip-turn region, a 1X casting of a whole bucket, and 1X castings of individual trailing edge cavities.

Introduction / Background

The trailing edge cavity of the ATS gas turbine second-stage bucket presents a challenge to designers because the trailing edge is very thin, see Figure 2.2.3.5.2-1. The resulting low aspect ratio cooling circuit cavity cannot use film cooling or trailing edge coolant bleed because of the closed-circuit cooling in the advanced gas turbine. Turbulators are

required in this cavity, both to increase the coolant heat transfer coefficient and to distribute the flow in the cavity so that all regions of the trailing edge are adequately cooled. Cooling the 180° turn at the bucket tip end of the trailing edge cavity is a unique challenge. The tip cap must be adequately cooled by internal cooling alone.

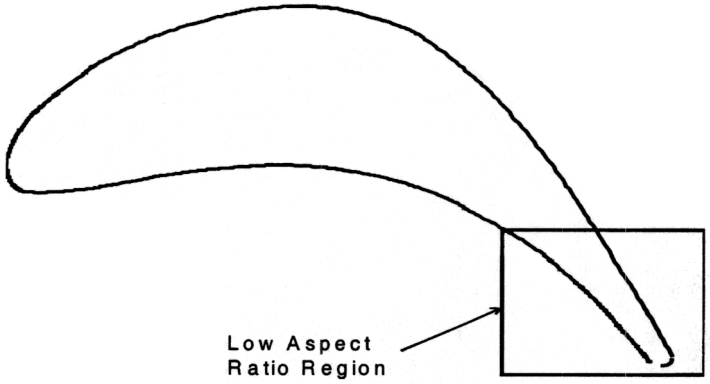

Figure 2.2.3.5.2-1. Bucket Trailing Edge

Discussion

Computational Fluid Dynamics

Work on this task began in April 1996. From April to June, the trailing edge cavity was modeled three-dimensionally using FLUENT, a commercial computational fluid dynamics (CFD) code. To help understand and fine-tune the flow distribution in the trailing edge cavity, the results of this modeling were compared to a flow network solution for the cooling circuit. Cooling the 180° turn at the bucket tip end of the trailing edge cavity also presents a challenge because film cooling cannot be used. The tip cap must be adequately cooled by internal cooling alone, with the trailing edge portion of the tip cap presenting a special challenge, shown in Figure 2.2.3.5.2-2. A 2D model of the 180° turn was created with FLUENT to provide qualitative insight into the flow there. Four configurations of tip turn cooling geometry were tested by the end of August. The 2D nature of the calculations limited the quantitative usefulness of the data, however.

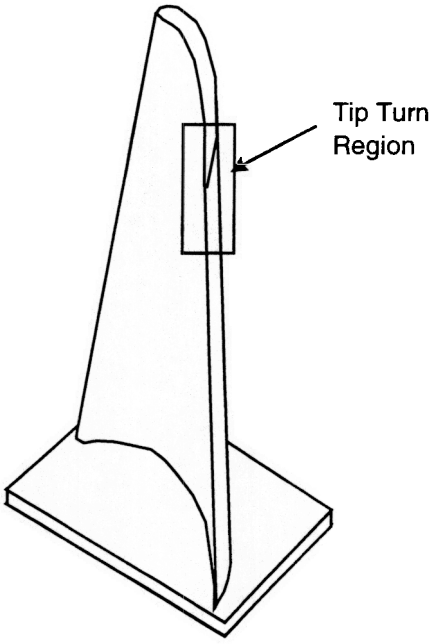

Figure 2.2.3.5.2-2. Bucket Tip Turn Region

Stationary Experimental Model Tests – First Model

The original plan for the experimental measurement of heat transfer coefficient distributions in the trailing edge/tip turn regions was to have a liquid crystal model of the region supplied to CRD for testing. The model was to be built by GEPS through a subcontract with a vendor. Since this model was never built, the work scope for this task was changed to include the construction of the model as well as the testing. It is a scale model of the two cooling cavities of the ATS gas turbine second-stage bucket nearest the trailing edge. It models half of the span of the bucket, from the pitch line to the tip. The model has a constant included angle for both cavities that is very close to the angle of the actual bucket. The tip geometry was modeled very carefully to match the same locations and relative angles of the ribs, tip cap, and turning vane.

Cooling air at room temperature and slightly above room pressure entered the model, (see Figure 2.2.3.5.2-3), from a plenum upstream of the trailing edge cavity, flowed up the trailing edge cavities, around the 180° turn, down the next cavity, and then discharged into the room. A thermocouple and a single static pressure tap in the inlet plenum measured inlet air conditions. Thin-foil heaters, thermochromic liquid crystals, and liquid crystal video thermography (LCVT) were used to measure the heat transfer coefficient distributions. This type of liquid crystal changes color with temperature, which allows temperature distributions to be measured by using the LCVT digital image processing system to convert the color distributions to temperature distributions.

Data were acquired for one turbulator/rib configuration and one mass flowrate. These results have been scaled to the actual advanced gas turbine conditions using the Dittus-Boelter correlation for smooth wall fully developed pipe flow:

$$Nu_{db} = {}^{h_{db} D_h}\!/_{k} = 0.023 \cdot Re_{Dh}^{0.8} \cdot Pr^{0.4} \quad (1)$$

Assuming that the flow distributions in both the model and the bucket are the same and follow the same dependence on *Re* and *Pr* as the Dittus-Boelter correlation, the model results are scaled using:

$$Nu_{bucket} = Nu_{model} \; {Re_{bucket}^{0.8} \cdot Pr_{bucket}^{0.4}}\Big/{Re_{model}^{0.8} \cdot Pr_{model}^{0.4}} \quad (2)$$

In the first of the three sets of tests to evaluate the effect of the turn guide vane, the model was modified to remove the turn guide vane from the trailing edge cavity. The model tested included separate cooling circuits to remove excess energy from the overlap region of the heater. The results showed a decrease in trailing edge tip heat transfer coefficient compared to the results observed with the turn guide vane present. In the second set of tests, the model was modified so that the turn guide vane in the trailing edge cavity matched the turn guide vane in the second-stage bucket core die. The results showed a decrease in trailing edge tip heat transfer coefficient compared to the results observed with the original turn guide vane design. In the third set of tests, the turn guide vane in the model was modified so that the ratio of passage areas on both sides of the turn guide vane matched the ratio of passage areas in the turbine bucket cooling circuit. The results showed heat transfer coefficients at the trailing edge that are similar in magnitude to those observed with the original turn guide vane design. The model was refurbished after the turn guide vane tests and the liquid crystals were replaced. The last turn guide vane test was repeated to ensure repeatability of results.

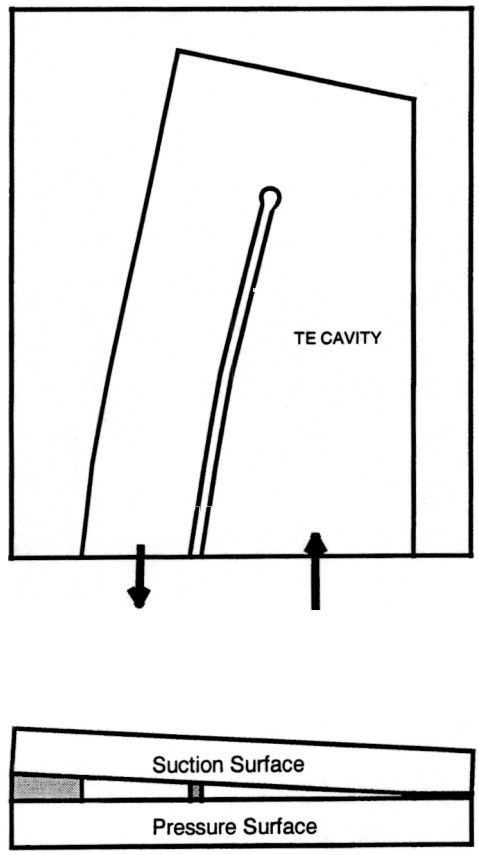

Figure 2.2.3.5.2-3. Bucket Trailing Edge Cavity Rig Flowpath

Rotating Model Tests

The trailing edge cavity of the ATS gas turbine second-stage bucket can be modeled by a smooth duct of narrow cross section. Experiments were planned to determine the effect of rotation on heat transfer in such a duct, oriented at oblique angles to the axis of rotation. In the experiments, a high-molecular-weight gas (Refrigerant-134A) at ambient pressure and temperature conditions was used to match the dimensionless parameters at engine conditions. Thin-foil heaters were used to produce a constant heat flux at the long sides of the duct; the narrow sides were unheated. Three duct cross-section orientations were evaluated: 0°, 45°, and 60° to the axis of rotation. The test results show the effect of rotation and orientation angle on duct leading and trailing side heat transfer.

Stationary Heat Transfer and Flow Tests – Second Model

Preliminary design reviews were held with GEPS design engineers in 1998 to gain an understanding of the revised final design geometry of the second-stage bucket trailing edge internal tip region and to determine key features for model tests. A new 2X acrylic test model was then designed and fabricated.

Testing was initiated using the nominal design for the passage geometry. First, tests were performed to determine the approximate extent and magnitude of heat transfer coefficients, the degree of overheat around the insulating ribs, and the amount of cooling air heat pickup through the test section. Once these preliminary results were obtained, additional air thermocouples were placed inside the flow passages to provide a better estimate of the local bulk coolant temperatures for determination of the heat transfer coefficients. Tests were also run to determine the heat loss from the test section via the thick model walls. Data testing was then performed for the maximum achievable Reynolds number that the model can obtain, which is approximately one-half of the design intent Reynolds number. Data were also obtained for two lesser Reynolds number conditions for the purpose of establishing a reasonable correlation, which may then be used to extrapolate to the design condition. Results indicate uniform heat transfer coefficient distributions in the passages approaching the tip turning region.

Tests were subsequently performed at three different passage average inlet Reynolds numbers on a 2X-scale acrylic test model designed and fabricated for use with the liquid crystal test technique. A consistent set of full-surface heat transfer coefficient data was obtained for the highest laboratory flow. These results were scaled to turbine operating conditions—including the conversion from laboratory air to steam—to provide a full set of thermal boundary conditions for design analysis. All results and conclusions regarding heat transfer distributions within the various regions of the passage, and their implications for the second-stage bucket design, were transmitted to GEPS Design Engineering.

The 2X-scale acrylic test model was then refitted with static pressure taps. Data were acquired at the same three Reynolds numbers for which heat transfer data were taken previously. These data were then compared to 1D flow predictions used by GEPS to model the internal cooling passages of the bucket. A fundamental change in modeling strategy was implemented as a result of these data, and overall agreement improved significantly.

Additional Follow-on Testing

One second-stage bucket casting, which had been flow tested previously, was refitted with many additional static pressure taps. The trailing-edge cavities of another second-stage bucket casting were cut away from the bucket to form individual, single-tube test pieces which were also fitted with pressure taps and tested. Detailed pressure and flow measurements were made. These measurements were submitted to GEPS engineers and were used to adjust and validate the 1D flow models for the cooling circuit.

An improved tip-turn internal cooling circuit configuration was identified, and the existing liquid crystal model retrofitted to the new configuration. Heat transfer measurements were made, and the results were submitted to GEPS engineers to adjust and validate the internal heat transfer boundary conditions.

Summary / Conclusion

Both heat transfer and flow testing has been performed to validate and calibrate the S2B trailing edge region design models. A number of different heat transfer tests were in order to examine the tip turning region in the restricted area region of the trailing edge,

such that a manufacturable and thermally acceptable design resulted. Small scale rotational testing determined any aspect ratio and orientation effects for the general turbulated region of the trailing edge.

Technology Application

The results of this task have been used to validate design predictions for the internal tip-turn region of the second-stage bucket trailing edge. Detailed local heat transfer coefficients were obtained for a more precise assessment of component cooling in this area. The test model also provided a vehicle to optimize the internal steam cooling in this tip region with minimal impact on the overall second-stage bucket design.

Section 2.2.3.5.3 (GTETIH04) S1N Outer Band Liquid Crystal Heat Transfer Tests [C]

Objective

The objective of this task was to perform heat transfer tests with a representative outer band impingement configuration and measure the heat transfer coefficient distributions underneath the impingement jets. The data were compared with the design calculations and expectations. A test rig was used to simulate the design impingement jet plate geometry as closely as possible. The test section walls were instrumented with three etched thin-foil heaters and a liquid crystal layer to measure the local wall temperature distributions as a function of flowrate and heat flux. The temperature data were then converted into heat transfer coefficient values.

Introduction / Background

In conventional turbine inlet nozzle design, impingement cooling is combined with film cooling to provide effective overall cooling for the life of the nozzle endwalls. Because the ATS turbine inlet nozzle utilizes closed-circuit steam cooling for both of its endwalls, film cooling is no longer available to provide design conservatism. Hence, determination of the precise internal flow divisions and endwall impingement arrangements must be accomplished for verification of cooling sufficiency. Such endwall regions must also be modeled in a manner which accounts for the source and sink flow locations and strengths due to the supply and return of steam cooling. The method of providing such design verification is to test a scaled model of the actual impingement cooling design.

Discussion

The manufactured test rig, shown in Figure 2.2.3.5.3-1, consists of an acrylic wall simulating the outer band impingement region. The jet impingement plate has all the detailed impingement jet geometries duplicated as closely as possible to the actual design. The impingement hole diameters, configurations, and row spacing vary from location to location to accommodate the local gas side thermal loads. A supply chamber feeds the cooling air to the impingement jets. The air flowrate is measured by calibrated venturi meters and the coolant supply chamber pressure and temperature are also recorded. The acrylic impingement surface is covered with a liquid crystal sheet and three etched thin-foil heaters that cover the leading edge region and the pressure and suction side regions

all the way to the trailing edge region. The impingement jet heat transfer patterns are recorded photographically, and the impingement heat transfer coefficients are calculated from the dissipated powers and the calibrated liquid crystal color spectra with temperature.

The first experiments consisted of flow visualization tests that were conducted by using wall tufts glued onto the jet plate and extending to the impingement surface. The flow directions visualized by the motion of the tufts were recorded on film by a video camera. Visual observations of the film frames showed that the flow directions in the various cooling regions of the outer end wall were qualitatively correct and the flow seemed to be following the directions assumed in the impingement design model calculations.

The test section was then instrumented and tests were conducted at two cooling-air flowrates, with the leading and trailing edge discharge regions open to atmosphere and the temperature field reflected by the liquid crystal color spectra which were recorded by a video camera and by the Liquid Crystal Video Thermography (LCVT) system. The impingement flow and heat transfer model was first used to calculate the total flowrates expected for the test supply and exit pressure flow conditions. The model predictions were within 3 percent of the experimentally measured total flowrates, indicating that the flow models were accurate.

Figure 2.2.3.5.3-1. S1N Outer Band Liquid Crystal Rig

Temperature photographs were recorded at several heat flux levels for the two total impingement flowrates investigated. The heat transfer coefficient distributions at the various regions were then compared with the design model predictions for each impingement region of interest. The agreement between the model and the test results was found to be acceptable.

To evaluate the effect of various discharge pressure levels at the leading and trailing edge discharge regions of the nozzle outer band region, a series of tests was conducted under the most extreme conditions, where first the leading edge discharge area was completely blocked and all the flow was forced to discharge through the trailing edge opening. Then the trailing edge discharge opening was completely blocked and all the flow was forced to discharge through the leading edge opening. The liquid crystal temperature distributions recorded showed that there is a significant variation in the heat transfer impingement pattern all along the outer band when these results are compared with the baseline results obtained when both discharge regions had the same exit pressures. The next series of tests was conducted with the leading edge discharge fully open and the trailing edge discharge blocked with three plugs with openings of various diameters. Similar tests were also conducted with the trailing edge opening fully open and the leading edge discharge equipped with three plugs with circular openings of various diameters. For the small opening diameters, the liquid crystal temperature distributions recorded showed that there is a variation in the heat transfer impingement pattern all along the outer band when these results are compared with the baseline results. The effect becomes less pronounced for the large-diameter holes. These tests showed that under extreme conditions, the discharge pressure has an effect on the impingement heat transfer coefficient distributions.

During the next series of tests, the effect of a single partitioning wall (a rib) in the impingement spent air region on the suction and pressure sides of the outer band was investigated. The rib separates the impingement spent air flow into two regions. Heat transfer tests were conducted with this separation rib in place with the leading edge discharge fully open and the trailing edge discharge blocked with three plugs with openings of various diameters. Similar tests were conducted with the trailing edge opening fully open and the leading edge discharge partially blocked with three plugs with circular openings of various diameters. The liquid crystal temperature distributions recorded showed that, for the same cooling flowrates, this second configuration resulted in lower impingement heat transfer coefficients in every region when compared with the case where there were no separation ribs.

Summary/Conclusion

The flow and heat transfer testing for the outer band impingement design verified the design procedure for the endwall regions of the Stage 1 Nozzle. Validation of the outer band is considered sufficient to allow proper design of the inner band region as well. Heat transfer magnitudes and distributions were obtained at lab scale conditions. Critical information about confined region heat transfer and flow in corners or along flow split lines was also obtained. The design data obtained in this task is used directly in the thermal analysis of the Stage 1 Nozzle, both for the preliminary design and for improved final design geometries.

Technology Application

The test results obtained with the flow and heat transfer tests showed that the design calculations and models were able to successfully predict the flow directions and heat transfer coefficients for the complicated impingement pattern of the ATS first-stage

nozzle outer band. The tests also showed that the heat transfer is dependent on the leading and trailing edge cavity discharge pressure levels. The data also showed that an impingement design without a separating rib is more effective than a design with a separating rib on the suction and pressure sides.

Section 2.2.3.5.4 (GTETIH04) S1N Convex Cavity Heat Transfer Tests [C]

Objective

The objective of this task was to perform flow and heat transfer tests in a simple test rig representative of a first-stage nozzle convectively cooled passage geometry with two different turbulator designs to determine the effect of corner radius on the heat transfer enhancements obtained with the turbulators. Two simplified plastic models of the cooling channel were constructed with the important geometric variables kept as close as possible to the actual design. An additional test section was also constructed to model the exact geometry of the convectively cooled cavity, which incorporated the area changes along the radial distance. The inside surfaces of the test pieces were coated with liquid crystal paint or a liquid crystal sheet, and transient and steady-state tests were run to determine the friction factors and local heat transfer coefficient distributions. The results were also compared with the CRD database. An additional flow test was conducted with a metallic test section manufactured with exactly the same dimensions as the prototypical passage to verify the flow models of the design.

Introduction/Background

As part of the design of the ATS turbine Stage 1 Nozzle, one of the steam cooled airfoil cavities is rather too small for the use of impingement jet arrays, and hence is cooled convectively with the addition of turbulators. Due in part to the 3D aerodynamics of the airfoil, this cavity retains a curved shape with a variable internal area. These aspects of this cooling cavity, as well as the very high Reynolds number of the steam flow, demand that the internal heat transfer and friction be verified by test, and compared to existing data for turbulated rectangular, straight channels. An additional aspect of such turbulated channels, indeed any cast turbulated featues, is that the specific rib roughening elements do not have ideal sharp edges, but rounded or radiused edges. This feature has also been included in the validation testing.

Discussion

Square and Rounded Turbulator Edge Test Sections

The first test sections were two simplified plastic models of the cooling channel constructed with the important geometric variables kept as close as possible to the actual design. One model had square turbulator edges and the other had rounded turbulator edges with a given radius at the corners. The inside surfaces of the test pieces were coated with a liquid crystal paint. A transient test was run to determine the local heat transfer coefficient distributions. The test began with a cold test section and then, at time zero, a hot gas stream was flowed through the cooling passage. The heating cycle was recorded by a VCR. The recorded images provided wall temperatures varying with time based on

the local heat transfer coefficient distributions. For the transient analysis, the recorded color fields were converted to local temperature values; then the 1D transient conduction solution was used to calculate the local heat transfer coefficient. The constant heat transfer coefficient lines (iso-h lines) were then combined to obtain area-averaged values for the heat transfer coefficients.

Because of concerns about the accuracy of the heat transfer measurements obtained with the transient technique at high values of the heat transfer coefficients, one turbulator test section was changed to accommodate a thin-foil heater and a liquid crystal sheet to run steady-state tests for additional data, and for comparison to the transient data.

Flow Tests with Machined Metallic Test Section

The convectively cooled cavity that was instrumented with static pressure taps is shown in Figure 2.2.3.5.4-1 below. Sixteen static pressure taps were distributed along the non-turbulated sides. Pressure drop tests were conducted at three flow rates and pressure ratios. To compare the results of the tests with the flow model calculations, a model of the flow circuit was prepared representing the various geometric parameters of the passage. The comparison shows that the total flow rates and the static pressure distributions were predicted accurately for the three flow rates investigated. The friction factors for the several turbulated regions were calculated from the CRD heat transfer database with the appropriate cooling cavity geometric parameters.

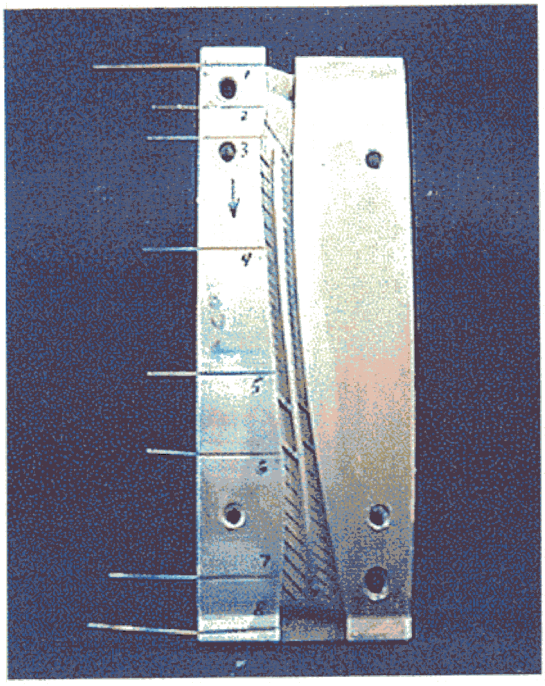

Figure 2.2.3.5.4-1. S1N Heat Transfer Test Section

Final Tests with Acrylic Test Section

The original design of the convectively cooled cavity has flow areas, passage geometries, and turbulators that vary in size from inlet (tip) to exit (root). To investigate the effect of the distributed turbulator height at different sections of the passage, an acrylic model of

the convectively cooled cavity was designed and constructed. This model has the two turbulated flow channels and prototypical turbulator heights. The test section was designed to keep the blockage ratio, the turbulator pitch, and the passage hydraulic diameters and aspect ratios as close as possible to the actual design – similar to the flow model photo above. A steady state technique with a thin-foil heater and a liquid crystal was used to record the local heat transfer coefficient distributions.

The new acrylic test section was used to run tests with the smooth passages with and without the partitioning rib. Two pressure taps were used to measure the pressure drop across the inlet and exit to calculate the friction coefficients and compare them with smooth duct correlations. A series of additional test were then performed with the variable sized turbulators in place.

Summary / Conclusion

For the specific geometry of this convectively cooled cavity in the Stage 1 Nozzle, design boundary conditions for heat transfer and friction factors, as well as inlet and entry loss factors, were obtained. Data on the behavior of the flow and heat transfer with sharp and rounded turbulators, as well as with smooth walls, allows extrapolation and comparison with existing turbulated channel data. Consistent results were obtained on both the generic and design specific levels.

Technology Application

The results of this series of tests were incorporated into the internal cooling design of the ATS turbine first-stage nozzle.

Section 2.2.3.5.5 (GTETIH05) Bucket Tip Closed Circuit Cooling [C]

Objective

The objective of this task was to measure non-rotating heat transfer and pressure drop in the 180° tip turn region of a two-pass serpentine bucket tip, and to evaluate the ability of an enhanced surface in the tip region to enhance the tip cooling without a substantial pressure drop penalty.

Introduction / Background

Conventional air-cooled turbine buckets utilize tip air discharge holes, or film cooling holes, to assure that the bucket tip section maintains its integrity. Again, for the ATS turbine buckets, steam cooling dictates that no coolant be released out the bucket tips. Hence, not only is an accurate knowledge of the external tip heat transfer required, but also a knowledge of the internal coolant side heat transfer. The tip portion of a bucket with serpentine cooling design is dominated by 180-degree turns. Such turns generally have high heat transfer due to coolant impingement, and minimal effects due to rotation, but may also contain small recirculation zones of lower heat transfer. Methods of enhancing this tip region cooling are desirable, but must be verified for design use.

Discussion

The effects of several parameters on the heat transfer and pressure drop in a two-pass, smooth rectangular channel with one 180° turn were investigated. The effects of flow rate and rib gap were determined. Two different endwall surfaces were tested for heat transfer and pressure drop. In order to achieve reasonable Reynolds numbers without sonic flow, a test rig, shown in Figure 2.2.3.5.5-1, was designed to be run at 3 atmospheres to keep test section velocity low.

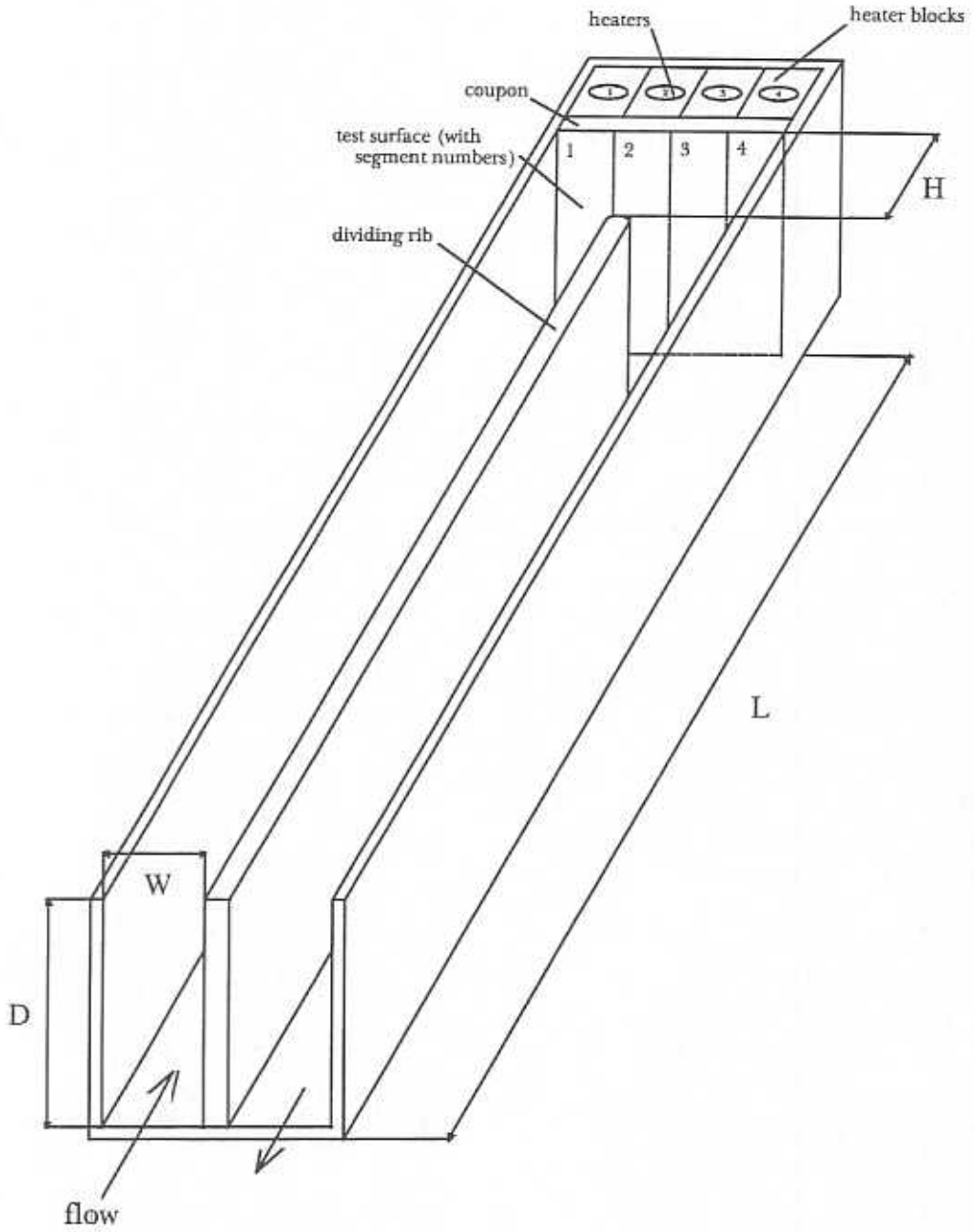

Figure 2.2.3.5.5-1. Bucket Tip Closed Circuit Cooling Rig Schematic

Two test surfaces were used, one smooth and one enhanced. Both coupons were made of cast, nickel-based superalloy. Each was permanently attached with thermal epoxy to a copper heater block, segmented into four equal pieces, each with its own individually controlled cartridge heater. Each heater had an attendant thermocouple, and there was a thermocouple directly above each heater in the base of the coupon, centered in the coupon. The heater power was set so that each heater thermocouple indicated the same temperature. The coupon thermocouples were then used to derive the local and average heat transfer.

Mass flow rates were measured using an orifice meter upstream of a settling plenum that supplied air to the test section. Four mass flow rates were chosen to cover the range applicable to the advanced gas turbine. Four rib gaps were tested at each flow rate with each of the two endwall surfaces. There was a pressure tap at the inlet and at the orifice plate, and a differential pressure tap from the inlet to the exit.

Examples of key results are shown in Figure 2.2.3.5.5-2 and Figure 2.2.3.5.5-3. For the smooth endwall coupon, heat transfer increased with increasing Reynolds number and decreasing rib gap. Surface enhancement increased the heat transfer over the smooth wall case without increasing pressure drop.

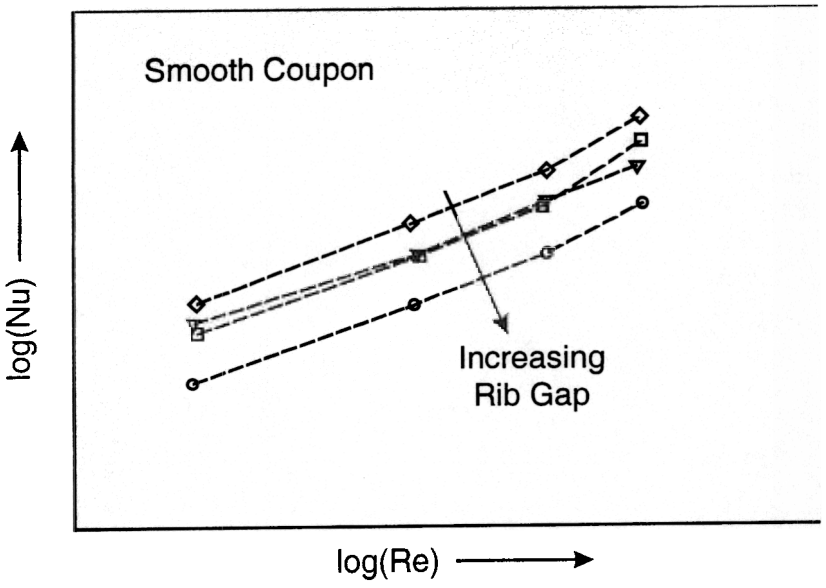

Figure 2.2.3.5.5-2. Smooth Tip Turn Endwall Heat Transfer.

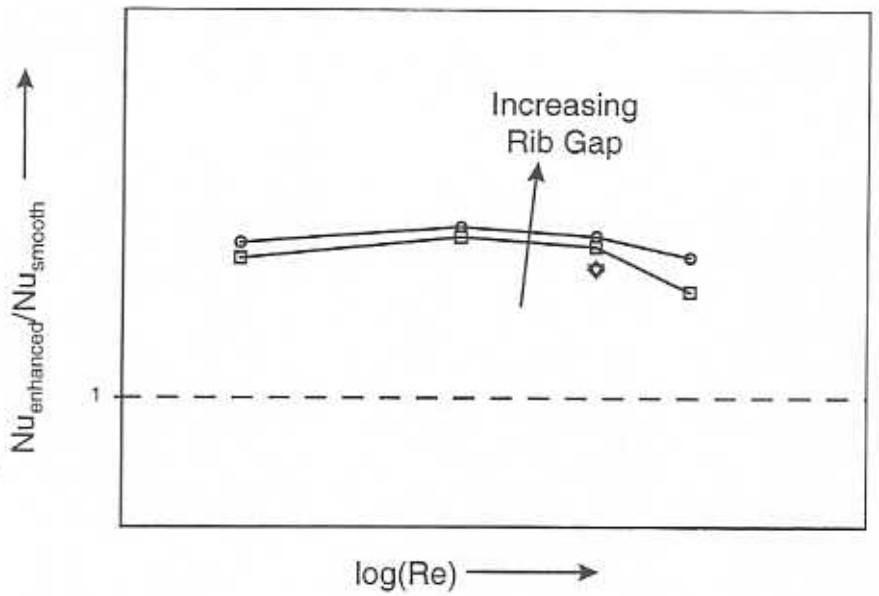

Figure 2.2.3.5.5-3. Surface Enhancement On Tip Turn Endwall Heat Transfer.

Summary / Conclusion

Heat transfer coefficient data has been obtained for the smooth tip turn case as a baseline result, followed by enhanced tip surfaces. The internal tip surface features have verified heat transfer enhancement factors substantially greater than unity, providing good benefit to the bucket designs. Pressure losses have not been increased by these new surface treatments, making these features high performance overall.

Technology Application

The results have been used by the designers of the ATS gas turbine buckets to design the tip turn regions of serpentine cooling circuits.

Section 2.2.3.5.6 (GTETLE) Bucket Leading Edge Heat Transfer Testing [C]

Objective

The objective of this task was to evaluate turbulator geometries for the first-stage bucket leading edge passage by performing non-rotating heat transfer and pressure drop tests at high Reynolds numbers on scaled models of the leading edge passage.

Introduction / Background

The majority of the existing database concerning heat transfer in turbulated flow passages for turbine airfoils has two common attributes, (1) it applies to rectangular cross section passages, and (2) it spans data over Reynolds numbers from 5000 to perhaps 80,000. The Stage 1 Bucket leading edge passage of the ATS turbine requires design data which is outside the established database in both respects. From tests that have been performed on curved cross section passages at lower Reynolds numbers, it is quite apparent that

specific data must be obtained for the specific passage shape of the leading edge intended for use.

Discussion

The original plan for this task was to measure local heat transfer coefficient distributions in a model of the ATS gas turbine first-stage bucket leading edge using the thin-foil heater/liquid crystal technique. The leading edge passage model is an acrylic, 2X scale, constant cross section, non-rotating model of that passage. This model was already available, having been built prior to the start of this task. The passage was modeled as shown in Figure 2.2.3.5.6-1, with one (curved) wall of acrylic forming the suction and pressure sides of the leading edge, and the other (straight) wall of acrylic forming the rib between the first and second cooling passage. This model runs with an atmospheric pressure discharge. At the Reynolds numbers of interest, however, the Mach number of the leading edge passage was sufficiently high that compressibility effects had to be considered. In all cases, the adiabatic wall recovery temperature was used as the reference temperature to define the heat transfer coefficient. To model the conditions of the ATS gas turbine, however, the acrylic rig had to be run at conditions where the correction from measured to adiabatic wall temperature was a significant fraction of the surface to freestream temperature difference. The resulting high uncertainty in measured h was unacceptable. A new rig was designed to eliminate this problem.

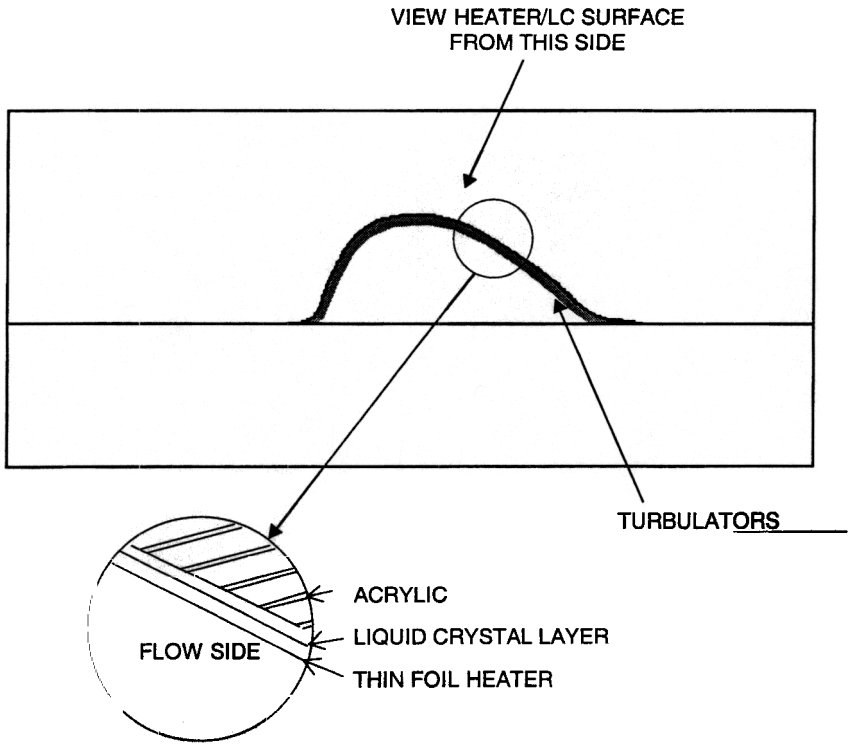

Figure 2.2.3.5.6-1. Bucket Leading Edge Heat Transfer Model

The new rig, shown in Figures 2.2.3.5.6-2 and 2.2.3.5.6-3, was designed and built to model the 50% span location of the first-stage bucket leading edge cavity. The cavity geometry for the bucket was used to make segmented heater blocks. These blocks have

been assembled inside of a rectangular, low-thermal-conductivity plastic shell to form a complete flow passage. The assembly has a $7.6D_H$ (7.6 times hydraulic diameter) unheated inlet region followed by 14 individually heated and instrumented segments. Each segment is $0.85D_H$ long for a total heated length of $12D_H$. For turbulent flow (especially with turbulated passages), this length is sufficient to establish fully developed heat transfer well before the end of the cavity model.

Each segmented heater block is heated by a cartridge heater. The rig is operated with a constant wall temperature boundary condition by individually controlling the power supplied to each block. The G7 plastic wall representing the rib side of the cavity is unheated. To prevent excessive heat loss by conduction to the unheated upstream and downstream regions, balsa wood segments have been used as insulation. The first and last heated sections act as guard heaters to prevent axial conduction from the center 12 segments to the unheated portions of the rig. In addition to the thermocouples in each block, the flow model has been instrumented with inlet and outlet air temperature thermocouples and with three pressure taps spaced evenly along the heated section on the rib side wall.

The entire flow model was placed inside of a pressure vessel at $P = 6$ atmospheres (90 psia). The pressure drop from the inside of the flow model to the inside of the pressure vessel did not exceed 0.5 atmosphere (8 psi) during operation. Operation at this elevated pressure level allows the high Reynolds number flow of the design to be obtained while keeping a low Mach number, and therefore incompressible flow condition.

Tests in the high Reynolds number, low Mach number leading edge cavity model were completed by the end of June 1996. Heat transfer and friction were measured over a range of Reynolds numbers applicable to the ATS gas turbine for both smooth walls and walls with five different turbulator geometries.

Summary / Conclusion

Design data heat transfer coefficients have been obtained spanning a generous Reynolds number range for the Stage 1 Bucket leading edge passage. The results have been compared to data at lower Reynolds numbers, showing that strict extrapolation of data would be insufficient for design accuracy.

Technology Application

The heat transfer and pressure drop results from this task have been used in the design of the first-stage bucket in the ATS gas turbine.

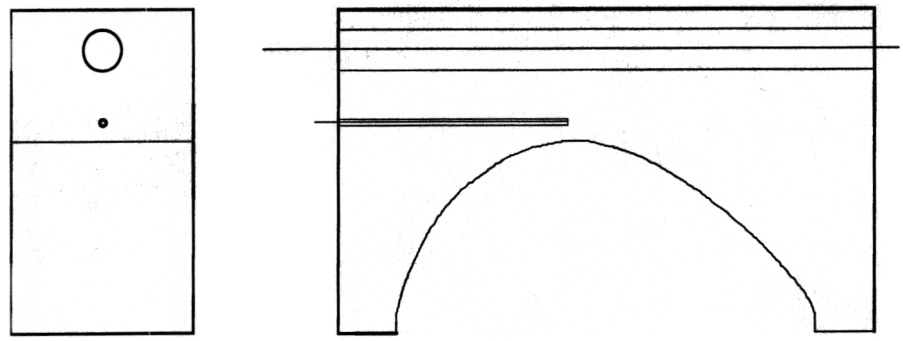

Figure 2.2.3.5.6-2. Copper block with geometry of leading edge formed by wire electrical discharge machining. The large-diameter hole accepts a cartridge heater, and a type K thermocouple is inserted in the smaller hole.

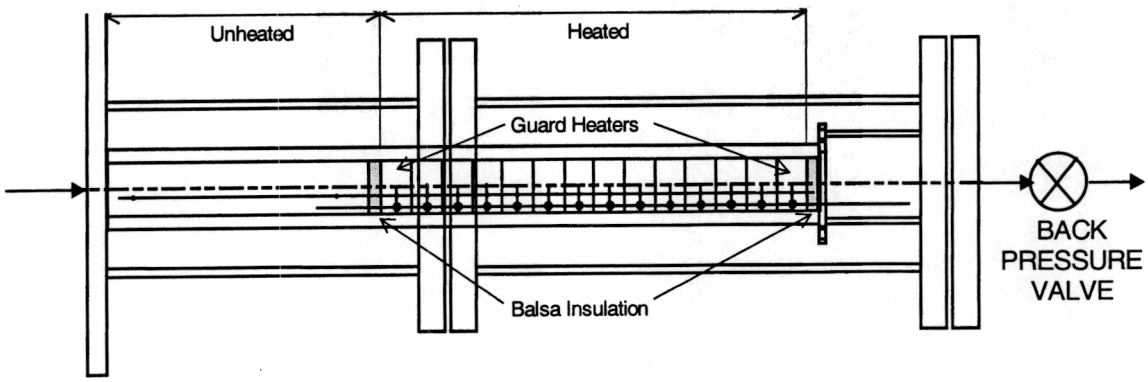

Figure 2.2.3.5.6-3. Test section consists of a stack-up of EDM'ed blocks inside of a low thermal conductivity G10 fiberglass board shell.

Section 2.2.3.5.7 (GTETIH03) S1N Surface Enhanced Internal Heat Transfer [C]

Objective

The objective of this task was to investigate and determine the heat transfer coefficient enhancements that could be generated under impingement jet cooling modules by adding surface roughness elements without increasing the total system pressure drop. The effect of bumps missing in some regions due to manufacturing problems was also investigated.

Introduction / Background

Impingement cooling is a wisely used method for enhancing the convective heat transfer capability of many components in gas turbines. This technique is especially practiced within the Stage 1 Nozzle of most advanced designs. While providing an very high degree of enhancement compared to purely convective flow, impingement also requires a generally higher pressure drop in the system, as well as the space to employ jet array

inserts. It is possible to increase the cooling effectiveness of jet impingement heat transfer even further through the use of surface roughness elements on the target surfaces. Literature provides examples of this with impingement onto rib rougheners, pedestals, and cubic elements. The surface roughness features must be manufacturable, must be repeatable for quality control, and must be cost effective. In any such case, the specific surface roughness elements must also be tested under the design Reynolds numbers and jet array configurations. The optimum element geometry is by no means obvious, nor is it constant under all conditions.

Discussion

Low Pressure Tests

To investigate the effect of missing bumps, the first series of three tests was conducted with a thin-foil heater and a liquid crystal sheet taped to a plain test surface. The impingement spent air was discharged into the atmospheric ambient. Three jet plates of interest were investigated. The cross flow effects of these jet plates are expected to be very strong and dominant. Several steady-state pictures of the liquid crystal surface were recorded at a given jet flow rate. The pictures were then analyzed by calculating the local heat transfer coefficients, which were superimposed to generate an overall heat transfer coefficient distribution map. Where the cross flow dominates, details of individual jets are not visible. In this case, the iso-h lines (lines of constant heat transfer coefficient) show high heat transfer underneath the first rows of jets. Where the cross flow diminishes, low heat transfer coefficients are found.

The next series of impingement tests consisted of recording the surface colors as a function of heat flux for a given impingement cooling flow rate. The color images were then digitized and the color (hue) field was converted into a temperature distribution by using the Liquid Crystal Video Thermography calibrator. With the heat flux, wall temperature distributions, and the coolant supply temperature known, the local heat transfer coefficients were calculated and averaged over the impingement surface. Tested smooth surface impingement heat transfer coefficients agree well with the Florschuetz & Metzger correlation used in the design, and with the heat transfer data that were obtained previously with the copper heater and the thermocouples imbedded in the test plates.

High Pressure Tests

The test section used for impingement heat transfer tests is enclosed in a high pressure enclosure that can be operated at pressures up to 10.2 atm (150 psia) by means of a back-pressure control valve. The impingement air is fed to a supply chamber equipped with a square impingement jet plate that can accommodate several hole configurations. The impingement test surface is in intimate contact with a copper block that is heated by four cartridge heaters. The impingement test plates, positioned at a controlled distance from the impingement jet plates, are instrumented with four embedded thermocouples that measure the plate temperature. Tests are conducted under high pressures to obtain high jet Reynolds numbers at low jet Mach numbers.

Tests were conducted at various jet Reynolds numbers and several jet plate geometries, including variations of the jet plate geometry, jet-to-target spacing, and many variations

of the specific geometry of surface roughness elements. Regionally averaged plate heat transfer coefficients were obtained in all cases as a function of average jet Reynolds number.

To investigate the effect of bumps missing in some regions, the high pressure containment was modified so that a window could be attached at one end. A thin-foil heater and a liquid crystal assembly were glued onto the impingement test plate and the color changes observed with the liquid crystal video thermography (LCVT) system. A three-dimensional ANSYS model of the bumpy surface was also prepared representing a 10 by 10 array of the bumps. The model was used for an analytical investigation of the effect of the missing bumps on the metal temperatures with convective boundary conditions that are similar to the actual design conditions.

Impingement test plates with missing bumps were prepared for testing to determine the heat transfer coefficient in the regions where bumps are missing and to determine with transient tests the smallest bump-free region that can be detected with a transient heating technique. Two test plates with regions of missing bumps were manufactured. The test specimen was tested with two techniques to try to detect the regions with the missing bumps. A transient technique was used to test the specimen. Pressurized air was bypassed from the impingement chamber supply to maintain a constant flow rate and temperature. The test specimen, coated with a liquid crystal on the face opposite to (backside of) the bumpy surface, was heated to an initial temperature that changed the color of the liquid crystal. At time zero, the cool air was diverted onto the enhanced test surface and the variation of the temperatures was recorded as a function of time by an RGB camera connected to an image acquisition and analysis system. Since the liquid crystal changes color within a narrow temperature range, the transient was caught only at a particular time interval when the surface temperature was in the liquid crystal's sensitive range. We then used a second technique, in which the surface of the test plate opposite to (on the backside of) the enhanced surface was painted with a black paint having a high and known emissivity. A similar test was conducted by heating the test plate to a high temperature and then suddenly turning the cooling air on and observing the painted surface with an infrared camera. The results observed were similar to the liquid crystal tests.

The second test plate prepared had a band of the bumps cleared all along the test plate. Steady-state heat transfer tests were conducted at several jet Reynolds numbers with several jet plates. Test results showed again that cross flow effects are important.

Summary / Conclusion

The design data obtained for a wide range of surface roughness elements has provided a database from which an optimum element geometry has been selected for the impingement applications in the ATS turbine Stage 1 Nozzle. The data also provides design specification limits, and sensitivity of heat transfer due to parameter variations. The effect of crossflow on impingement heat transfer has been shown to be significant for the rough surfaces in a similar manner to that previously known for smooth surfaces. The additional effect of missing or defective roughness elements has been determined, thereby providing a specification linked to quality of manufactured parts.

Technology Application

The experimental heat transfer coefficients for the optimum roughness elements as a function of Reynolds number and jet plate geometry have been incorporated into the S1N design. Non-optimum configuration data has been incorporated into the analysis of robustness for the design. The ANSYS analysis results provide the increases in wall temperature expected for various numbers of bumps missing. The acceptable temperature rise will determine the quality control criteria. The transient technique provides a nondestructive technique to check the non-uniformity of the cooling and the number of missing bumps.

Section 2.2.3.5.8 (GTETIH03) S1N Trailing Edge Flow and Heat Transfer Tests [C]

Objective

The first-stage nozzle trailing edge air-cooled cavity is a complicated cooling system involving turbulators, pin-fin-type pedestals, trailing edge film slots separated with ribs, and pressure and suction side film holes. The flow and heat transfer design calculations depend on empirical correlations and predictive tools that have to be verified. The objective of this task was to perform flow and heat transfer tests in a representative passage geometry of the trailing edge region of the first-stage nozzle using an acrylic model, and run flow tests with a cast prototype model of the cooling circuit. The results are compared with the design calculations.

An additional focus of this task, related to nozzle trailing edge heat transfer, is the performance of the trailing edge cooling passages. Short, partly turbulated STEM-drilled passages were used to cool the trailing edge of the first-stage nozzle. Since the inside diameters of these passages are relatively small (1 to 1.5 mm) they are outside of the CRD database. Two vendors manufactured these STEM-drilled passages. The objective of this subtask was to have each vendor manufacture a STEM-drilled passage so that the friction factors and heat transfer coefficients could be determined and compared.

Introduction/Background

While the first and second stage airfoils of the ATS turbine design are steam cooled in a closed-circuit fashion, the remains one region which requires more traditional air cooling in the Stage 1 Nozzle. This region is the trailing edge. Due to the very thin trailing edge profile required for efficient aerodynamics in the first turbine stage, it is of exceptional difficulty to provide closed-circuit cooling channels which meet both the heat loading and pressure drop system requirements with steam. In this case, the trailing edge region has been designed as an air-cooled segment which is integral to the overall airfoil casting, but fed by compressor discharge air in a conventional manner. The air comes into the trailing edge in a radial manner, and makes its way through thermal enhancement features to axial exits in the trailing edge. Limited film cooling holes bleed some of the air off the main cooling passage to provide external heat load reduction. Because this S1N trailing edge cooling configuration is unique in its overall design, being more compact in form, and also having no benefit of upstream airfoil film cooling, it is necessary to experimentally validate both the heat transfer and pressure losses.

Discussion

Flow Tests

The machined metallic test section was received at the end of 3Q96. A few flow tests were performed with the detailed test piece, where the pressure ratio across the inlet and exit of the passage and the flow rate were measured. The flow circuit was also modeled with a flow circuit model without the film holes. For the experimental pressure ratio, the measured total flow rate was within 10 percent of the flow rate calculated by the flow model. In addition to the total flow test, three additional tests were run with a third of the trailing edge slots open near the tip, a third open near the pitch, and a third open near the root. The measured flow rates for each case for the same pressure ratio between the supply and exit showed that the flow distribution was uniform with a third of the flow being measured in each one of the three tests.

A design change was incorporated near the root of the first-stage nozzle to improve castability. This change required additional trailing-edge cavity flow checks to the base case studies performed in 1996 in order to answer two questions: (1) how much does the cooling flow rate increase, and (2) can the pressure margin for the film holes in this region be maintained? To provide answers, the aluminum flow model used in 1996 was modified to reflect the casting changes. Flow tests were then conducted with the modified geometry. The detailed static pressure distributions measured were compared with the original model tests conducted in 1996. The results showed that the flow rate increased by 15% while maintaining the film pressure margin higher than the design requirement.

An additional updated version of the trailing edge flow circuit was also tested in early 2000. A cast Aluminum model of the entire air circuit was flow tested to determine the static pressure distributions at all film hole exits, verifying the internal pressure supply and film discharge margins used in the design.

Heat Transfer Tests

For the heat transfer tests, a conceptual design of the test section, shown in Figure 2.2.3.5.8-1, was prepared based on cross sections provided by Design Engineering. The model divides the cavity into several regions and matches the wetted perimeters and flow areas as closely as possible. These discrete cross sections were then connected with a linear variation of the passage geometry. A tool path program for a numerically controlled machine was prepared by the machine shop and an acrylic model of the test section was manufactured. Measurements were made on the acrylic model and compared with the model dimensions. After the dimension checks, one wall of the model was covered with a liquid crystal sheet and a thin-foil heater. The flow separation ribs, the pin fins, and the balsa wood turbulators were attached to the opposite wall with a clearance allowing for a gasket between the two faces.

Two series of heat transfer tests were conducted with the instrumented test section at two flow rates. The trailing edge holes were discharged to atmospheric pressure. The measured static pressure distributions agreed with the flow model predictions and showed a constant pressure all along the turbulated cavity that feeds the trailing edge holes. The calculated flow rates for both test pressure ratios were within 5% of the measured values.

The heat transfer tests were conducted by setting the flow rate and then setting the uniform heat flux to the thin-foil heater to a given value that started the color changes in the liquid crystal. Once steady state was reached, an image of the surface was recorded by liquid crystal video thermography (LCVT) system for future analysis. The heat flux was then increased in preset steps and the surface temperature distributions were recorded for each case. Twelve images were recorded and saved for analysis. The liquid crystal color versus temperature calibration was performed in the calibrator. The surface temperature results with the known uniform heat flux values were then used to convert them to heat transfer coefficient distribution data. The local heat transfer coefficients in the turbulated supply cavity and in the pin fin and turbulated trailing edge holes were measured.

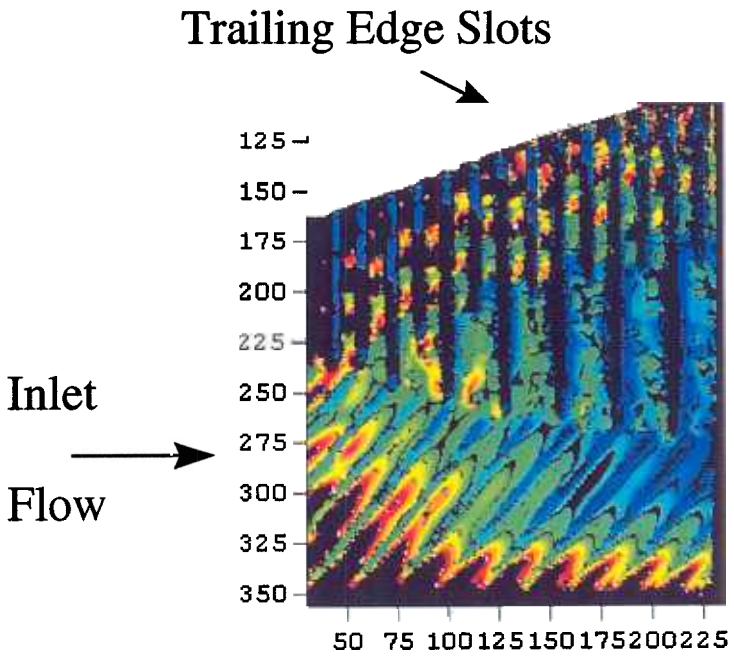

Figure 2.2.3.5.8-1. Lab-scale S1N Trailing Edge Model Liquid Crystal Test

A separate trailing edge cavity heat transfer test was conducted with an acrylic test section modified to form a 0.4-inch × 1-inch flow passage. The first series of tests was conducted with a smooth tube. The heat transfer coefficients measured with the smooth tube are within ±15% of the expected values. The second series of tests was conducted with turbulators. Additional tests were also conducted with medium height turbulators having square or rounded edges. The measured friction factor and the heat transfer coefficient enhancements were compared with the CRD database predictions. The friction factors at the low blockage ratios are close to the values in the database; the difference between the measured friction factors and the values in the database increases with the turbulator height. The heat transfer coefficient enhancements varied with the turbulator height and the flow Reynolds number.

The pin-fin-cooled region of the trailing edge was also investigated separately. First a model that can predict frictional losses and heat transfer coefficients for pin fins was

developed based on open literature data. The model calculations were then compared with those data. Although the heat transfer information compared favorably, the friction factors showed differences. A simple pin fin experimental setup was constructed. Pressure drop (friction factor) data were collected for the specific pin fin geometry of the trailing edge passage. The friction factor correlation was improved and the model is being used to optimize the present pin fin configurations and enhance the friction and heat transfer in the pin fin region.

Film Hole Discharge Coefficients

The film holes covering part of the trailing edge region near the rib are at an angle of 30° to the flow and drilled at an angle of 90° to the wall. Due to manufacturing constraints, these film holes are drilled in such a way that the film flows in the film holes are co-flowing with the supply cavity side feed flow in the airfoil half near the outer sidewall region. The film flows are counter-flowing to the supply cavity flow in the airfoil half near the inner sidewall region. Information in the open literature shows that the film hole discharge coefficients depend on the supply side velocity (Mach number) and orientation of the film holes with respect to the supply cross flow. A test facility was designed and experiments were conducted to measure the discharge coefficients of 30°-inclined film holes as a function of pressure ratio, supply side Mach numbers, and co- or counter-flowing supply flow with respect to the film flow direction. Additional film hole discharge coefficients were measured during 1Q99. The results showed the dependence of the discharge coefficients on three parameters: the supply flow Mach number, flow direction with respect to the film hole angle, and the ratio of the supply pressure to the discharge pressure across the film holes.

STEM Drilled Cooling Passages

For the work on cooling the trailing edge of the first-stage nozzle, each vendor manufactured one STEM-drilled turbulated passage. The test specimen provided was turned into a 0.25-inch OD tube. Before the tube was instrumented, a X-ray image was recorded to locate the beginning and end of the turbulated region. The test tubes were then instrumented with static pressure taps and imbedded thermocouples before the flow and heat transfer tests were run. The test results from one tube provided information that could be related to the existing data. The results obtained with the second tube did not agree with the expectations. The second tube was then cut along a diameter and visual observations revealed that the tube was not manufactured according to the specifications. While there was a plan to test a replacement tube for the vendor whose tube was out-of-specification, that action did not take place. The in-specification tube data were determined to be adequate.

Summary/Conclusion

All aspects of the internal heat transfer and pressure losses for the S1N air-cooled trailing edge have been investigated, both in their initial design form as well as updated / improved designs. No single mechanism within the cooling circuit is dominant, hence all features must be evaluated for design validation and calibration. Comparisons with

existing database information help to lay the foundation for any further design updates. Of vital importance is the validation of as-fabricated conditions.

Technology Application

The friction factor and heat transfer results obtained with the turbulated low aspect ratio passage have been used to validate the design tool predictions and form the basis for parametric evaluations. The testing of new concepts verifies the design assumptions with respect to the pressure drop and heat transfer coefficients. The friction factor and heat transfer information generated with the STEM-drilled tubes provides design information for these trailing edge tubes, and generates complementary information to the existing design database. Visual observations of the turbulators also allows a comparison between the process capabilities of vendors.

Section 2.2.3.5.9 (GTETBKHT) High Reynolds Number Turbulator Static Heat Transfer Test [C]

Objective

The objective of this task was to investigate and determine the heat transfer coefficient enhancements possible in the first-stage nozzle. Internal cooling is supplied by two different types of convection: one using impingement heat transfer within the internal airfoil cavities, the other using high Reynolds number turbulated heat transfer within the aftmost convective channel of the airfoil. This task concentrated on the latter type of heat transfer. Experimental work reported in the open literature on turbulator heat transfer enhancement and friction factors is limited to passage Reynolds numbers below 80,000. This task provided data and correlations to be used for advanced machine design conditions. Heat transfer and pressure drop data are required at far higher Reynolds numbers than previously tested with common turbulator geometries and passage aspect ratios.

Introduction / Background

Conventional turbulated cooling passages for use in air cooled gas turbine components typically use flows with Reynolds numbers ranging from 10,000 to 80,000. The existing literature data on heat transfer and friction for such channels is entirely limited to flows below Reynolds number of 80,000. Because the design for the ATS turbine Stage 1 Nozzle contains at least one steam-cooled passage with Reynolds number exceeding 100,000, it is necessary to extend the turbulated passage database to this region and beyond. This data provides design boundary conditions and also a basis for any design modifications, or use of high Reynolds number channels elsewhere in the ATS turbine.

Discussion

This task was initially subcontracted to Texas A&M University. The work was performed by Professor J. C. Han of Texas A&M's Turbomachinery Laboratory. Two test sections were designed which allow tests at three different aspect ratios. One test section has a square cross section; the other has a rectangular cross section that can be used to test both high and low aspect ratios by heating the narrow or wide walls of the passage,

respectively. As shown, forty individually heated and instrumented copper segments make up the inner walls of each test section, with ten segments per wall. The ten electric segment heaters on each wall are connected in series to one variable transformer, for a total of four variable transformers. Thus the power input to each wall can be varied independently. There are a total of fifty thermocouples for the test section, which are connected to a data logger and data acquisition computer. The complete flow loop at the Texas A&M Turbomachinery Laboratory is shown in Figures 2.2.3.5.9-1 through 2.2.3.5.9-3.

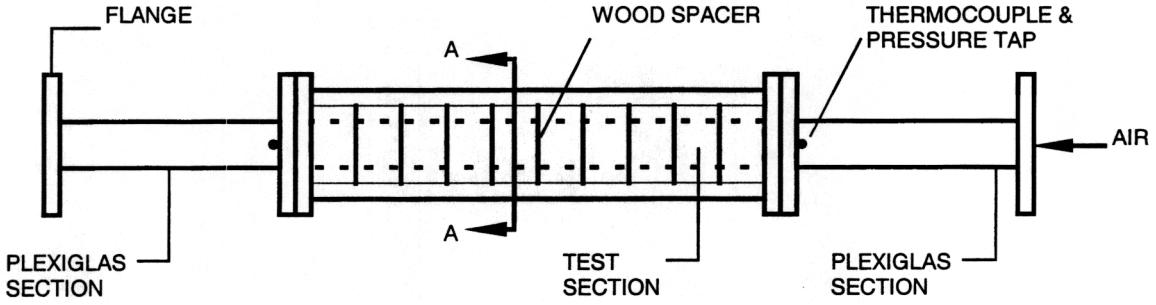

Figure 2.2.3.5.9-1. High Reynolds Number Turbulated Passage Test Section.

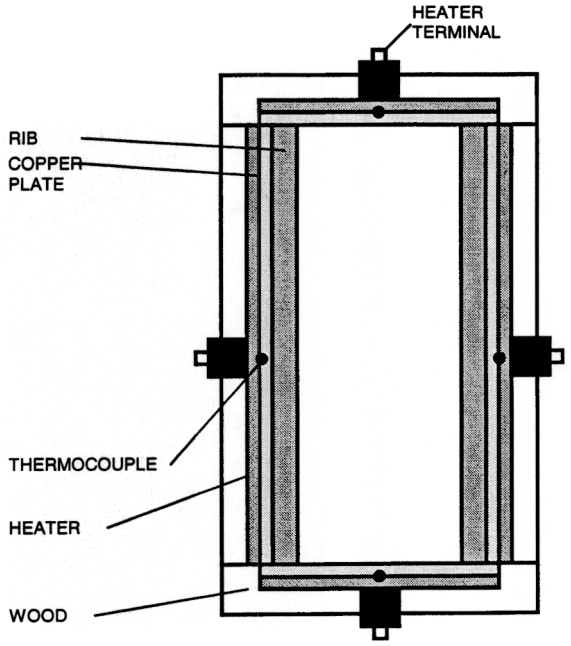

Figure 2.2.3.5.9-2. Section A-A Construction.

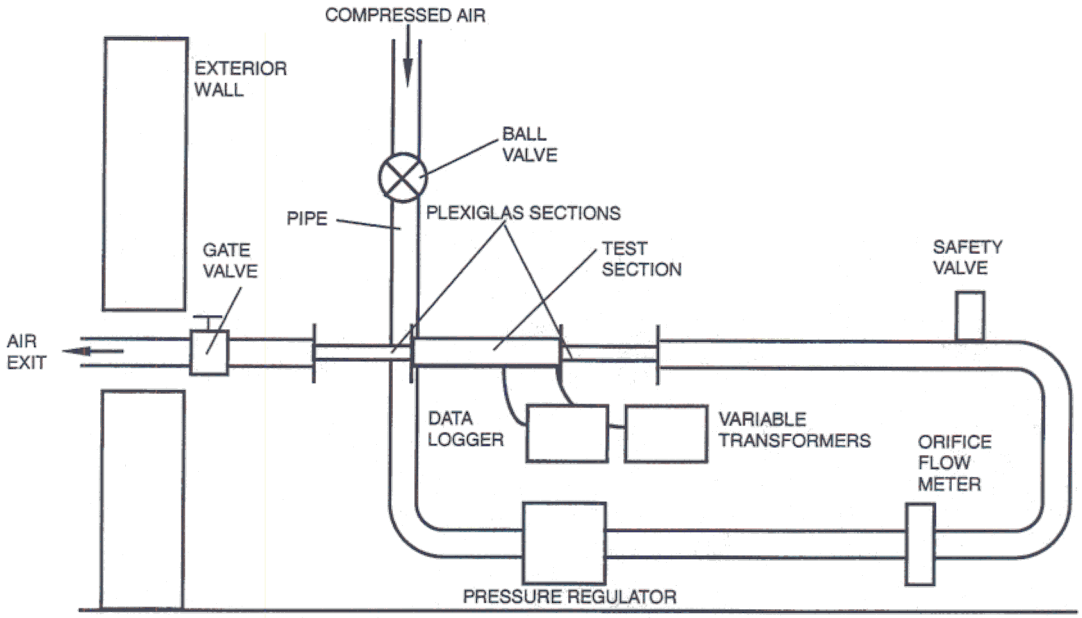

Figure 2.2.3.5.9-3. Flow Loop at Texas A&M's Turbomachinery Laboratory

Texas A&M tested both test sections with smooth and turbulated walls for heat transfer and pressure drop over a wide range of Reynolds numbers. The test sections are not capable of being pressurized to high levels, so at high Reynolds numbers compressibility effects can influence both the measured friction factors and heat transfer coefficients. While Texas A&M was advised to incorporate a pressure vessel in their design, this never materialized. As a consequence, not only were compressibility effects present, but also section leakages due to over-pressure at high Reynolds numbers. These unresolved issues caused the termination of this work at the university.

CRD Rig Tests

A very similar segmented / instrumented test section was fabricated and tested at CRD. In this case, a section of large diameter piping was used as the pressure vessel, allowing Reynolds numbers of as much as 1,000,000 to be obtained while maintaining incompressible Mach numbers. The channel was tested over the Reynolds number range of 50,000 to 1,000,000 with three configurations. The two main walls of the channel were tested as smooth surfaces, with 45-degree turbulators, and also with 90-degree turbulators. Both regional heat transfer coefficients and overall pressure loss data were obtained for all cases. This data was compared to the CRD database for turbulated channels, and allowed extension of that database to ATS turbine design conditions.

Summary / Conclusion

Reliable results have been obtained from the CRD test rig which extend the available database correlations for some turbulated cooling channels up to Reynolds numbers of 1,000,000. This data has been used directly in the design of the S1N convectively cooled channel, and in other regions where rotational effects are considered to be minor.

Technology Application

The results from this task are applicable to any non-rotating components in the advanced gas turbine that use turbulated passages for cooling. As long as rotational effects are accounted for, these results are also applicable to turbulated passage cooling of rotating components.

Section 2.2.3.5.10 (GTET) Impingement Degradation Effects [C]

Objective

The internal nozzle design verification tests conducted in 1996 with various impingement jet plates and test plates showed that the impingement heat transfer coefficients measured under the first and second rows of the impingement jets were lower than the open literature correlation predictions (Florschuetz & Metzger). Although this difference was not significant in some regions, it was important in others regions where accurate knowledge of the heat transfer coefficients under the first two impingement jets is important. The differences between the design verification test results and the correlation predictions were attributed to the fact that in the former tests the first row of jets was near a wall with zero velocity boundary conditions, while in the correlation tests the first row was adjacent to a constant pressure boundary condition. The objective of this task was to understand the physical phenomenon that causes the observed difference. The local static pressure distributions along the crossflow regions of the impinging jets will be measured for two inlet boundary conditions, one with a wall and the other with a constant pressure. Tests were also conducted with the cross flow discharging in one direction across the impingement jets and discharging in two directions symmetrically from the center row.

Introduction / Background

Impingement heat transfer is a well established cooling method in most respects. Many publications and company investigations document various aspects of impingement jets and arrays of jets. By far the most common data are for open jets and arrays of open jets impinging normal to a surface at various flow rates and spacings. When dealing with enclosed or confined geometries of impingement, the available data is very limited. This is the case because each confined geometry is design specific, involving many more parameters and boundary conditions. The established impingement array correlations, such as that of Florschuetz & Metzger, do not incorporate the same confinement conditions as the design of the ATS turbine Stage 1 Nozzle endwalls; they are in essence generic. In the course of some preliminary endwall impingement testing using a specific confinement geometry, certain lower than expected heat transfer magnitudes were exhibited in a liquid crystal test. This sparked the need to further investigate the confinement effect in order to assure correct boundary conditions for the S1N design.

Discussion

A series of tests was conducted to investigate the effect of the distance between the jet plate and the impingement test plate on the jet flow rate for a given constant pressure ratio. The results showed that, for the given pressure ratio, the flow rate increases and

reaches an asymptotic value as the distance between the plates increases. The impingement program developed for the design calculations appears to calculate the correct flow rates as long as the jet-to-plate distance is larger than 0.75 jet diameters.

To investigate the effects of the location of the first row of jets (i.e., near a wall with zero velocity boundary conditions or adjacent to a constant pressure boundary condition), the impingement test rig used in the enhanced surface heat transfer tests (2.2.3.5.7) was modified to accommodate static pressure taps along the jet cross flow regions. The impingement test plate was instrumented with a liquid crystal and a thin-foil heater. In addition to the impingement heat transfer coefficients distribution, the static pressure distributions were also measured along the side wall at the jet injection locations and in between jets. The first series of tests was conducted with the first row of jets impinging near a wall with a zero velocity boundary condition. A second series of tests was also conducted for comparison where the jet and test plates are left as above except that the first row of jets is moved away from the wall by 1 cm. An air cavity is left (with no flow) between the first row and the wall. Static pressure and heat transfer coefficient distributions were again measured.

Once again the data agreed with the model predictions. The heat transfer coefficients measured during these tests showed that the highest impingement heat transfer was occurring underneath the first jet and not the second jet as observed in 1996. The results confirmed the applicability of the Florschuetz & Metzger impingement heat transfer coefficient correlations and the model predictions for the design calculations. The difference between the 1997 and 1996 results may be due to some instability in the jet formation that was not manifested during the 1997 tests.

Summary / Conclusion

The appropriateness of the existing design correlations for use in the case of confined impingement jet arrays (eg. Stage 1 Nozzle endwall regions) has been confirmed. The nature of the earlier indication of sub-standard impingement heat transfer remains an unexplained phenomenon at this time.

Technology Application

The results obtained clarify the discrepancy between prior test results and those from open literature correlation predictions (Florschuetz & Metzger). The new data will improve the design of the first-stage nozzle internal cooling scheme.

Section 2.2.3.5.11 (GTETIH) Production Airfoil Flow Checks [C]

Objective

The cooling flow circuits of the first- and second-stage nozzles and buckets of the ATS gas turbine have complicated flow configurations. Design flow models involve several empirical friction factors and flow element head loss coefficients that were taken from the best knowledge available. The models need experimental verification with typical cast components. The objective of the flow checks, conducted with air, was to check the flow rates and static pressure distributions of typical cast first- and second-stage nozzle and

bucket components. The results were compared with the design flow model predictions. The measured overall coolant flow rates for a given overall inlet-to-exit pressure ratio also formed the basis for future quality flow tests to ensure that every component fulfills the flow design requirements.

Introduction/Background

An essential element to all turbine development programs is the validation of cooling for all turbine airfoils. While investment castings, after sufficient trials and development, meet the major specifications for dimensions and tolerances, this does not guarantee that the parts will flow the correct amount of coolant, nor that the parts will flow each individual circuit correctly. Due to the complexity of today's typical highly cooled turbine airfoils, the stack-up of casting tolerances will result in a variation in part-to-part flows. In addition, and perhaps of even greater importance, the ability of design to predict the precise internal flow resistances for such complex geometries is far from perfect. It is still required that each cooled part undergo flow checks to verify both overall flow, as well as to calibrate the component flow models for details of resistances. The steam-cooled parts of the ATS turbine contain impingement inserts, parallel flow paths, and many turbulated flow passages and turning regions. It is therefore imperative that detailed flow checks be performed both in the developmental stage and the production stage of all such components.

Discussion

Full-Scale Nozzle Cascade Component Flow Checks

As part of this airfoil flow checks task, two first-stage nozzles to be used in the first Full-Scale Nozzle Cascade (FSNC) low cycle fatigue (LCF) tests were flow checked. The two nozzles are similar to the ones which were flow checked in 1995 for the first FSNC heat transfer tests. The nozzles have steam circuits and two air-cooled cavities near the trailing edge. The flow checks were conducted in air, and the static pressure distributions were compared with the flow models and with the 1995 data. The comparison of data showed that the steam circuits of the LCF test nozzles and heat transfer test nozzles are similar. The air flow cavities differed somewhat, but those differences were corrected before the LCF test nozzles were installed.

The FSNC test setup at GE Aircraft Engines in Evendale, Ohio, has two fully instrumented airfoils which are air and steam cooled. Two water-cooled copper airfoils constitute the side walls of the test facility. These water-cooled airfoils form the pressure and suction side walls of the cascade facility. The water-cooling circuitry was flow tested to generate flow rate versus pressure drop data and compare them with the original design. The results showed that the overall measured flow rates were lower than the design intent for the given pressure differences. The test results obtained in the laboratory were also compared with the test data obtained in Evendale. Measures were taken to bring the water cooling up to design intent to assure a successful cascade test.

The flow tests on the first-stage nozzles of the 9H production FSNC (second cascade) used in the tests at GE Aircraft Engines, were initiated with available cast components. The first series of tests concentrated on determining the flow distribution underneath the

outer sidewall impingement plate. The post-impingement flow distributes itself between leading edge cavity 1 and cavities 6 and 7 in the trailing edge region. Tests were conducted with half and all the impingement holes open and the flow going through cavity 1 only, cavities 6 and 7 only, and all cavities. In addition to the overall flows, static pressures were also measured at thirteen locations at the outer sidewall post-impingement regions. Six impingement inserts for each of the six airfoil cavities were received from the manufacturer. Flow tests were conducted with and without the inlet metering plates. Two inserts were selected for each of the six cavities, which satisfies the design requirements for the two cascade airfoils. Also, with the first-stage nozzle cavity 1, 5, and 6 inserts in place, the flow distributions through the outer side wall impingement plate were investigated. Five series of tests were conducted to evaluate the assumptions made for the outer side wall impingement hole patterns and the flow distributions expected through these cavities. The test results showed that the stagnation line was well predicted and the flow distributions were close to expectations.

Flow Tests of Turbine Hardware

A prototype second-stage bucket was flow tested in 1997. In preparation for these flow tests, the SLA model of the bucket-cooling circuit was used to determine the location of the static pressure taps. The second-stage bucket YFT cooling-circuit flow model was run for the low-pressure air flow test conditions to evaluate the relative pressure drops and the flow rates involved in the testing. The vendor supplying the cast sample bucket provided the EDM-drilling of the static pressure taps.

In 1998, flow tests were completed for (1) the first- and second-stage bucket production castings, (2) four of the impingement inserts of the first-stage nozzle cooling circuits, without and with inlet metering orifices, and (3) the turbulated, convective cavities for two first-stage nozzles castings. Tests were also performed to verify the methods used in the design of the impingement inserts for the first-stage nozzle used in cooling cavities 1, 2, 3, and 4, as well as to measure the impingement jet supply pressure distributions along the inserts from root to tip. The nozzle parts tested at this time period were development parts.

Overall flow tests and static pressure distribution measurements were performed for the Stage 1 and 2 bucket castings for calibration of the flow models. To provide a proper baseline comparison, the YFT model of the second-stage bucket was modified to reflect differences between the bucket in service and the bucket in the flow tests. Those modifications included using room-temperature air instead of steam; no rotational effects; low inlet pressures; and venting to atmospheric pressure. The YFT code was then run with the modified case files to provide a comparison with the measured data. Several changes were proposed to the flow model to agree with the static pressure and flow measurements.

Similar flow tests were conducted with development and production impingement inserts for cavities 1, 2, and 3 for the second-stage nozzle. In addition to the insert flow test, a doublet of the second-stage nozzle was assembled with all the flow elements, and instrumented with pressure taps. The static pressure distributions at various circuit locations were measured with all cooling circuit elements assembled.

During 1999, flow tests were performed with cast 9H first- and second-stage nozzles and the various cooling circuit impingement inserts, without and with inlet metering orifices. Six first-stage nozzle impingement inserts were tested for steam cooling cavities 1 through 6. The objectives of these tests were (1) to verify the methods used in the design of the inserts and the impingement jet supply pressure distributions along the jet supply flow areas and (2) to compare the results of these production parts with the development parts tested earlier. The results showed that the average pin-checked jet diameters were close to the required values. The static pressure distributions at the various jet row locations were similar to those measured earlier on the development parts. Some variations in measuring insert flow rates with respect to design requirements were noted. The inserts were then incorporated into the cast airfoil, the inner and outer sidewall impingement plates and covers were assembled, and flow tests were run for the overall flow circuit. Similar flow tests were conducted with the impingement inserts of the second-stage nozzle without and with metering plates. The inserts were then incorporated into the cast airfoil, the inner and outer sidewall impingement plates and covers were assembled, and flow tests were conducted for the overall cooling circuit. Flow rates were measured as a function of inlet-to-discharge pressure ratio. Static pressure taps were positioned at key locations of the cooling circuit, and the pressure distributions were measured as a function of flow rate or pressure ratio.

The static pressure data and the flow rate data recorded for the first- and second-stage nozzles were compared with the flow models. The comparisons were used in altering the flow resistances where needed and to anchor the design predictions compared with the cast component flow data. In order to evaluate the effect of some of these changes on the resulting metal temperatures, GEPS staff applied the thermal conduction models of the nozzles with the empirically validated flows.

Flow tests were conducted, with and without the inlet metering plates, for a set of six airfoil impingement cavity inserts. These tests were conducted to determine the part-to-part variation in flows for sets of inserts.

An overall flow test at the design pressure ratio was conducted on a production complete first-stage nozzle casting received from GEPS. The measured flow was found to be just a few percent higher than the upper specification limit.

Summary / Conclusion

Overall and detailed flow checks have been a fundamental part of the development of the steam-cooled turbine airfoils. Only through the consistent use of such flow checks have the test, development, and production parts been qualified. Invaluable data has been gained with which the part flow models are calibrated. Many corrections and improvements results directly from these flow checks, which would have been difficult to foresee without this data. Such data is used not only in the production and quality control phases of this machine, but also in the design verification phase as the first units go into power production.

Technology Application

The flow and static pressure distributions results obtained with the cast components will verify the design flow model predictions and ensure that the predictions are correct and that there are no regions that have friction and head loss factors different from the design assumptions.

Section 2.2.3.5.12 (GTETIH) Nozzle Fillet Heat Transfer [C]

Objective

The objective of this task was to determine impingement heat transfer behavior in the fillet regions of the first-stage nozzle. There are two forms of internal fillet regions in the first-stage nozzle design: (1) the airfoil insert impingement into the spanwise cavity rib fillets and (2) the endwall perimeter edges, which represent the furthest extent of impingement into corners. Because thermal gradients make these fillet regions critical lifing areas, detailed heat transfer coefficients are required. A liquid crystal cooling model test was designed to determine heat transfer distributions with various geometries.

Introduction / Background

The bulk of the cooling surfaces within the steam-cooled airfoils of the ATS turbine utilize some form of impingement or convective heat transfer in a fairly uniform manner. There are, however, several specific areas of distinctly unique geometries, for which even rudimentary design correlations do not exist. This uniqueness is due to the closed-circuit cooling approach within geometrical regions that still conform to the conventional aerodynamic and mechanical designs of turbines. An example of such an area is in the Stage 1 Nozzle endwalls. Here, the steam coolant must still be contained, but must also cool the furthest extents of the endwall regions at the perimeter. This perimeter is essentially a corner or box end, which is cooled internally, but also performs other functions externally (eg. gas path sealing, component interface, etc.). The internal corner is known as a fillet, and is still subject to a substantial heat load from the hot gas path. As no correlations exist for such a geometry, or the variants on this geometry, it is necessary to perform validation tests to obtain the required design data.

Discussion

In 1998, CRD and the GEPS design team initiated this task by identifying the representative airfoil and endwall locations to be examined. Preliminary design reviews confirmed the key features and established the arrangement of the test models to be used. Two acrylic test models were designed, see Figure 2.2.3.5.12-1, each a 10X version of a representative fillet region. The models retain all the key surface features that may affect flow distribution and heat transfer. The detailed local heat transfer coefficient distributions are measured using the steady-state liquid crystal technique with thin-foil surface heaters. The 10X models achieve the same average Reynolds number conditions as expected in the turbine nozzle design, but with discharge of coolant to atmospheric pressure in the lab. Each model is similar in construction and data acquisition technique, but the inner and outer endwall fillet region geometries differ in the corner turning area to

an extent which requires separate test models. The differences lie in both the casting shapes and in the placement of the cooling impingement jets.

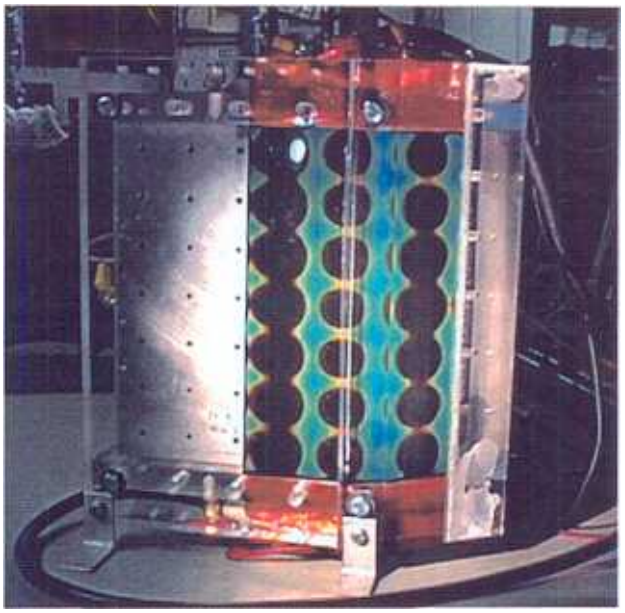

Figure 2.2.3.5.12-1. Example of 10X Fillet Region Impingement Test Model

Each model has been tested with three average jet impingement Reynolds numbers ranging from 8000 to 40,000, and at three impingement target spacings from roughly 4 to 11 jet diameters. Detailed maps of the cooling side heat transfer coefficients were obtained for the entire fillet flow turning region for each set of conditions. All of the data obtained has been transferred to the GEPS design team, along with the appropriate scaling factors to convert from the air-cooled model test data to the steam-cooled turbine heat transfer boundary conditions.

In 2000, the nozzle endwall edge region (perimeter) fillets have been re-designed for greater life capability. To obtain an accurate measure of the detailed heat transfer distribution in this updated configuration, a new 10X model has been designed and fabricated. This model has the ability to deliver two separate cooling flow supplies to allow full flexibility in the flow configurations to be tested. Both the fillet region and the flat array impingement region will be tested, including the effects of variable direction crossflow. An additional series of tests will model the inclusion of surface roughness elements for enhanced impingement heat transfer within this specific geometry. At the time of this report, this model is being assembled for initial tests.

Summary/Conclusion

Detailed heat transfer coefficient distributions for the Stage 1 Nozzle endwall fillet regions along the perimeters of the inner and outer endwalls has been obtained. This design data has been used in the first case to provide thermal-mechanical and lifing estimates for the nozzle, and also to help improve the design of the steam-cooled endwalls. There is a careful balance between the need for full cooling, and the available

supply of steam coolant. The level of heat transfer information supplied by these scaled-up test models assures that all cooled regions maintain the required integrity.

Technology Application

The first-stage nozzle endwall edge regions represent the furthest extent of impingement cooling within the steam circuit of the nozzle. These edge regions must balance the local cooling requirements with those of more inboard regions that experience cross-flow effects from the edge flow. The liquid crystal test models will provide detailed heat transfer coefficient distributions for the specific geometries of the endwalls. These data will be used to confirm design and component lifing. The models will provide vehicles to further optimize this cooling as required.

Section 2.2.3.5.13 (GTETIH) S1N and S2N Endwall Heat Transfer [C]

Objective

Additional high Reynolds number impingement heat transfer data with brazed microturbulator-roughened, enhanced surfaces are needed for possible application to the first- and second-stage nozzle outer and inner endwalls.

Introduction / Background

Impingement cooling is utilized heavily in both the ATS turbine S1N and S2N. While impingement is typically a very effective means of heat transfer, there are methods for the further enhancement of this technique. Surface roughness elements have been previously discussed in Section 2.2.3.5.7 as one convenient method for increasing the cooling effectiveness. Other methods have been explored for the formation of such surface roughness features, one of which is known as brazed microturbulators. The advantages of various forms of roughness, or application methods, comes in the quality of investment castings and the difficulty of placing roughness in certain regions. The microturbulators offer high levels of enhancement with convenience of placement location, but like all such roughness types must be investigated for its specific heat transfer enhancement values.

Discussion

The testing performed in this task utilizes the same impingement facility described in Section 2.2.3.5.7. Two 51-mm × 51-mm test plates were manufactured from GTD-222 and N5; both materials are Ni-based superalloys used for turbine airfoils. The test plates were coated with brazed microturbulators, a specific form of surface roughness elements for heat transfer enhancement. The roughness of each test plate was characterized by means of a cone stylus profilometer. The test plates were instrumented with imbedded thermocouples. The first tests were conducted with the GTD-222 rough test plate and two representative jet impingement array plates at several average jet Reynolds numbers. The jet-to-target surface spacing was 3 jet diameters. Baseline tests were also conducted with a HastX smooth test plate. The results provided heat transfer coefficient enhancement values at the test conditions.

The second series of tests were conducted with the N5 test plates and the same jet impingement array plates. In this case, the jet-to-target surface spacing was chosen as 5 jet diameters. The enhancement values obtained during these tests are lower than the ones measured earlier with similar rough surfaces. This difference is attributed to the effect of the distance between the impingement jet plate and the test plate.

Summary / Conclusion

The impingement heat transfer enhancement values obtained with the brazed microturbulators were reported to GEPS engineers for use in the design of selected regions of the turbine airfoils. At least comparable heat transfer enhancement values were obtained to those with roughness formed via investment casting.

Technology Application

The heat transfer information generated has been used in the cooling design of the inner and outer endwalls, where the enhanced surfaces formed by cast bumps could be replaced with the brazed microturbulators.

Section 2.2.3.5.14 (GTETIH) Production Stage 1 Nozzle Cooling Circuit Flow Checks [C]

Objective

The H machine stage 1 nozzle is a steam-cooled component and significantly different in thermal design than air-cooled nozzles. The objective of this task is to conduct flow checks of the stage 1 nozzle components which will be tested in the cascade tests to be carried out at Evendale later this year.

Introduction /Background

Air flow tests of individual 9H stage 1 production nozzle impingement inserts were completed in 1999, and some of these inserts tested were selected for use in the final (assembled) cascade test nozzles. Testing was conducted to study the flow as a function of pressure ratio characteristics of the internal (parallel) branches of the steam cooling circuits. This was also completed in 1999. Representative nozzle hardware was used in this test, but is not part of the final cascade test nozzles.

Discussion

Following the initial component flow tests, two production 9H stage 1 nozzles in a partially assembled condition were tested. The nozzle configuration included airfoil castings with the impingement inserts installed, and the outer sidewall cover assembly 'lightly' attached to the airfoil casting, (i.e. only the first weld pass of several planned was used for the attachment). This made the assembly strong enough for the low pressure flow test. All of the metal thermocouples, cooling circuit thermocouples, and cooling circuit static pressure tubing for the airfoil and outer cover assembly were included. The flow function as a function of pressure ratio was calculated. Tests of the airfoil leading edge and trailing edge internal flow circuits were measured separately, and then for both circuits flowing together in parallel. The inner sidewall cover assembly was omitted from this test.

The final air flow test of the steam cooling circuits was conducted to define the flow function vs. pressure ratio characteristics of both test nozzles, as well as the static pressure distribution within the flow circuits for the completely assembled nozzles.

Two airfoils were received early in 2000 with the inserts selected in 1999 installed in the nozzles. The outer sidewall covers were assembled but not the inner sidewall covers. The post impingement flow at the inlet distributes itself between the leading edge (cavity 1), and the two cavities (6 and 7) in the trailing edge region. Tests were conducted with all the impingement holes open and the flow going through cavity 1 only, cavities 6 and 7 only, and all cavities flowing. During these tests, it was determined that leaks existed between passage 1 and passage 2 through holes made for instrumentation routing and attachment. Passages 1, 6,and 7 were blocked and the leaks were quantified. The leaks were fixed and the nozzles were flow tested again. Tests were conducted with all of the impingement holes open, and the flow going through cavity 1 only, cavities 6 and 7 only, and with all cavities flowing

After the nozzle assemblies were completed, they were flow tested for the overall steam circuit. Results were compared with individual component flows. Final results for the nozzles flow measurement demonstrated satisfaction of the original test objective, as the leading and trailing edge flows measured separately agreed with the total measured nozzle inlet flow. During the GE Aircraft Engines - Evendale cascade test, only pressure ratios will be measured for the two circuits. From these pressure ratios, the two circuit flow rates can be determined and then added to obtain the total nozzle cooling flow.

Summary/Conclusions

This project demonstrated that using flows measured from individual components, the expected total flow of the assembled nozzle matched with the measured flow of overall nozzle. The flow functions measured on these two nozzles allow measurement of flow in the Evendale cascade tests.

Technology Application

Flow checks of these components will be compared with analytic predictions to validate design models. The data will also provide information on statistical scatter of nozzles due to manufacturing tolerances.

Section 2.2.3.6 (GTETEH) Surface Roughness and Combustor-Generated Flow Effects on Heat Transfer [C]

Objective

The effects of TBC surface roughness on external heat transfer have been characterized using flat plates tested in an atmospheric wind tunnel. An advantage of flat plates over airfoils is that TBCs can be applied easily and polished to uniform thickness and surface finish. Full mapping of the TBC surface topography was performed. Reynolds numbers spanned those expected in the ATS turbine inlet nozzle surface away from the leading edge. Tests included plates with and without leading edge step heights to model the effects of component interface misalignments.

Introduction/Background

The fundamental effects of surface roughness on heat transfer coefficients for external boundary layer flows is only modestly understood. The primary source for heat transfer knowledge connected to turbine airfoil surface roughness is engine experience. While predictive codes provide estimates of local heat transfer in the presence of roughness, it is the engine experience that must calibrate such predictive tools. The use of TBC surfaces introduces additional uncertainties into these predictive tools, since the TBC surfaces have different roughness characteristics than typical metallic surfaces or oxide deposits. This is further complicated by the fact that in-service roughness can depend upon the manufactured initial roughness of the surface. From both the aerodynamic and thermal

considerations, it is desired to introduce new surfaces into service as smooth as possible, but this is not always economically feasible or practical. With TBC surfaces, there is a point at which polishing will no longer produce a performance benefit. Experimental verification of the effect of different TBC roughness levels on heat transfer must be established for the particular TBC used on the ATS turbine airfoils. Because turbine components have interfaces which can never be perfectly aligned in-service, the associated effect of flow path steps for TBC surfaces is also required for design.

Discussion

In 1998, stainless steel test plates were installed in a cold-flow wind tunnel and heated from the backside via embedded cartridge heaters. Each plate was instrumented with several pairs of thermocouples arranged to form heat flux gauges. The test side of each plate was coated with TBC. One plate was left as an uncoated metal surface and served as the hydraulically smooth surface baseline.

The wind tunnel, shown in Figure 2.2.3.6-1, is a welded construction of steel plate with the exception of the test plate and viewing regions. Mainstream flow is provided at room temperature to an upstream pressure vessel (not shown) and then proceeds through an elliptical contraction entry piece into the channel of Figure 2.2.3.6-1. After an entry section spool piece, the flow is diverted around a symmetric splitter plate. The channel walls are of the same angle as the splitter plate so that dP/dx gradient remains essentially zero. In the present tests, the splitter plate also has trip strips of 50-mm height on both sides at intervals of 10 cm to periodically restart the boundary layer. The splitter plate provides a known length of unheated boundary layer, and is "adjustable" by the placement of trips. The freestream turbulence intensity level at the start of the test plate region was measured to be from 4.5 to 6.5% depending on the Reynolds number.

The test pieces are part of the removable cartridge assembly shown. Each test plate is made from stainless steel of 8.25-mm thickness, with a streamwise width of 7.62 cm and a total height of 15.2 cm. Only the lower 3 inches of the test plates reside in the flow stream; the upper portion of the plate transitions the instrumentation through the wind tunnel top wall and provides strain relief / splicing for the thermocouple leads. The test plate forms one side of the cartridge with the test surface exposed to the convective media. Behind the test plate is the heater block. The heater block is a solid piece of copper 7.6 x 7.6 cm and about 8.2-mm thick. Inside the copper are imbedded 6 cylindrical cartridge heaters of 300W each. The heater block and the test piece are pulled together by a series of 10 screws to retain good thermal contact. Thermal connection is further improved by the use of a 2-mil foil of Aluminum between the copper and test piece, which deforms into any surface irregularities. The opposite side of the heater block is covered by an insulating layer of G7, as are the sides of the assembly as well as the top and bottom. The heater block provides the heat flux and temperature level for the tests, with rejection of the heat to the mainstream air on either side of the test cartridge. The test cartridge is followed in the wind tunnel by a simple half-body of G7 material.

The test surface is viewed through a Sapphire window with an Infrared imaging camera. The Agema Thermovision 900 system was used for these tests, with "ATM" filter mode detecting the 3 to 4 micron wavelength range. Since the mainstream air was room

temperature in these tests, there was no need for any corrections to the images due to window thermal radiation contributions. Each plate has 20 imbedded K-type thermocouples, ungrounded. The thermocouples are all imbedded by wire-wedging in the pattern shown. The arrangement is seen to be mirror opposites on the two sides of the plate, thereby forming 10 thermocouple pairs, or heat flux gages. The primary gages used in the present tests are those along the centerline of the flow path. The first and last gages are ½-inch from the leading and trailing edges of the plate, and intermediate gages are at ½-inch spacings axially. The remaining heat flux gages monitor the uniformity of results away from centerline, the loss of energy out the top of the plate, and in at least one case provide backup data when a primary gage is damaged.

The test wind tunnel was designed and fabricated so that the test plates could be removed easily for detailed surface preparation and/or polishing. In addition, the design allowed for the provision of an adjustable step in the flowpath simulating the expected or potential component interfacial steps in the ATS turbine. Cold air-flow was provided over the heated test plates inducing a heat flux through the thickness of the plates, including the TBC, which was transferred to the air via convective heat transfer. An imaging infrared camera system was used to capture the steady-state surface temperature map of the entire plate, either metal or TBC surface. Separate calibration tests determined the individual heat flux gauge responses as a function of temperature level. The convective heat transfer coefficients were obtained for TBC surfaces of various roughnesses using the measured heat fluxes, the measured surface temperatures, and the measured air pressure, temperature, and mass flow rate.

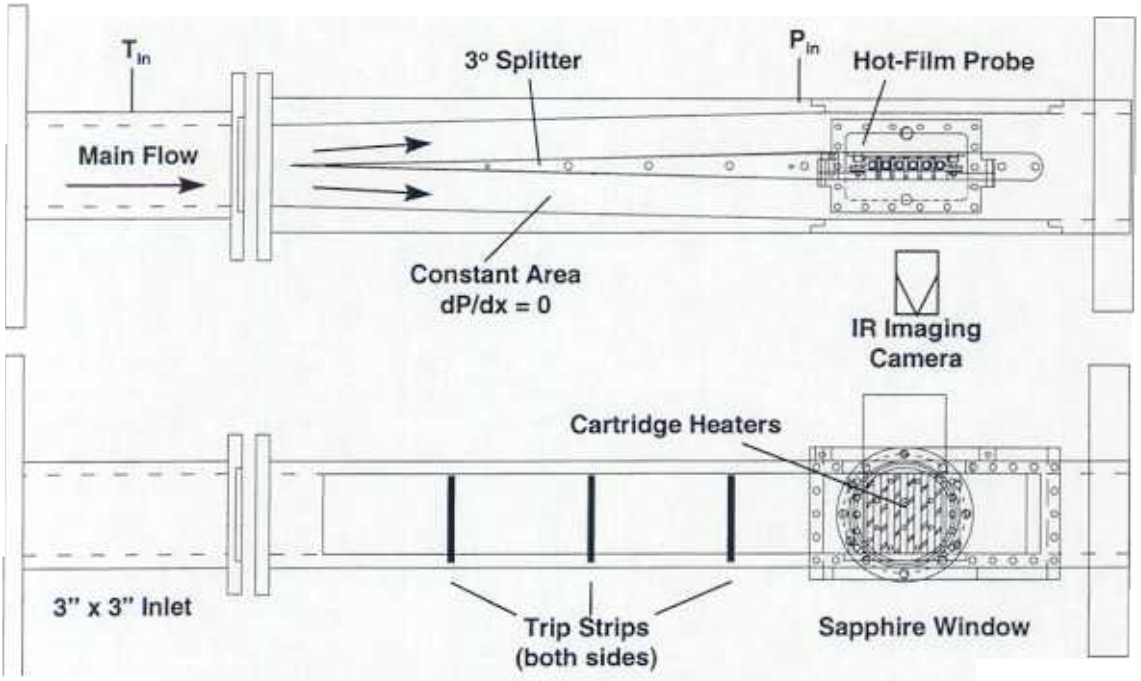

Figure 2.2.3.6-1. Cold Flow Wind Tunnel Cross Section Views

Test conditions covered a representative range of flow Reynolds numbers, surface roughnesses, and step-height-to-momentum boundary layer thickness ratios. Two TBC-coated plates and one hydraulically smooth metal plate were tested. Plate average Reynolds numbers ranged from 400,000 to 3,600,000. TBC surface roughness levels ranged from 1 to 10 microns (40 to 400 μinches). Step-height-to-momentum boundary layer thickness ratios from 0 to 20 were tested for each roughness level. Repeatability was found to be very good for the metal plate results and satisfactory for the TBC-coated plate results.

The results of this task show that, for the majority of the airfoil and endwall surfaces, polishing to a roughness level on the order of 2.5 to 3.0 microns (100 to 120 μinches) provides a significant reduction in heat transfer coefficients, whereas further polishing results in only minor improvements that were indistinguishable from the experimental uncertainty. The relative effects of flowpath steps were found to be essentially the same whether the surface is smooth or rough. Heat transfer enhancements of up to 2.5 may be expected at the leading edge of an endwall step. Roughness did tend to cause a more rapid decay of the heat transfer enhancement factor downstream of the steps.

Summary/Conclusion

These tests have determined the estimated break-even point for the required level of TBC surface roughness as it affects the resulting airfoil heat transfer. The data obtained are specific to the TBC type and application method used for the ATS turbine airfoils. The interaction of flow path interfacial steps, both smooth and rough, has also been determined. As-sprayed TBC surfaces are clearly unacceptable for the thermal performance of the turbine airfoils.

Technology Application

Data obtained from this task affects the design of turbine airfoils in two ways. Tests that measure the effect of TBC surface roughness on external heat transfer will be used to determine the extent of necessary polishing for new parts, and detailed quantification of the magnitude of heat transfer associated with actual, not modeled, TBC roughness will allow for greater accuracy in the initial design of airfoils. The data obtained on flowpath steps will be used directly in the design of the turbine nozzle endwalls to assess the impact and consequences of heat transfer enhancement due to steps, including the effect of TBC roughness as a possible mitigating factor.

Section 2.2.3.6.1 (GTETEH04) S1N Heat Transfer for Production Aero with TBC Spall Effects [C]

Objective

The objective of this task was the quantification of the external heat transfer coefficient distribution for the production aerodynamic design definition of the ATS turbine inlet nozzle airfoil.

Introduction / Background

A previous task begun in Phase 2 and completed under Phase 3 (2.2.3.1.2 and 2.2.3.6.2) quantified the external heat transfer distributions for the original aerodynamic design of the Stage 1 Nozzle, including effects due to roughness and turbulence intensity. The production aerodynamic design was sufficiently different in crucial regions to warrant a new series of tests, again including roughness and turbulence intensity effects. The new aerodynamic definition for the nozzle was specifically designed to lower the heat load on the airfoil. Results from the previous cascade tests were used on the new airfoil design, but with the assumed validity of local Reynolds number scaling of heat transfer coefficients. Since such scaling of results has no experimental basis for airfoils that deal with complex flows, it was deemed necessary to verify the new design.

Discussion

Results from the original series of tests were used to reduce the task efforts to a minimum. Most of the original apparatus hardware from the ATS Turbine Inlet Nozzle Cascade was reused for this task. Under this task, a more durable, single-piece nozzle cascade frame was fabricated for use in the second cascade test series. Beyond this effort, no further work was performed on this task, as the risk level for other issues was judged greater. A conservatism was placed on the Reynolds number scaled heat transfer coefficients for the new aerodynamic airfoil design.

Summary / Conclusion

The anticipated tests for the new Stage 1 Nozzle aerodynamic shape were not executed. The success of the method used to apply the original heat transfer coefficients to the new design will be born out in the second Full Scale Nozzle Cascade testing.

Technology Application

This task did not produce tangible results for application to the turbine design.

Section 2.2.3.6.2 (GTETEH03) Surface Roughness Effects on Heat Transfer [C]

Objective

The external heat loading for the ATS first-stage nozzle airfoil is heavily dependent upon the nonlinear effects of surface roughness, especially as the nozzle design cannot rely upon the workhorse of turbine heat load reduction, film cooling. Given the current state of turbine cooling technology, the only viable method for determining the nozzle heat load with roughness effects is experimental validation of the heat transfer distribution under non-dimensional engine-representative conditions.

The ATS Turbine Inlet Nozzle Cascade has been used to provide data on external heat transfer coefficients on airfoils with surface roughness. The cascade incorporates instrumented airfoils with flow conditions representative of the ATS inlet nozzle geometry. The appropriate non-dimensional parameters for dynamic similarity are close to those of the engine inlet nozzle. External heat transfer coefficient distributions were measured through the use of embedded thermocouples, with a constant surface heat flux

condition supplied by thin-foil heaters. Surface roughness elements of the appropriate size and distribution have been bonded onto the surface heaters. Data include various roughness levels, distributions, and types to allow for the calibration of predictive methods. Characterization of surface roughness effects included the interactive nature of roughness with fluid dynamic conditions such as acceleration. The cascade has also been used to assess the effects of transition piece wake shedding on airfoil heat transfer, the effect of extreme surface roughness representative of as-sprayed thermal barrier coatings, and the effect of modeled coating spallation on heat transfer enhancements.

Introduction / Background

The importance of airfoil surface roughness and freestream turbulence intensity on vane and blade heat loading characteristics has been known for many years. Both factors are considered to be major contributors to the undesirable but inevitable increase in airfoil heat loads from idealized conditions to engine representative conditions. In the past, turbine designers relied heavily upon engine experience to dictate the conservatism required to be incorporated into successive designs, such that surface roughness and turbulence intensity effects would be accounted for at least approximately. In more recent years, designs seeking to squeeze out every percent of efficiency require more detailed knowledge of the specific effects, the distributions with location, the alterations with flow conditions, and the interactions amongst effects. Of even more importance, is the concurrent requirement to design airfoils for full life and high reliability. The approaching goal is of course the ability to computationally predict such effects on heat transfer. While the effect of surface roughness, or surface finish, has been relatively well studied for its impact on aerodynamic performance, the effect on heat transfer has been mostly limited to idealized flat plate or tube geometries.

Several relevant flat plate heat transfer studies have been reported very recently, in which particular roughness types have been used to examine transition and heat transfer coefficients. The translation of such flat plate experiments to scaled airfoil tests is not straight forward in that the airfoil experiments must typically match certain required non-dimensional engine parameters, such as Re_C and Mach distribution. The difficulties of such testing have led to a more limited range of possible roughness elements for modeling surface roughness effects on airfoil heat transfer. Turner et al (1985) simulated engine type roughness due to depositions and oxidation by attaching abrasive powders to the surfaces of a blade in a stationary cascade. The maximum Re_C was $1.2 \cdot 10^6$ and the inlet freestream Tu was 7%. The powders were uniformly distributed, having element sizes of 50 to 250 μm; no statistical roughness measures were reported. Overall heat transfer was shown to increase with roughness, including the leading edge region, with an associated promotion of earlier suction side transition. Such roughness sizes are however very large in comparison to most turbine roughness. Blair (1994) tested roughness on a rotating blade surface in a stage-and-a half, large scale, ambient temperature annular turbine rig. He used liquid crystals to obtain a "smooth" surface with rms roughness of 0.33 μm and min-to-max roughness of 7.6 μm, flat black paint to achieve rms of 6.4 μm with min-to-max of 51 μm, and also a 660 μm grit size for a very rough surface. The axial chord based Re_{CX} was 2.3 to $5.8 \cdot 10^5$. Results showed dramatic increases of about

100% in heat transfer over the entire airfoil for the very rough case, so much so that heat transfer became independent of Re. Little change was noted between the smooth and near-smooth cases. Guo et al (1996) measured vane heat transfer in an annular rig using liquid crystals with a reported crystal roughness R_Z of 25 μm, and also a smooth surface R_Z of less than 1 μm with thin-film heat flux gages. Re_C was $2 \cdot 10^6$ with Tu of 13%. They also show heat transfer increases of up to 100% over much of the surface due to roughness, but with a very different type of roughness in the liquid crystals. Hoffs et al (1996) also used liquid crystals to form a rough airfoil surface in a linear vane cascade. Their "natural" crystals were measured as R_a of 7 μm and R_Z of 25 μm, and "polished" crystals with R_a of 4 μm and R_Z of 15 μm. In this facility, Re_C was varied from $3.2 \cdot 10^5$ to $1.6 \cdot 10^6$ with changing exit Mach number from 0.2 to 0.8, and Tu was 5.5 to 10%. They showed increased heat transfer with both Re and Tu, and hastened suction side transition with both Re and Tu increases.

The present experimental study utilizes a transonic linear vane cascade to obtain airfoil heat transfer coefficient distributions for a higher range of Re_{CX} representing larger, higher output gas turbines. A range of surface roughnesses from R_a of 0.4 to 4.5 μm is tested with varying Tu of 4 to 13%.

Discussion

This task was completed in June 1996. In the following summary of highlights for this task, Re_{CX} refers to the Reynolds number based on airfoil axial chord length and exit velocity, R_a is the average roughness, and R_Z is the average peak-to-peak roughness.

A linear vane cascade was tested to provide external airfoil heat transfer coefficient distributions over a range of high Re_{CX} with separate and combined effects due to surface roughness and inlet freestream turbulence intensity. The test facility is the same as that described in Section 2.2.3.1.2. The heat transfer test airfoil placed in the center location of the cascade, is a thin shell of stainless steel with a wall thickness of 1.27 mm. Inside the airfoil shell is air, with an estimated equivalent conductivity of about .05 W/mK, due to natural convection. A total of 38 cap-grounded, type-K thermocouples are embedded into grooves 0.64 mm square. The thermocouple junctions are placed at the airfoil midspan, and the region around each junction carefully filled by nichrome tackwelds to form a continuous metal bridge to the airfoil surface. Thermocouples are placed at uniform intervals of 0.75 cm starting from the airfoil flow stagnation point. This instrumented airfoil is covered with a double-sided adhesive film 0.1 mm thick. Over this adhesive is placed a thin-film surface heater. The heater is formed of a .0127 mm film of Inconel deposited onto a .09 mm thick substrate of Kapton, with additional .05 mm thick copper buss bars along the hub and tip perimeters for power distribution. The Kapton is placed on the adhesive and provides electrical isolation from the steel. Only the Inconel heater surface forms the new airfoil flowpath surface. This composite airfoil has the same external profile dimensions as the other cascade airfoils. This cascade is designed such that this airfoil is easily removed for application of new heaters or surface roughness. Inset into each cascade aluminum endwall is a phenolic piece which

completely encompasses the heated airfoil, and provides both thermal and electrical isolation from the metal endwalls. Operation of the heater is through an adjustable DC power supply, typically operated at conditions up to 6 volts with 200 amps. As many as ten power leads are soldered to the heater buss bars on each end to provide a uniform constant heat flux condition for the airfoil surface.

The Inconel heater is the smooth surface condition for this study. A Perthometer S5P profilometry unit was used to measure all roughnesses. The same cone type stylus was used in all cases. The smooth surface condition of the heater yields an average roughness R_a, or centerline average, value of 0.4 μm and an average peak-to-peak R_z value of 2.28 μm. Two elevated surface roughness conditions were obtained through the use of metal protection spray paints applied directly onto the heater. When sprayed from a sufficient distance, the paints deposit thin, uniform layers of particles on the surface. The paint layer is thin enough that the metal can still be "seen", and as such the thermal resistance of the paint is negligible. A high-heat grade of paint resulted in a surface roughness with R_a of 1.85 μm with R_z of 13.2 μm, and a peak spacing of about 70 μm. A common low grade metal paint resulted in a surface roughness with R_a of 4.5 μm with R_z of 27.8 μm, and a peak spacing of about 125 μm. These three roughness conditions were chosen as spanning representative engine design conditions when scaled from the cascade geometry and flow conditions. As an indication of the roughness regimes, the maximum Re_k value for each test surface can be estimated by assuming $k=R_a$ (the reader may use another conversion value if desired). For the smooth airfoil, the Re_{cx} range corresponds to maximum Re_k from 10 to 21 at the suction side trailing edge. For the case of R_a of 1.85 μm, maximum Re_k ranges from 44 to 100, and for the case of R_a of 4.5 μm, maximum Re_k ranges from 108 to 240. Local Re_k values on the airfoil cover magnitudes up to these maximums. These estimates indicate that the smooth airfoil probably lies in the mostly smooth regime, the moderately rough airfoil lies in the smooth to transitionally rough regime, and the very rough airfoil lies in the transitionally rough to fully rough regime.

Cascade test conditions and airfoil thermocouple data are monitored through an HP 3852 front end data acquisition computer providing updated information every 6 seconds. This unit and the Scanivalve are tied into an HP Vectra 486 PC with user interface graphics. When test conditions and airfoil thermocouples have reached steady-state, several sampling cycles are recorded, and the minimum, maximum, average, and standard deviation of each data channel computed. Lateral conduction effects within the thin-shell airfoil are corrected for by computing the lateral heat fluxes within the wall and adjusting the local heat fluxes accordingly. Thermal radiation and internal conduction losses are negligible. The local external heat transfer coefficients on the airfoil are defined as

$$h = Q_{corr} / A_{conv} (T_{wall} - T_{rec})$$

where Q_{corr} is the heater power per thermocouple corrected for lateral conduction, A_{conv} is the heater surface area per thermocouple, T_{wall} is the thermocouple reading, and T_{rec} is the local recovery temperature determined from the inlet total temperature and airfoil static pressure distribution using a recovery factor of 0.88 (this factor is assumed constant with no uncertainty included in the error estimate for heat transfer coefficient). Using the methods of Kline and McClintock (1953), the worst case uncertainty for the recovery temperature is estimated to be $\pm$ 1°C. This estimate includes both uncertainties and test duration standard deviations for the total temperature, total pressure, local static pressure, and local freestream velocity. Using the typical worst case (minimum) condition of a 17°C temperature potential between the wall temperature and the local recovery temperature, the estimated uncertainty in heat transfer coefficient is $\pm$ 8%.

Three surface roughnesses were tested: a smooth surface, a moderately rough surface, and a very rough surface. Turbulence intensity variation was generated with the use of perforated plates, and a cold flow mock combustor was used to provide large-scale turbulence. A series of smooth surface heat transfer results was presented that provides a full range of characteristic airfoil heat transfer behavior, with well-defined transition locations and lengths. The addition of surface roughness tends to hasten suction and pressure side transitions, though these still remain a strong function of Re_{cx}. Increased turbulence intensity also hastens suction side transition. At high roughness level, the typical cylinder-in-cross-flow heat transfer behavior disappears from the leading edge region, and suction side transition begins essentially from the stagnation point. Stagnation point heat transfer remains unchanged with roughness level under the tested conditions. Under rough surface conditions, the mock combustor is shown to produce the same airfoil heat transfer as that obtained with a perforated plate, lending some confidence to the common use of plate- or grid-type turbulence generators in heat transfer testing for application to turbine design. Results are shown in Figures 2.2.3.6.2-1 and 2.2.3.6.2-2.

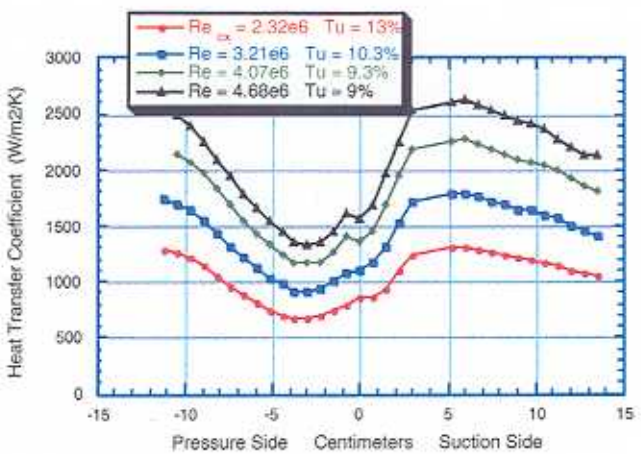

Figure 2.2.3.6.2-1. Airfoil Heat Transfer Coefficients with Ra = 4.5 Microns and High Tu.

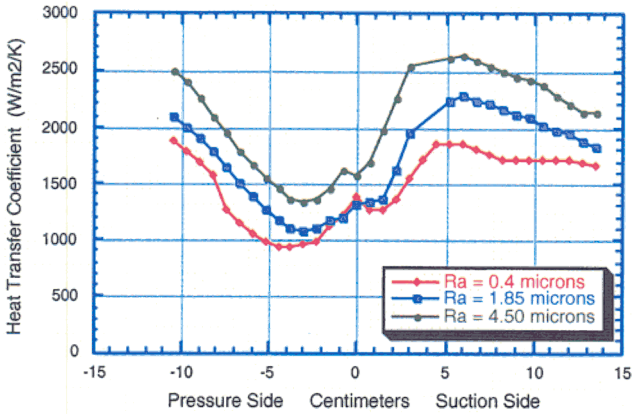

Figure 2.2.3.6.2-2. Effect of Surface Roughness with Re_{CX} = 4.7e6 and Tu = 9%.

The effects of discrete external surface disturbances on heat transfer coefficient distributions were measured with disturbances in various locations on the surface and Re_{CX}. Well-defined trip strips, (Figure 2.2.3.6.2-3), were applied to model the surface steps that might be present in the event of loss of airfoil protective coatings (e.g., thermal barrier coatings) with appropriate step-height-to-momentum thickness ratios. For external flows over very shallow cavities, or spalls, the assumption was made that the primary effect on heat transfer enhancement is due to the forward-facing step, not the backward-facing step. The validity of this assumption is supported in the results by the large enhancements observed far downstream of the usual reattachment region associated with backward-facing steps, or the point at which such reattachment enhancement would normally decay. Heat transfer coefficient enhancement factors were measured for five locations on the airfoil, with both smooth and rough surfaces, as a function of Re_{CX}. Pressure side mid-chord enhancements are very similar for low and high turbulence intensities as a result of decayed intensity from the inlet condition. All results (Figure 2.2.3.6.2-4), indicate that even more significant heat transfer enhancements may exist for airfoil designs with lower conditions of Re_{CX}, roughness, or turbulence intensity.

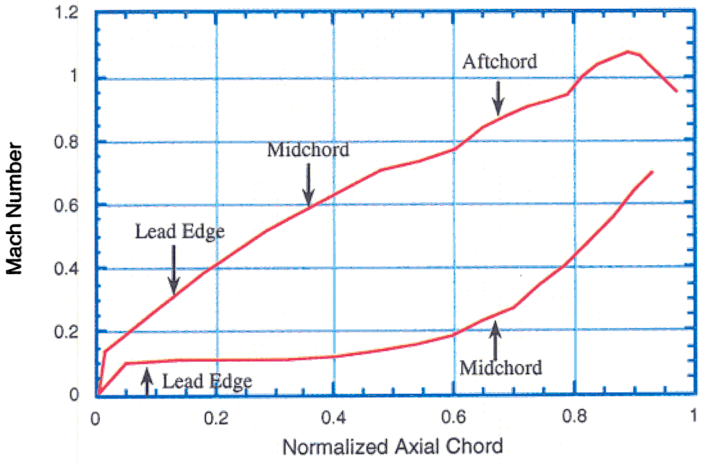

Figure 2.2.3.6.2-3. Airfoil Mach Distribution with Trip Locations.

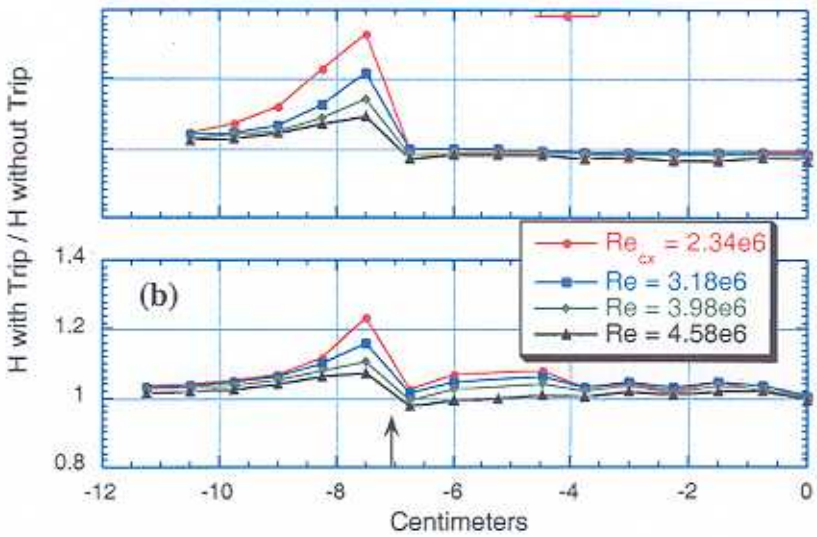

Figure 2.2.3.6.2-4. Effect of Modeled Spallation Trip on Pressure Side Heat Transfer

A tapered symmetric blockage airfoil was placed upstream of the cascade airfoil leading edge plane, in very close proximity, to simulate the presence of a combustor transition piece endwall. The location of this blockage element was varied in the turbine circumferential direction to determine the effect of wake shedding on the airfoil external heat transfer distribution. While there is no location where the wake effect is negligible, the optimal location was determined to be midway between two airfoil leading edges.

The linear cascade was also used in support of the Full Scale Nozzle Cascade test program by qualitatively determining the increase in external airfoil heat transfer due to the use of as-sprayed thermal barrier coating rather than polished coatings.

Summary/Conclusion

A linear vane cascade has been tested to provide external airfoil heat transfer coefficient distributions over a range of high Re_{CX} from 2.2 to 4.8 $\cdot 10^6$, with separate and combined effects due to surface roughness and inlet freestream turbulence intensity. Three surface roughnesses have been tested, a smooth surface with R_a of 0.4 μm and R_Z of 2.28 μm, a moderately rough surface with R_a of 1.85 μm and R_Z of 13.2 μm, and a very rough surface with R_a of 4.5 μm and R_Z of 27.8 μm. Turbulence intensities from 4 to 13% have been generated with the use of perforated plates, and a cold flow mock combustor has also been used to provide large scale turbulence. A series of smooth surface heat transfer results has been presented which provides a full range of characteristic airfoil heat transfer behavior, with well defined transition locations and lengths. For the smooth surface, heat transfer on both pressure side as well as suction side aft of transition follow a proportionality of $Re^{1.0}$. The addition of surface roughness tends to hasten suction and pressure side transitions, though these still remain a strong function of Re_{CX}. Increased Tu also hastens suction side transition. At moderate roughness, heat transfer aft of the

transition locations depends on $Re^{0.95}$. At high roughness level, the typical cylinder-in-crossflow heat transfer behavior disappears from the leading edge region, and suction side transition begins essentially from the stagnation point. With both elevated roughness and Tu, the entire airfoil heat transfer distribution shows a $Re^{0.9}$ dependence. Stagnation point heat transfer remains essentially unchanged with roughness level under the tested conditions.

Well defined trip strips have been applied to model the surface steps which might be present in the event of loss of airfoil protective coatings, such as thermal barrier coatings, with appropriate step height-to-momentum thickness ratios. For external flows over very shallow cavities, or spalls, the assumption has been made that the primary effect on heat transfer enhancement is due to the forward facing step, and not the backward facing step. The validity of this assumption is supported in the results by the large enhancements observed far downstream of the usual reattachment region associated with backward facing steps, or the point at which such reattachment enhancement would normally decay. Heat transfer coefficient enhancement factors have been measured for five locations on the airfoil, with both smooth and rough surfaces, as a function of Re_{cx}. Smooth pressure side leading edge enhancements range from 20 to 50%, decreasing with increased Re. Rough pressure side leading edge enhancements are only slightly less, again decreasing with Re. In this region, increased inlet freestream turbulence intensity tends to eliminate the Re dependence, showing the dominant effect of Tu here. Under conditions of elevated roughness and Tu, only a 10% enhancement in heat transfer is indicated locally. Pressure side midchord enhancements are very similar for low and high Tu as a result of decayed intensity from the inlet condition. The same trends in decreased enhancement with increasing Re are observed here, with 10 to 35% enhancement for a smooth surface and 10 to 25% enhancement for a rough surface. Suction side leading edge enhancements are in some cases as high as 50% over a large area, reflecting a trip-caused transition of the boundary layer. Corresponding rough enhancements are greatly reduced and decay rapidly, due to the existing turbulent boundary layer. Suction side midchord enhancement factors vary from 40 to 100% immediately after the disturbance (extrapolated) on a smooth surface, again decreasing with Re. Roughening the surface reduces these enhancements to about 40%, with no Re variation, showing that while roughness and Tu affect the transition location and strength, post-transition enhancement is virtually unaffected by roughness level under these conditions. Enhancement further aft on the suction side is reduced to 15 to 20%, with a slower decay rate. All results indicate that even more significant heat transfer enhancements may exist for airfoil designs with lower conditions of Re_{cx}, roughness, or turbulence intensity.

Further information on this task may be found in the publications:

Bunker, R.S., 1997, "Effect of Discrete Surface Disturbances on Vane External Heat Transfer", 97-GT-134, 1997 International Gas Turbine Conference, Orlando, FL.

Bunker, R.S., 1997, "Separate and Combined Effects of Surface Roughness and Turbulence Intensity on Vane Heat Transfer", 97-GT-135, 1997 International Gas Turbine Conference, Orlando, FL.

Technology Application

The test results have been used directly in the design of the ATS first-stage nozzle airfoil. Thus the cascade conditions for an appropriate rough surface condition, with elevated freestream turbulence intensity from a DLN combustor mockup, were used as the convective heat load definition for the nozzle airfoil (appropriately scaled to engine conditions). Since modeled spallation heat transfer enhancements were equal to or below the assumed enhancement levels for the nozzle design, the conservative nature of this portion of the design was verified. Cascade testing verified the requirement to polish the thermal barrier coating on the Full Scale Nozzle Cascade instrumented airfoils, thereby avoiding potential test problems in that task. The optimal relative location for the transition piece endwall segments, as determined through cascade testing, has been incorporated into the turbine design.

Section 2.2.3.7 (GTETCP) LCF Coupon Tests [C]

Section 2.2.3.7.1 (GTETCP) LCF Nozzle Coupon Life Validation Tests [C]

Objective

The primary objective of this task was the determination/verification of the ATS turbine first-stage nozzle low cycle fatigue (LCF) life. Tests were conducted to verify LCF life under conditions representative of the ATS turbine.

In addition to the high thermal gradient testing of superalloy coupons for LCF durability, this task assessed the crack propagation rate of N5 in the presence of steam. This was done in two ways: (1) isothermal, mechanically loaded testing of tubular specimens through which steam is passed and (2) high thermal gradient testing of a "tophat" specimen (Figure 2.2.3.7.1-1) in the presence of steam. Post-test evaluations of the metal conditions were performed. The data collected provide a basis for LCF life.

Introduction/Background

The Phase 2 task, "LCF Life and Crack Propagation," prepared the way for the Phase 3 task by performing most of the specimen design work, instrumentation evaluations, facility modifications in support of LCF testing, and early validation specimen testing. The earliest portion of the Phase 3 effort covered the design and installation of steam cooling to the E-beam facility in preparation for eventual testing with the same coolant as used in the ATS turbine. Additionally, tophat specimen castings, both plain and ribbed, were obtained from Howmet Whitehall for LCF testing.

LCF testing in the early part of 1996 concentrated primarily on three so-called "crack" specimens, which were specifically intended to test the potential for crack propagation into the metal substrate. In addition to the LCF concerns associated with the superalloy substrate material of the turbine first-stage components, the bond coat between the substrate and the TBC has been identified as a possible source of crack initiation and propagation to the substrate.

Discussion

Three tophat specimens were prepared with various bond coatings but without TBC. The test plan called for exposing each specimen to approximately 1500 cycles: 500 at moderate conditions and 1000 at elevated substrate stress conditions. None of these specimens was expected to fail under these conditions, but each one was expected to develop cracks within the bond coat. Post-test destructive measurements determined the nature and extent of such cracking, and whether the cracks from the bond coat may be expected to propagate into the substrate metal.

As a follow-up to Phase 2 activities, destructive evaluations were completed on an LCF specimen. This LCF test piece had received slightly over 500 cycles of very elevated exposure.

In 1997, The E-beam high thermal gradient test rig was brought back on-line after a lengthy down period resulting from power problems within the transformer array of the rig. An additional problem was encountered in the high voltage supply cable connecting the rig transformers to the E-beam gun. A replacement cable was installed after a short downtime.

Testing of LCF tophat specimens was resumed during this period with the first two of a set of specimens to be processed without single-point turning or other machining; i.e., the tophats were cast-to-dimensions and the TBC applied as in the turbine design process. The conditions for LCF testing in this facility exceeded the ATS turbine inlet nozzle design conditions for substrate/bond-coat interface stress but fell short of causing the quick plastic deformation seen in early specimens. Both specimens completed well over 3000 cycles of exposure with no apparent damage to the metal or TBC.

An analysis was run to determine test conditions for a tophat fillet specimen. The analysis was a pre-test prediction of thermal boundary conditions required to match design temperature and stress levels in the fillet. The analysis required that the tophat fillet specimen design be modified. The fabricated fillet specimen was instrumented with thermocouples. The specimen was given a coating that was found in previous tests to be a good qualitative guide to the location and magnitude of the strain pattern developed in the specimen. Tests were conducted that verified the strain pattern. E-beam cyclic testing of this specimen was initiated.

Evaluation of an LCF specimen that completed approximately 1850 cycles of E-beam testing was completed. One purpose of the evaluation was to help understand a mechanism that was proposed for the loss of TBC.

In 1998, a tophat specimen with a fillet geometry and a Pt/Al topcoat was thermally cycled for 200 cycles. The cracks in the topcoat became visible in a dye penetrant test. The pattern of the cracks is being interpreted as an indicator of the strain profile in the specimen. This information was used to establish whether the test conditions were as planned.

A TBC-coated fillet specimen was run and accumulated 2500 cycles. Data obtained from this test were analyzed. A specific objective of the analysis was to determine the thermal properties of the coating..

Summary/Conclusion

The E-beam high thermal gradient test facility was used to test several nickel-based superalloy (N5) coupons for LCF durability. The coupons were geometrically representative of a section of the turbine inlet nozzle airfoil containing hot and cold sides. Coupons were instrumented for the evaluation of the thermal conditions during testing. Tests were performed to evaluate metal durability under conditions of temperature, thermal gradient, and stress representative of the ATS turbine inlet nozzle. Testing was cyclic, developing cycles of exposure on the test coupons considered to be representative of engine cycles. Post-test evaluations of the TBC and metal conditions were performed. Data provided a basis for LCF life evaluations.

Technology Application

The results obtained have been of value in two ways. (1) The LCF testing, both for bond-coat/substrate systems and for TBC/bond-coat/substrate systems, indicates a minimum required life for the materials under high thermal gradient and stress conditions. These life indications provide a direct confirmation of the ATS turbine design. (2) Testing revealed many processing and preparation steps that must be controlled in order to maintain component quality. Determining the extent to which such processing steps are crucial and determining the effects of deviating from these procedures are equally valuable and necessary to design.

Section 2.2.3.8 (GTETSP) Steam Particulate Deposition [C])

Section 2.2.3.8.1 (GTETSP) Steam Particulate Rotational Deposition [C]

Objective

This task had four primary objectives. The first objective was to characterize the degradation of the steam filter to be employed in the ATS gas turbine.

The second objective of this task was to measure the rate and location of steam particulate deposition in bucket tip-turns and in two heat transfer structures to be employed within the ATS gas turbine nozzles and buckets. The information was to be translated into a steam purity specification and full-filter specification for the ATS gas turbine.

The third objective of this task was to define a test technique to quantify cleanliness.

The final objective was to explore the effectiveness of flushing the steam system with clean water, clean air, or some combination of the two in order to improve general cleanliness and move contamination away from critical surfaces (especially bucket tip-turns) when the engine is off-line

Introduction/Background

Cleanliness of the steam delivery system will be a significant factor in the performance of the ATS gas turbine. There are several aspects to this problem.

A filter is employed in the steam delivery system to provide an appropriate level of cleanliness. However, degradation of this filter with time could impair turbine performance. In order to assess this possibility, the original filter installed for ATS Phase 2 at the Ocean State Power plant was examined as part of this task.

Another critical issue in the durability of this system will be the rate of steam deposition in the bucket tip turns and other heat transfer structures. Characterization of this behavior can be translated into a steam purity specification and full-filter specification for the ATS gas turbine to establish an appropriate level of cleanliness. The approach employed to achieve this goal used gas turbine combined cycle (GTCC) steam flowing in series through a special filter specified for the ATS gas turbine, then through the tip-turns in a specially constructed centrifugal deposition rig, and finally through two static specimens consisting of turbulated and impingement-cooled specimens. Unfortunately, seal problems with the centrifuge deposition rig prevented its use in the test plan. Data was collected using the static specimens. Amounts and locations of deposits in these specimens were used to verify the predicted time-between-outages (TBO) results from ATS Phase 2 studies.

If cleanliness is to be a primary goal in the operation of the ATS gas turbine, there must be a method of quantifying component cleanliness. As a result a measurement technique was developed to quantify coolant duct surface cleanliness.

The ATS gas turbine cooling system cannot be chemically cleaned like a boiler because of the number of unwelded joints (e.g., spoolie/tube joints, interference fits) where chemicals could concentrate and create corrosion and wear problems. As a result, flushing with clean water, clean air, or some combination of the two in order to improve general cleanliness and move contamination away from critical surfaces was explored as an alternative. Effort was also focused on developing procedures for flushing the assembled cooling circuits at assembly and, to the extent possible, when the engine is fully assembled but off-line.

Discussion

Filter Exposure

The original filter installed for ATS Phase 2 remained on-line at the Ocean State Power plant. A visual inspection with a borescope showed there was no filter degradation with exposure, and there was no deposit adhering to the filter structure. Such particulates as were collected had clearly fallen off the vertically mounted cartridge and were swept out of the filter housing with the condensate that was drained on startup. These observations indicate that the collected particulates are friable and do not adhere to the selected two-micron-rated filter structure.

The steam filter exposure continued through 2Q97, when it was taken off-line for another examination after the centrifuge startup trials. The filter cartridge remained unchanged, and there was no change in its filtration performance after over 8,000 hours of steam exposure. In general the element had a mild discoloration due to thermal exposure, but there was no observable material degradation. Earlier the filter had been shown to be

resilient to small deformations, even after exposure. This filter design was carried forward to steam system design.

Rate of Steam Deposition

At the conclusion of ATS Phase 2 in 1Q96, the centrifuge deposition rig was assembled and tested, but the steam leak rate from the rotary shaft seals was well above expectations from design calculations. Cooler-than-planned shaft temperatures increased the gap. New seals were installed on the outboard ends of the shaft (nearest the bearings) in July 1996 and tested in August, but there was still too much leakage from the inboard seals (nearest the rotor).

The centrifuge apparatus went through three startup attempts with seal modifications before the last two. In the first case, the steam leakage was much too high to allow continuous running; in the second, the steam leakage was lower, but the machine rotating resistance was too high when steam was applied to the shaft. This resistance behaved as if the shaft was expanding to the carbon gap seals, forcing them to rotate until the steam pressure locked them to the stator. It was decided to make the system available for brush seal tests (reported on in Section 2.2.4.14.2, Brush Seals Development for Steam Box) in 3Q97 and 4Q97.

Testing to quantify rate of steam deposition continued using static specimens. Two static specimens were placed on-line downstream of the filter: an impingement specimen simulating cooling in the first-stage nozzle, and a convection specimen simulating a first-stage bucket cooling channel.

An examination of the specimens was conducted when a failed bucket specimen was replaced with a new one. No readout of the impingement holes was apparent on the target surface for impingement cooling, and no deposit was seen inside the distributor. This result is encouraging in that it continues to validate our expectation that any steam particulates breaking through the full-flow filter will not deposit in the steam cooling passages. However, longer exposures will be required to provide positive assurance.

The static specimens, impingement and turbulated, installed in 1996 were on-line for 31 and 38 weeks, respectively, with few outages. The specimens were again taken off-line at the end of 1Q97, when the steam system to which they were connected was shut down for a 7-year overhaul.

During 2Q97 the specimens were examined by borescope and sampled using remote manipulators in order to leave the specimens available for further exposure and to avoid disturbing any deposits as much as possible. The borescope analyses were recorded to videotape, and any removable deposits were analyzed for Cr, Mo, and Fe, since the plant superheater tubes were 2.25Cr, 1Mo, balance Fe.

The impingement specimen (portion of first-stage nozzle cooling) was very clean with no removable deposit observed at all. Only a slight darkening of the target wall adjacent to the distributor holes showed any relationship between the holes and the adjacent wall; that slight darkening was approximately the same diameter as the holes and was not removable.

In September 1998, the steam filter elements tested in this task were ordered as part of a complete steam filter assembly for the H-machine prototype plant. This was the major output of this ATS task, as the experience gained conducting the steam flow trials at the test power plant provided not only data on the suitability of this new filter style for handling the steam flow, but also valuable lessons in how to handle steam for this unique engine application. The steam particulate loading of magnetite was verified to originate in the superheater, and the filter was able to handle it. Off-condition operations, such as a plant condenser leak and load swings, indicated what is to be expected in these situations. Experiments with static flow specimens simulating bucket- and nozzle-channels, including both convection- and impingement-heat transfer, were successfully conducted on this program and provided guidance on ways to assure reliable system operation.

Surface Cleanliness Measurement

A new surface cleanliness test involving the measurement of reflectivities of cloth smears was developed and transitioned to the Greenville factory floor. Standard commercial cloth smears are mounted on special tools and used to collect contamination within masked areas on a surface following specified, but simple, procedures. The reduction in reflectivity of the smears is then related to the amount of sampled contamination by previous calibration. Calibrations and gauge R&R tests were conducted using two types of contamination found in the factory. The sampling and measurement equipment was mounted on a rolling 2-foot × 2-foot rack in Greenville, and it is now being used to establish cleanliness levels in the plant. Because the new measurement process is quick and easy to understand, it provides an archive record of the contamination on the labeled swatch.

Coolant System Flush

An apparatus was completed containing a first- and second-stage bucket pair, with cross-tube, rotor manifold, axial tube, and radial tube components to determine flush feasibility.

The apparatus is divided into two skids, a flush supply and a specimen rack sub-system. The two subsystems are connected by flexible feed- and return-hoses during experimental operation. The flush supply skid fabrication process was installed in the GEPS Houston Service Shop for use with production stator hardware.

Summary/Conclusion

In September 1998, the steam filter elements tested in this task were ordered as part of a complete steam filter assembly for the H-machine prototype plant. This was the major output of this ATS task. The experience gained conducting the steam flow trials at the test power plant provided not only data on the suitability of this new filter style for handling the steam flow, but also valuable lessons in how to handle steam for this unique engine application.

Experiments with static flow specimens simulating bucket- and nozzle-channels including both convection- and impingement-heat transfer were successfully conducted on this program and provided guidance on ways to assure reliable system operation.

The surface cleanliness measurement system provides a very effective approach to quantifying cleanliness in ATS turbine components. The new measurement process is quick and easy to understand, and it provides an archive record of the contamination on a labeled swatch.

A flush supply skid and process were defined and installed in the GEPS Houston Service Shop for use with production stator hardware.

Technology Application

Output of this task has contributed to the identification, experimental validation, and specifications for the on-line filter system ordered from the vendor for the first plant. The experimental program also provided the first-hand experience necessary to provide consultation on issues of condensate measurements and feedwater treatment systems. The development of the surface cleanliness measurement was quickly transitioned to the factory floor, where it is now in use providing go/no go decisions on whether parts are sufficiently clean to proceed with assembly. The successful demonstration of an ability to flush the cooling system components will reduce remnant contamination at first fire, and it will also assure that contamination will not limit time between outages for engine disassembly.

Section 2.2.4 (GTMT) Materials Technologies [S]

Section 2.2.4.1 (GTMTSE) Steam Effects on Mechanical Properties [S]

Objective

The objective of this task was to evaluate the candidate turbine materials for any effects due to operation in a steam environment. Tests of materials that are exposed to steam were performed to measure fatigue crack propagation, low cycle fatigue, and creep. Additional tests deemed necessary to meet design criteria were also performed. Comparisons were made to data collected in air. Where necessary, the program evaluated the roles of alternate heat treatments and/or surface treatments.

Introduction/Background

Steam effects on critical mechanical properties of turbine materials are required for proper lifing design of the components. The effects of steam was tested and new design curves issued.

Discussion

Crack Growth Rate Testing

Fatigue crack growth rate (FCGR) testing in steam of the first piece qualification (FPQ) and the Ingot 4 turbine wheel and spacer materials was performed at four temperature levels within the design operating range. It was found that the cycle dependent crack growth rates in air and steam were equivalent, but that the time-dependent crack growth rates in steam were higher than those in air.

Dynamic crack growth threshold testing and static crack growth threshold testing of FPQ and Ingot 4 material was performed in air and in steam. The dynamic thresholds in both environments were equal across the majority of test temperatures. However, at the higher temperatures, the dynamic threshold in steam was greater than that in air. It was also found that at higher testing temperatures, the steam static crack growth thresholds were also higher than those in air.

Optical microscopy, high resolution scanning electron microscopy (SEM), transmission electron microscopy (TEM), and Auger analysis were used to characterize the different oxide and metallic layers on the fracture surfaces of the various test specimens of forged IN718, as well as many different candidate turbine wheel and spacer alloys. The relationships between some of the observed differences and the different crack growth rates of the alloys when tested in steam are still under investigation.

Hold time sweep crack growth tests in steam were completed for coarse grain, fine grain and transition areas of cast 718 for steam delivery materials. It was found that there were no steam effects on coarse grain slabs or on grain size down to 50 mils in the fine grain slabs. However, steam effects were detected in the transition region, and in the fine grain

region. The crack growth rate in the fine grain region can be 1000X faster than in the coarse grain region at long hold times in steam, but is still in the order of wrought IN718 material.

Creep-Rupture Testing

Creep-rupture tests were performed in air and steam on both the FPQ material and the Ingot 4 turbine wheel and spacer material. Creep testing in steam for both materials was completed in 1998 for tests of up to 2000 hours to failure. Additional tests were performed in air and steam on both the FPQ material and the Ingot 4 material during 1998 and 1999 at temperature and stress levels resulting in 15,000 hours to failure in air. It was found that although long term rupture lives at higher temperatures were lower than those in air, the steam results were well within scatter of parametric rupture correlations.

Creep testing in air of FPQ and Ingot 4 IN718 turbine wheel and spacer material continued, with times in test currently at about 37,870 hours for the FPQ material and 27,000 hours for the Ingot 4 material; the goal is to continue these tests to 70,000 hours to ensure reliable extrapolation of data to design lifetimes in excess of 100,000 hours.

Low Cycle Fatigue Testing

Facilities were constructed to permit steam testing of low cycle fatigue (LCF) bars machined from the IN718 FPQ and Ingot 4 turbine wheel and spacer materials. Tests were conducted at four different temperatures. LCF life was observed to be reduced by a factor of approximately two at the highest test temperature, four at an intermediate temperature and much less than two at the lowest steam test temperature relative to air LCF lives.

Additional LCF tests were performed on forged IN718 turbine wheel and spacer material in both air and steam at an intermediate temperature. Specimens were machined with baseline "low stress ground and polished" (LSG&P) and "turned and shot peened" surfaces. It was found that the baseline surface normally used for design data generation resulted in equivalent continuous cycling LCF lives in air and in steam, and poorer LCF lives under hold time conditions in steam compared to air. This latter result is in agreement with crack growth results, i.e., higher time-dependent crack growth rates in steam. Although it is well known that turning reduces LCF life, the turned and shot peened surfaces representing shot peening conditions within the window of safe shot peening resulted in hold time LCF lives in excess of specimens representing the baseline LSG&P condition. This result is consistent with data in the open literature showing that shot peening restores LCF life for surfaces including machining damage.

For steam delivery materials, fine grain and coarse grain slab LCF tests in steam and in air without hold time tests were completed, and –3 sigma curves were generated. The results showed that grain size had no significant effect on LCF life, and the steam had no significant effect on LCF life at the no hold time condition.

Cyclic two minute hold time in air and in steam tests for coarse grain material were also conducted for steam delivery material. No pronounced steam effect was found.

LCF tests were conducted on TIG welded IN718 plate for steam delivery material. It was found that at 800F, the welded specimens outperformed the base metal. At 1100F, a maximum 2x reduction in life was observed compared with the base metal.

High Cycle Fatigue Testing

Facilities were constructed to permit high cycle fatigue (HCF) testing of specimens in steam. HCF specimens were manufactured of Ingot 4 IN718 forged turbine wheel and spacer material for HCF testing in air and in steam. HCF testing was concluded in 1999, and showed HCF lives in air and in steam to be equivalent. A draft report was written for Design Engineering.

High cycle fatigue tests were conducted on coarse grain cast IN718 material for the steam delivery material project. A Goodman diagram was generated and reported to Design Engineering.

Summary/Conclusions

Internal reports were issued documenting tensile, creep, LCF, HCF and crack growth rate curves for forged IN718 turbine wheel and spacer material. Design memoranda were also prepared for official communication of the resultant Design curves to Design Engineering that included the effects of steam on the mechanical properties.

Technology Application

This task evaluated the behavior of turbine materials in a steam environment in order to account for the introduction of steam cooling.

Section 2.2.4.2 (GTMTSO) Oxidation Due to Steam [S]

Objective

Testing of ATS materials in steam was performed to evaluate the long-term oxidation responses to this environment. Specimens were subjected to steam exposure in an autoclave and removed at specified intervals for examination of oxidation characteristics.

Introduction/Background

Steam presents a unique environment to turbine materials. The effect on oxidation behavior was investigated to aid in lifing design.

Discussion

Specimens, including four point bending, tensile, low cycle fatigue, and bulk aging blanks were machined. Retorts were constructed to provide exposure of specimens to steam.

Baseline testing was performed to provide the reference against which changes in properties induced by steam exposure could be measured. Four point bending specimens were exposed in both air and steam at upper limit steam operating temperature conditions. Bulk specimens were exposed in air and subsequently machined into test specimens. These specimens were tested to define the effects of bulk aging on the mechanical properties.

Summary/Conclusion

The results of the testing revealed no unique anomalies. The preliminary results were found to be adequate and testing was concluded.

Technology Application

This task evaluated the static behavior of turbine materials in a steam environment in order to account for the introduction of steam cooling.

Section 2.2.4.3 (GTMTCE) Corrosion Rate Evaluations of Airfoil Overlay Coatings [S]

Objective

The objective of this task was to evaluate the performance of various ATS overlay coatings and substrate materials in potentially corrosive environments. Initial evaluations were performed in small burner rigs burning fuels with known levels of contaminants. This allowed ranking of the of the oxidation and corrosion rates of materials and coatings. Subsequent testing was performed in facilities that better simulate gas turbine service conditions, for confirmation of the burner rig results.

Introduction/Background

The ATS design required the use of substrate alloys and coatings that have not heretofore been used in GE Power Generation gas turbines. Basic oxidation and corrosion data were therefore required for all such materials in order to estimate parts lives under varying environmental operating conditions. Oxidation data were obtained using burner rigs fired on clean natural gas. Corrosion data were obtained from rigs fired on distillate oil doped with prescribed levels of contaminants. Samples were exposed isothermally for varying lengths of time, with the rigs being run at several different temperatures that span the range of metal temperatures expected on the parts during service. Oxidation/corrosion rankings were established by metallographic measurement of the depth of oxidation/corrosion attack on the tested samples.

Discussion

Burner rig tests were run on five different substrate materials and fourteen different coating systems involving both compositional and processing variation. Exposure times were as long as 10,000 hrs. for some of the oxidation tests, and as great as 4,000 hrs. for some of the hot corrosion tests.

Samples were removed after prescribed exposure times, and were sectioned, mounted, and polished for metallographic evaluation. Measurements of corrosion/oxidation attack penetration were made from these samples. These data were plotted vs. time to provide the environmental damage rate curves from which coating and part lives estimates could be made. Some of the coated specimens were subjected to microprobe analysis to determine the compositional changes within the coating and the extent of interdiffusion with the substrate as a function of temperature and time.

Some of these coatings were also subjected to simple strain-to-crack type tests in which coated samples were deflected a known amount, from which the tensile strains imposed upon the coating surface were calculated. The purpose of this testing was to establish and explore the inevitable tradeoff between coating oxidation life and strain tolerance, since coatings which have superior oxidation lives also tend to have lower strain tolerance. Low coating strain tolerance can lead to excessive thermal fatigue cracking of the coating (i.e., craze cracking), a condition that is to be avoided if possible. These tests provided a ranking of strain tolerance as a function of temperature for the various coating systems. Availability of this type of information, along with the oxidation/corrosion data obtained from the burner rigs, was critical to the selection of the optimum coating systems where both life and resistance to craze cracking are desired characteristics.

Summary/Conclusion

The information gathered during this task has been used in the process to rank coating and alloy performance in environmental testing and to select coatings and bondcoats for ATS hot section components. In addition, the selection of new coatings for field testing in existing machines was augmented by the availability of this information. Evaluations of coating performance in these tests to date (evaluations being conducted under non-ATS funded programs) have not resulted in any changes to the performance rankings established by the testing conducted in this task. This has enhanced confidence that these relatively simple laboratory tests can provide good guidance in coating selections for advanced turbine designs.

Technology Application

This task evaluated potential airfoil coatings in environments that reflect planned turbine operating conditions.

Section 2.2.4.4 (GTMTBV) Compressor Blades and Vanes Materials and Processes [S]

Objective

This task examined potentially less expensive materials for use in blades and vanes in the latter stages of the ATS compressor. These evaluations of alternate materials were based on results of tests of mechanical properties, with emphasis on high cycle fatigue properties. For materials that have been selected, tests of critical properties were conducted under ATS-specific conditions. Component tests of selected parts were conducted for life verification purposes and establishment of final manufacturing parameters.

Introduction/Background

403Cb+ is a high strength 10 chrome class steel being considered for use as a latter stage compressor blade. Several test programs were conducted to develop data for design curves. Three lots of material were evaluated in the test programs. Material property curves were developed and issued from the data for use by Design Engineering.

Discussion

Tensile Property Program

Three heat lots of 403cb+ material were tested in the program. Tensile tests were conducted at room temperature, 500°F, 750°F, 850°F, 950°F and 1050°F. Property curves were developed from the data and issued.

HCF and LCF Test Programs

The following Tables 2.2.4.4-1 through 2.2.4.4-3 summarize the data collected in the program. Property curves were developed from the data in the tables and issued.

Table 2.2.4.4-1
403Cb+ LCF Test Matrix at 950°F, A=+1, frequency = 20 cpm

Spec. ID	$\Delta\varepsilon_{tot}$(%)
HT1-L3	1
HT1-L4	0.5
HT1-L5	1
HT1-L6	0.8
HT3-L3	0.8
HT3-L4	0.6
LN46-L3	0.8
LN46-L4	0.5

Table 2.2.4.4-2
403Cb+ LCF at 850°F, A=+1, frequency = 20 cpm

Spec. ID	$\Delta\varepsilon_{tot}(\%)$
HT1-L1	1
HT3-L1	1
LN46-L1	1
HT1-L2	0.5
HT3-L2	0.5
LN46-L2	0.6
HT3-L5	0.6

Table 2.2.4.4-3
403Cb+ HCF Test Matrix

Temp(°F)	Mean Stress (KSI)	Notch (Kt=2) or Smooth
850	0	N
850	30	N
850	0	S
850	30	S
950	0	N
950	30	N
950	0	S
950	30	S
1050	30	N
1050	30	S

Creep Test Program

Creep tests were conducted under the conditions shown in the following Table 2.2.4.4-4. Parameterized creep curves were generated and issued to Design Engineering.

Table 2.2.4.4-4
403Cb+ Creep Test Conditions

Stress (KSI)	Temp(°F) 950	1000	1050	1100	1150
40	X	X	X		X
30		X	X		X
25		X	X		
20			X	X	X
15			X	X	X

Summary/Conclusion

Design data curves for design use were issued from the test results.

Technology Application

This task characterized the mechanical behavior of existing and new blade/vane materials in more aggressive environments than past compressor operation.

Section 2.2.4.5 (GTMTVG) Compressor Variable Guide Vane System Design Support and Process Development [S]

Objective

Information to support selection of materials for the variable guide vane bushings and thrust washers was gathered to support a robust and reliable design. Testing was conducted to confirm materials selections, cover any parameters outside of existing data, and gather data for new materials.

Introduction/Background

GE's ATS compressor uses a grouping of variable guide vanes (VGV), rather than a single stage of inlet guide vanes, for the first time. This section of the development program was targeted to ensure the robustness of the VGV assembly.

Discussion

During 4Q95 consultations were held with Design Engineering and material suppliers to select the prime materials for the major components in the variable guide vane system. Under the guidance of Design Engineering, a list of candidate materials was prepared for the bushings and washers to undergo wear testing. The list included materials that were expected to have exceptional wear characteristics, and materials that offered potential cost savings and improved reliability over conventional bushing materials.

Over the next two quarters, specific material requirements were defined and a test matrix was drafted and agreed upon between Design Engineering and Materials Engineering. The project was reviewed with potential testing facilities and a test vendor was selected.

During 3Q96 all of the candidate bushing and washer materials were received. Pounding wear tests were initiated on the first set of potential bushing and washer materials being evaluated for durability improvements. Fixtures for oscillating tests were designed and procurement of the special tooling was initiated.

Summary/Conclusion

The oscillating wear tests continued into 1997 at increasing test temperatures until the test matrix was completed. The impact tests were also carried out into 1997 until the

complete array of samples and conditions had been evaluated for these samples. A report was written and the results were discussed Design Engineering. A final decision was made on the material selection of these components and applied to the compressor. This section of the overall materials evaluation of the ATS program was concluded in 1997.

Technology Application

This task will select materials with exceptional wear characteristics while offering a potential for cost savings and reliability over conventional bushing materials.

Section 2.2.4.6 (GTMTCS) Compressor Structural Materials and Process

Objective

Mechanical and physical property tests were performed on ATS compressor structural materials to provide an expanded mechanical and physical property database for design validation and enhancement. Material processing parameters for prototype manufacturing of the components were selected based on design requirements and discussions with vendors. When necessary, material and processing specifications were modified, or new ones written.

Introduction/Background

GE's ATS compressor operating conditions expanded the envelope from current practice. Testing performed in this section led to an understanding of the design parameters, and if necessary, any processing changes required to meet the design requirements.

Discussion

Mechanical testing of the various component materials was performed. LCF testing was performed on the cast compressor discharge casing material. Smooth bar HCF, notched bar HCF and LCF tests were performed on the compressor rotor material. HCF testing was performed on the compressor rotor wheel material.

Summary/Conclusion

The ultrasonic testing specification for the compressor rotor components was revised to take into account the unique configurations of the forgings. Various process specifications were revised to include the processing and acceptance requirements for the various components.

Technology Application

This task will continue characterization of compressor structural materials in test conditions that reflect service environments.

Section 2.2.4.7 (GTMTRF) Turbine Rotor Forging Materials and Processes [S]

Objective

Processing parameters of forged large turbine rotor components were optimized to achieve the desired forging attributes. These parameters included chemistry and processing temperatures, as well as post-processing surface treatments. Sub-size and full-size forgings were produced to verify and evaluate the processing approaches, and forging supplier process plans were developed for all components. Forging acoustic properties were determined by ultrasonic testing on test block and prototype parts. The attenuation, anisotropy, frequency bypass, and signal-to-noise ratio were measured and used in fracture mechanics analyses to support rotor design. Optimized inspection methods, any necessary software, and scan plans were developed based on the work with prototype parts. Property evaluations were conducted to ensure that material behavior models used for design accurately reflected those achieved in parts made by the manufacturing process selected.

Introduction/Background

The ATS gas turbine design called for a higher firing temperature than current production machines. This required a correspondingly higher temperature exposure of the turbine components. Evaluation of the current GE materials used in heavy-duty gas turbines found them to be inadequate for such operating conditions. Evaluation of other available materials indicated that none of them could be made into the large forgings that were needed for the turbine rotor components. It was therefore necessary to modify existing alloys, and then scale up the process in order to produce large parts in a robust manner. There were several concerns identified:

1. Ability to cast large ingots without segregation, cracking or other defects.
2. Convert the ingots into billets, which could be forged into the final shape. Issues identified were ability to homogenize the billet, and ability to convert the cast structure into uniform fine recrystallized grains.
3. Make the billet into a finished part as required by the design. Issues identified were whether the currently available presses could forge it, would it be free from forging defects, and would the final microstructure meet the design needs.
4. Have a suitable Non-Destructive Testing system, which could clearly and unambiguously locate and identify any defects in the finished part.
5. Would the mechanical properties of the finished part meet the requirements over the operating range of these components.

Discussion

Ingot Processing

An evaluation of available materials was done. The mechanism of formation of segregation, and the formation of other defects in the casting of large ingots, were identified. Small sub-scale ingots were cast which had their chemical compositions adjusted to reduce the propensity for segregation type defects.

Evaluations of the sub-scale ingots were satisfactory, and a scale-up was made to the full size ingots that were required. The processing parameters for the full size ingots were unknown. It was therefore decided to use an iterative type approach to arrive at the optimum processing parameters. Several ingots were melted with different melting conditions. The melting records for all these ingots were evaluated to first eliminate conditions that were not considered desirable, or were conditions of high risk. Samples from these ingots were given differential thermal analyses (DTA) to identify the melting range. This evaluation identified the range for homogenization studies. Small sections from the ingots were given different time and temperature homogenization treatments to identify the optimum range.

The full size ingots were then homogenized by the identified process, and the ingot was forged to a smaller diameter. The objective of forging was to get a feel for the forgeability of the ingots, and also to obtain a fully recrystallized structure, which could be ultrasonically tested for defects. The forged billets were machined to a smooth surface for ultrasonic testing. Immersion ultrasonic testing was performed on the entire billet. Any indications that were found were evaluated by metallographic sectioning. The billets were further cut into transverse sections and macro-etched. Uniformity of structure and presence/absence of any other unusual microstructural features of interest were identified.

After suitable processing parameters for the ingot were identified, additional melting trials were made to identify if the process was robust. The process of evaluating these was identical to the initial experiments, but the processing parameters were changed within the selected processing window. Evaluation of the ingots and billets found them to be satisfactory, and it was decided to go to the next step of the process.

Forging Process

The forging process of such large components has several issues, which are:

1. The part must forge adequately without cracking.
2. The part must be forgeable in the available presses in the world, (no new equipment).
3. The forging process must produce the microstructure and properties needed.

The first step of the forging process is to convert the ingot to a billet of uniform recrystallized grains. The experiment of converting the trial ingots to small diameter billets demonstrated that it was possible to do so. However the conversion needed for final forging requires a larger diameter, this required designing the process specifically for the diameter selected. Several different combination of steps were identified, each with specific temperatures, and upset ratios (change in selected billet dimension during forging). Specific tooling was designed for the steps of the process, and trial ingots were processed with these conditions. The ingots were photographed during the processing steps of these trials to evaluate details. The fully processed billets were evaluated for surface conditions and dimensions. The ends of the billet were sectioned and macro-etched to show the microstructural features of interest.

The design of the finished forging process involved several steps. The first step was to use small-scale laboratory specimens, which were upset isothermally at different temperatures and at different strain rates. This set of experiments provided the flow stress data needed for finite element modeling. The next set of lab specimens used specially designed lab specimens to evaluate the effect of strain and strain gradients in determining microstructural features. Finally, a third set of specimens were used to see the effect of multiple upsets on the structure. A DOE study of such tests established the desired operating parameters for finish forge processing.

Finite element modeling was used to determine if the desired operating conditions could be achieved in a full size component. The requirements were that the forging tonnage did not exceed the available press tonnage at GE suppliers. The characteristics of the actual forging press were used to get a more accurate answer.

Sub-scale parts at 1/3 of each dimension (1/9 the volume) of the finished part were then processed to the desired conditions. Modeling was also done for the sub-scale part so that it represented similar conditions as the full-scale parts. Additional sub –scale forgings of smaller size were made to optimize the heat treatment parameters. Sections from these forgings were given a range of heat treatments. Microstructural features and mechanical properties were compared for the different processes. Optimum heat treatment parameters were selected from this study. Extensive modeling of the heat treatment process was done to confirm that the selected parameters could be achieved in a full size forging. A full size forging was made to the dimensions required for the part. The processing data were compared with the models to ensure that they were similar. The part was heat treated to the selected process and tested.

Ultrasonic Test Development

The ultrasonic testing for these large parts required that special automated equipment and processes be developed. A special algorithm was developed so the part could be tested and analyzed at the same time without operator intervention. A new phased array ultrasonic testing system was developed to discriminate between benign and high-risk indications. To test this phased-array system, several small-scale ingots with known defects were prepared. These ingots were forged and heat-treated with processes similar

to full-scale parts. The automated ultrasonic system was used to first identify the locations of all indications. Each indication was then evaluated with the phased-array system to note its special signature. The indications were then extracted and sectioned and evaluated metallographically. Careful review and repetition of these tests and evaluations were able to identify specific types of defects with their characteristic signatures.

Mechanical Testing

At each step of the development process, mechanical test specimens were taken and tested. More extensive testing was done on the first forging. Testing was done at different locations to establish the effects of test locations. The mechanical properties were tested at room temperature and at elevated temperatures. A complete set of design curves was developed from this test data, ranging from room temperature to the operating temperature of these components.

Summary/Conclusion

1. A process was established for melting large ingots without segregation or defects in the selected alloy composition.
2. A robust process was developed for conversion of the ingot into a billet, and the subsequent finish forging into a turbine rotor component for the ATS gas turbine.
3. An ultrasonic testing system was developed to identify harmful sonic indications.
4. The mechanical properties of the large turbine components were optimized. The properties met the needs of the ATS turbine design.

Technology Application

This task will enhance process capabilities for manufacture of turbine rotor forgings.

Section 2.2.4.8 (GTMTRS) Turbine Rotor Spoolies and Transfer Devices Materials and Processes [S]

Objective

Although material selections for the cooling system delivery systems have been completed, this task performed testing to verify properties and identify potentially better materials. Any applicable or needed coatings or joint materials were also to be identified. Procedures for joining delivery components together and inspecting them were evaluated.

Introduction/Background

Components of the steam delivery system are one of a kind and have never been produced before. Therefore comprehensive part-specific process specifications were needed in order to define metallurgical requirements and production processes. New suppliers had to be selected and their processes had to be qualified.

Discussion

Five separate process specifications were written for spoolies, manifolds (cast and welded), elbows and for all other components. Welding processes (electron beam welding (EBW), gas tungsten arc welding (GTAW), and Flux Assisted GTAW) were developed for components such as the bore tube, rotor steam delivery manifolds and stationary steam piping manifolds. Also, casting processes were developed for components such as the rotor steam delivery manifolds and elbows. After the components were successfully produced and inspected in accordance with the process specifications, the suppliers' documentation was reviewed and approved.

Summary/Conclusion

Metallurgical requirements for steam delivery system components were defined in the process specifications and manufacturing processes for these extremely complex parts were successfully developed at the suppliers' facilities.

Technology Application

This task will develop processes and mechanical property data to optimize steam delivery hardware manufacture and subsequent operation.

Section 2.2.4.9 (GTMTSB) Structural Bolting [S]

Objective

Mechanical and physical property tests on two high strength bolting materials were conducted at ATS turbine conditions. If required, manufacturing trials would be conducted to optimize forming processes.

Introduction/Background

403Cb+ is a high strength 10 chrome class steel being considered for use as a candidate for bolting material. Several test programs were conducted to develop data for design curves. Three lots of material were evaluated in the test programs. Stress relaxation tests were conducted to supplement the data generated on this material in section 2.2.4.4. Material property curves were developed and issued from the data for use by Design Engineering.

Discussion

Stress Relaxation Program

Bolting alloy requirements include developing stress relaxation properties over the range of temperatures and strain levels applicable. Two heat lots of material were evaluated in the program under conditions shown in Table 2.2.4.9-1. Property curves were developed and issued to Design Engineering.

Table 2.2.4.9-1
403Cb+ Stress Relaxation Test Conditions

Strain(%)	600°F	700°F	800°F	900°F
0.10				X
0.15	X	X	X	X
0.20	X	X	X	X
0.25		X	X	X

Summary/Conclusions

Design data curves for design use were issued from the test results.

Technology Application

This task will increase the database for flange/flange and wheel/wheel bolting applications.

Section 2.2.4.10 (GTMTTA) Turbine Airfoils Materials and Processes [S]

Objective

Microstructure and mechanical properties were evaluated for full-size castings processed in this program. A comprehensive program yielded final specifications with appropriate heat treatments, and quantified the effects of ATS airfoil geometry and structure/property variability. Casting processes were developed for all airfoils utilizing developmental casting trials. Critical nozzle and bucket long-term material properties were measured at elevated temperatures. Metallic coating systems were developed for internal and external oxidation protection of the airfoils. Samples were coated using various techniques for optimization studies and process verification.

Introduction/Background

Successful ATS hot gas path designs will require high integrity turbine airfoil castings and thorough characterization of the cast materials at the expected component conditions. In large castings, careful attention to microstructural details is necessary in analyzing mechanical test results and, ultimately, in improving casting performance. To quantify and optimize prototype casting and airfoil materials, mechanical tests and microstructural

analyses need to be performed on component castings, including dendrite arm spacing (DAS) measurements and creep testing. DASs should be measured at various locations in several bucket castings and cast slabs of various ATS materials to determine consistency in the DASs of bucket castings and cast slabs for all alloys. Based on microstructural comparisons, findings from DAS measurements, and Laue diffraction results of the crystallographic orientations in prototype castings, material tests can be conducted on specimens machined from the cast slabs as well as from the buckets. The material tests should include all design allowable key mechanical properties to help achieve the performance goals of ATS. These include, but are not limited to, tensile, creep, rupture, low cycle fatigue, and high cycle fatigue. In addition, long-term creep tests need to be performed to ensure that the ATS durability goals are met. Mechanical test conditions should closely resemble those of component operating conditions and test materials should be representative of actual casting qualities. These include high temperatures, long hold times, and casting defects.

Discussion

To quantify and optimize prototype casting and airfoil materials, a number of tests and microstructural analyses were performed on bucket castings, including dendrite arm spacing (DAS) measurements and creep testing. DASs were measured at various locations in several buckets and cast slabs of various ATS materials. The results indicated reasonable consistency in the DASs of bucket castings for all alloys. Based on microstructural comparisons, findings from DAS measurements, and Laue diffraction results of the crystallographic orientations in prototype castings, creep tests were conducted on specimens machined from the buckets. The test results compared favorably with the results on slabs of the same material. Beyond standard specimen designs, samples were also used to assess geometry factors. Forty-three creep tests, covering four temperatures and a minimum of three stress levels, were completed on this program. Extensive microstructural investigations of twelve of the tested samples (six slab, six bucket) were conducted to better understand the mechanism of creep voiding. Stereomicroscopic evaluations were performed on the fracture surfaces of these samples.

Work was performed to better understand the behavior and castability of latter-stage bucket alloys. It included evaluation of the morphology of the material, deformation study, long-term aging experiment, and scanning electron microscopy (SEM). The long-term aging experiment was carried out on a cast slab to determine the extent of creep property degradation, if any. Other material was investigated following mechanical deformation and heat treatment at various temperatures to determine the propensity for recrystallization. Upon completion of the microstructural evaluation, the recrystallization temperature and heat treatment limits were defined for the large ATS buckets.

An experimental casting with chemistry modifications within specification was made at GE-CRD. Some of the material was sent out for machining and standard heat treatment. Subsequently, creep testing was conducted to determine the effect of the various element reductions on creep properties. Alternative heat treatments were also performed for this material to determine whether the reduction extended the heat treatment range. Creep tests were conducted at two different temperatures and stress levels to analyze the

properties from a latter-stage bucket casting. Results from this testing were compared to results from test slab material for correlation of actual component properties to handbook data. Creep evaluation was completed on a casting produced to study chemistry variations within specification limits. Six creep tests at three different temperatures (two tests at each temperature) were conducted to determine the effect by comparison to nominal chemistry creep data. This testing was conducted to finalize and optimize the alloy specification for the latter-stage buckets. Creep tests were conducted on several samples of the alloy with alternative heat treatments to determine the feasibility of the technique. Results of creep tests indicated a significantly longer time to 1% creep with the alternative heat treatment. Additional creep tests were conducted at two different temperatures and stress levels to analyze the properties from a latter-stage bucket casting. Results from this testing were compared to results from test slab material for correlation of actual component properties to handbook data.

Solidification processing experiments were conducted. The experiments were designed to cover a range of processing conditions, typical of those observed in large bucket and nozzle castings, to define the optimum processing window. The chemical compositions of the castings were analyzed at various locations along the length. The four castings were macroetched and analyzed for surface defects. Primary dendrite arm spacings (PDAS) were also measured. Differential thermal analyses (DTA) were also performed for determination of the alloy transformation temperatures relative to nominal chemistry material. The DTA information aided in setting heat treatment temperature limits. Microstructural evaluations of several samples of standard and non-standard material chemistries with various heat treatments were conducted. This was done to determine the effect of heat treatment on the strengthening phase precipitates. Additionally, experiments were conducted to gain an improved understanding of the solidification behavior and process defect map for latter-stage bucket materials. Fourteen experimental castings were made at a range of cooling rates.

An experiment was carried out to identify the process defect map for a bucket alloy. This experiment yielded a plot of gradient vs. withdrawal rate and identified the optimum process window. Examinations of chemistry variations within specification limits for latter-stage bucket materials were made using a developmental casting. Differential thermal analysis (DTA), heat treatment studies, and microstructural analysis were performed, as well as creep tests from samples with various heat treatments. Work on developmental heat treatments of the second-stage bucket material was performed with the goal of improving the solution heat treatment to enhance properties above current ATS-required values. Twelve creep tests were conducted. Metallographic evaluations of tested creep samples were conducted to determine the extent of creep voiding. SEM evaluations of several heat treatment microstructures were evaluated to determine and highlight any differences in microstructure morphology compared to the standard heat treatment.

Casting trials on the first- and second-stage nozzle and first-stage shroud configurations were made at casting suppliers to optimize the processing. Dimensional and metallurgical evaluations were made on the trial parts at the casting suppliers to assess and optimize the

casting processes. Metallurgical acceptance criteria for the buckets and nozzles were defined and submitted to the casting suppliers. A part specification for the first-stage inner shroud was written and submitted for review to the casting suppliers and design and manufacturing engineers. NDE techniques were developed to allow comprehensive inspections of the unique ATS configurations. Trials were conducted on both manufactured samples and full-size parts to determine the feasibility of various techniques to optimize production part inspections. The methods being examined were reviewed with the casting suppliers for feedback on special considerations for a production environment. A program was conducted with a casting supplier and a core supplier to better understand and improve core processing for bucket applications. An evaluation of a variety of cores was made.

Critical property mechanical tests were conducted on turbine bucket and nozzle alloys at various temperatures and stresses to cover a range of operating conditions expected for ATS components. These included tensile, creep, low cycle fatigue (LCF), high cycle fatigue (HCF), and thermal-mechanical fatigue (TMF) tests. Based on test results, various material property design curves were issued. Tensile tests were conducted on specimens removed from the shanks of the latter-stage buckets of three material types. Eight tensile tests were conducted on each of the three alloys at four temperatures. These tests were conducted to assure that the components possess expected properties. Various microstructural evaluations on prototype latter-stage buckets were performed. Porosity levels, heat treatment microstructure, and dendrite arm spacings were investigated. Creep-rupture and LCF tests were run on the first-stage airfoil material to analyze the effects of heat treatment, geometry, and coatings. Creep tests were conducted on standard bars as well as sheet specimens to assess geometry effects. After testing, specimens were examined both visually and metallographically. LCF tests with hold times were conducted on the second-stage bucket alloy on both notched and smooth bar specimens to evaluate the fatigue notch sensitivity factor (q). The notched specimens had double side notches resembling typical bucket dovetail geometries. Long-term creep tests were also conducted on various bucket and nozzle alloys. The total accumulated test hours ranged from 16,000-26,000 hours. These tests were aimed at addressing long-term durability issues and evaluating various orientation and geometry effects that may be present in ATS component material conditions. An effort was made to select the best post-cast processes. Samples of bucket materials were prepared, and LCF data on the effect of post-casting processes on the first- and second-stage bucket materials were obtained. The samples were evaluated metallography to determine the general microstructures. Also performed was a metallographic analysis of shaped cooling holes produced by a candidate manufacturing procedure.

Low Cycle Fatigue (LCF) tests were conducted on casting defect-containing first stage bucket material at five selected temperatures. In addition, creep and high cycle fatigue (HCF) tests were conducted on defect-containing first stage bucket material at one selected temperature. The defect types tested included low and high angle boundaries at varying angles of misorientation. LCF tests were also conducted on casting defect-containing stage two bucket material, similar to the test protocol for the first stage material. The defect types evaluated in this material included emergent and misoriented

grains. Based on test results, preliminary design curves were issued for defect-containing first stage and second stage bucket materials.

In addition, pressurized LCF tests were conducted on tubular samples intentionally cast with defects in the gauge section to evaluate their effects in ATS alloys. Nineteen (19) tests were run, and SEM fracture surface analysis was conducted on all 19 tested specimens. Defect sizes were measured from SEM micrographs for each specimen. More than 700 measurements were documented. Some defect-free specimens were also included for comparison. Test results were compared to solid bar design data. Microstructural evaluation of the tested specimens was also performed. LCF tests were also conducted on milled first stage airfoil material specimens to determine the effects of milling-induced recrystallization on LCF life. Three groups of LCF specimens were tested with the following surface finishes: 1) as-milled, 2) milled and polished, and 3) baseline low stress ground and polished. Specimens designed to accurately represent the actual component geometry factors and operating conditions of the first-stage airfoils were tested in LCF. Some samples were tested to evaluate various finishing operations, while others contained intentionally produced defects to evaluate the effect that casting defects have on properties in airfoils with ATS configurations. Four-thousand-hour air furnace exposure experiments were carried out on turbine bucket and nozzle alloys at one selected temperature to determine the effect, if any, of thermal exposure on microstructure and low cycle fatigue (LCF) life. Test results were analyzed and compared with existing design curves.

A number of candidate coating systems and application processes were examined to assess the viability and processes required to apply the best integrity internal and external (non-TBC) coatings on ATS-sized and configured airfoils. Buckets were prepared with various metallic coatings to obtain information on their application processes and subsequently to obtain performance information on full-size parts. Scale-up trials were performed. Forty-nine (49) buckets were coated with candidate improved coating systems and installed in a 6B at Mission Energy's Sargeant Canyon, California, facility for a field test. In addition to the bucket tests, laboratory information was generated in small burner rigs to evaluate the oxidation life and integrity of the coatings. In order to provide a relatively quick and inexpensive means of ranking coating susceptibility to cracking, laboratory tests were performed to measure the strain-to-cracking behavior of coatings as a function of temperature.

Summary/Conclusions

To quantify and optimize prototype casting and airfoil materials, a number of tests and microstructural analyses were performed on bucket castings, including dendrite arm spacing (DAS) measurements and creep testing. The results indicated reasonable consistency in the DASs of bucket castings for all alloys.

- Work was performed to better understand the behavior and castability of latter-stage bucket alloys. It included evaluation of the morphology of the material, deformation study, long-term aging experiment, and scanning electron microscopy.

- An experimental casting with chemistry modifications within specification was made at CRD, and creep testing was conducted to determine the effect of the various element reductions on creep properties. Alternative heat treatments were also performed for this material to determine whether the reduction extended the heat treatment range.

- Solidification processing experiments were conducted for a range of processing conditions, typical of those observed in large bucket and nozzle castings, to define the optimum processing window. The chemical compositions of the castings were analyzed at various locations along the length, and DTA was performed for determination of the alloy transformation temperatures.

- An experiment was carried out to identify the process defect map for a bucket alloy. This experiment yielded a plot of gradient vs. withdrawal rate and identified the optimum process window.

- Casting trials on the first- and second-stage nozzle and first-stage shroud configurations were made at casting suppliers to optimize the processing. Dimensional and metallurgical evaluations were made on the trial parts at the casting suppliers to assess and optimize the casting processes. Metallurgical acceptance criteria for the buckets and nozzles were defined, and NDE techniques were developed to allow comprehensive inspections of the unique ATS configurations.

- Critical property mechanical tests were conducted on turbine bucket and nozzle alloys at various temperatures and stresses to cover a range of operating conditions expected for ATS components. These included tensile, creep, low cycle fatigue (LCF), high cycle fatigue (HCF), and thermal-mechanical fatigue (TMF), and long-term creep tests. Based on test results, various material property design curves were issued.

- Casting defect-containing bucket materials were tested for key mechanical properties, including creep, LCF and HCF. The defect types tested included low and high angle boundaries at varying angles of misorientation, recrystallization, emergent and misoriented grains.

- Four-thousand-hour air furnace exposure experiments were carried out on turbine bucket and nozzle alloys at one selected temperature to determine the effect, if any, of thermal exposure on microstructure and low cycle fatigue (LCF) life. Test results were analyzed and compared with existing design curves.

- A number of candidate coating systems and application processes were examined to assess the viability and processes required to apply the best integrity internal and external (non-TBC) coatings on ATS-sized and configured airfoils. Work included a field test of coated buckets and laboratory burner rig and strain-to-crack tests to evaluate the oxidation life and mechanical integrity of the coatings.

Technology Application

This task will enhance the database of mechanical properties at service conditions for bucket, nozzle, and shroud materials.

Section 2.2.4.10.1 (GTMTTA) Airfoil NDE [C]

Objective

The objective of this task was to identify and prototype advanced methods of nondestructive evaluation (NDE) and metrology for the quality assurance of various hot gas path airfoils of the ATS gas turbine, especially the single crystal and directionally solidified castings used in the early turbine stages. Critical NDE and metrology requirements for the turbine airfoils include reliable detection of internal casting defects in the airfoil walls of first-stage bucket and nozzle airfoils, measurement of the wall thickness in the single-crystal and directionally-solidified castings, and inspection of the cover-to-airfoil welds in the turbine nozzle assemblies.

Introduction/Background

The higher firing temperatures and steam cooling required for the ATS gas turbine have placed stringent dimensional and structural requirements on the turbine airfoils, particularly as compared with previous generation gas turbine technology. In many cases, the inspection and metrology requirements that have evolved for the ATS turbine airfoils exceed the available capability of the inspection and metrology methods traditionally used for nickel superalloy investment castings. Accordingly, it was necessary to develop new NDE methods to assess various critical-to-quality parameters on the ATS turbine airfoils, particularly the first- and second-stage buckets and nozzles.

Airfoil wall thickness, internal casting integrity, and airfoil-to-cover weld integrity are major areas of focus for airfoil quality. Ultrasonic (UT) and infra-red (IR) test methods were developed for airfoil wall thickness measurement. X-ray inspection using digital radiography (DR) and immersion UT were investigated for detection of internal casting defects. Immersion and contact UT techniques were refined for inspection of critical welds in the first- and second-stage nozzles.

Discussion

Wall Thickness Measurement

Commercially available ultrasonic thickness gauges traditionally are used for wall thickness measurement in airfoil castings. This measurement approach assumes that the ultrasonic longitudinal wave velocity is known accurately at each measurement point, an assumption that holds fairly well in polycrystalline materials. However, these gauges do not afford the measurement accuracy required to operate reliably within the close tolerances specified for the single crystal and directionally solidified castings used in the early stages of the ATS machine. The anisotropic nature of these materials results in a large variation in ultrasonic velocity that in turn translates into unacceptable uncertainty in wall thickness measurement.

To address this limitation, a more sophisticated UT wall thickness measurement method was developed that employed an algorithm to calculate the ultrasonic velocity at each measurement point on a single crystal airfoil casting. By accounting for the variation in ultrasonic velocity, this method permitted wall thickness measurement with the necessary accuracy and precision that was not possible with off-the-shelf UT thickness gauging. A photo of the prototype measurement system is shown in Fig. 2.2.4.10.1-1, illustrating the fixturing used to position and hold the ultrasonic transducers on a curved airfoil wall. Measurements are made on an inspection grid that is superimposed on the airfoil, as with traditional thickness measurement approaches. This coarse sampling grid unfortunately does not give the full picture of thickness variation in the airfoil wall.

In order to provide a full field view of the wall thickness, quantitative infra-red (IR) imaging methods were modified for the inspection of single-crystal and directionally solidified nickel superalloy castings. This method involves pulse heating of the airfoil surface via a bank of flashlamps and then recording the temporal signature of the surface temperature of the part using an IR focal plane array camera as the airfoil cools down. A photo of the prototype measurement system is shown in Fig. 2.2.4.10.1-2.

Processing of the raw data frame-by-frame yields a full-field thickness image of the airfoil wall that permits rapid identification of localized thickness variations and verification of the heat transfer structures interior to the airfoil.

Volumetric Inspection of Turbine Airfoil Castings

Traditional X-ray inspection methods for castings lack the capability necessary for the first- and second-stage buckets and nozzles of the ATS gas turbine, so digital radiography and immersion ultrasonic imaging were developed to provide enhanced inspection capability for these castings.

This task established digital radiography as a practical method for enhanced inspection of ATS gas turbine airfoil castings for internal casting integrity. Both amorphous Selenium and amorphous Silicon digital radiographic imaging systems were tested in inspection capability trials on the first-stage turbine airfoils (both bucket and nozzle) for the ATS gas turbine. Test samples were prepared by machining "pore-like" blind holes (depth = diameter) in the airfoil and fillets of actual ATS gas turbine airfoil castings. Probability of detection (POD) was estimated from the inspection capability data for the digital radiography inspection methods and benchmarked against that for conventional film radiography. Figure 2.2.4.10.1-3 shows a typical digital radiograph of a portion of a single crystal casting, illustrating the image resolution of several of the machined pores under 0.020 inch in dimension.

Immersion UT inspection was developed using a 5-axis robotic scanning system to permit the ultrasonic transducer to track the complex contour of an airfoil. This inspection method was refined to the point where it can provide volumetric data on the casting integrity of the airfoil walls for characterization and optimization of the casting process capability. However, the level of measurement complexity and the length of time required to inspect an entire airfoil with sufficient resolution was determined to be impractical for 100% inspection of production parts at this time.

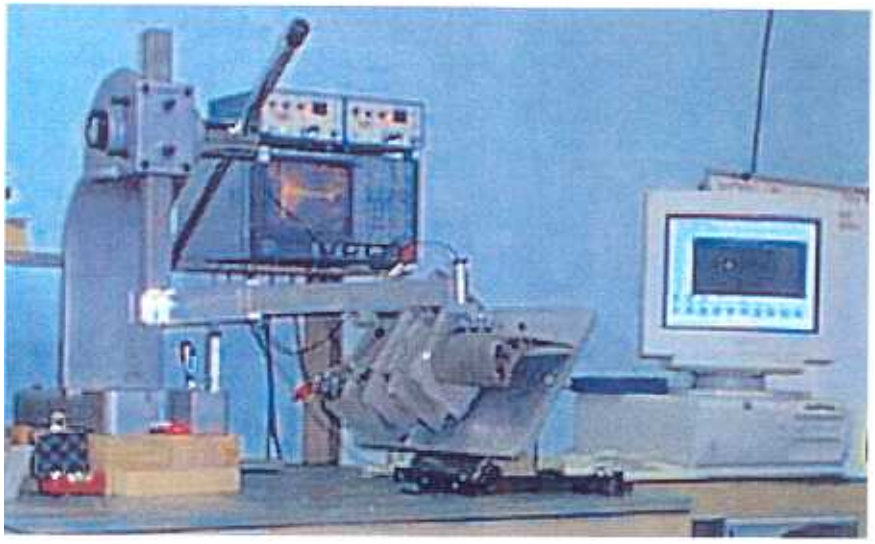

Figure 2.2.4.10.1-1. Photograph of a prototype ultrasonic system for wall thickness measurement in single crystal nickel-based super-alloy turbine airfoils for the ATS gas turbine.

Figure 2.2.4.10.1-2. Photograph of a prototype IR system for wall thickness measurement in single crystal and directionally solidified nickel-based super-alloy turbine airfoils for the ATS gas turbine.

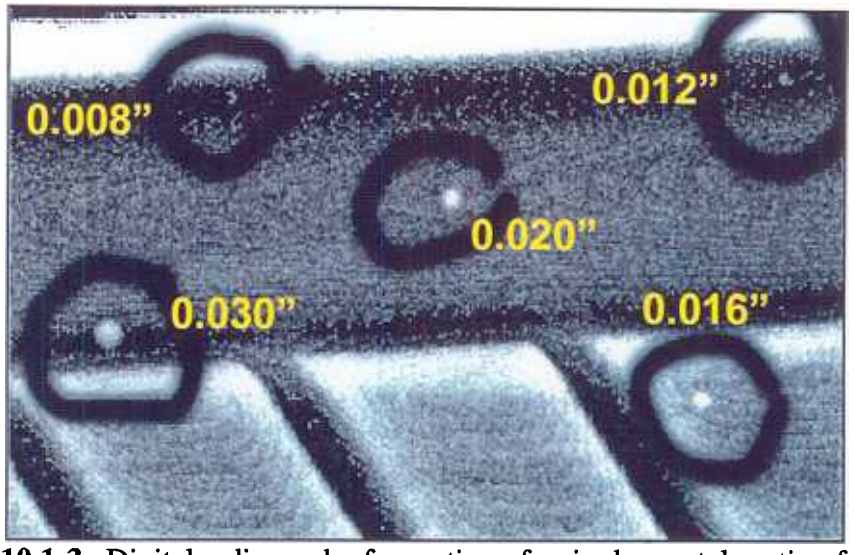

Figure 2.2.4.10.1-3. Digital radiograph of a portion of a single crystal casting for the ATS gas turbine, illustrating the image resolution of several machined pore-like features under 0.020 inch in dimension.

Turbine Airfoil Weld Inspection

Ultrasonic inspection methods were developed and implemented to assess the integrity of the cover-to-airfoil welds in the first and second stage nozzle assemblies for the ATS gas turbine. These inspections provided key data during the studies to optimize the various welding processes, and were used for the initial sets of nozzle assemblies.

Summary/Conclusion

Improved methods for nondestructive inspection and metrology have been developed that exceed the capability offered by traditional commercially available inspection technology and contribute to improved quality for the ATS turbine airfoils. This development effort has resulted in prototype UT and IR systems for airfoil wall thickness measurements, both of which have seen use on the first round of castings and are slated for use at the casting vendor for inspection of production castings of single crystal and directionally solidified airfoils. This development effort also has quantified the advantages of DR X-ray inspection over film-based radiography for airfoil castings, contributing to the acceptance of this emerging technology at the casting vendor and within the manufacturing engineering community. It is anticipated that DR inspection will soon be in use for production superalloy airfoil castings for the ATS gas turbine. This development effort also has resulted in effective UT inspection methods for critical cover-to-airfoil welds in the turbine nozzles that have provided the necessary data to support optimization of the welding processes and verification of the structural integrity of the welds on the initial production airfoils.

Technology Application

The NDE and metrology methods prototyped during this task will be integrated into the overall quality assurance program for the ATS gas turbine airfoils to provide the necessary data to the design staff for more accurate life predictions for critical single-crystal and directionally solidified turbine airfoils.

Section 2.2.4.11 (GTMTCB) Combustion Materials and Processes [S]

Objective

Properties of materials for combustion components were evaluated at ATS conditions. Where necessary, trial components were made in order to acquire material of the appropriate size using full-scale manufacturing processes.

Introduction/Background

The combustion components were based on the commercial DLN2 combustion system, with modifications to accommodate 7H and 9H operating conditions. Where possible, use of existing DLN2 combustion system materials and processes was leveraged. New materials and methods of manufacture were explored for the combustion liner and transition piece only, with property studies completed to support these components.

Discussion

A comprehensive review of applicable mechanical property data was performed for all potential materials at ATS conditions. Where appropriate, creep and low cycle fatigue studies of new candidate alloys were initiated for the test conditions of interest. Comparisons were made to enable material selection activities for the critical components.

For the combustion liner component activity, prototype tooling was completed to produce cast combustion liners of alloy GTD-222. Wax patterns were successfully injected using the prototype tooling. Two cast liners were produced, incorporating features that are typically welded on in subsequent fabrication operations. While these demonstrations were successful, the production liners produced for 7H and 9H utilized a wrought version of the alloy using conventional fabrication techniques.

For the transition piece activity, casting trials were pursued for both the transition piece body shape and the aft frame. Following successful prototyping and part casting, a complete set of transition pieces was produced from cast alloy GTD-222.

Summary/Conclusion

The production liners produced for the 7H and 9H utilized wrought materials and conventional fabrication techniques. The ATS program afforded an opportunity to explore casting processes and both combustion liners and transition pieces were shown to be producible. Further use of cast combustion components will depend on life cycle cost factors.

Technology Application

This task will enhance processes and mechanical property data to optimize combustion hardware manufacture and subsequent operation.

Section 2.2.4.12 (GTMTST) Turbine Structures Materials and Process [S]

Objective

Producibility evaluations for the turbine structures included selection of materials processing parameters and chemistry, and preparation of material and process specifications. Processing trials were be used to confirm producibility and verify capabilities of suppliers. Testing was conducted where necessary to evaluate the materials under ATS conditions.

Introduction/Background

GE's ATS turbine operating conditions expanded the envelope from current practice. Testing performed in this section led to an understanding of the design parameters, and if necessary, processing changes to meet the design requirements.

Discussion

Steam gland producibility was reviewed with potential suppliers. A review of the processing capabilities, material response and post-cast processing limitations was conducted in support of the final design efforts.

Summary/Conclusion

Various process specifications were revised to include the processing and acceptance requirements for the various components.

Technology Application

This task will continue characterization of turbine structure materials in test conditions that reflect service environment.

Section 2.2.4.13 (GTMTSH) Turbine Shells [S]

Objective

Materials and processes were identified for production of the turbine shells. Specifications were defined after material property testing and process verification/optimization trials were conducted to achieve the best quality part to meet all design criteria.

Introduction/Background

GE's ATS turbine operating conditions expanded the envelope from current practice. Testing performed in this section led to an increased understanding of the design parameters, and if necessary, processing changes to meet the design requirements.

Summary/Conclusion

Coefficient of friction testing for components of the turbine shell system was performed. Coefficient of thermal expansion testing was completed on two possible shell material. Fabrication options for producing the inner shell were reviewed and evaluated for design. Various process specifications were revised to include the processing and acceptance requirements for the various components.

Technology Application

This task will enhance characterization of turbine shell materials in test conditions that reflect service environments.

Section 2.2.4.14 (GTMTSR) Seal Technology [S]

Objective

Improved gas path seals will be developed for the ATS turbine using seal technology from aircraft engine components where applicable. The technology will be evaluated using developmental hardware and samples. These advanced seals will provide evolutionary advances in machine performance.

Introduction/Background

Hot gas path seals include a variety of intersegment spline seals, honeycomb seals for turbine shrouds and hardfacing materials for latter stage bucket interlocks. A series of design and manufacturing reviews was completed for each sealing system of interest to identify opportunities for enhancements in materials or processes.

Discussion

Intersegment seals for nozzles were developed and demonstrated on the nozzles for the cascade test using conventional materials and processes.

Honeycomb seals for turbine shrouds were produced using a highly oxidation resistant material first used by aircraft engine components. Brazing methods for these shrouds were developed using industry-wide practices.

Hardfacing for bucket tip shroud interlocks was demonstrated. The 7H, which utilized new alloy GTD-444 in the latter stages, required welding development for the hardfacing. This was completed and successfully demonstrated for FSNL hardware.

Summary/Conclusion

A variety of hot gas path sealing systems were successfully demonstrated with appropriate manufacturing plans and specifications completed. As anticipated, hot gas path sealing efforts were evolutionary in nature.

Technology Application

This task optimized seal attachment processes focused at airflow leakage restrictions to enhance performance.

Section 2.2.4.14.1 (GTFFTSESV) Hot Gas Path and Transition Piece Cloth Seals [C]

Objective

One objective of this task was to develop and test hot gas path seals that meet both leakage performance and life requirements. Specifically, improved sealing performance that reduces the equivalent gap of the seal was sought by replacing the current Q-tip seals with a cloth sealing system. The cloth seals also need to meet the same full-life requirement applied to current seal technologies.

The other objective of this task was to develop and test transition piece cloth seals that met both leakage performance and life requirements. Life consistent with the prescribed inspection interval is required.

Introduction/Background

Seals between the hot gas path turbine components are required to help meet the ATS combined cycle efficiency target. A turbine stator (shroud) is built up of several annular segments that are packed together at circumferential and axial junctions. The junctions between these segments need to be sealed in order to maintain high efficiency. Typically such junctions have slots on the mating edges. Seals are used in the slots, bridging adjacent members, to block off any leakage, (see Figure 2.2.4.14.1-1). Current turbine designs do not have any seals for the curved, circumferential junctions. Straight, axial junction (dogbone) seals are used in some newer machines. These seals do have a drawback, however; they chatter under low pressure drops, causing wear and degradation

of the sealing interface. Additionally, they are not flexible enough to withstand thermal/mechanical distortions and deformations. Cloth seals offer superior sealing ability with the added benefits of flexibility, good performance at low pressure differentials, and good damping (both fluid and structural).

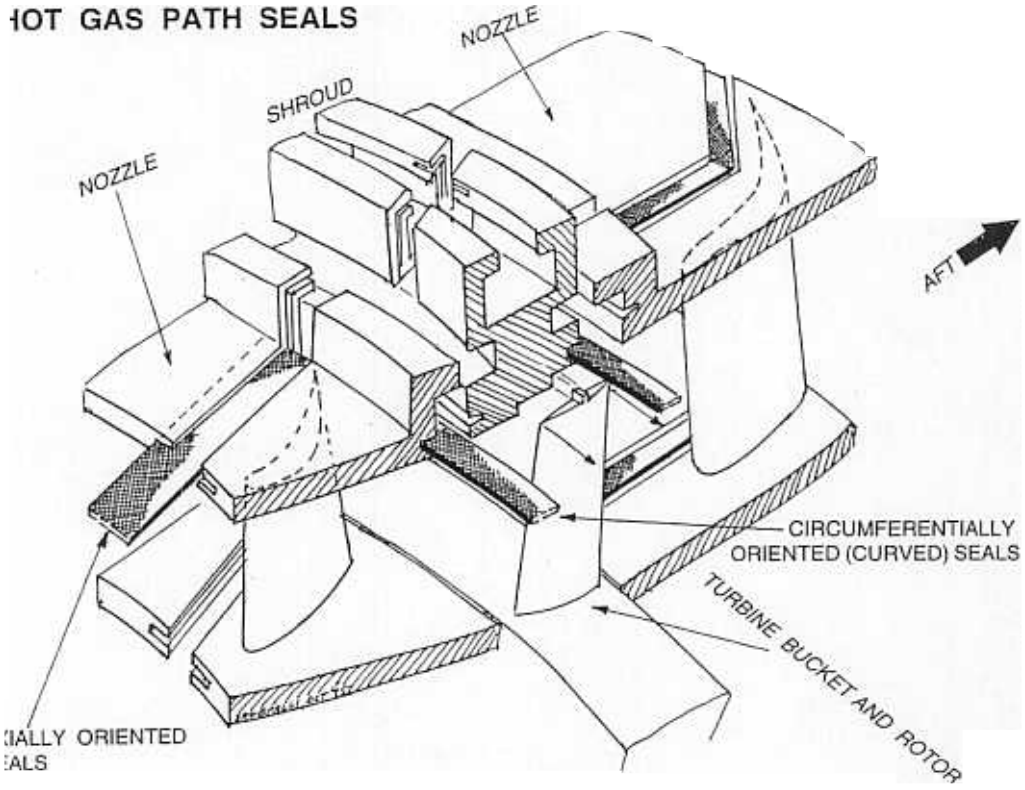

Figure 2.2.4.14.1-1. Hot Gas Path Seals in a Turbine

Seals between the combustor transition piece and the first-stage nozzle were required to help meet the ATS combined cycle efficiency target. The first-stage nozzle undergoes large (thermal) motion relative to the transition piece end frame under various machine conditions (e.g., fire-up; full speed, no load; steady-state). The cloth seal is required to maintain contact at the joint under all these conditions without yielding. In addition, under repeated load-unload cycling, the seal materials (cloth, shim) are expected to retain their functional properties (wear resistance, elasticity).

The general approach applied in this task was to develop advanced seals by designing and analyzing proposed seal concepts, fabricating preferred choices, and finally testing, back-to-back, a variety of advanced seal concepts using the "Shoebox" rig. The Shoebox test rig system is useful for testing many "standard" length seals at various temperatures and pressures to determine their sealing effectiveness. The rig has adjustable seal jaws that

can be assembled at specific values of gap, offset, and mismatch, representative of the relative thermal/mechanical growth between mating members in a machine.

Discussion

Hot Gas Path Seals

Extensive testing was done to identify the best cloth material and weave with respect to wear, sealing, and formability considerations, and detailed FEM analysis of various shim designs was done. Based on test and analysis results, a particular weave of a cobalt-based superalloy cloth and a nickel-based shim were selected for the seal. Typically, a cloth seal comprises a pair of high-strength shims sandwiched between two layers of cloth. The high-temperature "Shoebox" rig at CRD was used to test various seal designs over a range of controlled gap, offset, and mismatch conditions typical of those encountered between mating members in a turbine. After a number of designs were evaluated under controlled conditions of pressure and misalignment, a single-shim, crimped cloth seal was selected.

The relatively stiff strip (dogbone) seals now used for hot gas path sealing cannot be bent or curved easily for corner leakage applications. In current turbine designs, a typical inner+outer shroud arrangement uses straight seal segments that meet at corners, and there is usually leakage between segments. Because of their flexibility, cloth seals permit the design of continuous, curved sealing sections. Tests at ATS gas turbine conditions of temperature, pressure, and pressure drop were conducted on corner junctions using both continuous curved cloth seals and segmented straight seals. The continuous curved seals performed better than the straight two-piece corner junctions in all tests.

High-temperature oxidation tests of the seal material were also conducted. Many candidate superalloy samples were tested in both wire and sheet forms. A few of the materials that appear to work well under ATS gas turbine conditions will have to be investigated to evaluate seal producibility.

Transition Piece Cloth Seals

The seal and shelf contour geometries were carefully selected to achieve the objective of maintaining contact at the joint under all operating conditions without yielding. In addition, under repeated load-unload cycling, the seal materials (cloth, shim) are expected to retain their functional properties (wear resistance, elasticity). Finite element analyses were conducted to ensure that there will be no material failure.

Extensive high-temperature wear tests were conducted between standard cloth samples and corresponding solid surfaces representing the mating surface (shelf). On the basis of the results of these tests, materials were selected for the cloth and shim portion of the seal. High-temperature low cycle fatigue (LCF) testing and high-temperature material characterization testing were done on the fabricated seals to evaluate their performance. A special high-temperature rig and oven were fabricated for the LCF test. The rig provided a controlled high-temperature environment and an oscillating mechanism to permit low cycle deformation of the seals being tested. LCF tests were conducted on an outer cloth seal sample The range of motion used in testing the cloth seal sample was

representative of the relative movement between the ATS transition piece and the first-stage nozzle in going from fire-up to FSNL conditions.

The LCF tests were run for 1600 cycles. Leakage measurements were made before, during, and after the 1600 cycles. No appreciable deterioration in sealing occurred after 1600 cycles in the FSNL and steady-state conditions. A permanent set in the cloth seal was observed at fire-up conditions.

High-temperature leakage tests were conducted on the outer cloth seal using the Shoebox rig, which measures seal leakage under controlled conditions of pressure, pressure drop, and temperature of a "standard" length seal sample. Seal leakage was considerably lower than the leakage measured with conventional "Floating Seals."

Summary/Conclusion

A turbine stator (shroud) is built up of several annular segments that are packed together at circumferential and axial junctions. The junctions between these segments need to be sealed in order to minimize leakage and maintain high efficiency. Typically such junctions have slots on the mating edges. Seals are used in the slots, bridging adjacent members, to block off any leakage. Current turbine designs do not have any seals for the curved circumferential junctions. Straight axial junction (dogbone) seals are used in some newer machines. Cloth seals provide the capacity to reduce seal leakage significantly.

Technology Application

Seal technology and designs developed as part of this task will be applied to significantly reduce leakage in both the hot gas path and the combustor transition piece. Performance will be enhanced.

Section 2.2.4.14.2 (GTETBS) Steam Gland Brush Seals [C]

Objective

The objective of this task was to develop brush seals to minimize steam leakage in the steam gland.

Introduction

The brush seal design that was the objective of this task was made up of a wide range of tests and analyses. System behavior had to be defined first in order to define the environment to which the seals would be exposed. Fundamental material tests had to be carried out to determine effect of steam on materials. A variety of analytical tools were used to design the seals including CFD analysis. Finally, wear tests were conducted and leakage measurements were made to determine the effectiveness of the final design.

Discussion

A number of preliminary system analyses were carried out to determine the deformations that the seals will encounter during machine operation. Maximum radial excursion was calculated in order to set the seal fence height. This maximum radial excursion includes

thermal transients, rotor, vibration, and tolerance stack-up. Based on all these excursions, the exact axial location of the brush seal was chosen. The transient time history of the brush seal clearance was also determined and sub-scale wear tests were planned.

Fundamental material issues were also addressed with tests. The material for the brush seal bristles was selected on the basis of wear testing. Tensile tests were used to determine that the bristle material did not degrade in the presence of steam. Potential coatings were identified and tests were conducted to establish that they were not affected by the presence of steam.

The seal design itself consists of two elements: the seal cross section design and the design of the geometry between the seal stages. The seal parameters required to meet the machine operating conditions – i.e., fence height, bristle diameter, seal height, and cant angle – were all established. Once these parameters were chosen, tests were conducted on a single-stage and on a double-stage seal with room temperature air. Data were collected over a range of pressure ratios and clearances simulating the expected environment. Both air and steam maps were developed.

There are two seal locations to be considered: aft of the steam scroll is a leakage flow with a low-pressure drop; forward of the scroll is a leakage flow with a high-pressure drop. A single-stage brush seal design was developed for the first location and a two-stage brush seal for the second. Static leakage tests were used to determine the leakage performance under operating conditions. Computational fluid dynamics (CFD) modeling was used to design the geometry of the two-stage seal. Since most wear is assumed to occur during transients, the wear life was determined by testing under conditions based on extreme transient conditions. The design was validated by sub-scale rotary tests under operating conditions.

The objective of the interstage geometry design for the two-stage seals is to ensure that the flows exiting the first stage do not damage the second-stage seal. The jet velocity must be attenuated and the flow along the upstream bristles of the second stage must be radially inward rather than outward.

The CFD modeling work has shown that a space of at least 38.1 mm (1.5 inches) between the last labyrinth tooth and the second-stage brush is enough to ensure favorable flows into the second-stage brush. The seal is designed with a space of 44.5 mm (1.75 inches) between the last labyrinth tooth and the second-stage brush. Since the flow pattern appears to be insensitive to the number of labyrinth teeth, similar flow patterns are expected in the H machine with 20 teeth and the steam deposition rig, which has 4 teeth.

Wear and dynamic leakage tests are two of the most important final subtasks of seal design. A sub-scale wear test was designed and a dynamic leakage test was conducted to establish final performance of the seals.

The objective of the sub-scale wear test conducted in this task was to determine the wear characteristics of the brush seal at machine operating conditions. The brush seal vendor completed a 20-hour sub-scale wear test of the brush seal. The predicted transient conditions in the turbine call for wear conditions that exceed the capability of the test rig. The seal-to-shaft interference in the test rig was increased in order to partially compensate for the lower pressure difference across the seal. The larger interference

increased the contact pressure between the bristles and shaft. Wear rate on the brush seal was very low. No wear was observed on the IN718 rotor.

During the time this task was being carried out, the decision was made to change the material of the H machine aft stub shaft to a Cr-Mo-V. It was determined that this would result in reduced wear rate on the brush seal bristles and a slightly increased wear rate on the shaft.

Dynamic leak tests were also carried out. The objective of the dynamic leakage test is to measure seal leakage during rotation and to determine the durability of the two-stage seal design in a high-pressure steam environment. Brush seals, seal holders, and a new test rig rotor were designed, manufactured, and installed in the steam deposition test rig. Modifications were made to the steam piping system to accept larger steam flow. The steam deposition test rig was modified to accommodate a total of 4 brush seals: one brush seal set consists of unsegmented seals; the other set is segmented, with the segment end design similar to that of the H machine. Both sets of brush seals have 4 labyrinth teeth between the brush seal stages and a 44.5-mm (1.75-inch) space between the last tooth and the second brush seal. Orifice plates and additional instrumentation were added in order to measure flow through the unsegmented and segmented brush seals. The data acquisition system was modified to record additional test parameters for the brush seal test.

After these modifications the leakage tests were completed. Seal leakage was measured with and without shaft rotation. The static leakage data agreed well with predicted flowrates. Seal durability was also demonstrated. Inspection of the brush seals showed no flow-related damage.

Summary/Conclusion

The brush seals developed under this task will significantly reduce steam leakage in the steam gland. This leakage reduction increased the efficiency of the ATS gas turbine. The successful implementation of brush seals in the steam gland also allowed for a reduction in the axial length of the steam gland. This shorter length will result in a manufacturing cost reduction.

Technology Application

The results of this task constitute design specification for steam gland brush seals on the ATS gas turbine.

Section 2.2.4.14.3 (GTEBS) 7H Stage 3 Nozzle Brush Seals [C]

Objective

Preliminary analysis indicates that the application of brush seals to the 3rd stage diaphragm of the 7H gas turbine would improve turbine efficiency and heat rate and, as a consequence, increase both combined cycle efficiency and power. The objective of this task is to carry out the necessary development work to define the design that will be most effective for the 3rd stage diaphragm of the 7H gas turbine.

Introduction/Background

One way to improve a gas turbine's efficiency and output is to reduce the leakage flows of the secondary flow system. The performance analysis of the 7H gas turbine indicated that a potential 0.3% W2 flow saving can be achieved by improving the sealing at the stage 3 nozzle/diaphragm area; this savings comes to 0.05 point combined cycle efficiency and 0.4% combined cycle output. Brush seals were chosen to improve the sealing in combination with the original honeycomb seals as shown in Figure 2.2.4.14.3-1. In addition to the performance benefit, brush seals will also improve the life of the third stage buckets because they reduce the variation of the bucket cooling flow.

The development of the 7H brush seals started in 1998. A preliminary design was completed in 1999. Because the 7H application exceeds previous brush seal experience in terms of surface speed (> 1000 ft/s), interference (> 0.08"), and flow field (oscillation), extensive tests were performed in 2000 to validate the preliminary seal design. The results of these tests confirmed the benefits of the brush seals, and provided guidelines for further design improvements of the brush seals. The final seal design will be completed based on the results of the validation tests.

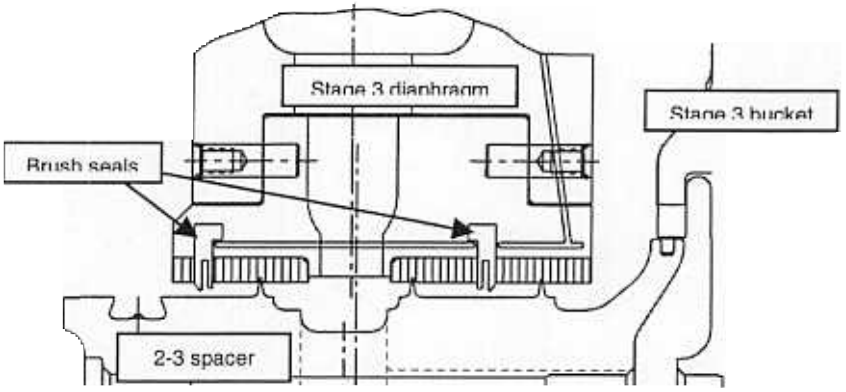

Figure 2.2.4.14.3-1: Brush Seals Configuration for 7H S3N

Discussion

The preliminary seal design consists of 20 segments for each seal, one segment per diaphragm/inducer block. Both seals use low hysteresis and long front plate design without damper shims. Inducer blocks and 2-3 spacers were modified for the brush seal application. To validate the seal design and retire risks associated with the brush seal application, instrumentation was added to the 7H FSNL1 test, and a series of small scale tests were carried out. Two of the most import tests are the endurance test and the stability test.

Endurance Test

A preliminary design review was held at the beginning of the year with the Chief Engineer's office to assess plans for a number of tests scheduled to collect data for the design of the 3rd stage diaphragm brush seal. The review resulted in several revisions to the planned endurance and stability tests. The final test plans were reviewed with

vendors, and a series of tests, including performance, hysteresis, endurance and seal blow-down, were completed. The endurance test revealed that the wear rate at the 7H machine speeds was higher than expected, and the seal design is being revised to reflect this latest data. A follow-up test has been recommended. At fully-deteriorated conditions, test results and complementary flow analyses show that the brush seals exhibit better performance than fully-deteriorated honeycomb seals.

Seals and rotors from the first endurance test were carefully examined to identify any evidence of material changes in grain structure or micro hardness as a result of wear during the test. No indication of serious problems was observed.

Preparation for the follow up endurance test continued. This test will examine effects of shot peening of the 2-3 spacer on surface wear. Final design conditions for brush stiffness and interference level will be examined. The final brush seal design will be completed and a detailed design review will be held.

Stability Tests

Due to the large difference in scale, it is very difficult to generate the same level of flow oscillation in a small-scale rig as in the actual turbine. Extensive CFD work was performed to evaluate the rig design for the stability test, and the results were reported on the preliminary design review. Based on the CFD results and recommendation from the preliminary design review, the test rig design for seal stability was finalized. Detailed hardware design was completed by the vendor, and design analyses for the brush seal stability test were completed and hardware was fabricated.

The brush seal stability tests were completed. Two seals with different stiffness characteristics were tested at various pressure conditions associated with 7H operating conditions. Stability-pressure maps were generated for each test seal. Results of the test indicated that both the forward and the aft seals will operate in stable regions of the stability map for the designed seal stiffness. The design has also been shown to be robust relative to the cant angle of the bristles.

Summary/Conclusion

Brush seals can improve the stage 3 diaphragm sealing over the original seal design. At fully deteriorated condition, the brush seals save 0.3% W2 flow, and more flow is saved with new brush seals. Brush seals also improve the life of the 3rd stage bucket by reducing the cooling flow variation.

Due to the high speed and large interference, the bristle wear rate is high compared to previous brush seal applications. The test results showed no sign of any serious problem to the rotor at the engine operating condition.

The oscillating flow generated by the wavy surface in the rotor cavity may cause potential instability of the bristles if the seals are not designed properly. By locating the brush seals behind honeycomb seal teeth and properly designing the seal stiffness, stable brush seals can be achieved at the locations.

Technology Application

The results of this task will be used to specify requirements and characteristics for brush seals to be installed in the 3rd stage diaphragm of the 7H turbine so that it can be tested during a no-load pre-shipment test of the full scale machine.

Section 2.2.4.15 (GTMTAR) Airfoil Repair [S]

Objective

Existing techniques were evaluated and adapted for the material/geometry combinations unique to the ATS turbine airfoils to extend component life.

Introduction/Background

Advanced high strength nickel base superalloys selected for turbine airfoils are inherently difficult to weld. Conventional salvage techniques used on production airfoils are not viable for steam cooled components. This task explored potential repair techniques and other opportunities to leverage advances in superalloy joining.

Discussion

An extensive analysis was made of the current GE airfoil repair processes and their applicability to ATS components. In particular, efforts were launched to pursue repair of single crystal alloys. Both diffusion and fusion methods were considered, with feasibility studies and property tests conducted for single crystal alloy N5. Potential repair methods for directionally solidified and equiaxed materials used on the steam cooled components were also identified.

When airfoil casting results and airfoil fabrication manufacturing methods were in place, airfoil repair needs for the 7H and 9H hardware were more clearly identified. Braze-type repairs in low stress areas of components and weld repair of more highly stressed locations were implemented in a few select components and locations. Much of the repair needs were driven by defects in the investment castings which were uncovered during post-cast joining and machining operations. All repairs for FSNL hardware were documented so an understanding of repair performance during component testing could be made.

Summary/Conclusion

A few specific airfoils repair techniques were developed and used on 9H and 7H hardware. These represented material salvage opportunities, and have been successful in FSNL testing conducted to date. These techniques can also be leveraged for post-service repair needs identified in the future to enhance life cycle cost of the components.

Technology Application

Repair processes applied to components will make them cost effective for commercial operation.

Section 2.2.5 (GTTT) Thermal Barrier Coating Technology [S]

Section 2.2.5.1 (GTTTSD) Coating System Development [S]

Objective

Thermal Barrier Coating (TBC) coating deposition processes were developed for specific ATS turbine and combustor components. Computer simulations, motion trials on part replicas and spray trials on parts were used for improving robot path planning accuracy. Coating evaluations consisted of metallography, properties measurements, and thermal cycling exposure tests. Improved process monitoring were developed to increase process repeatability and control.

The TBC Manufacturing Technologies portion of the task focused on integration and compatibility between TBC processing and other component manufacturing steps. Techniques to prepare components for spraying were defined. Fixturing and masking, surface finishing techniques, drilling or masking of cooling holes, and methods to protect instrumentation were developed as required.

The TBC Process and Diagnostics portion of the task focused on improving GE's fundamental understanding of the TBC deposition processes. Evaluation of alternative plasma spray guns to the Metco 7MB were performed. As part of this evaluation, specific process conditions critical to meeting the coating thickness and properties requirements on ATS components were studied. Continuing work identified the controlling process parameters for the ceramic top coat and metallic bond coat; i.e., those parameters which most strongly influence process variation and TBC quality.

The TBC Non-destructive Evaluation (NDE) portion of the task developed techniques to measure attributes and properties of TBCs on turbine hardware that are relevant to manufacturing and service. The primary focus was on development of methods to measure coating thickness. A secondary focus was on development of methods to evaluate coating adhesion and microstructure.

Introduction/Background

Yttria-Stabilized Zirconia (YSZ) TBC top coat, deposited by the Air Plasma Spray (APS) process, was selected at the start of the ATS program; for reasons of process flexibility and low capital cost of manufacturing equipment. Figure 2.2.5.1-1 shows the principal variations in YSZ coating microstructure that can be achieved by various deposition processes. Conventional APS processes produce the TBC microstructure shown in the left-hand photo in Figure 2.2.5.1-1. This type of TBC, although widely used on combustion hardware in other GE gas turbines, was not considered to be durable enough for use on ATS turbine and combustor components. TBC deposited using Electron Beam Physical Vapor Deposition (EB-PVD), shown in the center photo in Figure 2.2.5.1-1, is extremely durable due to a highly columnar microstructure. This TBC is widely used on aircraft engine components, but is difficult to apply uniformly to large and complex components, particularly turbine nozzles.

GE developed the process for depositing "Dense Vertically Cracked" or "DVC" TBC, shown in the right-hand photo in Figure 2.2.5.1-1, on turbine shrouds prior to the start of the ATS program. This TBC is deposited using an advanced APS process that was invented and patented by GECRD. The main goal for the ATS program was to develop methods to deposit this DVC TBC on the ATS turbine and combustor components.

Discussion

Robotics Motion Control and Programming Methods for ATS Turbine Airfoils

The ATS turbine buckets and nozzles require simultaneous movement of the spray tool and part motion to properly access all part surfaces and satisfy the coating process requirements for surface velocity, standoff distance, and spray angle. The robotic manipulation scheme is shown in Figure 2.2.5.1-2. Four on-line methods for robotics motion control and programming were developed and evaluated. The first two methods are based on FANUC Robotics products called Teach Pendant (TP) and Karel programming. These two approaches are forms of Tool Center Point (TCP) motion control, and require stationary targets in order to define motion paths along the part surface. These two approaches were shown to be inadequate for coating ATS turbine buckets and nozzles, due primarily to the geometric complexity of these parts.

The other two robotics motion programming methods are forms of Inverse Time (IT), which accounts for simultaneous movement of the spray tool and part motion. The first is a FANUC Robotics product called Segment Time Programming (STP), which utilizes the built-in path planning capabilities of the RJ2 controller. The second is a custom form of IT developed for GE by FANUC Robotics. Both STP and IT were shown to have acceptable motion control performance for coating ATS turbine buckets and nozzles. STP motion control/programming is preferred because it is a standard product from FANUC Robotics and is fully supported in industry.

Two off-line software tools were also developed, primarily for robotics motion modeling and simulation, although they are capable of being used for robotics motion programming as well. The first system is a Tecnomatix product called ROBCAD™, which supports full 3D modeling of robotics motion, with capabilities for detecting motion limits (position and velocity) and gun-part collisions. The standard ROBCAD product supports TP and Karel motion programming (TCP motion only). ROBCAD development for GE focused on integration of IT modeling capabilities, based on FANUC Robotics STP control. The primary robotics programming package being used for coating ATS turbine buckets and nozzles is a hybrid ROBCAD/STP software tool.

The second programming approach utilizes a custom product developed by GECRD, called Coordination through Short Motion Programming (CSMP). CSMP takes into account the robotics system capabilities for motion position, velocity, and acceleration; is based on equipment characterization studies performed at GECRD; and can be used to model robotics motion based on the TP, Karel, STP, and IT programming approaches. The CSMP model incorporates the measured performance limits for the M710i/RJ2

robotics system, including motion dynamics for each axis (position, velocity, and acceleration limits). The M710i/RJ2 has performed very systematically and gave excellent agreement with the CSMP model. Experiments performed included both constant and variable speed motions on a 2D airfoil replica shape and a pre-production ATS turbine nozzle. Coating process requirements were met or exceeded in nearly all tests. Version 1.0 of the CSMP-ROBCAD Advisor software was delivered to GEPS, which is used as an off-line tool for checking robot motions programmed using ROBCAD/STP.

GE's Six-Sigma process tools and methods have been extensively leveraged in the ATS program. The major thrust of this effort involved identifying and controlling the sources of process variation. A filter to correct the robot paths for the effects of variation in true part position, due to part-to-part dimensional variation and part-fixture alignment variation, was developed by GECRD. An off-line simulation tool to predict coating thickness and microstructure distributions on ATS turbine parts is being developed by GECRD in collaboration with several universities. Development began by using a GECRD-developed software tool used to predict the thickness distributions of metallic overlay coatings applied to turbine buckets using the Vacuum Plasma Spray (VPS) process. The VPS process requires only two degrees of freedom, whereas the Air Plasma Spray (APS) process used for coating ATS turbine buckets and nozzles requires at least seven degrees of freedom. The new tool is needed to further reduce the cycle for developing robotics motions, improve powder deposition efficiency, and achieve more uniform coating thickness and properties distributions. Additional use of Six-Sigma process tools is discussed in the TBC Process and Diagnostics section.

Eleven GE thermal spray cells are capable of coating ATS turbine buckets and nozzles using FANUC Robotics M710i/RJ2 systems. There are plans for an additional fifteen installations by 2001, which will bring the total number of GE thermal spray cells capable of coating ATS airfoils to 26, located worldwide. As part of this initiative, standards for thermal spray and advanced robotics systems have been established; including installation, calibration, and programming. A robotics users group was established within GE to assure that process transfer among the different cells can be readily accomplished, as well as facilitate sharing of TBC manufacturing best practices throughout GE. The users group also includes representatives from FANUC Robotics and Dynalog, Inc.

Other ATS program development efforts involved increasing manufacturing productivity. Robotics alignment and calibration times were reduced by a factor of four using the new DynaCal™ System from Dynalog, Inc. The thermal spray cell configuration included a six-axis robot and two-axis turntable, which were optimized for coating turbine buckets, nozzles and shrouds, but were sub-optimal for coating combustor liners and transition pieces due to physical space limitations. Coating these parts required only the six-axis robot, and was accomplished in the current spray cells when the turntable was removed. A unique interface was developed jointly by GE and FANUC Robotics, which enabled the robotics system to operate in this configuration.

Coating Processes for ATS Components

Air Plasma Spray (APS) and High Velocity Oxy-Fuel (HVOF) coating processes were developed and qualified for deposition of TBC on the following ATS components:

- Stage One Nozzle
- Stage Two Nozzle
- Stage One Bucket
- Stage Two Bucket
- Stage One Shroud
- Stage Two Shroud
- Combustor Liner
- Transition Piece

The APS process was used for the TBC top coats, while both the APS and HVOF processes were used for the TBC bond coats, as discussed below. The deposition of top coat on the ATS stage one nozzle at GECRD is shown in Figure 2.2.5.1-3. The coated stage one nozzle is shown in Figure 2.2.5.1-.4. Associated manufacturing processes and Non-destructive Evaluation (NDE) methods were also developed, as described in subsequent sections.

Bond Coat Processes

A variety of candidate bond coat materials and processes were evaluated for ATS turbine and combustor components. The bond coat must perform several functions: provide an adherent layer for the ceramic top coat, as well as provide protection to the substrate alloy against the effects of oxidation and, possibly, hot corrosion. Specifications were written for one-layer bond coats applied using the Vacuum Plasma Spray (VPS) and High Velocity Oxy-Fuel (HVOF) processes, and two-layer bond coats applied using the HVOF and Air Plasma Spray (APS) processes.

One-layer NiCrAlY bond coats applied by APS provided excellent TBC adherence and thermal cycling performance, and were used extensively on the first production ATS turbine airfoils and transition pieces. However, this bond coat is relatively porous, and therefore, not sufficiently protective to most substrate alloys to meet full ATS component life requirements. Therefore, two-layer bond coats are being considered for future ATS part generations. Both thermal spray (APS, HVOF) and braze-Infiltrated APS (IAPS) NiCrAlY bond coats will continue to be evaluated using furnace cycling and oxidation burner rig exposure testing, as well as rainbow testing in commercial gas turbines.

Two types of IAPS coatings were developed: Type 1 coatings are brazed oxidation barriers applied to the alloy substrate, followed by APS bond coat and TBC. Type 2 coatings are mixtures of braze and bond coat alloy co-sprayed by APS, followed by TBC. Improvements in thermal cycling life of up to 5X over the single-layer APS bond coat have been shown for some substrate alloys. However, IAPS bond coats have not been

previously used by GE on turbine or combustor components, so the long-term effects upon the substrate alloys are being thoroughly evaluated.

A new HVOF spray gun was implemented in manufacturing, requiring modifications to the spray process developed for some ATS components. Design of experiments and other six sigma tools were utilized to generate transfer functions between critical spray parameters and coating performance.

Coatings for CMAS Mitigation (development was conducted under non-ATS programs)

TBC protective coatings were developed to extend turbine service conditions beyond those currently allowable by improving the resistance of TBC to deposits of Calcium-Magnesium-Aluminum-Silicate (CMAS). An optimized multi-layer coating system deposited by Chemical Vapor Deposition (CVD) was developed. Long-term durability testing was performed using a combustion thermal gradient test rig. An improvement in TBC life of greater than 50X compared to unprotected TBC was demonstrated at conditions more severe than the ATS gas turbine requirements.

A pilot CVD coating reactor, shown in Figure 2.2.5.1-5, was installed at GECRD to coat ATS nozzles for cascade testing. ATS stage one nozzles with and without CMAS protective coating are shown in Figure 2.2.5.1-6.

TBC Manufacturing Technologies:

Manufacturing procedures for each ATS component were established; which include Manufacturing Process Plans (MPPs), Operations Methods, Quality Data Collection (QDC), Non-Destructive Testing (NDT) operations, and Final Audit. Local TBC repair procedures were developed and qualified. APS coating processes were developed for applying bond coat and top coat to the welded joint of the ATS stage two nozzle doublets. Techniques were developed for masking cooling holes in ATS turbine airfoils, as well as removal of excess coating from unmasked cooling holes. Techniques were developed to deposit coatings over instrumentation (thermocouples, strain gages).

The first production ATS turbine airfoils were surface finished using manual abrasive polishing methods. However, these methods are not capable of maintaining final coating thickness within the limits required on full-life ATS components. Conventional finishing techniques, such as tumbling and grit blasting, were also not acceptable because coating thickness uniformity cannot be maintained due to varying coating removal rates at locations such as fillets and leading edges of airfoils.

Continuous numeric control (CNC) grinding methods were developed by GE and Huffman Corp. to ensure both acceptable surface finish and uniform material removal over all regions of the ATS airfoils, fillets, sidewalls (nozzles), and platforms (buckets). The apparatus consisted of a modified Huffman 6-Axis grinder with an integrated coordinate measuring machine (CMM), GE diamond grinding wheels, and a GE eddy current system for on-line TBC thickness measurements. The process steps for using CNC grinding to create the desired ceramic top coat thickness profiles on ATS turbine components are shown in Figure 2.2.5.1-7. The as-sprayed coating thickness distribution is determined using Eddy Current (EC) measurements in combination with CMM Touch Probe (TP) measurements, which is required for acceptable control of the final coating

thickness. Software for integrating these data was developed by GECRD and provided to Huffman. Gage Repeatability and Reproducibility (R&R) studies were satisfactorily performed for both the EC and TP measurement systems.

TBC Process and Diagnostics

The TAFA Plazjet gun was selected for the next generation TBC process. This gun has the capability of achieving similar or better TBC properties than the Metco 7MB gun at longer standoff distances and up to 5X higher powder injection rates. Plazjet guns were installed in eight GE spray cells, and will be used for development and production of the next generation of ATS turbine components. A new spray process for this gun was developed by GECRD and successfully transitioned to manufacturing, resulting in improved TBC thickness and surface finish, as well as reductions in process cycle time of nearly 3X for F-class gas turbine components, which are now in volume production.

The Plazjet spray process development was greatly accelerated by leveraging several process diagnostic tools developed by GECRD during a recently concluded Advanced Technology Program sponsored by NIST. The program was conducted under the Intelligent Processing of Materials (IPM) banner, and focused on development of a closed-loop plasma spray controller. The basic approach used is shown in Figure 2.2.5.1-8; process sensors were developed for measuring key deposition process conditions, which can ultimately be used to control the plasma spray process via the controller. Three-sigma improvements in process capability for several key TBC mechanical properties were demonstrated on flat plates sprayed during the IPM program. The technology was demonstrated in 2000 on production turbine components.

A comprehensive TBC process/properties database was accumulated under both the ATS and IPM programs; including tensile strength, modulus, deposition rate, thermal conductivity, surface roughness, and furnace cycle life. Regression models to predict TBC properties, including both mean and standard deviation, from the controlling process parameters are now being developed as part of the GE "Design for Six Sigma" (DFSS) initiative. The core of the DFSS initiative is the quality flowdown and flowup, as shown in Figure 2.2.5.1-9. Additionally, a TBC thermal conductivity model will be developed through a two year collaborative effort with NIST, which began in the first quarter 2000.

GECRD is an industrial member of the Thermal Spray Consortium at the University of Toronto, which is developing transfer functions to predict TBC microstructure evolution using advanced experimental, numerical and statistical methodologies. Simulation software developed by the consortium will be beta tested by GECRD in 2000.

Non-destructive Measurement of TBC Thickness:

An automated ceramic coating thickness measurement system was developed, consisting of a flexible Eddy Current (EC) probe in combination with a three- or four-axis CMM. Several hundred inspection points can be measured in under fifteen minutes, which reduces inspection time by over 5X compared to manual measurements. The measurement software is capable of automatic archiving of data into the Quality Data Collection (QDC) system used by gas turbine manufacturing in Greenville.

Reference EC specimens were manufactured, which include bond coats and substrates for all ATS turbine buckets and nozzles. An improved flexible EC probe was recently developed, both to reduce cost and improve durability. A probe contact simulator, consisting of a single axis actuator with a servo controller, was developed in order to test probe life. An improvement in probe life by a factor of 20X was demonstrated.

A six-axis CMM system was constructed, which is capable of both on- and off-line programming via PC-DMIS. This system allows for development and simulation of the measurement process directly from CAD files (UG, IGES, etc.) without using actual parts or fixtures. PC-DMIS also supports reverse engineering of complex shapes, such as the ATS turbine buckets and nozzles.

Non-destructive Evaluation of TBC Adhesion:

Several Non-destructive Evaluation (NDE) techniques were developed for determination of coating adhesion and mechanical integrity. Infrared (IR) thermal imaging can be used to detect separation of one coating layer from another, or from the substrate; i.e., coating delamination. The basic technique uses the principle of measuring the temperature change at the coating surface following heating using a thermal source. The rate of temperature change is controlled by heat conduction, which depends on the thermal mass and diffusivity of the coating and underlying substrate, as well as the contact resistance between the coating and the substrate. When a coating delamination is present, the contact resistance is very high, and the coating above the delamination cools more slowly due to reduced heat conduction than does a well adhered coating.

The Laser Ultrasound Test (LUT) was developed to evaluate TBC adhesion in a different way from IR. A Nd:YAG laser is used to produce a shaped source beam on the target coated part, generating an ultrasonic Lamb wave that propagates almost completely within the ceramic top coat. A laser interferometer senses the propagating wave signal, which is stored on a computer and analyzed for frequency dispersion content; i.e., ultrasonic velocity as a function of frequency. Young's modulus and tensile properties are extracted from the measured signal, which correlate very well with destructive data from coupon tests. This technique can be used to distinguish strongly adhered coatings from coatings that are weakly adhered or delaminated. As such, it is a more powerful inspection technique than IR thermal imaging. However, the propagating ultrasonic wave can be strongly attenuated by the vertical crack network in the DVC TBC, reducing signal-to-noise ratio and inspection sensitivity, as described below.

The ATS Cascade Nozzles, (used in the GEAE-Evendale test rig), as well as production buckets and thermo-mechanical fatigue test specimens, were extensively evaluated to validate and refine the LUT correlations. However, some of the microstructural variation present on the components resulted in loss of signal due to attenuation, as well as a different transfer function from that obtained on the coupons. As a result of these inconsistencies, software for coating "fingerprint" evaluation was developed. This software compares the LUT signature for an unknown coating with a database of signatures from coatings of different microstructures. The signature that most closely matches the unknown coating is selected from the database, resulting in predictive accuracy for coating tensile strength of 10-20%.

Discussions were held with two universities (University of Connecticut, University of California-Santa Barbara) developing laser fluorescence "piezospectroscopy" as a possible technique for coating evaluation. These universities are funded under the Advanced Gas Turbine Systems Research (AGTSR) program. Collaborative research and development between GECRD and these universities could be performed under appropriate terms and conditions, outside the scope of the AGTSR contracts.

Summary/Conclusions

Thermal Barrier Coating (TBC) coating deposition processes were developed for specific ATS turbine and combustor components. Computer simulations, motion trials on part replicas and spray trials on parts were used for improving robot path planning accuracy. Coating evaluations consisted of metallography, properties measurements, and thermal cycling exposure tests. Improved process monitoring were developed to increase process repeatability and control.

The TBC Manufacturing Technologies portion of the task developed techniques to prepare components for spraying. Fixturing and masking, surface finishing techniques, drilling or masking of cooling holes, and methods to protect instrumentation were developed.

The TBC Process and Diagnostics portion of the task focused on improving GE's fundamental understanding of the TBC deposition processes, evaluation of alternative plasma spray guns to the Metco 7MB. As part of this evaluation, specific process conditions critical to meeting the coating thickness and properties requirements on ATS components were studied.

The TBC Non-destructive Evaluation (NDE) portion of the task developed techniques to measure attributes and properties of TBCs on turbine hardware that are relevant to manufacturing and service. The primary focus was on development of methods to measure coating thickness, with a secondary focus on development of methods to evaluate coating adhesion and microstructure.

Technology Application

The process for applying air plasma spray TBC to ATS turbine and combustor components was defined. This process defined the baseline upon which coating durability would be evaluated, and evolutionary improvements would be made.

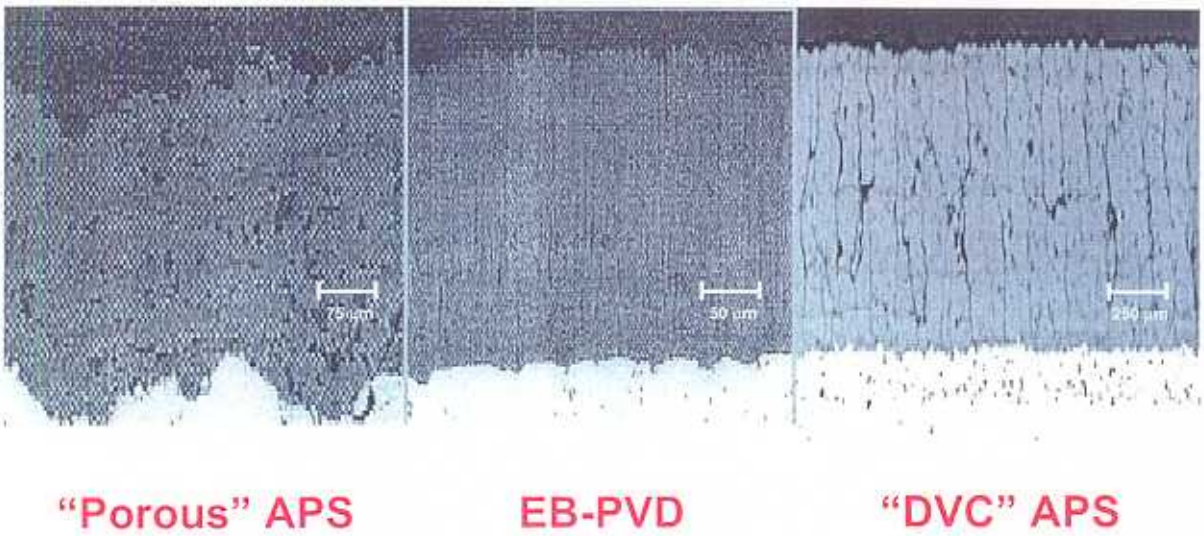

Figure 2.2.5.1-1. Thermal Barrier Coating Microstructures

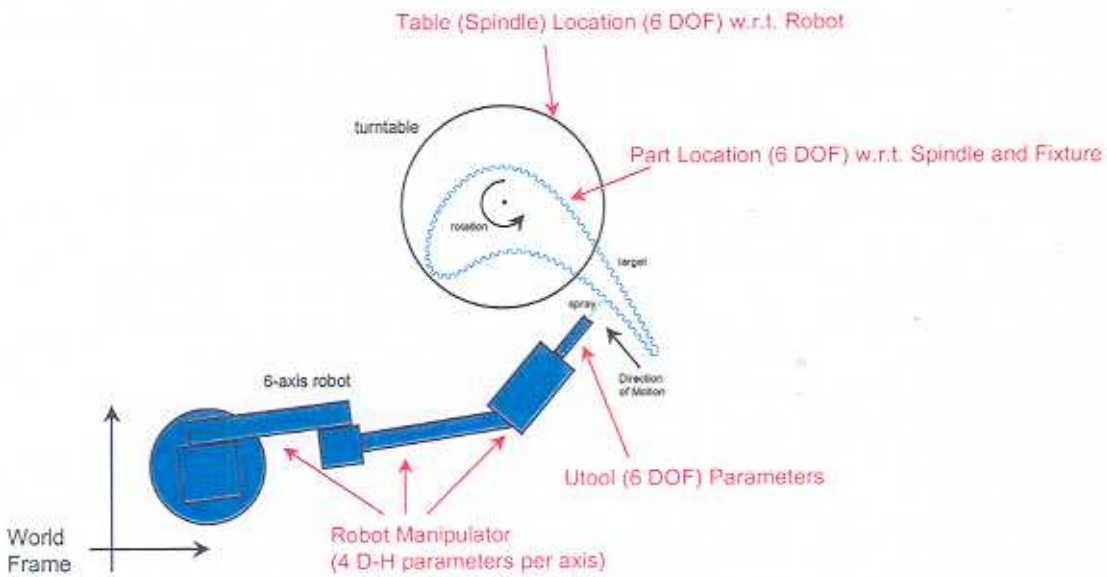

Figure 2.2.5.1-2. Robotic Manipulation Scheme for Coating Advanced Turbine Systems Components

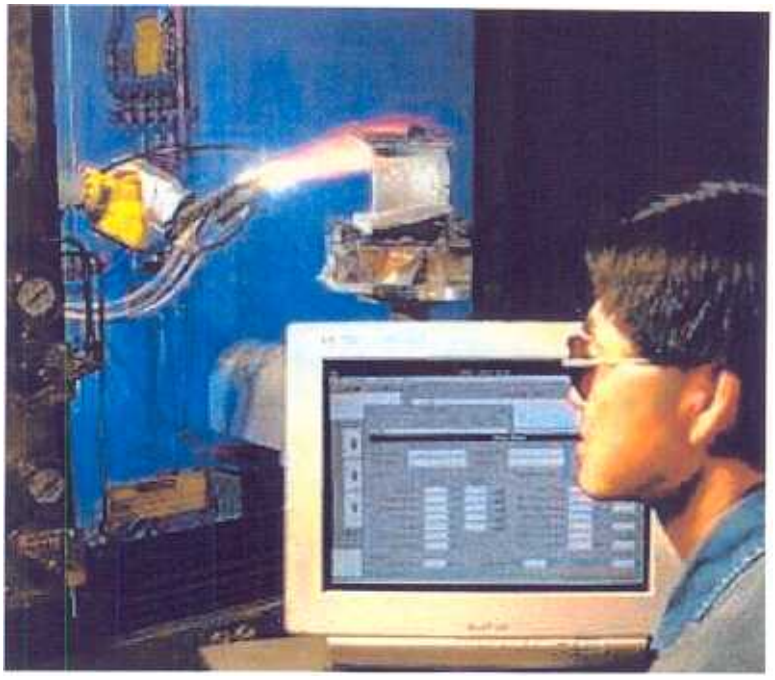

Figure 2.2.5.1-3. Deposition of Thermal Barrier Coating on the ATS Stage One Nozzle at GE-CRD

Figure 2.2.5.1-4. ATS Stage One Nozzle After Deposition of Thermal Barrier Coating

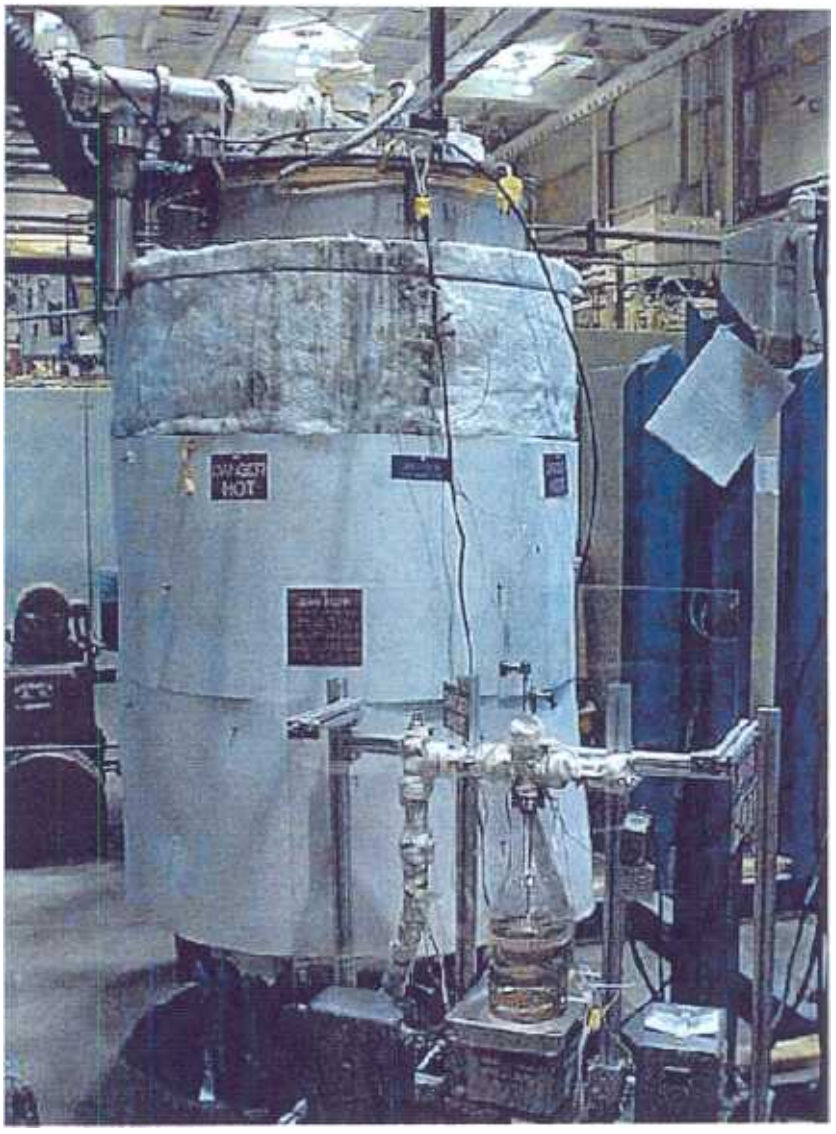

Figure 2.2.5.1-5. Reactor for Depositing CMAS Protective Coating at GE-CRD

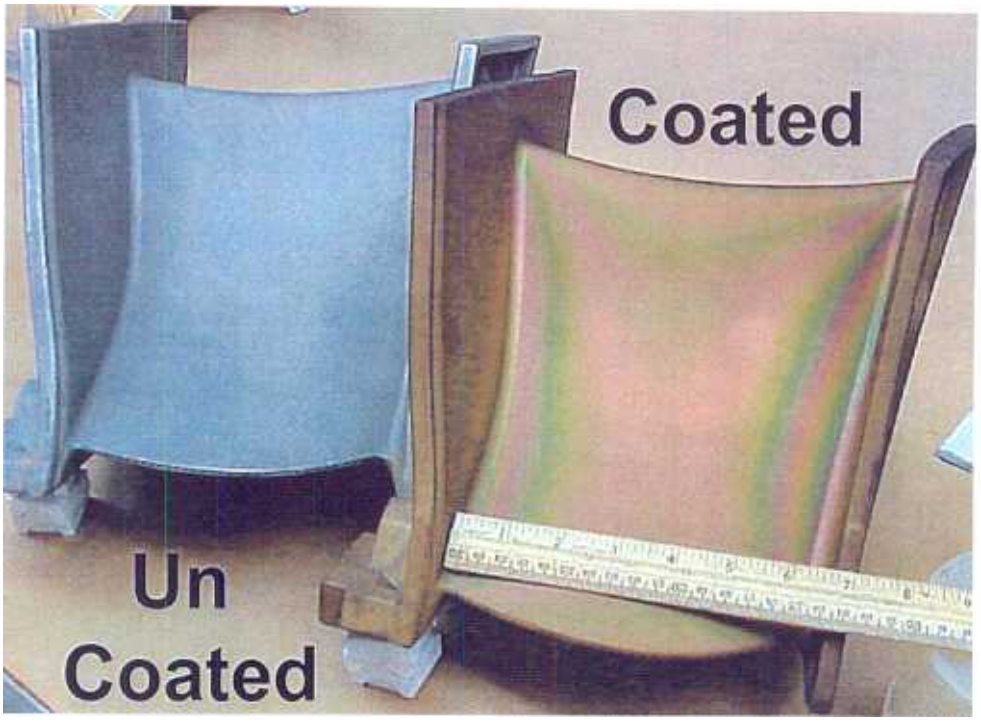

Figure 2.2.5.1-6. ATS Stage One Nozzle Before and After Deposition of CMAS Protective Coating

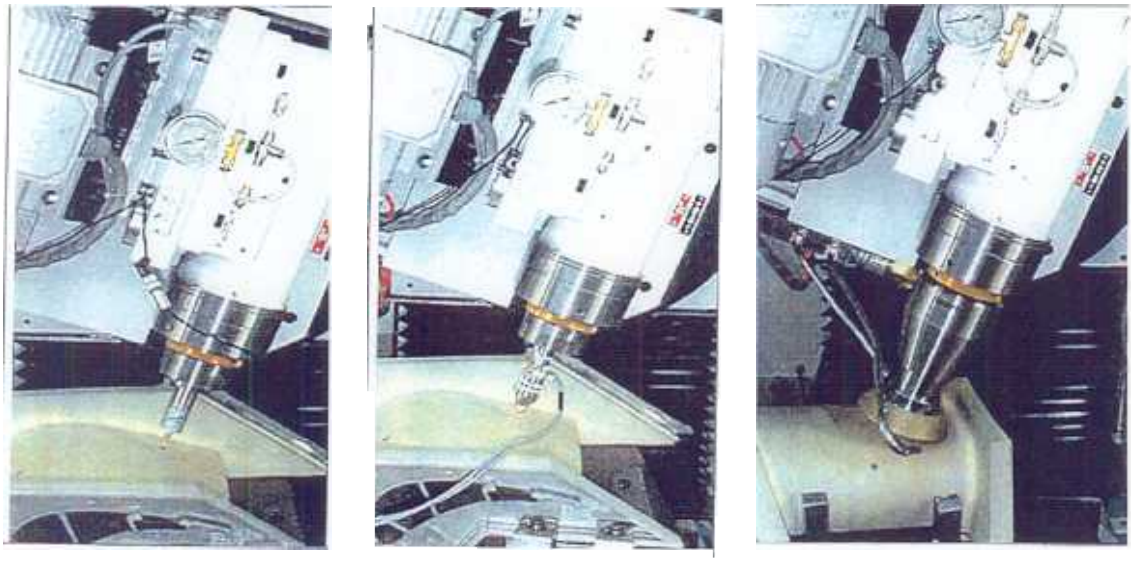

CMM probing for initial surface | **EC probing for ceramic thickness** | **CNC grinding to desired ceramic thickness**

Figure 2.2.5.1-7. Process Steps for Using CNC Grinding to Create the Desired Ceramic Coating Thickness Profiles on ATS Turbine Components

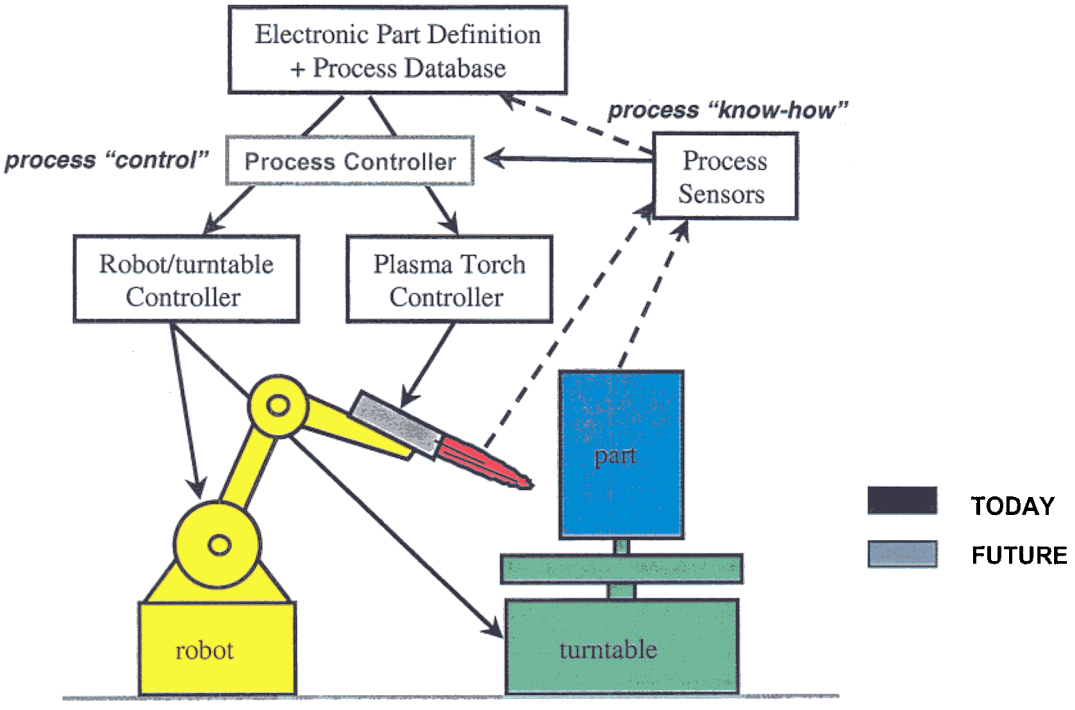

Figure 2.2.5.1-8. Control of Air Plasma Deposition Process for Thermal Barrier Coating

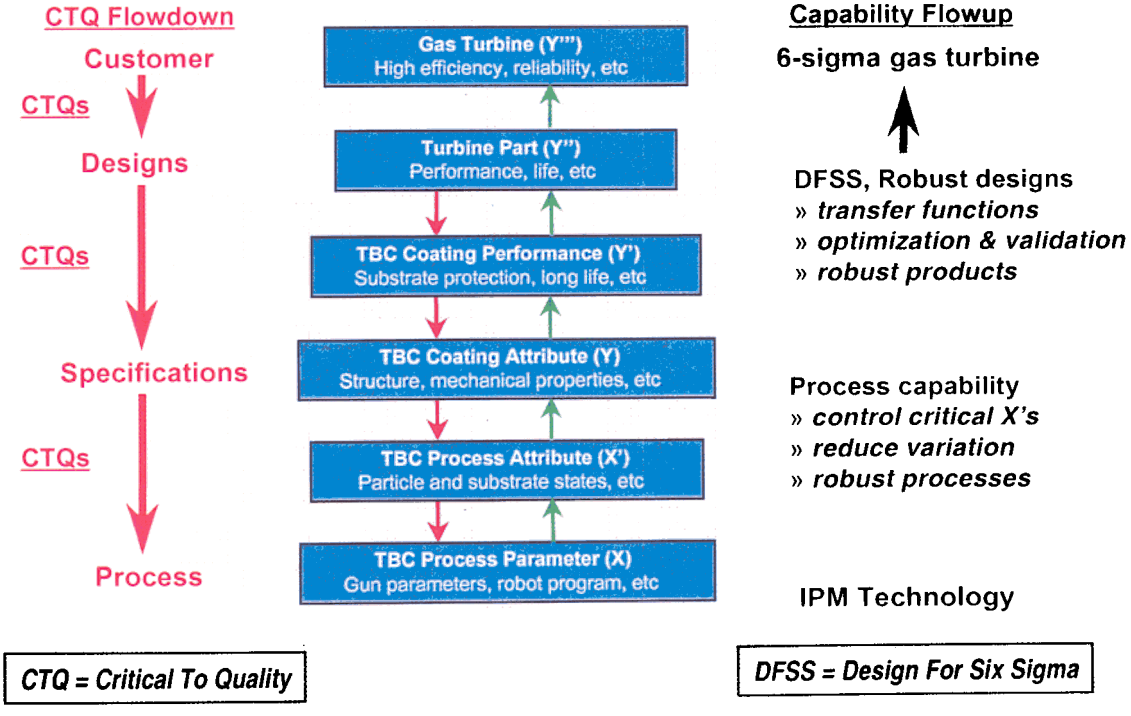

Figure 2.2.5.1-9. Quality Flowdown and Flowup as Applied to Development of Thermal Barrier Coating for the Advanced Turbine System

Section 2.2.5.1.1 (GTTTSD) Effects of TBC Surface Finish on Drag [C]

Objective

TBC coatings are used on the nozzles and buckets in the H turbine. Current TBC surface finish specifications call for polishing the TBC coatings from an as-applied finish (approximately 400 micro-inches) down to 60 micro-inches in order to reduce aerodynamic drag. The current specification of 60 micro-inches is based on design practices with metallic surfaces. Polished TBC surface finishes are physically different from machined metallic finishes, however, and there are no data that relate TBC surface finishes to the aerodynamic drag they produce. Polishing TBC-coated surfaces down to 60 micro-inches is both challenging and costly and may not be necessary. This task will experimentally determine the effect that TBC surface finish has on drag so that an informed, appropriate surface finish specification can be established.

Introduction/Background

As discussed in the Objective above, this task experimentally determined the effect that TBC surface finish had on drag so that an informed, appropriate surface finish specification could be established.

Discussion

Note: Testing was funded under an internal GE (non-ATS) program, and results are reported to maintain continuity in the overall H-technology program.

Wind tunnel airfoil drag testing of the smooth airfoil was completed. The airfoil TBC spray fixture was designed and built. The airfoil TBC spray coating path programming was completed. The airfoil was coated with TBC at a new GEPS coating facility in Schenectady, NY. Due to start-up problems in the new facility, delays were encountered in spraying the airfoil. Coating quality was closely controlled so that the coating was equal to production bucket coatings in terms of thickness and roughness pattern. Wind tunnel testing of the rough, as sprayed, airfoil was then completed.

Due to unavoidable delays in the coating process, no additional tests were run in year 2000. As noted above, the funding for this program came from an internal GE (non-ATS) source. As of this writing, work in 2001 has not been authorized, and testing has been halted. Efforts are being made to obtain authorization to continue the work as defined in the objectives.

Summary/Conclusion

Wind tunnel airfoil drag testing of the smooth airfoil was completed. The airfoil was then coated with TBC, and run in the wind tunnel. Data analysis has not been completed, so no final determination has been made for the TBC surface finish requirement.

Technology Application

The results of this test will provide data for determining a surface finish design specification for TBC-coated turbine nozzles and buckets. The data can be also be used to calculate tradeoffs of finishing costs and turbine efficiency.

Section 2.2.5.2 (GTTTRR) TBC Risk Reduction [S]

Objective

TBC durability was evaluated under conditions very similar to the surface temperature, thermal gradient, and stress state of TBCs on ATS gas turbine components. An electron-beam rig capable of inducing high thermal gradients was used to assess the relative durability of various TBCs, and the controlling mechanisms of TBC failure were characterized. TBCs with a spectrum of microstructures were tested. The effects of Calcium-Magnesium-Aluminum-Silicate (CMAS) environmental contaminant on TBC performance in high thermal gradient conditions was investigated. Numerical modeling was used to determine the stress, strain, and thermal gradient conditions in the various TBCs during the tests.
TBC-coated nozzles tested in the ATS Turbine Nozzle Cascade rig at GEAE-Evendale, were evaluated following completion of cascade testing.

Introduction/Background

TBCs provide essential insulation and protection of the metal substrate from high temperature combustion gases. It is essential that the TBC be able to remain intact for engine operation between planned overhauls. TBC durability is an important consideration in the development of any TBC coating system.

Discussion

Electron-Beam High Thermal Gradient Tests

A 25-kW electron beam high thermal gradient apparatus was constructed by GE-CRD to simulate the temperature, temperature gradient, and stress conditions on limiting regions of the steam-cooled ATS turbine components. The electron beam's power was controlled by the TBC surface temperature, as measured using an Infrared (IR) optical pyrometer. The test apparatus is shown in Figure 2.2.5.2-1. The following studies were conducted:

A) Flat tophat specimens (bare)

The flat "tophat" specimen was designed to simulate the thermal and mechanical stress conditions in the TBC near critical "high-C" region of the ATS stage one turbine nozzle. This specimen and its mounting arrangement in the test rig are shown in Figure 2.2.5.2-2. No TBC damage was observed and no systematic decrease in TBC mechanical properties was measured following testing for 100 hours, 2500 cycles at full ATS conditions. This was the case for unaged tophats as well as for tophats that were furnace aged to 50% and 75% of expected ATS TBC life.

TBC degradation during this testing was evaluated by comparing the microstructure and compressive-shear failure strains between hot and cold regions of the tested tophats. No systematic difference in TBC horizontal cracking, bond coat oxide thickness or TBC residual strain to failure was observed between the hot and cold sections of the tophats. In addition, no systematic difference in TBC residual strain to failure was measured between tophats with different pre-test furnace aging.

B) Flat Tophat specimens (CMAS)

Two CMAS-coated flat tophats were tested under conditions that produced partial CMAS infiltration into the TBC. In the first test, no TBC spallation occurred after 87 two-minute cycles, although melting and infiltration of CMAS was confirmed by destructive evaluation. However, TBC spallation occurred in the second test after only 22 cycles. It is believed that the IR emissivity of the TBC changed considerably during CMAS infiltration, which may explain the difference in results between the two tests.

C) Fillet Tophat specimens

One fillet tophat was tested under full ATS conditions for 2500 cycles. The sample was designed to simulate the thermal and mechanical stress conditions in the TBC near the critical fillet region of the ATS stage one turbine nozzle. The TBC was machined to produce a uniform thickness in the fillet region. No spalls or hot spots were observed during the testing; however, the TBC top surface ran hotter and the metal ran colder than expected due to increased thermal resistance of the coatings in the fillet, as discussed below.

Thermal conductivity measurements of the free-standing bond coat and top coat removed from this fillet tophat were performed. The thermal conductivity of both the bond coat and top coat were each approximately 25% lower than that of the same coatings applied to planar samples. The higher thermal resistance is caused by high coating porosity and poor splat-to-splat bonding, which are caused by geometric effects that adversely affect the spray process.

Cascade Nozzle Evaluations

Destructive and non-destructive evaluations were performed on four nozzles coated in an identical manner: UN004 (untested), HT14 (heat transfer test – no spalling observed), LCF47 (low cycle fatigue testing – TBC spall at leading edge) and LCF50 (low cycle fatigue test – TBC spall at leading edge).

Approximately 80 specimens were removed from each of the four nozzles using waterjet cutting. Mechanical properties were measured from three regions of the nozzles: convex side, concave side, and leading edge. Thermal conductivity measurements are described in a separate section. Four mechanical properties were characterized: tensile strength (mechanical test), tensile strength (transfer function from image analysis), compressive shear (mechanical test), and in-plane modulus (transfer function from image analysis). Significant degradation of the mechanical properties of the unspalled TBC on nozzles HT14, LCF47 and LCF50 was confirmed by these tests.

Laser Ultrasound Test (LUT) measurements were taken at each specimen location before the nozzles were sectioned. The untested nozzle was scanned non-destructively using both LUT and IR thermal imaging.

Summary/Conclusion

TBC durability was evaluated under conditions very similar to the surface temperature, thermal gradient, and stress state of TBCs on ATS gas turbine components using an electron-beam rig capable of inducing high thermal gradients. The effects of Calcium-Magnesium-Aluminum-Silicate (CMAS) environmental contaminant on TBC performance in high thermal gradient conditions was investigated. Numerical modeling was used to determine the stress, strain, and thermal gradient conditions in the various TBCs during the tests.

TBC-coated nozzles tested in the ATS Turbine Nozzle Cascade rig at GEAE-Evendale, were evaluated following completion of cascade testing.

Technology Application

Durability of the baseline TBC system in an environment simulating that of the ATS turbine will be evaluated. These results will establish confidence that the TBC will provide acceptable minimum durability for safe and reliable operation of the ATS turbine within the time frame of the first inspection interval.

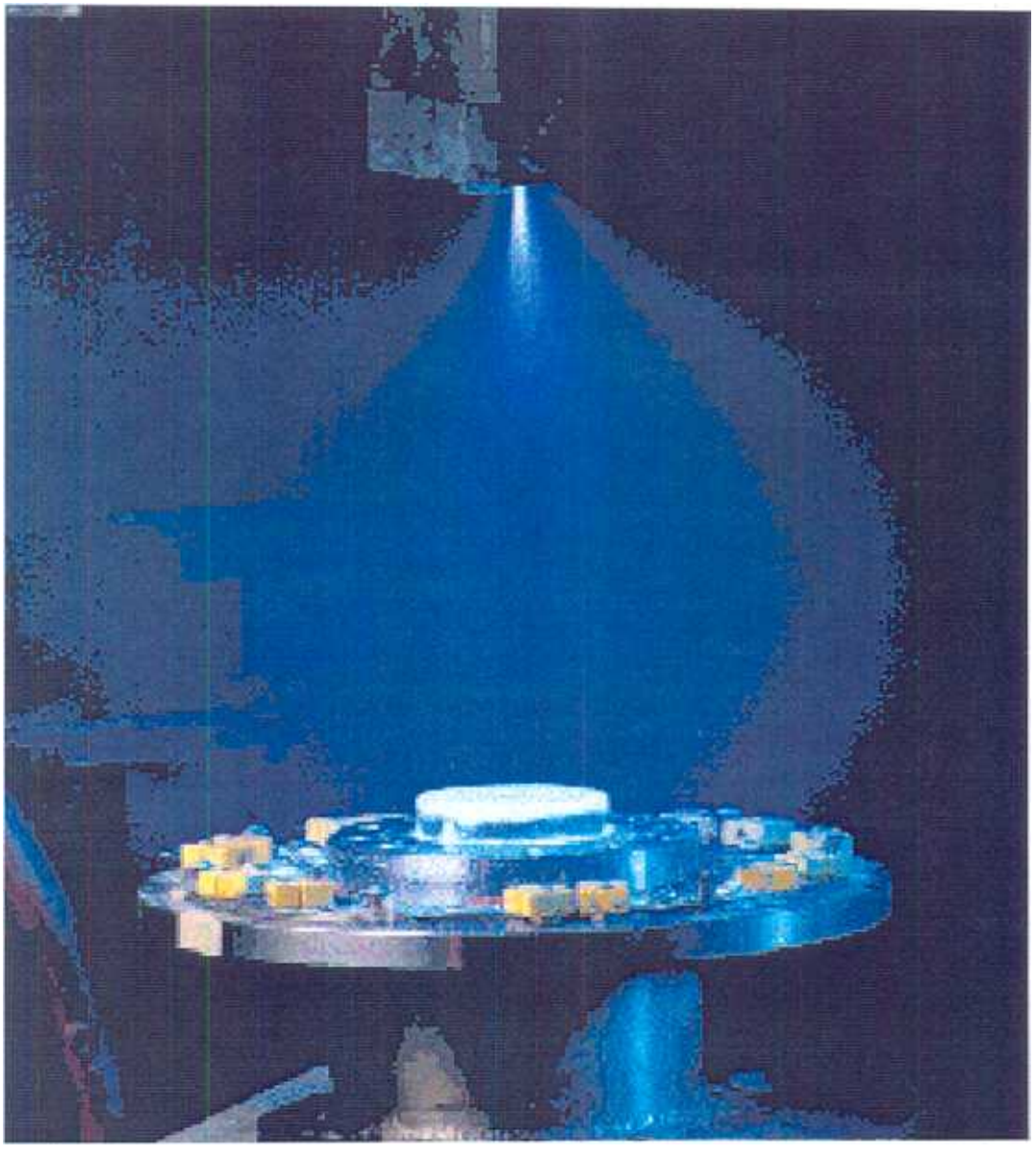

Figure 2.2.5.2-1. Electron Beam High Thermal Gradient Test Rig

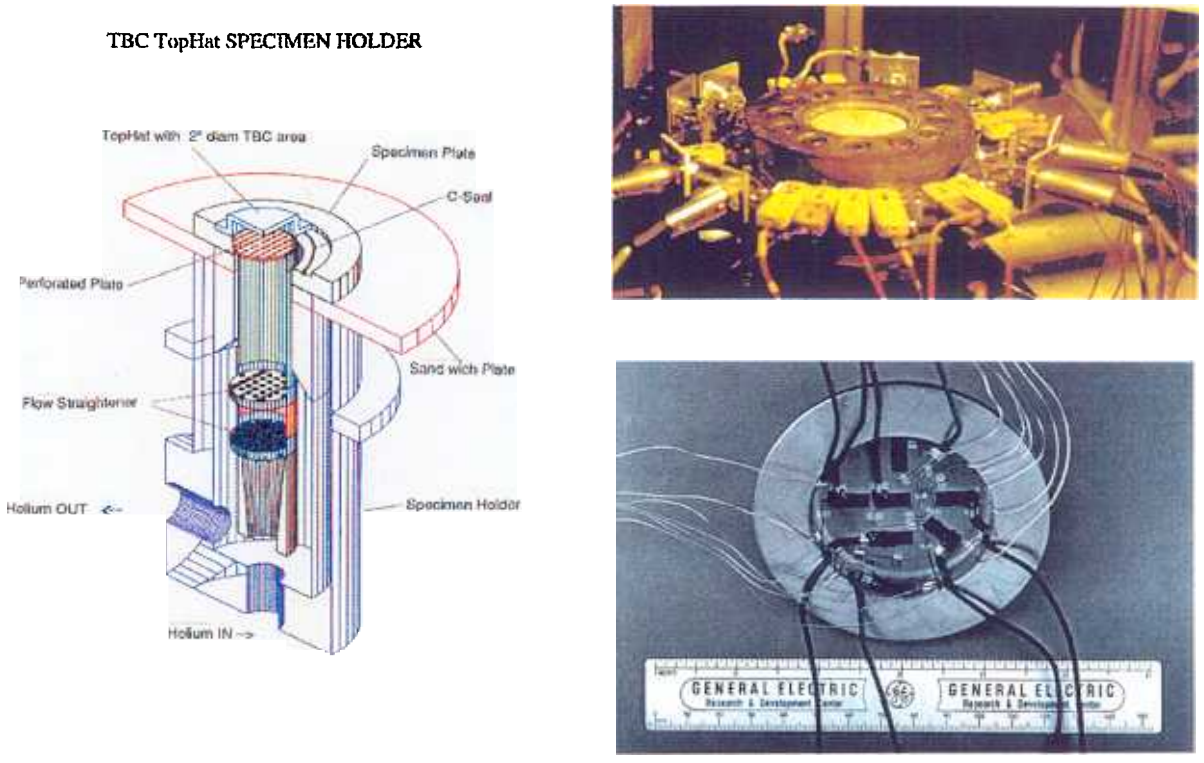

Figure 2.2.5.2-2. Electron Beam High Thermal Gradient "Tophat" Test Specimen

Section 2.2.5.3 (GTTTDD) TBC Design Data and Life Analyses [S]

Objective

Failure modes in advanced TBCs were identified, classified, and defined using empirical methods. Experiments were performed to find key relationships among plasma spray processing variables, coating microstructure, coating physical and mechanical properties, and coating performance under simulated ATS conditions.

The relative contribution of oxidation and cyclic damage to the failure of different substrate / bond coat / top coat systems was evaluated in order to estimate the TBC life in the ATS gas turbine. This was accomplished by furnace cycle testing TBC systems using a series of dwell times per cycle and dwell temperatures and incorporating the results into an existing cumulative damage model. Accelerated testing at temperatures below 1037°C (1900°F) was accomplished using a tensile thermo-mechanical fatigue test, which superimposed cyclic mechanical strain upon the cyclic thermal strain. In support of the modeling approach, microstructural features of the ceramic top coat and metallic bond coat were examined.

Numerical analyses were performed to determine TBC stress states expected in ATS turbine components and in laboratory thermal cycling tests. The influence of the TBC stresses on TBC failure modes was examined. Specially developed finite elements were used for modeling the behavior of the interface cracks and free-edge stress singularities. The effects of bond coat roughness on TBC stress state, crack driving forces, and delamination failure were examined. Parametric studies to determine the effects of bond coat and top coat properties on the TBC stress states were performed.

The spatial and run-to-run variability of TBC thermal conductivity was evaluated. Improved understanding of this variability is essential, because the variation in TBC thermal conductivity can be several times greater than that seen in metals due to variations in TBC microstructure, leading to design inaccuracy. Different methods of measuring thermal diffusivity and conductivity on flat and curved samples were developed. The effect of thermal aging and the gas pressure dependence of thermal conductivity as functions of temperature were measured. The results were used to estimate the thermal conductivity of TBC at ATS turbine conditions.

Introduction/Background

TBC degradation and ultimate failure can occur in the gas turbine via several mechanisms, as shown schematically in Figure 2.2.5.3-1. Impact accounts for localized loss of TBC from turbine components; if the impact energy is low and/or the ceramic-metal bond is strong, then crushing and internal fracture occurs in the ceramic top coat due to Hertzian contact stresses. However, if the impact energy is high and/or the ceramic-metal bond is weak, then complete delamination of the ceramic top coat can occur. This is indicated by the dashed arrow in Figure 2.2.5.3-1. Erosion, on the other hand, occurs progressively from the coating surface, as indicated by the short solid arrow in Figure 2.2.5.3-1. Another surface-degradation mode is wetting of the Yttria-Stabilized Zirconia (YSZ) ceramic by a contaminating liquid material, such as molten deposits of

Calcium-Magnesium-Aluminum-Silicate (CMAS). This is again indicated by the short solid arrow in Figure 2.2.5.3-1.

The mechanism of TBC degradation most thoroughly studied is termed "thermo-mechanical fatigue" or "TMF," which encompasses both time-dependent and cycle-dependent damage mechanisms. It was found in a parallel GE program that this damage mechanism is controlled by the temperature and stress at the ceramic-metal interface, and results in delamination of the ceramic top coat, as indicated by the long solid arrow in Figure 2.2.5.3-1. The majority of the stress is the result of the thermal expansion difference between the nickel-based superalloy substrate and the YSZ ceramic, with the bond coat serving to reduce this stress by only a small fraction. In most cases, the time-dependent damage is dominated by the formation of an interfacial oxide that grows between the YSZ and the bond coat. Sintering of YSZ is another contribution to time-dependent damage, but this effect is minor in a Dense Vertically Cracked (DVC) TBC because the vertical cracks accommodate the shrinkage caused by sintering of the solid material in the columns. The cycle-dependent damage is due to fatigue mechanisms, which may act upon either the YSZ or the interfacial oxide, depending on the mechanical properties of these constituents.

Discussion

The path to developing coating life prediction models is shown in Figure 2.2.5.3-2. The dashed line indicates the current knowledge level within the gas turbine industry. Ongoing work by GE, national labs and universities will eventually move this line down; however, this will not occur until the effects of coating deposition process variation on gas turbine components are statistically accounted for in the models. Figure 2.2.5.3-3 shows the various tests used for predicting TMF life of thermal barrier coating. Within the ATS program, the relative contributions of time-dependent (oxidation) damage and cycle-dependent (fatigue) damage to ultimate failure of the TBC were evaluated using thermo-mechanical fatigue (TMF) data and Furnace Cycle Test (FCT) data, as well as metallurgical and NDE evaluations. Other mechanical tests; which included compression shear, tensile, ballistic impact, and hardness tests; were performed in parallel programs.

Test specimens were prepared comprising four different substrate / bond coat / top coat systems, representing different ATS gas turbine components. One of the TBC systems is a duplication of the TBC applied to the ATS Cascade Nozzles. This TBC was deposited using certain process conditions which deviated from standard practice, and may have contributed to the early TBC spallation observed on some nozzles. Specimens were machined from Rene N5, GTD111, GTD222 alloys. Two types of specimen were prepared: 1.00 inch diameter x 0.125 inch thick buttons and 7 inch long x 0.250 inch thick TMF bars. After completion of TBC deposition, the test samples were heat treated in vacuum as per the requirements for the respective substrate alloys. Some samples were thermally aged in air in order to study the influence of exposure on the TBC properties and impact behavior. All GTD111 and GTD222 specimens were overaluminided using a NiAl coating to protect the substrate metal from oxidation during high temperature testing. The coating life and thermal performance evaluations focused upon during the ATS program are described in greater detail below:

Furnace Cycle Testing (FCT)

FCT of conventional ("porous") and advanced ("dense vertically cracked" or "DVC") TBC specimens were conducted at 1148°C (2100°F) and 1093°C (2000°F) using dwell times of 0.1, 0.75, 10, and 20 hours per cycle. The majority of specimens were cycled to failure, although some specimens were removed at intermediate times for tensile adhesion testing and laser ultrasound measurements. A small number of specimens were intentionally exposed to two different dwell times in order to test the influence of thermal history on remaining TBC life. Ongoing tests are being conducted at 1038°C (1900°F).

The data were fit using a cumulative damage model for the cases of parabolic and cyclic oxidation. In both cases, reasonable fits were obtained to the FCT data; however, the two curve fits yielded markedly different estimates for the TBC spallation lives at low temperatures. Examination of the oxide growth kinetics at 1093°C (2000°F) indicated that a two-stage parabolic oxidation damage model is appropriate for one TBC system.

Thermo-Mechanical Fatigue (TMF)

TMF testing was performed by Materials Characterization Laboratory (Scotia, NY). Development included construction of a collapsible hot surface ignitor furnace for sample heating/cooling, writing TMF test software modules, setting up a data acquisition system, and setting up a digital camera for recording TBC surface conditions during testing. A GE Specification was prepared for TMF testing coated superalloys.

Trial TMF tests revealed that the initial test specimen geometry was susceptible to buckling under compressive loading. A new gripping method was developed, which eliminated buckling for compression strain ranges up to -0.5%. Modifications to the furnace and grips were also made following the first tests to improve durability. The test rig can be used for both in-phase (maximum stress/strain coincides with maximum temperature) and out-of-phase (maximum stress/strain coincides with minimum temperature) tests.

Two in-phase TMF tests were performed on single crystal N5 coated with APS NiCrAlY bond coat and APS DVC top coat, at maximum conditions of 982°C (1800°F) and -0.3% or -0.5% strain. The tests were terminated after 946 and 315 cycles, respectively, without TBC failure. The condition of the TBC applied to the TMF specimens was evaluated using non-destructive laser ultrasound and infrared thermal imaging techniques. Measurable TBC degradation did occur during TMF testing, even though the TBC remained visibly intact.

Two in-phase TMF tests were performed at maximum conditions of 1066°C (1950°F) and -0.5% strain. TBC failure occurred by top coat delamination without specimen buckling. Non-destructive and metallographic examinations were performed. Metallographic examination showed that the bond coat exhibited minor oxidation, but significant additional damage occurred in both the top coat and bond coat due to the superimposed mechanical strain. This effect resulted in a significant reduction in TBC life compared with FCT data at the same temperature and dwell time, which is consistent with the cumulative damage model prediction.

Thermal Conductivity

Thermal conductivity characterization studies of the YSZ ceramic coatings were performed by GE-CRD. A laser flash thermal diffusivity measurement apparatus and a furnace capable of testing thermal diffusivity at pressures up to 30 atmospheres were installed at GE-CRD. Techniques for obtaining free-standing YSZ specimens from flat coupons and coated components were developed. Opaque surface coatings were developed for repeated measurement and exposure of samples to high temperature. The following results were obtained:

A) Planar samples from coupons

Measurement of YSZ thermal conductivity was completed on samples aged at 1038, 1204 and 1315°C (1900, 2200 and 2400°F) for 10, 100 and 1000 hours to create new design curves. The gas pressure effect over 1-25 atmospheres was evaluated for the aged samples. These data are in agreement with predictions published by GE-CRD in 1997 (Mogro-Campero et al., *Surface and Coatings Technology* 94-95, 102-105, 1997).

Thermal conductivity was measured as a function of TBC thickness. A positive, but minor correlation was observed with increasing thickness, which is consistent with the presence of a radiation heat transfer component. Variation in TBC thermal conductivity caused by differences in raw materials was evaluated. Ceramic powder from three suppliers was used to prepare test samples. Some samples were minimally aged and others were aged at 1315°C (2400°F) for 100 hours prior to measurement. The thermal conductivity of unaged and aged samples differed at most by 3% and 4%, respectively, which is close to the uncertainty of the measurement. Therefore, it was concluded that ceramic powder supplier has no measurable effect on YSZ TBC thermal conductivity.

B) Curved samples from components

Evaluations of as-deposited and aged free-standing TBC from ATS Cascade nozzles and field returned buckets and shrouds were performed. Samples of as-deposited TBC are being prepared from an ATS bucket. Systematic variation in thermal conductivity was observed on the nozzles according to location. The source of this variation was the TBC microstructure, which is strongly dependent upon the spray gun motions and local part temperature. An improved waterjet sectioning technique was developed for obtaining specimens from nozzle fillets.

Summary/Conclusion

Failure modes in advanced TBCs were identified, classified, and defined using empirical methods. Experiments were performed to find key relationships among plasma spray processing variables, coating microstructure, coating physical and mechanical properties, and coating performance under simulated ATS conditions.

The relative contribution of oxidation and cyclic damage to the failure of different substrate / bond coat / top coat systems was evaluated in order to estimate the TBC life in the ATS gas turbine. In support of the modeling approach, microstructural features of the ceramic top coat and metallic bond coat were examined.

Numerical analyses were performed to determine TBC stress states expected in ATS turbine components and in laboratory thermal cycling tests. Parametric studies were performed to determine the effects of bond coat and top coat properties on the TBC stress states.

The spatial and run-to-run variability of TBC thermal conductivity was evaluated. The effect of thermal aging and the gas pressure dependence of thermal conductivity as functions of temperature were measured. The results were used to estimate the thermal conductivity of TBC at ATS turbine conditions.

Technology Application

The results of this task are used to update the design databases. In addition, a database will be established which will link TBC properties and durability in laboratory tests to TBC durability in the ATS gas turbine. This database will be used ultimately be used to predict TBC life as a function of temperature and strain at specific locations on ATS gas turbine components. The database will also be used to identify process improvements to the baseline TBC that will result in improved coating properties and durability.

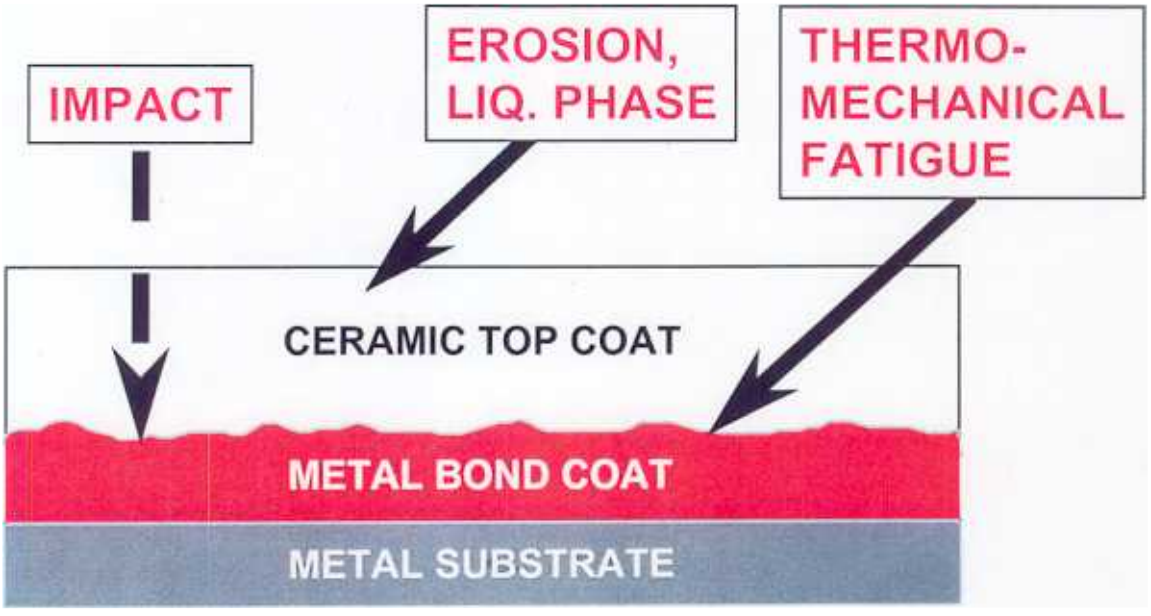

Figure 2.2.5.3-1. Degradation Modes for Thermal Barrier Coating

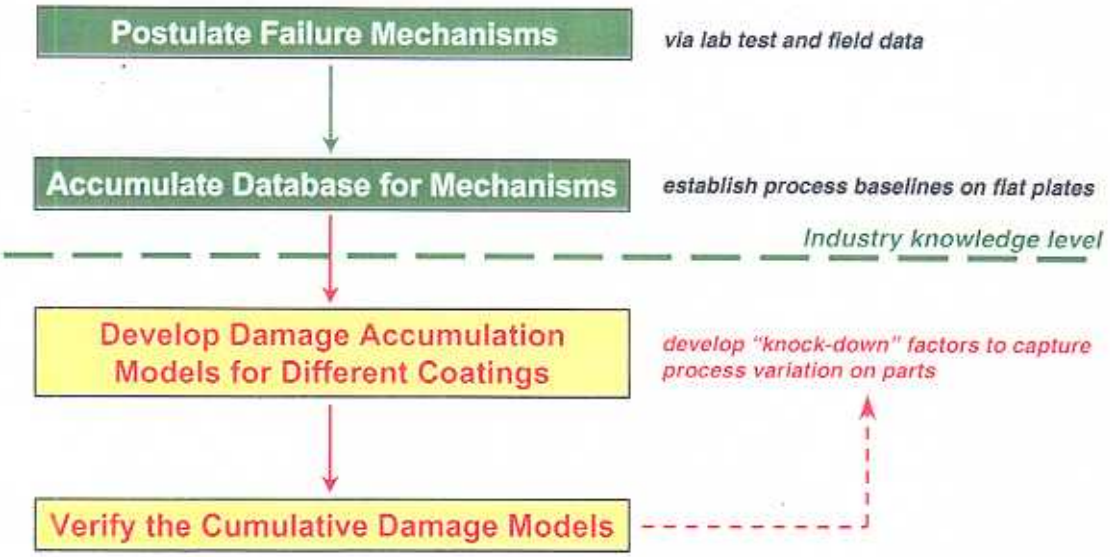

Figure 2.2.5.3-2. Path to Develop Coating Life Prediction Models

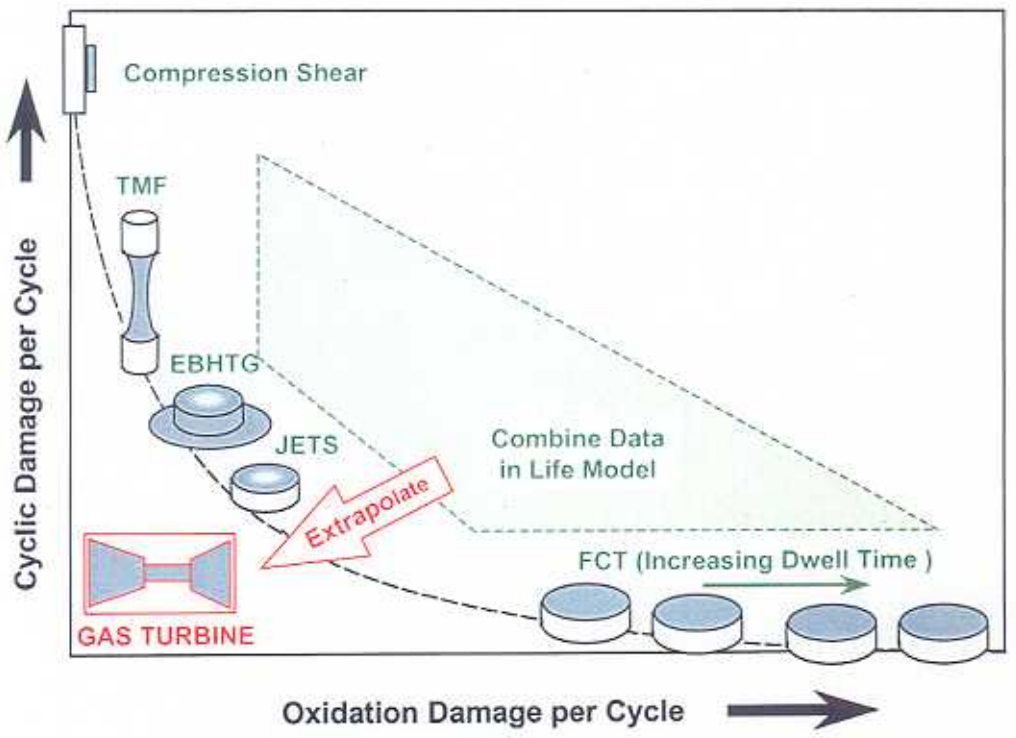

Figure 2.2.5.3-3. Tests Used for Predicting Thermo-Mechanical Fatigue Life of Thermal Barrier Coating on Gas Turbine Components

Section 2.2.5.3.1 (GTFFTB) Bucket TBC Roughness and Spall Characterization [C]

Objective

This task quantified the external airfoil heat transfer coefficients associated with the roughness characteristic of TBCs. Special attention was paid to the roughness associated with TBC structure, which can be very different from that of metallic surfaces or coatings. Typical average roughness measurements made on surfaces cannot fully distinguish between metal finishes, artificial rough surfaces, and applied or polished TBC surfaces. While the measured average roughness values of such surfaces may be the same, the effect on external heat transfer may be quite different due to the specific character of the roughness. This task used CRD's Transient Heat Transfer Cascade to test an airfoil coated with TBC that had been polished to various levels, and assessed the effect of TBC-type roughness.

Introduction / Background

The fundamental effects of surface roughness on heat transfer coefficients for external boundary layer flows is only modestly understood. The primary source for heat transfer knowledge connected to turbine airfoil surface roughness is engine experience. Experimental verification of the effect of different TBC roughness levels on heat transfer must be established for the particular TBC used on the ATS turbine airfoils. Section 2.2.3.6 described a series of flat plate tests aimed at the quantification of TBC roughness effects on heat transfer. The present task is very similar in nature, but utilizes instead an actual turbine nozzle cascade to include the full effects of boundary layer transition, freestream acceleration, and turbulence as these affect the airfoil TBC surface heat transfer.

Discussion

The first several months of effort dealt with the fabrication and coating of the instrumented test airfoil. A linear airfoil, of the shape required for the Transient Cascade, was obtained from GE Aircraft Engines. The exterior surface of the airfoil was first milled to remove material uniformly, except at the very trailing edge. This material was removed to accommodate the later application of coatings, such that the airfoil shape would be brought back to the original aerodynamics. The airfoil was then coated with TBC. GE Power Systems performed the coating operations after a number of trial runs and programming on slave airfoils of the same shape. GEPS also performed eddy current thickness measurements on the coatings, as well as CMM measurements. The bulk of the inside of the airfoil was then removed by electro-discharge machining. During this same operation, the internal grooves for the thermocouples were cut. The airfoil was then nickel flash coated on the interior surfaces, and the thermocouples brazed into place. During these operations, no TBC damage occurred. All thermocouples survived brazing.

The instrumented and TBC-coated airfoil was fixtured into the Transient Heat Transfer Cascade rig at CRD. Profilometer surface roughness measurements were made prior to cascade installation to determine the distribution of both centerline average roughness (R_a) and average peak-to-peak roughness (R_Z). An initial set of transient tests was run with four different mainstream Reynolds numbers. The initial data reduction used a

lumped parameter model for the metal/bond-coat/TBC airfoil structure and indicates a very consistent external heat transfer distribution with Reynolds number changes. For each series of tests at a roughness level, four airfoil mainflow Reynolds numbers (Re) were run. Based on exit conditions and airfoil axial chord length these Re were 6.5e5, 1.25e6, 1.9e6, and 2.4e6.

Summary/Conclusion

The results of these tests were:

- For each series, all heat transfer results were consistent in behavior, showing the appropriate variation with Reynolds number.
- Polishing of the TBC surface from as-sprayed roughness to removal of the peak elements resulted in about a 25% overall decrease in the heat transfer, fairly uniformly distributed over the entire airfoil surface.
- Polishing of the TBC further resulted in about a 12% overall decrease in the heat transfer, again fairly uniformly distributed over the entire airfoil surface, with the exception of the leading edge stagnation point which remained unchanged.
- At the smoothest condition of average roughness, the heat transfer levels on the pressure side of the airfoil agree quite well with previous results obtained in the same facility using a metallic airfoil having a similar average roughness level. Further comparison of these cases shows the suction side transition locations to agree for each Reynolds numner tested. The suction side heat transfer level does not agree, but is self-consistent.
- Spall testing results show the heat transfer enhancement at a location of about midchord to be moderate regardless of Reynolds number.

Technology Application

The results from this task were analyzed for consistency among the various roughness levels tested. The results were also compared to other, similar tests run in the same facility that used metallic rough surfaces. If the complete set of available data shows a consistent and clear effect of TBC surface roughness on external heat transfer, these data will be used to determine an equivalent TBC roughness for use in the design heat load predictions on the ATS turbine airfoils.

2.3 Combined Cycle Integration [S]

2.3.1 (CCUA) Unit Accessories [S]

Objective

Development of four new unit accessories – fuel heating, cooling air cooling, steam cooling, and clearance control-is critical to the development of the ATS gas turbine in order that the gas turbine meets its performance goals and function properly. The ATS turbine employs a DLN combustion system that requires the gas fuel to be heated in order to achieve the overall ATS efficiency goal. The cooling air cooling system is required to maintain the temperature in sections of the gas turbine within acceptable limits. The steam cooling system is required to cool the turbine hot gas path parts while meeting performance goals for the ATS turbine. The clearance control system enables the gas turbine to operate at a higher efficiency than would otherwise be possible without the system. The exhaust diffuser will be designed so that maximum possible pressure recovery will be realized, thus increasing the performance of the ATS gas turbine. Designs of remaining accessory systems will be conventional.

Design of the heat exchanger and piping for the hot fuel will take into consideration the need to avoid coking. Deposit formation will be investigated. The effectiveness of coke barrier coatings, which have been under development for liquid-fueled systems, will be evaluated in long-term tests.

Introduction/Background

The task of the Accessory Systems development has been to ensure the design and production of accessory systems to support the gas turbine and power plant. All four systems (cooling air cooling, steam cooling system, exhaust diffuser, and clearance control system), have a direct impact on gas turbine and plant efficiency and as such are critical for the H technology and ATS engine to meet its goals.

The accessory system development necessitated constant interaction with the gas turbine department to achieve the requirements. The accessory system department turned these requirements into working hardware.

Discussion

Cooling Air Cooling System (CAC)

The CAC system performs three functions: it provides cooling air to the gas turbine rotor to maintain the required rotor temperature, cooling air to cool the second stage turbine nozzles and wheel spaces, and it provides a source of cool air for use in the gas purge system. The skid has an air-to-water heat exchanger, which is used to cool the air sent to the rotor and purge system, and to produce steam that is sent to the HRSG for use in the steam cooling cycle. The ATS power plant cannot run without the operation of this system, resulting in extremely important reliability and performance requirements for CAC.

Since it's initial development, the system has gone through an extensive design evolution. Initial plans called for the system to be integrated with the gas fuel heating system. However,

to allow for more commercial flexibility (since an essential system like Cooling Air Cooling would be integrated to a system that could change with different fuel performance), the systems were separated. Because the reliability of this design is so critical, one of the first steps in the design of the skid was a reliability analysis. The analysis (also performed for Steam Cooling system and Clearance Control System) was done in conjunction with the GE Power Systems Reliability Organization, GE Corporate Research and Development, and the Engineering Department of Stanford University. The report focused on the production of Failure Mode Effects Analysis (FMEA) to ensure the elimination of single-point failures, structure the design to improve reliability, and how to mitigate the effects of those failures that could not be wholly eliminated. This input was then incorporated into the design, and at this stage a Process & Instrumentation Diagram (P&ID) was produced that allowed more detailed design and fabrication issues to be addressed.

One of the detailed issues that required resolution was the source of water for the heat exchanger located on the skid (used to cool the air sent to the gas turbine and gas purge). Initially, the source of this water was the HRSG high pressure drum. However, the high-pressure water resulted in a high system cost, and therefore a design using intermediate pressure water was developed. This design was determined to be viable, and the P&ID was updated. As the P&ID also contains device information, the control philosophy development could be initiated. With the system configuration complete, initial analysis was begun with a Flowmaster model of the system, incorporating the rotor cooling line, gas purge system and CAC skid. The results from this model were especially useful in determining the gas purge pressure ratios, and for validating the flows through the CAC skid. The model has been updated as the design has evolved, especially when the 9H FSNL and FSFL pre-shipment tests were run. With good definition of the system and skid components, a functional specification was written to allow sourcing to begin working to find a suppliers, and the supplier was chosen in 4Q97.

Work proceeded on integrating the skid into the power plant. At this point it was found that the optimum solution for the system lay in a change in the skid's location in order to minimize the pressure drop in the interconnect piping. This change, which improved overall system performance, required a change in the internal piping, and this design alteration was achieved by 3Q98. With the piping and skid layout defined a full piping thermal/structural analysis was completed, and which validated the design. At this point long-lead items were ordered.

A further development for the H Program in 2Q98 was the completion of the 9H FSNL test. This test, which used a simplified CAC skid, validated the design used and produced invaluable data on the gas turbine cooling flows. This test used an air-to-air heat exchanger and validated the air side of the system. With the validation of this portion of the system, the analysis could focus on the untested part of the system, the air-to-water heat exchanger.

Construction of the skid progressed to completion in 3Q99 (see Figure 2.3.1-1). At this time a team of GE personnel travelled to the vendor to conduct an inspection, which went successfully.

With the completion of the 9H skid, preparations for the design of the 7H skid began. The reliability analysis had focused on the heat exchanger, and a change in location of the skid

from the initial position for the 9H allowed for a change in the type of heat exchanger used, which will produce a more robust design. The successful completion in 4Q99 of the 7H FSNL test produced the data needed for the cooling flow to the gas turbine, and also validation of the design decision to mix CAC discharge air with another source of air to allow for greater coolant flow to the gas turbine.

Figure 2.3.1-1. Completed 9H Cooling Air Cooling Skid for Baglan Bay.

Summary/Conclusion

The cooling air cooling system has demonstrated the following critical functions:

- Provide cooled air to the gas turbine rotor.
- Provide cooled air to the second stage turbine nozzles.
- Provide cooled air to the gas purge system.
- Produce this cooled air through an air-to-water heat exchanger that will then produce high-quality steam for use in the steam cooling circuit.

The finished hardware must not only accomplish all four functions, but most also do so with the highest possible reliability. Based on the analysis to date, these requirements have been met.

For the 7H design a key improvement will be a change in the heat exchanger to ensure longer life components.

Discusion

Steam Cooling System

The steam cooling system represents the major technological advance of the ATS gas turbine. The system takes steam from the HRSG and steam turbine and routes it through interconnecting piping to the gas turbine. In this piping, the steam must be cleaned through a series of filters, and controlled through dozens of valves and the Mark VI control system. These valves and filters, with the associated control system, represent the main output of the accessory systems for the steam cooling circuit.

Initial design considerations for the system focused on the fact that it is the most important technological advance of the ATS gas turbine. Because of this, reliability became an important consideration, and the steam cooling system was studied in the reliability report commissioned by the Controls, Accessories, and Systems Engineering (CASE) group with Stanford University. The efforts were focused on the production of a failure modes effects analysis (FMEA), which is especially important because this system is the most widely integrated of all the accessory systems. Stakeholders in all parts of the power plant, including the architectural engineer (AE) who designs and engineers much of the interconnect piping and balance of plant equipment, are dependant on the steam cooling system. A failure mode in one piece of equipment may affect, or require correction by hardware or controls, in different section of the plant, designed and procured by another section of GE or the AE. Efforts to ensure proper integrate this system have been ongoing since that time.

One of the main deliverables were the datablocks. Datablocks are the analysis of the how the entire ATS power plant operates, and as such contain the information necessary to design the steam cooling system. The datablocks, reflecting the integration efforts, have been ongoing as the ATS power plant has been better understood through analysis and simulation efforts. These have given an increasingly more accurate definition of the system requirements and responses.

Coupled with this was the production of an initial process and interface drawing (P&ID), which describes the arrangement of the steam cooling valves and filters in the piping and within the power plant. This allowed determination of an initial list of components necessary to the system, and then the selection of a supplier. Because the long engineering cycle time to design the system, the agreement with the supplier was specifically written to allow complete engineering support from the supplier in advance of the production of actual hardware.

With this basis the design could now be refined. The P&ID was updated to show the temperature and flows that were defined through refinement of the datablocks. Outline

drawings of the valves and filter were produced, which also helped the piping designers to begin designing the interconnect piping. The control philosophy was defined, focusing on the type and quantity of flow meters needed to accurately monitor the system.

In 1999 the datablocks were finalized, validating the design of the steam valves and filter. Work since that time have focused on integrating efforts with the rest of power plant, ensuring smooth installation of the hardware at the site and proper fit-up in the field, and monitoring fabrication to support the delivery dates for the first 9H at Baglan Bay. The efforts expended will ensure a much shorter cycle time for the 7H work.

Summary/Conclusion

The steam cooling system is expected to provide the critical technical feature of the ATS gas turbine power plant. To this there are several important accomplishments:

- The system must provide cooling steam to the gas turbine in order that the ATS power plant to obtain the higher performance and firing temperature goals.
- Because the ATS power plant cannot run without the steam cooling system, reliability must be extremely high.
- The system, as noted previously, is integrated within the entire power plant and as such can only be successful if the design and fabrication of hardware is also accomplished in an integrated method.

Through the control and dynamic simulations done to date, as well as the extensive design reviews, these objectives will be met.

Discussion

Exhaust Diffuser

The exhaust diffuser for the ATS power plant was completely redesigned from GE's mature technology. Current technology called for a pair of expansion joints at the fore and aft of the diffuser to absorb the large thermal growths and stresses. The ATS design eliminated the front end joint to increase the reliability of the design. Further planned advances include an improved aerodynamic design to realize greater pressure drop recovery to increase ATS performance.

The front expansion joint was eliminated in response to field problems experienced on GE's F class technology, (the predecessor to the ATS power plant). Accessory system engineering undertook to understand the lessons learned from the field problems and concluded that since the expansion joint was the physically weakest part of the exhaust diffuser hardware, it would be better if one of the two joints was eliminated, and the remaining joint improved.

To improve the pressure recovery of the system, the entire system geometry was redesigned. To validate this, a scaled model of the diffuser was tested at GE Corporate Research and Development. The first series of tests, run in 1Q and 2Q97, were inconclusive, so an additional run was performed later that year. Based on results of these tests, the redesigned

diffuser is fully expected to meet the pressure recovery target needed for the ATS gas turbine to meet performance goals.

Based on the successful completion of the above two critical issues, a supplier was then selected to perform the detail design work and fabricate the diffuser. This was completed by the end of 1997.

Work then focused on how the diffuser interfaced with the rest of the power train. The diffuser has multiple pipe connections running through it, which require careful attention because of the elevated temperatures encountered by the pipes and the diffuser. The pipe bellows installed in the diffuser should resolve any difficulties.

Efforts at this point are now on the fabrication and installation of the diffuser. There is a diffuser test fabrication planned for 3/4Q00 to validate the fabrication approach. This erection will be videotaped for possible use at the site, and the field installation personnel will be present.

Summary/Conclusion

The goals of the diffuser were two-fold:

- Ensure reliable operation of the ATS power plant
- Realize pressure recovery to increase performance of ATS power plant.

The first ATS diffuser goal has been met, as the new design has been tested on GE machines in the field. The second goal has been validated through the model testing completed at CRD.

Discussion

Clearance Control System (CCS)

The purpose of the Clearance Control System is to provide heated and cooled air to the ATS gas turbine inner shell in order to control tip clearances on the blades. As such it is a critical component to meet efficiency goals.

Initial efforts focused on definition of the system's scope – initially the CCS was only to provide air to the turbine, but during the initial phases of the design development this was expanded to include the compressor as well. With this definition, the system was put through the same rigorous reliability assessment with Stanford University. It was with the FMEA produced in mind that the initial P&ID was completed. This showed the overall system configuration and reflected the initial design configuration.

Initial efforts focused on the production of the skid for use in the 9H FSNL test in 2Q98. Because of the expansion in scope of the system, the air supply source was changed from plant air to a pair of reciprocating compressors in order to be sure of adequate air for the proper operation. This work continued to the fabrication of the skid, which ran successfully during the 9H FSNL test, and has been used in the subsequent FSNL tests for both the 9H and 7H.

Data from the testing were then evaluated, resulting in a final design for the CCS skid to be used in initial 9H power plant development testing at Baglan Bay. One immediate change was planned for the production units: the replacement of the reciprocating compressors with centrifugal compressors, for acoustic and reliability reasons.

A supplier was chosen for the first CCS production unit at Baglan Bay. The design was built to reflect the improvements made during FSNL testing. One problem occurred during the 9H FSFL pre-shipment test, and again during the 7H FSNL test, when a strainer, which functioned correctly during the 9H FSNL testing, broke down during each of the subsequent tests. Based on this, a tougher strainer will be in place for the Baglan Bay test program, and in all future units.

At the completion of fabrication of the unit for Baglan Bay, GE engineers visited the supplier to verify the proper operation and fabrication of the skid.

Summary/Conclusion

The Clearance Control system has one requirement:

- Provide cooler/heating air to the ATS gas turbine to improve tip clearances, and therefore performance.

The system, while still in development, already has site experience through the successful completion of the 9H FSNL and FSFL pre-shipment, and 7H FSNL tests. The system to be used at Baglan Bay, and then for the 7H, incorporates improvements on these already successful designs.

Technology Application

Development of the cooling air cooling system, the steam cooling system, the clearance control system, and the exhaust diffuser are all critical to successful operation of the ATS gas turbine. Each system is also critical to the high efficiency rating that the ATS gas turbine will achieve. Therefore, development of these systems will continue in order that the ATS gas turbine will meet these design goals.

Section 2.3.2 (CCCL) Controls [S]

Objective

An integrated plant control system will be developed and designed that will be suitable for the advanced gas turbine combined cycle power plant. Specifications of control equipment requirements will be prepared. Control and protection strategies will be developed for gas turbine steam cooling and integration with the steam turbine and heat recovery steam generator (HRSG). Control system dynamic behaviors will be studied by dynamic simulations. Specifications of control algorithms will be prepared for implementation in the control system program.

Introduction/Background

A control system was developed to meet the requirements of the complex functions of the advanced gas turbine. These complex functions included its close integration in a combined cycle power plant. Key features required include modularity of design for flexibility, triple redundant controllers and sensors for high reliability, and integration and expansion capabilities for total control of combined cycle plant equipment. Control and protection strategies were developed for new functions such as cooling steam, cooled cooling air, fuel heating and clearance control. The development program included dynamic simulation studies to validate controllability and to optimize startup and shutdown sequences.

Discussion

The control system for the advanced gas turbine was developed to meet the requirements for flexibility, reliability, and expandability. The architecture accommodates the complexity of the advanced gas turbine and the integrated controls of the steam turbine and HRSG in a combined cycle power plant. In addition, the control system is designed with expansion capabilities that can include controls of balanced of plant equipment, for a total plant control solution, shown in Figure 2.3.2-1. This control system platform successfully controlled the 9H and 7H advanced gas turbines during the initial full speed no load tests. Continued field testing of this control system at a test site has demonstrated high reliability and availability.

The complex thermodynamic cycle of the advanced gas turbine presents challenges in the developments of control and protection strategies. The gas turbine cooling steam flow requires accurate control and monitoring to ensure proper operation. Process parameters such as flow, pressure, and temperature provide data for analysis of fault conditions. Operational sequence logic manages control valves to position them for a variety of modes during start up, on-line, and shutdown operations, shown in Figure 2.3.2-2. The gas turbine starts in air-cooled operation, (the hot gas path components are cooled by air from compressor discharge). During the initial loading phase, (Figure 2.3.2-3), control sequence logic manipulates valves to transfer from air to steam cooling, supplied by the startup steam source. After the steam turbine is placed on-line, control logic automatically transfers to the turbine discharge steam for normal loading operation. On a

unit shutdown, the control system reverses the sequence, where the cooling steam source reverts to the startup steam supply as the steam turbine shuts down. The gas turbine returns to air cooling as speed decreases in the final phase of shutdown.

Simulation environments have been developed to study the dynamic behaviors of control loops. These environments also provide engineers means to optimize equipment sequences. A non-real time environment is developed which couples equipment models to control system models, shown in Figure 2.3.2-4. In this environment, control strategies are formulated, control logic and control loop validated and operational sequences are optimized to meet equipment requirements. A real time environment is also in place to provide validation of the control hardware and software, shown in Figure 2.3.2-5. In this environment, the control program and actual control hardware are coupled to equipment models to perform further validations of the control and protection algorithms. Selected failure modes are studied to determine system reactions. These simulation environments will serve as engineering tools for dynamic studies as the gas turbine prepares for its first application.

Summary / Conclusions

A controls system has been developed to meet the complex requirements of the advanced gas turbine system. This control system has the flexibility and expandability to provide a total integrated combined cycle plant control solution. This control platform has been field tested and high reliability has been demonstrated.

New control algorithms have been developed to meet the complex functions of the advanced gas turbine; such as steam cooling, clearance control, and gas fuel heating. These algorithms are validated in simulation environments to ensure controllability and operability. Control software and simulation activities will continue as preparations proceed toward the first application of the advanced gas turbine H system.

Technology Application

The integrated plant control system conceptual design for the STAG 109H configuration will be very similar to that of the STAG 107H ATS plant.

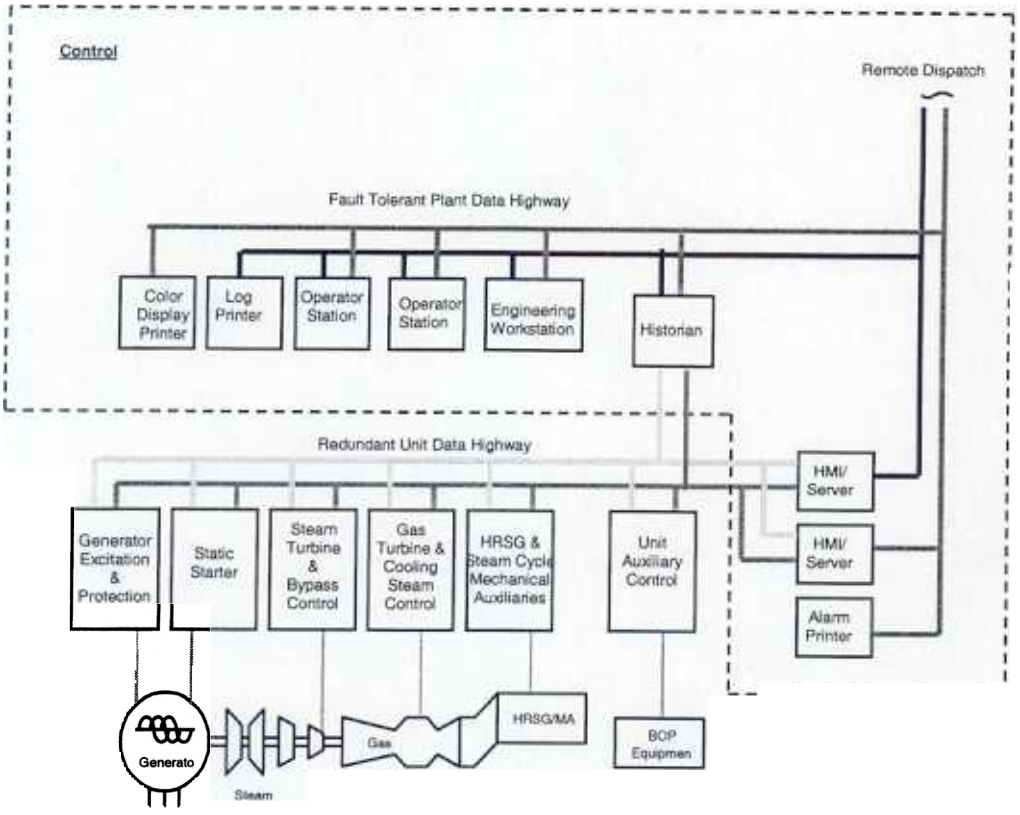

Figure 2.3.2-1. Integrated Control System

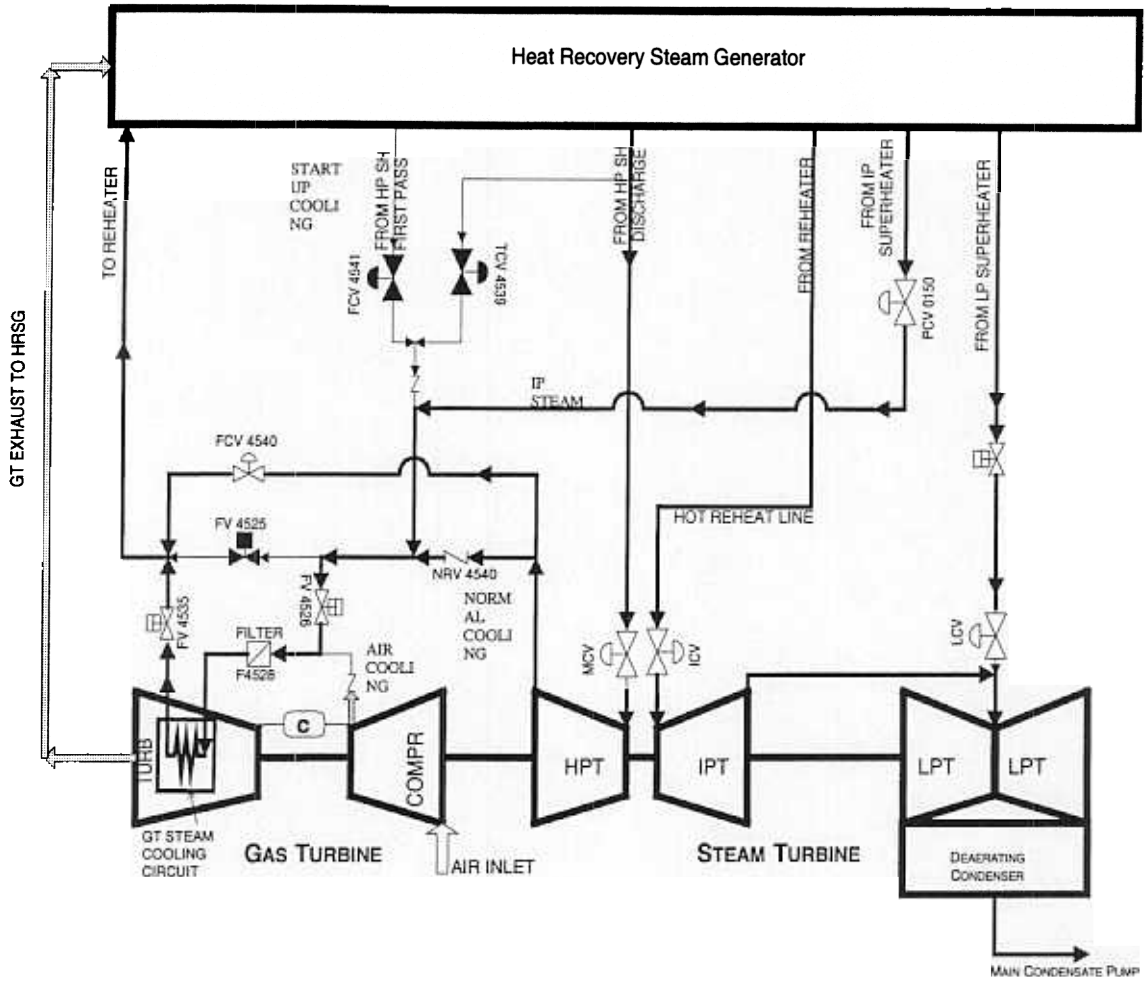

Figure 2.3.2-2. H System Complex Cycle

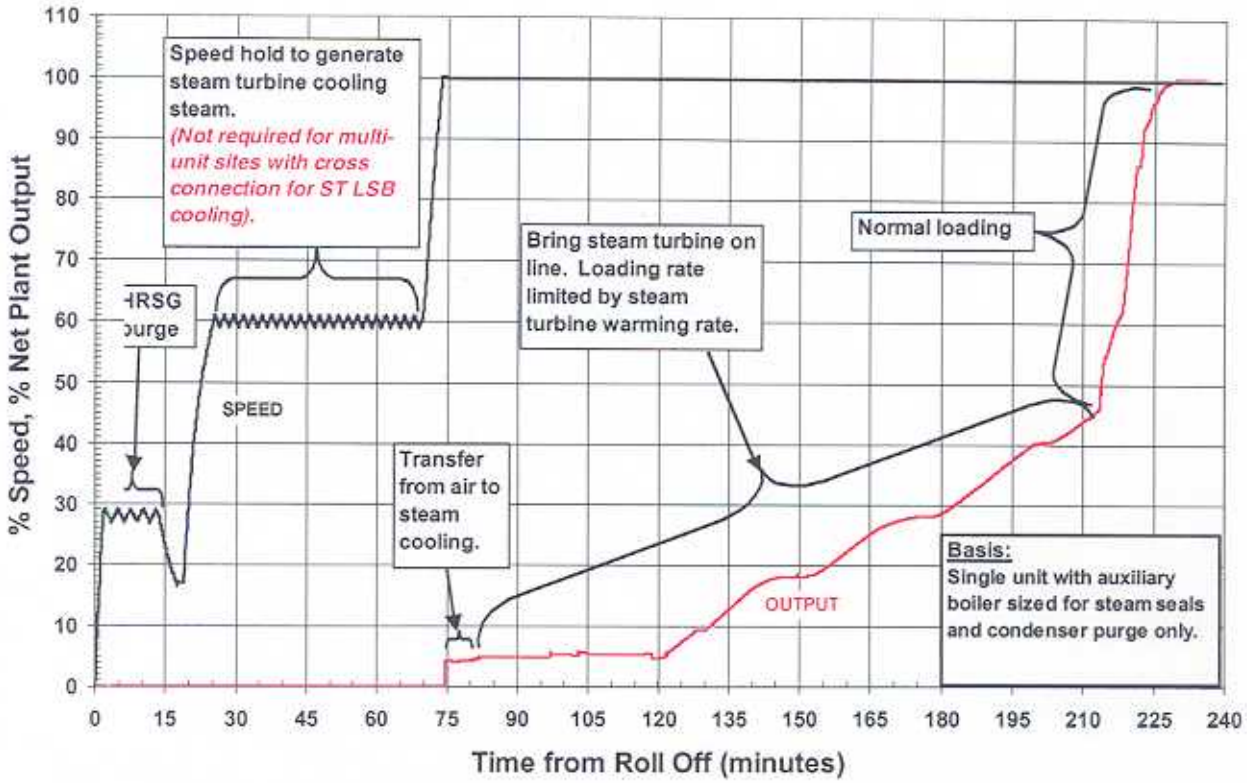

Figure 2.3.2-3. S107H/S109H Cold Start Loading Profile, Single Unit

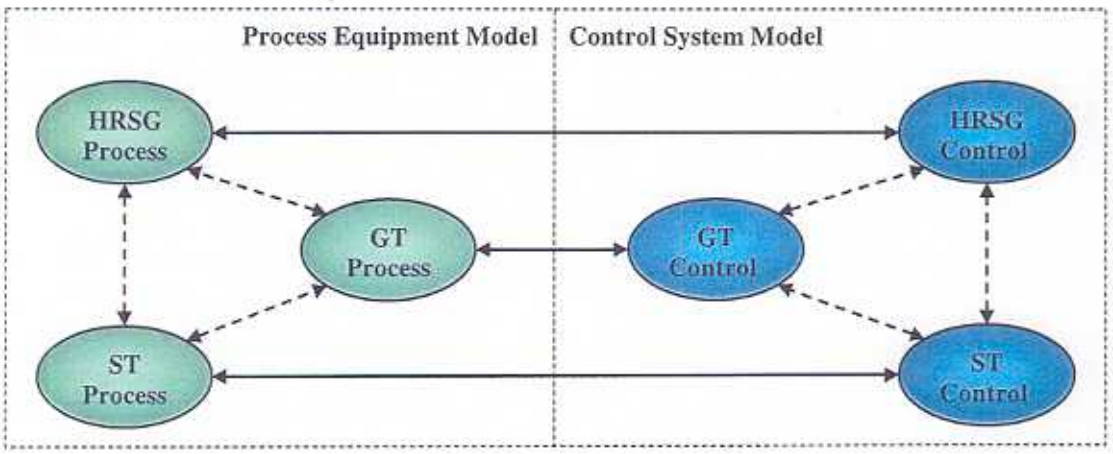

Figure 2.3.2-4. Integrated 9H Simulation Model Non-Real Time

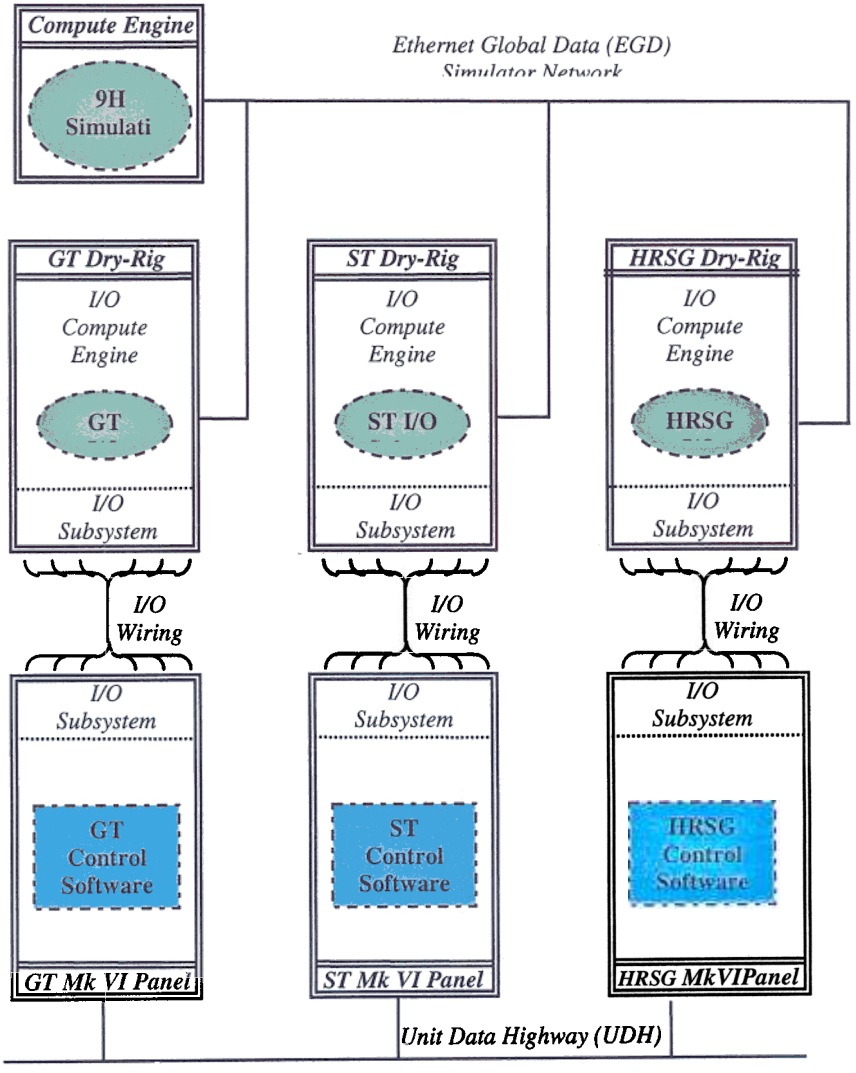

Figure 2.3.2-5. Integrated 9H Simulation Model Non-Real Time

Section 2.3.3 (CCRA) Reliability, Availability, and Maintainability (RAM) Analysis [S]

Objective

An evaluation of the reliability, availability, and maintainability (RAM) of the 7H equipment will be performed. The basis for the work will be the Electric Power Research Institute (EPRI) High Reliability Controls and Accessories Study. The RAM analysis will include: the flange-to-flange gas turbine, heat recovery steam generator, steam turbine, controls and accessories, electrical generator, and balance of plant equipment. A Failure Modes Effects Analysis (FMEA) will be included.

Introduction

As technology has advanced to provide higher performance equipment, engineering tools have advanced to provide better analysis of the hardware component performance. GE's Engineering Design Standards have likewise evolved to provide better and more comprehensive design guidance. The design of the new *H System™* has particularly benefited from a validation strategy utilized as a best practice in GE's Aircraft Engine (GEAE) business, and from ongoing GEPS design experience and an extensive installed engine data base. The result is that the *H System™* has a higher probability of rapidly achieving its design expectations than other "new technology" offerings of past decades.

The development of the *H System™* combined cycle power plant implemented a Design For Reliability (DFR) process utilized previously on the GE MS7001F new design in the 1980's, as documented by the EPRI High Reliability Controls and Accessories Study (AP-5823). For the *H System™* combined cycle plant, this process was utilized to identify the high level plant goals for Reliability, Availability, and Maintainability (RAM), allocate them to the various systems and components, perform reliability assessments, and make design changes to improve reliability. A formal Design for Reliability process was constructed, as shown in Figure 2.3.3-1.

Discussion

The initial effort was to review historical RAM data for GE combined cycle plant equipment from the Operational Reliability Analysis Program (ORAP) RAM database, operated and maintained for GE Power Systems by Strategic Power Systems, Inc. This effort provided a statistical analysis of the RAM experience of GE equipment at the following levels: plant, major systems, and systems. The analysis also provided a review of historical RAM of combined cycle plants, including; average, "best in class", and a breakdown by operational duty.

Based on this analysis, the overall plant Reliability, Availability, and Starting Reliability goals were established to ensure that the *H System™* is consistent with the current levels of today's "F" class combined cycle power plants. The definition of these goals also included a review of what new advanced technologies were associated with the *H System™*, and their potential impact on RAM.

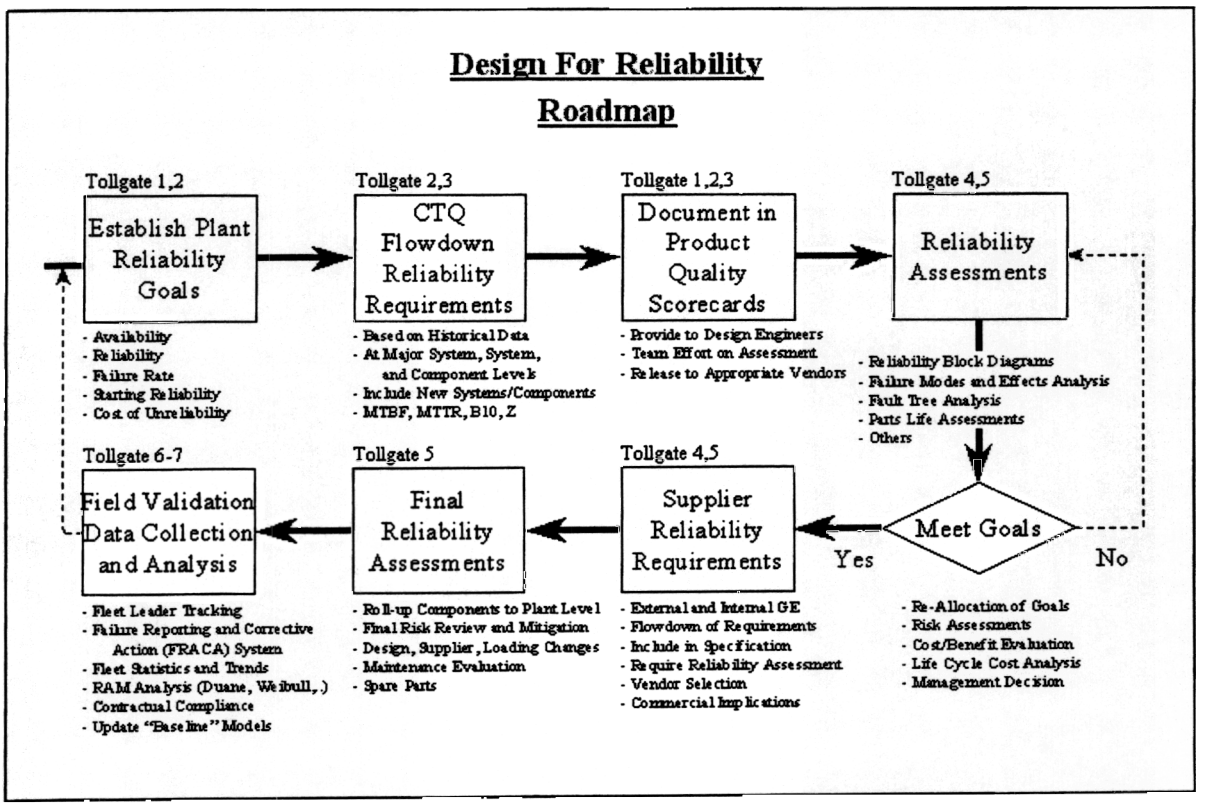

Figure 2.3.3-1. Design For Reliability (DFR) Process Map

Once the high level RAM goals were established for the plant, a flowdown of these requirements to the major systems, systems, and components was performed. This process provided specific goals that each design group was required to address during the design. As the design teams went through each system and component, an assessment of the calculated RAM was compared with the established goals.

One initial effort performed by the gas turbine design engineers was to complete Failure Modes and Effects Analyses for the major components in the flange-to-flange design. This process followed standard industry practice for identifying the potential failure modes of each component, the level of severity, the probability of occurrence, and the merit of the current methods of detection and prevention. Any potential failure modes that were not adequately addressed by current detection and prevention methods, were addressed during the design process. FMEA forms (sample shown in Figure 2.3.3-2) were developed to document these evaluations.

Failure Modes and Effects Analysis (FMEA)		Assembly: Part Name: Hardware Owner: Engineer:				Model/Year: Vendor Name: Scheduled Product Release Date: Schedule Part Release Date:						FMEA #: Analysis #: Page #: Date:	
Part Functions	Potential Failure Modes	Potential Effects of Failure on End Product & End User	Severity	Reference #	Potential Causes of Failure	Occurrence	Likelihood	RPKNP	In-Place & Scheduled Cause Preventions or Detections	Ideal	RPN	Actions Recommended to Eliminate Cause & to Enhance Prevention or Detection	Responsibility
								0			0.0		
								0			0.0		
								0			0.0		
								0			0.0		
								0			0.0		
								0			0.0		
								0			0.0		
								0			0.0		
								0			0.0		
								0			0.0		
								0			0.0		
								0			0.0		
								0			0.0		
								0			0.0		
								0			0.0		
								0			0.0		
								0			0.0		
								0			0.0		
								0			0.0		
								0			0.0		
								0			0.0		
								0			0.0		
								0			0.0		
								0			0.0		
								0			0.0		

Figure 2.3.3-2. Failure Modes and Effects Analysis (FMEA) Form

Another critical part of the Design For Reliability process was to complete reliability assessments for the controls and accessories systems (including balance of plant equipment). For each critical system, a Reliability Block Diagram (RBD) was created based on the system design to assess the reliability and availability. The following (Figure 2.3.3-3) provides an example of a RBD for the lube oil system.

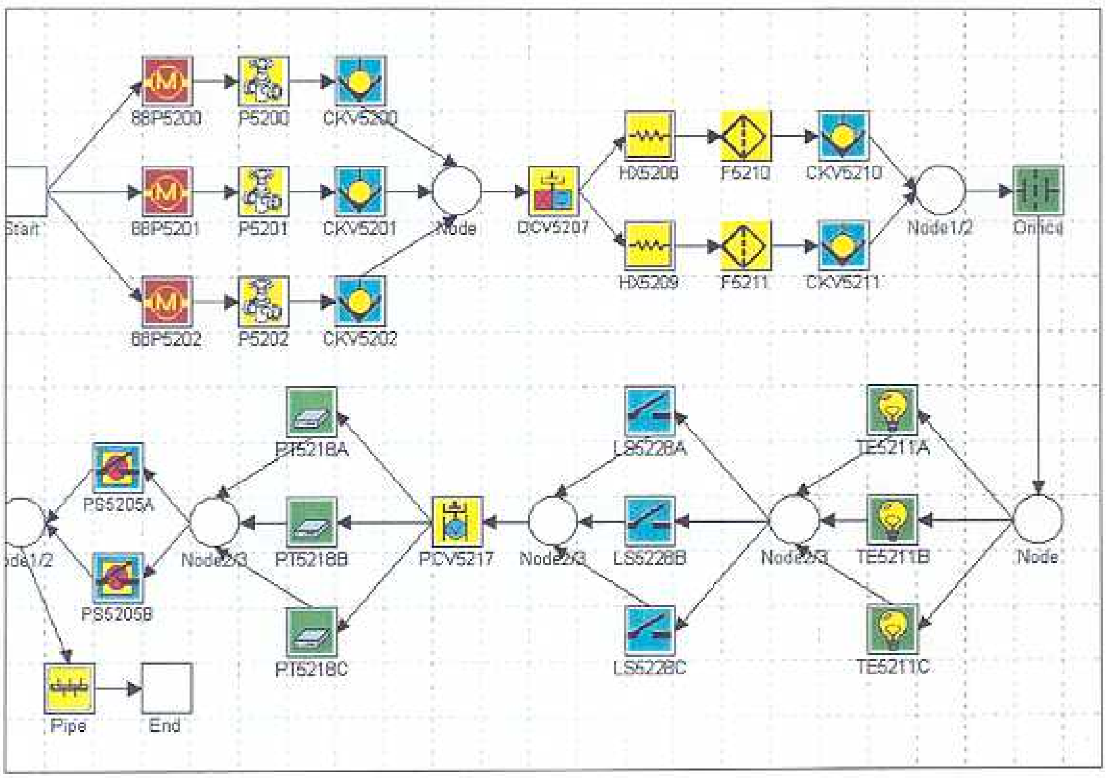

Figure 2.3.3-3. Lube Oil System Reliability Block Diagram Model

For each accessories and balance of plant system, the current design was compared to the system goals. Modifications to the design to address single point failure modes identified during the reliability study were also performed, assessing both control logic and design changes. These assessments also focused on the maintainability concerns for specific components within these systems.

For major equipment provided to GE by suppliers (i.e. Heat Recovery Steam Generator), reliability requirements were also provided. This equipment can impact the combined cycle plant RAM, and GE has required the suppliers to provide the following information;

- Historical RAM experience on similar equipment
- Acceptance of RAM as a technical requirement
- Reliability assessments performed on the design

GE will be collecting operational, failure, and maintenance data from the *H System™* combined cycle testing at the Baglan Energy Park launch site in the United Kingdom for the 9H (50 Hz) machine, and later at Sithe Energies Heritage Station site in upstate New York for the 7H (60 Hz) machine, to validate the RAM of the overall design, and the individual major systems and systems. This is part of the Verification Task. The RAM data tracking will be performed at the system and component level, to validate the calculated RAM that was done during the design process. This statistical data will be provided to the design teams.

Summary/Conclusion

The Design For Reliability process implemented for the 9H combined-cycle plant was based on the EPRI High Reliability Controls and Accessories Study performed on the 7F in the 1980's, but was improved and extended to the entire combined cycle system. RAM goals for the combined cycle plant and the allocations to systems and components provided the design teams with a focus on reliability from the beginning of the design process.

FMEA's were performed on the flange-to-flange components early in the design stages to identify potential reliability issues, which could be addressed during the detailed design phase. Reliability Block Diagrams were performed on accessories and balance of plant systems, which compared the system RAM of the current design with the RAM goals. Design changes to address single point failures, and the overall system design were reviewed and are being implemented.

Much of the *H System™* design is based on proven, established technologies. The major technologies of the combined cycle powertrain, including the bearing designs, the evaluation methods for rotor dynamics, the compressor and turbine blading designs, and the generator field construction methods are all either direct applications of proven design technology, or evolutionary refinement of existing designs. It is for these reasons that GE expects that the reliability of the new *H System™* combined cycle system will be fully

commensurate with the levels associated with today's "F" Class combined cycle power plants. With maintenance and operations performed at "best practice" levels, the new *H System™* plants should reach its full reliability potential of 97.0% or better.

RAM data collection will be performed during pre-commercial and commercial phases of the H system operation to track the Reliability, Availability, and Starting Reliability to ensure that these RAM goals are met.

Technology Application

The FMEA results will be applied to the design of the 9H and 7H hardware, with special emphasis on the components involved with the steam-cooling aspects of the design. The reliability assessments will affect the design of various systems across the H combined-cycle plant.

Section 2.3.4 (CCSD) Combined Cycle Systems Design [S]

Objective

Combined cycle system optimization analyses will be performed for cost/performance characteristics of the total plant. Steady-state modeling will be used to calculate the detailed plant performance. Dynamic modeling of load change sequences (e.g., startup and load rejection) will be used to specify control system design and assess operability.

Introduction/Background

At the inception of the ATS program it was recognized that adoption of closed circuit steam cooled technology would require complete integration of the gas turbine and steam cycle systems to achieve the desired result. While closed circuit steam cooling technology offered a path to improved efficiency and lower cost of electricity (with single digit NOx emissions), it was imperative to maintain operability and reliability equal to the best current air-cooled gas turbine combined cycles. Accordingly a team was established to develop the steam cycle configuration and associated models, track its performance and cost, and assure its operability and reliability.

Discussion

Following is an overview of the ATS single-shaft combined cycle system, as well as its features and operating characteristics which illustrates the end result of extensive combined cycle system design activities in support of the ATS program.

Figure 2.3.4-1 shows an overview of the three-pressure, reheat steam cycle and its integration with the gas turbine cooling system.

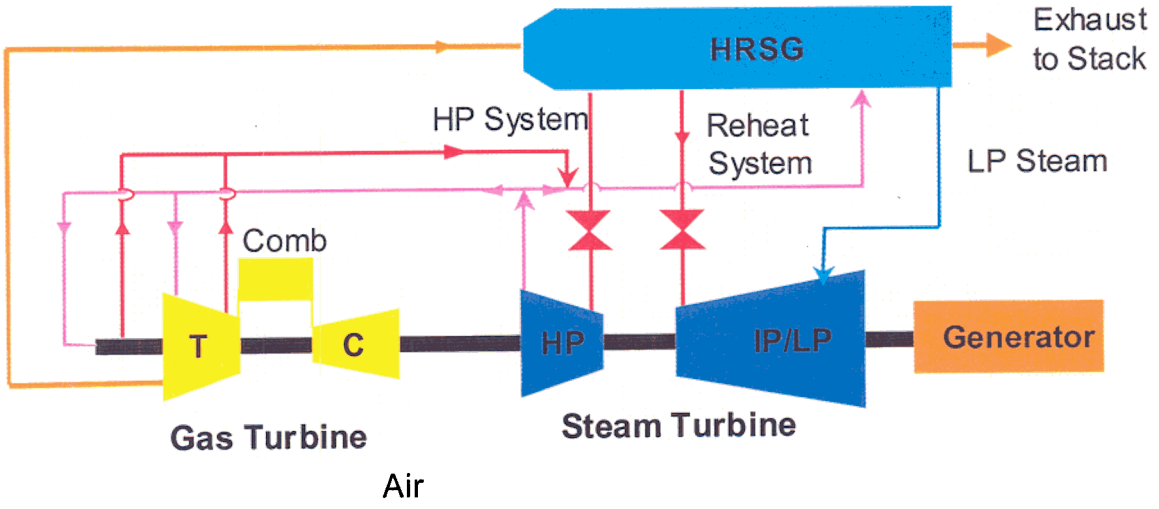

Figure 2.3.4-1. Overview of the GEPS ATS Integrated Steam Cooling System

Steam is supplied from the high pressure (HP) steam turbine exhaust and the HRSG intermediate pressure (IP) superheater to the closed circuit system that cools the gas turbine stage 1 and 2 nozzles and buckets. The gas turbine steam cooling system

operates in series with the reheater, with gas turbine cooling steam returned to the steam cycle cold reheat line.

During unit acceleration to rated speed and operation at low load, the gas turbine is cooled by air extracted from the compressor discharge. The air is filtered prior to supply to the cooling system. The cooling air from the gas turbine cooling circuit is discharged to the gas turbine exhaust. During air cooled gas turbine operation steam flow is established through the steam supply system to warm the steam lines and stabilize the steam supply conditions prior to admission of steam to the gas turbine cooling system. This steam is discharged via the reheater to the condenser through the IP bypass valve, which is modulated to maintain the pressure of the cooling steam above the gas turbine compressor discharge pressure to preclude gas leakage into the steam cycle. Appropriate shutoff valves isolate the gas turbine cooling circuit from the steam cycle while it is operating with air cooling. These cooling steam shutoff valves are included in the trip circuit such that the system is transferred to air cooling immediately upon an emergency shutdown to purge steam from the cooling system.

Initial cooling steam supply and line warming steam is supplied from the HRSG. Steam is extracted from the HP superheater after the first pass and mixed with steam from the HP superheater discharge to supply steam to the cooling steam system at the required temperature. In addition to providing start-up cooling steam supply to the gas turbine cooling steam circuit, the HP steam extraction after the first superheater pass is used to cool the LP steam turbine from ~70% speed until steam turbine loading is underway.

The sequencing system automatically starts the unit from a ready-to-start condition and loads it to gas turbine base load or a preset load. Starting time from initiation to full load are as follows:

Start Designation	Standby Period (hrs)	Time to Full Load (min)
Hot	0-12	60
Warm	12-48	120
Cold	>48	180

Figure 2.3.4-2 presents an overview of the starting and loading sequence for a hot start.

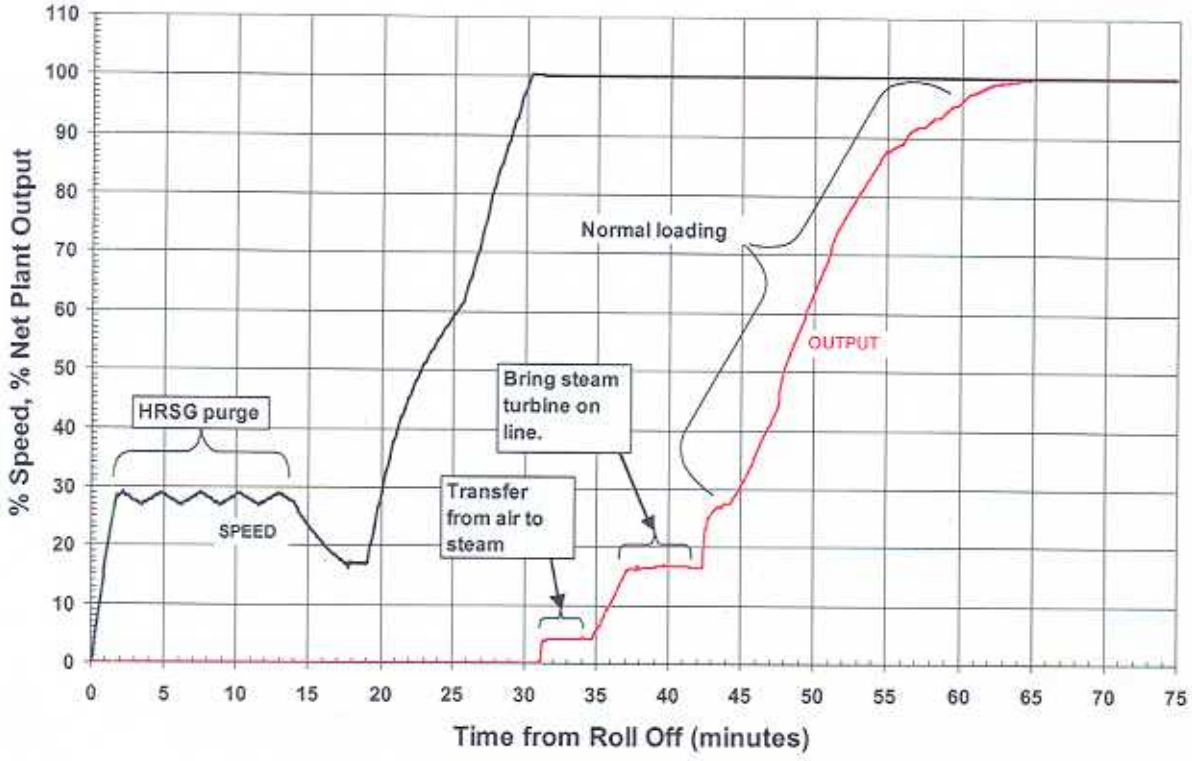

Figure 2.3.4-2. Typical S107H/S109H Hot Start Loading Profile

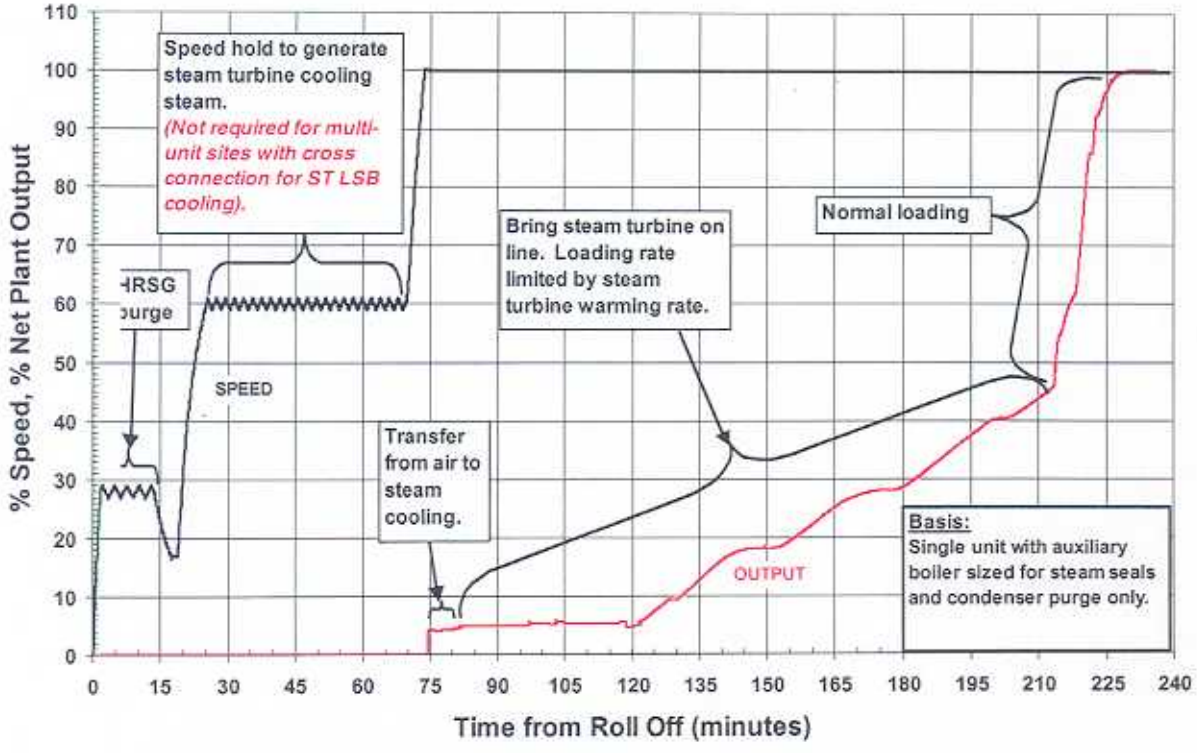

Figure 2.3.4-3. Typical S107H/S109H Cold Start Loading Profile, Single Unit

Figure 2.3.4-3 is a similar presentation of the cold start sequence of a single unit. Note the speed hold shown for developing steam for steam turbine cooling, which is not required in multi-unit installations where running units can be used to support steam turbine cooling needs of the starting unit.

Supply of high purity steam to the gas turbine cooling system is an essential requirement of the system for efficient long-term plant operation with high availability. Features included in the system to accomplish this requirement are:

- A reliable condenser leakage detection system with redundant condensate conductivity sensors and automated protection logic.
- Full flow feedwater filtration.
- All cooling steam is purified by evaporation in a steam drum with continuous monitoring of drum water purity.
- HP steam temperature control by steam attemperation.
- Full flow steam filtration.
- Application of non-corrosive materials in piping, filters and equipment downstream of the cooling steam shut-off valves.

The STAG 107H and STAG 109H are offered in a single-shaft combined cycle configuration, with two different LP steam turbines being offered. This configuration complements the cycle integration between the steam-cooled gas turbine and the steam bottoming cycle, and simplifies operation of the cooling steam supply system.

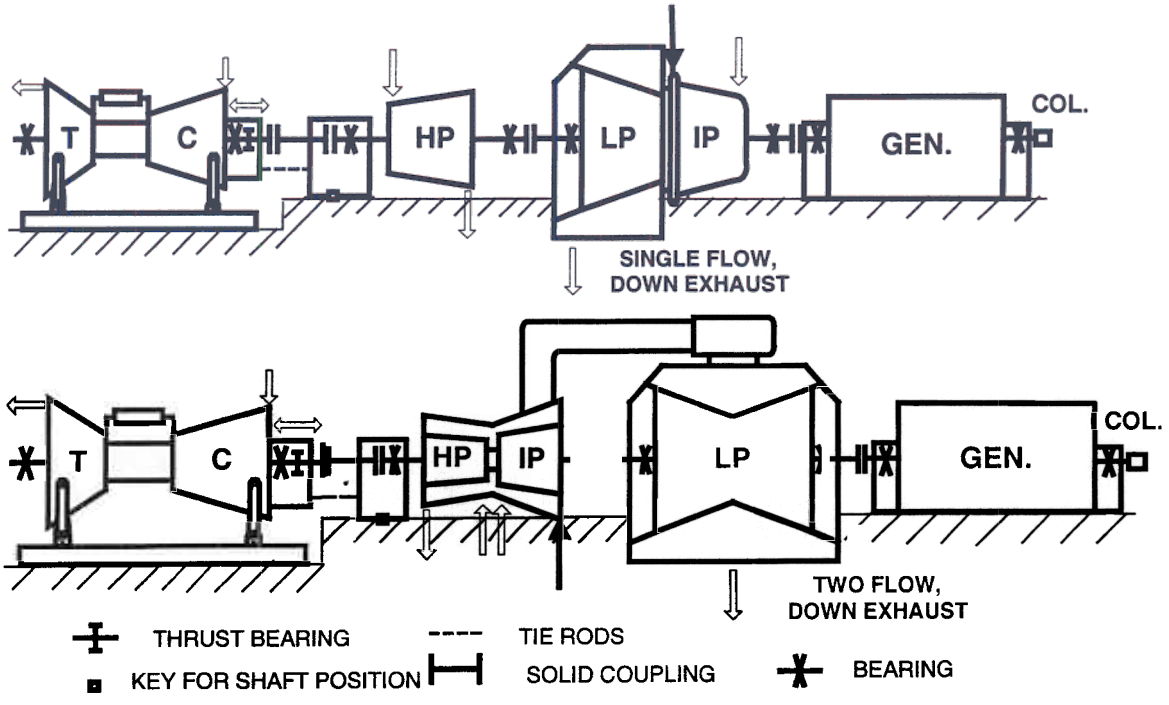

Figure 2.3.4-4. GEPS H Combined Cycle Configuration, Showing Two Different Steam Turbines.

The single-shaft power train is configured with the gas turbine on one end, the steam turbine in the middle and the generator on the other end, as shown in Figure 2.3.4-4. This close coupling of the steam and gas turbines permits full mechanical integration as a single prime mover with a single thrust bearing, thus minimizing the overall machine length. Use of all solid rotor couplings provides maximum reliability and simplifies the control, overspeed protection, and auxiliary systems.

The thrust bearing is located in the gas turbine inlet end bearing housing, which permits independent operation of the gas turbine for testing in the factory. This location is at the high pressure end of the steam turbine, which minimizes differential expansion, and permits use of small axial clearances throughout the HP and IP sections. The steam turbine contribution to the shaft thrust load is low, and is in the opposite direction to that of the gas turbine, so that the thrust bearing is lightly loaded under all operating conditions.

A single lubricating oil system with ac and dc powered pumps provides oil to all shaft bearings and to the generator hydrogen seals. Similarly, a single high-pressure hydraulic fluid system is used for all control and protective devices.

Summary/Conclusion

The combined cycle system design described in the previous section is the result of extensive analytical studies of numerous alternative configurations in terms of performance, operability, capital cost, operating cost, and reliability. These analyses often required development and validation of complex system models far more complex than prior combined cycle system designs. These evaluations were necessarily highly cross functional to assure a design that balanced the demanding requirements of the overall system against the constraints of individual components and sub-systems. This work will continue through the field testing of the S109H and S107H launch units to assure the successful commercialization of the ATS.

Technology Application

Operability evaluation of the STAG 109H configuration will be directly applicable to the STAG 107H ATS plant. Plant layout and piping design configuration, cooling-air cooling, plant control and protection strategies, and fuel heating system conceptual designs will be very similar for the STAG 107H ATS plant.

Section 2.4 (MF) Manufacturing Equipment and Tooling [G]

Objective

The materials, equipment, tooling and processes required to produce the 7H and 9H gas turbines will be identified, designed and procured. Manufacturing schedules will be established to support ATS pre-commercial demonstration goals. Manufacturing schedules and costs will be defined. Manufacturing will be conducted to these plans.

Introduction/Background

As part of the initial design phase of the project, Manufacturing Engineers were assigned to the design teams to assess the availability of material, equipment, and tooling to produce each component of the H gas turbines. This information was reviewed with the design teams and plans for design changes, development programs, and cost reductions were established. These plans were used to estimate the development, procurement and manufacturing cycles for each component. These cycles were used to construct a manufacturing schedule for each machine. The manufacturing schedule was then used to develop a schedule of the Engineering Design deliverables required to construct the H gas turbines. This information was used to determine when the H gas turbines could be produced for the FSNL testing, and for delivery to a power plant site.

Discussion

For the 9H and 7H gas turbines, the material, tooling, equipment, and Greenville manufacturing facility requirements were estimated, and potential sources for all required items were identified. Where no current GE suppliers were identified, industry searches were conducted to identify new suppliers. In cases where no suppliers were located, development programs and/or design changes were implemented to alleviate the situation. Since the 9H machine was developed first, all facility, tooling and equipment decisions on the 9H were made to also accommodate the 7H design to the greatest extent possible. A summary of the major program activities is as follows:

- Long-lead Material - Material development programs were put in place to develop large Inconel-718 rotor forgings, Cr-Mo-V rotor shaft forgings that exceeded existing sizes, N5 thinwall investment turbine airfoil castings, large compressor airfoil forgings, and material for numerous steam system components (spoolies, manifolds, bore tubes, elbows, and radial tubes). In addition to the development parts, suppliers were identified with capacity and capability to produce the larger size and more complex shaped iron and steel stator casing sand castings.

- Tooling - A significant amount of new tooling was required to build the 9H and 7H gas turbines.

  Tooling was purchased for the following starting materials:
  - Large Inconel-718 rotor forgings
  - Wooden patterns for stator sand castings

- Wax and core tooling for numerous airfoil investment castings
- Forging dies for compressor airfoils
- Casting tooling for steam system components

Manufacturing tooling for machining:

- Significant investment in fixtures and tooling for processing of airfoil castings into final configuration (Positioning fixtures, gauges, dovetail tooling, EDM fixtures, custom cutters and drilling equipment)
- Broach tooling, fixtures, positioning plates, gauges, special cutters and drill monitoring equipment for rotor forgings.
- Fixtures, gauges and cutting tools for compressor airfoils
- Tooling for close tolerance processing of steam system components

Tooling for special processes and inspection:

- Welding and brazing tooling for numerous airfoil processing steps
- Coating tooling for airfoils, rotor forgings, compressor airfoils, and steam system components
- Pressure testing of steam system components
- Welding and machining tooling for turbine Inner Shell fabrication
- Balancing and moment weigh fixtures for rotating components
- Coordinate measuring machine and gauging fixtures for numerous components
- Non-destructive testing fixtures and tooling
- Tooling, fixtures and balance tooling for steam bore tube manufacture

- Equipment for component manufacture- the following types of equipment were purchased for component manufacture:
  - Specialized ultrasonic equipment for inspection of Inconel-718 forgings
  - Numerous coordinate measurement machines for component inspection
  - EDM machines for airfoil machining
  - Laser, EDM and other welding machines for airfoil processing
  - 5-axis milling equipment for compressor airfoil machining
  - TBC coating equipment for airfoils
  - Specialized non-destructive test equipment for airfoil castings (Liquid penetrant, infra-red imaging, video boroscopes and wall thickness measurement)
  - Lathe pedestals, lifting fixtures and beams, broach plates and balancing equipment for rotor components

- Equipment for rotor and unit assembly:
  - Modifications to stack stands, balance machines, lift beams and lathe pedestals for rotor assembly.
  - Special tooling for tensioning rotor bolting
  - Ultrasonic equipment for measuring rotor bolt stretch during stack
  - Special tooling for assembly of rotor steam system

- Rail extension and floor modification to create assembly work station
- Special work platforms for 9H and 7H gas turbines
- Lifting pedestals to accommodate weight of H gas turbines
  Special equipment for installing and aligning Inner Shell into unit
- Alignment and tensioning equipment for unit assembly
- Assembly fixtures & stands, pressure test equipment and lifting equipment for Inner Shell assembly and testing.
- Shipping fixtures for rotors and Inner Shell
- Counterweight system for installing combustion

- Test Stand and equipment: - the H gas turbines required construction of a larger test stand in Greenville. This was a major construction effort to accommodate the advanced system interfaces and size of the H gas turbines. A modern control room with the latest monitoring, control and test technology is part of this facility. To accommodate this test stand, new rail track extensions, transfer cars and utility additions (electrical power, water and drain lines and a natural gas compressor) were required.

- Manufacturing schedules: - detailed manufacturing were developed for both the 9H and 7H gas turbines. These schedules linked the tooling, development, procurement and engineering schedules to the component and assembly schedule to show the required dates for all activities to support FSNL testing and shipment in time to meet delivery to power plant construction sites where pre-commercial demonstration testing has been arranged. These integrated schedules have been used to monitor status of engineering and manufacturing activities throughout the project. Periodic reports were issued from this schedule; highlighting activities that were behind schedule. These status reports resulted in changes to assembly sequencing, revised component workscopes, supplier changes, and numerous expediting actions to optimize the 9H and 7H gas turbine completion schedules. This process was followed throughout the program to continually monitor progress and take timely actions.

Summary/Conclusion

In summary all of the material, equipment, tooling and processes to design and manufacture the 9H and 7H gas turbines were identified, designed and procured. This was a significant effort requiring development of many new manufacturing processes, tooling concepts and assembly techniques. Numerous new and existing suppliers were involved in this process. In many cases, new and innovative tooling, gauging, processing and assembly methods were developed. Some of these can now be incorporated into existing gas turbine designs to improve performance and reduce cycle and cost.

The scheduling process developed for running these projects had to be designed to accommodate numerous development schedules and be flexible enough to work around the inherent changes that are part of new technology programs. To date both the 9H

and 7H gas turbines have completed FSNL1 testing, and the 9H has completed FSNL2 testing and is being processed for delivery in 2000.

Technology Application

Development of the turbine wheel forging dies and the ultrasonic inspection techniques are the first application in forgings of this size and will be used to provide high-strength, high-temperature material that is compatible with the steam cooling environment in the ATS turbine rotor. The mockups are being used to ensure fit-up of all components in very restrictive areas of the turbine. An electronic simulation of these areas is being done in parallel to develop simulation technology for future applications. The TBC robot controllers will provide the thickness control for the TBC coating that is required for proper heat transfer properties in the steam-cooled turbine airfoil components.

Section 2.5 (IG) Integrated Gasification and Biomass Fuel [S]

Objective

An assessment of the ATS will be performed as part of an efficient and environmentally compatible Integrated Gasification Combined Cycle (IGCC) power generation system. Modifications to the gas turbine to accommodate the low heating value fuel gas and nitrogen injection for low NOx emissions will be identified. Analyses will be run to optimize the integration of the steam cycle with one oxygen-blown entrained flow gasifier and gas cleanup system and integration of the gas turbine with the air separation unit. IGCC system performance will be analyzed for one coal composition at ISO ambient air conditions.

Background

GE Power Systems has been a major participant in the demonstration of Integrated Gasification Combined Cycle (IGCC) power generation technology starting with the Coolwater demonstration in the early 1980's with 7E-level gas turbine technology. This was followed with the Public Service of Indiana (PSI) and Tampa Electric (TECo) Clean Coal Technology projects in the early 1990's with 7F based gas turbine technology. The 7F gas turbines at PSI and TECo have been successfully operating at 192 MWe on coal-derived syngas.

This following describes the configuration optimization study result of an IGCC power plant design, integrating General Electric's (GE) single shaft combined steam and gas (STAG) 109H combined cycle unit with Texaco's heat recovery coal gasification unit, and Praxair's elevated pressure (EP) air separation unit (ASU). The full heat recovery IGCC design is preferred for high cost fuels, where high efficiency is important. The cycle analysis and system optimization were performed jointly by GE, Texaco, and Praxair as part of a larger study where the results were presented at the October 1999 Pittsburgh Coal Conference. The approach of this study is directly applicable to the 7H ATS 60 Hz configuration.

The oxygen blown type gasification process with conventional low temperature gas cleaning was selected for *H System*™ IGCC over the optional air blown type gasification process with hot gas clean-up, since the air blown systems at present are impractical for this size machine.

Discussion

Study Basis

The study was conducted at ISO ambient conditions using a typical sub-bituminous coal. The design basis is given in Table 2.5-1.

Table 2.5-1: DESIGN BASIS

1. **ISO Ambient (59^{O}F, 14.7 PSIA, 60% Relative Humidity)**
2. **Bayswater, Australian Sub-Bituminous Coal, 1% Sulfur, 12559 Btu/LB HHV**
3. **Single Train Gasifier (3940 tpd), Combined Cycle and Air Separation Unit**
4. **Optimized Air Integration To Give Ambient Range 32 To 95 ^{O}F**
5. **Low Emissions < 25 PPM NOx, SOx < 5 PPM**
6. **Zero Process Waste Discharge**
7. **Base Load Operation, 50 To 100% Load Range Capability**
8. **Total Plant Availability 95%, (85% On Gasifier Fuel)**
9. **Natural Gas as Start Up and Back Up Fuel**
10. **Sea Water Cooling supplied at 68^{O}F with 12.6^{O}F Temperature Rise**

The performance study is based on a single train consisting of the following units:

- Coal feed preparation
- Air Separation
- Gasification (with high temperature syngas cooling)
- Low temperature gas cooling and energy recovery
- Saturation and heating
- Syngas scrubbing for particulate removal
- Solids handling
- Acid gas removal
- Sulfur removal and tail gas treating
- Nitrogen compression, saturation, heating and injection
- Combined cycle power system

The block flow diagram as depicted in Figure 2.5-1 represents the H-technology IGCC system configuration.

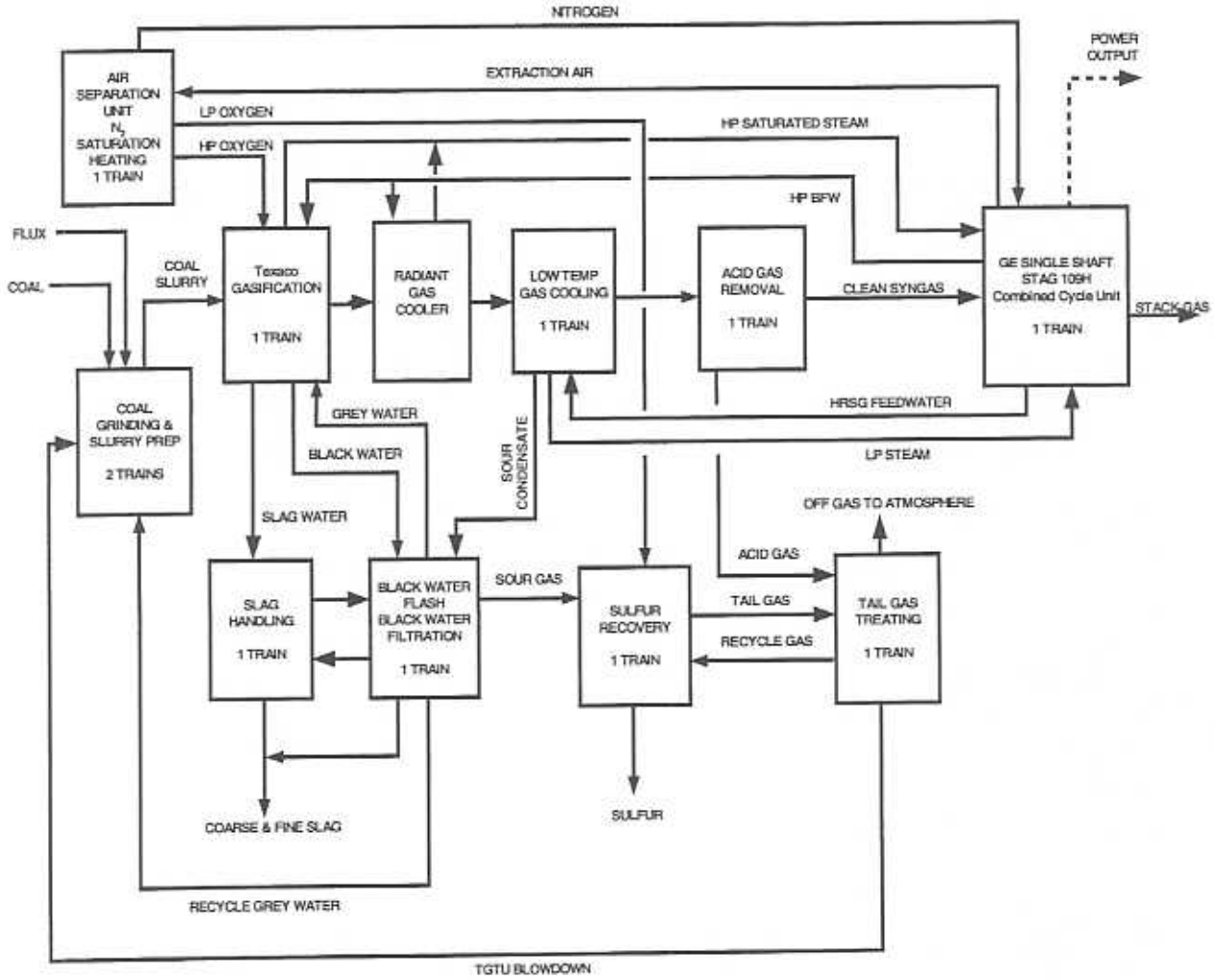

Figure 2.5-1. Heat Recovery (HR) IGCC Design Block Flow Diagram

Gasification Unit

The Texaco Gasification Process can be designed for a broad range of pressure levels, depending on the requirements of the application that the unit is being designed for. This makes it suitable for integrating with the higher-pressure ratio 9H gas turbine. In this study, the operating pressure selected was set based on the fuel pressure requirement of the gas turbine. It is preferred that the heat recovery system operates at gas turbine based pressures, because the heat transfer equipment becomes prohibitively more expensive at higher pressures.

The heat recovery IGCC design configuration uses only radiant syngas coolers (RSC) for the coal feed. Recognizing the experience of Tampa Electric's Polk Power Station, it was decided by the joint study team to pursue only a radiant syngas cooler for the high temperature syngas cooling. The gasifier operates at 570 psia in order to provide syngas at the pressure level required by the 9H gas turbine.

High-pressure (HP) steam at 2000 psia is produced in the radiant syngas coolers for export to the combined cycle unit. The syngas is quenched at the exit of the radiant cooler, thus requiring the import of hot HP economizer water from the HRSG.

The heat recovery in the low temperature gas cooling section involves syngas cooling through heat exchange with the cleaned saturated syngas and the scrubber return condensate. After the condensate is collected in a knockout drum, the syngas is heated with HRSG intermediate pressure (IP) economizer water before passing through a carbonal sulfide (COS) hydrolysis unit. The syngas is further cooled to saturate clean syngas fuel and generate LP steam.

Steam cycle integration between combined cycle HRSG and heat recovery gasification units involves the export of HP syngas cooler steam to the HRSG generated from HP economizer feed water. No HP steam is produced or exported to the combined cycle unit.

Air Separation Unit

The air separation unit (ASU) selected as the basis for this study is an elevated pressure ASU designed to operate with a feed pressure consistent with the gas turbine extraction air pressure. All of the ASU air feed is supplied by the gas turbine. This, along with the requirement to return all of the nitrogen from the ASU to the gas turbine, resulted in an elevated pressure ASU as the most efficient and cost effective selection.

The pressure of the extraction air from the 9H (320 psia) is significantly higher than the air feed pressure of a typical ASU (80 psia). At these pressures, a traditional double column air separation process can not efficiently separate the air. However, by adding a third distillation column that is thermally linked with the double column arrangement, high separation efficiencies can be achieved.

One of the benefits of elevated pressure operation is that both the oxygen and nitrogen products are produced from the separation process at elevated pressures. This results in

lower capital and operating costs for the product compression by reducing the number of product compression stages. A second benefit of elevated pressure operation is a significant reduction in power (relative to low pressure ASUs) when all of the products (oxygen and nitrogen) are required at pressure. The oxygen pressure from the separation process was adjusted to optimize the capital and operating costs of the system. In all cases, the nitrogen pressure from the process is dependent on the ASU air feed pressure.

Combined Cycle Unit

The *H System*™ single shaft combined cycle configurations incorporate proven combined cycle features for high efficiency and outstanding operability, in addition to integration with a gasification and cleanup system to enable operation on syngas efficiently, and with minimum effort on the environment. For more extensive analysis, please refer to Section 2.3.4, Combined Cycle System Design.

The gas turbine analyzed was specifically configured to burn the cleaned gas from the oxygen blown Texaco gasifier. The gas turbine was also integrated with the ASU, supplying all of its compressed air, and using nitrogen from the ASU to increase output and reduce NO_x emissions.

The steam cycle was integrated with the gasification and gas cleanup systems to maximize thermal efficiency. It was designed for operating simplicity, high reliability and convenient maintenance. The accessory systems and controls were integrated to be consistent with the requirement for high reliability and maintainability.

The combined cycle equipment consisted of a single shaft gas turbine - steam turbine - generator unit, and an unfired three pressure level natural circulation heat recovery steam generator (HRSG) unit. Natural gas was used as a start-up and back-up fuel to the gas turbine.

This analysis represented a special case for the STAG 109H system, and involved a careful study of matching the combined cycle's steam bottoming cycle, the gas turbine's steam cooling requirements, and the need for operation of the IGCC design with natural gas startup and backup fuel.

***H System*™ Provisions for IGCC**

The *H System*™ machines will be capable of being modified to accommodate IGCC with minimum change from the natural gas fired configuration. The IGCC modifications for the STAG 109H combined cycle have been identified and consist of the following:

- Dual fuel, diffusion flame, gas turbine combustion system
- High temperature gas turbine syngas fuel skid, piping and manifolds
- Nitrogen injection control skid, piping and manifolds
- Air extraction control skid, piping and manifolds
- Syngas nitrogen purge system
- Fuel control integration with gasification process
- Turbine enclosure modifications for high H2 syngas fuel

- Gas turbine cooling steam temperature control for both syngas and natural gas
- Thermal integration of syngas heating system
- Larger steam turbine for accommodating added IGCC steam flow
- Larger generator for accommodating increased IGCC output

A multi-nozzle, diffusion flame, reverse flow, can annular, IGCC combustion system derived from the Sierra Pacific/Pinion Pine F class combustor would be used for the syngas fired 9H. The high hydrogen content of the coal derived low-BTU syngas precludes a DLN type combustion system as is used in the current H machines. Also, since the compressor discharge temperature of the H machines is above the auto-ignition temperature of hydrogen, a diffusion/heterogeneous combustion system is the most technically feasible at this time.

Air extractions for integration with the ASU will be taken from each combustor can casing to assure adequate air cooling of the combustor transition piece. Nitrogen injection shall be introduced into the head-end of the combustor for NOx abatement.

The reheat, condensing steam turbine with an integral HP/IP opposed flow section requires a four flow LP section and is rated for nominal inlet steam conditions up to 1800 psig/1050°F/1050°F. The high and intermediate pressure sections are combined in one casing connected by a single crossover to the center of the double/four flow, low-pressure section. The design of the LP section and last stage bucket size may vary with different steam turbine exhaust flows and pressures.

***H System*™ IGCC System Performance**

Table 2.5-2 displays the overall IGCC performance of the 9H based on a coal feedstock. Comments to the performance are the following:

- The standard GE MS9001H gas turbine configuration was used in this performance analysis, retrofitted with IGCC combustors, accessories, and piping to enable it to be integrated with the rest of the IGCC system. No other changes to the flange-to-flange gas turbine including hot gas path, compressor, and rotor were used in the analysis.
- Firing temperature was limited by adherence to hot gas path operating temperatures consistent with projections for natural gas fired operation such that hot parts lives are unaffected by IGCC operation.
- All of the air required by the ASU was extracted from the gas turbine without disturbing the combustor and turbine hot gas path cooling requirements.
- Resultant turbine flow and pressure ratio after extracting ASU air, re-injection of nitrogen, and syngas flow are close to the natural gas fired DLN 9H.
- Full air extraction reduced the ASU power consumption and capital cost.
- NOx emissions from the combined cycle using diffusion flame combustors were estimated with the humidified syngas and residual humidified nitrogen injection from the ASU. This was done using "F-technology" data and correcting it for the higher combustor pressure and temperatures of the H.

- It is expected that improvements in *H System*™ IGCC performance will be realized as development engine test data analysis becomes incorporated into the design and performance data base.
- No additional torque enhancements have been imposed on the gas turbine rotor.

Table 2.5-2. Overall 9H IGCC Performance

Estimated Overall IGCC Performance Texaco Heat Recovery Coal Gasification Process Praxair Elevated Air Separation Unit GE STAG 109H Combined Cycle Unit 59 F / 60% R.H. / 0 Ft. / 68 F Tcw		
Energy Input:		
	Coke Feed Rate (sTPD):	3,940
	Coke LHV (Btu/Lb):	12,136
	HHV (Btu/Lb):	12,559
	Energy In, LHV (MMBtu/h):	3,985
	HHV (MMBtu/h):	4,124
	Clean Gas to GT, LHV (MMBtu/h):	2,922
	HHV (MMBtu/h):	3,123
Energy Output:		
	Combined Cycle Gross Output - MW	572.3
	Power Island Auxiliary Power - MW	10.0
	ASU and Gas Plant Aux Power - MW	33.0
	Balance of Plant Aux Power - MW	3.6
	Total Power Consumption - MW	46.6
	Net Plant Power Output - MW	525.7
Performance:		
	Net Heat Rate, LHV (Btu/kWh):	7,572
	HHV (Btu/kWh):	7,836
	Net Efficiency, LHV (%):	45.1
	HHV (%):	43.6
Heat Rejection:		
	To Cooling Water (MMBtu/h):	1,457
	From HRSG Stack (MMBtu/h):	311
Emissions:		
	NOx at 15% O2 (ppmvd):	<25
	SOx (Lb/MMBtu):	0.02
	CO2 (Lb/MMBtu):	204
	Sulfur (sTPD):	39.4
	Solid Waste (sTPD):	394.2

Summary/Conclusions

The study of adapting the *H System*™ to utilize coal derived fuel gas in an IGCC configuration has yielded the following conclusions:

- The *H System*™ machines should be capable of operating on both coal derived fuel gas and natural gas.
- The hot gas path parts are expected to have the same life expectancy and inspection intervals as those of the base natural gas fired machines.
- Power output for a single train *H System*™ machine appears to be of the same scale as conventional utility based coal fired power plants.
- Further system optimization work will be needed to improve the overall efficiency of the *H System*™ machines to achieve the desired 50+% (LHV) overall net IGCC efficiency level.

Future work should be directed toward the following activities:

- Additional study of operability issues related to operation of the *H System*™ IGCC configurations with natural gas fuel (steam integration issues).
- Further examination of *H System*™ gas turbine compressor capabilities over a range of ambient air temperature operation with low BTU syngas fuel.
- Confirmation of emission estimates through combustion testing at *H System*™ level pressures and temperatures with syngas in diffusion flame combustor designs proposed for the *H System*™ gas turbine.
- Study of hot gas path material and coatings compatibility with coal derived syngas.

  Additional combined cycle system analysis to be performed on the *H System*™ machines to investigate the effects of operating a system designed for IGCC operation on a natural gas back-up/start-up fuel.
- Review of the *H System*™ machines Integrated Control System to confirm added I/O capability for IGCC control integration.

  Examine *H System*™ gas turbine system design modifications needed to enhance overall compatibility with IGCC operation.

Technology Application

Integrated gasification combined cycle (IGCC) and biomass fuel based applications are potential uses for the ATS machine as part of an economical and environmentally compatible power generation system.

Section 2.6 (DE) Pre-Commercial Demonstration

Objective

This task is deleted.

Section 2.7 (PM) Program Management [S]

Objective

Within GEPG Engineering, an ATS Program Office will be established, and a Program Manager and a Contract Administrator will be assigned. The Program Manager will direct the overall activities of the Program Office and will have responsibility for reporting to DOE and ensuring that the program goals are achieved. The Program Office is responsible for communicating contract requirements, authorizing applied labor and expenses for material and services, scheduling, monitoring, and reporting cost and technical performance. Additional responsibilities include coordinating ATS activities with CRD and GEAE. The assigned Contract Administrator will support the Program Manager in all administrative matters. All materials and equipment acquisitions will be closely monitored by the Program Office with support from the Finance and Sourcing organizations.

Actual scope, schedule, and budget will be tracked against plan. An integrated Program Plan will be maintained, including a detailed Work Breakdown Structure, that accurately describes the planned work, reflecting all changes in work scope or schedule. The integrated program plan includes the implementation and coordination of all program support procedures and initiatives such as Target Costing, Key Quality, and Design for Manufacturing.

Reports will be prepared to serve both DOE and GE needs for oversight and monitoring, including quarterly reports, annual reports, and topical reports. A final report will be prepared at the completion of the Cooperative Agreement. Reports specified in the Cooperative Agreement's Financial Assistance Reporting Requirements Checklist will be supplied. Technical papers will be submitted for presentation to professional society meetings.

Discussion

An ATS Program Office was established at GEPS, and a Program Manager and Contract Administrator were assigned. The ATS Program Office delivered all contractually required reporting to DOE on schedule, including monthly, quarterly, and annual technical, program, and financial status reports. Quarterly Program Reviews were held with the DOE Contracting Officer's Representative (COR).

The Program Office communicated contract requirements to the responsible Engineering Design management regarding contract and reporting requirements. The Program Office also prepared annual Continuation Applications to DOE. These provided comprehensive

cost-to-complete program estimates, by task, and included applied labor, and purchased material and services at GE Power Systems, and corresponding vendor quotes from GE Corporate Research and Development (CRD), and GE aircraft Engines (GEAE). In addition, the Program Office managed the technical progress of the activities at CRD and GEAE.

The program scope, schedule, and budget were tracked against the plan, and reported to DOE each quarter, as required. An integrated Program Plan was maintained, which included a detailed Work Breakdown Structure (WBS) that accurately described the planned work, and reflected all changes in the work scope and schedule. The integrated Program Plan included the implementation and coordination of all program support procedures and initiatives, and reflected all activities involved in the WBS.

As mentioned above, all contractually required reporting to DOE was delivered on schedule. This reporting included monthly, quarterly, and annual technical, program, and financial status reports. Quarterly reviews were held with the DOE COR at various GE locations (GEPS - Schenectady, NY, Greenville, SC; GE-CRD, Niskayuna, NY; GE Aircraft Engines - Evendale, OH) to update program status, and to view the various test facilities associated with the ATS development and testing programs.

GEPS participated in each ATS Annual Program Review, presenting a status update report, and writing an abstract and paper for the Meeting Proceedings. In addition, GEPS presented a paper at a technical conference or symposium each year during the contract.

GEPS completed the required Topical Report for Phase 3R, which included the Environmental, Health, and Safety information required for DOE to prepare an Environmental Assessment for the Greenville, SC manufacturing and test facility, resulting in DOE's issuing of a Finding of No Significant Impact (FONSI). In addition, a Topical Report on "Predicted Reliability, Availability, Maintainability for the General Electric 7H Gas Turbine" was produced.

The final report was produced as part of the normal reporting process, and provided a technical accounting of the total work performed on the project. The report summarized all topical reports, and technical progress reports, and provided the original Objective for each WBS element, along with Introduction/Background, Discussion, Summary/Conclusion, and Technology Application. The total report contained an Executive Summary, Overview, and above mentioned task by task reviews.